Management of Reinforcement Corrosion

A Thermodynamic Approach

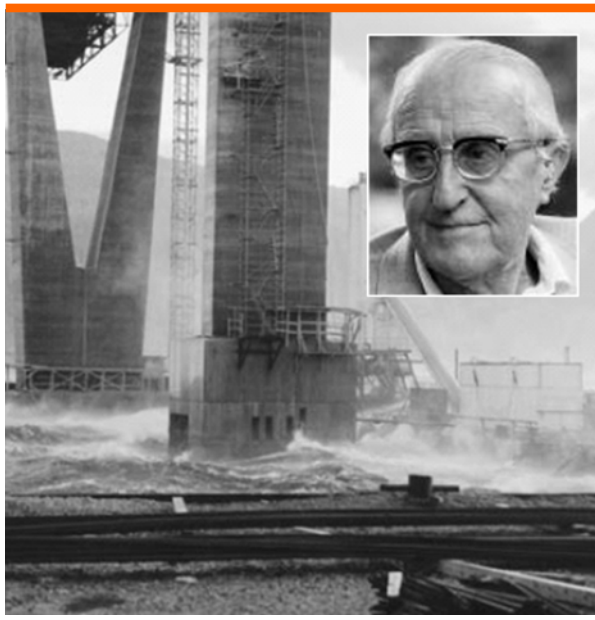

André Küter

PhD Thesis

Department of Civil Engineering

2009

DTU Civil Engineering Report R-228 (UK)
April 2009

DTU Civil Engineering
Department of Civil Engineering

Management of Reinforcement Corrosion

A Thermodynamic Approach

André Küter

PhD Thesis

Department of Civil Engineering
Technical University of Denmark

2009

Photos front page:
Construction of Helgeland Bridge, Leirfjorden, Norway [COWI, 2007a]
Marcel Pourbaix, Russia/Belgium, 1904-1998 [HUJI, 2007]

Management of Reinforcement Corrosion
A Thermodynamic Approach

Printed by Rosendahls-Schultz Grafisk
Department of Civil Engineering
Technical University of Denmark
ISBN 9788778773074
ISSN 1601-2917

Preface

This thesis is submitted as a partial fulfilment of the requirements of the Danish PhD degree. The thesis is based on the theoretical studies and experimental investigations conducted during the PhD project "Management of Reinforcement Corrosion" in the period from October 2003 through September 2007 at the Department of Civil Engineering (DTU Byg) of the Technical University of Denmark (DTU), Kgs. Lyngby, Denmark. The project period was intermitted by altogether one year of leave for projects that were not related to the PhD studies.

The principal supervisor of the PhD project was Associate Professor Mette R. Geiker from DTU Byg and Professor Per Møller from the Department of Mechanical Engineering (DTU Mekanik) at DTU acted as co-supervisor. The experimental work was carried out at DTU Byg and at DTU Mekanik as well as during an external research stay at the Department of Materials Science and Engineering at Northwestern University, Evanston, IL, USA, where the research was supervised by Professor Thomas O. Mason.

Acknowledgments

I owe the outcome of this PhD project to my supervisors Mette R. Geiker and Per Møller. I regard the last years as a unique educational journey, through which I have acquired valuable knowledge from them, and with them. They were always there when needed, for either inspiration or help. I would like to thank Mette and Per most sincerely for that.

At the same time, I also wish to express my gratitude to all my colleagues at DTU Byg and DTU Mekanik for their professional work and for helping to make my project both productive and enjoyable.

I would also like to thank Professor Thomas O. Mason and his group at Northwestern University for the valuable input, a great time, and for letting me use the facilities at the Department.

Furthermore, I would like to thank Helle Fiedler and Karl-Johan Hansen from Hempel A/S in Kgs. Lyngby, Mads C. Nielsen and Christina Pedersen from Lemvigh-Müller Stål A/S in Copenhagen, Leif Brunckhorst from Condor Kemi A/S in Glostrup, and Thomas Petersen from M Seals A/S in Espergærde (all in Denmark), and Rainer Olschok from Drahtwerk Elisental in Neuenrade, Germany, for advice and free-of-charge provision of experimental equipment and materials.

I also wish to express my gratitude to the sponsors of my external stay and of two of the conferences I participated in. My external stay at Northwestern University was funded by the Knud Højgaard Foundation, Kgs. Lyngby, Denmark, my participation in ConMat'05, Vancouver, BC, Canada, was financed by the Otto Mønsteds Fond, Hellerup, Denmark, and by the Research and Innovation Committee of DTU Byg, and the airfare for my participation in NKM13, Reykjavik, Iceland, was sponsored by the University of Iceland, Reykjavik.

Moreover, I would like to gratefully acknowledge the financial support of COWIfonden, Kgs. Lyngby, Denmark, for the establishment of a high-capacity exposure and monitoring system for testing of reinforcement corrosion.

Finally, I would like to thank my parents, Ute and Wolfgang, and my wife Mareike for their constant encouragement and care.

Abstract

Several measures to combat reinforcement corrosion have been proposed during the past decades; these comprise both preventive and rehabilitation measures. Around 50 patents pertaining to limiting corrosion of steel in concrete have been submitted in 2007 alone. Some of these patents relate to corrosion inhibitors, others take account of surface modifications, cathodic protection, or replacement of carbon steel reinforcement with alternative materials. Often it is difficult to evaluate the value of such proposals, since their effectiveness is largely governed by the given conditions, i.e. the microstructure of the concrete, the concrete-steel interface, and not least the surrounding environment.

Only a few methods, as the use of stainless steels and cathodic protection, are considered to be effective corrosion countermeasures, but these methods cannot always be justified for economical or technical reasons. Thus, there is – even after decades of research and development in the area of corrosion protection – still demand for both preventive and rehabilitation measures, which are effective and in particular cost-efficient.

The lack of performance of some countermeasures can be explained by conceptual weaknesses from a thermodynamic perspective, as the descriptions of the mechanisms are inconsistent or incomplete. That holds particularly for formation of macrocells and thus concentration cells, where the corrosion mechanisms in combination with the cement chemistry can easily be quite complex, e.g. the mechanisms for the formation of green rust.

With the above as point of origin, in the present thesis a consistent thermodynamic basis is established for the description of corrosion processes as well as for the evaluation of existing and the development of new corrosion countermeasures. The work covers: a) the adaptation of available thermodynamic principles to the area of reinforcement corrosion, b) thermodynamically consistent descriptions of the diverse corrosion states of steel in concrete, c) a review and evaluation of available measures for corrosion protection, and d) the development of theoretical concepts for new cost-efficient countermeasures. In addition to the theoretical considerations, two implementation principles of the developed concepts are proposed and one of these tested by means of custom-designed setups and measurement methods.

The two proposed principles relate to the use of ordinary carbon steel reinforcement and can be applied for both new and existing structures. The first principle is based on a surface modification of carbon steel reinforcement, whereas the second principle employs new concepts for sacrificial anodes. Both principles are expected to significantly improve the corrosion protection of carbon steel reinforcement in carbonated or chloride contaminated concrete.

Both principles of implementation aim at obtaining targeted low corrosion potentials. The materials concepts are based on processes that introduce magnesium and zinc in combination with supplementary electrochemically active compounds to the concrete-steel system. In addition to the provision of low corrosion potentials, the first principle also enables an improvement of the concrete-steel interface.

An experimental setup was established for investigating the first principle of implementation. The experiments were performed on reinforcing bars embedded in either mortar or cement paste. Mortar specimens with cast-in electrodes were applied for obtaining comprehensive electrochemical data for the reinforcement and the mortar matrix. An automated system based on cluster measurements allowed for detailed monitoring of multiple specimens. Monitoring of the corrosion potential and macrocell current was performed continuously and frequently supplemented by electrochemical impedance spectroscopy. The cement paste specimens, which could be produced in large amount, were used for initial as well as destructive measurements, e.g. anodic polarisation curves. In addition to the electrochemical techniques, chemical analyses were applied for e.g. the determination of chloride contents or pH alterations. Microscopy and energy dispersive X-ray spectroscopy were used to obtain extensive data for a comprehensive thermodynamic performance evaluation.

Selected experimental results are used in this thesis as illustration and documentation of the proposed mechanisms and concepts. With regard to expected patent possibilities, certain central concepts and results from the experimental investigations concerning the implementation of new countermeasures are not included in the present thesis; they will be dealt with in future publications.

Resumé (in Danish)

Adskillelige metoder til begrænsning af armeringskorrosion er blevet foreslået gennem de seneste årtier; disse omfatter både forebyggende og udbedrende foranstaltninger. Alene i 2007 er der indgivet ca. 50 patenter med relation til minimering af korrosion af stål i beton. Nogle af disse patenter tager udgangspunkt i anvendelse af korrosionsinhibitorer, andre omhandler overflademodificeringer, katodisk beskyttelse eller udskiftning af kulstofstålarmering med alternative materialer. Det er ofte vanskeligt at vurdere værdien af sådanne tiltag, da deres effektivitet i høj grad er styret af konkrete forhold, dvs. betonens mikrostruktur, grænsefladen mellem beton og stål og ikke mindst det omgivende miljø.

Kun få metoder, som brug af rustfrie ståltyper og katodisk beskyttelse, regnes for at være effektive foranstaltninger mod armeringskorrosion; men disse metoder kan af økonomiske eller tekniske årsager ikke altid berettiges. Der er således – selv efter årtiers forskning og udvikling af metoder til imødegåelse af armeringskorrosion – stadig efterspørgsel efter både forebyggende og udbedrende løsninger, som er effektive og især økonomisk attraktive.

Den manglende effekt af nogle foranstaltninger kan forklares ved, at de besidder konceptuelle svagheder set fra et termodynamisk synspunkt, idet beskrivelserne af mekanismerne fremstår termodynamisk set inkonsekvente eller ufuldstændige. Her tænkes specielt på dannelsen af makroceller og dermed koncentrationsceller, hvor korrosionsmekanismerne i kombinationen med cementkemien let bliver meget komplekse, f.eks. mekanismerne for dannelsen af grøn rust.

Med udgangspunkt i ovenstående er det formålet med denne afhandling at etablere en sammenhængende termodynamisk basis til beskrivelse af korrosionsprocesser samt vurdering af eksisterende og udvikling af nye foranstaltninger mod korrosion. Der er foretaget a) tilpasning af tilgængelige termodynamiske principper til området korrosionsbeskyttelse af stål i beton, b) opstilling af en termodynamisk konsistent beskrivelse af de forskellige korrosionstilstande for stål i beton, c) granskning og evaluering af nuværende foranstaltninger til korrosionsbeskyttelse og d) udviklingen af teoretiske koncepter for nye omkostningseffektive foranstaltninger. Som supplement til de teoretiske betragtninger er to anvendelser af de teoretiske koncepter blevet foreslået og én af disse afprøvet ved hjælp af specielt udviklede forsøgsopstillinger og målemetoder.

De to foreslåede korrosionsbeskyttelsesprincipper er udviklet til beskyttelse af almindeligt kulstofstålarmering og er anvendelige til beskyttelse af armering i såvel nye som eksisterende konstruktioner. Det første princip er baseret på overflademodifikation af armeringen, mens det andet princip anvender nye koncepter for offeranoder. Begge principper forventes i betydelig grad at forbedre beskyttelsen af kulstofstålarmering i carbonatiseret eller chloridholdig beton.

Begge beskyttelsesprincipper har til formål at etablere et tilpasset lavt korrosionspotentiale. Materialekoncepterne bygger på processer, der introducerer magnesium og zink sammen med andre elektrokemisk aktive materialer i beton-stål systemet. Foruden at etablere et lavt korrosionspotentiale forbedrer det første princip også grænsefladen mellem beton og stål.

Der er etableret en forsøgsopstilling til eksperimentel undersøgelse af det første korrosionsbeskyttelsesprincip. Forsøgene blev udført på armeringsstænger omstøbt med enten mørtel eller cementpasta. Mørtelprøverne med indstøbte elektroder blev brugt til bestemmelse af omfattende elektrokemiske data for armeringen og mørtelmatrixen. Et automatiseret system baseret på "cluster measurements" tillod detaljeret monitering af adskillige prøver. Måling af korrosionspotentiale og makrocellestrøm blev udført kontinueret og hyppigt suppleret med elektrokemisk impedans spektroskopi. Cementpastaprøverne, som kunne produceres i stort antal, blev anvendt til indledende og destruktive målinger, f.eks. til bestemmelse af anodiske polariseringskurver. Foruden de elektrokemiske teknikker, blev kemiske metoder anvendt til f.eks. bestemmelse af kloridindhold og ændringer i pH-værdi. Mikroskopi og energidispersiv røntgenspektroskopi blev brugt til at indsamle afgørende data til den omfattende termodynamiske evaluering af effekten af korrosionsbeskyttelsen.

Udvalgte eksperimentelle resultater er i rapporten anvendt som illustration og dokumentation af de foreslåede mekanismer og koncepter. På grund af forventede patentmuligheder er nogle af de teoretiske koncepter og eksperimentelle resultater ikke inkluderet i denne afhandling; de vil blive inkluderet i fremtidige publikationer.

Symbols and Abbreviations

For the purpose of this thesis the symbols and abbreviations in the below table apply. The list is in alphabetical order (first Latin, then Greek).

Throughout this thesis these symbols and abbreviations are indicated by single quotes, but the single quotes are omitted in equations and figures. A small type "s" is added to the symbol or abbreviation, if it is referred to in plural.

Symbol or abbreviation	Standard unit	Definition
'a'	mol/L	Activity (in terms of concentration)
'ASR'	-	Alkali-silica-reaction
'b'	-	Tafel constant[*]
'C'	mol/L	Concentration of a chemical species
'C_{dl}'	A×s/V	Double layer capacitance
'CE'	-	Counter electrode
'C_p'	J/(mol×K)	Heat capacity at constant pressure (specific heat)
'CP'	-	Cathodic protection
'CPre'		Cathodic prevention
'C-S-H'	-	Calcium-silicate-hydrate
'D'	m^2/s	Diffusion coefficient
'E'	V_{SHE}	Electrode potential (see Chapter 'TaD')
'E_0'	V_{SHE}	Equilibrium potential[*, †] (see Chapter 'TaD')
'EDS'	-	Energy dispersive X-ray spectroscopy
'EEW'	-	Embedded electrode wire
'ECat'	-	External cathode
'E_{corr}'	V_{SHE}	Corrosion potential (see Chapter 'TaD')
'ECR'	-	Electrochemical chloride removal
'EIS'	-	Electrochemical impedance spectroscopy
'$El_{\#}$'	-	Arbitrary element with index specified by "#"[†]
'EMF'	V_{SHE}	Electromotive force (see Chapter 'TaD')
'E_{pp}'	V_{SHE}	Primary passivation potential
'E_{pit}'	V_{SHE}	Pitting potential (see Chapter 'TaD')
'ERA'	-	Electrochemical realkalisation
'F'	A×s/mol	Faraday constant (96.485×10^3 A×s/mol)
'FRP'	-	Fibre reinforced polymer
'G'	J	Gibbs free energy[†, ‡] (see Chapter 'TaD')
'G_f'	J/mol	Gibbs free energy of formation[†, ‡]
'GR1'	-	Green rust one
'H'	J/mol	Enthalpy[†, ‡]

Symbol or abbreviation	Standard unit	Definition
'HSC'	-	Software Outokumpu HSC Chemistry
'HPC'	-	High performance concrete
'I' ('i')	A (A/m^2)	Current (density)[*]
'I' ('i_0')	A (A/m^2)	Exchange current (density)
'I_{cc}' ('i_{cc}')	A (A/m^2)	Critical current (density)
'I_{corr}' ('i_{corr}')	A (A/m^2)	Corrosion current (density)
'I/O'	-	Input/output
'I_p'('i_p')	A (A/m^2)	Passive current (density)
'LOM'	-	Light optical microscopy
'LPR'	-	Linear polarisation resistance
'ITZ'	-	Interfacial transition zone
'$Me_{\#}$'	-	Arbitrary metal with index specified by "#"[†]
'Me^{n+}'	-	Species of 'Me' in 'n' times higher oxidation state
'MEPD'	-	Multi element Pourbaix diagram[*] (see Chapter 'TaD')
'p'	N/m^2	Partial gas pressure
'$P_{\#}$'	-	Arbitrary product with index specified by "#"[§]
'Principle I'		Principle of implementation I (cf. Section 7.2.3)
'Principle II'		Principle of implementation II (cf. Section 7.2.3)
'R'	J/(K×mol)	Gas constant (8.314 J/(K×mol))
'RE'	-	Reference electrode
'$R_{\#}$'	-	Arbitrary reactant with index specified by "#"[§]
'R_p'	Ω	Polarisation resistance
'R_Ω'	Ω×m	Solution or electrolyte resistance
'S'	J/(mol×K)	Entropy[†, ‡]
'SCE'	-	Saturated calomel electrode
'SEM'	-	Scanning electron microscopy
'SEPD'	-	Single-element Pourbaix diagram (see Chapter 'TaD')
'SHE'	-	Standard hydrogen electrode
'SIPD'	-	Superimposed Pourbaix diagram (see Chapter 'TaD')
't'	S	Time
'T'	K	Temperature
'TaD'	-	Chapter "Terminology and Definitions" in this thesis
'Test I'	-	Experimental investigations I (cf. Section 1.9.3)
'Test II'	-	Experimental investigations II (cf. Section 1.9.4)
'v'	-	Stoichiometric coefficient
'W'	$\Omega \times s^{-½}$	Warburg impedance
'WE'	-	Working electrode
'w/c'	-	Water-to-cement ratio
'w/w'	-	Weight-by-weight [††]
'x'	M	Distance, length, or depth
'Z'	Ω	Impedance[**]

Symbol or abbreviation	Standard unit	Definition
'ΔE'	V	Potential difference (see Chapter 'TaD')
'ΔE_0'	V	Equilibrium potential difference (see Chapter 'TaD')
'ΔE_p'	V	Potential perturbation
'ΔI_p' ('Δi_p')	A (A/m^2)	Current (density) response
'η'	V	Overpotential[*, ‡‡]
'φ'	- (rad)	Phase angle shift
'ω'	1/s (in rad/s)	Angular frequency

[*] The subscripts "a" and "b" refer to the anodic and the cathodic parameter, respectively.

[†] The superscript "0" refers to the parameter at standard state.

[‡] The prefix "Δ" refers to the change of the parameter.

[§] The index "#" represents any integer or "z" that corresponds to the end of a list; "#" is omitted, if the associated parameter is limited to one instance.

[**] The subscripts "j" and "r" refer to the imaginary and the real part of impendence.

[††] The subscripts "co" and "ce" refer to oven-dry concrete and to the cement content, respectively.

[‡‡] The subscripts "act", "con", and "res" refer to the activation, the concentration, and the resistance overpotential, respectively.

SI units are used throughout this thesis. Numerical values are given based on convenient scales, e.g. potentials [mV_{SHE}], energies [kJ], currents [mA], pressure [bar], temperature [°C] and lengths, areas, volumes in any appropriate order of magnitude.

Only symbols and abbreviations that are of relevance throughout this thesis are included in the above table. Standard abbreviations, symbols with marginal importance, or alternative symbols or abbreviations, which differ from the ones defined in the above table (included for information purposes only), are stated in parenthesis with single quotes, i.e. ('symbol or abbreviation').

The formulas of the most important chemical species mentioned in this thesis are listed together with the names of the corresponding elements or compounds at the end of this thesis (Chapter "List of Chemical Species"). In contrast to the above listed abbreviations, formulas of chemical species are not marked by single quotes. The same holds for elements with a subscript "ia", which indicates that the ion activity of the associated element is referred to. It should also be noted that formulas and the corresponding names of elements or compounds are used interchangeably. Formulas used as subscript indicate that the parameter refers to that species, e.g. 'D_{Cl}' is the chloride diffusion coefficient and 'p_{O2}' is the partial oxygen pressure.

Standard abbreviations for organisations are neither marked by single quotes nor included in the above table, but the most important ones are elucidated by footnotes.

Terminology and Definitions

As far as possible and applicable, the electrochemical and chemical terminology and definitions used in this thesis correspond to the ones specified in [IUPAC, 2007][*] and in ASTM [ASTM G3, 2004][†] and to additional ASTM standards for the relevant test methods. The terminology used for the descriptions of concrete (e.g. constituents and properties) is largely in agreement with the one recommended in [ACI 116R, 2000][‡] and in [ASTM C125, 2005]. Moreover, some custom terminology and definitions are used. The most important terms and definitions, which are either not used in the literature or differ from the general use, are listed and described in the following:

- Referring to reactions

  The following terms are used to distinguish between three main groups of reactions that are relevant for the description of corrosion processes in this thesis:

  - Redox reactions

    Only those electrochemical reactions in which atoms have their oxidation state[§] changed and which are balanced for the charge transfer are referred to as redox (reduction/oxidation) reactions.

  - Acid-base reactions

    Chemical reactions that do not involve a change in oxidation state and only describe the exchange of bonds between the reacting chemical species depending on the electrolyte pH are referred to as acid-base reactions.

  - Half-cell reactions

    Electrochemical reactions which comprise a single part of a redox couple (reduction/oxidation), i.e. reactions with an electron on either side, are referred to as half-cell reactions. The prefix half-cell is omitted, when a half-cell reaction is referred to as an anodic or cathodic reaction and to as an oxidation or reduction reaction, since these terms imply that the associated reaction is a half-cell reaction (e.g. anodic reaction is used instead of anodic half-cell reaction).

  It should be noted that the above terms apply to *groups* of reactions as opposed to *types* of reactions. The term *type* is used to refer to a certain reaction in a *group* (e.g. the anodic reaction describing the reduction of ferrous ion to iron and the ca-

[*] International Union of Pure and Applied Chemistry (IUPAC), Research Triangle Park, NC, USA.

[†] ASTM International (ASTM), formerly known as the American Society for Testing and Materials, West Conshohocken, PA, USA.

[‡] American Concrete Institute (ACI), Farmington Hills, MI, USA.

[§] The term oxidation state is preferred to the terms valence or oxidation number and used throughout this thesis.

thodic reaction describing the reduction of ferric ion to iron are two different *types* of reactions that belong to the *group* of half-cell reactions).

- Referring to sequences of reactions

  A step by step sequence of reactions by which an overall change occurs is referred to as a reaction mechanism [March, 1992]. In this thesis, a reaction mechanism can also constitute a sequence of anodic reactions without taking into account the associated cathodic reactions. In this case, it is referred to as an anodic reaction mechanism.

- Thermodynamic states

  The following terminology, which is largely in agreement with the definitions given in [Pourbaix, 1974b], is used to describe and refer to the different thermodynamic states of a metal:

  - Immunity or immune state

    The terms immunity or immune state refer to the state of a metal in which corrosion is thermodynamically impossible in a given environment.

  - Corrosion, active corrosion, active (corrosion) state

    The terms corrosion, active corrosion, or active (corrosion) state refer to the reaction of a metal with its non-metallic environment that results in the continuing destruction of the metal.

  - Passivity or passive state

    The terms passivity or passive state refer to the state of a metal in which active corrosion in a given environment is prevented by the formation of a thin protective layer of its oxides, which is generally referred to as a passive layer in the present thesis.

  - Passivation

    The term passivation refers to the process that leads to more or less perfect passivity of a metal. Passivation can be obtained by electrochemical means (e.g. by anodic polarisation) or by chemical means (e.g. by changing the electrolyte pH).

- Standard state and non-standard state conditions

  - Standard state conditions correspond to:

    - An activity of 1 mol/L for each ion participating in the reaction
    - A temperature of 25°C (298.15 K)

- A pressure of 1 bar* (10^5 N/m^2) for each gas that takes part in the reaction
- All involved species are in their stable form under these conditions.

Standard state conditions are marked with a superscript "0".

- Activities 'a' for non-standard state conditions are approximated according to:
  - For gases 'a' corresponds to the partial pressure 'p' in [bar].
  - For solid matter and solvents 'a' corresponds to 1.
  - For dissolved matter (ionic species) 'a' corresponds to the ion concentration in [mol/L]. If not stated otherwise, the ion activity for numerical values stated for non-standard states and for Pourbaix diagrams corresponds to 10^{-6} mol/L.

- Referring to electrochemical potentials

  It appears that there are particular discrepancies when referring to electrochemical potential in the literature, which can be misleading. Therefore, the following terms are used consistently to distinguish between different types of the electrochemical potential:

  - Electrode potential 'E':

    The electrode potential 'E' is defined as the difference between the electrochemical potential of a metallic electrode in an electrolyte and the electrochemical potential of a reversible reference electrode in contact with this electrolyte [Pourbaix, 1974b]. The selected point of reference in this thesis corresponds to the standard hydrogen electrode 'SHE'.

  - Equilibrium potential:
    - Equilibrium potential 'E_0'

      The equilibrium potential 'E_0' is defined as 'E' at equilibrium.
    - Standard potential 'E_0^0'

      The standard potential 'E_0^0' is defined as 'E_0' at standard state conditions.

    In the literature the electrode and the equilibrium potential are often not distinguished and referred to as half-cell potential.

  - Potential difference:
    - Potential difference 'ΔE'

* In some literature the standard state pressure is defined as 1 atm (1.014×10^5 N/m^2). However, it is preferred to be consistent with SI units and [bar] is used, while the difference between [bar] and [atm] is considered negligible.

The electrode potential difference 'ΔE' is defined as the difference between two electrode potentials.

- Equilibrium potential difference 'ΔE_0'

  The equilibrium potential difference 'ΔE_0' is defined as 'ΔE' between two electrode potentials at equilibrium.

- Standard potential difference 'ΔE_0^0'

  The standard potential difference 'ΔE_0^0' is defined as 'ΔE_0' at standard state conditions.

The potential difference is in the literature usually referred to as electromotive force 'EMF'.

- Corrosion potential 'E_{corr}'

  The corrosion potential 'E_{corr}' is the mixed potential established between all anodic and cathodic reactions on a corroding surface or between two or more corroding surfaces in an electrolyte measured relative to a reference electrode. In the literature the corrosion potential is also referred to as rest potential, free corrosion potential, and open circuit potential ('OCP'). In relation to e.g. potential mapping [ASTM C876, 1999], 'E_{corr}' is also referred to as half-cell potential, which we regard to be particularly misleading. Therefore, the term corrosion potential is used throughout this thesis, also when referring to potentials in concrete.

  It should be emphasised that 'E_{corr}' includes mixed potentials established in macrocells or by galvanic (both embedded and external electrodes) polarisation as well as corrosion potentials resulting from polarisation by impressed current.

- Affinity of reactions

  The determined Gibbs free energy change 'ΔG' is stated for all chemical reactions throughout this thesis and correspondingly all half-cell reactions are assigned a calculated equilibrium potential 'E_0', while the following applies:

  - If not stated otherwise, the numerical values of 'ΔG' and 'E_0' are specified for the standard state, i.e. as 'ΔG^0' and 'E_0^0'.
  - According to the convention of Stockholm [IUPAC, 1953], values for 'E_0' are always specified as reduction potential, i.e. the sign for an oxidation reaction is not reversed.
  - If a numerical value for 'E_0^0' was found available in the literature, it is listed as the second value in the curly brackets ({...}). If not stated otherwise, this value was taken from [Jones, 1996].

- Analogies between reaction groups and electrochemical quantities

The above definitions allow the following analogies between the reaction groups and electrochemical quantities. The affinity of:

- Redox reactions can be expressed by 'ΔE_0' (or 'ΔG')
- Acid-base reactions can be expressed by 'ΔG'
- Half-cell reactions can be expressed by 'E_0'.

- Series of standard potentials

  The series of standard potentials is defined as a series of equilibrium potentials listed according to their magnitude of 'E_0^0'. In the literature such a list is usually referred to as the 'EMF' series.

- Comparing electrode potentials and metals in relation to the magnitude of 'E_{corr}'

  Both electrode potentials and metals are referred to as *noble* or *active* in relation to the magnitude of their associated 'E_{corr}' [ASTM G3, 2004]. Metals and electrode potentials with a high magnitude of 'E_{corr}' are referred to as *noble* and metals with a low magnitude of 'E_{corr}' are referred to as *active*. In the literature, *noble* is often referred to as passive, cathodic, or protected and *active* is often referred to as base, ignoble, anodic, or corroding. If two metals are compared in relation to their magnitude of 'E_{corr}', the terms *nobler* and *less noble* are used. If two electrode potentials are compared, the terms *higher* and *lower* are used. These refer to the full 'SHE' scale, i.e. from high positive to low negative, and not to the absolute (numerical) value of 'E_{corr}'.

- Types of Pourbaix diagrams

  The following terminology is used to distinguish between three distinct types of Pourbaix diagrams introduced in this thesis:

  - Single-element Pourbaix diagram 'SEPD'

    The term single-element Pourbaix diagram 'SEPD' refers to a Pourbaix diagram of an 'El'-H_2O system *covering only one element*. In this thesis, 'SEPDs' are normally limited to 'Me'-H_2O systems.

  - Multi-element Pourbaix diagram 'MEPD'

    The term multi-element Pourbaix diagram 'MEPD' refers to a Pourbaix diagram covering one main element ('El_1') in combination with other elements ('El_2'-'El_z'), i.e. an 'El_1'-'El_2'-…-'El_z'-H_2O system, which takes *all species that can be formed between the two or more elements* into account, as e.g. the Pourbaix diagram of the Fe-Zn-H_2O system.

  - Superimposed Pourbaix diagram 'SIPD'

    The term superimposed Pourbaix diagram 'SIPD' mainly refers to a superimposition of individual 'SEPDs', i.e. an 'El_1'-H_2O system on an 'El_2'-H_2O sys-

tem on an … on an 'El_z'-H_2O system (mainly superposition of a 'Me_1'-H_2O on a second 'Me_2'-H_2O system) *without taking into account the species that can be formed between the two elements* (e.g. the superposition of a Zn-H_2O system on a Fe-H_2O system). However, 'SIPDs' can also represent the superposition of two or more 'MEPDs' or any arbitrary combination of 'MEPDs' and 'SEPDs'. For instance, the superposition of the 'MEPD' of selected stainless steel alloys (e.g. the Cr-Fe-Ni-Mo-H_2O system) on the Fe-H_2O system is also referred to as 'SIPD'.

- Countermeasures

  The term countermeasures refers to all measures that have been proposed or are applied to improve the corrosion resistance of steel in concrete for both *new structures* (initial countermeasures) and *existing structures* (repair or rehabilitation of concrete structures). The following distinction is made in this thesis with regard to the principal aim of countermeasures for *new structures*:

  - Concrete countermeasures

    Concrete countermeasures include measures to reduce the permeability of the concrete bulk, concrete surface protection, integral corrosion inhibitors, and measures to improve the concrete-steel interface.

    Application of thermodynamics in relation to concrete countermeasures generally relates to the thermodynamic influence of other substances on iron in a Fe-'El_2'-…-'El_z'-H_2O system.

  - Reinforcement countermeasures

    Reinforcement countermeasures include non-metallic, organic-coated, more corrosion resistant, cladded, and galvanised reinforcement as well as cathodic prevention.

    Application of thermodynamics in relation to reinforcement countermeasures generally relates to the thermodynamic behaviour of a metal or a combination of metals in a 'Me'-'El_2'…-'El_z'-H_2O system.

  A general distinction between countermeasures for *existing structures* is not made.

Format and Style

Some general remarks on the format and style used in this thesis are given below:

- Active and passive voice

  The active voice has been used to indicate what *we* have done in this project and what *we* suggest or conclude in contrast to what has been done or suggested by *others* (i.e. in the literature). In doing so, "we" refers to the group of persons that have been involved in the project mentioned in the acknowledgements (mainly my supervisors and me), but it often includes other persons (everybody who assisted me, especially in the experimental part of this project).

- Italic text and quotes

  While single quotes are reserved for the symbols and abbreviations defined in the Chapter "Symbols and Abbreviations", the following applies to the use of italic text and double quotes throughout this thesis:

  - Italic text is used to emphasise certain words or sentences.
  - Double quotes indicate titles, particular denotations or uncustomary terms as well as indices of experimental specimens[*].
  - Italic text in double quotes indicates citations from the literature.

- Footnotes

  Footnotes are used for longer comments or supplementary information, which are not suitable within the text. Shorter comments and information are generally given in parenthesis.

- Chapters, sections, figures, tables, bullets, and equations

  - Referring to chapters, sections, figures, tables, and bullets

    The nine main parts of this thesis (cf. Section 1.8) are referenced to by "Chapter #", while the subsections are referenced to by "Section #". When reference is made to a "Chapter #" or a "Section #" as well as to a "Figure #", a "Table #", or a "Bullet #" (bullets are only numbered in Chapter 7) this terms are denoted with a capital letter. Reference to equations, i.e. mathematical equations or chemical reactions, is indicated by square brackets ([...]) and made in a descriptive manner (see Chapter 'TaD') without capitalisation.

  - Numbering of equations, figures, and tables

    Equations, figures, and tables are numbered continuously for each chapter. The chapter number and the number of the equation, figure, or table in the associated chapter are separated by a "dot". Contrary to figures and tables, which

[*] Curly brackets indicate a list of specimens, e.g. "C-1{A, B}" corresponds to "C1-A" and "C1-B".

are assigned a unique number, equations are repeated when convenient and are assigned a new number. Hence, equations do not have a unique number.

- References to the literature and list of references

  References in the text and the list of references in the end of this thesis are formatted according to a slightly modified APA* style [APA, 2001].

  - References in the text are indicated by square brackets and given as follows:
    - One author: [last name of author, year]
    - Two authors: [last name of first author & last name of second author, year]
    - More than two authors: [last name of first author et al., year]
    - Associations, e.g. standards [abbreviation of association standard number without year, year of publication or reapproval].
    - A semicolon is used as a separator for a list of references, i.e. [reference 1; reference 2], and the references are listed chronologically
  - List of references

    The list of references is sorted after the last name of the first author followed by the last name of other authors, the year, and the title of the reference. The reference used in the text precedes each full reference in the list of references.

- Standards and guidelines

  Apart from the actual materials and methods applied in the experimental investigations that were generally based on DS† or CEN‡ standards and specifications (cf. Section 1.9), it is referred to both the associated European, i.e. mainly CEN standards, and the corresponding US standards or guidelines, i.e. ASTM standards or ACI publications. CEN standards are generally (with few exceptions, which are not or not yet available in Denmark) referred to as DS/EN publications. If available, ASTM and ACI standards and guidelines are referred to as the metric issues. This is indicated by the letter "M" at the end of the associated standard number.

  If product types with different country-specific identifications are stated in this thesis, it is also referred to both European and US identification. For instance, stainless steel grades are specified according to CEN [VDEh, 1999; DS/EN 10088-1, 2005] as well as to [ASTM DS561, 2004].

* American Psychological Association (APA), Washington, DC, USA.

† Dansk Standard (DS), Danish Standard Association, Charlottenlund, Denmark.

‡ Comité Européen de Normalisation (CEN), European Committee for Standardisation, Brussels, Belgium.

Table of Contents

1 Introduction

At present, the application of certain thermodynamic principles in providing insights in the field of reinforcement corrosion appears to be quite limited. For instance, the use of Pourbaix diagrams is rather restricted and generally limited to exemplification purposes (e.g. to demonstrate the stability of iron in the concrete environment by means of the Fe-H_2O system). To our knowledge, Pourbaix diagrams have neither been used profoundly to investigate the electrochemistry of other metals or combinations of metals in concrete, nor to assess the influence of the concrete chemistry or of ingressing substances on the thermodynamics of steel or other metals in concrete. Moreover, the application of other thermodynamic principles (e.g. the establishment or evaluation of reaction mechanisms based on associated Gibbs free energy changes or the required electrode potentials) seems to be limited. Based on these principles some of the reaction mechanisms that have been postulated in the literature for the description of corrosion processes appear to be inconsistent or erroneous.

We think that there are a lot of unexploited possibilities in using thermodynamic principles not only for the description of the electrochemistry of steel in concrete, but also for the evaluation of existing and in particular for the design of new countermeasures. *The theoretical background of the design and implementation of new countermeasures as well as the establishment of experimental tests for verification of possible principles constitute the central arguments of this thesis.*

In this Chapter the motivation for the project and an introduction to related subjects are given. It comprises a brief introduction to reinforced concrete as a construction material (Section 1.1), to deterioration of reinforced concrete structures (Section 1.2) with emphasis on reinforcement corrosion (Section 1.3), to available countermeasures (Section 1.4), and to the proposed principles for the design of new countermeasures (Section 1.5).

The objectives, the scope, and an outline of this thesis are given in Sections 1.6, 1.7, and 1.8, respectively. An outline of the experimental investigations is provided in Section 1.9.

1.1 Success of Reinforced Concrete Structures

Throughout the world steel reinforced concrete is the most widely used manmade construction material. According to an estimate from the "Global Cement Report" around 1.6 billion tons of cement are produced every year [CemNet, 2007]. With the annual steel production of approximately 600 million tons and about 10% of that quantity being used for reinforcing steel [IISI, 2007], around 10.5 billion tons of structural concrete are produced every year [John, 2003]. Considering a world population of 6.4 billion this number is equivalent to a staggering 1.6 tons of structural concrete produced per capita each year.

The success of reinforced concrete is based on its mechanical strength, versatility, price, and durability. Among others, this is due to the following key characteristics of the concrete-steel composite system:

- Reinforced concrete structures can support 300-500 times their weight.
- Reinforced concrete can be moulded to a variety of shapes and finishes.
- The constituent materials are in general inexpensive and almost unrestricted.
- The physical characteristics of the concrete-steel composite are beneficial, in particular:
  - The cement paste conforms to the surface details of the reinforcing steel permitting efficient stress transmission between the two materials.
  - The similar thermal expansion coefficients provide durability with regard to temperature load.
- Besides the concrete acting as a physical barrier towards aggressors, its chemical environment enables protection of the reinforcing steel against corrosion.

However, several cases show that reinforced concrete structures do not always perform as intended, but deteriorate prematurely.

1.2 Deterioration of Reinforced Concrete Structures

Deterioration of concrete structures gives rise to concerns about structural safety, integrity, and serviceability and about the expenses spent on maintenance and repair. An interesting estimate is that nowadays the annual budget for maintenance and repair of existing structures compares to the one for new concrete structures [Li, 2004]. The following approximations of annual budgets for maintenance and repair of concrete structures illustrate the vast economical expenses:

- US > $ 1.6 trillion [Li, 2004]
- Asia > $ 2.0 trillion [Li, 2004]
- EU-15 > € 250 billion [Li, 2004]
- Denmark > DKK 25 billion [DBR, 2001].

A further increase in these budgets is expected due to the fact that an aging concrete infrastructure from the 1960s and 1970s construction boom is to be maintained and repaired during the next decades.

Yet, deterioration is not only a matter of economical concern. Deterioration of reinforced concrete structures also affects resources and energy consumption [fib, 2004]. The cement industry is responsible for about 3% of the global anthropogenic greenhouse gas emission and for about 5% of the global anthropogenic CO_2 emission [John, 2003]. The final, but most important, concern emerges when the structural in-

tegrity is compromised due to deterioration. In this case, safety is at risk and catastrophic failures may occur which in the worst case include the loss of human life.

Corrosion of the reinforcing steel has been estimated to be related to 90% of deterioration problems with concrete structures [Rendell et al., 2002]. However, there are various deterioration mechanisms that affect the concrete directly, e.g. freeze/thaw damage, sulphate attack, or alkali-silica reaction 'ASR'. The physical or chemo-physical nature of concrete deterioration mechanisms often leads to cracking of the concrete cover, which impairs the protection of the steel against corrosion. Thus, deterioration of reinforced concrete structures can often be attributed to a combination of mechanisms.

1.3 Reinforcement Corrosion

Steel embedded in uncracked and uncontaminated (uncarbonated and chloride-free) concrete is protected from corrosion by the alkaline environment provided by the pore solution and by the bulk of the surrounding concrete, which acts as a physical barrier towards aggressors. With availability of oxygen, a protective oxide layer is formed on the steel surface, i.e. the steel passivates. In the passive state the corrosion rate is negligible, although the steel is not thermodynamically immune. The passive state is retained, except when the protective environment of the concrete is disturbed either by neutralisation (mainly, due to carbonation) or by the ingress of depassivating ions (primarily, chloride ions); both are largely potentiated in cracked concrete.

Carbonation induced corrosion can generally be linked to a uniform corrosion attack. The corrosion products that form on the steel under these conditions are much larger in volume than the pure iron consumed in the corrosion reaction. The increase in volume around the rebar exerts disruptive tensile stress on the surrounding concrete. If these stresses exceed the concrete tensile strength, the concrete cracks or spalls.

Carbonation alone can generally be controlled with state-of-the-art concrete mixtures and design of adequate cover depth, whereas corrosion induced by ingress of chloride ions remains a major problem. Most often critical chloride contents arise with penetration of chlorides through the concrete cover, when the external surface of the structure is exposed to e.g. sea salt spray, direct seawater, or deicing salt. Also, chlorides may be incorporated in the original mix. They may be present in the constituent materials or, as accepted until the mid 1970s in Europe for acceleration of cement hydration, deliberately added as calcium chloride ($CaCl_2$). Depending on the availability of oxygen, chloride induced corrosion or the combination of chloride ingress and carbonation can lead to similar damage types as carbonation induced corrosion. Yet, chloride induced corrosion alone is often related to a notch-like shape attack of the reinforcement rebar. The tensional stress-strain relation of the rebar changes in the corroding area and its vicinity, when the notch grows to a sufficient size. The notch takes up all the deformation as tensile stress and the yield capacity of the rebar is reduced to yield-

ing in the notch [Frederiksen & Poulsen, 1997]. Under these circumstances, the corroding rebar acts as a brittle material and the consequence of brittle behaviour under simultaneous exposure to heavy load can be disastrous.

1.4 Available Corrosion Countermeasures

Suitable design, i.e. a dense and sufficiently deep concrete cover and an adequate crack width limitation, as well as appropriate execution are often sufficient to attain the required service life for concrete structures. However, certain concrete structures, e.g. structures under severe exposure conditions, with special service life requirements, or with architectural designs that do not allow for sufficient cover depths, require additional corrosion countermeasures to prevent premature deterioration.

Various approaches have been proposed to enhance the resistance of the concrete against carbonation and against the penetration of chloride ions as well as to improve the resistance of the reinforcement against corrosion initiation. For a given environment, the resistance of the concrete cover against carbonation and against the ingress of chloride ions is largely dependent on the physical properties of the concrete. Furthermore, chemical attributes of the concrete as well as the electrochemical properties of the reinforcement have a significant influence. The corrosion resistance of the reinforcement against carbonation and chloride induced corrosion is governed by a combination of all these factors, but in addition the characteristics of the concrete-steel interface play a major role.

The most important available corrosion countermeasures include, on the one hand, measures relating to the concrete (henceforth, concrete countermeasures), such as measures to reduce the permeability (e.g. high performance concrete 'HPC'), concrete surface protection, and integral corrosion inhibitors and, on the other hand, measures relating to the reinforcement (henceforth, reinforcement countermeasures), such as non-metallic, organic-coated, stainless steel, cladded, and galvanised reinforcement as well as cathodic prevention.

With the exception of non-metallic reinforcement, stainless steel reinforcement, and cathodic prevention, several cases of premature deterioration were reported during the past decades due to an insufficient performance of the above mentioned countermeasures, mainly in chloride environments. In particular, certain types of concrete surface protection and some integral inhibitors as well as galvanised and epoxy-coated reinforcement did not always perform up to the expectations[*].

The application of non-metallic reinforcement such as glass, aramid, or carbon fibre reinforced polymers 'FRP' is quite limited due to economical and particularly practi-

[*] Nevertheless, there is an ongoing discussion about the effectiveness of these countermeasures and apparently they are still largely promoted by the related industry, which does not always seem to acknowledge the related problems (cf. Section 6.3.2.5).

cal disadvantages. So, durability design of concrete structures for severe chloride exposure seems to adapt more and more to using stainless steel reinforcement. This development focuses mainly on using austenitic stainless steel grades, alone or selective (in combination with carbon steel reinforcement). At present, this solution seems to be the state-of-the-art and it is considered to be effective and infallible [Rostam, 2003; Rostam, 2007]. However, it comes at a price; the initial costs of specifying austenitic stainless reinforcement are normally 5-10 times higher than specifying carbon steel [Nürnberger, 1996; Bertolini et al., 2004]. The high price cannot always be justified and efforts have been made to cut costs by using cheaper stainless steel grades. Yet, the performance was generally observed to decrease more than the expenses [Nürnberger, 1996; Chowdhury, 2004]. Another way of cutting costs has been to clad carbon steel rebar with stainless steel, but the reductions in costs have been insufficient to make cladding an attractive option [Chowdhury, 2004]. Other recent approaches to develop less expensive reinforcing steels with an improved corrosion resistance included microcomposite steels and tungsten doped steels, for instance. Some developments may be promising, but there still is a lack of experience and documentation with regard to their durability.

Cathodic prevention ‘CPre’ is a relatively new initial countermeasure that is based on similar principles as the more familiar cathodic protection ‘CP’, which is generally related to repair or rehabilitation of existing structures. ‘CPre’ and ‘CP’ show promising results and are, in our opinion, reasonable approaches from a thermodynamic point of view. Besides ‘CP’, there are a number of other more or less prevalent countermeasures for existing structures, e.g. electrochemical realkalisation ‘ERA’ and chloride removal ‘ECR’, patch repair, concrete surface protection, crack injection, and diffusion inhibitors.

‘ERA’ and ‘ECR’ are based on similar principles as ‘CPre’ and ‘CP’, but the objective and the applied current densities differ. Besides possible negative side effects, such as hydrogen embrittlement, ‘ASR’, and loss of bond strength, ‘ERA’ and ‘ECR’ require rather elaborate installations and operation. Thus, we do not regard these techniques as an adequate solution for repair of common civil engineering structures. They can have beneficial application in the preservation of architectural landmarks, however.

The effectiveness of diffusion inhibitors appears to be questionable. The same holds for concrete surface protection and crack injection for repair of structures that are substantially contaminated by chloride or where corrosion has already initiated. Finally, traditional patch repair is often linked to the so-called ring-anode effect, which generally leads to corrosion initiation in the vicinity of the patch. Zinc-rich primers or sacrificial anodes are often used to prevent this effect.

1.5 Design of New Corrosion Countermeasures

The brief discussion in Section 1.4 shows that even nowadays (after constructing with reinforced concrete for more than a century and decades of extensive research and development) there still is an ongoing, oftentimes controversial, discussion about the effectiveness of available countermeasures for both new and existing structures.

It actually seems that, besides the developments in 'HPC' and corrosion inhibitors, research and durability design moves more and more towards promoting reinforcement with an increased corrosion resistance and thus further away from making use of the original benefits of the concrete-steel system, i.e. the physical and chemical protection that the concrete provides to embedded carbon steel. Stainless steel has a far superior corrosion resistance than carbon steel and the use of stainless steel reinforcement surely grants a major gain in durability of concrete structures. However, due to the increasing world market demand for stainless steels and its alloys (in particular, chromium) we expect that the present upward price tendency for stainless steel [MEPS, 2007] will persist in the future.

As mentioned, we think that there are a lot of unexploited possibilities in using thermodynamic principles for the design of new countermeasures. Yet, thermodynamic principles alone are not sufficient to ascertain whether the reinforcement will corrode under a given set of environmental conditions. On the one hand, even though the thermodynamic tendency for corrosion is high, active corrosion may not a problem, if the rate is insignificantly low. On the other hand, the thermodynamic tendency for formation of protective products may be high, but the reaction kinetics can be too slow to enable sufficient corrosion protection. Therefore, kinetic considerations as well as conclusive laboratory investigations are to be taken into due account in the design of new countermeasures. Moreover, general considerations, such as structural, economical, and ecological* aspects, further limit the available options. These considerations establish the basis of the proposed largely simplified methodology for the design and implementation of new countermeasures, see Figure 1.1.

General considerations (phase 1) establish the foundation of the methodology in close relation and constant interchange with thermodynamic considerations, kinetic considerations, and the associated production and implementation of the new countermeasure (phase 2). Preliminary laboratory investigations (phase 3), i.e. testing based on small scale specimens under accelerated conditions, is the next phase in the design hierarchy, which is also closely linked to phase 2 and in constant interchange with it.

* Ecological aspects might seem peculiar on the first glance, but considering e.g. the toxicity of chromates and nitrites, we regard them as relevant.

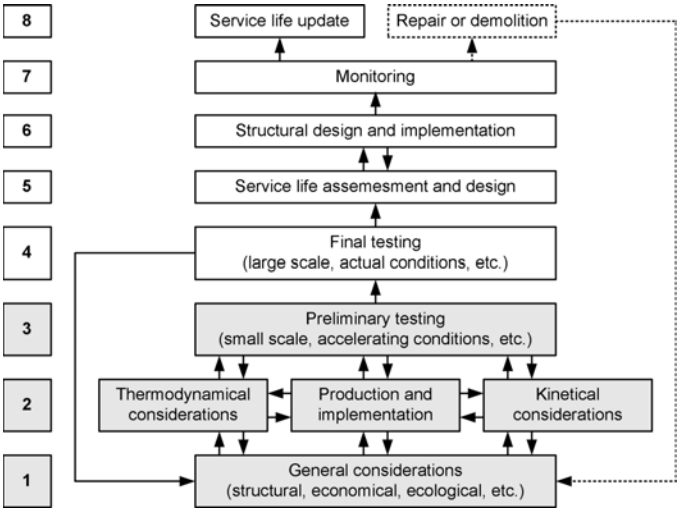

Figure 1.1: *Simplified flow chart for the design and implementation of new countermeasures. The grey shaded areas indicate the design phases of concern in this thesis, i.e. phases 1 to 3.*

If affirmative results are obtained from preliminary testing, comprehensive final investigations (phase 4) are to be performed on e.g. large scale specimens based on the actual materials under realistic exposure conditions. An obvious problem connected to such final investigations is that measures are to be taken to enable predictions for design service lives of 100 years or more within reasonable test duration, e.g. a few months or years. If the final investigations indicate problems, which have not been identified in the preliminary investigations, the general considerations are to be re-evaluated. This is illustrated by the solid backwards orientated arrow on the left hand side. If the final investigations confirm the effectiveness of the new countermeasure, service life assessment and design (phase 5) can be undertaken based on the corrosion protection characteristics determined by the final testing and with the design service life and actual exposure conditions as input parameters. Service life design is undertaken in close connection and constant interchange with structural design (phase 6) to determine the final detailing of the structure (or repair strategy).

Continuous monitoring (phase 7) during the service life provides feedback on the effectiveness of the implemented countermeasure. Taking into account the safety margins applied in durability and structural design, an update (phase 8) towards an extended service life is possible in the desirable case of the countermeasure performing effectively, based on the information obtained from monitoring. In the undesirable case of premature deterioration indicated by the monitoring, options of repair or demolition (phase 8) are to be considered and the design and implementation of the countermeasure is to be re-evaluated. This is indicated by the dashed backwards orientated arrow on the right hand side.

The proposed approach towards the first three design phases, i.e. general, thermodynamic, and kinetic considerations as well as the development of theoretical principles for processes and implementation of new countermeasures and the design of required test methods and setups constitute the central subject of this thesis.

1.6 Objectives of Thesis

This thesis is meant to establish a consistent thermodynamic basis for the description of corrosion processes as well as for the evaluation of existing and the development of new corrosion countermeasures. Hence, its central aims and contents are: the adaptation of available thermodynamic principles to the area of reinforcement corrosion, a thermodynamically consistent description of the diverse corrosion states of steel in concrete, a review and evaluation of available measures for corrosion protection, and the development of theoretical concepts for new cost-efficient countermeasures. In addition to these theoretical considerations, two practical implementations of the theoretical concepts are outlined and custom-designed setups and measurement methods for performance testing are discussed.

Although the largest part of this project was experimental, the major part of this thesis deals with theoretical principles (cf. Section 1.7). Selected experimental observations or results are referred to throughout this thesis in connection with the discussed theoretical concepts (cf. Section 1.9). *With regard to expected patent possibilities, some of the key theoretical concepts and most of the results of the experimental investigations are not included in the present thesis. This holds in particular for the production and implementation of the proposed new countermeasures (cf. Section 1.9.4 and Chapter 7). The related theoretical concepts and experimental results will be dealt with in future publications.*

1.7 Scope of Thesis

This thesis is meant for a reader with a background in either civil engineering or materials and chemical engineering. The intention is to introduce the underlying theory and concepts of corrosion science and concrete technology from a rather fundamental level to what is considered as the necessary theoretical background of the objectives of this thesis.

Most of the described theory concerning aqueous metallic corrosion, in particular the one concerning thermodynamics, is not or only marginally treated in the literature on reinforcement corrosion. Moreover, the terminology and the application of the theoretical models and tools used in this thesis differ to some extent from corrosion science. Therefore, the corrosion theory is explained starting from the basic concepts of aqueous metallic corrosion, which might appear trivial to the reader with a background in materials or chemical engineering. On the other hand, some of the background concerning concrete technology and structural concrete, which is considered

to be essential to understanding the complex physical and chemical properties of the concrete-steel composite system, might be trivial to the reader with a civil engineering background.

Emphasis is set on the application of electrochemical principles and essential aspects of concrete technology rather than on detailed theoretical background, e.g. derivation of the applied formulas. The treated subjects are thereby limited to what is considered to be relevant to comprehend our application of electrochemical principles in the area of reinforcement corrosion. Hence, the theoretical part of this thesis does by no means represent a complete summary of all aspects of the two broad and complex disciplines of corrosion science and concrete technology.

1.8 Outline of Thesis

This thesis comprises altogether nine main Chapters. After the "Introduction" in this Chapter, the contents of the subsequent Chapters can be summarised as follows:

- In **Chapter 2** an introduction to selected theoretical models and tools for the description of metallic corrosion is provided with emphasis on thermodynamics. In combination with the relevant information on concrete and carbon steel properties (Chapter 3), these tools are seen as the very fundamentals for the theoretical considerations (Chapters 4 to 7) and for the performed experimental investigations (Section 1.9 and Chapter 8).
- In **Chapter 3** the existing knowledge on concrete and carbon steel properties that are relevant for reinforcement corrosion is critically reviewed. Taking into account the multi-faceted chemistry of concrete and its particular physical characteristics as well as the metallurgical properties of the carbon steel, the concrete-steel system represents a complex chemical and electrochemical system. The description of corrosion processes in such system (Chapter 5), which we consider to be an important basis for the evaluation of existing (Chapter 6) and the design of new countermeasures (Chapter 7), requires a detailed understanding of the governing parameters.
- **Chapter 4** deals with our general understanding and application of thermodynamic data, models, and tools with primary focus on Pourbaix diagrams. The extension and application of the available aqueous metallic corrosion theory to the concrete environment is discussed in detail with special focus on the concrete-steel system (Chapter 3).
- **Chapter 5** demonstrates the application of the extended and adapted thermodynamic models established in Chapter 4 in combination with the theory on concrete and carbon steel (Chapter 3) for the description of different reinforcement corrosion processes. After some general notes on our concept of the electrochemistry of steel in concrete, our proposed models are verified against and compared to de-

scriptions that have been postulated in the literature. Emphasis is set on the thermodynamic models, whereas other aspects are dealt with rather briefly.

- **Chapter 6** gives an introduction to durability design and descriptions and evaluations of the most important available countermeasures as well as selected marginal techniques, which are of relevance to the new proposed countermeasures (Chapter 7). The underlying principles and the most important aspects of the described countermeasures are discussed and evaluated based on a critical review of the literature as well as on own theoretical considerations and experimental observations. The application of thermodynamic models and tools is indicated, but not elaborated in detail (as e.g. in Chapter 5).
- In **Chapter 7** design requirements are formulated and our proposed theoretical and practical concepts for the design of new countermeasures is summarised. It presents the final application of the available theory given in Chapters 2 and 3, which was extended and transferred to the description of reinforcement corrosion processes and to the evaluation and design of countermeasures throughout Chapters 4 to 6. While most of the available countermeasures investigated in Chapter 6 are ruled out from further consideration, the underlying principles of some available countermeasures contribute to the concepts of the new proposed countermeasures. This Chapter contains the central objective of this thesis (cf. Section 1.6). However, with regard to the expected patent possibilities only limited information on the theoretical concepts as well as on production and implementation of the countermeasures is given (cf. Section 1.6). Finally, requirements for laboratory testing of countermeasures are discussed.
- **Chapter 8** describes our approach towards testing of available and new countermeasures based on the requirements formulated in Chapter 7 with focus on electrochemical testing and evaluation. The design and features of the applied specimen types, the central aspects of the high-capacity exposure and monitoring setup used for electrochemical testing as well as the implementation of the required monitoring and measurement techniques (cf. Chapters 2, 3, and 7) are described in detail.
- Finally, **Chapter 9** summarises the most important findings of Chapters 4 to 8 and provides recommendations for future investigations.

1.9 Outline of Experimental Investigations

In this Section the most important experimental investigations, parameters, and performances are very briefly summarised to provide the background of the observations and results referred to in this thesis. It is important to note that *this Section should be understood as a reference to be consulted in connection with the observations and results referred to throughout the thesis*, rather than a complete introduction to the

experimental performances. A more detailed introduction to the experimental setup and performances is given in Chapter 8.

The experimental performances included in the present thesis are related to the practical realisation of the proposed new countermeasures as well as to their testing and comparison to available countermeasures. Furthermore, the design, manufacture, and testing of suitable experimental setups and measuring techniques constituted a major part of the practical work and the experimental performances. The final test setup for electrochemical investigations is described in detail in Chapter 8, which also provides information on the applied electrochemical measurements and their customisation. Supplementary experimental methods included microscopic and X-ray analyses as well as chemical analyses. These methods are described in connection with the investigated parameters in Chapter 3 (in relation to general properties of concrete and carbon steel reinforcement) and in Chapter 5 (in relation to reinforcement corrosion).

In Section 1.9.1 the basic principles of the final electrochemical test setup and the most important features of the applied specimens are summarised. The relevant parameters concerning the materials used for the test specimens and the exposure conditions are given in Section 1.9.2. This information in combination with a brief overview of the main parameters of two investigations (Sections 1.9.3 and 1.9.4) provides the central information for the experimental observations and results mentioned and referred to throughout this thesis.

The experimental investigations included in this thesis dealt with:

- The thermodynamic properties of different steel qualities and carbon steel surface *treatments* embedded in mortar (henceforth, 'Test I') (Section 1.9.3)
- The thermodynamic properties of different steel qualities and carbon steel surface *modifications* (including the first implementations of the proposed new countermeasures) embedded in mortar and in cement paste (henceforth, 'Test II') (Section 1.9.4).

In correspondence with the proposed design methodology for corrosion countermeasures and the stages of concern in this project (cf. Figure 1.1 in Section 1.5), small scale samples and accelerating conditions were used for all experiments. Due to associated size limitations and in order to eliminate undesirable influences on the measurements, *mortar and cement paste were used instead of concrete during all experimental investigations*.

1.9.1 Test Setup and Electrochemical Measurements

A central part of the project was the development of a test setup for comprehensive monitoring of multiple test specimens. Instrumented specimens for extensive testing as well as simple specimens that allowed for mass production were tested on a high-capacity exposure setup by means of an automated monitoring system.

In all experiments *focus was set on chloride induced corrosion*, whereas the resistance of available and the proposed new countermeasures to carbonation induced corrosion was treated theoretically only. Electrochemical tests were mainly based on combined monitoring of the corrosion potential 'E_{corr}' and the macrocell current 'i_{mac}' as well as on electrochemical impedance spectroscopy 'EIS' and polarisation curve measurements (cf. Sections 7.5.1 and 8.4.1). The concept for comprehensive 'E_{corr}' and 'i_{mac}' monitoring is exemplified in Figure 1.2 based on one set of an instrumented mortar specimen and its associated external cathode 'ECat'.

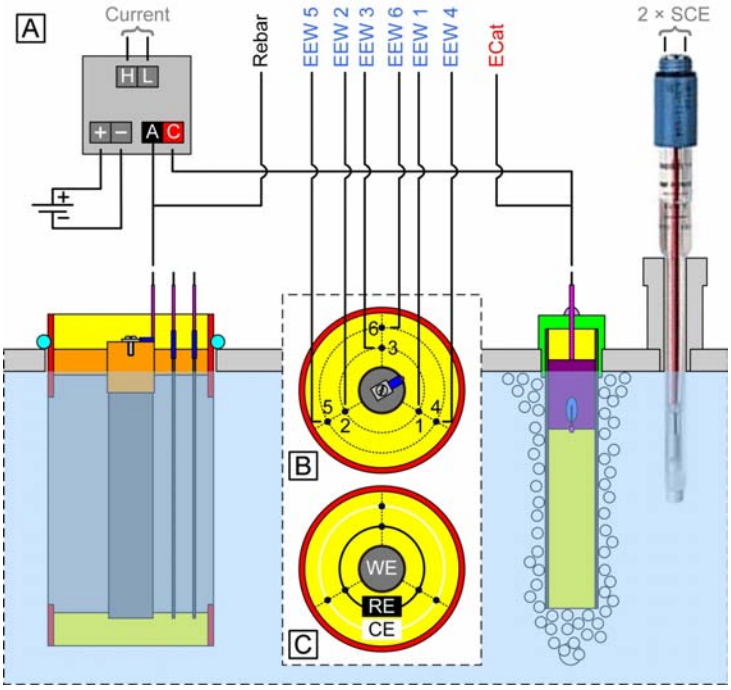

Figure 1.2: [A]: *Idealised test setup showing one set of instrumented mortar specimen and aerated external cathode and the monitored signals. ('H'): high terminal and ('L'): low terminal (of datalogger). ('A'): anode and ('C'): cathode connection for macrocell current monitoring. 'ECat': external cathode and 'SCE': saturated calomel electrode.* [B]: *Top view of instrumented mortar specimen with identification of embedded electrode wires 'EEWs'.* [C]: *As [B] with illustration of using 'EEWs' as electrodes for electrochemical impedance spectroscopy 'EIS'. 'WE': working electrode, 'RE': reference electrode, and 'CE': counter electrode. Apart from the 'EEWs', the colours used for the connections agree with the colour code used in Section 8.*

As indicated in Figure 1.2 [A] and [B], eight signals from each instrumented mortar specimen were recorded during long-term exposure. When the macrocell was activated, i.e. the rebar was connected to the aerated 'ECat', the current flowing between

the rebar and the cathode 'i_{mac}' was also monitored. The associated signals were diverted into 24 monitoring channels. These comprised the 'i_{mac}' reading, two times eight signals (rebar, 'ECat', and the six embedded electrode wires 'EEWs') against the two shared saturated calomel electrodes 'SCEs', as well as the signals from the 'ECat' and 'EEWs' against the rebar. Moreover, the 'EEWs' could act as both reference electrode 'RE' and counter electrode 'CE' during 'EIS'; the rebar represented the working electrode 'WE', see Figure 1.2 [C]. In the standard layout, both the 'ECat' and the 'EEWs' consisted of Ru/Ir mixed metal oxide ('MMO') activated titanium (cf. Section 8.1.1).

'E_{corr}' and 'i_{mac}' monitoring was automated and undertaken by means of cluster measurements. Cluster measurements made it possible to monitor multiple specimens by subdividing the test batch into clusters, which were measured one after the other. In the final configuration, 54 instrumented mortar specimens could be monitored with 24 channels each. A standard plug connected to each instrumented mortar specimen gave the option of additional electrochemical methods for corrosion testing. This standard plug connection was primary used for 'EIS', but could be easily adapted to polarisation curve measurements or other potentiostatic methods as well as conductivity measurements between different 'EEWs' and/or the rebar. The monitoring concept and the implementation of the principal electrochemical measurement methods are described in detail in Sections 8.3 and 8.4.1, respectively.

In addition to the instrumented mortar specimen, two simple specimen designs were used as reference specimens for electrochemical measurements, which aimed at the assessment of the thermodynamic state of the rebar only:

- Simple mortar specimen

  The simple mortar specimen was based on the same layout as the instrumented mortar specimen, but without 'EEWs'. A photograph of a 'Test II' simple mortar specimen at the end of its exposure period is shown in Figure 5.14 [A] in Section 5.2.2.2.

- Cement paste specimens

  The cement paste specimen was based on a rebar with the same diameter and exposure area as the mortar specimens, but the rebar was dip-coated with cement paste instead of cast into mortar. The production process of the cement paste specimen allowed for mass production.

The simple mortar and the cement paste specimen were monitored in the same way as the instrumented mortar specimen, but leaving out the 'EEW' connections. The unused 'EEW' connections could be applied for 'E_{corr}' monitoring of additional specimens. Among others, these connections were used for 'E_{corr}' monitoring of supplementary cement paste specimens. Yet, the major part of the cement paste specimens was used for destructive measurements, mainly full-scale anodic polarisation.

The manufacture and the special features of these three types of specimens, i.e. the instrumented and the simple mortar specimen as well as the cement paste specimen, are described in detail in Section 8.1.2. Besides these specimen types, which established the principal part of the test batches for all test series, a number of other specimen layouts were used for supplementary measurements. Among others, these included instrumented mortar specimens with carbon steel 'EEWs' that enabled monitoring of the chloride ingress, instrumented mortar specimens without rebar that were used as a reference for monitoring the 'E_{corr}' of the activated titanium wire, as well as plain mortar specimens (simple mortar specimens without rebar) that were used as a reference for chemical analysis, e.g. for testing of mortar pH (cf. Sections 3.1.7.2 and 5.2.2.2) and chloride ingress (cf. Section 3.1.7.3).

Based on the above described specimen layouts and a total of 1296 (54 × 24) channels available for monitoring, altogether 84 specimens were monitored at a time in two exposure containers in the final configuration of the experimental setup; 56 specimens in chloride solution and 28 specimens in potable water (cf. Sections 1.9.4 and 8.2). For exemplification purposes, the arrangement of specimens in the chloride solution exposure container used during 'Test II' is shown in Figure 1.3.

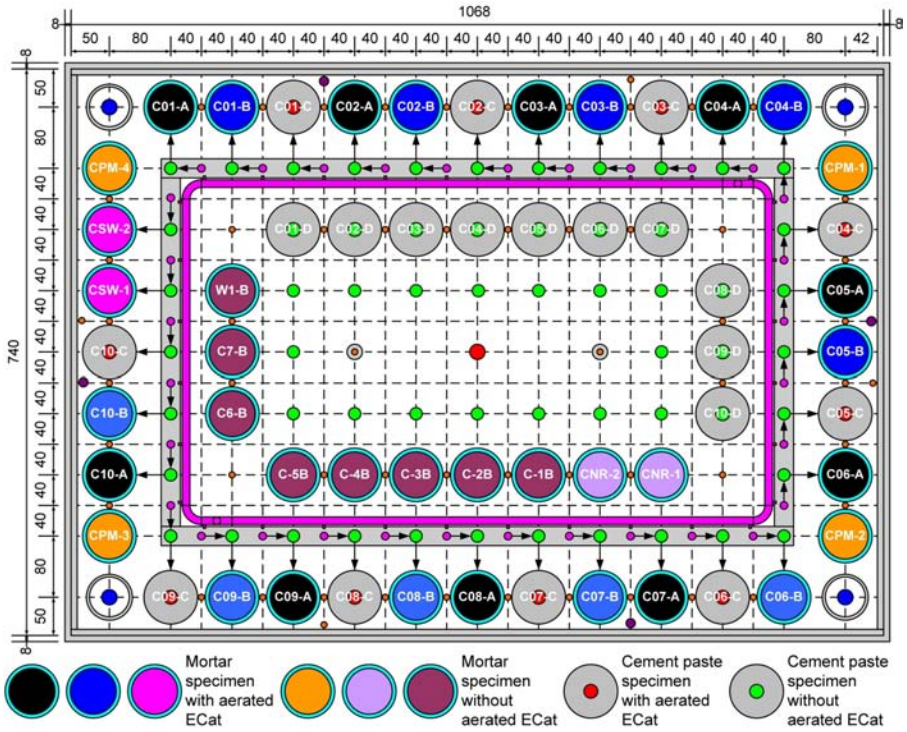

Figure 1.3: *Exemplification of the arrangement of specimens tested in the chloride exposure setup for the concluding experiments (cf. Section 1.9.4). 'ECat': external cathode.*

The reference container for exposure in potable water is presented in Figure 8.7 in Section 8.2. The equipment of the exposure containers, which is also shown in Figure 1.3, is described in connection with Figure 8.7 in Section 8.2.

1.9.2 Materials and Exposure Conditions

In this Section the most important materials properties, i.e. properties concerning corrosion performance, of the specimens tested in 'Test I' (cf. Section 1.9.4) and 'Test II' (cf. Section 1.9.3) as well as the exposure conditions applied in these experimental investigations are summarised:

- Cement and mixing water

  Rapid hardening Portland cement CEM I 52.5 [DS/EN 197-1, 2001] from Aalborg Portland[*] was used as the standard cement in all experimental investigations. A chemical analysis of the applied cement type is given in Table 3.1 in Section 3.1.1. Standard potable water complying with [DS/EN 1008, 2002] was used as mixing water for all specimens.

- Mortar specimens

  Two mortars compositions (A) and (B) were used. Both compositions were based on the same water-to-cement ratio 'w/c' of 0.5 and 0.1% weight-by-weight of cement 'w/w_{ce}' superplasticiser was added to both mixes to improve the workability. Different types of sand, cement-to-sand ratios, and types of superplasticisers were used for the two mortars:

  - Mortar (A):

    0/4 mm sand of type Betonsand kl. A (concrete sand class A) with a cement-to-sand ratio of 1/3.6. Peramin F from Fosroc[†] was used as superplasticiser. This mortar composition corresponded to a mortar used in earlier investigations at DTU Byg (e.g. [Nielsen, 2001; Küter, 2005]).

  - Mortar (B):

    0/2 mm sand of type Søsand kl. E (sea sand class E) with a cement-to-sand ratio of 1/3. Viskocrete 34 from Sika[‡] was used as superplasticiser. Apart from the addition of superplasticiser, this composition was based on the proportioning specified in [DS/EN 197-1, 2001].

[*] Aalborg Portland A/S, Aalborg, Denmark.

[†] Fosroc A/S, Rødding, Denmark.

[‡] Sika Danmark A/S, Fredensborg, Denmark.

Both types of sand complied with [DS/EN 12620, 2004] specifications and were obtained from Sten & Grus*. For 'Test I' both mortars (A) and (B) were applied, while 'Test II' was based on mortar (B) only.

Mixing of the mortar was conducted in a Hobart planetary mixer in accordance with [DS/EN 196-1, 1995]. Two specimens (instrumented plus simple or plain) and one mortar cylinder were cast at the same time. The samples were compacted by vibration in three steps during and after filling of the moulds (cf. Section 8.1.2.1). The specimens were cured vertically in the moulds at 20°C for 48 hours. During the first 24 hours the specimens were cured top-side-up, then the bottom lid was removed for casting of the bottom layer of epoxy (cf. Section 8.1.2.1) and the specimens were cured top-side-down for another 24 hours before demoulding on a pneumatic press. The exposure for both 'Test I' and 'Test II' started 28 days after casting, but the treatment during the 26 days between demoulding and exposure differed between the two test batches:

- Treatment between demoulding and exposure of 'Test I' specimens

  Immediately after demoulding, the specimens were sealed in plastic foil. After 5 days of transportation (from DTU Byg to Northwestern University) with unknown temperature conditions, the sealed specimens were stored at a temperature of 20°C ± 3°C.

- Treatment between demoulding and exposure of 'Test II' specimens

  The specimens were stored unsealed in a controlled indoor climate at a temperature of 20°C ± 3°C and an ambient relative humidity of 50% ± 10%.

- Cement paste specimens

  The cement paste specimens were based on cement paste with a 'w/c' of 0.4. Mixing of the cement paste was conducted in a food processor. The schedule specified in [DS/EN 196-1, 1995] was followed for the timing of the mixing. 400 ml of cement paste were mixed at a time to dip-coat six specimens. After dip-coating the cement paste specimens were mounted on a slowly rotating spinning wheel, while being sealed in plastic bottles and cured for 12-24 hours (cf. Figure 8.5 [B] in Section 8.1.2.2). Depending on the surface modification of the rebar, the coating/curing process was performed two to three times with an adequate number of dips to achieve a thickness of 3 ± 0.5 mm on the exposed surface, which was measured by means of a vernier calliper gauge. When the desired thickness was attained and the specimens were hardened, they were moist cured in saturated $Ca(OH)_2$ solution (cf. Figure 8.5 [C] in Section 8.1.2.2).

  Cement paste specimens were not used in 'Test I'. The 'Test II' cement paste specimens *for monitoring* were exposed in the chloride and potable water contain-

* Sten & Grus Prøvestenen A/S, Copenhagen, Denmark.

ers (cf. Section 8.2) 28 days after the final dip-coating (specimens with indices ending with "C" and "D", cf. Section 1.9.4). The 'Test II' cement paste specimens *for destructive measurements*, i.e. full-scale anodic polarisation curves, were tested at different time intervals, but with a minimum age of 7 days after the final dip-coating (specimens with indices ending with "E" to "P", cf. Section 1.9.4). The specimen production and testing was scheduled, so that measurements that were to be compared, e.g. to quantify the performance of different countermeasures at a certain exposure time, were taken at the same cement paste age (after the final dip-coating).

- Reinforcing steel qualities

  For 'Test I' ribbed rebar qualities were used to investigate actual conditions, e.g. concerning the effect on rolling and ribs for corrosion initiation (cf. Section 3.2). For 'Test II' emphasis was set on homogeneity to allow exact quantification of the effect of different surface modification and thus smooth rebars were used. The following ribbed and smooth carbon steel and stainless steel qualities were used; all in diameter of 16 mm:

  - Ribbed carbon steel rebar of type K550TS [LMG, 2004a] corresponding to B550AR+AC [DS 13080, 2001]
  - Ribbed stainless steel rebar of grade 1.4436 / 316 [DS/EN 10088-1, 2005] / [ASTM DS561, 2004]
  - Smooth carbon steel bar (structural steel) of type S235JR [DS/EN 10025-1, 2004; DS/EN 10025-2, 2004]
  - Smooth stainless steel bar (structural steel) of grade 1.4301 / 304 [DS/EN 10088-1, 2005] / [ASTM DS561, 2004].

  Details on the composition and the metallurgical properties of the applied ribbed reinforcement steel qualities are given in Section 3.2.2.2 for carbon steel and in Section 6.3.2.3 for stainless steel rebars.

- Exposure conditions

  As mentioned in Section 1.9.1, during the experimental investigations focus was set on chloride induced corrosion. However, no chloride or other depassivating species were cast into the mortar or cement specimens, since the thermodynamic conditions during both passivity and active corrosion were to be investigated and particularly the breakdown of passivity was of interest (cf. Sections 2.1.9 and 5.2.1.1). Hence, corrosion initiation and propagation was solely based on exposure to chloride solution. During all experimental investigations exposure solutions corresponded to 10% weight-by-weight 'w/w' chloride solution (165 g NaCl per litre solution) in accordance with NT build 443 [Frederiksen, 1997] and to potable water as reference exposure solution (the chloride solution was based on the same potable water). In accordance with NT build 443 the temperature of all exposure

solutions was kept at 23 ± 2 °C. Further details on the exposure conditions are given in Section 8.2 concerning chloride solution and potable water containers of the testing setup and in Section 8.4.1.4 concerning a supplementary setup for destructive electrochemical testing.

1.9.3 Investigations on Steel Qualities and Surface Treatments

The experimental setup used and selected results from the first experimental investigations concerning the thermodynamic properties of different steel qualities and carbon steel surface treatments (i.e. 'Test I') are described in [Küter et al., 2004; Küter et al., 2005b]. Besides investigating thermodynamic properties, these initial test aimed at verifying the design of the instrumented mortar specimen (in particular with regard to 'EIS') and to calibrate the applied measurement techniques.

The following steel qualities and surface treatments were examined based on the instrumented mortar specimen:

- Ribbed carbon steel rebars:
  - As-received. Indices: "C-1{A, B}"
  - Weathered according to [ASTM B117, 2007]. Indices: "C-2{A, B}"
  - Grit-blasted (grit roughness 10-15 µm). Indices: "C-3{A, B}"
  - Degreased (alkaline anodic, cf. Section 2.6.1.1). Indices: "C-4{A, B}"
  - HCl etched (cf. Section 2.6.1.2). Indices: "C-5{A, B}" and "W-5{A, B}"
  - Galvanised (HCl etched and 2 µm* zinc layer applied electrolytically, cf. Section 2.6.2). Indices: "C-6{A, B}".
- Ribbed stainless steel rebars:
  - Degreased (alkaline cathodic, Section 2.6.1.1). Indices: "C-7{A, B}".

For monitoring chloride ingress, instrumented mortar specimens with carbon steel 'EEWs' were produced based on the HCl etched specimens ("C-5S{1, 2}"). Moreover, plain mortar specimens ("C-P{1-4}" and "W-P{1-2}") and instrumented specimens without rebar ("C-N{1, 2}" and "W-N{1, 2}") were tested (cf. Section 1.9.1).

1.9.4 Investigations on Steel Qualities and Surface Modifications

The following steel qualities and surface modifications were examined based on instrumented mortar specimens (indices ending on "A"), simple mortar specimens (indices ending on "B"), and cement paste specimens (indices ending on "C" and "D"):

- Smooth carbon steel rebars:

* The thickness of the zinc layer was measured according to [Weidmann, 2002].

  - Grit-blasted (grit roughness 10-15µm}. Indices: "C01-{A-D}" and "W01-{A, D}"
  - Galvanised (grit-blasted and 2 µm zinc layer applied electrolytically, cf. Section 2.6.2) without defect / with defect. Indices: "C03-{A-D}" and "W03-{A, D}" / "C04-{A-D}" and "W04-{A, D}".
  - Modification type {I-III} without defect / with defect. Indices modification type I: "C05-{A-D}" and "W05-{A, D}" / "C06-{A-D}" and "W06-{A, D}". Indices modification type II: "C07-{A-D}" and "W07-{A, D}" / "C08-{A-D}" and "W08-{A, D}". Indices modification type III: "C09-{A-D}" and "W09-{A, D}" / "C10-{A-D}" and "W10-{A, D}".

- Smooth stainless steel rebars
  - Electrochemically cleaned (alkaline cathodic, cf. Section 2.6.1.1)

Besides the above listed specimens, which were monitored and tested in the two exposure containers, twelve cement paste specimens corresponding to each surface modification and exposure situation (indices ending with "E" to "P") were tested destructively by means of full-scale anodic polarisation curve measurements in a separate three-point electrode setup (cf. Section 8.4.1.4). Details on the specimens tested in the exposure containers (cf. Section 8.2) during 'Test II' are given in Table 1.1.

Table 1.1: *Indices, surface modification, purpose, and amount of specimens tested in the exposure containers (cf. Section 8.2) during the concluding experiments for the investigations on steel qualities and surface modifications.*

Index	Surface modification	Purpose	Amount
Chloride solution exposure setup			
CPM-{1-4}	No rebar / no electrode	Chloride ingress by colour test	4
CNR-{1, 2}	No rebar	Activated Ti potential	2
CSW-{1, 2}	Grit-blasted / steel wires	Chloride ingress	2
C01-{A-D}	Grit-blasted	Corrosion properties	4
C02-{A-D}	Stainless steel	Corrosion properties	4
C03-{A-D}	Galvanised	Corrosion properties	4
C04-{A-D}	Galvanised, defect	Corrosion properties	4
C05-{A-D}	Modification type I	Corrosion properties	4
C06-{A-D}	Modification type I, defect	Corrosion properties	4
C07-{A-D}	Modification type II	Corrosion properties	4
C08-{A-D}	Modification type II, defect	Corrosion properties	4
C09-{A-D}	Modification type III	Corrosion properties	4
C10-{A-D}	Modification type III, defect	Corrosion properties	4
C{1-7}B	Ribbed rebar specimens (cf. Section 1.9.3)	Corrosion properties (continuation)	7
-	-	Reserved for short-term tests	1
Number of specimens in chloride solution container			**56**
Potable water exposure setup			
WPM-{1-4}	No rebar / no electrode	Chemical investigations reference	4
WNR-1	No rebar	Activated Ti potential reference	1
WSW-1	Grit-blasted / steel wires	Chloride ingress reference	1
W01-{A, D}	Grit-blasted	Corrosion properties reference	2
W02-{A, D}	Stainless steel	Corrosion properties reference	2
W03-{A, D}	Galvanised	Corrosion properties reference	2
W04-{A, D}	Galvanised, defect	Corrosion properties reference	2
W05-{A, D}	Modification type I	Corrosion properties reference	2
W06-{A, D}	Modification type I, defect	Corrosion properties reference	2
W07-{A, D}	Modification type II	Corrosion properties reference	2
W08-{A, D}	Modification type II, defect	Corrosion properties reference	2
W09-{A, D}	Modification type III	Corrosion properties reference	2
W10-{A, D}	Modification type III, defect	Corrosion properties reference	2
W5B	Ribbed rebar specimen (cf. Section 1.9.3)	Corrosion properties reference (continuation)	1
-	-	Reserved for short-term tests	1
Number of specimens exposed in potable water container			**28**
Total number of specimens in both containers			**84**

* The modifications types I-III are not described in detail, due to expected patent possibilities (cf. Section 1.6). However, all three surface modification types are related to the theoretical concepts proposed in Section 7, i.e. implementation of zinc and magnesium as principal electrochemical active compounds.

2 Aqueous Metallic Corrosion

Selected theory and analytical tools for the thermodynamic and kinetic description of aqueous metallic corrosion, which are introduced in Sections 2.1 and 2.2, respectively, constitute the major part of this Chapter. Furthermore, forms of metallic corrosion (Section 2.3), the correlation between thermodynamics and kinetics (Section 2.4), selected electrochemical measurement techniques (Section 2.5), and the application of electrochemistry in steel surface treatments (Section 2.6) are described.

This Chapter is limited to the theory of metallic corrosion in aqueous electrolytes. Other forms of corrosion are generally not taken into consideration in the present thesis. Most of the described theory is applicable to corrosion of metals in general, while special emphasis is set on iron (especially in the exemplifications), which we consider to represent sufficiently the electrochemical properties of carbon steel.

Aqueous metallic corrosion is an electrochemical process, which consists of a variety of electrochemical reactions involving the transfer from one chemical species to the other. In simple terms, thermodynamics provides information on the type of electrochemical reaction and its tendency to occur in a certain environment, whereas kinetics provides information on the rate at which the transfer occurs.

Chapter 3 deals with properties of concrete and carbon steel that relate to both thermodynamics and kinetics, while the subsequent Chapters 5, 6, and 7 covering thermodynamics of carbon steel reinforcement corrosion, available corrosion countermeasures, and the development of new countermeasures, respectively, largely deal with thermodynamics only. Kinetic considerations (especially polarisation curves) were essential in the experimental part of this project. Besides describing the necessary background of the experimental investigations, Section 2.2 illustrates the importance of kinetics and hence the limitations of thermodynamics.

2.1 Thermodynamics of Aqueous Metallic Corrosion

Thermodynamics provides an understanding of the energy changes involved in the electrochemical reactions of corrosion. These energy changes provide the driving force and control the spontaneous direction of a chemical reaction. Thus, thermodynamics may illustrate how conditions can be adjusted to make corrosion impossible. As outlined in Section 1.5, our intention was to use thermodynamic tools to describe corrosion mechanisms and to apply this knowledge in the evaluation of available and the design of new countermeasures.

In this Section the theoretical basis for thermodynamic considerations is explained in more detail, whereas the background on the fundamental electrochemistry of corrosion is dealt with rather briefly. The basic concepts regarding reaction mechanisms (in particular, verifications based on electrode potentials and the involved Gibbs free en-

ergy changes) and most importantly the Pourbaix diagram are explained in more detail, as these concepts are central in this thesis.

2.1.1 Reaction Mechanisms

Reaction mechanisms can be used to describe, understand, and verify corrosion processes and accordingly measures that can counteract corrosion. Therefore, detailed evaluation or establishment of descriptive reaction mechanisms is a fundamental principle for the evaluation of available and the design of new corrosion countermeasures.

The affinity of reactions can be assessed based on evaluating the equilibrium potential 'E_0' for half-cell reactions and the Gibbs free energy change 'ΔG' for chemical reactions (cf. Chapter 'TaD'). These two concepts are regarded as central for a thermodynamically consistent description of corrosion processes. The theoretical backgrounds to 'E_0' and 'ΔG' are given in Sections 2.1.5 and 2.1.3, respectively.

The benefits of reaction mechanisms in describing corrosion processes and the proposed terminology used to refer to reactions (cf. Chapter 'TaD') are exemplified by means of a frequently cited redox reaction describing the *atmospheric* corrosion of iron to form hematite (Fe_2O_3):

$$4Fe + 3O_2 \rightarrow 2Fe_2O_3 \quad \left(\Delta G^0 = -1485\,\text{kJ} \right) \qquad [2.1]$$

This redox reaction does not illustrate what is actually taking place at the metal-electrolyte interface, i.e. the detailed reaction mechanism. The reaction does not occur by a direct reaction between oxygen and iron atoms (as e.g. in combustion reactions), but by electron transfer from the metal to the water. In this Section it is demonstrated how the redox reaction can be broken down in its constituent reactions to assess the detailed reaction mechanism.

Half-cell reactions describe either the gain of electrons, which is referred to as reduction, or the loss of electrons, which is referred to as oxidation[*]:

- Reduction: An oxidant is reduced, i.e. the oxidation state is decreased (and electrons are gained)
- Oxidation: A reductant is oxidised, i.e. the oxidation state is increased (and electrons are lost)

Neither oxidation nor reduction can be realised alone (in condensed matter). The reduction must necessarily consume the electrons produced by the oxidation. Thus, the oxidation reaction must always be coupled to and balanced by the reduction reaction. The electrode (or site on the surface) where oxidation takes place is referred to as an-

[*] Although not truly correct, these definitions are sufficient for the scope of this thesis. Oxidation and reduction properly refer to a change in oxidation state, whereas the actual transfer of electrons may not occur, as e.g. for covalent bonds.

ode (or anodic site), and the electrode (or site on the surface) where reduction takes place is referred to as cathode (or cathodic site).

The redox reaction [2.1] comprises the below half-cell reactions, which provide a more accurate description of the actual reaction mechanism.

Iron is first oxidised to ferrous ion (Fe^{2+}) described by the half-cell reaction:

$$Fe \rightarrow Fe^{2+} + 2e^{-} \quad \left(E_0^0 = -475\{-447\}\,mV_{SHE} \right) \qquad [2.2]$$

Ferrous ion is further oxidised to ferric ion (Fe^{3+}) according to the half-cell reaction:

$$Fe^{2+} \rightarrow Fe^{3+} + e^{-} \quad \left(E_0^0 = 771\{771\}\,mV_{SHE} \right) \qquad [2.3]$$

The half-cell reactions [2.2] and [2.3] are also referred to as anodic reactions. It should be noted that iron can exist in two oxidation states “2+” and “3+”.

The electrons that were produced by these two anodic reactions are consumed by the half-cell reaction describing the reduction of dissolved oxygen in neutral and alkaline solutions, i.e. in neutral water:

$$O_2 + 2H_2O + 4e^{-} \rightarrow 4OH^{-} \quad \left(E_0^0 = 402\{401\}\,mV_{SHE} \right) \qquad [2.4]$$

The half-cell reaction [2.4] is also referred to as cathodic reaction.

It should be remarked that water is not only required for the cathodic reaction, but also as the carrier for the cations produced in the anodic reaction, i.e. the ferrous and the ferric ion.

Combining the half-cell reactions [2.2], [2.3], and [2.4] and balancing them for the number of electrons being transferred, the following redox reaction is obtained:

$$4Fe + 3O_2 + 6H_2O \rightarrow 4Fe^{3+} + 12OH^{-} \quad \left(\Delta G^0 = -178\ kJ \right) \qquad [2.5]$$

The free ferric ions and the hydroxide ions are not actual intermediates, but directly form a more stable phase under the liberation of water. As ferric ion and hematite are in the same oxidation state, this is described by the acid-base reaction:

$$2Fe^{3+} + 6OH^{-} \rightarrow Fe_2O_3 + 3H_2O \quad \left(\Delta G^0 = -476\ kJ \right) \qquad [2.6]$$

Inserting [2.6] into [2.5] leads to:

$$4Fe + 3O_2 + 6H_2O \rightarrow 2Fe_2O_3 + 6H_2O \quad \left(\Delta G^0 = -1485\ kJ \right) \qquad [2.7]$$

which corresponds to the original redox reaction [2.1].

In this way, the reaction mechanism that reflects the actual process summarised by the redox reaction [2.1] (but is not accessible through the same) can be evaluated step-by-step. As explained in more detail in Section 2.1.3 and Section 2.1.5, the step-by-step reaction mechanism can also be thermodynamically verified with regard to the

involved magnitudes of 'ΔG' and 'E_0'. Based on such verfication this reaction mechanism can be considered to be a reasonable description of the investigated corrosion process. In Chapter 5 selected examples from the literature show that *many reactions or reaction mechanisms, which have been postulated for the description of different reinforcement corrosion phenomena, do not fullfil these fundamental thermodynamic requirements*.

Besides that the original redox reaction [2.1] does not illustrate the detailed reaction mechanism, it indicates a further problem of such descriptions. Fe_2O_3 is not only the principal compound formed in active corrosion as the *undesirable corrosion product* commonly known as red rust, but it also is the major contributor to the generally *desired passivation* and hence to the passive state of iron (or steel) in alkaline media, such as uncontaminated concrete. Among others, the thermodynamic differentiation between the products formed in these two states, i.e. the active corrosion and the passive state, and their consequences in aqueous corrosion systems of steel and other metals are a central aspect in this thesis.

2.1.2 Anodic and Cathodic Reactions

In aqueous metallic corrosion the anodic reaction is invariably in the form of an oxidation reaction:

$$Me \rightarrow Me^{n+} + ne^- \qquad [2.8]$$

with 'Me' as an arbitrary metal and 'n' as the oxidation state of the metal 'Me'. 'Me' can also represent any compound of the metal, while 'Me^{n+}' represents any compound of the same metal in a higher oxidation state. This includes that the anodic reaction can form any oxide, hydroxide, or any other oxidised compound of the metal, as e.g. illustrated by the oxidation of iron to magnetite (Fe_3O_4):

$$3Fe + 4H_2O \rightarrow Fe_3O_4 + 8H^+ + 8e^- \quad \left(E_0^0 = -86\,mV_{SHE} \right) \qquad [2.9]$$

Thus, anodic reaction products are not at all limited to the formation of dissolved ions such as Fe^{2+} or Fe^{3+} (cf. half-cell reactions [2.2] and [2.3] in Section 2.1.1), but various compounds can be formed. This aspect, which appears to be not or only partly acknowledged in most textbooks on reinforcement corrosion, is a central aspect in our thermodynamic considerations. Products formed by anodic reactions are dealt with throughout this thesis, while the most important aspects are reasoned in Chapter 4 and discussed in detail with focus on reinforcement corrosion in Chapter 5.

In the corrosion literature, it is often remarked that half-cell reactions describing cathodic reactions are few in number[*]. The generally stated cathodic reactions comprise:

[*] In contrast to other electrochemical disciplines (e.g. electroplating, cf. Section 2.6.2) where the desired cathodic reactions include $Me^{n+} + ne^- \rightarrow Me$.

- Reduction of oxygen in acid solutions:

$$O_2 + 4H^+ + 4e^- \rightarrow 2H_2O \quad \left(E_0^0 = 1230\{1229\}\,mV_{SHE} \right) \qquad [2.10]$$

- Reduction of oxygen in neutral and alkaline solutions:

$$O_2 + 2H_2O + 4e^- \rightarrow 4OH^- \quad \left(E_0^0 = 402\{401\}\,mV_{SHE} \right) \qquad [2.11]$$

- Reduction of hydrogen ion (hydrogen evolution) in acid solutions:

$$2H^+ + 2e^- \rightarrow H_2 \quad \left(E_0^0 = 0\,mV_{SHE} \right) \qquad [2.12]$$

- Reduction of water (hydrogen evolution) in neutral and alkaline solutions (in absence of all other cathodic reactions):

$$2H_2O + 2e^- \rightarrow H_2 + 2OH^- \quad \left(E_0^0 = -828\{-828\}\,mV_{SHE} \right) \qquad [2.13]$$

Both terms reduction of hydrogen ion/hydrogen ion reduction and hydrogen evolution are used throughout this thesis. Hydrogen evolution (in the literature also referred to as hydrogen development or hydrogen formation) is used, if the *evolution* of hydrogen is of concern rather than the *cathodic action* (cf. half-cell reactions [2.12] and [2.13]).

It should be noted that from a thermodynamic point of view every reduction reaction, e.g. in analogy to the half-cell reaction [2.9], can be considered as a possible cathodic reaction:

$$Fe_3O_4 + 8H^+ + 8e^- \rightarrow 3Fe + 4H_2O \quad \left(E_0^0 = -86\,mV_{SHE} \right) \qquad [2.14]$$

So in principle, any anodic reaction can be reversed into the reduction direction and act as cathodic reaction, if the thermodynamic conditions are present. Yet, kinetics limits the reduction of oxides and hydroxides to a large extent, as is reasoned in Section 4.2.1 and, with particular regard to reinforcement corrosion, throughout Chapter 5. We suggest, however, that reduction of soluble species, such as reduction of ferric ion to ferrous ion (cf. [2.3] in Section 2.1.1), is kinetically favoured:

$$Fe^{3+} + e^- \rightarrow Fe^{2+} \quad \left(E_0^0 = 771\{771\}\,mV_{SHE} \right) \qquad [2.15]$$

Nevertheless, compared to the magnitude of the cathodic reactions [2.10] to [2.13], reduction of oxidised ions generally has in corrosion a smaller contribution to the cathodic processes. This and other aspects concerning cathodic reactions and their domains are dealt with throughout this thesis, in particular in Sections 2.1.10 as well as in Chapters 4 and 5.

2.1.3 Gibbs Free Energy

The driving force for any chemical reaction occurring under conditions of constant temperature and pressure can be measured by the negative Gibbs free energy* change 'ΔG', which accompanies the transformation of the reactants to the products.

'ΔG' can be defined as follows [Bardal, 2004]:

"When a system is transferred to one state from another at constant pressure and temperature, it is subjected to a change of free enthalpy (or Gibbs free energy) given by: 'ΔG' = − (maximum work available from the system through the state transition), when this work is given a positive sign."

The system tends to transform to a lower energy level by itself, i.e. a net reaction that occurs without any supply of energy is accompanied by a negative 'ΔG'. Accordingly, the meaning of the sign of 'ΔG' can be understood as follows:

- 'ΔG' < 0 means that the system can carry out work and releases energy. Hence, the chemical reaction that describes the system is spontaneous and irreversible, i.e. *the reaction is thermodynamically favoured.*
- 'ΔG' = 0 means the system is at equilibrium. Hence, the chemical reaction that describes the system is reversible and *neither the forward nor the reverse reaction prevails*.
- 'ΔG' > 0 means that energy must be supplied to the system to proceed. Hence, the chemical reaction that describes the system is non-spontaneous. That means that it proceeds in the opposite direction, i.e. *the reaction is thermodynamically unfavoured.*

It should be emphasised that there is a lot more theory to the concept of the Gibbs free energy, in particular with regard to its equivalences with other thermodynamic potentials such as internal energy, Helmholtz free energy, and enthalpy (cf. Section 4.1). The theory behind these parameters is intentionally omitted in this Section, as they are "indirect" parameters in thermodynamic calculations and we regard the related theory to be marginal for the scope of this thesis. The other thermodynamic definitions and fundamental correlations are, however, briefly dealt with in Section 4.1, since they are relevant to our application of e.g. thermodynamic software. For a detailed discussion of the concepts of Gibbs free energy and other thermodynamic potentials reference is made to the literature. Among standard thermodynamic or physical chemistry textbooks, reference is made to e.g. [Freiesleben Hansen, 1995; Møller, 2003a].

If 'ΔG' of a reaction is known, it is possible to predict whether or not the reaction is thermodynamically favoured. We use this statement only as a "negative indicator", i.e. if a chemical reaction displays a positive 'ΔG' and hence is thermodynamically unfavoured, it is considered impossible to take place. However, no clear statement can

* Named after Josiah Willard Gibbs, USA, 1839-1903 [Roberge, 2007].

be made on whether or not a chemical reaction with a negative 'ΔG' takes place, since the reaction kinetics plays an essential role as well. This also excludes statements of the probability of a reaction to occur based on the *magnitude* of its associated 'ΔG'.

For a reaction of the type:

$$v_{R_1} R_1 + ... + v_{R_z} R_z \rightarrow v_{P_1} P_1 + ... + v_{P_z} P_z \qquad [2.16]$$

where 'v' is the stoichiometric coefficient and 'R' and 'P' are the reactants and the products, respectively, 'ΔG' for the standard state 'ΔG^0' can be calculated according to:

$$\begin{aligned} \Delta G^0 &= \sum \Delta G^0_{f,P} - \sum \Delta G^0_{f,R} \\ \Delta G^0 &= \left(v_{P_1} \Delta G^0_{f,P_1} + ... + v_{P_z} \Delta G^0_{f,P_z} \right) - \left(v_{R_1} \Delta G^0_{f,R_1} + ... + v_{R_z} \Delta G^0_{f,R_z} \right) \end{aligned} \qquad [2.17]$$

'ΔG_f^0' of the reactants and the products is referred to as standard Gibbs free energy of formation *change*. 'ΔG_f^0' accompanies the formation of 1 mol of a compound from its component elements at their standard states. All pure isolated elements in their standard states (e.g. Fe, O_2, and H_2) have a 'ΔG_f^0' of zero, as there is no energy change involved in their formation. This is not true for values specified as standard Gibbs free energy of formation 'G_f^0', which refers to the so-called absolute scale [Barin, 1993]. Due to this divergence, we prefer to use and refer to 'ΔG_f^0' values. The meaning of the different scales and the transformation from one to the other are briefly dealt with in Section 4.1.

For almost any compound, 'ΔG_f^0' (or 'G_f^0') values can be obtained from various sources or calculated based on other thermodynamic parameters provided in the literature. The sources and other relevant parameters are discussed in Section 4.1. Within our project most of the applied 'ΔG_f^0' values were obtained from the thermodynamic database provided in the software Outokumpu 'HSC' Chemistry*, which was also used for calculating 'ΔG^0' of reactions [Ouku, 1999; Ouku, 2002]. However, in some cases, e.g. where the thermodynamic data provided in 'HSC' was found to be incomplete or we came across discrepancies in the specified values, additional sources were used. These aspects are further elaborated in Section 4.1.

The establishment of 'ΔG^0' based on 'ΔG_f^0' and 'G_f^0' values is briefly exemplified in the following by means of the acid-base reaction describing the precipitation of ferric ion as hematite (cf. reaction mechanism described in Section 2.1.1):

$$2Fe^{3+} + 6OH^- \rightarrow Fe_2O_3 + 3H_2O \quad \left(\Delta G^0 = -476\,\text{kJ} \right) \qquad [2.18]$$

The associated 'ΔG_f^0' and 'G_f^0' values are listed in Table 2.1.

* Both major versions 4 and 5 of 'HSC' were used throughout the project period. Apparently some database entries were incorrect in version 4 or wrongly updated in version 5. Thus, data for thermodynamic calculations was verified with other publications and between the two 'HSC' versions. More information is given in Section 4.1.

Table 2.1: *Standard Gibbs free energy of formation change 'ΔG_f^0' and standard Gibbs free energy of formation 'G_f^0' values for compounds involved in acid-base reaction [2.18].*

Compound	'ΔG_f^0'	'G_f^0'	Reference
	kJ/mol	kJ/mol	
Fe^{3+}	−17.183	33.126	[Shock & Korezky, 1993]
OH^-	−157.286	−226.830	[Shock & Helgeson, 1988]
Fe_2O_3	−741.044	−850.307	[Barin, 1993]
H_2O	−237.141	−306.686	[ESDU, 2007]

Based on these 'ΔG_f^0' values, 'ΔG^0' of the reaction can be calculated in accordance with equation [2.17] to:

$$\begin{aligned} \Delta G^0 &= \left[1\times(-741.044)+3\times(-237.141)\right]-\left[2\times(-17.183)+6\times(-157.286)\right] \\ \Delta G^0 &= -475\ \text{kJ} \end{aligned} \quad [2.19]$$

'ΔG^0' obtained in this way is in agreement with 'ΔG^0' calculated by 'HSC' for the acid-base reaction [2.18]. The equivalent calculation based on 'G_f^0' values shows that the same 'ΔG^0' is calculated based on standard Gibbs free energy of formation in the absolute scale, as the differences cancel each other out in the calculation:

$$\begin{aligned} \Delta G^0 &= \left[1\times(-850.307)+3\times(-306.686)\right]-\left[2\times 33.126+6\times(-226.830)\right] \\ \Delta G^0 &= -475\ \text{kJ} \end{aligned} \quad [2.20]$$

The concept of calculating 'ΔG^0' for a reaction at the standard state can be extended to arbitrary conditions (non-standard states) according to:

$$\Delta G = \Delta G^0 + R\times T\times \ln\left(K_{ma}\right) \quad [2.21]$$

where 'R' = 8.314 J/(K×mol) is the gas constant, 'T' is the absolute temperature, and ('K_{ma}') is the mass constant. A derivation of equation [2.21] goes beyond the scope of this thesis and reference is made to e.g. [Freiesleben Hansen, 1995; Møller, 2003a; Bardal, 2004].

At the standard state ('K_{ma}') is equal to 1, which (in accordance with equation [2.21]) means that 'ΔG' is equal to 'ΔG^0'. If the system is at equilibrium (the reaction is reversible), 'ΔG' is equal to zero and ('K_{ma}') corresponds to the equilibrium constant ('K_{eq}'). Hence, in correspondence with [2.21], 'ΔG^0' can be expressed as:

$$\Delta G^0 = -R\times T\times \ln\left(K_{eq}\right) \quad [2.22]$$

('K_{ma}') and ('K_{eq}') can be described as:

$$K_{ma} = K_{eq} = \prod_{i=1}^{z} a_i^{\nu_i} \quad [2.23]$$

where 'a' is the activity of the involved compounds. Thus, for a reaction of the type:

$$\nu_{R_1} R_1 + ... + \nu_{R_z} R_z \rightarrow \nu_{P_1} P_1 + ... + \nu_{P_z} P_z \quad [2.24]$$

('K_{ma}') and ('K_{eq}') can be written as:

$$K_{ma} = K_{eq} = \frac{\left(a_{P_1}\right)^{\nu_{P_1}} \times ... \times \left(a_{P_z}\right)^{\nu_{P_z}}}{\left(a_{R_1}\right)^{\nu_{R_1}} \times ... \times \left(a_{R_z}\right)^{\nu_{R_z}}} \quad [2.25]$$

The natural logarithm in equations [2.21] and [2.22] is generally transferred to a base-10 logarithm to express the quantities as function of the pH:

$$pH = -\log\left(a_{H^+}\right) = 14 + \log\left(a_{OH^-}\right) \quad [2.26]$$

Thus, with a conversion factor of 2.303 (ln to log) and [2.25] inserted, equations [2.21] and [2.22] can be rewritten as:

$$\Delta G = \Delta G^0 + 2.303 \times R \times T \times \log\left(\frac{\left(a_{P_1}\right)^{\nu_{P_1}} \times ... \times \left(a_{P_z}\right)^{\nu_{P_z}}}{\left(a_{R_1}\right)^{\nu_{R_1}} \times ... \times \left(a_{R_z}\right)^{\nu_{R_z}}}\right) \quad [2.27]$$

and

$$\Delta G^0 = -2.303 \times R \times T \times \log\left(\frac{\left(a_{P_1}\right)^{\nu_{P_1}} \times ... \times \left(a_{P_z}\right)^{\nu_{P_z}}}{\left(a_{R_1}\right)^{\nu_{R_1}} \times ... \times \left(a_{R_z}\right)^{\nu_{R_z}}}\right) \quad [2.28]$$

For a standard state temperature 'T' of 25°C (cf. Chapter 'TaD'), equations [2.27] and [2.28] correspond to:

$$\Delta G = \Delta G^0 + 5705.974 \times \log\left(\frac{\left(a_{P_1}\right)^{\nu_{P_1}} \times ... \times \left(a_{P_z}\right)^{\nu_{P_z}}}{\left(a_{R_1}\right)^{\nu_{R_1}} \times ... \times \left(a_{R_z}\right)^{\nu_{R_z}}}\right) \quad [2.29]$$

and

$$\Delta G^0 = -5705.974 \times \log\left(\frac{\left(a_{P_1}\right)^{\nu_{P_1}} \times ... \times \left(a_{P_z}\right)^{\nu_{P_z}}}{\left(a_{R_1}\right)^{\nu_{R_1}} \times ... \times \left(a_{R_z}\right)^{\nu_{R_z}}}\right) \quad [2.30]$$

where 5705.974 is a factor created from '$R \times T$ [K]' times the conversion factor (ln to log).

Equations [2.29] and [2.30] are of central importance in the present thesis. Among others, equation [2.29] is used throughout this thesis to transfer 'ΔG^0' values (calcu-

lated by means of 'HSC') to the conditions under consideration*. Equation [2.30] plays an important role in calculating acid-base equilibria, e.g. for the establishment of Pourbaix diagrams (cf. Section 2.1.10).

The final input parameter for equations [2.29] and [2.30] are the activities 'a', which (apart from *ion* activities) can be treated in a rather simple approach when dealing with customary aqueous corrosion systems (including corrosion of steel in concrete). For such electrochemical systems, we think that it is satisfactory to base the calculations on the following assumptions concerning the activities 'a' (cf. Chapter 'TaD'):

- For gases, 'a' corresponds to the partial pressure 'p' in [bar].
- For solid matter and solvents, 'a' corresponds to 1.
- For dissolved matter (ionic species), 'a' corresponds to the ion concentration in [mol/L].

The choice of representative ion activities is hence a critical parameter and a central aspect in our project. This aspect is dealt with throughout this thesis and with particular regard to the establishment of Pourbaix diagrams in Section 4.2.1. *If not stated otherwise, the ion activity for numerical values (non-standard states) and for Pourbaix diagrams corresponds to 10^{-6} mol/L.*

2.1.4 Equilibrium Potential Difference

In a galvanic cell at equilibrium, the equilibrium potential difference 'ΔE_0' (in the literature also referred to as electromotive force 'EMF', cf. Chapter 'TaD') can be measured as the difference between the individual equilibrium potentials of two electrodes. Under standard state conditions, the equilibrium potential difference is referred to as 'ΔE_0^0' in the present thesis.

The detailed theory on how metals attain their equilibrium potential and the reason for the difference in equilibrium potentials is complex and beyond the scope of this thesis. A brief and simplified note on this topic is given in Section 2.1.5.

According to the convention of Stockholm, 'ΔE_0' of a spontaneous system is defined to be positive [IUPAC, 1953]:

$$\Delta E_0 = E_{0,2} - E_{0,1} \quad \text{for} \quad E_{0,1} < E_{0,2} \qquad [2.31]$$

'ΔE_0' is the force that drives electrons in a reversible cell and accordingly a measure of the corresponding redox reaction, i.e. the combination of the anodic and cathodic reactions.

* Unfortunately, 'HSC' does not provide for calculations of *individual* thermodynamic parameters for non-standard states. However, non-standard state conditions are represented in the equilibria calculated for e.g. the establishment of Pourbaix diagrams (Section 2.1.10) by means of 'HSC'.

Hence, the two quantities 'ΔE_0' and 'ΔG' are proportional to each other and the general definitions for 'ΔG' given in Section 2.1.3 can be transferred. The maximum useful work is equivalent to the maximum electrical energy that can be achieved from a reversible cell. The maximum achievable electrical energy corresponds to 'ΔE_0' times the charge ('Q'). According to Faraday's law*, a charge equal to 'n' times the Faraday constant 'F' = 96.485×10^3 C/mol is passed per mole of a species (in the oxidation state 'n'). That leads to:

$$Q = n \times F \qquad [2.32]$$

Accordingly, the thermodynamic relation between 'ΔE_0' and 'ΔG' can be expressed as:

$$\Delta G = -n \times F \times \Delta E_0 \qquad [2.33]$$

The negative sign in equation [2.33] confirms the definition that positive work, i.e. a positive 'ΔE_0' results in a negative 'ΔG'. Therefore, in accordance with the classifications for 'ΔG' in Section 2.1.3, the following holds for 'ΔE_0':

- 'ΔE_0' > 0 means that the reversible cell produces energy. Hence, *the associated redox reaction is spontaneous*.
- 'ΔE_0' < 0 means that energy must be supplied to the system. Hence, *the associated redox reaction is non-spontaneous*.

2.1.5 Reference, Reduction, Equilibrium, and Standard Potential

As mentioned in Section 2.1.4, 'ΔE_0' can be measured in a system at equilibrium as the difference between the individual equilibrium potentials. However, it is impossible to measure the absolute value of any equilibrium potential (the electrode potential associated with a single half-cell reaction), because the two half-cell reactions in a galvanic cell are not independent of each other. Only the 'ΔE_0' between two half-cell reactions (i.e. a redox couple) is measurable and a certain electrode potential must be selected as the reference. In accordance with the zero or reference point of the standard electromotive force series and other thermodynamic tools (in particular the Pourbaix diagram, cf. Section 2.1.10), the reference point for electrode potentials in this thesis is chosen as the electrode potential of the hydrogen half-cell reaction at standard state:

$$2H^+ + 2e^- \rightarrow H_2 \quad \left(E_0^0 \equiv 0\,mV_{SHE} \right) \qquad [2.34]$$

This reference point is also known as the electrode potential of the standard hydrogen electrode 'SHE' (in the literature also referred to as normal hydrogen electrode ('NHE')). This is a common choice in the literature on corrosion science, whereas most of the literature dealing exclusively with reinforcement corrosion refers to other

* Named after Michael Faraday, UK, 1791-1867 [Roberge, 2007].

reference potentials, often to the one of the saturated calomel electrode 'SCE'. Half-cell reactions and the corresponding electrode potentials of the most important other reference electrodes used in corrosion and reinforcement corrosion science are discussed in Section 2.1.7.

By defining a reference point, the electrode potential can be used equivalently to the 'ΔE_0' in equation [2.33] to express the thermodynamic relation between 'ΔG' and the equilibrium potential 'E_0':

$$\Delta G = -z \times F \times E_0 \qquad [2.35]$$

For a half-cell reaction at its equilibrium potential 'E_0', reduction and oxidation reactions occur at the same rate, i.e. the half-cell reaction is reversible. For example, at 'E_0' an iron electrode releases ions from the surface and discharges them on the surface at the same rate. This is often indicated by a double arrow in the literature:

$$Fe \rightleftarrows Fe^{2+} + 2e^- \quad \left(E_0^0 = 475\{447\}\,mV_{SHE} \right) \qquad [2.36]$$

This notation is omitted in the present thesis. Considering the reversibility of half-cell reactions, there also is a sign problem for the electrode potential. For the reduction potential '$E_{0,red}$' and the oxidation potential '$E_{0,oxi}$' the numeric value is identical, but the sign is opposed, as illustrated by the half-cell reactions [2.37] and [2.38]:

Reduction reaction:

$$Fe^{2+} + 2e^- \rightarrow Fe \quad \left(E_{0,red}^0 = -475\{-447\}\,mV_{SHE} \right) \qquad [2.37]$$

Oxidation reaction:

$$Fe \rightarrow Fe^{2+} + 2e^- \quad \left(E_{0,oxi}^0 = 475\{447\}\,mV_{SHE} \right) \qquad [2.38]$$

In this thesis, all half-cell reactions and specified equilibrium potentials are given in the notation according to the convention of Stockholm [IUPAC, 1953]: The equilibrium potential *"... is defined as the reduction potential and all half-reactions are read in the sense of the reduction."*

That means that the sign of the equilibrium potential 'E_0' is defined as the sign of the reduction potential '$E_{0,red}$':

$$E_0 = E_{0,red} \qquad [2.39]$$

This definition includes that, if not stated otherwise, in the present thesis 'E_0' for an oxidation reaction *always* refers to the reduction potential. Accordingly, [2.38] corresponds to:

$$Fe \rightarrow Fe^{2+} + 2e^- \quad \left(E_0^0 = -475\{-447\}\,mV_{SHE} \right) \qquad [2.40]$$

It should be noted that the exemplification given in Section 2.1.1 corresponds to this definition.

Among the benefits of consistency with e.g. Pourbaix diagrams (cf. Section 2.1.10), the specification of the equilibrium potential as the reduction potential (regardless of the direction of the half-cell reaction) provides the major advantage that the *numerical values match the polarity of experimentally measured potentials* (cf. Chapter 5).

As in most other literature, the sign of the electrode potential of any species compared to the 'SHE' is defined as follows in the present thesis [Bardal, 2004]:

"The half-cell potential of a reaction X referred to the 'SHE' corresponds to the voltage of the cell in which the hydrogen reaction proceeds as oxidation and X as reduction."

This means that any electrode or environment accepting electrons from the 'SHE' is defined to be at a positive electrode potential, whereas any electrode or environment donating electrons to the 'SHE' is defined to be at a negative electrode potential.

An exemplification for the relation between 'ΔE_0', 'ΔG', and 'E_0' (based on oxidation of ferrous ion as anodic reaction and hydrogen ion reduction as cathodic reaction) is given in the following. In this case, it is assumed that the half-cell reactions take place at the same rate. This is a theoretical assumption and not true in practice (cf. Section 2.2).

Anodic reaction:

$$\mathrm{Fe} \rightarrow \mathrm{Fe^{2+}} + 2\mathrm{e^-} \quad \left(\mathrm{E_0^0} = -475\,\{447\}\,\mathrm{mV_{SHE}} \right) \qquad [2.41]$$

Cathodic reaction:

$$2\mathrm{H^+} + 2\mathrm{e^-} \rightarrow \mathrm{H_2} \quad \left(\mathrm{E_0^0} = 0\,\mathrm{mV_{SHE}} \right) \qquad [2.42]$$

According to [2.31], 'ΔE_0^0' of this system is obtained to:

$$\Delta \mathrm{E_0^0} = \mathrm{E_{0,c}^0} - \mathrm{E_{0,a}^0} = 0 - (-0.475) = 0.475\ \mathrm{V} \qquad [2.43]$$

The sum of [2.41] and [2.42] leads to the corresponding redox reaction:

$$\mathrm{Fe} + 2\mathrm{H^+} \rightarrow \mathrm{Fe^{+2}} + \mathrm{H_2} \quad \left(\Delta \mathrm{G^0} = -92\,\mathrm{kJ} \right) \qquad [2.44]$$

With [2.33] rewritten as

$$\Delta \mathrm{E_0} = -\frac{\Delta \mathrm{G}}{\mathrm{n} \times \mathrm{F}} \qquad [2.45]$$

and 'ΔG^0', 'n', and 'F' inserted, 'ΔE_0^0' of the reversible cell is obtained to:

$$\Delta \mathrm{E_0^0} = -\frac{-91,625}{2 \times 96,485} = 0.475\ \mathrm{V} \qquad [2.46]$$

Thus, 'ΔE_0^0' obtained from [2.46] corresponds to 'ΔE_0^0' obtained from [2.43], which exemplifies the thermodynamic relation between 'ΔE_0' and 'ΔG'. Moreover, it can be

observed that 'E_0^{0}' specified in the half-cell reaction [2.41] corresponds to 'ΔE_0^{0}' calculated in [2.43] and [2.46], as reduction of hydrogen was chosen as cathodic reaction.

The definition of a reference point *allows comparison of standard potentials of different half-cell reactions* (cf. Section 2.1.6) and enables (e.g. based on measured electrode potentials) conclusions on the direction of the evaluated half-cell reactions:

If the electrode potential is lower than the equilibrium potential of the associated half-cell reaction, the half-cell reaction goes into the reduction direction. If the electrode potential is higher, the associated half-cell reaction goes into the oxidation direction.

In correspondence with the calculation of 'ΔG^{0}' values (cf. Section 2.1.3), all 'E_0^{0}' stated in the present thesis have been calculated using 'HSC' and most are based on the included thermodynamic database [Ouku, 1999; Ouku, 2002]. If a numerical value for 'E_0^{0}' was found available in the literature, it is listed as the second value in the curly brackets ({...}). If not stated otherwise, this value was taken from [Jones, 1996] (cf. Chapter 'TaD').

In case of incomplete or identified erroneous entries, additional sources were used and verifications were performed. In Section 4.1, such a verification is exemplified for the 'E_0^{0}' of the reduction of ferrous ion, which shows a considerable deviation between the calculated value ('HSC': 'E_0^{0}' = −475 mV_{SHE}) and the literature value ([Jones, 1996] and most other literature: 'E_0^{0}' = −447 mV_{SHE}).

2.1.6 Relevant Half-Cell Reactions and Standard Potentials

A list of half-cell reactions sorted according to their associated standard potentials is often referred to as the electromotive force 'EMF' series. 'EMF' series can be found in the literature, e.g. [Jones, 1996; Bardal, 2004]. Generally, half-cell reactions in the 'EMF' series are written from the left to the right as reduction potentials versus 'SHE' (in accordance with the sign conventions defined in Section 2.1.5) and sorted according to their ability to be reduced, i.e. from noble to active reduction potentials. In accordance with [ASTM G3, 2004], the upper boundary is referred to as noble and the lower boundary is referred to as active in the present thesis (cf. Chapter 'TaD').

In the following, selected half-cell reactions (of relevance in this thesis), are listed (according to their ability to be reduced) together with their calculated 'E_0^{0}' and their literature 'E_0^{0}' [Jones, 1996]:

- Reduction of oxygen in acid solutions:

$$O_2 + 4H^+ + 4e^- \rightarrow 2H_2O \quad \left(E_0^0 = 1230\{1229\}\ mV_{SHE} \right) \qquad [2.47]$$

- Reduction of ferric ion:

$$Fe^{3+} + e^- \rightarrow Fe^{2+} \quad \left(E_0^0 = 771\{771\}\ mV_{SHE} \right) \qquad [2.48]$$

- Reduction of cupric ion:

$$Cu^{2+} + 2e^- \rightarrow Cu \quad \left(E_0^0 = 340\,\{342\}\,mV_{SHE} \right) \qquad [2.49]$$

- Reduction of hydrogen ion in acid solutions:

$$2H^+ + 2e^- \rightarrow H_2 \quad \left(E_0^0 = 0\,mV_{SHE} \right) \qquad [2.50]$$

- Reduction of nickelous ion:

$$Ni^{2+} + e^- \rightarrow Ni \quad \left(E_0^0 = -237\,\{-250\}\,mV_{SHE} \right) \qquad [2.51]$$

- Reduction of ferrous ion:

$$Fe^{2+} + e^- \rightarrow Fe \quad \left(E_0^0 = -475\,\{-447\}\,mV_{SHE} \right) \qquad [2.52]$$

- Reduction of chromic ion:

$$Cr^{3+} + 3e^- \rightarrow Cr \quad \left(E_0^0 = -714\,\{-744\}\,mV_{SHE} \right) \qquad [2.53]$$

- Reduction of zinc ion:

$$Zn^{2+} + 2e^- \rightarrow Zn \quad \left(E_0^0 = -764\,\{-726\}\,mV_{SHE} \right) \qquad [2.54]$$

- Reduction of chromous ion*:

$$Cr^{2+} + 2e^- \rightarrow Cr \quad \left(E_0^0 = -855\,mV_{SHE} \right) \qquad [2.55]$$

- Reduction of magnesium ion:

$$Mg^{2+} + 2e^- \rightarrow Mg \quad \left(E_0^0 = -2354\,\{-2372\}\,mV_{SHE} \right) \qquad [2.56]$$

The two half-cell reactions describing the reduction of oxygen [2.47] and of hydrogen [2.50] illustrate that hydrogen ions are necessary for the reactions to take place. Sufficient supply of H^+ is provided in acid solutions only, but both reactions can also take place in neutral or alkaline solutions, as they can be supported by continuous dissociation of water:

$$H_2O \rightarrow H^+ + OH^- \quad \left(\Delta G^0 = 80\,kJ \right) \qquad [2.57]$$

Adding the dissociation of water [2.57] to oxygen reduction [2.47] leads to the half-cell reaction describing reduction of dissolved oxygen in neutral and alkaline solutions, which was already mentioned in Section 2.1.1:

$$O_2 + 2H_2O + 4e^- \rightarrow 4OH^- \quad \left(E_0^0 = 402\,\{401\}\,mV_{SHE} \right) \qquad [2.58]$$

* Reduction of chromous ion is normally not included in standard 'EMF' series in the literature, e.g. [Jones, 1996; Bardal, 2004]. This is probably due to the fact that it is easily oxidised to chromic ion. However, we think that chromous ion can play an important role in crevice corrosion (cf. Section 2.3.4) of stainless steel and it is thus included in this list.

Similarly, adding [2.57] to hydrogen ion reduction [2.50] leads to the half-cell reaction describing the reduction of water in neutral and alkaline solutions:

$$2H_2O + 2e^- \rightarrow H_2 + 2OH^- \quad \left(E_0^0 = -828\,\{-828\}\ mV_{SHE} \right) \qquad [2.59]$$

Once more, it should be emphasised that (in accordance with Section 2.1.5) an electrode potential 'E' lower than 'E_0' means that the associated half-cell reaction takes place in the reduction direction, whereas a higher 'E' means that the reaction takes place in the oxidation direction.

The above listed reactions and standard potentials are only valid for the active corrosion state. Moreover, the listed equilibrium potentials only reflect standard state conditions, which is (in particular, with regard to pH variations) a major limitation in the information provided in the 'EMF' series. The literature on reinforcement corrosion does generally not provide 'EMF' series, which might be due to the above mentioned limitations. However, restrictions with regard to standard state conditions can be conveniently addressed by applying the Nernst equation (cf. Section 2.1.8) to verify potential ranges at a certain pH of concern, i.e. for non-standard states.

The Pourbaix diagram (cf. Section 2.1.10) overcomes both limitations and allows considerations on the possible reactions (depending on 'E' and pH) to evaluate the formation of any anodic corrosion product (including passive compounds, cf. Section 2.1.9) or the reduction of oxidised species.

Moreover, it should be emphasised that 'E' required for any half-cell reaction to occur is largely affected by various kinetic aspects. Especially, overpotentials* have a large effect on 'E' required for oxygen and hydrogen ion reduction to take place as cathodic reaction. The theoretical background of overpotentials and their practical meaning are discussed in Sections 2.2.3 and 2.2.4. In some literature the overpotential is partly acknowledged when stating reaction equations. For instance, for the frequently cited half-cell reaction describing the reduction of hydrogen in acid solutions [2.50], H_2 is often replaced by ('H_{ad}') or ('H_{ads}') to acknowledge the formation of an adsorbed hydrogen atom prior to formation of a hydrogen molecule. This aspect surely represents a major contribution in the magnitude of the hydrogen overpotential. However, this notation is omitted in this thesis, as there are other steps involved in the reaction, which also contribute to the magnitude of hydrogen overpotentials (cf. Section 2.2.4.1). So, throughout the present thesis only "complete" reactions are stated, while the contribution of overpotentials is kept in mind.

Based on the above listed half-cell reactions, indicative conclusions for a metal's affinity to be oxidised or reduced by any other metal or environment can be drawn for the standard state. The higher 'E_0^0' the easier the species is reduced, i.e. the metal or

* The term overpotential is in the literature commonly referred to as overvoltage. We prefer to refer to it as overpotential, because this term is more consistent with the term potential.

environment is a better oxidant. The lower 'E_0^0' the easier the species is oxidised, i.e. the metal or environment is a better reductant.

For example, ferric ion is reduced at 771 mV_{SHE} and magnesium ion is reduced at −2354 mV_{SHE}. So, ferric ion is easily reduced and thus is a good oxidant, whereas magnesium rather undergoes oxidation and thus is a good reductant. Zinc ion with 'E_0^0' equal to −764 mV_{SHE} is oxidised by any other metal or environment with 'E_0^0' higher than −764 mV_{SHE} (e.g. oxygen, ferric ion, and ferrous ion) and reduced by any other metal or environment with 'E_0^0' lower than −764 mV_{SHE} (e.g. magnesium). At the same time, zinc and even more magnesium have a high affinity to reduce oxygen. Some of these *simplified primary indications* were of importance in the development of the proposed new countermeasures (cf. Chapter 7).

It should also be remarked that the ability to be reduced (the corrosion tendency), does generally *not allow conclusions on the corrosion rate* of the associated metal. For instance, 'E_0^0' of zinc (−764 mV_{SHE}) is much lower than 'E_0^0' of ferrous ion (−475 mV_{SHE}) and zinc could be expected to corrode at a higher rate than iron, as it is oxidised much easier. However, as discussed in more detail in Section 2.2.2, the exchange current density of zinc is much lower than the one of iron and hence zinc corrodes at a much lower rate.

The list of half-cell reactions and standard potentials also allows some general conclusions concerning the corrosion potential 'E_{corr}' (cf. Chapter 'TaD'), e.g. to determine the preferentially corroded metal, if two dissimilar metals are submerged in an electrolyte and electrically connected (i.e. a galvanic cell). Yet, it should be emphasised once more that the above listed equilibrium potentials are limited to active corrosion in the standard state and do normally not reflect the actual state of a metal in a certain environment. This is of particular importance with regard to whether or not passivation is possible (cf. Section 2.1.9). When the preferentially corroded metal is to be determined (e.g. to estimate the effect of galvanic coupling) conclusions cannot be drawn based on the 'EMF' series, but the so-called galvanic series for the environment in question is to be used.* Often the galvanic series provided in the literature refer to seawater conditions, e.g. [Jones, 1996; Callister & Callister, 2000]. It is important to emphasise that galvanic series are strictly limited to one particular environment, which seems to be often overlooked in the literature. The characteristics of the environment do not only concern the pH, 'E_{corr}', and e.g. the content of depassivating species; any present substance that interferes with the electrochemistry of the regarded metals has an influence. The theory behind the corrosion potential 'E_{corr}' (i.e. the mixed potential theory) is outlined in Section 2.2.3 and galvanic coupling with special focus on the concrete environment is discussed throughout Chapters 6 and 7. In these

* Nevertheless, some literature refers to the 'EMF' series when specifying the preferentially corroded metal (e.g. to conclude on the effect of galvanic coupling).

Sections it will also be demonstrated that Pourbaix diagrams (cf. Section 2.1.10) can be beneficially utilised in investigations on the effect of galvanic coupling.

With regard to 'E_{corr}', the electrochemical interaction between an aqueous environment and a metal surface (i.e. the mixed potential established between the associated anodic and cathodic reactions) is even more important, since it basically concerns all common metal applications. Reducing environments lower 'E_{corr}', whereas oxidising environments raise it, which is explained in Section 2.2.3 and discussed in more detail based on carbon steel in Section 5.1.2. Yet, taking this information into consideration, preliminary conclusions concerning corrosion protection can also be drawn based on the above listed standard potentials. For instance, relatively noble metals (e.g. copper and nickel, and alloys based on these metals) are generally compatible with reducing environments. If any of the above listed metals is to be used in oxidising environment, however, the corrosion resistance depends upon passivity (cf. Section 2.1.9), as e.g. chromium or chromium alloys in many applications (cf. Section 6.3.2.3). As indicated in Section 1.3, also the durability of carbon steel in intact and uncontaminated concrete is based on the formation of a passive layer. Nevertheless, half-cell reactions and the associated standard potentials describing passivity are generally not included in 'EMF' series.

Hence, *the 'EMF' series may provide information for limited preliminary conclusions, but we consider it to be insufficient for the description of corrosion processes and even more as a basis for evaluation of existing and design of new countermeasures.* We suggest using other more refined thermodynamic tools for these tasks, in particular verification of reaction mechanisms (cf. Section 2.1.1) and customised and representative Pourbaix diagrams (cf. Sections 2.1.10 and 4.2).

Finally, a short note on the theory behind 'E_0' and the reason for the differences in '$E_0^{\,0}$' between the diverse metals. In simple terms, the attainment of certain equilibrium potential could be understood as follows. If a metal is submerged in an electrolyte that does not contain cations of this metal, the metal has the tendency to release ions, i.e. to dissolve. Thus, the metal surface becomes more negative due to the surplus of electrons. At the same time, the activity of positive metal ions in the liquid increases, causing an increasing number of dissolved ions to be discharged on the metal surface. These processes continue until the transport is equal in both directions. At this stage, the metal is in equilibrium with its own ions in the solution and hence at its equilibrium potential 'E_0' for the given ion activity [Jones, 1996; Bardal, 2004].

So, the *differences in the 'E_0'of the metals could be understood to be based on the different abilities to be dissolved*, which is, in our opinion, a more tangible concept. For instance, magnesium has a strong ability to be dissolved. Thus, magnesium has to be charged relatively negative, i.e. has to be at relatively active potential, to balance the dissolution of cations with the discharge of cations from the electrolyte on the surface.

2.1.7 Reference Electrodes

In practice, electrode potentials are usually measured against other reference electrodes than the 'SHE'. For laboratory measurements the 'SCE' (mercury-mercury chloride (calomel, Hg/Hg_2Cl_2) and the silver-silver chloride (Ag/AgCl) electrode, e.g. for calibration purposes in pH buffered solutions, are often used due to their convenience and reliability*. For measurements in the area of reinforcement corrosion, where robust and oftentimes embeddable construction are favoured over higher precision, e.g. the copper-cupric sulphate ($Cu/CuSO_4$) electrode [ASTM C876, 1999] and the manganese dioxide-manganese trioxide (Mn_2O_3/MnO_2) electrode [Arup & Sørensen, 1992] play an important role. The half-cell reactions corresponding to these reference electrodes are listed below together with their associated 'E_0^0' according to their ability to be reduced:

- Half-cell reaction corresponding to the MnO_2-Mn_2O_3 electrode:

$$2MnO_2 + 2H^+ + 2e^- \rightarrow Mn_2O_3 + H_2O \quad \left(E_0^0 = 964\,mV_{SHE} \right) \qquad [2.60]$$

- Half-cell reaction corresponding to the Cu-$CuSO_4$ electrode:

$$CuSO_4 + 2e^- \rightarrow Cu + SO_4^{2-} \quad \left(E_0^0 = 338\,\{318\}\,mV_{SHE} \right) \qquad [2.61]$$

- Half-cell reaction corresponding to the 'SCE':

$$Hg_2Cl_2 + 2e^- \rightarrow 2Hg + 2Cl^- \quad \left(E_0^0 = 269\,\{268\}\,mV_{SHE} \right) \qquad [2.62]$$

- Half-cell reaction corresponding to the Ag/AgCl electrode:

$$AgCl + e^- = Ag + Cl^- \quad \left(E_0^0 = 223\,\{222\}\,mV_{SHE} \right) \qquad [2.63]$$

The actual electrode potential of the 'SCE' is specified to 244 mV_{SHE} [RA, 2006b] and accordingly somewhat lower than the calculated 'E_0^0' of 269 mV_{SHE} of the associated half-cell reaction, which is considered to be due to the higher chloride ion activity at saturation (larger than unity). The same holds for the Ag/AgCl electrode used for calibration purposes in the experimental part of this project. For a filling solution of 3 M potassium chloride solution (KCl) the electrode potential of this electrode is specified to 207 mV_{SHE} [RA, 2006a] compared to the calculated 'E_0^0' of 223 mV_{SHE}.

2.1.8 Nernst Equation

As shown in Section 2.1.7, there is a *discrepancy between the standard potential 'E_0^0' of the half-cell reactions corresponding to the reference electrodes and their actual equilibrium potentials 'E_0'*. In principle, this is due to the ion activities of the reference electrodes deviating from the standard state (cf. Chapter 'TaD'). All equilibrium potentials for the half-cell reactions [2.47] to [2.63] were specified for standard state

* 'SCE' and Ag/AgCl electrodes have also been used in the experimental part of this project.

conditions. However, electrochemical reactions generally take place under arbitrary, i.e. non-standard conditions. Besides variations in the ion activity, non-standard state conditions mainly involve variations in temperature and the gas pressure from the standard state, as specified in Chapter 'TaD'. Even in the area of reinforcement corrosion, where generally only ambient temperatures are of concern (as opposed to e.g. high-temperature corrosion), the influence of the temperature can play a significant role (cf. Section 3.1.10). The gas pressure is of particular relevance with regard to cathodic reactions, which are discussed in more detail throughout Chapters 3, 4, and 5. However, for the purpose of this thesis the most important aspect is the influence of the ion activity on the thermodynamics of the system under investigation, which is discussed throughout Chapters 4 to 7.

The variation of equilibrium potentials in non-standard states is treated by the Nernst equation*. The Nernst equation can be derived based on the expression of 'ΔG' for non-standard states (cf. Section 2.1.3):

$$\Delta G = \Delta G^0 + 2.303 \times R \times T \times \log\left(\frac{\left(a_{P_1}\right)^{\nu_{P_1}} \times \ldots \times \left(a_{P_z}\right)^{\nu_{P_z}}}{\left(a_{R_1}\right)^{\nu_{R_1}} \times \ldots \times \left(a_{R_z}\right)^{\nu_{R_z}}}\right) \quad [2.64]$$

Inserting the thermodynamic relation between 'ΔG' and the reduction potential 'E_0^0' (cf. Section 2.1.5), which can be rewritten as:

$$\Delta G^0 = -n \times F \times E_0^0 \quad [2.65]$$

into [2.64], establishes the Nernst equation:

$$E_0 = E_0^0 - \frac{2.303 \times R \times T}{n \times F} \times \log\left(\frac{\left(a_{P_1}\right)^{\nu_{P_1}} \times \ldots \times \left(a_{P_z}\right)^{\nu_{P_z}}}{\left(a_{R_1}\right)^{\nu_{R_1}} \times \ldots \times \left(a_{R_z}\right)^{\nu_{R_z}}}\right) \quad [2.66]$$

Thus, the Nernst equation relates the equilibrium potential 'E_0' for non-standard states to 'E_0^0' and to the activities of the products and reactants involved in the associated half-cell reaction.

In correspondence with the simplification of the expression of 'ΔG' for non-standard states at a temperature 'T' of 25°C (cf. Section 2.1.3), [2.66] can be written as:

$$E_0 = E_0^0 - \frac{0.059}{n} \times \log\left(\frac{\left(a_{P_1}\right)^{\nu_{P_1}} \times \ldots \times \left(a_{P_z}\right)^{\nu_{P_z}}}{\left(a_{R_1}\right)^{\nu_{R_1}} \times \ldots \times \left(a_{R_z}\right)^{\nu_{R_z}}}\right) \quad [2.67]$$

where 0.059 is a factor created from $R \times F \times T\,[K] \times 2.303$ (the conversion factor from ln to log). For this expression, the same assumptions concerning the activities 'a' for

* Named after Walther Hermann Nernst, Germany, 1864-1941 [Roberge, 2007].

gases, solids, liquids, and ions (as defined in Section 2.1.3) apply throughout this thesis.

Before discussing in Section 2.1.10 the theory of the Pourbaix diagram, which can be understood as a graphical representation of the Nernst equation and the expression of 'ΔG' for non-standard states, a theoretically as well as practically highly important aspect of thermodynamics, the state of passivity and the breakdown of passivity, is dealt with in Section 2.1.9.

2.1.9 Passivity and Breakdown of Passivity

As indicated in Section 1.3, carbon steel in intact and uncontaminated concrete is thermodynamically unstable but in the passive state. Passivity is a crucial factor controlling both the corrosion tendency, i.e. the thermodynamics, and the corrosion rate, i.e. the corrosion kinetics, in many fields of metal application [Jones, 1996; Callister & Callister, 2000; Bardal, 2004]. According to most textbooks, controversy still exists concerning the exact mechanisms that lead to the existence of the phenomenon of passivity on metals. In a publication as early as 1844, Faraday (cf. Section 2.1.4) assumed that passivity was caused by an oxide film or a process that can be imagined as adsorption of oxygen on the metal surface [Kaesche, 1979]. These two possibilities have been the basis for two competing theories of passivity. Strong arguments for the oxide film theory were found by the experimental demonstration of existing oxide films in connection with passivity and a reasonably good correlation between passivity indicated by polarisation curves (cf. Section 2.2.5) and thermodynamic stability domains of metal oxides, e.g. [Pourbaix, 1974a; Pourbaix, 1974b]. However, passive layers are very thin and they can be formed via stages of oxygen adsorption, so that there is no practical controversy between these two theories [Bardal, 2004]. For the scope of this thesis, it is sufficient to acknowledge these theories and to regard *passivity as the presence of a protective oxide layer on the metal surface that significantly lowers the rate of corrosion, even though the metal is thermodynamically unstable*.

Yet, it is crucial to take one central notion concerning passivity into account: According to [Bardal, 2004], *passive layers "are not formed by deposition of corrosion products from the liquid, as this usually gives more or less porous surface layers, but ... the oxide is directly formed in close connection with the crystal structure of the metal."* This notion constitutes a central aspect in our understanding and description of corrosion mechanisms of steel in concrete (cf. Chapter 5), which differ to quite some extent from the traditional understanding and description of reinforcement corrosion in the literature. Naturally, this notion also governs our general interpretation and application of thermodynamic tools (cf. Chapter 4) and hence our understanding and description of available countermeasures (cf. Chapter 6) and design strategies for new countermeasures (cf. Chapter 7).

Due to the above and their limited thickness, some passive layers allow transfer of electrons, so that certain electrochemical reactions can occur on the external face of the oxide. In order to understand the practical meaning of this aspect, it is, especially with regard to the evaluation of available and the design of new countermeasures, important to distinguish between the related characteristics of passive layers of different metals. Concerning these characteristics, in principle, three major groups of surface layers on metal with passivating properties can be distinguished [Bardal, 2004]:

- The first group of passive layers impede anodic reactions effectively, but not the cathodic reaction. This means that the passive layer is electron conducting, but not ion conducting (cf. Section 2.1.2). Examples for this group of passive layers are iron, nickel, chrome, and their alloys, e.g. stainless steel (cf. Section 6.3.2.3).
- The second group of passive layers impede both the anodic and the cathodic reaction to a large extent, i.e. the passive layer impedes conduction of both electrons and ions. A typical example for formation of such passive layers is aluminium, which, contrary to iron, nickel, and chrome, forms a passive layer with high resistance against electron transfer[*]. Furthermore, the passive layer of zinc is generally considered to largely prevent both anodic and cathodic reactions [Zhang, 1996; Roberge, 2007].
- The third group comprises porous surface layers, e.g. deposited rust and salts. In principle, these are no passive layers. However, such layers may reduce both anodic and cathodic reactions, but not sufficiently to provide efficient passivity. The cathodic reaction may take place on the metal surface in the bottom of pores of the porous layer, and it is hindered to a certain extent by the resistance of the deposit against oxygen diffusion. At the same time, the pores allow the anodic reaction, but it is also largely hindered by the deposit.

So, to be effective *a passive layer must provide low ionic conductivity and low solubility. In addition, it must have sufficient toughness and adhesion to the metal to avoid cracking, wear, and/or disbonding. Moreover, resistance to breakdown (i.e. the deterioration of the passive layer) depends on its resistance to depassivating species.* Depassivating species normally lead to a localised breakdown of the passive layer. Localised breakdown results in several forms of localised corrosion phenomena for carbon and stainless steels, e.g. pitting, crevice, and intergranular corrosion (cf. Section 2.3). Unfortunately, one of the major species causing the breakdown of passivity for many metals is chloride, which is abundantly available in nature. Mechanisms postulated for the breakdown of the passive layer by chloride ions are briefly described in Section 5.2.2.2.

[*] However, in practice natural oxides on aluminium generally have a large number of defects that allow some electron conductance and hence cathodic activity.

A repassivation process competes with the breakdown process of the passive layer. Thus, an effective metal for resisting localised corrosion not only forms an effective passive layer, but is also capable of repassivating at a rate sufficiently high that exposure to a corrosive environment is minimal once breakdown has occurred. [Jones, 1996; Callister & Callister, 2000; Kruger, 2001; Bardal, 2004].

If the thermodynamic requirements for passivation are fulfilled and the passive layer meets the above requirements, anodic dissolution is largely impeded. For instance, for steel in concrete, the corrosion rate under this condition has been estimated to about 0.1 µm/y [Arup, 1983]. This is practically negligible, although steel (or more precisely iron) is not thermodynamically immune (cf. Section 1.3). The slow dissolution can only be assessed electrochemically, e.g. by measurements to determine the passive current density 'i_p' (cf. Section 2.2.5.3). The current density is an important kinetic parameter that is dealt with throughout Chapter 2, while the theoretical background is mainly described in Section 2.2.5.3.

With regard to passivity and kinetics, it should be emphasised that the appropriate thermodynamic conditions do not necessarily guarantee the occurrence of passivation. The actual occurrence of passivation depends also on kinetic conditions. While thermodynamic conditions determine whether formation of a passivation layer is possible, kinetic conditions govern the chemistry near the electrode surface and hence the characteristics of the formed passive layer, which is, due to the largely hindered ingress of substances and ion mobility in the concrete bulk, a particularly central aspect in reinforcement corrosion. Ingress into and ion mobility in concrete are dealt with in Section 3.1.7 and the consequences for reinforcement corrosion are discussed throughout Chapter 5.

2.1.10 Pourbaix Diagram

Most metals experience a change of thermodynamic stability with a change of the pH of the environment. However, not only the pH of the environment, but also its oxidising power, i.e. the electrochemical potential, governs the formation of different chemical species of a metal, i.e. the pure metal, soluble ions, or oxides. The Pourbaix diagram* is a predominance diagram that combines these two factors by mapping out the various possible species of an aqueous electrochemical system depending on the pH and the electrode potential 'E'. The pH and 'E' are represented on the X-axis and Y-axis, respectively. The domains of favoured thermodynamic stability of the different species (henceforth, stability domains) are bounded by lines that represent equilibrium conditions between the two adjacent thermodynamically favoured species (henceforth, equilibrium lines). These lines represent the various possible reactions of the aqueous electrochemical system and are derived from the expression of 'ΔG' for

* Named after Marcel Pourbaix, Russia/Belgium, 1904-1998 [Roberge, 2007]. In the literature also referred to as equilibrium diagram, potential/pH diagram, E-pH diagram, or E_h-pH diagram.

non-standard states (cf. Section 2.1.3) as well as the Nernst equation (cf. Section 2.1.8). Hence, the Pourbaix diagram can be understood as a graphical representation of these equations.

The equilibrium lines are obtained by inserting 'ΔG^0' or '$E_0{}^0$' of the reaction describing the equilibrium between two adjacent stability domains and the associated activities in the expression of 'ΔG' for non-standard states [2.27] or the Nernst equation [2.66], respectively. Hence, the pH dependency or the equilibrium pH of an equilibrium line is determined from the participation of H^+ or OH^- in the reaction. This leads to the following types of equilibrium lines in the Pourbaix diagram:

- Equilibrium lines of *half-cell reactions with participation of H^+ or OH^-*, which correspond to inclined lines in the Pourbaix diagram (equilibrium line type I)
- Equilibrium lines of *half-cell reactions without participation of H^+ or OH^-*, which correspond to horizontal lines in the Pourbaix diagram (equilibrium line type II)
- Equilibrium lines of *acid-base reactions with participation of H^+ or OH^-*, which correspond to vertical lines in the Pourbaix diagram (equilibrium line type III).

Pourbaix diagrams can be constructed for all variations in temperature, in gas pressure, and in the activity of the species (cf. equations [2.27] and [2.66]). However, as mentioned, mainly the variations in the activity of the soluble ions are of importance in this thesis.

For exemplification purposes, a Pourbaix diagram for the Fe-H_2O system* based on a preselection of species according to Table 2.2 and an iron ion activity of 10^{-6} mol/L is shown in Figure 2.1 [A].

Table 2.2: *Species preselected for the Pourbaix diagram of the general Fe-H_2O system*†.

Solid	Fe	Fe_2O_3	Fe_3O_4
Soluble	Fe^{2+}	Fe^{3+}	$HFeO_2^-$

The stability domains corresponding to the preselection in Table 2.2 are given in Figure 2.1 [A], while Figure 2.1 [B] illustrates the corresponding thermodynamic states and provides the labels for the exemplifications concerning the construction of the equilibrium lines.

* This type of Pourbaix diagram is referred to as single element Pourbaix diagram 'SEPD', when it is relevant to differentiate between different types of diagrams, which will be further elaborated in Section 4.1 (cf. Chapter 'TaD').

† The preselected species are listed in alphabetical order for solid and soluble species. This system is kept up throughout this thesis for tables illustrating the preselection for all types of Pourbaix diagrams (cf. Section 4.2.1).

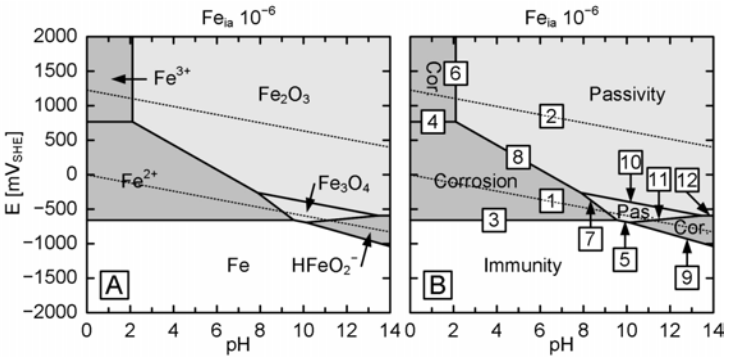

Figure 2.1: *Fe-H_2O Pourbaix diagram based on Table 2.2 with $Fe_{ia} = 10^{-6}$ mol/L.* [A]: *Dominant species in their associated stability domains.* [B]: *Identification of immune, passive, and corrosive domains and labelling for description of equilibrium lines.*

Besides the choice of activities of soluble species, the preselection of species to be taken into consideration in the establishment of the diagram is the absolute central aspect in the Pourbaix diagram. *The diagram will only represent an electrochemical system, if all species that have a tendency to be formed are considered and species that will not be formed are deselected.* This crucial information is not implemented in 'HSC' (or, to our knowledge, in any other thermodynamic software) and solely based on user input.

This Section only deals with the analytical background of Pourbaix diagrams. Ion activities and the preselection of species as well as other aspects (in particular, relating to the validity of the Pourbaix diagram in the concrete environment) are discussed in detail in Chapter 4.

As summarised in Table 2.2, solely ferrous ion, ferric ion, and bihypoferrite ion ($HFeO_2^-$) are selected as soluble species (ions), while magnetite and hematite are selected as the only solid compounds besides pure iron. Figure 2.1 illustrates that the stability domains of the soluble ions (Fe^{2+}, Fe^{3+}, and $HFeO_2^-$) can be associated with corrosion (dark grey), the stability domains where formation of solid species other than pure iron (Fe_3O_4 and Fe_2O_3) is thermodynamically favoured give rise to passivity (light grey), and the area where iron is thermodynamically stable can be associated with immunity (white); cf. Chapter 'TaD' for the definition of these thermodynamic states.

Since the Pourbaix diagram is based on reduction potentials, the direction of the reactions (reduction or oxidation) in the associated stability domains of the Fe-H_2O system can be interpreted as described for half-cell reactions (cf. Section 2.1.5). This also holds for the stability of area of water, which is indicated by the dashed lines. Water is theoretically stable between the equilibrium lines 1 and 2. Equilibrium line 1 corresponds to the half-cell reaction describing hydrogen ion reduction in acid solutions:

$$2H^+ + 2e^- \rightarrow H_2 \quad \left(E_0^0 = 0\ \{0\}\ mV_{SHE} \right) \qquad [2.68]$$

By means of the Nernst equation for standard temperature on 25°C (cf. Section 2.1.8):

$$E_0 = E_0^0 - \frac{0.059}{n} \times \log\left(\frac{\left(a_{P_1}\right)^{\nu_{P_1}} \times \ldots \times \left(a_{P_z}\right)^{\nu_{P_z}}}{\left(a_{R_1}\right)^{\nu_{R_1}} \times \ldots \times \left(a_{R_z}\right)^{\nu_{R_z}}} \right) \qquad [2.69]$$

the functions for the equilibrium lines, i.e. the equilibrium potential lines, for half-cell reactions (type I and II) can be calculated. Considering the partial hydrogen pressure 'p_{H2}' equal to 1 and inserting the corresponding 'E_0^0' and the involved activities and coefficients into the Nernst equation [2.69] leads to the pH dependent type I equilibrium line 1:

$$\begin{aligned} E_{0,H^+/H_2} &= E_0^0 - \frac{0.059}{n} \times \log\left(\frac{\left(a_{H_2}\right)^{\nu_{H_2}}}{\left(a_{H^+}\right)^{\nu_{H^+}}} \right) \\ E_{0,H^+/H_2} &= 0 - \frac{0.059}{2} \times \log\left(\frac{(1)^1}{\left(a_{H^+}\right)^2} \right) \\ E_{0,H^+/H_2} &= -0.059 \times pH \end{aligned} \qquad [2.70]$$

Equilibrium line 1 can be derived accordingly for the equivalent hydrogen ion reduction reaction for the neutral and alkaline environment, which is obtained by adding sufficient hydroxyl to both sides of half-cell reaction [2.68]:

$$2H_2O + 2e^- \rightarrow H_2 + 2OH^- \quad \left(E_0^0 = -828\ \{-828\}\ mV_{SHE} \right) \qquad [2.71]$$

Hence, the Y-axis intercept at pH 0 agrees with the 'E_0^0' of the hydrogen ion reduction reaction in acid solutions [2.68] and the Y-axis intercept at pH 14 corresponds to the 'E_0^0' of the hydrogen ion reduction reaction in neutral and alkaline solutions [2.71].

Theoretically, equilibrium line 1 represents the reduction potential of water saturated with H_2 at 1 bar, i.e. the oxygen-deprived or a reducing environment (cf. Section 2.1.6). Thus, at any potential lower than equilibrium line 1, water is theoretically thermodynamically unstable and H_2 is formed. Starting in acid solution, H^+ is first consumed according to the half-cell reaction [2.68] until the pH increases sufficiently so that water is decomposed directly to H_2 as described by half-cell reaction [2.71]. Correspondingly, above equilibrium line 1, H_2 is oxidised to H^+ or water. Thus, below equilibrium line 2 any water present is steadily reduced to H_2. This means that water at any pH is reduced to H_2 by any dissolved reductant with a potential lower than $-828\ mV_{SHE}$. However, as indicated in Section 2.1.5, in practice kinetic effects influence the actual electrode potential for hydrogen ion reduction (cf. Sections 2.2.3 and

2.2.4). A so-called hydrogen overpotential can be considered to displace equilibrium line 1 by about 500 mV in the active direction [WOU, 2007].

Equilibrium line 2 corresponds to the half-cell reaction describing reduction of oxygen in the acid solutions:

$$O_2 + 4H^+ + 4e^- \rightarrow 2H_2O \quad \left(E_0^0 = 1230\,\{1229\}\,mV_{SHE} \right) \qquad [2.72]$$

Considering the oxygen partial pressure 'p_{O2}' equal to 1 and inserting the corresponding 'E_0^{0}' and the involved activities and coefficients into [2.69] leads to the pH dependent type I equilibrium line 2:

$$E_{0,O_2/H_2O} = E_0^0 - \frac{0.059}{n} \times \log\left(\frac{\left(a_{H_2O}\right)^{\nu_{H_2O}}}{\left(a_{O_2}\right)^{\nu_{O_2}} \times \left(a_{H^+}\right)^{\nu_{H^+}}} \right)$$

$$E_{0,O_2/H_2O} = 1.230 - \frac{0.059}{4} \times \log\left(\frac{(1)^2}{(1)^1 \times \left(a_{H^+}\right)^4} \right) \qquad [2.73]$$

$$E_{0,O_2/H_2O} = 1.230 - 0.059 \times pH$$

In analogy to equilibrium line 1, equilibrium line 2 can also be derived for the equivalent oxygen reduction reaction for the neutral and alkaline environment, which is obtained by adding sufficient hydroxyl to both sides of half-cell reaction [2.72]:

$$O_2 + 2H_2O + 4e^- \rightarrow 4OH^- \quad \left(E_0^0 = 402\,\{401\}\,mV_{SHE} \right) \qquad [2.74]$$

Moreover, as for equilibrium line 1, the Y-axis intercept at pH 0 agrees with the 'E_0^{0}' of the oxygen reduction reaction in acid solutions [2.72] and the Y-axis intercept at pH 14 corresponds to the 'E_0^{0}' of the oxygen reduction reaction in neutral and alkaline solutions [2.74].

Theoretically, equilibrium line 2 represents the reduction potential of water saturated with O_2 at 1 bar, i.e. an oxygen-rich or oxidising environment (cf. Section 2.1.6). At any potential higher than equilibrium line 2, water is in theory thermodynamically unstable and O_2 is formed. Thus, above this equilibrium line any water present is steadily oxidised to O_2. This means that water at any pH is oxidised to O_2 by any dissolved oxidant with a potential higher than 1230 mV_{SHE}. However, in correspondence with equilibrium line 1, in practice a so-called oxygen overpotential displaces equilibrium line 2 in the noble direction (cf. Sections 2.2.3 and 2.2.4). According to [WOU, 2007] the magnitude of this displacement for Fe-H_2O system can be also considered to be in the range of 500 mV.

Accordingly, the diagram can be subdivided into three regions of major importance, among others for the acting cathodic reactions and accordingly the corrosion rate. With regard to the theory on cathodic reactions described in Section 2.1.2 and the cathodic reactions listed in Section 2.1.6, it can be concluded that *reduction of oxygen is*

the only possible cathodic reaction in the stability domain of water and hence the dominant cathodic reaction for steel in an aqueous system. For hydrogen reaction to contribute in the cathodic process, the electrode potential (cf. Section 2.2.3) would at least need to be lower than equilibrium line 1 minus the hydrogen overpotential displacement of about 500 mV.

The equilibrium lines bounding the stability domains of the iron species are determined in the same way, as exemplified for the hydrogen and oxygen equilibrium line. In the following the establishment of the two other types of equilibrium lines as well as for all possible equilibria between soluble and solid species is exemplified.

Equilibrium line 3 represents the equilibrium between the soluble species Fe^{2+} and the solid state Fe, i.e. between corrosion and immunity, respectively. It corresponds to the half-cell reaction describing reduction of ferrous ion:

$$Fe^{2+} + 2e^- \rightarrow Fe \quad \left(E_0^0 = -475\{-447\}\,mV_{SHE} \right) \qquad [2.75]$$

Inserting the corresponding 'E_0^0' and the involved activities and coefficients into [2.69] leads to the pH independent, i.e. horizontal, type II equilibrium line 3:

$$\begin{aligned} E_{0,Fe^{2+}/Fe} &= E_0^0 - \frac{0.059}{2} \times \log\left(\frac{(a_{Fe})^{v_{Fe}}}{(a_{Fe^{2+}})^{v_{Fe^{2+}}}} \right) \\ E_{0,Fe^{2+}/Fe} &= -0.475 - \frac{0.059}{2} \times \log\left(\frac{(1)^1}{(10^{-6})^1} \right) \\ E_{0,Fe^{2+}/Fe} &= -0.651 \end{aligned} \qquad [2.76]$$

That means that at a potential of −651 mV_{SHE} half of the 10^{-6} mol/L of Fe is corroding as soluble Fe^{2+}, while the other half remains immune. Soluble Fe^{2+} dominates and corrosion takes place, if the potential is higher than −651 mV_{SHE}, and solid immune Fe dominates if the potential lower than −651 mV_{SHE}.

Equilibrium line 4 is another type II equilibrium line, which represents the equilibrium between the two soluble species Fe^{3+} and Fe^{2+}, i.e. both adjacent stability domains are thermodynamically favoured to be corrosive. It corresponds to the half-cell reaction describing the reduction of ferric ion:

$$Fe^{3+} + e^- \rightarrow Fe^{2+} \quad \left(E_0^0 = 771\{771\}\,mV_{SHE} \right) \qquad [2.77]$$

In analogy to the above, the equilibrium line is obtained by inserting the corresponding 'E_0^0' and the involved activities and coefficients into [2.69] which leads to:

$$E_{0,Fe^{3+}/Fe^{2+}} = 0.771 \qquad [2.78]$$

The type I equilibrium line 5 between immunity and passivity represents the equilibrium between the two solid compounds Fe and Fe_3O_4:

$$Fe_3O_4 + 8H^+ + 8e^- \rightarrow 3Fe + 4H_2O \quad \left(E_0^0 = -86\,mV_{SHE} \right) \qquad [2.79]$$

Inserting the involved activities and the corresponding 'E_0^0' into [2.69] leads to the equilibrium line between passive compound Fe_3O_4 and immune Fe:

$$E_{0,Fe_3O_4/Fe} = -0.086 - 0.059 \times pH \qquad [2.80]$$

The type III equilibrium line 6 between the two species in the same oxidation state, soluble Fe^{3+} and passive Fe_2O_3. It corresponds to the acid-base reaction:

$$Fe_2O_3 + 6H^+ \rightarrow 2Fe^{3+} + 3H_2O \quad \left(\Delta G^0 = -3\,kJ \right) \qquad [2.81]$$

For the calculation of equilibrium lines of acid-base reactions based on a known 'ΔG^0', the equilibrium pH can be calculated based on the equation for 'ΔG^0' for non-standard states derived in Section 2.1.3:

$$\Delta G^0 = -5705.974 \times \log\left(\frac{\left(a_{P_1}\right)^{\nu_{P_1}} \times ... \times \left(a_{P_z}\right)^{\nu_{P_z}}}{\left(a_{R_1}\right)^{\nu_{R_1}} \times ... \times \left(a_{R_z}\right)^{\nu_{R_z}}} \right) \qquad [2.82]$$

Inserting the involved activities and the corresponding 'ΔG^0' into [2.82] leads to the pH value that defines the position of the vertical equilibrium line:

$$\Delta G^0 = -5705.974 \times \log\left(\frac{\left(a_{Fe^{3+}}\right)^{\nu_{Fe^{3+}}} \times \left(a_{H_2O}\right)^{\nu_{H_2O}}}{\left(a_{Fe_2O_3}\right)^{\nu_{Fe_2O_3}} \times \left(a_{H^+}\right)^{\nu_{H^+}}} \right)$$

$$-3495 = -5705.974 \times \log \frac{\left(10^{-6}\right)^2 \times (1)^3}{(1)^1 \times \left(H^+\right)^6} \qquad [2.83]$$

$$pH_{Fe_2O_2/Fe^{3+}} = 2.102$$

The above exemplifications cover all possible combinations for the establishment of the equilibrium lines in the Fe-H_2O Pourbaix diagram. The half-cell reactions determining the remaining equilibrium lines, which are all of type I, are listed below together with their label according to Figure 2.1 [B] and their associated 'E_0^0':

7: $Fe_3O_4 + 8H^+ + 2e^- \rightarrow 3Fe^{2+} + 4H_2O \quad \left(E_0^0 = 1078\,mV_{SHE} \right)$ [2.84]

8: $Fe_2O_3 + 6H^+ + 2e^- \rightarrow 2Fe^{2+} + 3H_2O \quad \left(E_0^0 = 789\,mV_{SHE} \right)$ [2.85]

9: $HFeO_2^- + 3H^+ + 2e^- \rightarrow Fe + 2H_2O \quad \left(E_0^0 = 391\,mV_{SHE} \right)$ [2.86]

10: $3Fe_2O_3 + 2H^+ + 2e^- \rightarrow 2Fe_3O_4 + H_2O \quad \left(E_0^0 = 211\,mV_{SHE} \right)$ [2.87]

11: $Fe_3O_4 + 2H_2O + 2e^- \rightarrow 3HFeO_2^- + H^+ \quad \left(E_0^0 = -1518\,mV_{SHE} \right)$ [2.88]

12: $Fe_2O_3 + H_2O + 2e^- \rightarrow 2HFeO_2^- \quad \left(E_0^0 = -941\,mV_{SHE} \right)$ [2.89]

Based on these equilibrium lines, which are represented in combination with the associated stability domains in Figure 2.1 [B], some obvious preliminary conclusions on the thermodynamics of iron can be made. These are extended and correlated with other aspects of Fe-H_2O systems as well as Pourbaix diagrams for other metals and elements and transferred to the concrete environment (cf. Chapters 4 to 7). For instance, it is notable that the distance between the equilibrium lines 3, 5, and 9, which limit the immune area, and equilibrium line 1, which limits the stability domain of water, decreases with increasing pH. This indicates that the corrosion rate of iron decreases with increasing solution pH. Moreover, it can be observed that in alkaline to neutral solutions with dissolved oxygen, the potential is lifted into the passive region, but below neutrality the passive layer is not stable and dissolved oxygen increases the corrosion rate. Thus, besides providing more oxidation power, acid environments do not allow for passivation of iron and hence lead to high corrosion rates, which is an issue in aqueous corrosion of many metals. Some more general observations on equilibrium lines in the Pourbaix diagram for general 'Me'-H_2O systems and, the associated stability domains include:

- The position of acid-base equilibria is dependent on the selected concentration.
- In more dilute solutions, the stability domains of soluble species are generally larger.
- Diagonal boundaries generally slope from upper left to lower right, as alkaline solutions tend to favour the species in a higher oxidation state.

Furthermore, some *general limitations* concerning the Pourbaix diagram are listed:

- The Pourbaix diagram does only reflect the thermodynamic state of the selected environment for a certain situation, i.e. concentration, temperature and pressure. The effects that influence the actual conditions at e.g. the surface of a metal cannot be directly assessed and only be estimated by the input parameters.
- The Pourbaix diagram does not provide information on the kinetics of the investigated system and it does necessarily reflect it either. For instance, for stability domains, where corrosion is thermodynamically favoured, no predictions on the corrosion rates can be made. Corrosion rates can be high or low considering the moderate temperatures which are regarded in the present thesis.[*]
- The Pourbaix diagram does not provide information on the actual protective function, i.e. the structure and denseness, of the passive layer, which gives rise to stability domains, where passivation is thermodynamically favoured.

[*] As opposed to e.g. high temperature corrosion, where the equilibrium is reached quite rapidly and corrosion rates are generally high.

Besides the above listed *general limitations*, *other restrictions and/or inadequacies* are often postulated in the literature in connection with the Pourbaix diagram. Among several others, the most important rejections include:

- Pourbaix diagrams are limited to Me-H_2O systems, i.e. one metal in pure water, and do not take into consideration the influence of other substances, which can affect the thermodynamics of the system to a large extent.
- Species could be thermodynamically favoured, but the kinetics of its formation is so slow that it does not play any role in the investigated system or thermodynamically unstable species are present because of slow decomposition.
- The choice of ion activity is arbitrary and does not reflect the actual conditions in the system. Even if the ion activity of the bulk solution is known and applied, it will largely deviate from the actual concentration on the metal surface, where the electrochemical reactions take place and hence the thermodynamic characteristics of the system are determined.

While the *general limitations* always apply to Pourbaix diagrams and we take them into due consideration in our interpretation, we suggest that the frequently stated *other restrictions and/or inadequacies* can be overcome by the proposed approach for the establishment and application of customised Pourbaix diagrams, which is discussed in-depth in Chapter 4. This approach comprises a central aspect in our thermodynamic approach towards the management of reinforcement, since it governs our understanding and description of corrosion processes of steel in concrete (cf. Chapter 5) as well as our evaluation of existing and design of new countermeasures (Chapters 6 and 7, respectively). In particular, the influence of other substances on the reactions can be of major importance in the complex chemistry of the concrete environment.

In conclusion it can be said that, although the theory behind the Pourbaix diagram is rather simple, its establishment is calculation intensive. Furthermore, the validity of the diagram for the investigated system is strongly affected by the preselection of species and the choice of ion activity, which are rather complex aspects (cf. Chapter 4), in particular with regard to the physical properties of concrete and the multifaceted chemistry and electrochemistry of a concrete-metal system. Besides the thermodynamic aspects, these parameters are largely governed by the reaction kinetics of the electrochemical system under investigation.

However, as indicated throughout this Section*, reactions kinetics does not only concern the establishment and interpretation of Pourbaix diagrams, but the application of thermodynamic theory and tools in general.* Selected theoretical and practical aspects of reaction kinetics of aqueous metallic corrosion, which we consider to be most important for the purpose of this thesis, are dealt with in Section 2.2.

2.2 Kinetics of Aqueous Metallic Corrosion

In Section 2.1 it was shown that the application of thermodynamics, i.e. the assessment of the 'E_0^0' or 'ΔG^0' of reactions and in particular the information that can be obtained from the Pourbaix diagram, provides a useful basis for predicting conditions under which certain reactions are liable to influence the corrosion behaviour of metals. Based on this information, the relative tendencies of the metal reactivity can be assessed and countermeasures can be verified or designed. However, as indicated in Section 2.1.10, it is necessary to recognise that this approach has certain limitations. In thermodynamics redox couples, i.e. the charge balanced combination of anodic and cathodic reactions, are considered to be at equilibrium. Yet, in practice this is generally not the case and it is, therefore, impossible to predict whether a thermodynamically favoured half-cell reaction occurs at a significant rate. Hence, assessment of the kinetics of electrochemical reactions is important in asserting the extent to which a metal corrodes, i.e. its corrosion rate.

So, in the present thesis focus is set on thermodynamic principles. But it should be kept in mind that it is crucial to take kinetics into due account in describing corrosion mechanisms (cf. Chapter 5) as well as in the evaluation of existing (cf. Chapter 6) and the design of new countermeasures (cf. Chapter 7). Moreover, the kinetics theory dealt with in this Section establishes the basis for some of the electrochemical measurement techniques used in the experimental part of this project (cf. Sections 1.9, 7.5.1, and 8.4.1).

2.2.1 Electrical Double Layer

The so-called electrical double layer is an essential concept in corrosion kinetics. This layer is formed by each conducting metal in contact with an aqueous solution. For detailed description of this complex interface reference is made to the literature, e.g. [Freiesleben Hansen, 1995; Jones, 1996; Callister & Callister, 2000]. In simple terms, the most important features of the double layer can be described as follows. The conductive metal surface attracts unsymmetrical, polar water molecules, which form an oriented solvent layer. This layer prevents close approach of ions from the bulk solution. Charged ions in the bulk solution also attract their own sheath of polar water-solvent molecules, which further insulate them from the metal surface. The plane of closest approach of positively charged cations to the negatively charged metal surface is generally referred to as the outer Helmholtz* plane. The result is an interface with separated negative and positive charge, which is commonly referred to as the electrical double layer. The electrical double layer is generally considered to behave like a charged capacitor. The electrical field created by the double layer prevents easy charge transfer, which, thereby, limits electrochemical reactions on the metal surface.

* Named after Hermann Ludwig Ferdinand von Helmholtz, Germany, 1821-1894 [Roberge, 2007].

[Jones, 1996]. A useful electrochemical measuring technique providing information on the governing parameters of the electrical double layer is 'EIS' (cf. Section 2.5.6), which played a central role in our experimental investigations (cf. Sections 1.9.1, 7.5.1.3, and 8.4.1.3).

2.2.2 Exchange Current Density

For a half-cell reaction at its equilibrium potential 'E_0', i.e. a reversible cell, reduction and oxidation reactions occur at the same rate (cf. Section 2.1.5). The reaction rate in each direction can also be expressed by the transportation rate of electric charges, i.e. by the exchange current 'I_0' or by the exchange current density 'i_0'. The net reaction rate and the net current density are zero. The magnitude of the exchange current density 'i_0' depends on the type of half-cell reaction, the electrode material and the electrolyte and also significantly on the temperature and concentrations. The exchange current density has a strong influence on actual corrosion rates and is, therefore, an important parameter in corrosion kinetics.

Data for certain half-cell reactions in selected electrolytes with certain concentrations is provided in the literature, e.g. [Jones, 1996; Bardal, 2004]. Most data is available based on hydrogen ion reduction as cathodic reaction:

$$2H^+ + 2e^- \rightarrow H_2 \quad \left(E_0^0 = 0\,mV_{SHE} \right) \qquad [2.90]$$

for metals in acid electrolytes, e.g. the 'i_0' for the reduction of ferrous ion:

$$Fe^{2+} + e^- \rightarrow Fe \quad \left(E_0^0 = -475\{-447\}\,mV_{SHE} \right) \qquad [2.91]$$

in 1 N hydrochloric acid is e.g. given to 10^{-6} A/cm^2 [Bardal, 2004] or 10^{-5} A/cm^2 [Jones, 1996], whereas the 'i_0' for the reduction of zinc ion:

$$Zn^{2+} + 2e^- \rightarrow Zn \quad \left(E_0^0 = -764\{-726\}\,mV_{SHE} \right) \qquad [2.92]$$

in 1 N sulphuric acid (H_2SO_4) was determined to be much lower to 1.6×10^{-11} A/cm^2 [Bardal, 2004] or 2×10^{-11} A/cm^2 [Jones, 1996].

The above example indicates the importance of the exchange current density and accordingly kinetics in the assessment of corrosion. Based on the magnitude of '$E_0{}^0$', i.e. the ability to be reduced, zinc could be expected to have a higher corrosion rate than iron (cf. Section 2.1.6), but the lower exchange current density shows that the corrosion rate is much lower than the one of iron.

The difference of corrosion rates due to the different magnitudes in the current densities, especially of iron and zinc, are of major relevance to the discussion of existing (cf. Chapter 6) and the development of new countermeasures (cf. Chapter 7). Moreover, the exchange current density also played a significant role in the experimental part of the project, e.g. with regard to the choice of material for external and embed-

dable electrodes. For instance, the selection of Ru/Ti activated titanium (cf. Section 8.1.1) as base material for different electrode types in the experimental investigations in this project was primarily based on its provision for high exchange currents density, while being relatively unreactive itself.

Thus, we understand the exchange current density 'i_0' as the fundamental *kinetic* parameter corresponding to 'E_0' and 'ΔG' as the fundamental *thermodynamic* parameters.

2.2.3 Corrosion Potential, Polarisation, and Overpotential

In practice, half-cell reactions are generally not at equilibrium and proceed only at finite rates, which is among others due to the formation of the electrical double layer outlined in Section 2.2.1. For a redox reaction to occur all involved anodic and cathodic reactions are moved away from their equilibrium potential 'E_0' as a result of the net electrode reaction occurring, i.e. a net electric current flowing through the interface between the metal and the electrolyte. Thus, when "corrosion" takes place on a metal surface, *the actual potential adapts to a value somewhere between the equilibrium potential of the cathodic and anodic reactions, i.e. a mixed potential. That way, the so-called corrosion potential 'E_{corr}'* is established.*

The deviation from 'E_0' is called polarisation, and the electrode is referred to as polarised. A measure of polarisation is the overpotential, i.e. the difference between 'E_{corr}' and the equilibrium potentials of the involved half-cell reactions.

With '$E_{0,a}$' as the equilibrium potential for the anodic reaction and '$E_{0,c}$' as the equilibrium potential of the cathodic reaction, the anodic overpotential 'η_a' and the cathodic 'η_c' can be expressed as†:

$$\eta_a = E_{corr} - E_{0,a} > 0 \qquad [2.93]$$

$$\eta_c = E_{corr} - E_{0,c} < 0 \qquad [2.94]$$

[Jones, 1996; Bardal, 2004].

The tendency for corrosion increases with the magnitude of anodic polarisation. Thus, anodic polarisation represents a driving force for corrosion by the anodic reaction. That means, if the potential on the metal surface rises, the oxidising power, and hence

* 'E_{corr}' is in the literature also referred to as rest potential, free corrosion potential, and open circuit potential ('OCP'). In relation to e.g. potential mapping [ASTM C876, 1999], 'E_{corr}' is also referred to as half-cell potential, which we consider to be particularly misleading. Therefore, the term corrosion potential is used throughout this thesis, also when referring to potentials in concrete, which might appear unusual (cf. Chapter 'TaD').

† In the literature the symbol 'η' is used for both polarisation and overpotential (overvoltage). In this thesis 'η' is only used for overpotentials , which is considered to be the measureable result of polarisation.

the corrosion rate, of the solution increases, because the anodic polarisation is larger. Among others, this effect can be investigated by so-called polarisation curves, which provide various details on the reaction kinetics of a corroding system (cf. Section 2.2.5).

The theoretical basis to these important parameters, the so-called mixed potential theory, was established in 1938 by Wagner* and Traud in their fundamental paper "Über die Deutung von Korrosionsvorgängen durch Überlagerung von Elektrochemischen Teilvorgängen und über die Potentiallbildung an Mischelektroden" ("On the Interpretation of Corrosion Processes through the Superposition of Electrochemical Partial Processes and on the Potential of Mixed Electrodes") [Wagner & Traud, 1938].

2.2.4 Types of Polarisation and Overpotential

When the half-cell reactions are moved away from their equilibrium, a net current is obtained in either one or the other direction. A certain resistance always counteracts that current flow across the electrode interface and an overpotential of a certain magnitude is required to overcome this resistance. Depending on the type of resistance, which limits the reaction rate, three different types of polarisation can be distinguished:

- Activation polarisation (cf. Section 2.2.4.1)
- Concentration polarisation (cf. Section 2.2.4.2)
- Resistance polarisation (cf. Section 2.2.4.3).

2.2.4.1 Activation Polarisation and Overpotential

In principle, activation polarisation resulting in an activation overpotential 'η_{act}' is caused by the energy barrier limiting the electrochemical reaction at the metal-electrolyte interface. This is partly due to the electrical field created by the double layer that prevents easy charge transfer (cf. Section 2.2.1), but the rate determining step largely depends on the conversion of species involved in the electrochemical reaction.

For instance, in terms of hydrogen ion reduction as cathodic reaction (cf. Section 2.1.2):

$$2H^+ + 2e^- \rightarrow H_2 \quad \left(E_0^0 = 0\,mV_{SHE} \right) \qquad [2.95]$$

the transformation occurs in three major steps. First H^+ reacts with an electron from the metal:

$$H^+ + e^- \rightarrow H_{ads} \qquad [2.96]$$

* Carl Wagner, Germany, 1901-1977 [Wikimedia, 2007].

to form an adsorbed hydrogen atom 'H_{ads}' at the surface. In the second step, two of these adsorbed atoms must react to form a hydrogen molecule:

$$H_{ads} + H_{ads} \rightarrow H_2 \qquad [2.97]$$

and the third step requires sufficient molecules to combine and nucleate a hydrogen bubble at the metal surface. Any one of these three steps controls the rate [2.95] and thus contributes to activation polarisation. [Jones, 1996].

For activation polarisation the relationship between the current density 'i' and the activation overpotential 'η_{act}' is given by the Tafel equation*:

$$\eta_{act} = \pm b \times \log\left(\frac{i}{i_0}\right) \qquad [2.98]$$

For the anode:

$$\eta_{act,\,a} = \pm b_a \times \log\left(\frac{i_a}{i_0}\right) \qquad [2.99]$$

For the cathode:

$$\eta_{act,\,c} = \pm b_c \times \log\left(\frac{i_c}{i_0}\right) \qquad [2.100]$$

where 'b_a' and 'b_c' are the anodic and cathodic Tafel constants (in the literature also referred to as Tafel slopes). The Tafel constants can be determined by:

$$b = \frac{2.3 \times R \times T}{\alpha \times n \times F} \qquad [2.101]$$

with ('α') as a constant determined by the shape of the energy barrier, i.e. mainly the electrical double layer (cf. Section 2.2.1). [Bardal, 2004].

Accordingly, the Tafel equation gives straight lines in a diagram plotting the electrode potential 'E' as a function of the logarithm of the current density 'i', see Figure 2.2.

These types of diagrams are commonly referred to as Tafel diagrams and correspondingly the lines are known as Tafel lines.

* Named after Julius Tafel, Germany, 1862-1918 [Roberge, 2007].

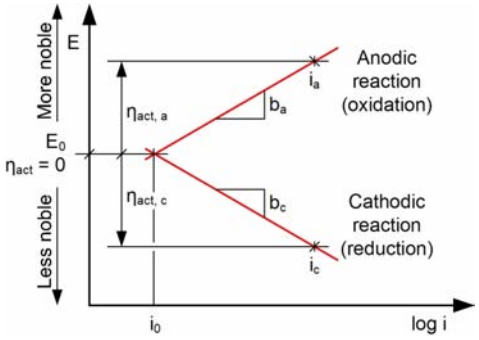

Figure 2.2: *Plot of 'E' as function of log of current density 'i' illustrating the activation overpotential 'η_{act}'. 'E_0': equilibrium potential, 'i_0': exchange current density, and 'b': Tafel constant. Indices 'a' and 'c' denote anodic and cathodic reactions, respectively. For 'i_a' = 'i_c' = 'i_0' is 'η_{act}' = 0. After combined information from [Jones, 1996; Møller, 2003b; Bardal, 2004].*

2.2.4.2 Concentration Polarisation and Overpotential

Concentration polarisation leading to a concentration overpotential 'η_{con}' is due to the limited mass transport within the electrolyte that often determines the rate of the electrochemical reactions at the metal-electrolyte interface. Cathodic reduction reactions tend to deplete the electrolyte at the metal-electrolyte interface of the dissolved species that is reduced. Reduction usually implies that the reactants, i.e. ions or molecules, are transported from the electrolyte to the electrode surface, whereas for the anodic reaction, the reactants are directly available from the metal. Therefore, concentration polarisation influences the theoretical hydrogen and oxygen equilibrium lines in the Pourbaix diagram, as indicated in Section 2.1.10.

For instance, from the equilibrium line of hydrogen ion reduction in acid solution that was derived in equation [2.70] it is obvious that the equilibrium potential decreases with depletion of H^+ at the metal-electrolyte interface:

$$E_{0,H^+/H_2} = 0 - \frac{0.059}{2} \times \log\left(\frac{(1)^1}{\left(a_{H^+}\right)^2}\right) \qquad [2.102]$$

Based on the general Nernst equation [2.66], the concentration overpotential 'η_{con}' can be expressed for any system as a function of the current density by:

$$\eta_{con} = \frac{2.3 \times R \times T}{n \times F} \times \log\left(1 - \frac{i}{i_L}\right) \qquad [2.103]$$

where ('i_L') is the so-called limiting current density that can be expressed by implementing Faraday's law (cf. Section 2.1.4) as:

$$i_L = n \times F \times D \times \frac{C}{x} \qquad [2.104]$$

with 'D' as the diffusion coefficient, 'C' as the concentration of the reacting species in the electrolyte, and 'x' as the length of the diffusion domain*. [Jones, 1996; Bardal, 2004]. A quantitative graph of the concentration overpotential 'η_{con}' as expressed by equation [2.103] is shown in Figure 2.3.

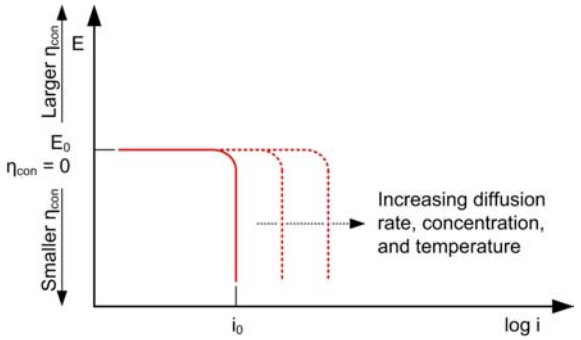

Figure 2.3: *Plot of the electrode potential 'E' as function of the log of the current density 'i' illustrating the (cathodic) concentration overpotential 'η_{con}'. The dotted lines indicate the effect of solution conditions. After combined information from [Jones, 1996; Møller, 2003b].*

For a detailed derivation of concentration overpotential as a function of the current density and the limiting current density, reference is made to the literature, e.g. [Jones, 1996; Bardal, 2004].

The concentration overpotential is of particular importance in the area of reinforcement corrosion. The transport of reactants from the outside environment to the embedded reinforcement by diffusion through the concrete bulk is rather complex and depends on various factors. Diffusion and other transport mechanisms as well as factors determining the ingress rates are discussed in detail in Chapter 3.

2.2.4.3 Resistance Polarisation and Overpotential

Resistance (in the literature also referred to as ohmic) polarisation and accordingly the resistance overpotential 'η_{res}' result from the passive layers (or other surface layers) that can have a considerable ohmic resistance†, even if the layer is very thin (cf. Section 2.1.9). Anodic resistance polarisation is known to affect anodic dissolution and hence the corrosion potential 'E_{corr}' on the passivated metal surfaces, while it only af-

* The diffusion domain is the area between the metal-electrolyte interface, where the reactant is consumed, and the bulk of the electrolyte where transport of the reactant is governed by convection, i.e. the concentration of the reactant is equal to 'C'.

† Named after Georg Simon Ohm, Germany, 1789-1854 [Roberge, 2007].

fects the cathodic reactions for the second group of passive layers (cf. Section 2.1.9). [Jones, 1996; Møller, 2003b; Bardal, 2004].

When a current 'I' or the current density 'i' is flowing through the film, there will be an ohmic drop according to Ohm's law. Thus, the resistance overpotential 'η_{res}' can be expressed by:

$$\eta_{res} = R_{pas} \times I = r_{pas} \times i \qquad [2.105]$$

Where ('R_{pas}') and ('r_{pas}') are the resistances of the passive layer on the total electrode surface and on 1 cm^2 of the electrode surface, respectively.

As indicated by Ohm's law in equation [2.105] the plot of the 'η_{res}' is represented by a straight line with a slope determined by the ohmic resistance of the passive layer.

2.2.4.4 Appearance and Combination of Polarisation and Overpotentials

In practice the discussed polarisation effects do generally not occur individually, but a combination of all three polarisation effects on the investigated electrochemical system is observed. For anodic reactions, activation polarisation is usually dominating, except when passivation takes place. Accordingly, the relationship between the overpotential and the current density for anodic reactions can generally be expressed by:

$$\eta_{act,\,a} = \pm b_a \times \log\left(\frac{i_a}{i_0}\right) \qquad [2.106]$$

For cathodic reactions, the reaction rate is usually governed by both activation and concentration polarisation. Thus, the relationship between the overpotential and current density for cathodic reactions can be expressed as the sum of equations [2.100] and [2.103] by:

$$\eta_{act,\,c} + \eta_{conc,\,c} = \pm b_c \times \log\left(\frac{i_c}{i_0}\right) + \frac{2.3 \times R \times T}{n \times F} \times \log\left(1 - \frac{i_c}{i_L}\right) \qquad [2.107]$$

If a passivated metal surface is investigated, the effect of resistance polarisation can additionally be taken into account, as described in Section 2.2.4.4.

2.2.5 Polarisation Curves

The presence and the effect of the types of polarisation described in Section 2.2.4 as well as the passivation and depassivation behaviour of a metal can be determined by so-called polarisation curves. For a polarisation curve, the electrode potential 'E' is plotted on the Y-axis as a function of the current density 'i' on the X-axis. In correspondence with the Tafel lines (cf. Section 2.2.4.1), the applied current is generally plotted on a logarithmic scale.

In accordance with the definitions for anodic and cathodic polarisation described in Section 2.2.3, a polarisation curve is referred to as anodic or cathodic polarisation curve, if the metal is polarised in positive or negative direction, respectively. Thus, *anodic polarisations curves represent anodic reactions*, e.g. metal dissolution, and cathodic *polarisation curves represent cathodic reactions*, e.g. oxygen or hydrogen ion reduction (cf. Section 2.1.2).

Hence, a polarisation curve is a measure of how the rates of the anodic and the cathodic reactions are limited by activation, concentration, and resistance polarisation, i.e. the variation of the potential as a function of the current enables to visualise the effect of polarisation processes on the rate at which the anodic or cathodic reactions can give up or accept electrons. Polarisation curves can be beneficially applied to determine the rate of the reactions that are involved in the corrosion process, i.e. the corrosion rate. *Yet, contrary to the Pourbaix diagram, a single polarisation curve represents the corrosion processes for one certain pH of the electrolyte*. Moreover, it should be emphasised that in practice the pH at the metal-electrolyte interface can deviate largely from the bulk electrolyte pH and further experience changes during the measurement due to reactions on the metal surface, which is particularly relevant for the study of localised corrosion phenomena, e.g. pitting and crevice corrosion (cf. Section 2.3).

2.2.5.1 Tafel Lines

Figure 2.4 shows a schematic exemplification of a polarisation curve around the area of 'E_{corr}' based on oxidation of iron as anodic reaction and hydrogen ion reduction as cathodic reaction.

The associated anodic overpotential curve representing oxidation of iron to ferrous ion and the cathodic overpotential curve representing hydrogen ion reduction (red lines) are determined by their associated Tafel constants 'b' as well as 'E_0' and 'i_0'. As mentioned in Section 2.2.4.4, both the anodic reaction, i.e. oxidation of iron, and the cathodic reaction, i.e. hydrogen ion reduction, are in this potential range predominately controlled by activation polarisation. The overpotential curves, i.e. the Tafel lines, are asymptotes to the anodic and cathodic polarisation curves (blue lines). The deviation between the polarisation curves and the Tafel lines is due to the fact that the anodic and cathodic reactions occur simultaneously close to 'E_{corr}' [Bardal, 2004]. In Section 2.2.5.3 it is shown that the anodic overpotential curve and the anodic polarisation curve are essentially identical at higher potentials except for very noble potentials, where oxidation of water, i.e. oxygen evolution, interferes with the anodic dissolution of iron.

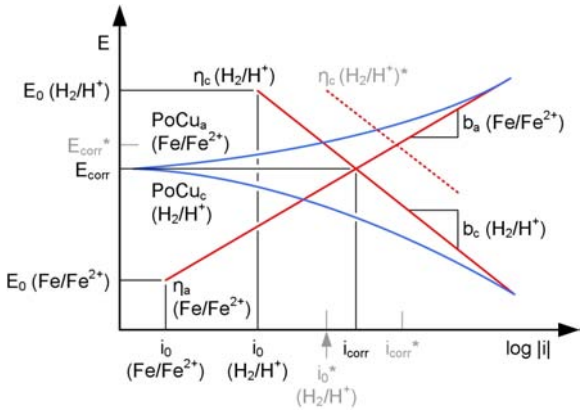

Figure 2.4: *Plot of the electrode potential 'E' as function of the log of the current density 'i' illustrating a schematic polarisation curve in the vicinity of the corrosion potential 'E_{corr}'. 'E_0': equilibrium potential, 'i_0': exchange current density, 'i_{corr}': corrosion current density, 'η' overpotential, 'b': Tafel constant, and ('PoCu'): polarisation curve. Indices 'a' and 'c' denote anodic and cathodic reactions, respectively. The effect of an assumed increased '$i_{0,c}$' on 'i_{corr}' is illustrated by asterisks. After combined information from [Jones, 1996; Kruger, 2001; Bardal, 2004].*

It should be noted that the polarisation curves, but not the Tafel constants are generally obtained by experiments. The measured polarisation curves are used to determine the overpotential curves and with that the parameters, i.e. the Tafel constants 'b', and not vice versa. As explained in more detail in Section 2.5.4, the logarithm is taken from the absolute value of the current density, if the polarisation curve is determined experimentally. Section 2.5.4 provides information on the experimental determination of polarisation curves for general aqueous corrosion systems, whereas the application of polarisation curves in reinforcement corrosion is described in Section 7.5.1.4.

The intercept of the extrapolation of the Tafel lines in Figure 2.4, which under ideal conditions is in line with the corrosion potential 'E_{corr}', represents the logarithm of the corrosion current density 'i_{corr}', which expresses the inherent corrosion rate of the redox couple.

As mentioned in Section 2.2.2, the magnitudes of the exchange current densities for the cathodic and anodic reactions have a major effect on the corrosion rate. This can be illustrated by considering a higher exchange current density ('i_0*') for the cathodic reaction, while assuming that the equilibrium potential is constant. The increased corrosion current ('i_{corr}*') shows that the corrosion rate increases with increasing exchange current density.

2.2.5.2 Evans Diagram

The extrapolations of the anodic and cathodic Tafel lines are often used to produce so-called Evans diagrams*, which are exemplified in Figure 2.5.

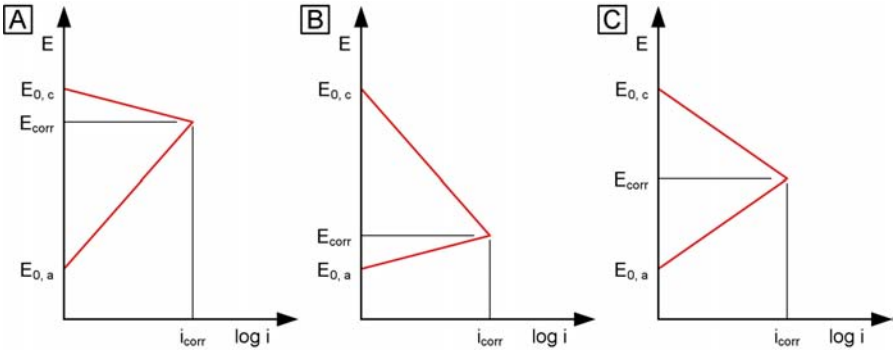

Figure 2.5: *Plot of the electrode potential 'E' as function of the log of the current density 'i' presenting Evans diagrams to illustrate three options of corrosion control. 'E_0': equilibrium potential, 'E_{corr}': corrosion potential, 'i_{corr}': corrosion current density. Indices 'a' and 'c' denote anodic and cathodic reactions, respectively.* [A]: *Anodic control.* [B]: *Cathodic control.* [C]: *Mixed mode. After [Kruger, 2001].*

The relative slopes of the extrapolated Tafel lines obtained from anodic and cathodic polarisation curves determine whether the anodic, cathodic, or both reactions control the rate of the corrosion process. Figure 2.5 [A] represents a system under anodic control, Figure 2.5 [B] denotes to a system under cathodic control, and the slopes in Figure 2.5 [C] indicate that the system is controlled by both the anodic and cathodic reactions, i.e. a mixed mode†. Evans diagrams can be beneficially applied to evaluate the effect of various factors on the corrosion rate in an electrochemical system. [Kruger, 2001; Møller, 2003b].

2.2.5.3 Passivity

Anodic polarisation curves can be used to visualise the passivation and depassivation behaviour of metals. Figure 2.6 shows a hypothetical cathodic and anodic polarisation curve for a passive metal. Moreover, the terminology and abbreviations for the description of polarisation curves as recommended by ASTM [ASTM G3, 2004] are introduced.

---

* Named after Ulick Richardson Evans, UK, 1889-1980 [Roberge, 2007].

† The terms anodic control and cathodic control are used in correspondence with Figure 2.5 throughout this thesis, although we think that this terminology can be misleading, e.g. with regard to the influence of the anodic and cathodic processes on the development of 'E_{corr}' (cf. Section 5.1.2).

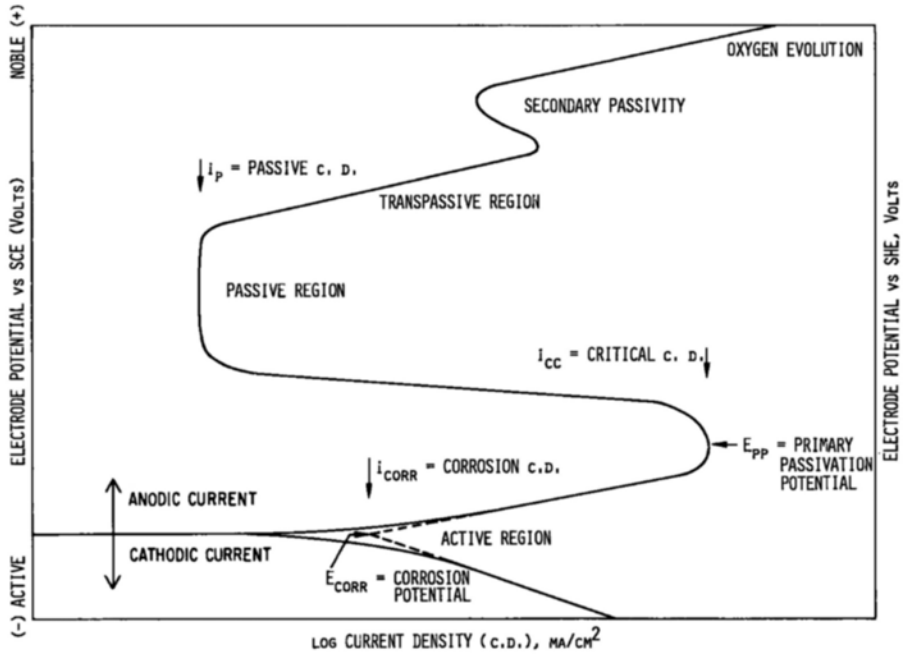

Figure 2.6: *Hypothetical cathodic and anodic polarisation curve of an active-passive metal with recommended terminology and abbreviations for the description of polarisation curves. From [ASTM G3, 2004].*

The cathodic polarisation curve and the linear anodic branch above 'E_{corr}' as well as the Tafel lines (dashed lines) have been introduced in Section 2.2.5. If the potential is raised in anodic direction from 'E_{corr}', the polarisation curve and the overpotential curve approach each other to become identical, as metal dissolution is the only anodic reaction taking place. In the first linear part, the current density increases corresponding to the slope of the Tafel line, i.e. controlled by activation polarisation. With further increment of 'E', the increase in current density ceases and the polarisation curve starts to deviate from the slope determined by activation polarisation. The cease in current increment is due to the fact that the high corrosion rates lead to a high concentration of metal ions at the metal-electrolyte interface*, which leads to concentration polarisation increasing the equilibrium potential of the dissolution reaction (cf. Section 2.2.4.2). With further increment of the potential, the critical current density 'i_{cc}' is reached. The critical current density 'i_{cc}' is the maximum corrosion current density of the system at the primary passivation potential 'E_{pp}' (in the literature also referred to as passivation potential ('E_{pass}')). This is followed by a major decrease in the current density, which is caused by the formation of a passive layer on the metal surface (cf.

* The measured deviation from the Tafel line is normally larger than the actual one due to the potential drop between the reference electrode and the investigated metal sample at the high current density [Bardal, 2004].

Section 2.1.9). In the passive region the current remains low at the almost constant passive current density 'i_p', which is governed by the ohmic resistance of the passive layer (i.e. its resistance polarisation, cf. Section 2.2.4.3). With further potential increment certain metals in certain electrolytes show a transpassive region with increasing current density before another decrease in the current density is measured, which is referred to as secondary passivity. Other metals and/or other electrolytes remain at a more or less constant 'i_p' until transpassivity oxygen evolution leads to a sharp rise in the current density.

Besides the above mentioned parameters, the pitting potential 'E_{pit}' (cf. Section 2.3.2) is often used as an additional characteristic parameter for the quantification of corrosion initiation, in particular in environments containing depassivating ions.

2.3 Forms of Corrosion

Before interrelations between thermodynamics and kinetics are dealt with in Section 2.4, selected forms of aqueous metallic corrosion that are relevant in the present thesis are summarised. More detailed descriptions of these and other forms of corrosion can be found in the literature on corrosion science, e.g. [Kaesche, 1979; Jones, 1996; Bardal, 2004] or in textbooks on materials science or related subjects, e.g. [Callister & Callister, 2000; Møller, 2003c].

2.3.1 Uniform corrosion

Uniform (in the literature also referred to as general) corrosion occurs, when anodic and cathodic reactions take place on the entire metal surface, but not simultaneously at the same place, i.e. the anodic and cathodic sites constantly shift places. That requires that there are no significant macroscopic concentration differences in the electrolyte and along the metal surface or, in terms of reinforcement corrosion, at the concrete steel interface and along the surface of the reinforcement (cf. Sections 3.2 and 3.3). Hence, uniform corrosion is relatively evenly distributed over the surface and thus results in a uniform thickness reduction. Homogeneous materials without a significant passivation tendency in the present environment are liable to uniform corrosion, e.g. reinforcing steel in carbonated concrete (cf. Section 5.2.2.1).

2.3.2 Pitting corrosion

Unlike uniform corrosion, pitting corrosion is localised and corrosion pits can have different sizes and depths and usually appear randomly distributed. In terms of reinforcement corrosion, pitting corrosion is generally associated with a notch-like attack with a depth equal or greater than the surface diameter of the notch (cf. Section 5.2.2.2). Pitting begins when surface (or interface) defects, certain particles, or other variations in the metal (or interface) lead to a fixation of anodic and cathodic sites on

the metal surface (cf. Sections 3.2 and 3.3). The nature of pitting often makes it difficult to estimate the amount of damage. As indicated in Section 2.2.5.3, pitting can be associated with a premature breakdown of passivity. The electrode potential, where the breakdown of the passive layers occurs is commonly referred to as pitting potential 'E_{pit}', see Figure 2.7 [A].

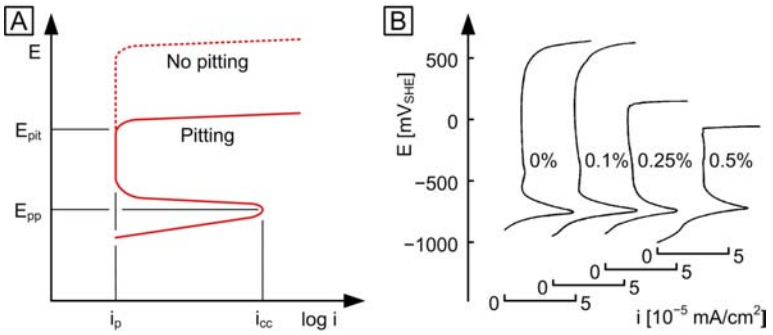

Figure 2.7: [A]: *Anodic polarisation curve for an active-passive metal in an environment causing pitting corrosion. 'E_{pit}': pitting potential, 'E_{pp}': primary passivation potential, 'i_p': passive current density, and 'i_{cc}': critical current density (cf. Section 2.2.5.3). After [Bardal, 2004]*. [B]: *Potentiodynamic anodic polarisation curves (scan rate = 1 mV/s) of carbon steel in saturated $Ca(OH)_2$ solution containing various percentages of $CaCl_2$. After [Page & Treadaway, 1982]*.

Pitting corrosion occurs on more or less passivated metals in environments containing depassivating ions, among others chloride ions (cf. Section 2.1.9). For instance, carbon steel in chloride contaminated concrete or stainless steel in environments with higher chloride contents are susceptible to pitting. As shown in Figure 2.7 [B], 'E_{pit}' decreases drastically with increasing concentration of depassivating ions, in this case $CaCl_2$ [Page & Treadaway, 1982]. It should be emphasised that 'E_{pit}' is not a thermodynamic parameter, but rather a kinetic one. Among others, this is sustained by the fact that 'E_{pit}' is largely affected by the scan rate (in the literature also referred to as sweep rate) used to record the polarisation curve (cf. Section 2.5.4).

2.3.3 Galvanic Corrosion

Galvanic corrosion takes place if a metallic contact is made between a nobler and a less noble metal (cf. Chapter 'TaD') under the condition that there also is an electrolytic connection between the metals, so that a closed circuit, i.e. a galvanic cell, is established. If 'ΔE' between two metals in a galvanic cell is large, the nobler metal does generally not take part in the corrosion process with its own ions. Under this condition, 'E_0' of the nobler metal does not play any role [Bardal, 2004]. As mentioned in Section 2.1.6, the EMF series allows only preliminary conclusions about preferentially corroded metal, and *conclusive information can only be obtained from the gal-*

vanic series for the particular environment under investigation. For instance, the galvanic series for seawater, which is often provided in the corrosion literature, e.g. [Jones, 1996; Bardal, 2004], does not allow conclusion about the behaviour of e.g. certain metals in carbonated and chloride contaminated concrete.* The complex chemical environment of concrete (cf. Section 3.1) interacts with the thermodynamics, so that not only the pH and the chloride content play a role. For instance, this aspect is evident in the thermodynamic interaction between calcium and magnesium (cf. Section 7.3.2).

2.3.4 Crevice Corrosion

Crevice corrosion is a specialised form of pitting corrosion that particularly attacks metals or alloys, which are protected by passive layers. Crevice corrosion results from a relative lack of oxygen in a crevice, where the metal becomes anodic towards the metal outside the crevice. Corrosion can take place, if the crevice is large enough to admit the electrolyte, but small enough to suffer from oxygen depletion.

2.3.5 Intergranular Corrosion

Intergranular (in the literature also referred to as intercrystalline) corrosion can occur between the grains (in the literature also referred to as crystals) that are formed during the solidification of a metal. The composition of the areas between the grains differs from the one of the grains themselves, and these boundaries are often subjected to intergranular corrosion. Grains and grain boundaries in carbon steel are discussed in detail in Section 3.2.2. Grains and grain boundaries in stainless steel, which are known to be particularly sensitive to intergranular corrosion in the vicinity of welds, are dealt with in Section 6.3.2.3.

2.3.6 Hydrogen Embrittlement

In principle, hydrogen embrittlement is not an actual form of metallic corrosion, but rather a possibly harmful result of metallic corrosion reactions. It is interconnected with corrosion mechanisms and an important aspect that we took into due consideration, in particular in the design of new countermeasures (cf. Chapter 7). Thus, it is briefly described in this Section.

Hydrogen embrittlement results from diffusion of hydrogen atoms into the metal. The hydrogen atoms recombine in the minuscule voids of the metal matrix to hydrogen molecules and create pressure from inside the cavity. This pressure can increase to levels that reduce the ductility and tensile strength of the metal and can eventually lead to the so-called hydrogen induced cracking. Among other metals, high-strength

* The galvanic series in seawater can even be misleading in supposedly equivalent environments, e.g. due to the different behaviour of certain metals in simulated and in actual seawater.

steels are known to be particularly susceptible to hydrogen embrittlement. Hydrogen embrittlement can occur during different stages of manufacturing or operation, e.g. caused by 'CP' and/or galvanic coupling, which are central parameters in our design approach to new countermeasures.

2.4 Interrelations between Thermodynamics and Kinetics

In Sections 2.1 and 2.2 the importance of thermodynamic and kinetic parameters for the understanding and description of corrosion processes was illustrated and the interrelations between the two approaches were indicated. A convenient and illustrative way of presenting these interrelations is the comparison of Pourbaix diagrams with polarisation curves, since both identify domains of immunity, corrosion, and passivity, see Figure 2.8.

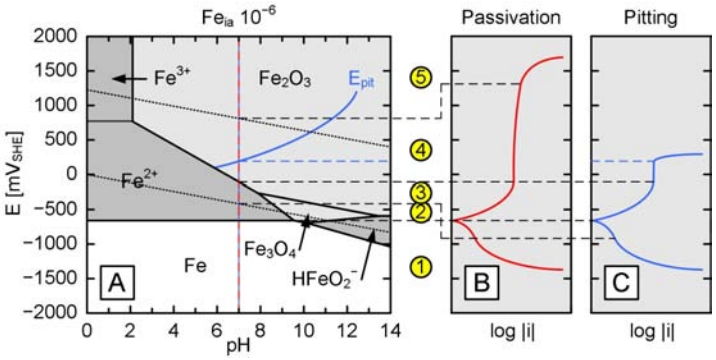

Figure 2.8: *Comparison of Pourbaix diagram and selected polarisation curves to illustrate interrelations between thermodynamics and kinetics. After combined information from [Pourbaix, 1974a; Møller, 2003b; Bardal, 2004; KAIST, 2007]. The distinguished regions in the Pourbaix diagram and the polarisation curves are indicated by the dashed lines (and the dotted-and-dashed line for 'E_{pit}') and indexed 1-5 in the yellow circles, which is referred to in Table 2.3.* [A]: *Fe-H_2O Pourbaix based on Table 2.2 and $Fe_{ia} = 10^{-6}$ mol/L (cf. Figure 2.1). The selected pH of 7 for the establishment of polarisation curves is marked by the red/blue dashed line and a hypothetical pitting potential 'E_{pit}' is marked by the blue line.* [B]: *Qualitative polarisation curve for passivation without premature depassivation.* [C]: *Qualitative polarisation curve for premature depassivation in relation to the hypothetical 'E_{pit}' in [A].*

To provide additional information to Figure 2.8, the relevant anodic and cathodic half-cell reactions and their direction, i.e. reduction or oxidation (as written or reversed, cf. Section 2.1.5), associated with the regions 1 to 5 (indicated by the yellow circles in Figure 2.8) are listed in Table 2.3.

Table 2.3: *Half-cell reactions, associated equilibrium potentials, and reaction directions (reduction: as written, oxidation (bold): reversed) corresponding to the essential regions identified in the Pourbaix diagram and the polarisation curves for the selected pH of 7 by the yellow circles in Figure 2.8.*

Region	Half-cell reaction			
	I	II	III	IV
1	Reduction	Reduction	Reduction	Reduction
2	**Oxidation**	Reduction	Reduction	Reduction
3	**Oxidation**	Reduction	Reduction	**Oxidation**
4	**Oxidation**	**Oxidation**	Reduction	**Oxidation**
5	**Oxidation**	**Oxidation**	**Oxidation**	**Oxidation**
Anodic reactions				
I	$Fe^{2+} + e^- \rightarrow Fe \quad \left(E_0^0 = -475\,\{-447\}\ mV_{SHE} \right)$			
II	$Fe_2O_3 + 6H^+ + 2e^- \rightarrow 2Fe^{2+} + 3H_2O \quad \left(E_0^0 = 789\ mV_{SHE} \right)$			
Cathodic reactions				
III	$O_2 + 4H^+ + 4e^- \rightarrow 2H_2O \quad \left(E_0^0 = 1230\,\{1229\}\ mV_{SHE} \right)$			
IV	$2H^+ + 2e^- \rightarrow H_2 \quad \left(E_0^0 = 0\ mV_{SHE} \right)$			

The theory for the establishment of the Pourbaix diagram, which was described in detail in Section 2.1.10, can be summarised for the selected pH of 7 by Figure 2.8 [A] and the information given in Table 2.3. The anodic branch of the qualitative polarisation curve without depassivation in Figure 2.8 [B] reflects passivation, which is for selected pH of 7 mainly characterised by the thermodynamic stability of the passive oxide Fe_2O_3 (cf. Section 2.1.9). The drastic effect of depassivating ions in a certain (threshold) concentration, which is represented by a *hypothetical* 'E_{pit}' in the Pourbaix diagram, on the polarisation curve is illustrated by the premature sharp rise in corrosion current, as indicated in Figure 2.8 [C] (cf. Section 2.3.2). Besides those features, other important kinetic aspects, such as the effect of the hydrogen and oxygen overpotentials (cf. Section 2.2.3) and the influence of H_2 and O_2 evolution (cf. Section 2.1.10) on the cathodic and anodic branch of the polarisation curve as well as other general characteristics introduced for the anodic branch of polarisation curves (cf. Section 2.2.5.3) are e.g. represented in Figure 2.8 [B].

Thus, many important aspects of the theory described in Sections 2.1 and 2.2 are represented by Figure 2.8 in combination with the information provided in Table 2.3. Furthermore, the comparison between the Pourbaix diagram and polarisation curves in Figure 2.8 draws attention to some of the central benefits and drawbacks of thermodynamics and kinetics, respectively, which were also pointed out throughout Sections 2.1 and 2.2:

- On the one hand, the Pourbaix diagram (representing thermodynamics) can provide the full picture concerning the corrosion tendencies of a certain metal in a certain environment (given that the established diagram appropriately reflects the system under investigation). So, the full pH scale is represented, but the picture is limited to corrosion tendencies, i.e. no information on the rates of corrosion is obtained. On the other hand, polarisation curves (representing kinetics) can provide for detailed information on the rates, but the picture is limited to a certain pH.
- Pourbaix diagrams can be established based on theoretical considerations and hence allow predictions (e.g. with regard to the design of new countermeasures), while polarisation curves have to be determined experimentally.

Based on the above, we suggest that thermodynamic considerations established on the basis of appropriate and representative Pourbaix diagrams, which are founded on reasonable kinetic considerations and interpreted with due regard to kinetics, allow for the description of corrosion mechanisms (Chapter 5) as well as for the evaluation of existing (Chapter 6) and the design of new countermeasures (Chapter 7). Among these central Chapters, the approach towards the establishment of the required appropriate and representative Pourbaix diagrams is a central part of this thesis (Chapter 4).

2.5 Electrochemical Measurement Techniques

The theoretical background of selected measurement and online monitoring techniques to assess the corrosion tendency and rate experimentally is briefly outlined in this Section. The selected techniques relate to the experimental part of this project. Special aspects of these techniques in the area of reinforcement corrosion and our adaptation concerning the customisation to the applied experimental setups are discussed in Sections 7.5.1 and 8.4, respectively. In our own experimental investigations and in the analysis of the results we used the conventions described in [ASTM G3, 2004] as far as possible, while some of the applied measurement techniques were custom-designed and hence not standardised.

2.5.1 Corrosion Potential Measurements and Monitoring

The measurement or the continuous monitoring of 'E_{corr}' are fundamental non-destructive techniques to access the thermodynamic state of the investigated system. As described in Section 2.2.3, the corrosion potential 'E_{corr}' represents the electrode potential, where the rates of the anode and cathode reactions are in equilibrium. 'E_{corr}' can be assessed by simply measuring the potential difference between a reference

electrode, e.g. a 'SCE', and the metal surface.* The 'RE' is connected to the ground terminal and the 'WE' (i.e. the investigated metal sample) is connected to the positive terminal of a high-impedance voltmeter. Results can be analysed, for instance, based on the Pourbaix diagram by transferring the measured potential to the 'SHE' scale, e.g. by simply adding 244 mV to the measured value [RA, 2006b], if a 'SCE' is used as reference electrode at 25°C (cf. Section 2.1.5).

2.5.2 Macrocell Current Measurements and Monitoring

Macrocell current measurements or the continuous monitoring of the macrocell current are non-destructive techniques that aim at accessing the current passing between two dissimilar metals (or the same metal at a different 'E_{corr}') in a galvanic cell (cf. Section 2.3.3). The electrical connection between the two metals can be established over a resistor, and the macrocell current is measured as the proportional potential over the resistor, or even better, over a zero-impedance-ammeter, i.e. without introducing resistance to the system. In case of continuous monitoring, the recorded current can be integrated to represent the total charge passed, which can be plotted as a function of time and hence interrelated with the material loss. It should be emphasised, however, that *only the macrocell current between the two dissimilar metals is measured and consequently the micro- and macrocell corrosion activity on the preferentially corroding metal surface is not reflected*. Hence, the application of macrocell current techniques may be limited in some areas of aqueous metallic corrosion. Nevertheless, it is frequently used in the area of reinforcement corrosion, because of its simplicity and the clear indication of corrosion initiation by a sharp increase in macrocell current with depassivation of the reinforcement acting as anodic member in the galvanic cell (cf. Sections 2.1.9 and 2.2.5.3).

To indicate that the macrocell current does not account for microcell and macrocell corrosion activity on the preferentially corroding metal surface, it is referred to as 'i_{mac}' (not 'i_{corr}') in the present thesis. In accordance with the definitions in Chapter 'TaD' the mixed corrosion potential established between the two dissimilar metals is referred to as 'E_{corr}', however.

2.5.3 Potentiostatic and Galvanostatic Measurements and Monitoring

For potentiostatic and galvanostatic measurements or monitoring a potentiostat is used to keep either the potential constant while recording the current necessary to maintain the potential, i.e. so-called potentiostatic monitoring, or to apply a constant current to

* As mentioned in Section 2.5.1, 'E_{corr}' measured in such way is generally referred to as half-cell potential. However, we consider this term to be rather misleading in this connection, since the mixed potential between the anodic and cathodic reactions (cf. Section 2.2.3) on the metal surface is measured. The term half-cell potential may actually have led to some misinterpretations regarding the development of 'E_{corr}' for steel in concrete, which will be dealt with in detail in Section 5.1.2.

the working electrode while recording the potential of the same, i.e. so-called galvanostatic monitoring. *In the potentiostatic mode a sharp increase in current is indicative of corrosion, whereas a sharp decrease in potential to lower values is the indication for corrosion activities in the galvanostatic mode.*

Depending on the degree of polarisation, potentiostatic and galvanostatic measurements or monitoring techniques can be regarded as non-destructive, but we think that these techniques interfere largely with the system by either polarising the 'WE' or restricting it to maintain a constant 'E_{corr}'.

2.5.4 Polarisation Curve Measurements

The theory behind and the interpretation of potential curves was outlined in Section 2.2.5 and a standard reference test method for measuring anodic polarisation curves is specified in [ASTM G5, 2004].

In practice polarisation curve measurements are performed by means of a three-electrode setup, i.e. a 'WE', a 'CE', and a 'RE', in combination with a potentiostat. The potentiostat is used to control the potential of the 'WE', i.e. *it supplies voltage to the cell consisting of the 'WE' and the 'RE' by delivering and measuring the necessary current between the 'CE' and the 'WE', which represents an external current to the 'WE'*. No external current is supplied, if the electrode potential of the 'WE' is equal to 'E_{corr}'. Application of positive current to the 'WE' leads to anodic polarisation, and application of negative current provides cathodic polarisation curves (cf. Sections 2.2.5 and 2.4). Thus, as mentioned in Section 2.2.5, the absolute value of the current density 'i' is to be used for the graphical representation of the measured polarisation curves to allow for the logarithmic scale that corresponds to the Tafel line representation.

As indicated in Section 2.3.2, the scan rate used to obtain polarisation curves can have a significant effect on the determination of 'E_{pit}', as e.g. significant variations of the pH and chloride concentration are introduced on the metal surface. Thus, the scan rate is a critical parameter and to be selected appropriately, in particular for a system with "slow chemistry", such as for metals embedded in concrete (cf. Sections 3.1 and 7.5.1.4). Various other obstacles, such as the solution (or concrete bulk) resistance and changing surface conditions, complicate polarisation curve measurements and their interpretation. This also holds for measurements that are based on "limited" polarisation, such as linear polarisation resistance 'LPR' measurements (cf. Section 2.5.5) or electrochemical impedance spectroscopy 'EIS' (cf. Section 2.5.6). A detailed discussion on all possible obstacles goes beyond the scope of this thesis, and reference is made to the literature, e.g. [Berke & Hicks, 1990; Kelly et al., 2003]. The most important effects to be taken into account for measuring steel in concrete and our related approaches are dealt with in Sections 7.5.1 and 8.4, respectively. Finally, it should be noted that in contrast to 'LPR' and 'EIS', full-scale polarisation interferes with the

system and thus polarisation curve measurements are regarded as destructive techniques.

2.5.5 Linear Polarisation Resistance Measurements

Linear polarisation resistance 'LPR' measurements are based on the fact that the polarisation curve close to 'E_{corr}' approximates linearity, i.e. the anodic and cathodic currents are almost equal in magnitude (cf. Section 2.2.5). A three-electrode setup in combination with a potentiostat capable of performing 'LPR' routines is applied to impose a small potential perturbation 'ΔE_p' defined with respect to the corrosion potential:

$$\Delta E_p = E - E_{corr} \qquad [2.108]$$

to the metal sample and the resulting current density response 'Δi_p' is recorded. Since the magnitude of 'ΔE_p' is small, the electrochemical system is not significantly affected and 'LPR' can, thus, be considered to be a non-destructive technique. The polarisation resistance 'R_p' of a corroding electrode can then be defined as:

$$R_p = \frac{\Delta E_p}{\Delta i_p} \qquad [2.109]$$

The corrosion current 'i_{corr}' can be expressed in relation to 'R_p' by the Stern-Geary equation [Stern & Geary, 1957]:

$$i_{corr} = \frac{B}{R_p} \qquad [2.110]$$

with ('B') as the so-called Stern-Geary coefficient. The Stern-Geary coefficient can be related to the anodic and cathodic Tafel lines 'b_a' and 'b_c' by:

$$B = \frac{b_a \times b_c}{2.303 \times (b_a + b_c)} \qquad [2.111]$$

For the derivation of the above equation and the method for estimating Tafel slopes based on the measured data, reference is made to [ASTM G102, 1999]. A standard reference test method for performing 'LPR' measurements is provided in [ASTM G59, 2003]. The ASTM standard practice for calculation of corrosion rates and related information from electrochemical measurements [ASTM G102, 1999] also provides means to calculate the corrosion rate of different metals, e.g. expressed in millimetres of material loss per year, based on 'i_{corr}' determined by 'LPR' or qualitatively by macrocell current monitoring (taking into account the limitation of this method described in 2.5.2). *It should be noted that the measurement of the current, which is required to maintain a constant potential under potentiostatic control (cf. Section 2.5.3), does not allow conclusions about the corrosion rate, since this current does not at all reflect 'i_{corr}'.*

2.5.6 Electrochemical Impedance Spectroscopy

Electrochemical impedance spectroscopy 'EIS' is based on the same principles as 'LPR' measurements with the difference that the current density response 'Δi_p' of the potential perturbation 'ΔE_p' is measured at *varying frequencies*. As 'LPR', 'EIS' is based on a three-electrode setup in combination with a potentiostat that is capable of performing 'EIS'. Otherwise, a frequency response analyzer ('FRP') can be used in combination with an electrochemical interface to perform 'EIS'. ASTM provides a standard practice for verification of algorithm and equipment for electrochemical impedance measurements [ASTM G106, 1999], which also contains an appendix reviewing the details of this measurement technique. The most important theory for the purpose of this thesis concerning 'EIS' and the analysis of the associated measurement data is based on the descriptions in [ASTM G106, 1999] as well as additional literature, e.g. [Gabrielli, 1984; Jones, 1996; Cottis & Turgoose, 1999; Kelly et al., 2003; AutoLab, 2005; Gamry, 2006] that are briefly summarised in this Section.

During 'EIS' runs, a small amplitude sinusoidal '$\Delta E_p(t)$' is applied to the 'WE' at a number of frequencies 'ω' (expressed as angular frequency) by superimposing it on the supplied direct current ('DC') polarisation potential, which maintains the 'WE' at 'E_{corr}' during the 'EIS' run.* At each one of these frequencies the resulting current density waveform exhibits a sinusoidal response '$\Delta i_p(t)$' that is out of phase with the applied '$\Delta E_p(t)$' by a magnitude determined upon the circuit parameters of the metal-electrolyte interface of the 'WE'. Among other possible parameters, the electrical double layer tends to act as capacitor (cf. Section 2.2.1), whereas a passive layer functions as a resistor in 'EIS' (cf. Sections 2.1.9 and 2.2.4.3). The current amplitude is inversely proportional to the electrochemical impedance of the interface '$Z(\omega)$'. Thus, '$Z(\omega)$' is the frequency dependent proportionality factor of the electrochemical system that can be expressed by the quotient of '$\Delta E_p(t)$' and '$\Delta i_p(t)$':

$$Z(\omega) = \frac{\Delta E_p(t)}{\Delta i_p(t)} \qquad [2.112]$$

where '$\Delta E_p(\omega)$' can be expressed as:

$$\Delta E_p(t) = \Delta E_p \times \sin(\omega \times t) \qquad [2.113]$$

and correspondingly '$\Delta i_p(t)$' with the phase shift 'φ':

$$\Delta i_p(t) = \Delta i_p \times \sin(\omega \times t + \varphi) \qquad [2.114]$$

The impedance of the system '$Z(\omega)$' is a complex quantity and can be represented in polar as well as Cartesian coordinates. In polar coordinates '$Z(\omega)$' is given by:

* In our own experimental trials, we found out that it is crucial to supply a direct current to maintain 'E_{corr}'. Even if very small amplitudes were used for the potential perturbation, 'E_{corr}' was largely affected by perturbation without control of 'E_{corr}'.

$$Z(\omega) = |Z(\omega)| \times e^{\varphi(\omega)} \qquad [2.115]$$

and in Cartesian coordinates it can be expressed as:

$$Z(\omega) = Z_r(\omega) + j \times Z_j(\omega) \qquad [2.116]$$

where '$Z_r(\omega)$' is the real part of the impedance and '$Z_j(\omega)$' is the imaginary part of the impedance with ('j') as the square root of −1. [Jones, 1996; Kelly et al., 2003; AutoLab, 2005; ASTM G106, 1999].

The plot of '$Z_j(\omega)$'on the Y-axis versus '$Z_r(\omega)$' in the *same scale* on the X-axis results in a so-called Nyquist plot*. The advantage of Nyquist plots is that they provide a beneficial overview of the data allowing rapid qualitative interpretations. The disadvantage is that information on the frequency is normally not included, but the curve can additionally be labelled with so-called frequency markers.

An alternative to Nyquist plots for the representation of 'EIS' data are Bode plots†. In Bode plots the absolute values of 'Z' and the phase shift 'φ' are plotted as a function of the frequency 'ω' by two individual curves. Generally, all axes in Bode plots are given in the log scale.

The relationship between the two ways of representing plots can be described as follows [AutoLab, 2005]:

$$\begin{aligned} |Z(\omega)|^2 &= (Z_r(\omega))^2 + (Z_j(\omega))^2 \\ \varphi &= \tan^{-1}\left(\frac{Z_j(\omega)}{Z_r(\omega)}\right) \end{aligned} \qquad [2.117]$$

or:

$$\begin{aligned} Z_r(\omega) &= |Z(\omega)| \times \cos\varphi \\ Z_j(\omega) &= |Z(\omega)| \times \sin\varphi \end{aligned} \qquad [2.118]$$

In our analysis of 'EIS' data, we used Bode plots only marginally, e.g. for the verification of measurement data, and favoured Nyquist plots for the interpretation of results. The qualitative overview in Nyquist plots provides various beneficial means, in particular with regard to comparing data, e.g. comparison between "different specimens at the same exposure time" or "the same specimen at different exposure times" [Küter et al., 2005b]. Hence, the Bode plot representation will not be dealt with in detail in this thesis and reference is made to the above mentioned literature. Selected Nyquist plots are shown in Figure 2.9 together with their associated equivalent circuits for a brief summary of the underlying theory of this approach in analysing 'EIS' data.

* Named after Harry Nyquist, Sweden/USA, 1889-1976 [Roberge, 2007].

† Named after Hendrik Wade Bode, USA, 1905-1982 [Roberge, 2007]).

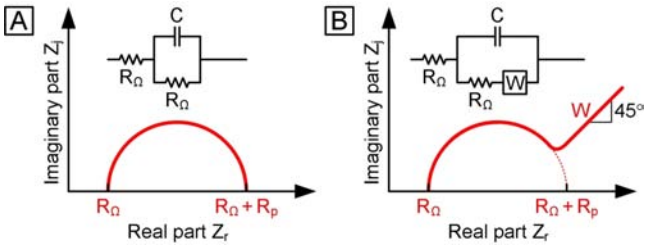

Figure 2.9: *Graphical representation of electrochemical impedance spectroscopy data by schematic Nyquist plots with associated equivalent circuits. After [Jones, 1996].* [A]: *Corroding interface simulated by solution resistance 'R_Ω' in series with parallel connected polarisation resistance 'R_p' and double layer capacitance 'C_{dl}'.* [B]: *As [A] and Warburg impedance 'W' connected in series after 'R_p' added to the equivalent circuit.*

An equivalent circuit representing a corroding interface by the solution resistance 'R_Ω' in series with parallel connected polarisation resistance 'R_p' and double layer capacitance 'C_{dl}'(cf. Section 2.2.1), which often is an adequate representation of a corroding surface with activation polarisation in aqueous corrosion (cf. Section 2.2.4.1), and its corresponding Nyquist plot are shown in Figure 2.9. The Nyquist plot consists of a semicircle with increasing frequency 'ω' in a counterclockwise direction. At very high frequencies, 'Z_j' disappears leaving only 'R_Ω'. At very low frequencies, 'Z_j' again disappears leaving a sum of 'R_Ω' and 'R_p'. It is evident from Figure 2.9 [A] that the 'R_Ω' measured at high frequencies can be subtracted from the sum of '$R_p + R_\Omega$' at low frequencies to give a compensated value of 'R_p' free of ohmic interferences. This 'R_p' can be used for the determination of 'i_{corr}' and hence for estimates on the corrosion rate as described in Section 2.5.5.

In the frequent case of limited diffusion in the electrolyte, i.e. presence of concentration polarisation (cf. Section 2.2.4.2), which is of particular importance in the concrete environment (cf. Section 3.1), an additional resistive element, the so-called Warburg impedance 'W', can be included in the equivalent circuit, see Figure 2.9 [B]. In the Nyquist plot 'W' is recognised by a straight line with an angle of 45° in the lower frequency region. This representation is often referred to as the Randles circuit*.

In investigations on aqueous metallic corrosion systems, typical 'EIS' frequency ranges are in the order of 100 kHz to 0.1 Hz [AutoLab, 2005; Gamry, 2006].

2.6 Chemical and Electrochemical Surface Modifications

Although per se no corrosion processes, many chemical and electrochemical surface modifications are based on the theory of aqueous metallic corrosion. Among other

* Named after John E. B. Randles, England, 1912-1998 [HUJI, 2007].

surface cleaning processes, degreasing and etching have been investigated in the experimental part of this project. These techniques as well as electrolytic plating are briefly outlined in this Section. Besides these standard processes, a number of special material concepts and surface treatments/modifications have been designed and tested experimentally in relation to the development of new countermeasures (Chapter 7). However, with regard to the expected patent possibilities (cf. Section 1.6), descriptions of these custom-designed processes are not included in the present thesis.

2.6.1 Surface Cleaning

As far as possible, the surface cleaning methods we applied in the experimental part of this project were based on [ASTM B322, 2004]. Surface cleaning of reinforcing steel is used as a pretreatment in connection with reinforcement countermeasures involving surface modifications, such as galvanisation, organic coating, or cladding (cf. Section 6.3.2), but it is generally not applied as a single treatment in practice, as the gain in corrosion protection is technically insignificant.* Nevertheless, *the condition of the embedded metal surface has a significant effect on the electrochemistry in concrete,* e.g. concerning 'E_{corr}' and 'R_p' [Küter et al., 2005b]. We think that these aspects allow for a better understanding of the thermodynamic parameters and thus allow for certain considerations for the design of new countermeasures. Hence, we quantified the surface and metallurgical characteristics of different reinforcement steel qualities and investigated the effect of diverse carbon steel surface treatments on the thermodynamics of steel in concrete in an experimental study that also included other steel qualities and galvanisation. The investigated steel surface treatments and steel qualities are briefly described in Section 1.9.3 and selected results of the metallurgical and thermodynamic investigations are given in Sections 3.2.2.2 (carbon steel) and 6.3.2.3.2 (stainless steel). Both investigations were performed in close relation to the theory on the metallurgical and surface properties of carbon steel, which is dealt with Section 3.2.

2.6.1.1 Degreasing

The degreasing process aims at removal of oil and loose defilement from the surface. Degreasing is normally performed as a twofold process, consisting of dip-degreasing and electrolytic degreasing. Dip-degreasing removes loose oil and defilement from the metal surface, before electrolytic degreasing is applied to remove the remaining thin grease film. Thick films can generally not be removed by electrolytic degreasing only, since the current transfer is limited [Streeb & Hoffmann, 1969].

* On the contrary, reinforcing steel is often intentionally exposed to the atmosphere to attain a certain degree of precorrosion, which supposedly increases the roughness and thus leads to better bond properties. However, considering that almost all reinforcement is produced from ribbed bars nowadays, we think that the gain in bond obtained from precorrosion is rather negligible, as the interlocking between the concrete and the steel achieved by the ribs provides for effective force transfer.

The dip-degreasing solution contains different base components (builders) and an advanced system of detergents. The detergent consisting of a hydrophilic and a hydrophobic part, see Figure 2.10 [A] emulsifies oil and grease in water. The hydrophilic part of the molecule is a chemical compound, commonly an acid group that presents a large affinity to water, while the hydrophobic part has a strong affinity to oil. The hydrophobic part intrudes into oil and grease to extract it as well as other loose defilement into the water, as illustrated in Figure 2.10 [B] and [C]. [Møller, 2003c].

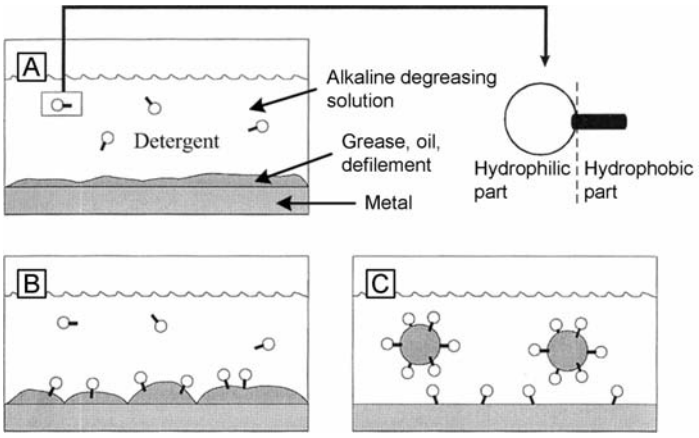

Figure 2.10: *Degreasing in alkaline bath. After [Møller, 2003c]*. [A]: *Detergent consisting of compound with hydrophilic and hydrophobic part.* [B]: *Hydrophobic part intrudes oil and grease.* [C]: *Hydrophobic part emulsifies oil and grease and other loose defilement.*

The function of the builders is to suspend the particles in the solution and to avoid that these precipitate on the metal surface again. Builders are normally composed of stable mixtures of silicate compounds and polyphosphates. [Møller, 2003c].

While dip-degreasing is merely based on chemical principles, electrolytic degreasing is largely based on the electrochemical theory described throughout Sections 2.1 and 2.2. During electrolytic degreasing the metal is submerged in an alkaline electrolyte and either cathodically or anodically polarised (cf. Section 2.2.4). That way, either hydrogen or oxygen evolution takes place on the metal surface (cf. Section 2.1.10), which "bursts off" remaining grease, oil, and defilement. The following half-cell reactions take place on the metal surface:

Anodic degreasing:

$$4OH^- \rightarrow O_2 + 2H_2O + 4e^- \quad \left(E_0^0 = 402\,\{401\}\,mV_{SHE} \right) \qquad [2.119]$$

Cathodic degreasing:

$$2H_2O + 2e^- \rightarrow H_2 + 2OH^- \quad \left(E_0^0 = -828\,\{-828\}\,mV_{SHE} \right) \qquad [2.120]$$

For carbon steel degreasing is always performed anodic, since the cathodic process often involves reduction of solved heavy metals on the surface, which might lead to a sludge-like deposition. However, cathodic degreasing is often applied for nobler metals, e.g. stainless steel. [Møller, 2003c].

An example for anodic degreasing of carbon steel samples with intense hydrogen evolution on the cathode is shown in Figure 2.11 [A].

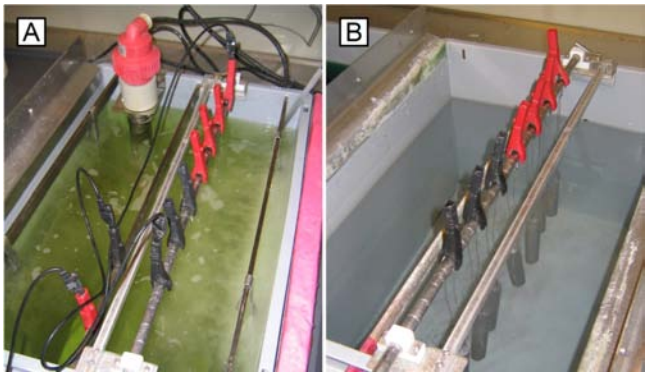

Figure 2.11: *Electrolytic degreasing of carbon steel samples.* [A]: *Anodic degreasing of rebar samples in alkaline bath.* [B]: *Acid pickling of rebar samples.*

After electrolytic degreasing and water rinsing (after each step in the process) a neutralisation process in an acid bath, generally referred to as acid pickling, is performed. In this process reaming alkaline products and oxides (in principle, passive layers, cf. Section 2.1.9), which might have evolved with oxygen evolution during the anodic cleaning process, are removed. The applied neutralisation solutions are often based on sulphate buffer systems ($HSO_4^- \leftrightarrow SO_4^{2-}$) with a pH around 2 and fluoride salts. Such solutions are effective for removal of thin oxide layers, as they immediately transform iron oxides to soluble fluoride complexes of iron, e.g.:

$$Fe_2O_3 + 6H^+ + 4F^- \rightarrow 2FeF_2^+ + 3H_2O \quad \left(\Delta G^0 = -100\,\text{kJ} \right) \qquad [2.121]$$

An example for acid pickling of carbon steel samples with moderate oxygen evolution on the metal surface is given in Figure 2.11 [B].

2.6.1.2 Etching

Besides sulphuric acid, hydrochloric acid, which was also applied in the experimental part of this project, is the most important etching agent for steel. Generally, solutions in concentrations from 10% to 25% are used for sulphuric and hydrochloric acid etching [Straschill, 1972]. The following chemical processes are considered to take place during etching of carbon steel [Møller, 2003c]:

- Sulphuric acid etching:

$$Fe_2O_3 + 3H_2SO_4 \rightarrow Fe_2(SO_4)_3 + 3H_2O \quad \left(\Delta G^0 = -162\ \text{kJ} \right) \qquad [2.122]$$

$$FeO + H_2SO_4 \rightarrow FeSO_4 + H_2O \quad \left(\Delta G^0 = -126\ \text{kJ} \right) \qquad [2.123]$$

$$Fe + H_2SO_4 \rightarrow FeSO_4 + H_2 \quad \left(\Delta G^0 = -135\ \text{kJ} \right) \qquad [2.124]$$

- Hydrochloric acid etching:

$$Fe_2O_3 + 6HCl \rightarrow 2FeCl_2^+ + 2Cl^- + 3H_2O \quad \left(\Delta G^0 = -166\ \text{kJ} \right) \qquad [2.125]$$

$$FeO + 2HCl \rightarrow FeCl_2 + H_2O \quad \left(\Delta G^0 = -39\ \text{kJ} \right) \qquad [2.126]$$

$$Fe + 2HCl \rightarrow FeCl_2 + H_2 \quad \left(\Delta G^0 = -47\ \text{kJ} \right) \qquad [2.127]$$

The dissolution of iron described by reaction [2.127] can be damped by addition of etching inhibitors, which are capable of slowing down the iron dissolution hydrogen ion reduction. [Møller, 2003c].

2.6.2 Electrolytic Plating

Electrolytic plating (henceforth, electroplating) is another beneficial application of electrochemical "corrosion" processes. This section provides a simplified description of the electroplating processes applied in the experimental part of this project.

In an electroplating cell, the plating metal is used as anode and the cathode corresponds to the metal to be plated. The required anodic and cathodic polarisation (cf. Section 2.2.3) is achieved by an external supply of direct current ('DC'), i.e. the anode is connected to the positive terminal of a current supply, and the cathode is connected to the negative (ground) terminal, see Figure 2.12.

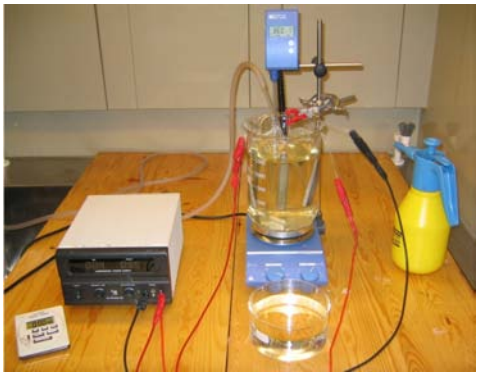

Figure 2.12: *Electroplating of zinc on grit-blasted smooth carbon steel rebar sample (cf. specimen types "C03/W03" and "C04/W04" in Section 1.9.4).*

When current is supplied to the cell, the metal anode is oxidised from the zero oxidation state to form cations with a positive charge (cf. Section 2.1.2):

$$Me \rightarrow Me^{n+} + ne^{-} \quad [2.128]$$

The metal cations associate with anions in the electrolyte and are eventually reduced at the cathode to deposit in the metallic form on its surface:

$$Me^{n+} + ne^{-} \rightarrow Me \quad [2.129]$$

Many plating baths include cyanides of the metal to be deposited as well as cyanides of other metals, e.g. potassium cyanide. These free cyanides facilitate dissolution at the anode and thereby facilitate to maintain a constant metal ion level in the electrolyte and contribute to the conductivity of the bath. Additionally, non-metal chemicals such as carbonates and phosphates are often added to increase the conductivity. [Møller, 2003c]. Besides these standard compounds, plating baths can contain various other substances, e.g. to achieve certain characteristics of the plating. Hence, the chemical equilibria in the baths become rather complex. For detailed information on these and other aspects, reference is made to standard books concerning electroplating (e.g. [Kanani, 2000]) or general surface technology (e.g. [Møller, 2003c]).

The current density has a major influence on the deposition rate, plating adherence, and plating quality. Moreover, the current density varies significantly over the cathode surface; outside surfaces tend to have a higher current density than inside surfaces (e.g. holes, bores, etc.). The higher the current density, the faster the deposition rate, but there is a practical limit enforced by poor adhesion and plating quality, when the deposition rate is too high. Recommended current densities for different metals and electrolytes can be found in the literature, e.g. [Kanani, 2000]. Finally, it should be noted that current densities applied in electroplating deviate largely from the exchange current densities mentioned in Section 2.2.2. For instance, the dissolution of zinc in sulphuric acid take places with about 2×10^{-11} A/cm^2 (cf. Section 2.2.2) compared to 6×10^{-2} A/cm^2 for deposition of zinc in an acid bath [Møller, 2003c].

In the experimental part of the project, zinc coating of carbon steel rebar was one of the applied electroplating processes. Electroplating was preferred to other galvanisation processes, i.e. hot-dipping or thermal spraying (cf. Section 6.3.2.5), due to its low process temperature and the possible precise control of the layer thickness. These two aspects were important, as application of thin and controlled layers was feasible without interference and hence allowing for performance comparison with other surface treatments/modifications (cf. Section 1.9). The Zn-Fe layer (cf. Section 6.3.2.5), as formed in hot-dip galvanising, does not exist beneath electroplated zinc. So, Zn-Fe complexes, which we consider to provide for largely improved corrosion resistance, can only be formed from ions of the zinc layer (with a very limited thickness of 2 µm in our investigations, cf. Sections 1.9.3 and 1.9.4) combining with iron ions from the substrate. These and other aspects of zinc are described with particular regard to application in the concrete environment in Sections 6.3.2.5 (general theory and available countermeasures) and 7.3.1 (our application in the proposed new countermeasures).

3 Properties of Concrete and Reinforcing Steel

Considering the multi-faceted chemistry of concrete and its particular physical characteristics as well as the metallurgical and surface properties of carbon steel, the concrete steel system represents a complex chemical/electrochemical system. The description of corrosion processes in such a complex system as well as the evaluation and the design of solutions for corrosion protection, i.e. countermeasures, require a profound knowledge on all decisive parameters concerning the concrete and the steel alone as well as on the interaction between the two materials from a physical, chemical, and electrochemical point of view. Furthermore, detailed knowledge on the manifold parameters concerning the application of the reinforced concrete member (in particular, with regard to structural and exposure conditions) is essential.

This Section summarises the above mentioned aspects, while focussing on the most important parameters that are of relevance for the purpose of this thesis. A brief description of selected properties of Portland cement concrete and carbon steel reinforcement is given, which is limited to the essential information concerning properties in relation to corrosion. Concerning concrete, emphasis is on the concrete porosity and the associated transport properties as well as the composition of the pore solution (Section 3.1). Concerning carbon steel reinforcement, emphasis is set on the metallurgical and surface properties (Section 3.2). The influence of both the concrete and the carbon steel properties on the concrete-steel interface is dealt with in the separate Section 3.3.

3.1 Portland Cement Concrete

Concrete is a composite material composed of granular material, i.e. the aggregate, embedded in a more or less dense matrix of cement paste that fills the space between the aggregate particles and glues them together. The cement paste consists of the reaction products and possible remains of the reactants, cement, and mixing water.

Aggregates can be obtained from different kinds of materials, but predominantly natural materials, i.e. sand and gravel, are used. Sand and gravel are generally inert and non-porous, but often contain low concentrations of chlorides. Concrete deterioration by ‘ASR’ (cf. Section 6.1) can be of concern, if certain reactive aggregates containing amorphous silica are used. Potable water with varying compositions depending on the local properties is generally used as mixing water.

Cements are fine mineral powders that, when mixed with water, form a paste that sets and hardens due to hydration reactions. Cement is a generic term and can apply to dif-

ferent classes of binders. The present thesis is focused on Portland cement* concrete, which is used for most civil engineering structures [Mindess et al., 2003]. However, mineral additions and chemical admixtures to obtain specific concrete properties are briefly dealt with in Section 6.3.1.1.

The following terms are used to distinguish between Portland cement based compositions with regard to their aggregate content:

- Concrete: A composite material of fine and coarse aggregates, i.e. sand (grain size ≤ 4 mm) and gravel (grain size > 4 mm), Portland cement, and water
- Mortar: A composite material of fine aggregates, i.e. sand (grain size ≤ 4 mm), Portland cement, and water
- Cement paste: A composite material of Portland cement and water.

The most important European standards concerning the specification, performance, and production of structural concrete are [DS/EN 206-1, 2002], which is complemented by additional national rules (e.g. [DS 2426, 2004] for Denmark), and, besides the cement specifications (cf. Section 3.1.1), supplemented by the standards for aggregates for concrete [DS/EN 12620, 2004] and mixing water [DS/EN 1008, 2002]. The corresponding US equivalents are the standard specifications for structural concrete [ACI 301M, 2005], concrete aggregates [ASTM C33, 2007], and mixing water [ASTM C1602M, 2006].

3.1.1 Portland Cement

In simple terms, Portland cement is produced by grinding clinker, which is obtained by burning a suitable mixture of limestone, clay and other suitable materials. The burning takes place in a kiln at 1400°C to 1600°C, which is the temperature range in which the two materials interact chemically [Mindess et al., 2003].

The main components of Portland cement are tricalcium silicate ($3CaO{\cdot}SiO_2$), dicalcium silicate ($2CaO{\cdot}SiO_2$), tricalcium aluminate ($3CaO{\cdot}Al_2O_3$), and tetracalcium ferroaluminate ($4CaO{\cdot}Al_2O_3{\cdot}Fe_2O_3$). Gypsum ($CaSO_4{\cdot}2H_2O$) is added to the clinker before or during grinding to control the rate of hydration of the aluminates [Neville, 1995].

Portland cements are specified in [DS/EN 197-1, 2001; ASTM C150, 2007]. The chemical analysis in Table 3.1 presents a typical cement composition of rapid Portland cement Type I [DS/EN 197-1, 2001; ASTM C150, 2007], which is the cement that was used in the experimental investigations of this project.

* Portland cement refers to a family of calcium silicate cements. The prefix "Portland" was coined by Joseph Aspdin (UK, 1778-1855), because of the real or fancied similarity of the hardened cement to a popular, naturally occurring limestone quarried at the Isle of Portland, UK, which was used in many 18th and 19th century buildings in southern England [Mindess et al., 2003; Wikimedia, 2007].

Table 3.1: *Chemical analysis of rapid hardening Portland cement CEM I 52.5. From (AP, 2005). This cement type was used as the standard cement in all experimental investigations (cf. Section 1.9.2).*

Component	Unit	Amount	Component	Unit	Amount
SiO_2	%	19.78	As	mg/kg	< 30*
Al_2O_3	%	5.09	Co	mg/kg	< 20*
Fe_2O_3	%	3.79	Cd	mg/kg	< 10*
CaO	%	63.64	Sb	mg/kg	< 20*
P_2O_5	%	0.34	Cu	mg/kg	108
MgO	%	0.87	Pb	mg/kg	< 20*
SO_3	%	3.19	Zn	mg/kg	151
Cl	%	0.026	V	mg/kg	75
K_2O	%	0.41	Cr	mg/kg	40
Na_2O	%	0.27	Mn	mg/kg	248
Ignition loss	%	2.15	Ni	mg/kg	42

* The value is below detection limit.

3.1.2 Hydration

During hydration the gross volume of the cement paste (cf. Section 3.1.3) remains practically unchanged and the initial volume, which corresponds to the sum of the volumes of the mixing water and the cement, is equal to the volume of the hardened cement paste. The hardened cement paste consists of the sum of the volume of cement that has not yet reacted, the hydrated cement, and the capillary pores that are filled by water or by air. The volume of the products of hydration can be assumed to be roughly double that of the cement. Hence, the hydration products fill the space previously occupied by the cement and part of the surrounding space initially occupied by water. If the cement paste is kept moist during curing, the hydration proceeds and the capillary pore volume decreases and reaches a minimum, when the hydration of the cement is completed. [Neville, 1995; Boulfiza et al., 2003].

In conclusion, the volume of the capillary pores in the cement paste increases with increasing ‘w/c’ and decreases with increasing degree of hydration. In principle, the effect of hydration on the diffusion coefficient can be considered to be of importance during the first six maturity month after casting [Nielsen, 2001]. The rate of chemical reactions between water and cement is also dependent on the temperature. An increased temperature will accelerate the hydration. However, increased curing temperature can also lead to a coarser and an increased porosity of the hardened cement paste.

3.1.3 Cement Paste

Given that dense and inert aggregates are used, the structure and composition of the cement paste to a large extent determines the strength, the durability, and accordingly the long-term performance of the concrete.

The development of strength, i.e. the hardening of cement paste, which follows solidification, is governed by the hydration of silicates. The hydration of tricalcium silicates and dicalcium silicates results in calcium silicates hydrates forming a rigid gel, commonly referred to as 'C-S-H', i.e. calcium-silicate-hydrate. 'C-S-H' is composed of extremely small particles with a layer structure that aggregates in formations of a few μm in dimension, characterised by interlayer spaces of smaller dimensions (< 2 nm) and by a large surface area (100-700 m^2/g). Hydration of calcium silicates also produces hexagonal crystals of $Ca(OH)_2$, also referred to as portlandite. The crystals are in the order of few μm in dimension and occupy 20 to 25% of the volume of solids. They do not contribute to the strength of the cement paste, except that they fill space. $Ca(OH)_2$ as well as NaOH and KOH, which are present in small amounts, are also important with regard to protecting the reinforcement, because they largely determine the composition of the pore solution (cf. Section 3.1.5). The hydration of tricalcium aluminate and tetracalcium ferroaluminate leads, among others, to hydrated calcium sulphoaluminates. [Neville, 1995; Mindess et al., 2003; Bertolini et al., 2004].

3.1.4 Porosity

A crucial property of concrete is its porosity, as it largely determines the strength and transport properties. Considering the aggregates to be non-porous, the cement paste determines the porosity of the concrete. The hydrated cement paste always contains pores of diverse dimensions.

The structure of 'C-S-H' gel and the nomenclature of the porosity is still a matter of debate. According to [Bertolini et al., 2004] the interlayer spacing between 'C-S-H' sheets, the so-called gel pores, ranges from fractions of one nm to several nm in dimensions and obtain a volume equal to about 28% of the gel. The smaller gel pores do not affect the durability of the concrete and its protective function for the reinforcement, as they are too small to allow significant transport of species (cf. Sections 3.1.6 and 3.1.7). The capillary voids are the pores, which are not filled by the solid hydration products in the hardened cement paste. They have dimensions of 10 to 50 nm, if the cement paste is well hydrated and produced using low 'w/c' ratios, but can reach up to 3-5 μm, if the concrete is based on high 'w/c' ratios or is not sufficiently hydrated. Larger pores of dimensions of up to some mm are the result of air bubbles and voids that were not removed by proper compaction of the fresh concrete. Air bubbles with diameters of about 0.05-0.2 mm can also be intentionally introduced in the cement paste by means of air-entraining admixtures to enhance the resistance to freeze-thaw cycles (cf. Section 6.1). Both capillary pores and air voids are relevant to the du-

rability of concrete and its protection of the reinforcement. [Neville, 1995; Mindess et al., 2003; Bertolini et al., 2004].

Not only the pore and void dimensions are of concern, when dealing with the ingress properties of concrete, but also their connectivity, i.e. the percolation characteristics, since ingress of species that penetrate the concrete from the outside requires an interconnected path. In relation to that, the so-called interfacial transition zone 'ITZ' is of importance. The 'ITZ' refers to the vicinity of the aggregates*, where the porosity of the paste is higher than in the remaining paste (bulk paste) due to restricted packing of the original cement grains. Thus, the 'ITZ' has an increased diffusivity, which according to [Jensen, 1999] can be up to 10 times higher than the diffusivity in the bulk cement paste.

3.1.5 Pore Solution

The chemical composition of the pore solution of the hydrated cement paste depends on the composition of the concrete, mainly on the type of cement, but also on the exposure conditions.

As shown in the first two rows of Table 3.2, in uncarbonated and chloride-free Portland cement concrete the pore solution consists mainly of sodium hydroxide and potassium hydroxide, while KOH is predominant. Depending on the composition of the cement, the pH of the pore solution is in the range of 13-14, while concrete containing pozzolans can have lower pH values. The concentration of hydroxyl ions varies from 0.1 mol/L to 0.9 mol/L. Other ions, e.g. calcium ions and sulphate ions (SO_4^{2-}), are also part of the pore solution, but in rather low concentrations.

Table 3.2: *Ionic concentration measured in the pore solution extracted from cement pastes and mortars made with Portland cement. After [Bertolini et al., 2004]. CO_2 represents carbonation and NaCl stands for sodium chloride added to the mix.*

Mix	'w/c'	CO_2	NaCl	Age	OH^-	Na^+	K^+	Ca^{2+}	SO_4^{2-}	Cl^-
			% 'w/w_{ce}'	days	10^{-3} mol/L					
Paste	0.5	No	0	28	834	271	629	1	31	-
Mortar	0.5	No	0	192	251	38	241	< 1	8	-
Paste	0.5	Yes	0	-	< 3	< 23	< 20	31	-	< 16
Paste	0.5	No	1%	-	458	580	208	-	-	227
Paste	0.5	Yes	1%	-	< 1	< 269	< 31	21	-	< 651

* In some literature the vicinity of the reinforcement is also referred to as 'ITZ'. However, due to the importance of this region with regard to reinforcement corrosion, it is referred to as concrete-steel interface throughout this thesis and hence distinguished from the 'ITZ' of aggregates.

Rows three to five show that the composition of the pore solution is largely affected by carbonation and by the penetration of chloride ions, which is discussed in Section 5.2.2.1 and Section 5.2.2.2, respectively.

3.1.6 Transport Mechanisms

The transport of gases, liquids, and ions through the cement paste gel is governed by a variety of physical and chemical mechanisms. The transport mechanisms that we consider to be most important with regard to reinforcement corrosion are:

- Diffusion (cf. Section 3.1.6.1)
- Capillary suction (cf. Section 3.1.6.2)
- Migration (cf. Section 3.1.6.3)
- Permeation, i.e. the transport of liquids or gases caused by a pressure head [Kropp & Hilsdorf, 1995]
- Transport induced by secondary mechanisms, e.g. freeze and thaw cycles [Geiker & Thaulow, 1996].

Diffusion, capillary suction, and migration are relevant for the purpose of this thesis and the theoretical background of these mechanisms is briefly described in Sections 3.1.6.1, 3.1.6.2, and 3.1.6.3, respectively.

3.1.6.1 Diffusion

Diffusion in concrete can be defined as the *"transfer of mass by random motion of free molecules or ions in the pore solution, resulting in a flow from regions of higher concentration to regions of lower concentration of the diffusing substance"* [Kropp & Hilsdorf, 1995].

To quantify and predict diffusion in concrete, models based on Fick's second law of diffusion are generally used. Fick's second law of diffusion is formulated as:

$$\frac{\partial C}{\partial t} = \frac{\partial}{\partial x}\left(D \times \frac{\partial C}{\partial t} \right) \qquad [3.1]$$

with 'C' as the concentration of the diffusing substance and 'D' as the associated diffusion coefficient.

For an infinite source of a diffusing substance the common error function solution to Fick's second law of diffusion solves the partial differential equation, assuming constant 'D' and surface concentration ('C_s'):

$$C(x,t) = C_s - (C_s - C_i) \times \mathrm{erf}\left(\frac{x}{2 \times \sqrt{D \times t}} \right) \qquad [3.2]$$

This means that the total concentration 'C' of a diffusing substance at a certain depth 'x' and time 't' can be determined based on the total concentration at the exposed surface ('C_s') and the initial concentration in the material ('C_i'). The error function ('erf') (in the literature also referred to as Gauss error function) is described as:

$$\mathrm{erf}(z) = \frac{2}{\sqrt{\pi}} \times \int_0^z \exp\left(-u^2\right) du \qquad [3.3]$$

3.1.6.2 Capillary Suction

Capillary suction (in the literature also referred to as sorption) can be defined as the *"transport of liquids in porous solids due to surface tension acting in capillaries"* [Volkwein, 1991]. The extent of capillary suction is largely influenced by the degree of saturation [Neville, 1995]. Moreover, capillary suction depends on the characteristics of the liquid, e.g. viscosity, density, and surface tension, as well as on the characteristics of the pore structure in the material, e.g. tortuosity, continuity, and radius [Kropp & Hilsdorf, 1995]. Under steady-state flow capillary suction, the flow of a liquid ('F_{liq}') in a pore system can be described by [Kropp & Hilsdorf, 1995]:

$$q = -\frac{k_p}{\eta_{vis}} \times \frac{\partial p_{pw}}{\partial x} \qquad [3.4]$$

where ('k_p') is the coefficient of moisture permeability, ('η_{vis}') is the viscosity of the liquid, and ('p_{pw}') is the pore water pressure.

However, due to the many irregularities in the pore system, the behaviour of concrete diverges largely from the theory, and empirical formulas are normally used to predict the effect of capillary suction.

3.1.6.3 Migration

Migration can be defined as the *"transport of ions in electrolytes due to the action of an electrical field as the driving force"* [Kropp & Hilsdorf, 1995].

The velocity of the ion movement is proportional to the strength of the electric field and the charge and size of the ion. The ion mobility ('u_i') can be directly related to the diffusion coefficient 'D' [Bertolini et al., 2004]:

$$D = \frac{R \times T \times u_i}{n \times F} \qquad [3.5]$$

The contribution of a certain ion to the ionic current through an electrolyte increases with the concentration and the mobility of the ion. *Hydrogen and hydroxyl ions show the highest ion mobilities, and their conductivity is much higher than the one of other ions due to their interaction with the solvent water* [Bertolini et al., 2004]. The transport of these ions does not require their actual displacement, but is rather based on a

series of breaks and modifications of bonds within the water molecules [Bertolini et al., 2004].

Cations, e.g. H^+, K^+, Na^+, and Ca^{2+}, migrate towards negative electrodes, i.e. cathodic sites, whereas anions, e.g. OH^-, SO_4^{2-}, and Cl^-, are attracted by positive electrodes, i.e. anodic sites. Based on this concept, ionic current "flow" in reinforcement corrosion should not be assigned a certain "direction" (as done in most textbooks). All ions present in the concrete bulk can discharge the cations and anions formed at the anodic and cathodic sites, respectively, and thus contribute in preserving the electrical neutrality. This also is a central aspect in the formation of macrocells (cf. Section 3.1.8). Moreover, based on the above and with regard to the mobilities of H^+ and OH^-, we question the common notion in the literature on reinforcement corrosion concerning the nature of ionic current, i.e. that the ionic current is established by migration of ferrous ion to cathodic sites combining with hydroxyl ions to form iron hydroxide (cf. Section 5.1.3). These considerations play a major role in the proposed description of corrosion processes of steel in concrete (cf. Chapter 5).

3.1.7 Ingress and Ion Mobility

A particular feature of reinforced concrete is that the concrete bulk itself provides the means to largely influence the reaction kinetics as well as the thermodynamic state of the embedded metallic reinforcement. On the hand, this influences the corrosion processes itself; on the other hand, this aspect provides various options for the implementation of countermeasures, which appear to be getting more and more out of sight in the present day countermeasure approaches. The special characteristics of the concrete bulk with regard to reinforcement corrosion are dealt with in this Section.

In Sections 3.1.1 to 3.1.6 the most important parameters determining the ingress and conductivity properties of concrete have been introduced. The influence of these parameters on the initiation and propagation of reinforcement corrosion is mainly governed by the exposure conditions and the quality and depth of the concrete cover, because these factors control the penetration of oxygen, carbon dioxide, and chloride ions as well as the mobility of ions, i.e. the conductivity. Hence, the resistance of the concrete cover against penetration of carbon dioxide and chloride ions largely determines the extent of the initiation phase. As described in more detail in Chapter 5, the penetration of oxygen and the mobility of ions also have a major contribution in the initiation phase, and they are the governing factors once active corrosion has been initiated, i.e. in the propagation phase. Thus, in principle, the characteristics of the concrete cover in relation to the exposure conditions govern the corrosion of the reinforcement.

In Section 1.3 the potentiating effect of cracks on the ingress of species and hence on the initiation and propagation of reinforcement corrosion was indicated. Cracking of concrete and the effect of cracks on the factors governing reinforcement corrosion are

dealt with in Section 3.1.11. In Sections 3.1.7.1, 3.1.7.2, 3.1.7.3, and 3.1.7.4, ingress of oxygen, ingress of carbon dioxide, ingress of chloride ions, and the ion mobility in concrete are summarised. For a more detailed description of these properties, in particular with regard to structural situations and real environmental conditions, which are only marginally treated in the present thesis, reference is made to standard textbooks, e.g. [Bentur et al., 1997; Cigna et al., 2003; Bertolini et al., 2004; Böhni et al., 2005; Raupach et al., 2007].

3.1.7.1 Ingress of Oxygen

The diffusion coefficient of oxygen through the cement paste has been specified to be in the range of 1×10^{-9} to 100×10^{-9} m^2/s, while the specific value is dependent on the pore structure and on the degree of saturation [Tuutti, 1982; Bentur et al., 1997; Bertolini et al., 2004; Böhni et al., 2005]. As mentioned in Section 3.1.2, the 'w/c' has a major effect on the pore structure. The effect of the 'w/c' and the degree of saturation on the oxygen diffusion can be exemplified by selected results from Figure 3.1 [A] and [B], respectively.

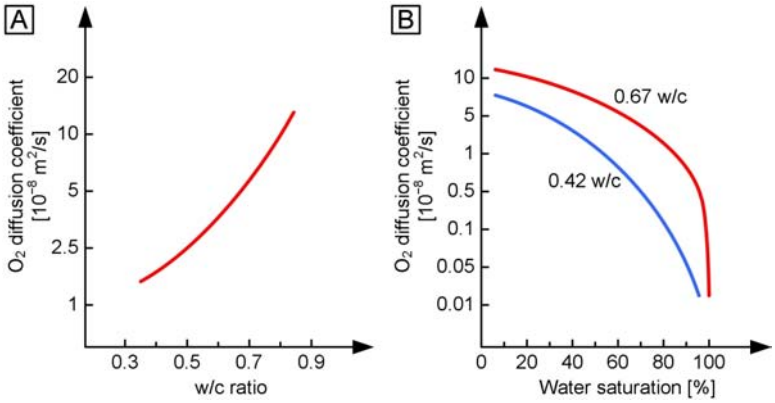

Figure 3.1: *Effect of cement paste properties on oxygen diffusion coefficient. After [Tuutti, 1982].* [A]: *Effect of 'w/c' on the oxygen diffusion coefficient in cement paste at 50% water saturation.* [B]: *Effect of water saturation on the oxygen diffusion coefficient of 0.42 and 0.67 'w/c' cement pastes.*

For example, from Figure 3.1 [A] it can be concluded that for cement paste at 50% saturation, the effective oxygen diffusion coefficient of 0.8 'w/c' paste is almost an order of magnitude higher than the one of 0.4 'w/c' paste. Figure 3.1 [B] shows that, for instance, a decrement of saturation from 100% to 50% increases the oxygen diffusion coefficient of 0.42 'w/c' paste more than an order of magnitude and the one of 0.67 'w/c' paste more than two orders of magnitude.

3.1.7.2 Ingress of Carbon Dioxide

Carbonation takes place in moist environments, where atmospheric CO_2 forms an acid aqueous solution that reacts with the hydrated cement paste and thereby neutralises the alkalinity of the concrete. Corrosion inducing conditions for carbon steel in concrete can generally be regarded to be attained at a pH approaching neutrality* at the level of the reinforcement, if the concrete is free of other corrosion promoting substances, in particular depassivating ions, i.e. most importantly chloride ions. So, if the carbonated concrete is not contaminated by chloride ions, the pore solution is almost composed of "pure water" (cf. row three of Table 3.2 in Section 3.1.5), which means that, in principle, carbon steel in humid carbonated concrete corrodes as in contact with water. Our model for the description of carbonation induced corrosion is given in Section 5.2.2.1. Another important consequence of carbonation is that chloride, which has been fixated in the paste (chloride binding, cf. Section 3.1.7.3), is liberated with decreasing pH, making the pore solution even more aggressive (cf. row five of Table 3.2 in Section 3.1.5).

The carbonation reaction starts at the external surface and penetrates into the concrete. As mentioned in Section 3.1.5, the alkaline constituents of concrete are mostly present in the pore liquid, mainly as sodium and potassium hydroxides, but also in the solid hydration products, e.g. $Ca(OH)_2$ or 'C-S-H'. Calcium hydroxide is the hydrate in the cement paste that reacts most readily with CO_2, e.g. described by [Freiesleben Hansen, 1995]:

$$CO_2 + Ca(OH)_2 \rightarrow CaCO_3 + H_2O \quad \left(\Delta G^0 = -73\,\text{kJ} \right) \qquad [3.6]$$

Carbonation does not cause any damage to Portland cement concrete itself, although it can cause the concrete to shrink, which can lead to cracking (cf. Section 3.1.11.1). Especially for Portland cement, carbonation can even reduce the porosity and lead to an increased strength. In contrast to that, the porosity of concrete with high slag content is increased by carbonation.

It has been suggested that the diffusion coefficient of carbon dioxide is similar to the one of oxygen [Tuutti, 1982; Bentur et al., 1997]. The time dependent penetration of carbonation is generally described by:

$$d = k_{car} \times t^{\frac{1}{n}} \qquad [3.7]$$

where ('d') is the depth of carbonation in [mm] and 't' is time in years and ('k_{car}') in [$mm/y^{1/n}$] is a constant which depends on the effective diffusivity of CO_2 in the concrete, the ambient CO_2 concentration, and the reactivity of the cement paste with CO_2

* It appears that there are different concepts concerning the critical pH in the literature. Some literature considers the critical pH as being close to neutrality, whereas other literature refers to pH 8 or even pH 9. We decided to base our considerations with regard to carbonation induced corrosion on a bulk pH of 8 (cf. Section 5.2.2.1).

under the prevailing moisture conditions. The inverse exponent ('n') is usually about 2. However, the rate of carbonation decreases with time, as the CO_2 has to diffuse through the pores of the already carbonated outer layers. In highly impervious concrete the carbonation rate even tends to become negligible after a certain time.

The chemical reaction rate of carbonation depends largely on the ambient relative humidity. As shown in Figure 3.2 [A], CO_2 will hardly react with completely dry concrete and CO_2 cannot penetrate fully saturated concrete. The interval which is most critical in promoting carbonation is from 60% to 70% relative humidity, i.e. moisture contents low enough to permit ready penetration by the CO_2 gas, but high enough so that there is sufficient water for CO_2 chemical reaction.

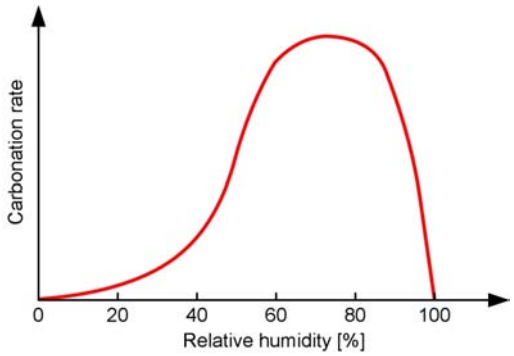

Figure 3.2: *Schematic representation of the rate of carbonation of concrete as a function of relative humidity. After [Bertolini et al., 2004].*

Measurement of the depth of carbonation are normally carried out by spraying an indicator on a freshly broken split faces, which are in practice often obtained from e.g. cores [Mays et al., 1992; Broomfield, 1997].

Normally, an alcoholic solution of phenolphthalein ($C_{20}H_{14}O_4$) is used as indicator. Such solutions, which are commercially also known as deep purple indicators (e.g. by Germann Instruments[*]), are qualitative (i.e. "positive-negative") indicators to determine location of the carbonation front. Areas where the pH exceeds 8.5 to 9.5 take on a pinkish colour, which is typical for phenolphthalein in a basic environment, whereas the colour of carbonated areas remains unchanged, see Table 3.3.

More sophisticated indicators (e.g. the rainbow indicator, which also is commercially available from Germann Instruments) provide a set of different colours that can be associated with certain ranges of concrete pH, as illustrated in Table 3.3.

[*] Germann Instruments A/S, Copenhagen, Denmark

Table 3.3: *Colour code for the deep purple and the rainbow indicator commercially available from Germann Instruments. After [Campbell et al., 1991; GI, 2006].*

Indicator	pH and associated colour				
Deep purple indicator	< 8.5-9.5			> 8.5-9.5	
Rainbow indicator	5	7	9	11	13

Both phenolphthalein and the rainbow indicator have been applied in our experimental investigations. However, the application aimed at estimation of the bulk pH and the pH in the vicinity of the concrete-steel interface (cf. Section 3.3) rather than on the characterisation of the carbonation front. Experimental results, which are based on the application of phenolphthalein and the rainbow indicator, are exemplified in Section 5.2.2.2.

3.1.7.3 Ingress of Chloride Ions

Most often critical chloride contents in concrete arise with penetration of chloride ions through the concrete cover from the outside, when the external surface of the structure is exposed to e.g. sea salt spray, direct seawater, or deicing salt. However, chlorides can also be incorporated into the original mix due to their presence in the constituent materials or, as accepted until the mid 1970s in Europe for acceleration of cement hydration, deliberately added as calcium chloride ($CaCl_2$). Nowadays, design codes for reinforced and prestressed structures impose restrictions on the amount of chloride introduced to the concrete mix from constituent materials. For instance, [DS/EN 206-1, 2002] limits the maximum chloride content to 0.2% and 0.4% 'w/w_{ce}' for reinforced and to 0.1% and 0.2% 'w/w_{ce}' for prestressed concrete structures. The chloride content class, which depends on the provisions valid in the place of use of the concrete, determines which of the two specified values is governing. Moreover, it is specified that calcium chloride and chloride based admixtures shall not be added to concrete containing steel reinforcement, prestressing steel reinforcement, or other embedded metal. For structures *"not containing steel reinforcement or other embedded metal with the exception of corrosion-resisting lifting devices"* [DS/EN 206-1, 2002] limits the chloride content to 1.0% 'w/w_{ce}'.

The chloride diffusion coefficient in concrete is lower than the one of oxygen and CO_2. It has been determined to be in the range from 10^{-13} m/s^2 to 10^{-11} m/s^2 [Tuutti, 1982; Nilsson et al., 1996; Bentur et al., 1997; Bertolini et al., 2004]. A method for the determination for the diffusion coefficients has been standardised in the Nordic countries, i.e. NT BUILD 443 [Frederiksen, 1997]. As for oxygen and CO_2 diffusion, the 'w/c' has a major effect on the chloride diffusion effect, which has been investigated and quantified in several studies. Selected results, which illustrate that the chloride diffusion coefficient increases largely with increasing 'w/c', are summarised for cement paste and concrete in Table 3.4.

Table 3.4: *Effective diffusion coefficient of chloride ions through cement paste and concrete in 10^{-12} m/s^2 from different sources.* [A]: *[Page et al., 1981]*. [B]: *[Tuutti, 1982]*. [C]: *[Berke & Hicks, 1992]*.

'w/c'	0.4	0.5	0.6	Source
Cement paste	2.6	4.5	12.4	[A]
Concrete	0.8-5	-	8-12	[B]
Concrete	2	11	-	[C]

It is difficult to acknowledge the significance of the variations in the diffusion coefficients without calculating concentration profiles at different ages. Selected results from the literature are shown in Figure 3.3 [A].

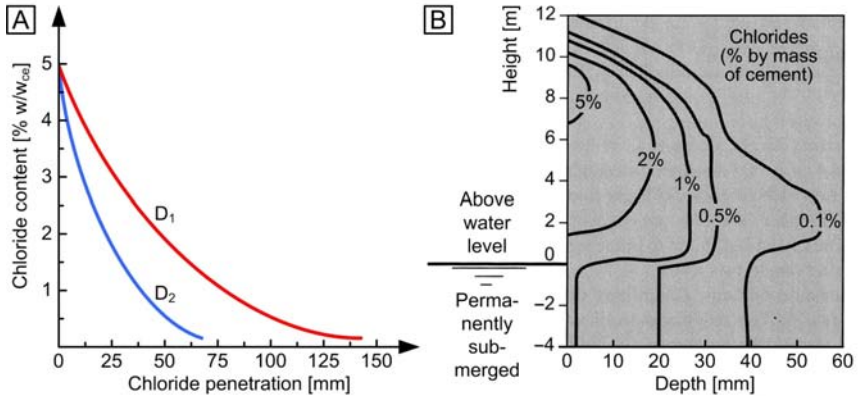

Figure 3.3: [A]: *Diffusion profiles of chloride ions in normal and high quality concrete with diffusion coefficients of 'D_1' = 5×10^{-12} m/s^2 and 'D_2' = 0.1×10^{-12} m/s^2, respectively. After 30 years of diffusion, assuming a constant chloride ion concentration of 5% 'w/w$_{ce}$' on the concrete surface (cf. Section 3.1.6.1). After [Bentur et al., 1997]*. [B]: *Example of chloride profiles in a marine structure as a function of the height above the seawater level. After [Bertolini et al., 2004]*.

Concentration profiles can be predicted based on Fick's second law, as described in Section 3.1.6.1. The profiles shown in Figure 3.3 [A] were calculated based on an initial surface chloride concentration of 5% 'w/w$_{ce}$' and diffusion coefficients of 5×10^{-12} m/s^2 representing normal concrete and 0.1×10^{-12} m/s^2 for high quality concrete [Bentur et al., 1997].

While such calculations are useful in predicting at least a lower bound to the expected service life, it should be emphasised that such profiles are only valid for concrete continuously and fully submerged in chloride-containing water, i.e. with diffusion as the sole transport mechanism. In practice, the exposure conditions are often much more complex. Depending on the exposure situation and the location of the structure or the

structural part, the ingress of chloride ions is predominately governed by one of transport mechanisms described listed in Section 3.1.6 or a combination of these.

For example, an exposure situation of major concern with regard to chloride induced corrosion is the so-called splash zone of marine structures, which is considered to be located between three meters above and three meters below the maximum and minimum sea level, respectively [Frederiksen & Poulsen, 1997]. In this zone, concrete is exposed to constant wetting by waves and tidal changes. Dry periods cause a progressive build-up of chloride on the surface of the concrete, sometimes to very high levels. As a result, when the concrete is rewetted, the chloride ingress rate is largely enhanced. Thus, a complex combination of transport mechanisms, mainly diffusion, capillary suction, and evaporation, leads to unpredictable chloride profiles as sketched in Figure 3.3 [B].

Part of the chlorides entering the concrete bulk will be fixated in the paste, where both 'C-S-H' and reaction products of alumina binds chlorides. This process is generally referred to as chloride binding. Chloride binding is reversible, e.g. carbonation causes release of fixated chlorides (cf. Section 3.1.7.2). The distribution of chlorides between the different phases and the pore solution can be calculated by means of thermodynamic models, given that information on solubility products is available for the relevant phases from assumed phase equilibria in hydrated Portland cement [Nielsen, 2004; Nielsen et al., 2005b; Nielsen et al., 2005a; Geiker et al., 2007]. The effect of chloride binding is of major importance with regard to the proportion between the total chloride content and the chloride content in the pore solution, which is generally considered to determine corrosion initiation and propagation. Concerning the chloride content in the pore solution, typical compositions are exemplified in rows four and five of Table 3.2 in Section 3.1.5 for chloride contaminated concrete without and with carbonation, respectively. Chloride contents for corrosion initiation and the proposed thermodynamic mechanism for chloride induced corrosion are discussed in Sections 3.1.9 and 5.2.2.2, respectively.

Chloride binding is also of major importance with regard to the determination of the chloride contents, which is a central part in the service life assessment of a reinforced concrete structure. For instance, actual chloride profiles determined from bore cores by profile grinding and subsequent titration can be used to calibrate the ingress models enabling a service life update (cf. Section 1.5). Standard methods for the chemical determination of the chloride content of hardened concrete are described e.g. in [DS/EN 14629, 2007]. In the experimental part of this project the so-called colour test [Frederiksen, 1997] was used to determine the depth of ingress. Similar to the phenolphthalein test described in Section 3.1.7.2, the colour test is a rapid, qualitative indication of the chloride content based on a colour change from a certain chloride concentration in the pore solution. For the colour test a 0.1 N silver nitrate ($AgNO_3$) solution is sprayed on a split face of the investigated concrete sample. $AgNO_3$ reacts with the chloride leading to pinkish-grey colour change for areas of the concrete, where the

content of chloride exceeds a certain concentration that depends among others on the chemical composition of the mortar. For instance, the chloride concentration for colour change of mortar (B), which was used as the "standard" mortar in our experimental investigations (cf. Section 1.9.2), was determined by profile grinding and titration to be in the range of 0.4% 'w/w_{ce}'.

3.1.7.4 Ion Mobility

For corrosion to be initiated and to propagate, the concrete in the vicinity of the steel also must provide a path for the ionic current between anodic and cathodic sites of the steel surface (cf. Section 3.1.6.3). The transport rate of this current can be the limiting factor for the corrosion rate, i.e. the propagation phase, but it also has a major influence on corrosion initiation, in particular with regard to the chloride threshold (cf. Section 3.1.9). The transport rate of ionic currents can be expressed in terms of the resistivity of the concrete, which, similar to the ingress properties, depends on its physical and chemical characteristics. The resistance to the ionic current flow, i.e. the resistivity of the concrete, is primarily influenced by three factors: the pore structure (cf. Section 3.1.2), the composition of the pore solution (cf. Section 3.1.5), and the moisture content, i.e. the degree of saturation.

As described in Section 3.1.2, concretes of low 'w/c' have a lower pore volume and thus fewer channels available for ion transport, so that the resistivity is higher than the one of concretes of high 'w/c'. Besides the effect of total pore volume, low 'w/c' concretes generally have smaller pores and pores which are more easily isolated by growth of hydration products at critical interconnections, so that the resistivity is further increased. Accordingly, the resistivity of the concrete is dependent on the same factors as the resistance against ingress of oxygen, carbon dioxide, and chloride ions that were described in Sections 3.1.7.1, 3.1.7.2, and 3.1.7.3, respectively.

The pore solution provides the primary medium for the ion transport. This solution generally has a sufficient concentration of alkali and hydroxide ions to be a satisfactory electrolyte. However, if the concrete dries out or self-desiccates and the water content and degree of saturation of the pores are reduced, the pore spaces are partly emptied and the difficulty of ion transport is consequently multiplied [Nielsen & Geiker, 2003]. This is true even though the actual concentration of electrolyte in the remaining solution may be increased. Under these reduced ion mobility conditions the resistivity is increased substantially.

Specific indications of the effects of 'w/c' and of saturation on the resistivity of concretes are provided in Figure 3.4 [A].

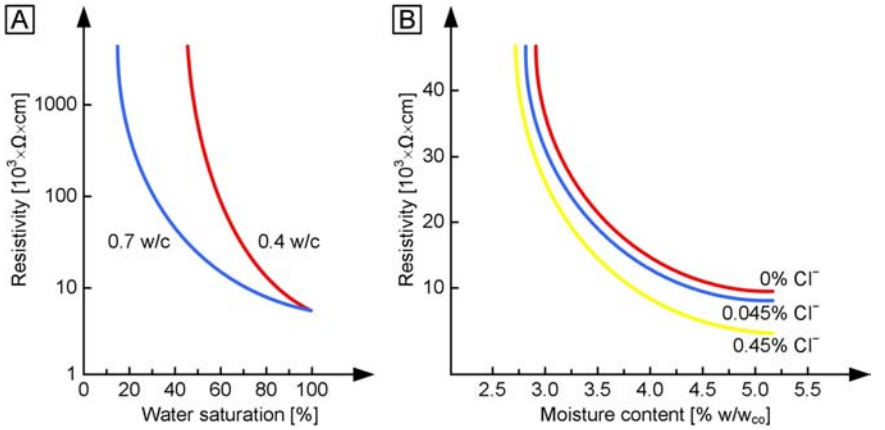

Figure 3.4: [A]: *Effect of water saturation and 'w/c' on the resistivity of concrete exemplified for concretes with 'w/c' ratios of 0.7 and 0.4. After [Tuutti, 1982]*. [B]: *Effect of chloride ion and moisture content on the resistivity of concrete exemplified for chloride contents of 0%, 0.045%, and 0.45% 'w/w_{co}'. After [Bentur et al., 1997]*.

Figure 3.4 [A] illustrates the great sensitivity of resistivity to the moisture level of the concrete. For instance, for a change in saturation from 100% to 50% an increase in resistivity of about an order of magnitude occurs. The 'w/c' has an effect of similar magnitude, especially at intermediate water saturation levels.

Figure 3.4 [B] depicts the specific effect of increasing chloride ion concentration in the pore solution. Addition of chloride decreases the resistivity to a certain extent, but contrary to the opinion commonly expressed in the literature, we consider the effect to be rather small in comparison to the influence of the moisture content.

It can be concluded that for a given concrete an increase in resistance is an indication of a decrease in saturation or a decrease in concrete porosity or both. We think that increasing the resistance against ionic transport in the vicinity of the rebar can be a major key in controlling reinforcement corrosion (cf. Chapter 7).

3.1.8 Formation of Macrocells

Macrocell corrosion refers to a situation where the anodic and cathodic processes take place on separate sites of the reinforcement preferentially. Formation of macrocells represents a particular risk, because large cathodic areas can drive the dissolution in localised small anodic areas formed in pitting corrosion (cf. Section 2.3.2), while the cathodic reaction can take place on the passive carbon steel surface (cf. Section 2.1.9). As mentioned in Section 2.3.2, pitting corrosion is of particular concern with regard to chloride induced corrosion, and macrocell formation is, hence, exemplified in relation to chloride induced corrosion in the splash zone (cf. Section 3.1.7.3).

Two more exposure zones can be distinguished for concrete structures in the marine environment according to their location in relation to the sea surface, the atmospheric and the submerged zone. In correspondence with the splash zone, the atmospheric zone is defined to be located from three metres above the maximum sea level and the submerged zone begins three metres below the minimum sea level [Frederiksen & Poulsen, 1997]. In these exposure zones, the conditions controlling the appearance and the effect of the various possible transport mechanisms, discussed in Section 3.1.6, differ from conditions in the splash zone and thus the magnitude of chloride and oxygen ingress varies largely.

The ion mobility plays a significant role in the formation of macrocells. Thus, the exposure zones can be subdivided into four corrosion zones with regard to the conductivity of the concrete [Wilkins & Sharp, 1990], as illustrated in Figure 3.5.

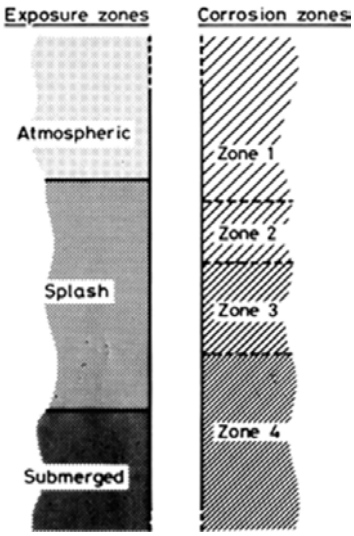

Figure 3.5: *Exposure and corrosion zones in marine environment. From [Wilkins & Sharp, 1990].*

In these zones the concrete becomes progressively more conductive as the degree of saturation increases. Accordingly, the cathodic area that is available for a local anode to form a macrocell is increased. This is counteracted by the decreasing oxygen permeability, which restricts the cathode reaction.

As indicated in Figure 3.5, the atmospheric zone is covered by corrosion zone 1. In this zone the concrete resistance is high and formation of macrocells is not favoured. The splash zone is suggested to be divided into two corrosion zones. In corrosion zone 2, which covers the top of the splash zone, corrosion may occur, but the probability compared to corrosion zone 3 is considered to be small. The middle and lower parts of the splash zone are considered to be covered by corrosion zone 3. In this zone the outermost layer of the concrete cover is exposed to large moisture and temperature varia-

tions and chloride initiated corrosion is likely to occur. The concrete conductivity even in good quality concrete is considered to be high enough to allow formation of large corrosion cells resulting in a severe corrosion attack in this zone. The oxygen diffusion towards the reinforcement cannot be expected to be greatly restricted, as the concrete is frequently exposed to the air environment. The submerged zone is saturated and hence the transport of oxygen towards the reinforcement is largely restricted. Even if the reinforcement fails to maintain the overall passivity under this condition, only slow uniform corrosion will occur, due to the lack of oxygen. However, large macrocells with intense pitting corrosion can be developed in cracks or similar defects, if areas of passive reinforcement can act as cathode. [Wilkins & Sharp, 1990].

Thus, macrocell formation leads to a complex corrosion mechanism that is controlled by the various transportation mechanisms into and within the concrete, which are interconnected with the concrete properties and the environmental exposure conditions.

3.1.9 Chloride Threshold

The chloride threshold can be seen as the highest possible chloride concentration at the concrete-steel interface before corrosion on the reinforcing steel is initiated, i.e. full passivity is retained. Several reviews on the chloride threshold can be found in the literature, e.g. [Glass & Buenfeld, 1997; Nygaard, 2003]. In terms of the concrete cover properties, the chloride threshold is, in principle, dependent on the same factors as macrocell corrosion and further interconnected with macrocell corrosion itself. The influence of these factors expressed as concrete quality, degree of carbonation, and moisture content can be illustrated as shown in Figure 3.6.

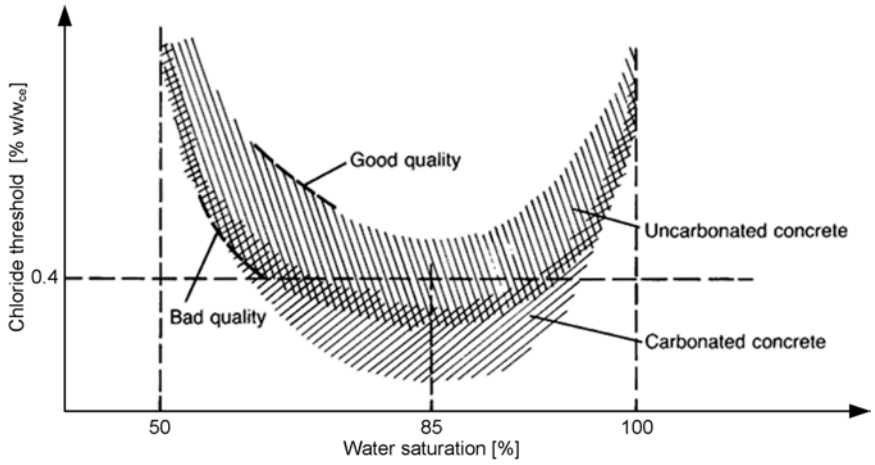

Figure 3.6: *Qualitative dependence of chloride threshold on concrete properties and exposure conditions. After [fib, 1992].*

Based on the description of interrelated factors controlling the ingress and ion mobility in concrete, the effect of the factors covered in Figure 3.6 is obvious. The transport rate of oxygen in concrete is dependent on the moisture content, since oxygen diffusion in gases is orders of magnitude higher than in aqueous solutions. The transport rate of oxygen in concrete decreases largely, when the capillary pores are water filled (cf. Section 3.1.7.1). On the other hand, a dry concrete impedes the electrolytic process by limiting the passage of ionic current through the concrete (cf. Section 3.1.7.4). Therefore, the chloride threshold is largely affected by the exposure conditions. High chloride thresholds are determined for steel in fully submerged concrete, while cyclic wetting and drying leads to low threshold values [Schießl & Raupach, 1997].

The saturation of the concrete, i.e. the oxygen availability, does not only control the ingress properties of other species and the ion mobility, but it also controls the cathodic reaction and thus the potential of the reinforcement. As mentioned in Section 2.3.2 and discussed in more detail in Chapter 5, chloride induced corrosion can be related to a pitting potential and corrosion initiation is strongly dependent on the electrode potential. In some reinforcement corrosion literature, the chloride threshold is therefore defined as the highest possible chloride content before corrosion initiation at *a given potential*. However, in the present thesis the definition given in the beginning of this Section is preferred, because the electrode potential is obviously interconnected with all above mentioned factors. Typical chloride thresholds for carbon-steel in uncarbonated concrete of a reasonable quality are in the range of 0.4% to 1% 'w/w_{ce}' [fib, 1992], cf. Figure 3.6 . Alternatively, the chloride threshold is in the literature sometimes expressed as Cl^-/OH^- ratio (also referred to as Hausmann criterion); typical ratios are in the range of 0.6 [Hausmann, 1967; Gouda, 1970; Gouda & Halaka, 1970; Saremi & Mahallati, 2002; Nielsen, 2004].

3.1.10 Influence of Temperature

The effect of the temperature is only of marginal interest in the present thesis. It is mentioned nonetheless, because it can have a drastic effect on corrosion initiation and propagation.

As indicated in Section 2.1, the expression for ΔG for non-standard states and accordingly the Nernst equation are dependent on the temperature, which illustrates that the temperature contributes to all types of thermodynamic reaction that are taken into account in the present thesis. In Section 2.2 the effect of the temperature on the reaction kinetics was indicated, e.g. the influence on the exchange current densities and the related polarisation phenomena that were all, except resistance polarisation, expressed as a function of the temperature. Finally, in Section 3.1.10 it was shown that the velocity of the ion movement is also dependent on the temperature. So, all these factors are influenced by the temperature and in principle it can be said that increasing temperature accelerates all thermodynamic reactions, all reaction kinetics as well as the

movement of ions into and within the concrete. The result of this acceleration is that even a more or less moderate increase in temperature can have a considerable effect for reinforcement corrosion, which is obvious when comparing e.g. the performance of concrete structures in Nordic countries to the performance in the Middle East [Rostam, 2003].

For more details on the effect of the temperature on the reinforcement corrosion, reference is made to e.g. [Schießl & Raupach, 1995; Nilsson et al., 1996; Østvik, 2005].

3.1.11 Cracking and Effect of Cracks

Cracking of the concrete cover is a major factor in altering ingress properties and most concrete cracks in practice, despite the best efforts to avoid it [Bentz et al., 2001]. So, knowledge on the extent of cracking, i.e. the typical crack sizes, as well as on the effect of concrete cracks on the corrosion mechanisms is a crucial background concerning corrosion countermeasures.

3.1.11.1 Extent, Appearance, and Causes of Cracking

According to [Nilsson et al., 1997], microcracks (< 0.01 mm) should be considered as a natural part of concrete and their effect is to be included, when properties of the material are tested. Larger cracks, e.g. cracks resulting from mechanical loading, shrinkage, or temperature induced stresses, should be regarded as defects and their effect is to be quantified separately. Typical crack sizes and causes can be classified as listed in Table 3.5.

Table 3.5: *Typical crack classifications, widths, causes, depths, and distances. After [Nilsson et al., 1997].*

Classification	Microcrack	Intermediate crack	Macrocrack
Width	< 0.01 mm	0.01-0.1 mm	> 0.1 mm
Cause	Self-desiccation	Shrinkage/temperature	Mechanical loading
Depth	< 2 mm	< 50 mm	> 100 mm
Distance	5-40 mm	10-200 mm	30-200 mm

In principle, concrete cracks are caused by either mechanical load or by restrained movements.

Load-induced cracking can often be regarded as an inherent characteristic of reinforced concrete structures, since the maximum tensile strain that the concrete can support is often exceeded to use the steel reinforcement efficiently. Actually, design specifications require the complete elimination of cracks only for special structural applications, which is then normally achieved by prestressed or post-tensioned reinforced concrete. Cracks due to mechanical load are often flexural cracks that tend to be tapered and to run perpendicular to the main reinforcement. Under large deforma-

tions, flexural cracks can lead to debonding along the concrete steel-interface, see Figure 3.7 [A].

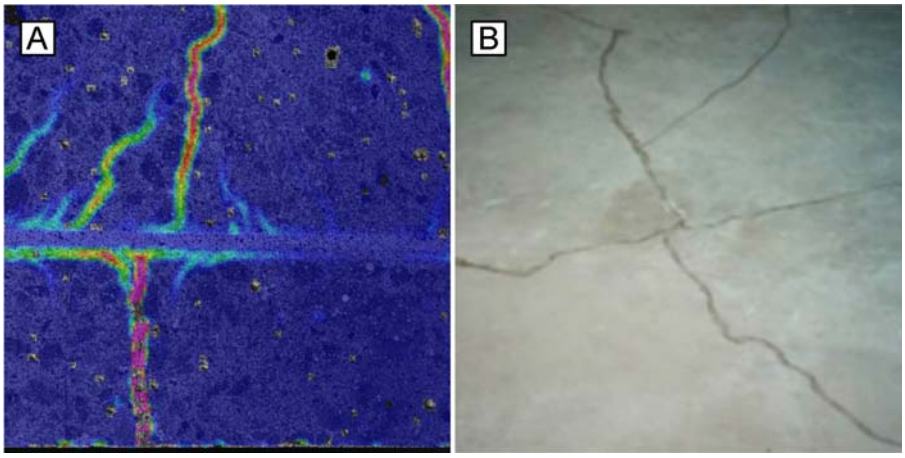

Figure 3.7: [A]: *Perpendicular cracks and debonding along the rebar of a beam under flexural loading. From research at DTU Byg [Pease et al., 2006] using ARAMIS 3D deformation analysis [GOM, 2007]*. [B]: *Shrinkage cracks in concrete slab. From [Friedmann, 2007]*.

Restraint movements cause tensile stresses, and the concrete cracks, when the tensile strength is exceeded. Restraints are either introduced by internal restraints, e.g. aggregates and reinforcement, or arise from external constraints, e.g. earlier castings. Cracks due to restraint movement usually run through large parts of the cross section and can also occur parallel to the main reinforcement, see Figure 3.7 [B]. Concrete is particularly prone to cracking during the transition phase from fresh concrete to hardening concrete, since this is a critical period with low tensile strength and low deformability. Two distinct causes for cracking, plastic shrinkage, and plastic settlement, are of concern during this period:

- Plastic shrinkage cracking caused by capillary tension in the pore water, when the water loss by evaporation exceeds the supply of bleeding water [fib, 1992]
- Plastic settlement cracking caused by hampered settlement [fib, 1992].

Three mechanisms, self-desiccation, drying shrinkage, and temperature differences, dominate cracking after the set of concrete:

- Self-desiccation caused by the menisci at the interfaces between the water-filled and empty pores [Bentz et al., 2001]
- Drying shrinkage cracking by the contraction of a hardened concrete mixture due to the loss of capillary water
- Carbonation shrinkage (cf. Section 3.1.7.2)

- Thermal cracking caused by restraint stresses from thermal gradients, in particular due to the exothermic reactions during concrete hydration.

3.1.11.2 Effect of Cracking on Ingress and Reinforcement Corrosion

Based on the description of the extent, appearance, and causes of cracking in Section 3.1.11.1, concrete covers must generally be regarded to contain cracks to a smaller or larger extent. Thus, when taking into account the protective function of the concrete cover for the reinforcement, the effects of cracks is to be considered. As mentioned in the introduction, also the corrosion process itself often results in cracking of the cover, which further complicates the situation.

Cracks in the concrete cover present at least the following three effects with regard to reinforcement corrosion:

- If a certain width is exceeded, cracks act as high velocity paths and enable carbonation and chloride ions to reach the reinforcing steel in a fraction of the time compared to an uncracked cover. Accordingly, the duration of the initiation phase is largely decreased.
- Increased transport of oxygen through cracks enables or accelerates the cathodic reaction, so that corrosion rate is increased after corrosion initiation.
- Cracks produce substantial non-uniformities in the physical and chemical environment around the reinforcement. The non-uniformities can provide conditions leading to the development of concentration cells, which can enable a galvanic corrosion process.

The influence of cracks on the permeability of concrete was evaluated by e.g. [Wang et al., 1997; Aldea et al., 1999; Aldea et al., 2000], while the time dependent counteracting effect of crack healing due to the formation of calcium carbonate ($CaCO_3$) that was determined to largely hamper the ingress rate was quantified by e.g. [Schießl et al., 1995; Edvardsen, 1999]. As indicated in Section 1.3 and explained in more detail in Chapter 5, the effect of chloride induced corrosion is generally much more severe than the effect of carbonation induced corrosion. Thus, cracks with access to chloride ions are of particular concern in durability design, and the crack width is a significant design parameter. Accordingly, several studies have dealt with the ingress of chlorides in cracked concrete, e.g. [Place Hansen de, 1999; Schutter, 1999; Gowripalan et al., 2000; Boulfiza et al., 2003; Rodriguez & Hooton, 2003; Win et al., 2004; Küter et al., 2005a]. The effect of cracks on the initiation and propagation of reinforcement corrosion has been investigated by several authors as well, e.g. [Schießl, 1986; Rehm et al., 1988; Raupach, 1992; CS, 1995; Schießl & Raupach, 1997]. A discussion of these investigations goes beyond the scope of this thesis, but there is a general agreement in the literature that cracks exceeding a certain width present a major risk, especially under chloride exposure. However, there are different, sometimes con-

troversial opinions expressed about the exact magnitude of crack width that leads to an increased corrosion risk.

Although there is a general agreement that even microcracking increases the diffusion coefficient and thus reduces the initiation phase of both chloride and carbonation induced corrosion, many investigations have shown that there is no precise correlation between the crack widths and the risk for corrosion [Gautefall & Vennesland, 1983; Schießl, 1988; Francois & Arliguie, 1998; Mohammed et al., 2001; Audenaert et al., 2007]. For small crack widths the corrosion risk depends largely on the same factors as uncracked concrete, i.e. the depth, porosity and the degree of saturation of the concrete cover. For example in dry concrete (high resistance), as well as in saturated concrete (low oxygen content), the corrosion rate remains negligible, even if there are cracks of a considerable width. The environmental conditions for e.g. the marine splash zone (cf. Section 3.1.7.4) or parking decks fall between these limits, and the effect of cracks is, therefore, substantial in these structural situations, so that special corrosion preventive measures are required.

For other structural situations, limiting the oxygen supply for the cathodic reaction and the transport of ionic current in the concrete between the cracks is often considered to be more beneficial from a corrosion protection point of view than limiting the maximum crack width. For instance, as illustrated in Figure 3.8, it was shown that a dense and thick concrete cover omits the formation of macrocells by limiting diffusion of oxygen and migration of hydroxyl ions [Schießl & Raupach, 1997].

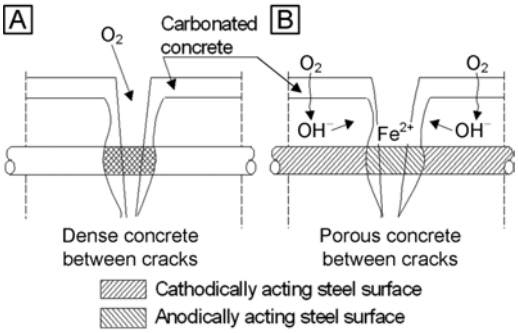

Figure 3.8: *Effect of concrete quality on corrosion mechanism for cracks. After [Schießl & Raupach, 1997].* [A]: *Dense concrete leading to microcell corrosion with cathode reaction limited to crack.* [B]: *Porous concrete leading to macrocell corrosion with cathode reaction possible in uncracked concrete.*

As shown in Figure 3.8 [A], the cathodic reaction can be limited to the exposed steel surface in the crack, if the concrete between the cracks is dense. In contrast, a macrocell with a high corrosion rate can be formed between the steel surface in the uncracked, but porous concrete between cracks, which enables oxygen diffusion and

OH^- migration. Thus, the quality of the concrete between the cracks and the thickness of concrete cover can play a major role in the corrosion risk related to cracking.

It should be noted that this factor has a major impact on structural and durability design. Designing for small crack width inevitably involves a higher reinforcing degree, which can, besides economical disadvantages, lead to improper compaction and hence a more porous concrete between the cracks. Furthermore, a deeper concrete cover that limits oxygen diffusion generally leads to larger crack widths.

Maximum crack widths for different environments are specified in the national building codes and guidelines for concrete structures, i.e. Eurocode 2 [DS/EN 1992-1-1, 2005] and [ACI 224R, 2001]. In the absence of prestressing or specific requirements, e.g. water-tightness, the national codes generally limit the maximum crack width to 0.2 mm or up to 0.4 mm. However, the actual exposure conditions and the design service lives of many special civil engineering structures, e.g. offshore structures and car parks, are generally not covered by the general reinforced concrete codes and often special guidelines are provided, e.g. [ACI 357R, 1984] for offshore structures and [ACI 362.1R, 1997; ACI 365.1R, 2000] for car parks. Moreover, special models for service life design exist. These models and the most important countermeasures, which can be taken to ensure the attainment of the design service life, are briefly discussed in Chapter 6.

3.2 Carbon Steel Reinforcement

Information on the exact materials properties of carbon steel reinforcement is scarce, but literature on the metallurgical properties of carbon steel is abundant. Reference is made to the various extensive textbooks, e.g. [Davis, 1998; Bhadeshia & Honeycombe, 2006]. The detailed physical and metallurgical properties of carbon steel, in particular concerning the strength development, are beyond the scope of this thesis. General electrochemical properties of carbon and stainless steel have been dealt with throughout Chapter 3 and the electrochemistry of steel in concrete is discussed in detail in Chapter 5.

Specifications and requirements for carbon steel rebars are standardised in [DS/EN 10080, 2006][*] and [ASTM A615M, 2007] as well as in [ISO 6935-1, 2007] for smooth rebars and, more importantly, in [ISO 6935-2, 2007] for ribbed bars.

In Sections 3.2.1, a short overview is given of the production process of carbon steel reinforcement. In Section 3.2.2, the metallurgical and surface properties relevant for corrosion are summarised.

[*] According to [CIEG, 2007], there is a strong possibility that EN 10080 [DS/EN 10080, 2006] will be withdrawn from the list of references of harmonised standards published in the Official Journal of the European Union ('OJEU'), because it is considered not to meet the requirements of a harmonised standard.

3.2.1 Production Process

Until the mid 1930s no special steels were used for reinforcement. The bars and profiles used for reinforcing steel had a yield strength of around 250 MPa and a smooth surface. The activation of the bearing function was achieved by hooks and loops at the ends. (Russwurm & Schäfer, 2001).

Nowadays, ordinary carbon reinforcing steels have a yielding strength in the range of 400 to 500 MPa. From the end of the 1970s reinforcing steel was mainly produced by the Thermex or the Tempcore process [Scholz et al., 1999]. By means of these processes weldable reinforcing steel based on a simple analysis with a carbon content of about 0.2% and a manganese content ranging from 0.5% to 1.1% can be produced [Davis, 1998].

Nowadays, reinforcing steel is produced from 100% of recycled material, i.e. ferrous scrap, and, according to an estimate of the steel recycling institute [CRSI, 2002], over 45% of reinforcing steel from the demolition of reinforced concrete structures is recycled, see Figure 3.9.

Figure 3.9: *Salvage separation for recycling of reinforced concrete in Chicago, IL, USA. From [Brandenburg, 2005].*

The reinforced concrete salvage is separated for recycling. The reinforcement is sold as ferrous scrap, and the concrete is normally crushed and used e.g. as road base material, as a concrete aggregate, or even as a raw material for the cement production. [Brandenburg, 2005].

To provide for interlocking between the concrete and the steel, which enables effective force transfer between the reinforcement and the concrete bulk, ribs (in the literature also referred to as ridges, deformations, or cross hatchings) are rolled on the rebars. These ribs normally have a maximal height of 4.5% and a maximal distance of 60% in relation to the diameter of the reinforcing [Scholz et al., 1999].

3.2.2 Metallurgical and Surface Properties

According to [Bardal, 2004], *a metal is usually most corrosion resistant when it contains the smallest possible amounts of impurities*. In this Section, this notion is related to metallurgical and surface properties of carbon steel reinforcement. The theoretical background is briefly described in Section 3.2.2.1. Results from own investigations on the metallurgical and surface properties of as-received carbon steel rebar are summarised in Section 3.2.2.2.

3.2.2.1 Theory

Anodic and cathodic sites (cf. Section 2.1.1) are created on the carbon steel surface due to compositional variations from one site to another or due to certain variations in the concrete-steel interface (cf. Section 3.3). Such differences cause some sites to be more electrochemically active than others and create potential gradients. Active sites become anodes, whereas less active sites tend to act as cathodes.

Carbon steel is heterogeneous on a microscopic scale. Two different types of phases, the α-Fe phase, referred to as ferrite, and an iron carbide compound (Fe_3C,), referred to as cementite, are generally taken into account, when corrosion properties are dealt with. The ferrite phase tends to develop a more active potential than the cementite phase. However, potential gradients can also develop in areas of uniform composition, since the atoms at or near the grain boundaries tend to be significantly more active than the atoms within the bulk of the grains and thus the grain boundary regions tend to be anodic. Therefore, the reinforcing steel surface can be considered to consist of clusters of numerous local corrosion cells. If the concrete is dry, ionic charge transfer is ceased (cf. Section 3.1.7.4) and the corrosion reaction cannot take place. However, if the surface has access to an ionic solution, i.e. the pore solution, currents can flow and the corrosion reactions between the local cells can occur. [Bentur et al., 1997].

On a larger scale, stresses induced by cold working can lead to considerable inhomogeneities. The metal in the strained zones is more active and tends to behave anodically, whereas the unstrained metal tends to function as cathode. [Bentur et al., 1997].

We assume that especially rolling of ribs produces major stress concentrations leading to considerable potential gradients. Furthermore, we think that other variations in the surface conditions, e.g. caused by oxides or inclusions of other species, have a major effect on formation of corrosion cells on the steel surface, which appears not to be taken into much consideration in the literature. Therefore, we have analysed the surface and metallurgical properties of as-received carbon steel. This investigation was also of importance with regard to the proposed new countermeasures, because one principle for the implementation is based on concrete-steel interface modification (cf. Section 7.2.3). Selected results from the investigation are given in Section 3.2.2.2, while results from a comparative analysis performed for stainless steel reinforcement

are summarised in Section 6.3.2.3.2. The practical relevance of such analyses with regard to surface modifications of carbon steel is exemplified by the influence of silicon on the quality of hot-dip galvanisation in Section 6.3.2.5.

3.2.2.2 Experimental Investigations

As-received ribbed carbon steel rebar K550TS [LMG, 2004a], i.e. B550AR+AC [DS 13080, 2001] (cf. Section 1.9.2), was investigated based on light optical microscopy 'LOM', scanning electron microscopy 'SEM', and energy dispersive X-ray spectroscopy 'EDS'. Selected results are summarised after a short note on the sample preparation and measurement techniques.

3.2.2.2.1 Sample Preparation and Measurement Techniques

The metallographic sample containing cross and longitudinal sections of as-received ribbed stainless steel rebar with a diameter of 8 mm was prepared by means of a suitable grinding and polishing sequence according to [Bjerregaard et al., 2000]. 'LOM' was performed on the specimen before and after etching with 2% nital, as described in [Weidmann & Guesnier, 2006]. Besides 'LOM', the metallurgical properties of the specimen have been investigated by 'SEM' and 'EDS' according to [ASTM E2142, 2001] and [ASTM E1508, 2003], respectively. Before 'SEM' and 'EDS' analyses a conducting thin film of carbon was applied on the surface of the metallographic specimen.

3.2.2.2.2 Light Optical Microscopy

Photographs from low magnification 'LOM' of the cross and longitudinal section from the etched carbon steel sample are shown in Figure 3.10 [A] and [B], respectively. The lighter inside with an even lighter ring is apparent in both photos. We assume that this appearance results from the hardening and the hot-rolling process. Cooling from the outside during hardening might push certain alloying elements that solidify later towards the centre and therefore lead to decisive differences in the composition.

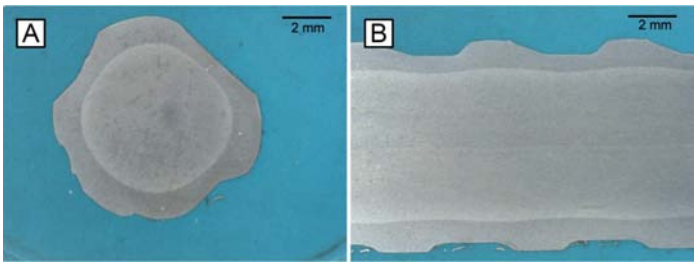

Figure 3.10: *Low resolution light optical microscopy of etched carbon steel sample.* [A]: *Cross section.* [B]: *Longitudinal section.*

Figure 3.11 [A] and [B] show photos from the 'LOM' before etching of the cross and the longitudinal section, respectively. Dotted inclusions can be identified in the cross section, whereas the inclusions in the longitudinal sections are "stretched" due to the rolling process. We think that these inclusions consist of oxides, e.g. Fe_2O_3 or SiO_2, sulphates, or sulphites (cf. Section 3.2).

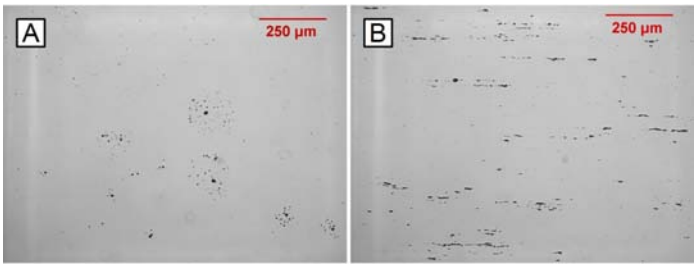

Figure 3.11: *Light optical microscopy of unetched carbon steel sample.* [A]: *Cross section.* [B]: *Longitudinal section.*

Selected photographs from high magnification 'LOM' on the etched carbon steel sample are presented in Figure 3.12. All photos were taken along the edge of the longitudinal section.

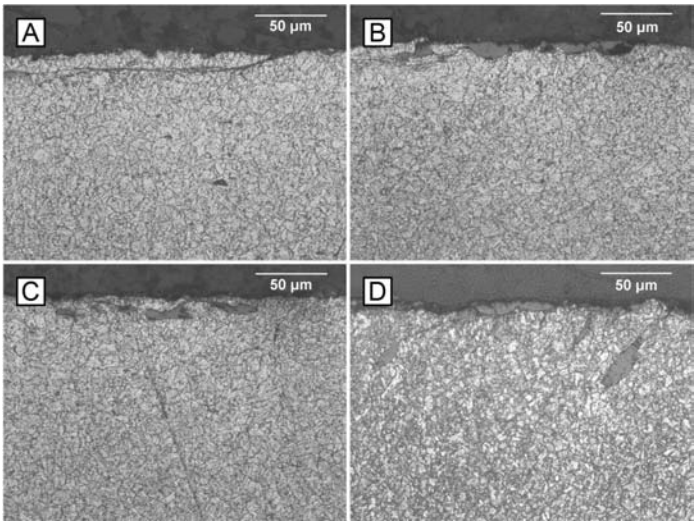

Figure 3.12: *High magnification light optical microscopy of longitudinal section of etched carbon steel sample.*

Besides the clearly visible microstructure, all photos exhibit surface defects and inclusions. Figure 3.12 [A] shows a surface crack that might result from over-rolling. We assume that corrosion is likely to be initiated in such a crack, in particular with regard to the mechanisms described for crevice corrosion (cf. Section 2.3.4). Figure 3.12 [B], [C], and [D] show locations, where corrosion products were formed. While the products in Figure 3.12 [B] were found at the surface, Figure 3.12 [C] and [D] represent

locations, where the corrosion products were rolled into the bulk. We suggest that such scale rolled on and into the surface interacts very precious and electrochemically active to endorse regions for corrosion initiation.

3.2.2.2.3 Scanning Electron Microscopy

Figure 3.13 shows secondary electron ([A] and [C]) and backscattered ([B] and [D]) 'SEM' photographs from the edge of the etched cross section of the carbon steel sample. The previously discussed rolled-in corrosion products are clearly visible as black inclusions in the bulk of the backscattered 'SEM' photo in Figure 3.13 [B]. Figure 3.13 [C] and [D] show a magnification of the dots of scale previously identified as oxide, sulphate, or sulphite inclusions (cf. Section 3.2.2.2.2).

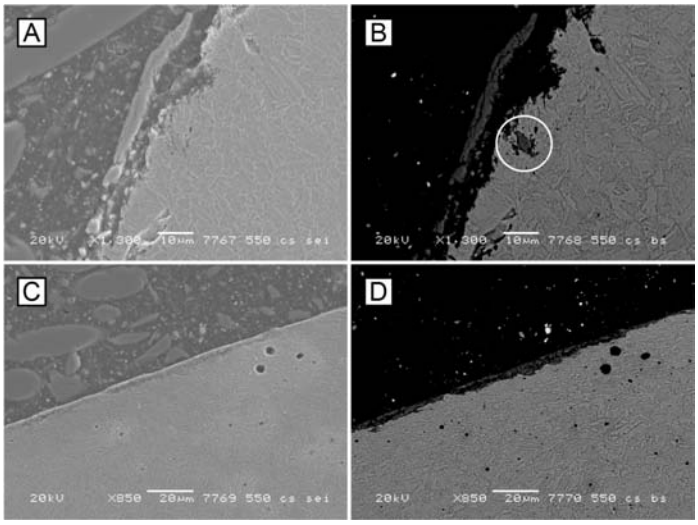

Figure 3.13: *Scanning electron microscopy of edge of cross section of etched carbon steel sample.* [A] and [C]: *Secondary electron.* [B] and [D]: *Backscattered.*

3.2.2.2.4 Energy Dispersive X-Ray Spectroscopy

The specified [LMG, 2004b] and measured values from the chemical analysis of the investigated carbon steel are listed in Table 3.6. The measured quantities for the bulk are taken from the average of the 'EDS' spectra from the middle and close to the edge of the longitudinal section. Additionally, a chemical analysis for the inclusion marked by the white circle in the cross section in Figure 3.13 [B] was performed. It should be noted that the detection of carbon is not feasible with the 'EDS' equipment at DTU Byg.

Besides iron the only two elements detected by 'EDS' in the bulk of the longitudinal section (columns 3 and 4) were silicon and manganese. Both measured averages ex-

ceed the specified values by about 50%. However, the deviational quantities are rather small (< 0.4%) and considered to be within the error margin of the equipment for detection of these elements. The quantities specified for the other elements are, apart from copper, rather small. Therefore, these elements might remain undetected in the spectra.

Table 3.6: *Specified [LMG, 2004b] and averaged measured composition of investigated carbon steel sample. ('LL'): longitudinal section. ('CS'): cross section.*

Element	Specified [LMG, 2004b] [%]	Avg. measured ('LL'), middle [%]	Avg. measured ('LL'), edge [%]	Avg. measured ('CS'), inclusion [%]
Iron	-	98.603	98.537	87.745
Manganese	0.700	1.055	1.095	1.340
Copper	0.320	-	-	-
Silicon	0.220	0.307	0.367	0.395
Carbon	0.180	-	-	-
Nickel	0.150	-	-	-
Chromium	0.110	-	-	-
Tin	0.025	-	-	-
Molybdenum	0.020	-	-	-
Phosphorus	0.017	-	-	-
Zinc	0.011	-	-	-
Nitrogen	0.010	-	-	-
Aluminium	0.006	-	-	-
Niobium	0.003	-	-	-
Lead	0.002	-	-	-
Sulphur	0.002	-	-	-
Vanadium	0.002	-	-	-
Titanium	0.001	-	-	-
Oxygen	-	-	-	11.155
Calcium	-	-	-	0.230

Silicon and manganese are detected in similar quantities in the averaged measurements of the spectra for the inclusion (column 5). Furthermore, a large quantity of oxygen (ca. 11%) was detected on expense of the quantity of iron, which was found to be reduced to about 88%. This indicates that the investigated inclusion is composed of iron oxide, i.e. a corrosion product rolled in from the surface. Additionally, a small quantity of calcium (ca. 0.2%) was detected in the inclusion.

3.3 Concrete-Steel Interface

While Section 3.1 largely dealt with the decisive properties of the bulk concrete cover, the concrete-steel interface, i.e. the physical adhesion between the cement paste and the passive layer on the steel surface, is treated in this Section. The concrete-steel interface is dealt with in a separate Section, because it relates to both the concrete bulk and the steel surface properties and its particular properties are a decisive factor for the initiation and propagation of corrosion, especially in the case of chloride induced corrosion.

The factors described for the bulk concrete have an obvious influence on the properties of the concrete-steel interface and also cracking, load-induced or initial, clearly impairs its protective functions for the reinforcing steel. Furthermore, the often observed settlement of the concrete beneath horizontal reinforcement, which does not necessarily involve cracking, affects this protective function drastically. So, from a corrosion protection perspective, the same principles apply for the concrete-steel interface as for the bulk concrete, i.e. the more dense, the better the corrosion protection. However, in practice, air voids at the concrete-steel interface and other interface defects cannot be omitted and will always be present to a smaller or larger extent. The magnitude of voids and defects is not only determined by the concrete mix or the steel surface properties, but largely dependent on the execution, in particular the compaction of the concrete. The voids and defects have, in principle, two major effects. The first relates to the formation of potential gradients on the surface of the reinforcing steel (cf. Section 3.2.2), while the second relates to the chloride threshold (cf. Section 3.1.9).

As mentioned in Section 3.2.2, potential gradients on the steel surface are formed either due to metallurgical dissimilarities on the steel surface or due to differences in the in the environment surrounding different areas on the same steel. It is important to note that a potential gradient due to environmental differences would even be formed, if the steel itself was entirely homogeneous (which is practically impossible).

We think that the potential gradients on the steel surface resulting from the inevitable voids and interface defects have a much more pronounced effect than the potential gradients resulting from the metallurgical dissimilarities of the steel itself. The potential gradients from the voids and interface defects are primarily due to the differences in the concentration of dissolved oxygen. Areas with imperfections or voids have a larger availability of oxygen and become cathodic, whereas a dense concrete-steel interface limits oxygen availability and the associated areas become anodic sites. However, the formation of anodic and cathodic sites is not only associated with oxygen. Basically, any dissolved species can lead to concentration cells and thus to the formation of anodic and cathodic sites, which localise dependent on the given condition of the concrete-steel interface. For instance, local variations in the alkalinity can play a significant role in the formation of potential gradients.

The above factors relate to potential gradients, which do generally not lead to problems as long as the steel is in the passive state. After depassivation these gradients obviously increase the corrosion rate by enhancing the cathodic reaction. However, we think that voids and defects at the concrete-steel interface are of even more importance with regard to the effect on the chloride threshold. The effect of interfacial air voids on the chloride threshold is by the red line in Figure 3.14.

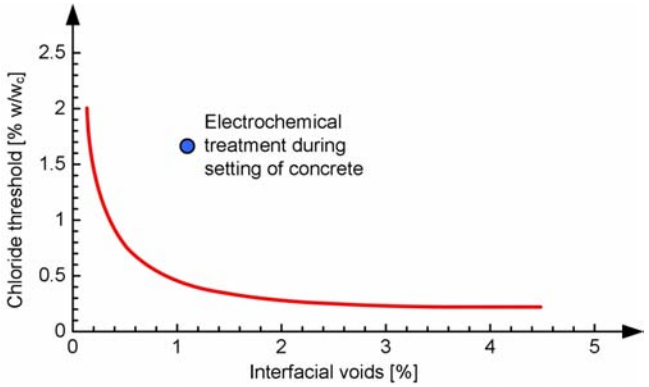

Figure 3.14: *Chloride threshold as function of interfacial voids. A qualitative average of untreated reference samples is given by the red line. The blue dot indicates the threshold measured for samples that have been electrochemically treated during setting of the concrete (cf. Section 6.3.1.5). After [Buenfeld et al., 2004].*

As illustrated in Figure 3.14, it has been determined that the chloride threshold could be largely increased, if the percentage of interfacial voids was brought below 0.8%. Chloride thresholds up to 2% 'w/w_{ce}' could be reached by reducing the percentage of interfacial voids to about 0.1%. On the other hand, an increase in the percentage of interfacial voids to more than 1% decreased the chloride threshold largely and values as low as 0.2% 'w/w_{ce}' have been measured.

Thus, it can be concluded that the properties of the concrete-steel interface have a major influence on chloride induced reinforcement corrosion. We think that these physical properties of the concrete-steel interface are of major importance and regard voids or interface defects as a necessary condition for corrosion initiation. Yet, we consider a reduction in the percentage of interfacial voids to values below 0.1% to be practically impossible to achieve by conventional techniques. Considerations on alternative ways, i.e. electrochemical and chemical methods, to reduce voids at the concrete-steel interface to the minimum play a major role in the development of the proposed new countermeasures (cf. Section 6.3.1.5 and Chapter 7).

4 Application of Thermodynamics

In this Chapter the proposed application of the thermodynamic principles and tools introduced in Section 2.1 is summarised and their validity in the area of reinforcement corrosion is discussed. As indicated throughout Section 2.1, we think that *thermodynamic principles and tools provide several beneficial means for the understanding and description of corrosion processes and, even more important for the purpose of this thesis, allow theoretically based predictions on the behaviour of systems*. From a theoretical point of view, the underlying principles for thermodynamic descriptions and predictions are rather simple (cf. Section 2.1), but the assumptions for the establishment of appropriate and representative models for the description and prediction of a system are rather complex. That holds in particular for the multifaceted physical, chemical, and electrochemical properties of the concrete-steel system (cf. Chapter 3). Our thermodynamic models are based on the establishment of reaction mechanisms (cf. Section 2.1.1) and in particular on the application of the Pourbaix diagram (cf. Section 2.1.10). So, in this Chapter, special focus is set on the establishment of appropriate and representative Pourbaix diagrams.

In Section 4.1 selected information on thermodynamic data and the way we dealt with encountered thermodynamic discrepancies is summarised. In Section 4.2 our suggested method for the establishment and application of Pourbaix diagrams is discussed in detail.

4.1 Thermodynamic Data

As mentioned in Section 2.1, all numerical thermodynamic data as well as all equilibria for the Pourbaix diagrams have been calculated using 'HSC', and they are, hence, largely based on the thermodynamic database provided in 'HSC' [Ouku, 1999; Ouku, 2002]. Thermodynamic calculations in 'HSC' are based on the *three fundamental parameters that describe the thermodynamic properties of a chemical species: enthalpy 'H', entropy 'S', and heat capacity 'C_p'*.[*] The theory behind these parameters was intentionally omitted in Section 2.1, because they are "indirect" parameters in the thermodynamic calculations included in this thesis and the related theory is considered to be marginal for its scope. For a detailed introduction to the theoretical background of these fundamental parameters, reference is made to e.g. [Freiesleben Hansen, 1995; Schroeder, 2000; Møller, 2003a]. However, a certain extent of knowledge on and application of these parameters was required in the theoretical part of this project, e.g. to utilise thermodynamic data from different sources, and the relevant background is introduced in a brief and largely simplified summary in the following:

- Enthalpy and heat capacity of chemical species

[*] Thus, the name 'HSC' for the applied software.

The enthalpy 'H' of a system can be defined as [IUPAC, 2007]: *"Internal energy of a system plus the product of pressure and volume. Its change in a system is equal to the heat brought to the system at constant pressure."* Similar to electrode potentials (cf. Section 2.1) absolute values of the enthalpy of chemical species cannot be measured, but enthalpy differences between two temperatures can be determined with a calorimeter. In order to achieve this, the heat capacity at constant pressure 'C_p', the so-called specific heat, is to be determined. The heat capacity of a system can be defined as [IUPAC, 2007]: *"Heat brought to a system to increase its temperature divided by that temperature increase."* Thus, 'C_p' can be calculated from calorimetric data according to:

$$C_p(T) = \left(\frac{\partial H}{\partial T}\right)_p \qquad [4.1]$$

This allows the calculation of the enthalpy 'H' of a chemical species according to:

$$H(T) = H^0 + \int_{298.15}^{T} C_p(T)\,dT \qquad [4.2]$$

where 'H^0' is the enthalpy at standard state conditions. All pure isolated elements in their standard states, e.g. Fe, O_2, and H_2, have a 'H^0' of zero. [Freiesleben Hansen, 1995].

- Entropy of chemical species

  The entropy 'S' of a system can be defined as [IUPAC, 2007]: *"Quantity of the change which is equal to the heat brought to the system in a reversible process at constant temperature divided by that temperature. Entropy is zero for an ideally ordered crystal at 0 K."* Absolute entropies can be calculated from experimentally determined values according to:

$$S(T) = S(0) + \int_{0}^{T} \frac{C_p(T)}{T}\,dT + \sum \frac{\Delta H}{T} \qquad [4.3]$$

  where '$S(0)$' is the entropy of a chemical species at 0 K and 'ΔH' is the enthalpy of phase transformation, i.e. the enthalpy change.

Thus, 'H', 'S', and 'C_p' can all be derived from experimental investigations. Many experimental and theoretical methods are available for determination of these parameters. Usually a critical analysis of the values is based on a thorough simultaneous cross-correlation of thermochemical data from different sources, experimental measurement, e.g. calorimetric, spectroscopic, electromotive force, and solubility measurements, as well as on theoretical calculations. A detailed discussion on these methods goes beyond the scope of this thesis. Among standard textbooks on physical chemistry and thermodynamics, reference is made to [Freiesleben Hansen, 1995; Schroeder, 2000; Roine, 2002].

In principle, all thermodynamic parameters in this thesis were calculated based on these parameters using the fundamental definition of the Gibbs energy (in the literature also referred to as free energy, free enthalpy, Gibbs free energy, or Gibbs function) 'G'* [IUPAC, 2007]: *"Enthalpy minus the product of thermodynamic temperature and entropy"*, which corresponds to:

$$G \equiv H - T \times S \qquad [4.4]$$

Equation [4.4] can be expressed in terms of 'ΔG', i.e. relating to the delta scale, as:

$$\Delta G = \Delta H - \Delta(T \times S) \qquad [4.5]$$

which under constant temperature and pressure corresponds to:

$$\Delta G = \Delta H - T \times \Delta S \qquad [4.6]$$

with 'ΔH' and 'ΔS' as the change of enthalpy and entropy of phase transformation, respectively. Finally, 'ΔG' can be related to the equilibrium potential 'E_0', as derived in Section 2.1:

$$\Delta G = -n \times F \times E_0 \qquad [4.7]$$

So, the numerical values of 'ΔG' and 'E_0' as well as the equilibrium lines in the Pourbaix diagram can be determined from the enthalpies and entropies of the species present in the system under investigation. Enthalpy and entropy values are provided in various literature including handbooks containing thermodynamic data (e.g. [Naumov, 1974; Wagman et al., 1982; Barin, 1993; Freiesleben Hansen, 1995; Lide, 2002]) and online databases (e.g. [THDA, 2007; Yaws, 2003]). These extensive lists are constantly complemented and updated by publications, e.g. [Shock & Helgeson, 1988; Shock & Korezky, 1993; Shock et al., 1997]. Furthermore, thermodynamic software generally provides databases with extensive lists of entropies and enthalpies of various chemical species referring to standard textbooks and publications, e.g. [Ouku, 1999; Ouku, 2002] as used in the theoretical part of this project.

According to [Roine, 2002] thermodynamic data of chemical species always contains certain errors, which can have a significant effect on the results, especially if the driving forces of the associated reactions are small. So, it is often useful to verify the applied thermodynamic data with other literature. Moreover, it should be noted that the thermodynamic database of 'HSC' is extensive, but certainly not complete. Thus, often it is necessary to add data to the 'HSC' database. Most thermodynamic data miss-

* In older chemistry literature, the Gibbs energy is also abbreviated by ('F'). However, 'G', as used in this thesis, is recommended in [IUPAC, 2007] to avoid confusion with the Helmholtz free energy, which is often abbreviated by ('F'), in particular in physics.

ing in 'HSC' can be found in the literature (as described above), but for some species that we came across in this project data appeared not to be available.*

As indicated in Section 2.1.3, two different scales for thermodynamic data exist: the delta scale [Wagman et al., 1982] and the absolute scale [Barin, 1993]. *The different scales do not interfere with the calculation of 'ΔG' values of reactions*, which has been exemplified in Section 2.1.3. However, besides the difference in the 'ΔG_f^0' (delta scale) and 'G_f^0' (absolute scale) values of species (that cancel each other down in the calculation of 'ΔG' for reactions), the diverse scales lead to differences in the database entries for 'H' and 'S'. 'HSC' provides an option for output in both scales, but its database is based on the absolute scale. So, if entries from a delta scale database (e.g. [Wagman et al., 1982]) are to be implemented in 'HSC', the following equations apply:

$$\begin{aligned} \Delta H &= H(\text{species}) - \sum H(\text{elements}) \\ \Delta S &= S(\text{species}) - \sum S(\text{elements}) \\ \Delta G &= G(\text{species}) - \sum G(\text{elements}) \\ \Delta G &= G(\text{ions}) - \sum G(\text{elements}) + \frac{z}{2} \times G(H_2) - z \times G(H^+) \end{aligned} \qquad [4.8]$$

It should be emphasised that the mutual stability of chemical species cannot be compared based on the enthalpy in either scale. Thus, the concept of the Gibbs free energy and its application in terms of 'ΔG^0' or '$\Delta G_f^{0'}$ as a measure for the affinity of reactions and formation, respectively, is crucial. These concepts are applicable for systems, where the processes occur under constant temperature and pressure, which is a common assumption in chemistry.

Systems with other so-called natural variables, i.e. variables that are assumed to be constant in the process, require considerations based on other thermodynamic potentials. Besides 'G' and 'H', the most important thermodynamic potentials are the internal energy ('U') (with 'S' and volume as natural variables) and the Helmholtz free energy ('A')† (with 'T' and volume as natural variables). The theoretical background of these potentials is not relevant for the purpose of this thesis. With regard to the relationships between these important thermodynamic potentials, the often cited mnemonic diagram in Figure 4.1 can be useful.

---

* For general investigations related to aqueous metallic corrosion, i.e. 'Me'-H_2O systems or 'Me_1'-'Me_2'-…-'Me_z'-H_2O systems, data for relevant species is generally included in 'HSC' or can be obtained from other sources (cf. Section 4.1). For systems involving various non-metallic elements alone or in combination with metals, thermodynamic data is often not available. However, as will be described in more detail in Section 4.2.1, these considerations and the associated 'MEPDs' are not included in the present thesis due to the expected patent possibilities (cf. Section 1.6).

† IUPAC recommends the symbol ('A') for the Helmholtz free energy to avoid confusion with the Gibbs free energy. However, the abbreviation ('F') is in frequent use, in particular in physics.

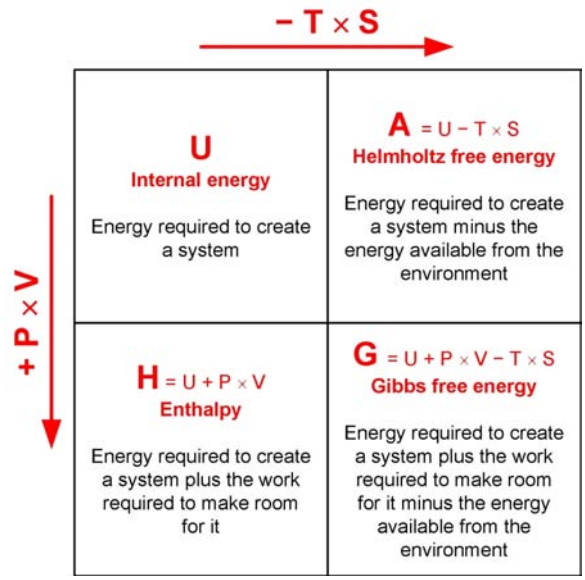

Figure 4.1: *Relationship between the four thermodynamic potentials internal energy ('U'), Helmholtz free energy ('A'), enthalpy 'H', and Gibbs free energy 'G' expressed by offsets of the energy from the environment, i.e. the product 'T'×'S', and the expansion work, i.e. the product ('P')×('V'). After [Schroeder, 2000].*

For a detailed description of the relationships between and the background of these thermodynamic potentials, reference is made to e.g. [Freiesleben Hansen, 1995; Schroeder, 2000; Møller, 2003a; GSU, 2007].

Based on the above, the deviations determined between the calculated 'E_0^0' values and the ones cited from the literature [Jones, 1996] for some of the half-cell reactions mentioned throughout this thesis are briefly analysed in the following.

The frequently stated half-cell reaction describing the reduction of ferrous ion:

$$Fe \rightarrow Fe^{2+} + 2e^- \quad \left(E_0^0 = -475\{447\}\,mV_{SHE} \right) \qquad [4.9]$$

is chosen for that purpose. The analysis is based on a comparison of the 'E_0^0' calculated based on the thermodynamic data provided in [Wagman et al., 1982], which corresponds to the data provided in the 'HSC' database, the thermodynamic data from [Freiesleben Hansen, 1995] and the data provided in [Pourbaix, 1974b] as well as in [Jones, 1996], see Table 4.1.

Table 4.1: *Thermodynamic data (delta scale) of ferrous ion from the 'HSC' database [Wagman et al., 1982] and from [Freiesleben Hansen, 1995] with 'ΔG^0' and '$E_0{}^0$' for reduction of ferrous ion calculated on that basis, '$\Delta G_f{}^0$' from [Pourbaix, 1974b] with 'ΔG^0' and '$E_0{}^0$' for reduction of ferrous ion calculated on that basis, and '$E_0{}^0$' as specified by [Jones, 1996] and other literature.*[*]

Fe^{2+}			$Fe^{2+} + 2e^- \rightarrow Fe$		Source
'ΔH^0'	'ΔS^0'	'$\Delta G_f{}^0$'	'ΔG^0'	'$E_0{}^0$'	
kJ/mol	J/(mol×K)	kJ/mol	kJ	mV	
−92.26	−2.46	−91.53	92	−475	[Wagman et al., 1982]
−89.10	−34.20	−78.90	79	−409	[Freiesleben Hansen, 1995]
-	-	−84.99	85	−440	[Pourbaix, 1974b]
-	-	-	-	−447	[Jones, 1996]

It can be observed that there is quite a large discrepancy between the values for 'ΔH^0' and especially for 'ΔS^0' specified in [Wagman et al., 1982] and in [Freiesleben Hansen, 1995]. These values lead to a considerable difference in 'ΔG^0' for the reduction of ferrous ion and accordingly for '$E_0{}^0$'. The '$E_0{}^0$' calculated based on the data from [Wagman et al., 1982] is 28 mV lower and the '$E_0{}^0$' calculated based on the data from [Freiesleben Hansen, 1995] is 38 mV higher than the value given in [Jones, 1996] and most other literature. We think that these deviations might be due to the two oxidation states of iron and the fact that ferrous ion is easily oxidised to ferric ion, so that both the measurement of 'H', 'S', and 'C_p' and the direct measurement of the equilibrium potential could be affected by impurities. *Disregarding, the probable insignificance in practice, the deviation is rather high from a theoretical point of view and we suggest that it is worth to be further investigated in the future*.

The '$E_0{}^0$' calculated based on the '$\Delta G_f{}^0$' taken from [Pourbaix, 1974b], which is based on a seemingly rounded value of the chemical standard potential specified for ferrous ion in calories, is the closest match to the value specified by [Jones, 1996]. However, it is unclear, if the numerical value for '$\Delta G_f{}^0$' in [Pourbaix, 1974b] was determined based on different 'H' and 'S' values or based on a given '$E_0{}^0$'. Moreover, the original source of the '$E_0{}^0$' for the reduction of ferrous ion is unknown.

Hence, we decided to base our considerations for ferrous ion and other species for which limited discrepancies between the calculated and literature values were observed on [Wagman et al., 1982]. The thermodynamic data of Fe^{2+} in [Wagman et al., 1982] was also confirmed by [Shock et al., 1997] and according to [Gurvich, 1989] the information provided in [Wagman et al., 1982], which is also referred to as the

[*] 'ΔG^0' corresponds to '$\Delta G_f{}^0$' (in the delta scale) for this half-cell reaction, as the '$\Delta G_f{}^0$' for Fe is 0 kJ. *This is not true for the normal scale*. We consider this correspondence to be a further benefit of the delta scale, but of course 'ΔG^0' and '$\Delta G_f{}^0$' differ, if other species are involved in a half-cell reaction, e.g. H_2O, H^+, or OH^-.

"NBS* Tables", is recommended by IUPAC as the standard source of thermodynamic data.

4.2 Pourbaix Diagram

We consider the Pourbaix diagram to be of particular benefit in describing and predicting the characteristics of a system, since it provides an insightful representation of its thermodynamic states. However, *Pourbaix diagrams only represent the actual thermodynamic conditions of a system, if due regard is given to the choice of elements, the associated ion activities, and the preselection of the chemical species, which are known or postulated to exist in the system under investigation. If these presumptions do not agree with actual conditions of the system under investigation, conclusions based on the Pourbaix diagram are inadequate and can be extremely misleading.* Taking into account the rather complex chemistry of the concrete environment, the limited application of the Pourbaix diagram in this area might be explained. In this Section the proposed way of establishing and using appropriate and representative Pourbaix diagrams for the description of reinforcement corrosion mechanisms (cf. Chapter 5) as well as the evaluation of available and the design of new countermeasures (cf. Chapters 6 and 7, respectively) is reasoned. Section 4.2.1 provides some general notes on our thermodynamic presumptions and applications concerning the Pourbaix diagram. Section 4.2.2 focuses on the applicability in the area of reinforcement corrosion.

4.2.1 Establishment and Application of Pourbaix Diagrams

Traditionally, Pourbaix diagrams have been obtained from the literature, and many corrosion science textbooks that deal with related subjects cite the diagrams as they have been originally established and published by Pourbaix and his colleagues at CEBELCOR† as the essential part of the famous "Atlas of Electrochemical Equilibria" [Pourbaix, 1974b], which was first published as an English edition in 1966. Moreover, Pourbaix also published an extended paper dealing with "Applications of electrochemistry in corrosion science and practice" [Pourbaix, 1974a], where various applications of thermodynamics are reviewed (including a short note on reinforcement corrosion, cf. Chapter 7). However, the *Pourbaix diagrams provided in these original publications and hence in the literature referring to it, are generally limited to a single element in an aqueous system, i.e. an 'El'-H_2O system, at standard state temperature and pressure*.

* National Institute of Standards and Technology (NIST), formerly known as the National Bureau of Standards (NBS), Gaithersburg, MD, USA.

† Centre Belge d'Étude de la Corrosion (CEBELCOR), Belgian Centre for Corrosion Study, Waterloo, Belgium.

As described in Section 3.1.10, the temperature has a significant effect on the thermodynamics and the kinetics of corrosion processes and variations in 'p_{H2}' and 'p_{O2}' have an important influence on cathodic reactions (cf. Section 2.1.10). However, being aware of the temperature and the pressure effect and taking their influence into account in particular in the design of new countermeasures[*], we think that *the most critical aspect in existing Pourbaix diagrams is the limitation to 'El'-H_2O systems*. Pourbaix diagrams covering only one element can be useful, but limitations apply, if one or more chemical species present in the system under investigation affect its thermodynamic conditions and hence alter the electrochemistry of the system, which is of particular importance in a system as chemically complex as the concrete-steel system (cf. Section 3). So, custom-made Pourbaix diagrams are necessary, if a complex chemical system, as e.g. a concrete-metal system, is to be investigated. Also, often the combination of two or more metals, e.g. galvanic coupling, is to be analysed.

As a fundamental and central task in this project, we have devised and tested principles for the establishment of custom-made Pourbaix diagrams that can be applied to describe complex systems or to investigate the effect of e.g. combination of diverse metals. With regard to this, we propose the following diffraction between three distinct types of Pourbaix diagrams for which the following terminology is used in the remaining part of this thesis (cf. Chapter 'TaD'):

- Single-element Pourbaix diagram 'SEPD'

  The term single-element Pourbaix diagram 'SEPD' refers to a Pourbaix diagram of an 'El'-H_2O system *covering only one element*. In this thesis, 'SEPDs' are normally limited to 'Me'-H_2O systems. However, Pourbaix diagrams are not at all limited to considerations on metals. In particular, in the design of the proposed new countermeasures (Chapter 7) focus is set on investigations concerning other elements as well as the thermodynamics of metals in combination with other elements[†].

  In Figures an 'SEPD' appears with only one ion activity above the diagram, e.g. "$Fe_{ia}\ 10^{-6}$" indicates a Pourbaix diagram for the Fe-H_2O system with an iron ion activity of 10^{-6} mol/L.

- Multi-element Pourbaix diagram 'MEPD'

  The term multi-element Pourbaix diagram 'MEPD' refers to a Pourbaix diagram covering one main element ('El_1') in combination with other elements ('El_2'-'El_z'), i.e. an 'El_1'-'El_2'-…-'El_z'-H_2O system, which takes *all species that can be*

[*] Temperature effects are taken into account in the proposed new countermeasures. Nonetheless, all Pourbaix diagrams in the present thesis are given for the standard state temperature of 25°C, in order to reduce the amount of variables.

[†] These considerations and the associated Pourbaix diagrams are not included in the present thesis with regard to the expected patent possibilities (cf. Section 1.6).

formed between the two or more elements into account, as e.g. the Pourbaix diagram of the Fe-Zn-H_2O system.

In Figures an 'MEPD' is indicated by separating the concentrations of the involved elements with commas, while the main element is named first. For instance, "Fe_{ia} 10^{-6}, Zn_{ia} 10^{-6}" indicates a Pourbaix diagram for the Fe-Zn-H_2O system, where Fe is the main element and the ion activities of both Fe and Zn are 10^{-6} mol/L.

- Superimposed Pourbaix diagram 'SIPD'

  The term superimposed Pourbaix diagram 'SIPD' mainly refers to a superimposition of individual 'SEPDs', i.e. an 'El_1'-H_2O system on an 'El_2'-H_2O system on an … on an 'El_z'-H_2O system (mainly superposition of a 'Me_1'-H_2O on a second 'Me_2'-H_2O system) *without taking into account the species that can be formed between the two elements* (e.g. the superposition of a Zn-H_2O system on a Fe-H_2O system). However, 'SIPDs' can also represent the superposition of two or more 'MEPDs' or any arbitrary combination of 'MEPDs' and 'SEPDs'. For instance, the superposition of the 'MEPD' of selected stainless steel alloys (e.g. the Cr-Fe-Ni-Mo-H_2O system) on the Fe-H_2O system is also referred to as 'SIPD'.

  In Figures an 'SIPD' is indicated by separating the concentrations of the involved elements with a slash, while the overlying 'SEPD' is listed first (e.g. "Zn_{ia} 10^{-6} / Fe_{ia} 10^{-6}" indicates superposition of the 'SEPD' of the Zn-H_2O system with an ion activity of 10^{-6} mol/L on an 'SEPD' of the Fe-H_2O system with the same ion activity). Superposition involving 'MEPDs' follows the same scheme, e.g. "Cr_{ia} 10^{-6}, Fe_{ia} 10^{-6}, Ni_{ia} 10^{-6}, Mo_{ia} 10^{-6} / Fe_{ia} 10^{-6}" indicates the superposition of the Cr-Fe-Ni-Mo-H_2O system (Cr as main element) on the Fe-H_2O system with the ion activities of all involved metals corresponding to 10^{-6} mol/L. For better visualisation the underlying diagram is generally coloured in blue, red, and yellow which correspond to the immune, corrosion, and passive domain, respectively. Depending on the effect to be exemplified, selected domains of the superimposed diagram are displayed transparently.

To our knowledge, neither 'MEPDs' nor 'SIPDs' have been applied in the area of reinforcement corrosion. As indicated in Chapter 1, the use of the Pourbaix diagrams in this area appears to be limited to the Fe-H_2O system, mainly for exemplification purposes. Considering, for instance, the application of galvanised steel or 'CP' for reinforced concrete structures, we think that such tools have a lot of potential in this area and should not be disregarded in particular concerning verification and design of countermeasures (cf. Chapter 6 and 7, respectively).

Some 'SIPDs' can be found in the literature on corrosion science and are used successfully in various areas, e.g. with regard to galvanic coupling of metals, especially concerning metal coatings and cladding or 'CP' by sacrificial anodes. However, even in general corrosion science, there seems to be certain reluctance towards the use of

'MEPDs'. This reluctance might be related to the complexity of systems where formation of multiple species is possible, since those species have to be carefully considered and preselected.

For the preselection, it is not sufficient to take into account whether or not a species is thermodynamically favoured based on the associated 'ΔG_f^0'. Formation of several, in particular complex species, can be thermodynamically possible or even favoured, but such species may not play a role in the system under investigation. Even if a species is thermodynamically favoured, kinetics can largely impede or entirely prevent formation, if the activation energy for formation of the species, which is principally a function of the temperature, is out of the range in the system under investigation. The activation energy (in the literature also referred to as Arrhenius* activation energy) is defined as [IUPAC, 2007]: *"An empirical parameter ('E_a') characterizing the exponential temperature dependence of the rate coefficient ('k'):*

$$E_a = R \times T^2 \times \left(\frac{\partial(\ln(k))}{\partial T} \right) \qquad [4.10]$$

where 'R' is the gas constant and 'T' the thermodynamic temperature".

Besides this "basic case", another option is possible. Given that certain initially present reactants can form two diverse species with different 'ΔG_f^0', the species with the lower 'ΔG_f^0' could be formed faster than the one with the higher 'ΔG_f^0' and eventually formation of the species with the higher 'ΔG_f^0' is thermodynamically impossible based on the "transformed reactants".

Such kinetic aspects can generally not be assessed and neither the rate coefficient nor the activation energy for most of the chemical species of concern in this thesis is available in the literature, so that information on the temperature of formation cannot be deduced. With regard to this, it is crucial to emphasise that *neither the reaction kinetics nor the activation energy of a species are by any means reflected by the associated 'ΔG_f^0'*, which is exemplified in 4.2.2.2. So, the choice of species to be formed is critical and rather complex in the establishment of custom-made Pourbaix diagrams, especially for 'MEPDs', and additional means are to be used to obtain necessary information on the actual likelihood of formation of the various thermodynamically favoured species.

Besides some general understanding of the chemistry and electrochemistry of the system under investigation, additional means that we applied for deducing information on likelihood of formation of the various thermodynamically possible species include the following:

- Sources containing Pourbaix diagrams

* Named after Svante August Arrhenius, Sweden, 1859-1927 [Wikimedia, 2007].

In principle, the use of literature containing a wider selection of Pourbaix diagrams is largely limited to [Pourbaix, 1974b], as various subsequent publications dealing with Pourbaix diagrams cite these diagrams with or without modifications. As mentioned, the diagrams provided in [Pourbaix, 1974b] are generally limited to 'SEPDs', but they provide some fundamental notions for species to be taken into consideration for 'MEPDs'. However, some publications deal with thermodynamic properties of relevant species and postulate the associated thermodynamic data or the corresponding regions in the Pourbaix diagram. For instance, theoretical and experimental data on iron species formed under carbonation and chloride induced corrosion has been published in e.g. [Refait & Génin, 1993; Sagoe-Crentsil & Glasser, 1993; Drissi et al., 1995; Refait et al., 1998].

- Sources containing information on the chemistry of materials

  Species that do not involve complex combinations of elements can often be deduced from information on the chemistry of the base material provided in textbooks or publications. For metals, information from standard textbooks (e.g. [Davis, 1998; Bhadeshia & Honeycombe, 2006] for iron or e.g. [Zhang, 1996] for zinc) can be applied, whereas standard textbooks on cement and concrete chemistry (e.g. [Taylor, 1997]) and various journal papers (e.g. [Lothenbach & Winnefeld, 2006; Matschei et al., 2007b; Matschei et al., 2007a]), or databases (e.g. [EMPA, 2007]) provide information on chemical species formed in concrete (cf. Section 3.1). Furthermore, standard chemistry or materials science textbooks (e.g. [Freiesleben Hansen, 1995; Callister & Callister, 2000]) or mineral and chemical databases (e.g. [MinDat, 2007; MinGal, 2007; WebEle, 2007; WebMin, 2007]) may be consulted.

- Sources containing information on corrosion products formed in a certain environment and conditions for formation of compounds between different species

  The above mentioned textbooks on metals also contain general information on corrosion products, while corrosion products formed in the concrete environment are generally not covered and many scientific papers deal with the formation of corrosion products under atmospheric or submerged conditions often in connection with chloride exposure, e.g. [Refait & Génin, 1997; Antunes et al., 2003; Rémazeilles & Refait, 2007]. Information on corrosion products observed in concrete can be found in publications dealing exclusively with this topic (e.g. [Raharinaivo et al., 1987; Sagoe-Crentsil & Glasser, 1989; Sandberg, 1998; Koleva et al., 2006; CeFrCo, 2007; Marcotte & Hansson, 2007] concerning carbon steel or e.g. [fib, 1995a; Popov, 2007] concerning zinc in concrete) mostly with regard to chloride induced corrosion. Besides such sources, literature on minerals or online mineral databases (e.g. [MinDat, 2007; MinGal, 2007; WebMin, 2007]) can often be applied beneficially, since species formed between different elements often exhibit mineralogical characteristics, especially for metals in the concrete environment.

In principle, the above listed sources are used as positive indicators for the formation of species. Our general concept in the preselection of species based on these sources is that if a thermodynamically favoured species has been observed to be formed "in nature" under comparable conditions, i.e. similar chemical substances, pressure, and temperature, the species is taken into account in the establishment of a Pourbaix diagram. In the case of absence of information on formation of a certain species under investigation in the above listed sources, we used negative indicators to confirm that this certain species can be "safely" excluded from the Pourbaix diagram. Negative indicators include, for instance, descriptions of high temperature or plasma technique processes, which are necessary for formation of the species under investigation, i.e. that its formation requires an activation energy that is out of range for steel in concrete. Such negative indicators can be found in various sources, e.g. in some of the above mentioned textbooks, publications, or online.

Besides the above mentioned sources for positive and negative indicators, we used own experimental observations to verify the input parameters, i.e. the choice of elements and the preselection of species, as well as the output of the Pourbaix diagram.

If one or more species are determined to be potentially formed by means of the above described approach and are located in the same stability domain and no other indicators for a favoured formation are available, we preselect the species with the lowest 'ΔG_f^0' value, i.e. with the highest thermodynamically probability to be formed.

In this project, we applied 'HSC' to establish custom Pourbaix diagrams. Our application of 'HSC' was limited to its thermodynamic database and on the calculation of the equilibria. Based on the exemplification of the Pourbaix diagram in Section 2.1.10, it is obvious that the required calculations are rather elaborate without using chemical reaction and equilibrium software, even if limited to preselected species.

All calculations required for the establishment of Pourbaix diagrams in 'HSC' are based on the thermodynamic parameters and relations introduced in Section 4.1 and performed by the so-called STABCAL routine. The theory behind this routine and its application in 'HSC' is beyond the scope of this thesis and reference is made to [Haung & Cuentas, 1989a; Haung & Cuentas, 1989b; Roine, 2002].

The STABCAL routine does not account for 'ΔG_f^0' of the individual species and establishes all possible equilibria of the system. So, as long as the equilibrium conditions are fulfilled, 'HSC' will produce a Pourbaix diagram disregarding the reasonability of the preselected species.[*] Therefore, an appropriate preselection of species is absolutely crucial for the establishment of *appropriate and representative* Pourbaix

[*] In civil engineering terms, the establishment of the Pourbaix diagrams can be e.g. compared to using FEM software in structural analysis. In finite elements analysis, a result will always be obtained as long as the static or dynamic equilibria can be fulfilled. However, the result only reflects the actual behaviour of a system, if due consideration is given to e.g. the input of appropriate boundary conditions and material properties as well as to a representative choice of finite elements.

diagrams. Since the STABCAL routine does not account for the magnitude of 'ΔG_f^{0}', *the preselection of species for all Pourbaix diagrams in this thesis is narrowed down to the species that are necessary for the establishment of the certain Pourbaix diagram*. For 'SEPDs' this means that only such species need to be preselected, which are *actually present* in the Pourbaix diagram (cf. for instance Table 4.2 and Figure 4.2). However, for 'MEPDs' that means that all species that are *necessary to form the preselected species (including all combined species) as well as their associated equilibrium lines* are preselected (cf. for instance Table 5.1 and Figure 5.4 [C] in Section 5.2.1.1 or Table 5.4 and Figure 5.9 [B] in Section 5.2.2.2). So, in this thesis the *Tables that introduce the preselected species of the associated Pourbaix diagram do by no means represent all thermodynamically possible or favoured species*. In particular, for 'MEPDs' the amount of thermodynamically favoured species can be in the range of several decades, while the amount of species that we consider to play a role in the system under investigation can generally be narrowed down to a maximum of e.g. ten.

A final important issue in the application of Pourbaix diagrams is the choice of ion activities for the elements to be investigated. As mentioned in Section 2.1.10, where the Pourbaix diagram was introduced, the conservative choice for the iron ion activity for passivity in the associated stability domains is 10^{-6} mol/L for the Fe-H_2O system.

The 'SEPD' for this choice of iron ion activity is shown in Figure 4.2 [A], which is identical with the Pourbaix diagram and the preselection of species as used for introduction to the theory of the Pourbaix diagram in Section 2.1.10. The same holds for Table 4.2, which lists the preselected solid and soluble species.

Table 4.2: *Species preselected for the 'SEPD' of the general Fe-H_2O system.*

Solid	Fe	Fe_3O_4	Fe_2O_3
Soluble	Fe^{2+}	Fe^{3+}	$HFeO_2^-$

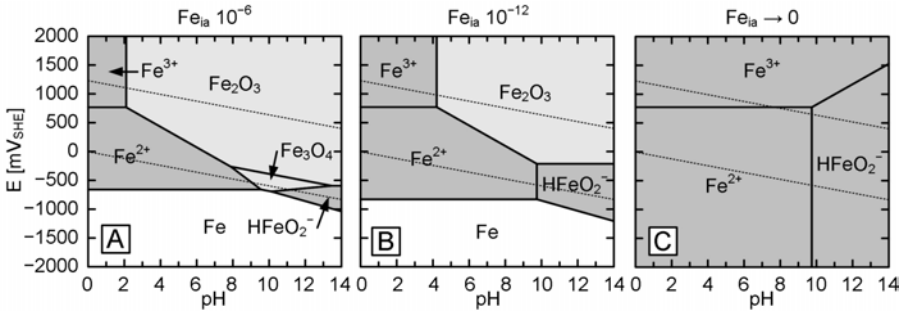

Figure 4.2: *Fe-H_2O 'SEPDs' based on Table 4.2 and different Fe_{ia}.* [A]: *Fe_{ia} = 10^{-6} mol/L as conservative value for passive stability domains.* [B]: *Fe_{ia} = 10^{-12} mol/L.* [C]: *Fe_{ia} → 0 mol/L, i.e. predominance domains of iron ions. Diagrams [B] and [C] are for exemplification purposes only and do not represent actual conditions.*

Based on the Nernst equation and the theory of the Pourbaix diagram in Section 2.1.10, it could be concluded that a decrease in iron ion activity below 10^{-6} mol/L affects the Pourbaix diagram by increasing the stability domains of the soluble compounds on expense of the domains of solid compounds. Figure 4.2 [B] exemplifies the theoretical consequence for the Fe-H_2O 'SEPD' based on $Fe_{ia} = 10^{-12}$ mol/L and the result of $Fe_{ia} \rightarrow 0$ mol/L, which corresponds to the predominance domains of ions in the Fe-H_2O system, is illustrated in Figure 4.2 [C]. However, the diagrams in Figure 4.2 [B] and [C] are for the theoretical exemplification purpose only and of *no practical relevance* in this thesis. Based on the literature and on own observations, we consider the Fe-H_2O Pourbaix diagram for an ion activity of 10^{-6} mol/L to be a reasonable lower limit for the thermodynamically favoured formation of oxide layers in the associated stability domains. A detailed discussion on this topic is beyond the scope of this thesis, but the theoretical value has been verified and calibrated for corrosion in aqueous solution by means of an extensive research program based on e.g. polarisation curves and studies on oxide solubilities [Pourbaix, 1974b], which furthermore illustrates the importance of kinetics in thermodynamic considerations.

Some metals require other considerations, but an ion activity of 10^{-6} mol/L has also been determined to be a reasonable conservative value for formation of passive layers in the associated stability domains for zinc and magnesium [Pourbaix, 1974b]. The electrochemistry of these two metals is of major importance in the considerations for the proposed new countermeasures (cf. Section 7).

So, as a basis for all following considerations in this thesis, we assume that the passive domains indicated in the Pourbaix diagrams for iron, zinc, and magnesium based on ion activities of 10^{-6} mol/L represent the actual passive domains of these metals. This means in practice that if a piece of pure iron, zinc, or magnesium is submerged in an *unlimited supply of H_2O containing none of their ions*, these metals *at least* passivate in the stability domains determined by the Pourbaix diagram of the respective Me-H_2O system with an ion activity of 10^{-6} mol/L.

However, we postulate that contrary to this limitation of the Pourbaix diagram with decreasing the ion activity below 10^{-6} mol/L, *no such limitation applies to the Pourbaix diagram with increasing ion activity above 10^{-6} mol/L.*

In other words, we assume that the equilibrium lines in the Pourbaix diagram with increasing ion activity *above 10^{-6} mol/L are without exceptions determined by the Nernst equation* (cf. Section 2.1.10). This is exemplified in Figure 4.3, which shows the effect of increasing the iron ion activity in the Fe-H_2O 'SEPD' from 10^{-6} mol/L (Figure 4.3 [A]) to 10^{-3} mol/L (Figure 4.3 [B]) and to 1 mol/L (Figure 4.3 [C]).

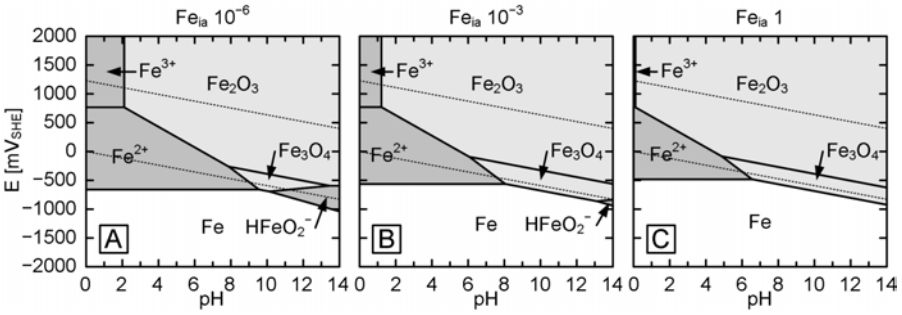

Figure 4.3: *Fe-H_2O 'SEPDs' based on Table 4.2 with Fe_{ia}.* [A]: *$Fe_{ia} = 10^{-6}$ mol/L.* [B]: *$Fe_{ia} = 10^{-3}$ mol/L.* [C]: *$Fe_{ia} = 1$ mol/L.*

In the 'SEPDs' in Figure 4.3 it can be observed that the immune and passive domains enlarge with increasing iron ion activity at the iron-electrolyte interface on expense of the corrosion domains. Based on this thermodynamic aspect, it can be concluded that the electrochemistry of the Fe-H_2O system can be largely influenced by the iron ion activity at the iron-electrolyte interface. In Chapter 7 it is shown that the same holds for zinc and magnesium. We think that this is a central aspect in the description of reinforcement corrosion and in the design of countermeasures, which appears to be disregarded. Different to metals directly exposed to the environment, metals in concrete benefit from the "built in" diffusion control of the concrete. We think that there are different ways of further improving the diffusion limitations of metal ions and other ions at the concrete-metal interface. This is a central aspect in the underlying principles of the proposed new countermeasures, which are discussed in detail in Chapter 7.

Apart from information on the composition of pore solutions (cf. Table 3.2 in Section 3.1.5), no experimental data is available to evaluate the effect of the concentrations of different species in the concrete with regard to the electrochemistry of the embedded steel or, more general, the embedded metal. We think that it is important to realise that the environment that actually affects the electrochemistry of a metal embedded in concrete corresponds to the micro-environmental conditions, i.e. the local environment at the concrete-metal interface. It is known that for metallic corrosion in aqueous solutions the electrolyte composition at the metal surface largely differs from the one of the bulk electrolyte (cf. Section 2.2.5) and, due to the limited transport and mobility of species (cf. Section 3.1.7), we consider this effect to be even more pronounced in case of corrosion of metals in concrete. Moreover, the environment at the concrete-metal interface is a time dependent variable that largely changes with the electrochemical conditions, i.e. the reactions alter the environment and vice versa, and considerable concentration gradients may be developed, in particular after corrosion initiation. For instance, in case of chloride induced corrosion in uncracked concrete, the chloride threshold can be relatively precisely assessed for a given concrete composition, concrete-steel interface properties, and exposure conditions, cf. Chapter 3. However, as described in more detail in Section 5.2.2.2, after corrosion initiation corrosion

pits experience drastic changes in the pH and chloride concentration, so that the exact conditions cannot be predicted. Therefore, we decided to base our theoretical considerations, which relate to the effect of ion activity changes, on a rather *large scale of ion activities*, as given in Table 4.3.

Table 4.3: *Molar masses [Ouku, 1999; Ouku, 2002; WebEle, 2007] and ion activities in mol/L and mg/L taken into consideration in Pourbaix diagrams to evaluate the effect of changes in the ion activity.*

Element	Molar mass	Ion activity in Pourbaix diagrams		
		10^{-6} mol/L	10^{-3} mol/L	1 mol/L
	g/mol	mg/L		
Fe	55.85	0.06	55.85	55,845
Zn	65.41	0.07	65.38	65,409
Mg	24.31	0.02	24.31	24,305
Ca	40.08	0.04	40.08	40,078
C	12.01	0.01	12.01	12,011
Cl	35.45	0.04	35.45	35,453

In conclusion, we consider that Pourbaix diagrams established on the above described considerations to be a comprehensive and convenient tool for the illustration of the corrosion tendencies. Even if the assumed ion activities do not reflect the actual situation of the system, they give a clear indication of the *governing parameters* for immunity, passivity, and corrosion in the system under investigation, given that the Pourbaix diagram represents all factors that can have an effect on the associated stability domains. *We think that these parameters indicate how the conditions in the system can be manipulated to make corrosion thermodynamically impossible.*

It should be emphasised, however, that all information that can be obtained from the Pourbaix diagram and accordingly conclusions drawn upon that information, depend on the underlying assumptions. Thus, the Pourbaix diagram is only of benefit, if these assumptions apply to the system under investigation; otherwise, the diagram is meaningless.

4.2.2 Applicability of Pourbaix Diagram for Concrete-Steel System

In this Section, the most important aspects, which we considered with regard to the validity of the Pourbaix diagram for the description of the electrochemistry of the concrete-steel system, are summarised.

Concerns could be raised as to the validity of the Pourbaix diagram for the description of the electrochemistry of steel or other metals in concrete, i.e. if and to which extent the Pourbaix diagram reflects the complex electrochemistry at the concrete-metal interface. As mentioned in Section 4.2.1, the Pourbaix diagram for an 'El'-H_2O system is only valid in the absence of substances which can form soluble complexes or in-

soluble salts with the investigated element [Pourbaix, 1974b]. With regard to the complex chemistry of the pore solution and the solid phases of the concrete as well as the drastic change of the chemistry with carbonation and the ingress of chloride ions (cf. Section 3.1), this probably is the most critical limitation in the use of Pourbaix diagrams for the description of reinforcement corrosion and the design of countermeasures. Based on the proposed application of the Pourbaix diagram (cf. Section 4.2.1), we think that it is possible to establish custom-made, representative Pourbaix diagrams for the concrete-steel system, despite the complex chemistry of the concrete-environment and the various soluble and insoluble complexes that can be thermodynamically favoured to be formed in combination with the embedded metal. While certain limitations apply for "pure" magnesium and zinc in concrete (cf. Chapter 7), this holds in particular for carbon steel.

In principle, the considerations in this Section are limited to the electrochemistry of the metal and the chemistry of the environment, i.e. the influence of the concrete composition on the Pourbaix diagrams for the investigated metal. We presume that, with regard to the thermodynamics, all other electrochemical factors in the concrete environment are comparable to corrosion in aqueous electrolytes, whereas the kinetic conditions are entirely different. In other words, we assume that the concrete bulk and the concrete-metal interface behave like a complex electrolyte, in particular with regard to diffusion of chemical species. Yet, from a thermodynamic point of view, we consider the embedded metal to behave in the same way as submerged in an electrolyte that provides the same conditions, i.e. with regard to the composition, aeration, etc. Among others, this includes that the passivation behaviour of a metal embedded in concrete and the stability domain of water are considered to be reflected by a Pourbaix diagram, which describes the corresponding aqueous metallic corrosion process under the same condition. Thus, we postulate that the ion activity of 10^{-6} mol/L as a conservative value for passivation and the effect of increasing the ion activity above this value, as described in Section 4.2.1, are also valid for at least steel and zinc in concrete.

Based on the above assumptions, which are further elaborated in Chapter 5, the influence of the electrochemistry of the metal and the chemistry of the concrete "electrolyte" are the only parameters, which are left to be evaluated for a verification of the applicability of the Pourbaix for the description of a concrete-metal system. This evaluation, based on the Fe-H_2O system, is summarised in Sections 4.2.2.1 and 4.2.2.2. Selected notes are made with regard to the validity of the Pourbaix diagram for zinc and magnesium in concrete, while a detailed discussion on the zinc-concrete system and the magnesium-concrete system is provided in Section 7.3.1 and Section 7.3.2, respectively.

4.2.2.1 Fe-H_2O System and Electrochemistry of Carbon Steel

Due to the fact that steel is almost entirely composed of iron (cf. Section 3.2) we presume that iron adequately reflects the electrochemical properties of carbon steel reinforcement. Moreover, iron has been and is successfully used to describe the electrochemistry of steel. Thus, we assume that the Pourbaix diagram of the Fe-H_2O system applies for carbon steel reinforcement.

The above considerations are not necessary for the Zn-H_2O and the Mg-H_2O system, as application of zinc and magnesium in this project is based on the pure, i.e. the unalloyed, metal.

4.2.2.2 Fe-H_2O System and Chemistry in Concrete

The influence of the complex concrete chemistry on the formation of species, which potentially interfere with the Fe-H_2O system, is the most critical concern in establishing representative Pourbaix diagrams. Besides certain misconceptions of the thermodynamics of reinforcement corrosion, which are discussed in more detail in Chapter 5, this concern is probably the main reason for the reluctance in using the Pourbaix diagram in the area of reinforcement corrosion. We postulate that considerations on 'MEPDs', based on the approach described in Section 4.2.1 in combination with experimental verifications, allow the application of Pourbaix diagrams in complex chemical systems, including the concrete-steel system.

In the following, our most important considerations on this topic are given with respect to uncontaminated concrete, carbonated concrete, and chloride contaminated concrete:

- Uncontaminated concrete

  Based on theoretical considerations and verifications on the effect of formation of possible compounds in 'HSC', we assume that the electrochemistry of the Fe-H_2O system is from a thermodynamic point of view not significantly affected by the chemical properties of the concrete apart from the hydrogen and hydroxyl ion activity, i.e. the pH, which is reflected by the Pourbaix diagram. The concentrations of SO_4^{2-} and Cl^- are considered to be too low to affect the Fe-H_2O system in uncontaminated concrete (cf. Section 3.1). Na^+ and K^+ can form various thermodynamically favoured complexes with iron, in particular sodium and potassium ferrites. Yet, based on the proposed approach of positive and negative indicators for the preselection of the species, we found that the temperature of formation for these complexes is far beyond the temperature conditions in the concrete structures. Besides the absence of information on formation under natural conditions, processes described for the production of these complexes relate to high temperature and plasma techniques (e.g. [Randhawa & Sweety, 1998; Sofin & Jansen, 2005; Rousseau & Bernheim, 2007]), which are regarded as negative indicators. Hence, all complexes between iron and sodium or potassium are considered to be

insignificant for the establishment of the Pourbaix diagram for steel in uncontaminated concrete. Calcium is present in concrete in various complexes before and after hydration (cf. Section 3.1). The high reaction affinity of calcium is demonstrated by e.g. carbonation (cf. Section 3.1.7.2). Calcium carbonate ($CaCO_3$) was also observed as a constituent of the passive layer (e.g. [Poursaee & Hansson, 2007]). However, we do not think that $CaCO_3$ has a major effect on the passive domains of steel in concrete. A short note on the effect of calcite on the passivation is given in Section 5.2.1.1.

- Carbonated concrete

  We assume that besides the reduction in alkalinity the effect of carbonation can be considered by introducing carbon to the Fe-H_2O 'SEPD'. Based on evaluations of the thermodynamically favoured species in the Fe-C-H_2O system, we found that iron carbonate ($FeCO_3$), also known as siderite, is the only potentially formed species. $FeCO_3$ has a considerable effect on the passivation area in the 'MEPD' of the Fe-C-H_2O system. However, based on a comparison of the 'ΔG_f^0' values for the evaluation of the mutual formation, Fe_2O_3 ('ΔG_f^0' = −741 kJ/mol) is thermodynamically favoured over $FeCO_3$ ('ΔG_f^0' = −667 kJ/mol). This notion is confirmed by nature, since siderite as a natural mineral generally experiences a surface alteration to an iron oxide [MinGal, 2007]. Hence, we assume that $FeCO_3$ can be omitted from the Pourbaix diagram for carbonated concrete and thus steel in carbonated concrete can be treated in the same way as steel in uncontaminated concrete.

- Chloride contaminated concrete

  The potentially formed complexes between steel and *uncontaminated* and *carbonated* concrete are limited to insoluble salts, which can be formed in the corresponding passivity domain of the Fe-H_2O system or extend this domain, if preselected for formation in an 'MEPD'. Thus, we think that it to be on the safe side to exclude such species from the Pourbaix diagram. However, *the situation with adding chloride to the Fe-H_2O system is entirely different*. The thermodynamic effect of chloride addition is in the 'MEPD' of the Fe-Cl-H_2O system reflected by formation of soluble complexes of ferric chloride ($FeCl_2^+$) and, with higher chloride concentration, ferrous chloride ($FeCl^+$). The stability domains of these complexes are not limited to the corresponding ones of ferrous ion and ferric ion in the Fe-H_2O system, but, depending on the chloride concentration, they extend into the corresponding passive domains of the Fe-H_2O system. However, thermodynamic considerations alone are not sufficient in describing chloride induced corrosion.

  The localised breakdown of the passive layer under chloride initiated corrosion and the resulting of formation of corrosion pits is a kinetic aspect that is generally approached by the pitting potential 'E_{pit}' (cf. Section 2.3.2), which is further elaborated in Section 5.2.2.2. Nevertheless, we think that Fe-Cl-H_2O 'MEPDs'

can be advantageously applied to describe and understand corrosion propagation of chloride induced corrosion, as exemplified in Section 5.2.2.2.

In conclusion, we think that the 'SEPD' of the Fe-H_2O system sufficiently reflects the chemical properties of steel in uncontaminated and carbonated concrete, but chloride contaminated concrete requires special considerations. The Fe-Cl-H_2O 'MEPD' allows comprehensive and insightful considerations on the corrosion propagation. However, it should be emphasised that corrosion initiation by chloride ions cannot be reflected by thermodynamic principles alone.

Concerning zinc and magnesium, the same applies with regard to Na^+ and K^+, as described for iron in uncontaminated concrete. We suggest that neither of the two metals form complexes with sodium and potassium, which need to be taken into account in the Pourbaix diagram. However, the presence of calcium plays a major role for both for zinc and magnesium. An important complex to be taken into account for zinc in concrete is calcium hydroxyzincate, e.g. [fib, 1995a; Fratesi, 2002a; Bertolini et al., 2004; Yeomans, 2004]. We consider calcium hydroxyzincate to contribute to the passivity domain of zinc in concrete, but not to interfere with its electrochemistry otherwise. Yet, based on theoretical considerations and own experimental observations, we observed that calcium has an even more pronounced effect on the electrochemistry of magnesium, because formation of calcite prevents the passivation of magnesium in the concrete environment. Hence, magnesium requires special considerations. With regard to carbonation, we consider that e.g. the formation of zinc carbonate ($ZnCO_3$) contributes to the resistance of galvanised steel in carbonated concrete. Presence of chlorides requires special considerations for both zinc and magnesium. The parameters influencing the electrochemistry of zinc and magnesium in the concrete environment and the associated Pourbaix diagram are given in Chapter 7, which deals with the application of these metals for the proposed new countermeasures.

5 Thermodynamics of Reinforcement Corrosion

In Section 2.1 the necessary analytical tools to describe aqueous metallic corrosion on a thermodynamic basis were introduced and our use of these tools and their applicability were discussed in Chapter 4. In this Chapter the theory is applied in combination with the information on the complex physical, chemical, and electrochemical properties of the concrete-steel system, which has been summarised in Chapter 3, to describe the electrochemistry of steel in concrete on a thermodynamic basis.

It should be emphasised here that we disregard by no means the importance of kinetics in corrosion processes in general and in particular for corrosion of steel in concrete. Quite on the contrary, we regard kinetic considerations (cf. Section 2.2) to be essential and emphasise that conclusions based on thermodynamic considerations are pointless without taking reaction kinetics into due account. Kinetic considerations do not only exhibit the limitations of thermodynamic models, but they can also be beneficially applied to describe corrosion processes of steel in concrete. Especially polarisation curves can be used in an insightful manner for that purpose, as it has been done in e.g. [Bertolini et al., 2004].

However, as mentioned in Chapter 4, we think that thermodynamic considerations provide a lot of potential for the detailed understanding of corrosion mechanisms and, as opposed to kinetic considerations, allow predictions for the system based on theory. The reason for the apparently limited use of the Pourbaix diagram in this area seems to be due to the intricate assumptions, which are necessary to obtain representative results (cf. Section 4.2.1), or based on misconceptions with regard to its applicability (cf. Section 4.2.2).

In contrast to the rather limited application of Pourbaix diagrams in the area of reinforcement corrosion, reaction mechanisms have been postulated in the literature for the description of corrosion processes of steel in concrete. In standard textbooks the provision of reaction mechanisms is often limited to the fundamental corrosion mechanism for steel in concrete, which is further elaborated in Section 5.1.3. However, there are various other possible mechanisms for the different corrosion states of steel in concrete. Some of these mechanisms have been postulated in other literature, e.g. in scientific papers or theses. Yet, as is discussed in more detail in Section 5.2, many of the postulated mechanisms seem to exhibit thermodynamic inconsistencies.

Thermodynamics control the underlying principles in corrosion processes and hence a reaction does not occur, if thermodynamically impossible. Considerations based on the Pourbaix diagram and on reaction mechanisms allow to determine which reactions are thermodynamically possible or impossible in a certain system, given that they reflect the actual condition in the system under investigation. Thus, we think that there

is a need for a thermodynamically consistent description of the electrochemistry of steel in concrete. The proposed approach to that description is summarised in this Section, which differs to quite some extent from the description of carbon steel reinforcement corrosion in textbooks.

Before the different states and conditions of reinforcement corrosion are described based on reaction mechanisms and the Pourbaix diagram in Section 5.2, our general concept of the electrochemistry of steel in concrete and possible misconceptions in the literature are discussed in Section 5.1.

It should also be noted that this Chapter only deals with the thermodynamic principles that apply to carbon steel in ordinary Portland cement concrete. The electrochemistry of other reinforcement materials and the effect of mineral additions and/or chemical admixtures are summarised in Chapter 6.

Corrosion rates of steel in concrete are only marginally dealt with in this Chapter. Among abundant publications, reference is made to textbooks on reinforcement corrosion, e.g. [Schießl et al., 1988; Broomfield, 1997; Bentur et al., 1997; Cigna et al., 2003; Bertolini et al., 2004; Böhni et al., 2005; Raupach et al., 2007]. Also, structural aspects concerning corrosion and corrosion damage are treated rather marginally. Besides the theory on the most important structural aspects controlling reinforcement corrosion, which was briefly summarised in Chapter 3, reference is made to the above literature, where these subjects are generally dealt with in detail.

5.1 Electrochemistry of Steel in Concrete

According to [Schießl et al., 1988] it is (or, rather: it was) not uncommon to find the opinion expressed that concrete protects the reinforcing steel by preventing ingress of water and oxygen. This misconception, which might be due to observations of atmospheric steel corrosion (e.g. the mechanism described in Section 2.1.1) does probably not represent the present understanding of people in the concrete business, but it reflects some misunderstandings about the thermodynamics of steel in concrete, in particular with regard to the passive state and the development of the corrosion potential.

From Section 3.1 it can be concluded that concrete is neither watertight nor airtight. So, nowadays there is a general agreement that steel in uncontaminated concrete is protected by the formation of a stable and dense passive layer due to the high alkalinity of the pore solution (cf. Section 3.1.5). However, in some descriptions of the passive state in the literature on reinforcement corrosion, the character of the anodic and cathodic reactions leading to the formation of the passive layer and the fact that the layer is not formed *despite*, but *due* to the presence of oxygen and water seem not to be fully acknowledged. In relation to that, the effect of oxygen and water on the corrosion potential of steel in concrete seems to be misinterpreted in some literature.

5.1.1 Anodic Corrosion Products

In Section 2.1.9, it was mentioned that according to [Bardal, 2004]: *Passive layers "... are not formed by deposition of corrosion products from the liquid, as this usually gives more or less porous surface layers, but that the oxide is directly formed in close connection with the crystal structure of the metal."* However, this central aspect seems to be often overlooked in the description of the passive and active corrosion in some literature on reinforcement corrosion, in particular in textbooks. It appears that it is often not acknowledged that *the passive state is based on the same principles as active corrosion, i.e. a combination of anodic oxidation with one or more cathodic reduction reactions.* In principle, the only, but significant difference between the active and passive state is that different iron species are formed by the anodic reaction and the enormous difference in the corrosion rates, which is closely linked to the type of products formed. From a thermodynamic perspective, this difference is based on the fact that dissimilar species are favoured depending on the corrosion potential 'E_{corr}' and the pH at the steel-electrolyte interface. The similarity between active corrosion and passivity is exemplified by the standard 'SEPD' of the Fe-H_2O with an iron ion activity of 10^{-6} mol/L in Figure 5.1, which we assume to sufficiently reflect the chloride free concrete-steel environment (cf. Section 4.2.2).

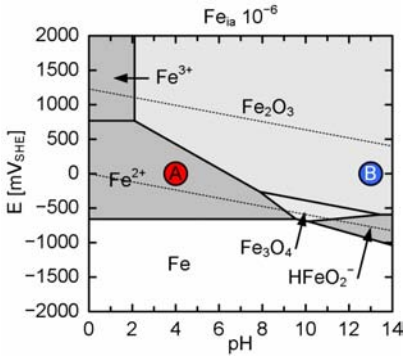

Figure 5.1: *Fe-H_2O 'SEPD' based on Table 4.2 and $Fe_{ia} = 10^{-6}$ mol/L. Identification of possible range of 'E_{corr}' and pH for carbon steel in (A) organic rich lake water and (B) uncontaminated semi-saturated concrete.*

Since this Pourbaix diagram is assumed to be valid for general aqueous corrosion, it is used to exemplify a passive and an active corrosion condition for a surface of iron and hematite, e.g. a piece of carbon steel* that was initially stored under atmospheric conditions and submerged in (A) organic rich lake water and (B) embedded in uncontaminated semi-saturated concrete. The following thermodynamic conditions apply in these two cases:

* We consider carbon steel to be interchangeable with iron in relation to their electrochemical properties (cf. Section 4.2.2.1).

- In case (A) the 'E_{corr}' can be assumed to be around 0 mV_{SHE} [WOU, 2007] and the pH at the steel-electrolyte interface to be around 4 [Møller, 2003b]. Under these conditions the iron on the surface will not start to dissolve abruptly, but will dissolve steadily to form soluble ferrous ion governed by the thermodynamically favoured reaction:

$$Fe \rightarrow Fe^{2+} + 2e^- \quad \left(E_0^0 = -475\{447\}\, mV_{SHE} \right) \qquad [5.1]$$

'E_{corr}' is in the theoretical stability domain of water and [5.1] proceeds along with reduction of oxygen in acid solutions as dominant cathodic reaction:

$$O_2 + 4H^+ + 4e^- \rightarrow 2H_2O \quad \left(E_0^0 = 1230\{1229\}\, mV_{SHE} \right) \qquad [5.2]$$

The reduction of oxygen [5.2] can be supported by the reduction of Fe_2O_3, which is initially present at the surface:

$$Fe_2O_3 + 6H^+ + 2e^- \rightarrow 2Fe^{2+} + 3H_2O \quad \left(E_0^0 = 789\, mV_{SHE} \right) \qquad [5.3]$$

- In case (B) the 'E_{corr}' can be assumed to also be around 0 mV_{SHE} and the pH at the steel-electrolyte interface in uncontaminated concrete to be around 13 (cf. Section 3.1.5). Under this condition the hematite on the surface is thermodynamically stable and the iron on the surface starts to be oxidised not abruptly, but steadily to form solid hematite governed by the thermodynamically favoured reaction:

$$2Fe + 3H_2O \rightarrow Fe_2O_3 + 6H^+ + 6e^- \quad \left(E_0^0 = -51\, mV_{SHE} \right) \qquad [5.4]$$

As in case (A), the 'E_{corr}' is in the theoretical stability domain of water and [5.4] proceeds with reduction of oxygen in the alkaline environment as cathodic reaction:

$$O_2 + 2H_2O + 4e^- \rightarrow 4OH^- \quad \left(E_0^0 = 402\{401\}\, mV_{SHE} \right) \qquad [5.5]$$

Thus, both active corrosion and passivity consist of anodic oxidation reactions. In the active corrosion case (A) iron is oxidised to form soluble Fe^{2+}, i.e. Fe is dissolved, whereas in the passivity case (B) iron is *directly* oxidised to solid Fe_2O_3, which constitutes the formation of the passive layer.

Disregarding the low potential corrosion domain, which favours formation of soluble $HFeO_2^-$ (cf. Section 5.2.1.2), from the Pourbaix diagram in Figure 5.1 it can be concluded that no soluble species are thermodynamically favoured to be formed in the pH range of uncontaminated concrete, i.e. pH 12-14 (cf. Section 3.1.5). However, with depassivation by carbonation or chloride induced corrosion (cf. Sections 5.2.2.1 and 5.2.2.2, respectively) the pH at the concrete-steel interface approaches values that favour the anodic dissolution reaction forming Fe^{2+} [5.1] to take place. Depending on the availability of oxygen, the soluble Fe^{2+} experiences further transformations, which are described in detail in Section 5.2.

As mentioned in Sections 2.1.9 and 2.2.5.3, the passive layer impedes the corrosion kinetics, which largely limits further anodic dissolution once a certain thickness and denseness is attained. These slow kinetics enable corrosion rates as low as 0.1 µm/y in the passive state [Arup, 1983], whereas corrosion rates up to 100 µm/y (concrete contaminated by chloride at 90%-95% saturation or carbonated concrete at 95%-98% saturation) or under the worst conditions up to even 1000 µm/y (concrete severely contaminated by chloride at 95%-98% saturation) have been observed for the active corrosion state [Bertolini et al., 2004].

In conclusion, it can be said that both the passive and the active corrosion state constitute anodic oxidation reactions, but the difference in the reaction kinetics, which, in principle, results from the difference in the products formed by the different anodic reaction, is enormous. This again, shows the importance of kinetic considerations in the area of reinforcement corrosion. However, the type of products formed by the anodic reaction, which we understand to be the fundamental parameter controlling the magnitude of the corrosion rate, is determined by the thermodynamics of the system. Thus, we suggest that a thermodynamically consistent description of reinforcement corrosion and a thermodynamically founded design of countermeasures based on this description is the key to counteract reinforcement corrosion.

5.1.2 Corrosion Potential

In both cases (A) and (B) of the exemplification in Section 5.1.1, the main cathodic reaction is reduction of oxygen. As is discussed in more detail in Section 5.2, we assume that the reduction of oxygen in the alkaline environment [5.5] is the dominant cathodic reaction for steel in concrete, especially in the passive state. As described in Section 2.1, an anodic reaction cannot proceed without a cathodic reaction and thus the passive compounds, i.e. the Fe_2O_3 in the anodic reaction [5.4], cannot be formed without the cathodic reaction [5.5], which involves consumption of oxygen and water to form hydroxyl. This aspect underlines that the corrosion protection offered by uncontaminated concrete to the embedded steel is not attained despite, but due the presence of oxygen and water.

Leaving out the influence of the oxygen and hydrogen overpotentials (cf. Sections 2.1.10 and 2.2.4) and reduction of oxidised iron species as supporting cathodic reactions, the following can be concluded from the Pourbaix diagram in Figure 5.1 with regard to possible cathodic reactions (cf. Sections 2.1.2 and 2.1.10):

- If the electrode potential in case (A) is lowered below the hydrogen equilibrium line, the reduction of oxygen in acid electrolytes [5.2] is supported by the hydrogen ion reduction in acid solutions:

$$2H^+ + 2e^- \rightarrow H_2 \quad \left(E_0^0 = 0\,mV_{SHE} \right) \qquad [5.6]$$

- If the electrode potential in case (B) is lowered below the hydrogen equilibrium line, the reduction of oxygen in alkaline electrolytes [5.5] is supported by the reduction of water in alkaline solutions:

$$2H_2O + 2e^- \rightarrow H_2 + 2OH^- \quad \left(E_0^0 = -828\,\{-828\}\ mV_{SHE} \right) \qquad [5.7]$$

- In both cases (A) and (B) raising the electrode potential above the oxygen equilibrium line leads to oxygen evolution as anodic reaction described by inverting reactions [5.2] and [5.5]:
  - Case (A), i.e. formation of oxygen in the acid environment:

$$2H_2O \rightarrow O_2 + 4H^+ + 4e^- \quad \left(E_0^0 = 1230\,\{1229\}\ mV_{SHE} \right) \qquad [5.8]$$

  - Case (B), i.e. formation of oxygen in the alkaline environment:

$$4OH^- \rightarrow O_2 + 2H_2O + 4e^- \quad \left(E_0^0 = 402\,\{401\}\ mV_{SHE} \right) \qquad [5.9]$$

An increase or decrease of the electrode potential could *theoretically* be obtained in both cases by addition of a reducing or oxidising agent (cf. Section 2.1.6) or cathodic or anodic polarisation (cf. Section 2.2.3), respectively.

The above considerations are based on the theoretical equilibrium lines limiting the stability domain of water. As mentioned in Section 2.1.10, in practice these lines will always be replaced by the hydrogen and oxygen overpotential. The practical meaning of these overpotentials, in particular with regard to hydrogen evolution, in the area of reinforcement corrosion is discussed in more detail in Chapters 6 and 7, as certain countermeasures require additional considerations on that subject.

For the purpose of this Section, we think that it is sufficient to state that reduction of oxygen in the alkaline environment [5.5] is the dominant cathodic reaction for unpolarised steel in uncontaminated concrete. In general, we expect the following to be true for steel in uncontaminated concrete at any degree of saturation (cf. Section 3.1.7):

- Without anodic polarisation electrode potentials leading to transpassivity (i.e. oxygen evolution) are not obtained for steel in concrete, i.e. the half-cell reactions [5.8] and [5.9] do generally not play a role in corrosion of steel in concrete. This includes (with certain exceptions) most available countermeasures (cf. Chapter 6). However, certain misconceptions about the transpassivity state of steel in concrete seem to exist in the literature, in particular with regard to the effect of stray currents. We generally agree that under certain conditions stray currents can polarise the reinforcing steel to very noble potentials, so that transpassivity can be attained. Yet, this condition does not lead to the dissolution of iron (i.e. active corrosion) in the first place, because the anodic reaction is oxygen evolution, which can take place on the surface of the passive layer (electron conducting, but not ion conducting, cf. Section 2.1.9). Nevertheless, if the half-cell reaction [5.8] is thermody-

namically favoured in the transpassivity state, H^+ is steadily formed, which can eventually lead to sufficient neutralisation for depassivation and hence initiation of active corrosion.

- Without cathodic polarisation electrode potentials leading to hydrogen ion reduction are generally not attained for steel in uncontaminated concrete (cf. Section 5.2.1). We assume that the oxygen depletion required to lower 'E_{corr}' to enable hydrogen ion reduction is, even under laboratory conditions, difficult to attain. Thus, we think that the reduction of water in alkaline electrolytes [5.7] does not play a significant role for the electrochemistry of carbon steel in uncontaminated concrete.

However, under certain circumstances hydrogen ion reduction can play a minor role in carbonated concrete and has a significant effect in chloride induced corrosion, which is further elaborated in Section 5.2.2. Moreover, we assume that oxygen reduction in acid electrolytes [5.2] can complement oxygen reduction in the alkaline environment [5.5] in case of chloride induced corrosion (cf. Section 5.2.2.2).

It is also important to note that some available countermeasures (cf. Section 6) and the proposed new countermeasures (cf. Section 7) include corrosion potentials that surpass the theoretical hydrogen equilibrium line, i.e. 'E_{corr}' is lower than (cf. Section 2.1.10):

$$E_{0,H^+/H_2} = -0.059 \times pH \qquad [5.10]$$

In these cases and for the conditions under chloride induced corrosion of carbon steel in concrete, special considerations on the hydrogen overpotential are necessary.

Related to the above considerations on the possible cathodic reactions, there seem to be common misconceptions in some literature on reinforcement corrosion related to the development of the corrosion potential 'E_{corr}' of steel in concrete. Therefore, the following should be emphasised:

- Development and magnitude of 'E_{corr}' in general

  As exemplified by the polarisation curves in Section 2.2.5, the corrosion current 'i_{corr}' in the passive state is determined by the anodic reaction. In corrosion science literature this condition is commonly referred to as being under anodic control [Bardal, 2004], because the anodic reaction limits the corrosion rate, disregarding the equilibrium potential of the cathodic reaction and thus the magnitude of the resulting corrosion potential 'E_{corr}'.

  With regard to the development and magnitude of 'E_{corr}', the term anodic control seems to be misleading, since the effect of the cathodic reaction on 'E_{corr}' often appears to be misinterpreted. Hence, the following should be noted:

- 'E_{corr}' is not a parameter of a certain metal in a certain electrolyte, but obtained as the mixed potential of the equilibrium potential of the anodic reaction '$E_{0,a}$' and the cathodic reaction '$E_{0,c}$' (cf. Section 2.2.3).
- The cathodic process raises 'E_{corr}', whereas the anodic process lowers 'E_{corr}'.

This notion can be comprehensibly illustrated by means of polarisation curves, as e.g. shown in Section 2.2.5. However, it can also be accessed by means of thermodynamic considerations by qualitative comparison of the equilibrium potentials. The 'E_0^{0}' of the anodic and cathodic reactions does naturally not reflect '$E_{0,a}$' and '$E_{0,c}$' that govern the equilibrium at a certain pH. However, 'E_0' of the half-cell reactions calculated by the Nernst equation can be applied for that purpose (cf. Section 2.1.8). This is shown based on the exemplifications given in Section 5.1.1, where an 'E_{corr}' of 0 mV_{SHE} was assumed for both cases (A) at pH 5 and (B) at pH 13:

- Anodic reaction in case (A):

$$\begin{aligned} &Fe \rightarrow Fe^{2+} + 2e^- \quad \left(E_0^0 = -475\,\{447\}\,mV_{SHE} \right) \\ &E_0(pH\,5) = -475\,mV_{SHE} \end{aligned} \qquad [5.11]$$

- Cathodic reactions in case (A):

$$\begin{aligned} &O_2 + 4H^+ + 4e^- \rightarrow 2H_2O \quad \left(E_0^0 = 1230\,\{1229\}\,mV_{SHE} \right) \\ &E_0(pH\,5) = 935\,mV_{SHE} \end{aligned} \qquad [5.12]$$

$$\begin{aligned} &Fe_2O_3 + 6H^+ + 2e^- \rightarrow 2Fe^{2+} + 3H_2O \quad \left(E_0^0 = 789\,mV_{SHE} \right) \\ &E_0(pH\,5) = 198\,mV_{SHE} \end{aligned} \qquad [5.13]$$

- Anodic reaction in case (B):

$$\begin{aligned} &2Fe + 3H_2O \rightarrow Fe_2O_3 + 6H^+ + 6e^- \quad \left(E_0^0 = -51\,mV_{SHE} \right) \\ &E_0(pH\,13) = -819\,mV_{SHE} \end{aligned} \qquad [5.14]$$

- Cathodic reaction in case (B):

$$\begin{aligned} &O_2 + 2H_2O + 4e^- \rightarrow 4OH^- \quad \left(E_0^0 = 402\,\{401\}\,mV_{SHE} \right) \\ &E_0(pH\,13) = 463\,mV_{SHE} \end{aligned} \qquad [5.15]$$

The differences in the magnitudes of 'E_0' at the associated pH values and the assumptions regarding the anodic and cathodic overpotentials (cf. Section 2.2.4) provide a beneficial indication on the thermodynamic condition of the system.

Organic rich lake water was chosen for the exemplification purpose to refer to a realistic 'E_{corr}' for steel in an aqueous solution with low potential that compares to an average 'E_{corr}' of steel in uncontaminated concrete, i.e. around

0 mV_{SHE}. If an aerated solution with the same pH had been considered instead of organic rich lake water the driving force for active corrosion would have been much higher.

Moreover, taking into account that polarisation curves are limited to a certain pH value, we consider the immediate presentation of the pH dependencies of these half-cell reactions, in particular for the most important cathodic reactions, i.e. oxygen and hydrogen ion reduction, to be a beneficial aspect in the Pourbaix diagram (cf. Figure 5.1). However, the equilibrium potentials of [5.11] and [5.13] are dependent on the assumed iron ion activity.

- The magnitude of '$E_{0,c}$' is controlled by the availability of oxygen

  With decreasing oxygen availability '$E_{0,c}$' decreases and hence the anodic polarisation and with that the oxidation power or corrosion tendency of the system goes down, and vice versa. This notion can also be comprehensibly illustrated by means of polarisation curves, as e.g. shown in Section 2.2.5. Yet, it can also be thermodynamically accessed by e.g. expressing the Nernst equation describing the oxygen equilibrium line (cf. Section 2.1.10) as a function of the pH and the partial oxygen pressure 'p_{O2}':

$$E_{0,O_2/H_2O} = 1.230 - 0.059 \times pH + 0.015 \times \log\left(p_{O_2}\right) \quad [5.16]$$

  As mentioned, 'p_{O2}' = 1 bar represents standard conditions, and it is obvious from [5.16] that '$E_{0,c}$' decreases with decreasing 'p_{O2}' and vice versa.

- Development and magnitude of 'E_{corr}' in the passive state

  As long as the steel is in the passive state we consider the following to be true with regard to the development and magnitude of 'E_{corr}':

  - 'E_{corr}' is dominated by the cathodic process. This is due to the anodic process being hampered by the passive layer, whereas the cathodic process can take place on the surface of the passive layer (the passive layer of steel is electron conducting, but not ion conducting, cf. Section 2.1.9).
  - In contrast to some literature, we consider the formation of products in all states to be "direct" and the product to be determined by the associated thermodynamically favoured anodic reaction. For the passive state that means, for instance, that formation of hematite as described by [5.14] involves no intermediate steps. If a sufficient amount of oxygen is available and the cathodic process "moves" 'E_{corr}' in the thermodynamic stability domain of Fe_2O_3, hematite is directly formed in the presence of water (cf. Figure 5.1 and half-cell reaction [5.14]). With lower oxygen content and consequently lower 'E_{corr}', formation of Fe_3O_4 or $HFeO_2^-$ can be favoured, which is dealt with in Sections 5.2.1.1 and 5.2.1.2, respectively.

- Given that the steel remains passive, 'E_{corr}' increases with decreasing alkalinity of the concrete and vice versa, which is due to '$E_{0,c}$' increasing with decreasing alkalinity (cf. equation [5.16] and the slope of the oxygen equilibrium line in Figure 5.1).

- Development and magnitude of 'E_{corr}' in the active corrosion state

  With initiation of active corrosion or corrosion propagation, we emphasise the following with regard to the development and magnitude of 'E_{corr}':

  - The often cited* drop of 'E_{corr}' with corrosion initiation, commonly referred to as potential drop, is not due to the change of '$E_{0,c}$' with formation of other products. For instance, the '$E_{0,a}$' values at pH 5 and pH 13:

$$\begin{aligned} &Fe \rightarrow Fe^{2+} + 2e^- \quad \left(E_0^0 = -475\{447\}\,mV_{SHE} \right) \\ &E_0(pH\,5) = -475\,mV_{SHE} \end{aligned} \qquad [5.17]$$

$$\begin{aligned} &2Fe + 3H_2O \rightarrow Fe_2O_3 + 6H^+ + 6e^- \quad \left(E_0^0 = -51\,mV_{SHE} \right) \\ &E_0(pH\,13) = -819\,mV_{SHE} \end{aligned} \qquad [5.18]$$

  show that '$E_{0,a}$' is actually lower in the passive state. The potential drop is also not due to a decrease in '$E_{0,c}$', which actually is lower in alkaline concrete, i.e. in the passive state (cf. Bullet "Development and magnitude of 'E_{corr}' in the passive state").

  - With corrosion initiation the passive layer is broken down and thus the depassivated steel surface is both electron and ion conducting (cf. Section 2.1.9), *so that the anodic reaction is unhampered and takes a larger contribution in the development of* 'E_{corr}'. That means a more active anodic process lowers 'E_{corr}' and vice versa (cf. Figure 2.5 in Section 2.2.5.2). We think that this notion is thermodynamically coherent with measuring higher corrosion potentials in the passive state than in the active state given that the availability of oxygen is the same in both states.

We regard these aspects to be central in understanding the fundamental principles of the thermodynamics of reinforcement corrosion. In conclusion, the above can be summarised as follows:

'E_{corr}' is determined as the mixed potential between '$E_{0,a}$' and '$E_{0,c}$'. '$E_{0,a}$' depends on the products formed by the anodic reaction and it is only slightly influenced by the iron ion activity at the concrete steel interface (cf. Section 4.2.1), whereas '$E_{0,c}$' is dependent on the oxygen availability. The anodic process decreases 'E_{corr}', while the cathodic process increases 'E_{corr}' and thus 'E_{corr}' increases with increasing oxygen availability and vice versa. '$E_{0,c}$' is dominant in controlling 'E_{corr}' in the passive

* In particular with regard to potential monitoring/mapping as an indication for corrosion initiation (cf. Section 7.5.1.1).

state, but the contribution of '$E_{0,\,a}$' to the development of 'E_{corr}' increases with depassivation, which can be measured as a more or less pronounced drop of 'E_{corr}'.

5.1.3 Fundamental Corrosion Mechanism

Taking into account the above mentioned aspects, we think that a modified concept to describe the underlying principles of the electrochemistry of steel in concrete is required to enable a thermodynamic understanding and hence a consistent description of processes in active corrosion and passivity.

Many textbooks on reinforcement corrosion introduce corrosion of steel in concrete by different variations of a sketch indicating a "closed circuit" that includes the dissolution of Fe to Fe^{2+} [5.1] as the anodic process and the reduction of oxygen in the alkaline environment [5.5] as the cathodic process. These reactions form an electric circuit as the combination of the electronic current through the reinforcement and the flow of ionic current through the concrete bulk, see Figure 5.2.

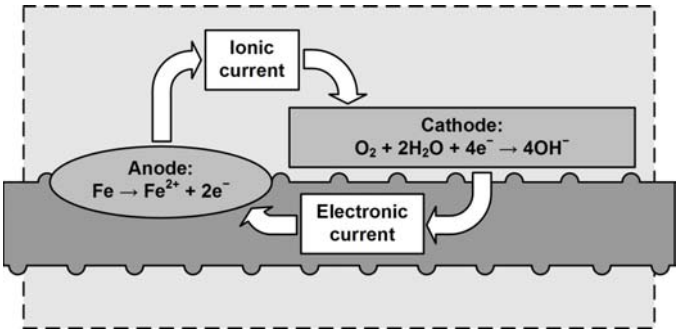

Figure 5.2: *Traditional fundamental mechanism for corrosion of steel in concrete. After [Broomfield, 1997]. This mechanism is proposed to be modified, see Figure 5.3.*

This mechanism is often referred to as the "fundamental mechanism" for corrosion of steel in concrete. Disregarding the possible thermodynamic inconsistency between the anodic and cathodic reaction (cf. Section 5.1.2), we think that this illustration does not adequately represent the corrosion process of steel in concrete, since it only indicates one of various possible anodic reactions that determine the active and passive state of steel in concrete. However, if this description of the "fundamental mechanism" is meant to include formation of e.g. passive iron oxides, we disagree to such description, since we consider passive species to be formed directly in the presence of water and oxygen (cf. Section 5.1.2). Furthermore, we think that it is important to point out that the character of the ionic current is misinterpreted or oversimplified in such description. Related to this concept of the "fundamental mechanism", the establishment of the ionic current is often described as the diffusion of Fe^{2+} from the anode to the cathode and diffusion of OH^- vice versa and the electrical neutrality is preserved this way (cf. Section 2.1.1). However, based on the theory on transport mechanisms, in-

gress, and ion mobility in concrete (cf. Sections 3.1.6 and 3.1.7), we assume that all ions present in the concrete pore solution can discharge the cations and anions formed at the anodic and cathodic sites, respectively, and thus contribute in preserving the electrical neutrality. Apart from being thermodynamically consistent with the formation of the passive layer, this concept of the ionic current is also accounting for macrocell formation (cf. Section 3.1.8), where e.g. Fe^{2+} diffuses away from the reinforcement and does not necessarily precipitate immediately (cf. Section 5.2.2.2). *The traditional fundamental mechanism does not account for these aspects*. We understand this description to be limited to carbonation induced corrosion and think that it neither covers passivity nor active macrocell corrosion and the often (if not always) related chloride induced corrosion. With regard to chloride induced corrosion, it should also be noted that formation of iron-chloride complexes, which we assume to be largely favoured under this condition, are not taken into account in the traditional description.

Based on the above and the statements in Section 5.1.1 and 5.1.2, we propose a modified concept for the description of the "fundamental mechanism" that accounts for *all states and causes for active corrosion and passivity* of steel in concrete, as shown in Figure 5.3.

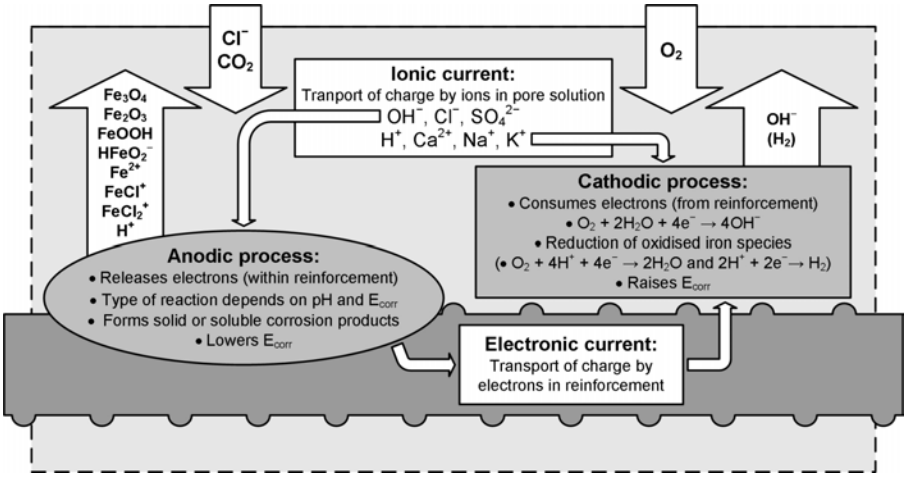

Figure 5.3: *Proposed fundamental mechanism for passive and active corrosion of steel in concrete.*

As mentioned in Section 3.1.6.3, we do not think that it is reasonable to assign a certain direction to the "flow" of ionic current. However, for the direction of electronic current we prefer, contrary to most literature, the concept that the electronic current "flows" from the anode to the cathode, because we consider this concept to be in better agreement with the release of electrons *within* the reinforcement at the anodic site and the consumption of electrons *from* the reinforcement at cathodic sites.

The proposed mechanism and the underlying theory described throughout Sections 5.1.1 and 5.1.2 is applied for a, in our opinion, thermodynamically consistent descrip-

tion of different states of active corrosion and passivity for carbon steel in concrete in Section 5.2 that deviates to quite some extent from the existing descriptions of reinforcement corrosion.

5.2 Reaction Mechanisms

In this Section the theory for a thermodynamically consistent description of the electrochemistry of reinforcement corrosion, which was proposed and exemplified in Section 5.1, is applied for the description of different conditions in the passive state (Section 5.2.1), the active corrosion state (Section 5.2.2), and the immune state (Section 5.2.3) by reaction mechanisms. As mentioned, apart from the fundamental mechanism for corrosion of steel in concrete, reaction mechanisms are generally not dealt with in detail even in extensive textbooks. Some common corrosion conditions have been described by reaction mechanisms in other literature, e.g. in scientific papers or theses. However, based on the theory described in Section 5.1, especially with regard to the thermodynamics involved in the formation of anodic products and the related cathodic reactions, we consider some of the reactions postulated in the literature to be erroneous or inconsistent on a thermodynamic basis. Other corrosion conditions, especially propagation of chloride induced corrosion have not been described in detail. In the following Sections alternative or new reaction mechanisms are proposed for the different states and conditions of active corrosion and passivity of carbon steel in concrete. In addition to that, the most important factors concerning the different states and/or conditions are briefly summarised.

5.2.1 Passive State

In this Section two conditions, passivity (Section 5.2.1.1) and low potential corrosion (Section 5.2.1.2), which we consider to be relevant in uncontaminated concrete, are described on a thermodynamic basis.

5.2.1.1 Passivity

In principle, the passive layer on steel in concrete can be considered to be 10^{-3} to 10^{-1} μm in thickness and to consist mainly of Fe_2O_3, while it also constitutes smaller portions of Fe_3O_4 and cement hydrates.* This definition is considered to be sufficient for the purposes of this thesis, but it should be emphasised that the composition, formation, and structure of the passive layer is much more complex. These issues are generally not dealt with in standard textbooks, but reference is made to journal papers,

* This description is simplified. In the literature, it is generally distinguished between different phases of Fe_2O_3, e.g. hematite (α-Fe_2O_3) and maghemite (γ-Fe_2O_3). This distinction is of marginal importance in the present thesis, and all phases of Fe_2O_3 are referred to as hematite. This is due to two reasons: Firstly, we do not think that this distinction is required, when electrochemistry is of concern, and secondly, there is no distinction between the phases in the available thermodynamic data.

e.g. [Andrade et al., 1995a; Sandberg, 1998; Sagoe-Crentsil & Glasser, 1989; Poursaee & Hansson, 2007]. Evidence for the existence of the passive layer of steel in concrete is indirect and largely based on electrochemical measurements (cf. Section 2.4), whereas its composition is can be directly assessed by e.g. Raman spectroscopy [Andor, 2007].

Traditionally, the reactions leading to the formation of the passive layer were believed to be quite rapid and to occur during the initial stages of cement hydration, e.g. [Sagoe-Crentsil & Glasser, 1989]. However, more recent publications suggest that the full development of the passive layer is only attained after a period of seven days or more [Poursaee & Hansson, 2007]. There is a general agreement that the driving force for the reactions forming the passive layer results from the potential gradients at the steel surface, introduced by the steel as a heterogeneous material itself (cf. Section 3.2.2), but even more by the inhomogeneity of the concrete-steel interface, due to the voids and the often related local variations in moisture content, the alkalinity, etc. (cf. Section 3.3), which divide the steel into several anodic and cathodic areas. The effect of these conditions on the initiation of active corrosion is discussed in more detail in Section 5.2.2.1.

Depending on the availability of oxygen, the corrosion potential 'E_{corr}' of passivated steel in concrete has been measured in a rather wide range of $-460\ mV_{SHE}$ to $440\ mV_{SHE}$ [Arup, 1983], but is within the theoretical stability domain of water in the pH range from at least 11-14, which we regard as a reasonable range for considerations on the passive state.

Hence, oxygen reduction in the alkaline environment can be assumed to be the dominant cathodic reaction (cf. Section 5.1.2):

$$O_2 + 2H_2O + 4e^- \rightarrow 4OH^- \quad \left(E_0^0 = 402\,\{401\}\ mV_{SHE} \right) \qquad [5.19]$$

We assume that, in the literature, there is a general agreement on the prevalence of this cathodic reaction, but apparently there are different concepts regarding the anodic reaction mechanism that leads to the formation of the passive layer. Two examples are given in the below.

The following set of anodic reactions for formation of Fe_2O_3 and Fe_3O_4 depending on the oxygen availability, i.e. Fe_3O_4 is favoured over Fe_2O_3 with low oxygen availability, was proposed in [Sandberg, 1998]:

$$Fe^{2+} \rightarrow Fe^{3+} + e^- \quad \left(E_0^0 = -771\ mV_{SHE} \right) \qquad [5.20]$$

$$O_2 + 4e^- \rightarrow 2O^{2-} \quad \left(E_0^0 = -5151\ mV_{SHE} \right) \qquad [5.21]$$

$$2Fe^{3+} + 3O^{2-} \rightarrow 2Fe_2O_3 \quad \left(\Delta G^0 = -3688\ kJ \right) \qquad [5.22]$$

$$2Fe^{3+} + Fe^{2+} + 4O^{2-} \rightarrow 2Fe_3O_4 \quad \left(\Delta G^0 = -4863\ kJ \right) \qquad [5.23]$$

In [Sagoe-Crentsil & Glasser, 1989] the following set of anodic reactions is proposed for the formation of the passive layer depending on the existence of an appropriate electrochemical potential:

$$Fe + 2H_2O \rightarrow Fe(OH)_2 + 2H^+ + 2e^- \quad \left(E_0^0 = -89\,mV_{SHE} \right) \qquad [5.24]$$

$$3Fe + 4H_2O \rightarrow Fe_3O_4 + 8H^+ + 8e^- \quad \left(E_0^0 = -86\,mV_{SHE} \right) \qquad [5.25]$$

and alternatively:

$$Fe \rightarrow Fe^{2+} + 2e^- \quad \left(E_0^0 = -475\,\{447\}\,mV_{SHE} \right) \qquad [5.26]$$

$$Fe + 2H_2O \rightarrow FeO(OH)^- + 3H^+ + 2e^- \quad \left(E_0^0 = 391\,mV_{SHE} \right)^* \qquad [5.27]$$

We think that the first set of anodic reactions ([5.20] to [5.23]) displays some major thermodynamic inconsistencies with regard to the concrete environment. The redox reactions for the formation of hematite [5.22] and magnetite [5.23] are thermodynamically favoured. However, the half-cell reaction [5.21], which forms the necessary reactant, i.e. the oxygen-(II)-ion, for these reactions to proceed, takes place at an 'E_0^0' of $-5151\ mV_{SHE}$. Such equilibrium potentials are not only out of range for passive reinforcing steel, but generally impossible to be attained in the concrete environment.†

We consider all reactions from the second set of anodic reactions ([5.24] to [5.27]) to be thermodynamically possible in the concrete environment, but apart from [5.25], which is the equivalent to the equilibrium line between iron and magnetite (cf. Section 2.1.10 and Figure 5.4 [A]), we do not think that they play a role in the formation of the passive layer.

The stability domain of $Fe(OH)_2$ postulated to be formed in [5.24] falls mainly into the stability domain of magnetite. A comparison of the 'ΔG_f^0' of both values, which we consider to be decisive, if both species are potentially formed (cf. Section 4.2.1), shows that formation of Fe_3O_4 ('ΔG_f^0' = −1162 kJ/mol) is favoured above formation of $Fe(OH)_2$ ('ΔG_f^0' = −491 kJ/mol). Moreover, Fe_3O_4 was identified to constitute to the passive layer, whereas no evidence was found for formation of $Fe(OH)_2$. Accordingly, we assume that $Fe(OH)_2$ does not play a considerable role for steel in concrete. Since an alternative Pourbaix diagram based on a preselection of Fe, $Fe(OH)_2$, and $Fe(OH)_3$ as solid species is proposed in [Pourbaix, 1974b], it should be mentioned here that we also exclude $Fe(OH)_3$ from our considerations for the same reasons. $Fe(OH)_3$ occupies, in principle, the same stability domain as Fe_2O_3, see Figure 5.4 [A]. With regard to the activation energy, we consider both to be potentially formed, but based on a comparison of the mutual formation, Fe_2O_3 ('ΔG_f^0' = −741 kJ/mol) is

* $FeO(OH)^-$ corresponds to bihypoferrite ion ($HFeO_2^-$).

† Potentials below $-5000\ mV_{SHE}$ and the associated formation of oxygen-(II)-ions, also referred to as superoxide ions, are known from fields such as high temperature oxidation and plasma technique, for instance.

thermodynamically favoured over $Fe(OH)_2$ ('ΔG_f^{0}' = −708 kJ/mol) and, contrary to $Fe(OH)_2$, there is experimental evidence for the formation of Fe_2O_3.

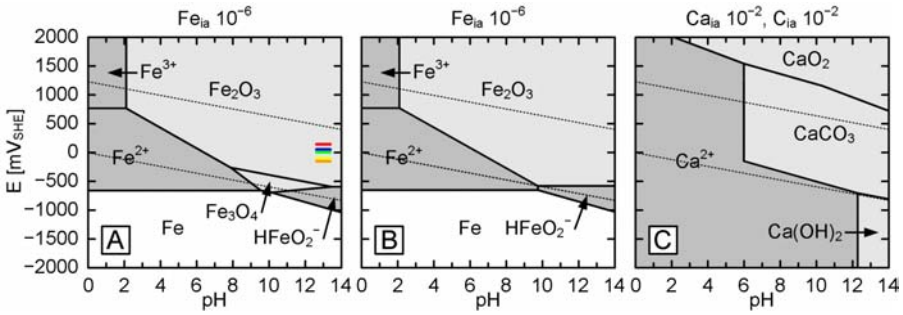

Figure 5.4: [A]: *Fe-H_2O 'SEPD' based on Table 4.2 and Fe_{ia} = 10^{-6} mol/L. Own measurements from 'Test I' of passive carbon steel with different surface properties embedded in mortar (cf. Section 1.9.3) are indicated by the coloured bars (top to bottom): weathered ("C-2A", red), as-received ("C-1A", blue), degreased ("C-4A", green), HCl etched ("C5-A", yellow), and grit-blasted ("C3-A", orange).* [B]: *As [A], but with deselection of Fe_3O_4 (for exemplification purposes only).* [C]: *Ca-C-H_2O 'MEPD' based on Table 5.1 and Ca_{ia} = 10^{-2} mol/L and C_{ia} = 10^{-2} mol/L.*

Table 5.1: *Species preselected for the 'MEPD' of the Ca-C-H_2O system.*

Solid	C	Ca	$CaCO_3$	CaO
	CaO_2	$Ca(OH)_2$	-	-
Soluble	Ca^{2+}	$Ca(OH)^{+}$	CO_3^{2-}	HCO_3^{-}

With regard to the alternative anodic reactions [5.26] and [5.27], the following should be noted. Although thermodynamically possible, we do not think that there is a relation between the formation of $FeO(OH)^{-}$, i.e. half-cell reaction [5.27], and the products that constitute the passive layer.

The thermodynamic inconsistency between the oxidation of iron to ferrous ion [5.26] and the formation of the passive layer was already discussed in Section 5.1.1, but it should be dealt with here again, since it appears to represent a common misconception in the thermodynamics of reinforcement corrosion. According to [Sagoe-Crentsil & Glasser, 1989] and several other publications, migration of the ferrous ion from:

$$Fe \rightarrow Fe^{2+} + 2e^{-} \quad \left(E_0^0 = -475\{447\}\,mV_{SHE} \right) \qquad [5.28]$$

towards the cathodic site forming OH^{-}:

$$O_2 + 2H_2O + 4e^{-} \rightarrow 4OH^{-} \quad \left(E_0^0 = 402\{401\}\,mV_{SHE} \right) \qquad [5.29]$$

leads to formation of iron oxide, which is not described by a reaction in [Sagoe-Crentsil & Glasser, 1989], but probably considered to take place according to:

$$Fe^{2+} + 2OH^- \rightarrow Fe(OH)_2 \quad (\Delta G^0 = -85\,kJ) \qquad [5.30]$$

The involved equilibrium potentials and the negative 'ΔG^0' of this mechanism illustrates that it is thermodynamically possible. However, as described in detail in Section 5.1.1, we assume that the anodic formation of Fe^{2+} is thermodynamically unfavoured in concrete pH above 10 (cf. Figure 5.4 [A]), which can generally be associated with conditions in the passive state.

In contrast to the above postulated reaction mechanisms and in accordance with our assumptions mentioned in Section 5.1, we propose the following set of reactions to sufficiently and thermodynamically consistently describe the passive state of carbon steel in concrete:

- Favoured anodic reaction under general conditions:

$$2Fe + 3H_2O \rightarrow Fe_2O_3 + 6H^+ + 6e^- \quad \left(E_0^0 = -51\,mV_{SHE}\right) \qquad [5.31]$$

- Additional anodic reaction under general conditions, if Fe_3O_4 is present:

$$2Fe_3O_4 + H_2O \rightarrow 3Fe_2O_3 + 2H^+ + 2e^- \quad \left(E_0^0 = 211\,mV_{SHE}\right) \qquad [5.32]$$

- Favoured anodic reaction with limited access to oxygen:

$$3Fe + 4H_2O \rightarrow Fe_3O_4 + 8H^+ + 8e^- \quad \left(E_0^0 = -86\,mV_{SHE}\right) \qquad [5.33]$$

- Dominant cathodic reaction:

$$O_2 + 2H_2O + 4e^- \rightarrow 4OH^- \quad \left(E_0^0 = 402\,\{401\}\,mV_{SHE}\right) \qquad [5.34]$$

- Additional cathodic reaction with limited access to oxygen, if Fe_2O_3 is present:

$$3Fe_2O_3 + 2H^+ + 2e^- \rightarrow 2Fe_3O_4 + H_2O \quad \left(E_0^0 = 211\,mV_{SHE}\right) \qquad [5.35]$$

With regard to the ionic current, from the proposed set of reactions it is obvious that the anodic reactions [5.31] to [5.33] form H^+, while the dominant cathodic reaction [5.34] forms OH^- and the possible supplementary cathodic reaction at low 'E_{corr}' consumes H^+ [5.35]. So, in contrast to the common notion of the ionic current being established by migration of ferrous ions to cathodic sites, where they combine with hydroxyl ions to form iron hydroxide (cf. reactions [5.28] to [5.30]), we understand the ionic current in the passive state to be primary established by migration of H^+ and OH^- that combine to form water or, less significantly, the ionic current can also be established by consumption of H^+, as e.g. described by half-cell reaction [5.35].

Besides the thermodynamic consistency of this concept of the ionic current, we assume that the migration of H^+ and OH^- is kinetically favoured over migration of e.g. Fe^{2+} for the establishment of the ionic current. This notion is based on the high ion

mobility of H^+ and OH^- due to their interaction with water, i.e. that no actual displacement is required (cf. Section 3.1.6.3).

As mentioned in Section 5.1.1, it can be concluded from the Pourbaix diagram that formation of the soluble species $HFeO_2^-$ can play a role with very low 'E_{corr}' values in the passive range. This is dealt with in Section 5.2.1.2.

A verification of the above described mechanism based on the involved equilibrium potentials 'E_0' in the pH range of concern is not necessary, since all involved half-cell reactions, apart from [5.31], are represented by the associated equilibrium lines in the Pourbaix diagram (cf. Figure 5.4 [A]).The equilibrium potential of [5.31] at e.g. pH 13 was given in Section 5.1.1 to:

$$\begin{aligned} &2Fe + 3H_2O \rightarrow Fe_2O_3 + 6H^+ + 6e^- \quad \left(E_0^0 = -51\,mV_{SHE} \right) \\ &E_0\left(pH\,13\right) = -819\,mV_{SHE} \end{aligned} \qquad [5.36]$$

With regard to half-cell reaction [5.36], it should be noted that in [Pourbaix, 1974b] an equilibrium between Fe and Fe_2O_3 is postulated to exist in the Fe-H_2O 'SEPD', if formation of Fe_3O_4 is not taken into account. However, based on the thermodynamic data in 'HSC' (cf. Section 4.1), this equilibrium does not exist. The stability domains of Fe^{2+} and $HFeO_2^-$ are favoured to extend in the associated "intersection" between Fe and Fe_2O_3 with deselection of Fe_3O_4 (cf. Figure 5.4 [B]). Yet, this notion is just of theoretical concern and insignificant in practice.

Before the influence of inclusions of cement hydrates in the passive layer and the thermodynamic consequences is briefly dealt with, a short note on own measurements included in Figure 5.4 [A] should be made. We consider the potential range and the "ranking" of weathered, as-received, degreased, HCl etched, and grit-blasted carbon steel rebar from higher to lower 'E_{corr}' to be in good agreement with the above discussed theory, the statements made throughout Sections 5.1.1 and 5.1.2, and the literature, e.g. [Gonzalez et al., 2007]. Thus, it can be concluded that a passive precorroded carbon steel surface is at a slightly higher 'E_{corr}' than a passive carbon steel surface without initial corrosion products.

As mentioned in Section 4.2.2.2, $CaCO_3$ has been observed as a constituent of the passive layer of steel in concrete [Poursaee & Hansson, 2007]. Although, the effect of calcite on the electrochemistry on steel in concrete cannot be directly thermodynamically verified (thermodynamic data of iron-calcite complexes is not available in [Ouku, 1999; Ouku, 2002] and has not been found elsewhere), the possibility of formation of $CaCO_3$ can be verified by means of the Ca-C-H_2O 'MEPD' in Figure 5.4 [C], which is based on the preselection given in Table 5.1. It can be observed that formation of calcite complexes is thermodynamically favoured in a stability domain that is associated with the pH and E_{corr} for passive steel in concrete. Thus, formation of such complexes is very likely. We assume that $CaCO_3$ does not interfere negatively

with the formation of a stable passive layer (as opposed to e.g. with the passivation of magnesium in concrete, cf. Section 7.3.2).

In conclusion it can be said that:

- Various chemical species are present and several complex phase transformations take place in the multifaceted chemistry of concrete, in particular during hydration (cf. Section 3.1), but we postulate that no other species or transformations than the ones that affect the H^+ and OH^- concentration (the pH) have a significant influence on the passivation of carbon steel in concrete.
- Moreover, from the above it can be deduced that "vice versa" the concrete chemistry is not significantly influenced (e.g. concerning hydration, cf. Section 3.1.2) by the presence of carbon steel.
- Given that the above is true, we postulate that the thermodynamics of the passive state is sufficiently (and thermodynamically consistently) reflected by the proposed set of reactions (in contrast to some reaction mechanisms postulated in the literature).

  We think that this also is confirmed by the good correspondence between the 'E_{corr}' values that can be deduced from the proposed anodic and cathodic reactions and actual values of 'E_{corr}' published in the literature or measured in own investigations.

We consider the above notions to be *central for the underlying principles as to "why and how" the concrete-steel system actually works*. From a theoretical and predictive perspective these notions can only be assessed by thermodynamic considerations, and we regard the Pourbaix diagram as a beneficial tool to base these considerations upon. However, it should be emphasised that the possibility of representing the electrochemistry of a metal in uncontaminated concrete by an 'SEPD' is, at least for the metals of concern in this thesis, limited to steel. The 'SEPD' representation is only partly appropriate for zinc and insufficient for magnesium (cf. Section 7.3).

5.2.1.2 Low Potential Corrosion

In the Pourbaix diagram of Figure 5.4 [A] (cf. Section 5.2.1.1) it can be observed that a domain of active corrosion exists in a pH range of 10-14 at very low potentials of around −800 mV_{SHE}. This corrosion state is generally referred to as low potential corrosion. It may occur for carbon steel in concrete with almost no availability of oxygen. However, as mentioned in Section 5.1.1, we assume that the associated magnitudes of 'E_{corr}' are difficult to attain (even under laboratory conditions), given that no

means of cathodic polarisation are present.* The actual 'E_{corr}' for this type of corrosion was measured to −760 mV_{SHE} [Arup, 1983], which is found in good agreement with the Pourbaix diagram and hence with thermodynamics. The corrosion rate under this condition was determined to be very low, i.e. as low or lower than in the passive state [Arup, 1983]. Accordingly, we regard this *thermodynamically active corrosion state as a passive state in terms of the actually very low corrosion rate*.

Information on corrosion mechanisms describing low potential corrosion in the literature is scarce, but the following set of reactions was postulated [Sandberg, 1998]:

$$Fe + 2H_2O \rightarrow HFeO_2^- + 3H^+ + 2e^- \quad \left(E_0^0 = 391\,mV_{SHE} \right) \qquad [5.37]$$

$$2Fe_2O_3 + 4OH^- \rightarrow 4HFeO_2^- + O_2 \quad \left(\Delta G^0 = 518\,kJ \right) \qquad [5.38]$$

We agree to half-cell reaction [5.37], which corresponds to the equilibrium line between Fe and bihypoferrite ion ($HFeO_2^-$) in the Pourbaix diagram of the Fe-H_2O system (cf. Section 2.1.10 and Figure 5.4 [A]). Yet, the redox reaction [5.38] displays a positive 'ΔG'. Moreover, this set of reactions does not account for possible constitutes of magnetite in the passive layer. So, in accordance with Section 5.2.1.1 and with particular regard to the proposed fundamental corrosion mechanism (cf. Section 5.1), we propose the following reaction mechanism for the description of active low potential corrosion:

- Favoured anodic reaction:

$$Fe + 2H_2O \rightarrow HFeO_2^- + 3H^+ + 2e^- \quad \left(E_0^0 = 391\,mV_{SHE} \right) \qquad [5.39]$$

- Dominant cathodic reactions†:

$$O_2 + 2H_2O + 4e^- \rightarrow 4OH^- \quad \left(E_0^0 = 402\,\{401\}\,mV_{SHE} \right) \qquad [5.40]$$

$$Fe_2O_3 + H_2O + 2e^- \rightarrow 2HFeO_2^- \quad \left(E_0^0 = -941\,mV_{SHE} \right) \qquad [5.41]$$

$$Fe_3O_4 + 2H_2O + 2e^- \rightarrow 3HFeO_2^- + H^+ \quad \left(E_0^0 = -1518\,mV_{SHE} \right) \qquad [5.42]$$

- Supplementary cathodic reaction, which we consider as rather unlikely with regard to the minimal 'E_{corr}' that can be obtained for unpolarised carbon steel in concrete and the existence of hydrogen overpotential in practice (cf. Sections 2.1.10 and 2.2.3):

---

* According to [Nygaard, 2007], corrosion monitoring at the Oresund Fixed Link between Copenhagen, Denmark, and Malmö, Sweden, revealed a very low polarisation resistance (i.e. active corrosion) based on 'LPR' measurements (cf. Section 2.5.5) at very low corrosion potentials of carbon steel in uncontaminated, very dense, and fully saturated concrete. We think that such observations can actually be addressed to low potential corrosion.

† The oxidation state of $HFeO_2^-$ is 2, whereas the oxidation states of Fe_3O_4 and Fe_2O_3 are 2.67 and 3, respectively.

$$2H_2O + 2e^- \rightarrow H_2 + 2OH^- \quad \left(E_0^0 = -828\,\{-828\}\ mV_{SHE} \right) \qquad [5.43]$$

With regard to the ionic current, we assume that principally the same applies to low potential corrosion as described in Section 5.2.1.1 for passivity, but we consider the effect of the cathodic reactions [5.41] and [5.42] to be of more relevance in low potential corrosion than in passivity. The surplus of H^+ [5.42] and the resulting pH drop in combination with possible alterations in oxygen availability will favour repassivation, soon after 'E_{corr}' fell into the stability domain $HFeO_2^-$ (cf. Figure 5.4 [A]).

5.2.2 Active Corrosion State

In this Section the description of carbonation and chloride induced active corrosion based on the Pourbaix diagram is exemplified in Section 5.2.2.1 and Section 5.2.2.2, respectively. While both corrosion initiation and propagation can be assessed thermodynamically for carbonation induced corrosion, the thermodynamic description of chloride induced corrosion is limited to the propagation stage. The propagation stage for carbonation induced corrosion is described for oxygen-rich concrete, whereas propagation under chloride induced corrosion is described for oxygen-deprived concrete, in order to cover both extremes and emphasise certain special characteristics.

Although these conditions can be regarded as somewhat "typical" for carbonation and chloride induced corrosion, it should be remarked that generally mixed forms of both initiation mechanisms, i.e. a combination of carbonation and chlorides, as well as to propagation, i.e. various levels of concrete saturation are generally present in practice. With regard to that, the interconnection between both initiation mechanisms should be emphasised. The degree of carbonation influences the chloride threshold (cf. Section 3.1.9) and, vice versa, the chloride concentration has an effect on the critical pH (cf. Section 3.1.7.2). Moreover, the influence on carbonation on the chloride binding capacity should be emphasised (cf. Section 3.1.7.2).

5.2.2.1 Carbonation Induced Corrosion in Oxygen-Rich Concrete

Corrosion initiation by carbonation might not be immediately obvious from the Pourbaix diagram, but we think that the mechanism can be conclusively explained based on the "standard" 'SEPD' of the Fe-H_2O system with an iron ion activity of 10^{-6} mol/L, as shown in Figure 5.5.

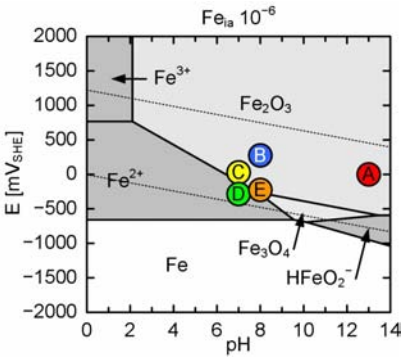

Figure 5.5: *Fe-H_2O 'SEPD' based on Table 4.2 and Fe_{ia} = 10^{-6} mol/L with proposed mechanism for carbonation induced corrosion in semi-saturated concrete. Identification of possible range of 'E_{corr}' and pH for (A) average of carbon steel in uncontaminated concrete, (B) average of carbon steel in carbonated concrete before corrosion initiation, (C) anodic sites of carbon steel in carbonated concrete at corrosion initiation, (D) anodic sites of carbon steel in carbonated concrete in corrosion propagation, and (E) cathodic sites of carbon steel in carbonated concrete in corrosion propagation.*

As discussed in Section 5.1.1, case (A) in Figure 5.5 can be regarded as representing the pH range (around pH 13) and the 'E_{corr}' (around 0 mV_{SHE}) of carbon steel in uncontaminated concrete. The lower boundary of case (A) might correspond to the 'E_{corr}' in concrete under the exposure conditions, which are most critical in promoting carbonation, i.e. 60% to 70% relative humidity (cf. Section 3.1.7.2).

With carbonation the pH of the bulk concrete can drop to values approaching neutrality (cf. Section 3.1.7.2 and Table 3.2 in Section 3.1.5). In this exemplification a bulk pH of around 8 is chosen that we assume to be reasonable. This pH and resulting increase in 'E_{corr}' of about 300 mV (cf. Section 5.1.2) is indicated by case (B) in the diagram.

However, cases (A) and (B) do only represent the average 'E_{corr}' of carbon steel reinforcement in concrete and do not reflect the localised conditions of the various anodic and cathodic sites on the carbon steel surface. In addition to that, the bulk pH does normally not represent the pH at the steel surface. The localised conditions of the anodic and cathodic sites differ to a certain extent with regard to both the localised potential and the localised pH due to the inhomogeneities of steel itself (cf. Section 3.2.2) and, more importantly, due to the inhomogeneities of the concrete-steel interface (cf. Section 3.3). Moreover, we assume that the H^+ and OH^- produced by the anodic and cathodic reactions in the passive state, which do not necessarily need to neutralise each other (cf. Section 5.1.3), contribute to these inhomogeneities.

A range of 'E_{corr}' and a pH that might be obtained at an anodic site are indicated in case (C). This situation leads to depassivation, i.e. corrosion initiation, which means, in accordance with the theory proposed in Section 5.1, that the formation of active corrosion products is favoured over the formation of passive products at the localised anodic site (cf. Figure 5.5). The condition at this localised site can be described by the following reaction mechanism:

- Favoured anodic reaction at the localised depassivated site:

$$Fe \rightarrow Fe^{2+} + 2e^- \quad \left(E_0^0 = -475\{447\}\,mV_{SHE} \right) \qquad [5.44]$$

- Dominant cathodic reactions, which can take place on the passive layer:

$$O_2 + 2H_2O + 4e^- \rightarrow 4OH^- \quad \left(E_0^0 = 402\{401\}\,mV_{SHE} \right)^* \qquad [5.45]$$

- Supplementary cathodic reactions that can take place at the localised depassivated sites, given that Fe_2O_3 and Fe_3O_4 are present:

$$Fe_2O_3 + 6H^+ + 2e^- \rightarrow 2Fe^{2+} + 3H_2O \quad \left(E_0^0 = 789\,mV_{SHE} \right) \qquad [5.46]$$

$$Fe_3O_4 + 8H^+ + 2e^- \rightarrow 3Fe^{2+} + 4H_2O \quad \left(E_0^0 = 1078\,mV_{SHE} \right) \qquad [5.47]$$

As described in Section 5.1.2, depassivation increases the rate of the anodic processes, which leads to a decrement of 'E_{corr}'. The decrement of 'E_{corr}' leads to an increment in the number of anodic sites, where formation of ferrous ion [5.44] is favoured over formation of passive products. Thus, more and more of the surface is depassivated until the carbon steel is at a pH and 'E_{corr}', where formation of ferrous ion is favoured on the entire steel surface. A new, lower "equilibrium" 'E_{corr}' between the various anodic and cathodic equilibrium potentials is obtained. In accordance with Section 5.1.2, this thermodynamic scenario corresponds to the potential drop under carbonation induced corrosion.

In Figure 5.5 the conditions after corrosion initiation, i.e. in the propagation phase, are illustrated by case (D) and case (E), which represent conditions at an anodic and at a cathodic site in corrosion propagation. It can be observed that the conditions for case (D) and case (E) were chosen to be close to the theoretical hydrogen line in the 'SEPD'. Even if the hydrogen line is at a higher potential in this pH range, we consider obtaining a magnitude of 'E_{corr}' low enough for hydrogen ion reduction under carbonation induced corrosion to be rather unlikely, when taking into account the hydrogen overpotential (cf. Section 2.1.10).

In principle, this is based on two notions. Firstly, also after corrosion initiation, 'E_{corr}' is dependent on the 'E_0' of oxygen reduction as the dominant cathodic reaction, which

* Different to the exemplification based on organic rich lake water, the reduction of oxygen in alkaline and neutral electrolytes is listed as dominant cathodic reaction in this case, as the pH is not considered to significantly drop below 7.

also is at higher potentials at this pH (both *the oxygen line and the hydrogen line have the same slope* of $-0.0059 \times \text{pH}$ (cf. Section 2.1.10 and Figure 5.5)). Secondly, a rather low oxygen content is required to obtain 'E_{corr}' in this range, and the associated degree of saturation counteracts the carbonation rate (cf. Section 3.1.7.2).

After corrosion initiation the *soluble* iron species Fe^{2+} is favoured to be formed at anodic sites, which we understand to be the major difference to passivity (cf. Section 5.1.1). *In contrast to passivity, where a dense layer of iron oxides is directly formed and the corrosion rate diminishes, the ferrous ion is released and available for further transformations*. For oxygen-rich concrete, these transformations are often described by a threefold mechanism leading to the formation of hydrated hematite [Broomfield, 1997; Sandberg, 1998]:

- Formation of ferrous hydroxide

$$Fe^{2+} + 2OH^- \rightarrow Fe(OH)_2 \quad \left(\Delta G^0 = -85\ \text{kJ} \right) \qquad [5.48]$$

- Formation of ferric hydroxide

$$4Fe(OH)_2 + O_2 + 2H_2O \rightarrow 4Fe(OH)_3 \quad \left(\Delta G^0 = -364\ \text{kJ} \right) \qquad [5.49]$$

- Formation of hydrated hematite

$$2Fe(OH)_3 \rightarrow Fe_2O_3 \cdot H_2O + 2H_2O \quad \left(\Delta G^0 = -57\ \text{kJ} \right) \qquad [5.50]$$

The reactions [5.48] to [5.50] in the described transformation illustrate a negative 'ΔG^0' and are, thus, thermodynamically possible. However, that this is not true for an alternative description of the electrolysis of iron that is often stated in the literature:

$$Fe^{2+} + 2H_2O \rightarrow Fe(OH)_2 + 2H^+ \quad \left(\Delta G^0 = 74\ \text{kJ} \right) \qquad [5.51]$$

Contrary to the general absence of descriptions for other corrosion states, this reaction mechanism is frequently cited in the literature and we generally agree to this mechanism as *one* thermodynamic option.

A constant shift between the anodic and cathodic sites is introduced by the formation of hydroxyl ions at the cathodic sites. As illustrated by case (E) in Figure 5.5, 'E_{corr}' at cathodic sites is initially slightly higher due to differences in oxygen concentrations and the increase in pH due to the presence of hydroxyl ions. With consumption of oxygen by the dominant cathodic reaction [5.45] and consumption of hydroxyl ions in the formation of ferrous hydroxide [5.48], case (E) will eventually change to anodic condition, i.e. shift towards case (D), while at a prior anodic site can develop cathodic conditions. This constant shift between anodic and cathodic sites leads to uniform corrosion (cf. Section 2.3.1).

Typical corrosion potentials for uniform corrosion have been observed to be in the range of −210 to −360 mV_{SHE} [Arup, 1983], which is in good agreement with the av-

erage potential range between case (D) and case (E) in the Pourbaix diagram (cf. Figure 5.5) and the notion that carbonation induced corrosion does generally not involve hydrogen ion reduction.

As mentioned in Section 5.2.1, the stability domains of $Fe(OH)_2$ and $Fe(OH)_3$ agree approximately with the stability domains of Fe_3O_4 and Fe_2O_3, respectively. The stability domain of $Fe_2O_3 \cdot H_2O$ corresponds to the stability domain of Fe_2O_3. So, the products formed in the mechanism described in [5.48] to [5.50] are stable in case (E) only. However, as discussed in Section 5.2.1 based on the evaluation of 'ΔG_f^0' values to compare the probability of mutual formation and on corrosion products described in the literature, we postulate that case (E) favours the formation of Fe_3O_4 and Fe_2O_3 over $Fe(OH)_2$ and $Fe(OH)_3$, respectively. So, the transformation of the dissolved ferrous ion can also be described as the inversion of the supplementary cathodic reactions [5.46] and [5.47]:

$$2Fe^{2+} + 3H_2O \rightarrow Fe_2O_3 + 6H^+ + 2e^- \quad \left(E_0^0 = 789\,mV_{SHE} \right) \qquad [5.52]$$

$$3Fe^{2+} + 4H_2O \rightarrow Fe_3O_4 + 8H^+ + 2e^- \quad \left(E_0^0 = 1078\,mV_{SHE} \right) \qquad [5.53]$$

which we consider to be thermodynamically favoured.

With regard to the formation of hydrated hematite, it should be noted that direct formation of Fe_2O_3 ('ΔG_f^0' = −741 kJ/mol) is favoured over $Fe_2O_3 \cdot H_2O$ (ΔG_f^0 = −24 kJ/mol) and that the formation of $Fe_2O_3 \cdot H_2O$ from Fe_2O_3 is not thermodynamically favoured:

$$Fe_2O_3 + H_2O \rightarrow Fe_2O_3 \cdot H_2O \quad \left(\Delta G^0 = 1002\,kJ \right) \qquad [5.54]$$

However, with sufficient supply of oxygen the formation of $Fe_2O_3 \cdot H_2O$ is thermodynamically favoured and assumed to be possible in oxygen-rich concrete, e.g. according to:

$$4Fe^{2+} + O_2 + 6H_2O \rightarrow 2Fe_2O_3 \cdot H_2O + 8H^+ \quad \left(\Delta G^0 = -163\,kJ \right) \qquad [5.55]$$

In either way, from a thermodynamically point of view the formation of iron oxides must take place at cathodic sites, so that the traditional notion of the establishment of the ionic current, i.e. migration of ferrous ion from anodic to cathodic sites to form an iron oxide, is applicable for carbonation induced corrosion. With regard to the ionic current it should also be noted that current transfer by "migration" of hydroxyl ions is largely limited due to the neutralisation of the concrete bulk, which reduces its conductivity (cf. Table 3.2 in Section 3.1.5 and Sections 3.1.6.3 and 3.1.7.4 with regard to migration and the ion mobility in concrete, respectively). We think that, among others, reduced conductivity is a factor for the relatively low corrosion rates under carbonation induced corrosion compared to chloride included corrosion (cf. Section 5.1.1).

Disregarding the supplementary cathodic reactions [5.46] and [5.47], which we understand to play a role in passivity, especially in low potential corrosion (cf. Section 5.2.1.2), but to be negligible in active corrosion, the traditional "fundamental mechanism" is, hence, applicable for the description of carbonation induced corrosion in oxygen-rich concrete. Yet, once more it should be emphasised that we consider this concept to be limited to these corrosion conditions. We think that *the formation of Fe^{2+} and its migration to form solid products is the central difference between the active state and the passive state, where solid products are directly formed on the carbon steel surface*.

Disregarding the type of iron oxides formed in the process of active uniform corrosion, the iron oxides occupy a larger volume than the pure iron that is consumed in the corrosion reaction, e.g. [Herholdt et al., 1985; Alonso et al., 1998; Marcotte & Hansson, 2007]. The increase in volume around the rebar exerts disruptive tensile stress on the surrounding concrete. If these stresses exceed the concrete tensile strength, the concrete cracks, spalls, or the concrete cover delaminates, see Figure 5.6, depending on the exposure as well as on the structural conditions.

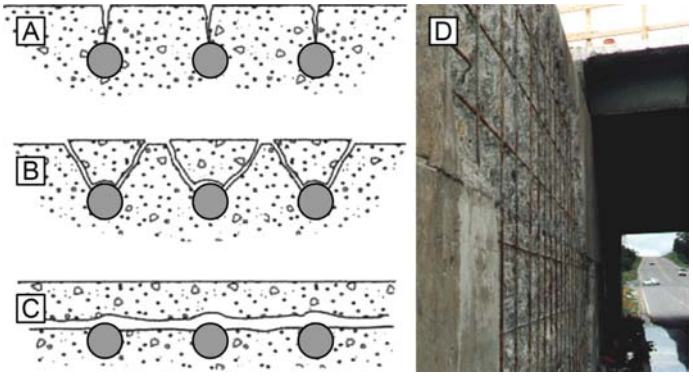

Figure 5.6: *Damage types resulting from reinforcement corrosion in oxygen-rich concrete.* [A]: *Cracking.* [B]: *Spalling.* [C]: *Delamination.* [D]: *Combination of damage types at concrete bridge. After [SSR, 2007].*

It should be noted that corrosion cracks (see Figure 5.6 [A]) are often parallel to the reinforcement and therefore quite distinct from load induced cracks.

With regard to both the exact corrosion products formed and the respective volumes, there seem to be different notions in the literature on reinforcement corrosion. In the experimental part of this project, we did not deal with carbonation induced corrosion and quantified neither the exact composition of the products nor their volume for chloride induced corrosion. Yet, based on theoretical considerations, we think that formation of Fe_3O_4 and Fe_2O_3 is favoured over formation of $Fe(OH)_2$ and $Fe(OH)_3$, respectively. This also excludes formation of $Fe_2O_3 \cdot H_2O$ from Fe_2O_3 combining with water, whereas the direct formation of hydrated hematite is possible with sufficient supply of oxygen, as described by the redox reaction [5.55].

Considerations on the volumes of the products are marginal in this project, since we aim at avoiding corrosion rather than controlling corrosion propagation. However, knowledge on the exact volumes and consequently on the actual products formed, is crucial in e.g. mathematical modelling of corrosion propagation. It appears that in some models the underlying assumptions for the volumes of corrosion products are based on preferential formation of $Fe_2O_3 \cdot H_2O$ [Andrade et al., 1993; Molina et al., 1993; Isgor & Razaqpur, 2006]. Based on thermodynamics, we think that this assumption is inaccurate to some extent, as was also indicated in [Marcotte & Hansson, 2007].

For the purpose of this thesis, where volumes of corrosion products are marginal, we regard it to be sufficient to refer to the often cited values from [Herholdt et al., 1985], which are listed in Table 5.2.

Table 5.2: *Volumes of corrosion products based on 1 cm^3 iron (7.86 g Fe). Values estimated from bar chart in [Herholdt et al., 1985].*

Product	**FeO**	**Fe_3O_4**	**Fe_2O_3**	**$Fe(OH)_2$**	**$Fe(OH)_3$**	**$Fe(OH)_3 \cdot H_2O$**
Volume ratio	1.7	2.0	2.1	3.6	4.2	6.3

While we postulate that the situation is rather different under chloride induced corrosion, especially in oxygen-deprived concrete, we assume that under carbonation induced corrosion in oxygen-rich concrete most of the ferrous ion formed at the anodic sites will precipitate as a certain type of iron oxide in the vicinity of the reinforcement as long as the concrete is uncracked. Based on the Pourbaix diagram in Figure 5.5, this can be reasoned by considering that the oxygen content and pH will approach conditions of the bulk concrete as indicated by case (B), so that the ferrous ion will precipitate as an iron oxide, i.e. as Fe_2O_3 according to the proposed concept of the dominant species. However, in cases where the concrete is saturated, the ferrous ion could stay in solution and diffuse towards the surface or in the direction of an electrical field, e.g. in the case of macrocell corrosion.

Control of carbonation induced corrosion is dealt with in Chapters 6 and 7 with regard to available and the proposed new countermeasures, respectively.

5.2.2.2 Chloride Induced Corrosion in Oxygen-Deprived Concrete

As mentioned in Section 4.2.2.2, the initiation of chloride induced corrosion is largely dependent on kinetic parameters and cannot be assessed by thermodynamic considerations only. However, we think that the effect of chlorides *during the propagation stage* can be thermodynamically assessed and represented by a combination of the Fe-Cl-H_2O 'MEPD' and associated reaction mechanisms. Among others, we think that the proposed model enables us to understand why corrosion rates are significantly higher under chloride induced corrosion than under carbonation induced corrosion,

e.g. by a factor of about 10 (cf. Section 5.1.1). And, even more importantly, we consider that a thermodynamic assessment enables us *to design specific, targeted measures that are able to counteract the corrosion processes.*

Before the proposed model for the description of corrosion propagation under chloride induced corrosion is discussed in detail, the present understanding of corrosion initiation and propagation in chloride contaminated concrete is reviewed.

As described in Section 2.1.9, chloride ions trigger the dissolution of the passive layer. The attack starts with pitting corrosion (cf. Section 2.3.2) at a site, where the passive layer is most vulnerable. Vulnerable sites may be caused by the heterogeneity of the steel itself (cf. Section 3.2.2), but research showed that *voids or defects at the concrete-steel interface (cf. Section 3.3) are particularly vulnerable to chloride induced corrosion*, e.g. [Glass & Buenfeld, 1997; Buenfeld et al., 2004; Nygaard & Geiker, 2005]. Moreover, we think that *localised concentration differences and potential differences along the concrete-steel interface due to the different products formed by the anodic and cathodic reactions in the passive state (cf. Section 5.2.1) have a considerable effect on the formation of vulnerable sites as well as on the diffusion of chloride ions during the initiation stage*. For instance, anodic sites will attract chloride ions and thus experience higher concentrations due to the influence on the migration of anions (cf. Section 3.1.6.3).

Similar to the incomplete understanding of the exact mechanisms for the establishment of passive layers on metals (cf. Section 2.1.9), the detailed mechanisms of the breakdown of the passive layer by chloride ions appear to be not fully understood to date. In principle, there are three theories to explain the effect of chloride ions on initiation of corrosion [Foley, 1970; ACI 222R, 2001]:

- Oxide film theory
- Adsorption theory
- Transitory complex theory

A detailed description of the postulated mechanism goes beyond the scope of this thesis and reference is made to the literature. [ACI 222R, 2001] provides a short summary on this theories and an extensive review of these hypotheses can be found in e.g. [Foley, 1970].

As mentioned in Section 2.3.2, the breakdown of the passive layer is generally assessed by the pitting potential 'E_{pit}', which also determines the chloride threshold (cf. Section 3.1.9). The presence of chloride ions in concrete leads to changes of the anodic behaviour of the embedded steel, which largely interferes with the anodic polarisation curve (cf. Figure 2.7 in Section 2.3.2). The passivity range is reduced, i.e. its upper limit 'E_{pit}' decreases with increasing chloride content. So, the passivity range is reduced from corrosion potentials representing oxygen evolution in uncontaminated

concrete (cf. Section 5.2.1.1) to values of −200 mV_{SHE} and below in concrete with high chloride concentrations [Page & Treadaway, 1982].

As mentioned in Section 3.1.9, one way of understanding the chloride threshold is to relate it to a given potential of the steel, i.e. the highest chloride content compatible with conditions of passivity at that potential. For concrete structures exposed to the atmosphere 'E_{corr}' of the embedded steel can be assumed to be at around 0 V_{SHE} and the chloride threshold is normally in the range of 0.4% to 1% 'w/w_{ce}' (cf. Section 3.1.9). For submerged structures or members the reinforcement steel is at a much lower potential, e.g. around −400 to −500 mV_{SHE}, or for reinforcement that is cathodically polarised for any reason the chloride threshold can be much higher.

Pitting corrosion is likely to develop in concrete with a high conductivity, high alkalinity, i.e. uncarbonated, and a concentration of chloride ions in excess of the threshold value. Therefore, pitting corrosion can be regarded as a chloride induced corrosion phenomenon. An approach to implement the kinetic parameter 'E_{pit}' in the Pourbaix diagram is shown in Figure 5.7 [A], which illustrates the dependency of the pitting potential on the pH and on chloride concentration by superimposing curves (as function of the pH) on the 'SEPD'* of the Fe-H_2O system. These curves are referred to as pitting potential curves in the present thesis.

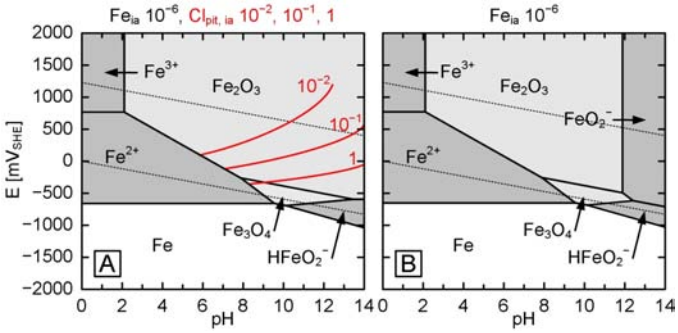

Figure 5.7: [A]: *Fe-H_2O 'SEPD' based on Table 4.2 and $Fe_{ia} = 10^{-6}$ mol/L with superimposed pitting potential curves for different chloride concentrations: $Cl_{pit, ia} = 10^{-2}$ mol/L, $Cl_{pit, ia} = 10^{-1}$ mol/L, and $Cl_{pit, ia} = 1$ mol/L. After [Nilsson et al., 1996; Sandberg, 1998]*. [B]: *Fe-H_2O 'SEPD' based on Table 4.2 and $Fe_{ia} = 10^{-6}$ mol/L with additional selection of FeO_2^-. Diagram [B] is for exemplification purposes only and does not represent actual conditions.*

At corrosion potentials higher than 'E_{pit}', the chloride ions induce the localised breakdown of the passive layer. For electrode potentials below 'E_{pit}', the action of chloride

* A Pourbaix diagram with superimposed pitting potential curves is not referred to as 'MEPD' in this thesis, since the curves neither represent thermodynamic parameters nor can they be determined by thermodynamics (alone) (cf. Section 2.3.2).

is, in principle, negligible. Considering a constant chloride content, it can be concluded from Figure 5.7 [A] that 'E_{pit}' decreases with decreasing pH, which corresponds to the general thermodynamic characteristics of steel, i.e. higher corrosion risk and rate with decreasing pH (cf. Section 2.1.10). We generally agree with the description of conditions for initiation of corrosion by superimposing pitting potential curves on a Pourbaix diagram, as proposed in e.g. [Nilsson et al., 1996; Sandberg, 1998]. Yet, as mentioned, in practice 'E_{pit}' is dependent on various parameters concerning the concrete and steel (in particular, on the conditions at the concrete-steel interface, cf. Section 3.3) and on the measurement, i.e. mainly the scan rate during polarisation (cf. Section 2.5.4). Nevertheless, it should be kept in mind that also Pourbaix diagrams for the concrete-steel system are established on an approximate basis (cf. Section 4.2.2).

Figure 5.7 [A] exemplifies how pitting potential curves are projected on the Fe-H_2O 'SEPD' in the literature [Nilsson et al., 1996; Sandberg, 1998]. We consider this to be thermodynamically inconsistent to some extent, since chloride (and accordingly the formation of iron-chloride compounds) is not taken into account in the underlying diagram. An important thermodynamic aspect of the Fe-Cl-H_2O system, i.e. the effect of chloride on the stability domains of iron, is not reflected and no representative information on corrosion propagation can be obtained.

In Figure 5.7 [A] it can also be observed that, in contrast to carbonation induced corrosion, where a "global" pH drop takes place (cf. Section 5.2.2.1), active corrosion after depassivation is not thermodynamically favoured in the system reflected by the Fe-H_2O 'SEPD'. This mismatch is underlined by a particular reinforcement corrosion phenomenon. Under chloride induced corrosion in oxygen-deprived concrete, formation of rust stains on the concrete surface is observed. Undoubtedly, such stains result from precipitation of soluble iron that diffuses outwards from the corroding carbon steel reinforcement. *However, from the Fe-H_2O 'SEPD' in Figure 5.7 [A] it can be concluded that diffusion of soluble iron species through an uncarbonated concrete cover is thermodynamically impossible.* The 'SEPD' clearly indicates that any dissolved ferrous ion is oxidised and precipitated as Fe_3O_4 or Fe_2O_3 (depending on the oxygen availability) in concrete with a pH of 10 and above.

Rust stains are observed at concrete exposed to the atmosphere, so that conditions corresponding to low potential corrosion, i.e. formation of soluble bihypoferrite ion can be safely excluded. With regard to this, it should be noted that we exclude formation of other soluble iron species in the alkaline region. For instance, formation of ferrite ion (FeO_2^-) could be (mistakenly) taken into consideration for the establishment of the Fe-H_2O 'SEPD'. The effect of such misleading assumptions is exemplified in the 'SEPD' in Figure 5.7 [B], which is only used for exemplification purposes and without practical relevance for the area of concern in this thesis.

Formation of ferrite ion can be described by:

$$2Fe_2O_3 + O^{2-} \rightarrow 2FeO_2^- \quad \left(\Delta G^0 = -1026\,kJ \right) \qquad [5.56]$$

which is, as indicated by the negative 'ΔG^0', a thermodynamically favoured acid-base reaction. However, as exemplified in Section 5.2.1.1 for the doubtful reaction descriptions of the passive state (cf. reactions [5.22] and [5.23]), reactions involving oxygen-(II)-ion have a strong thermodynamic tendency to occur, but the formation of the necessary oxygen-(II)-ion requires electrode potentials, which are regarded to be entirely out of range for reinforced concrete. So, we exclude ferrite ion and any other soluble species in the alkaline region, except from $HFeO_2^-$, from our assumptions concerning the Fe-H_2O system. This is also confirmed by investigating positive and negative indicators in the literature (cf. Section 4.2.1). While no positive indicators for the existence of such species under conditions comparable to the concrete environment have been reported, formation of ferrite ion is normally discussed in connection with high temperature corrosion, e.g. corrosion in Kraft recovery boilers [Colwell, 1992], which we regard as negative indicators for the existence in customary concrete-steel systems.

Thus, it can be concluded that the frequently observed outwards diffusion of iron species in chloride contaminated uncarbonated concrete is thermodynamically impossible, without other thermodynamic relevant changes taking part. We suggest that the *only possible explanation for outwards diffusion of iron ions is a change of pH in the associated areas of the concrete cover*.

Most of the literature dealing with diffusion of dissolved iron ions in oxygen-deprived concrete simply explains this phenomenon by referring to macrocell corrosion (cf. Section 3.1.8) and postulates that dissolved iron stays in solution, because there is no oxygen available for further transformations. However, the Pourbaix diagram and the corresponding reactions for the pH and 'E_{corr}' of concern clearly indicate that thermodynamically no additional supply of oxygen is necessary for ferrous iron to precipitate in alkaline solutions:

$$2Fe^{2+} + 3H_2O \rightarrow Fe_2O_3 + 6H^+ + 2e^- \quad \left(E_0^0 = 789\,mV_{SHE} \right) \qquad [5.57]$$

$$3Fe^{2+} + 4H_2O \rightarrow Fe_3O_4 + 8H^+ + 2e^- \quad \left(E_0^0 = 1078\,mV_{SHE} \right) \qquad [5.58]$$

So, we regard the mechanism for diffusion of dissolved iron in uncarbonated chloride contaminated concrete to be more complex.

While the conditions of formation as well as the composition and characteristics of compounds formed during propagation of chloride induced corrosion are generally not dealt with in standard textbooks on reinforcement corrosion, there are various other publications, e.g. theses and journal papers, dealing exclusively with this topic. In several of these publications evidence of the formation of soluble complexes of ferrous chloride has been reported. It has been suggested that chlorides bound in these complexes can be released by the conversion of the complexes to ferric hydroxide,

which leave the chloride ions free for a new attack on the passive layer. Moreover, it has been indicated that these iron-chloride complexes, which are stable only in the absence of oxygen, can involve both ferrous and ferric ion. [Refait & Génin, 1993; Sagoe-Crentsil & Glasser, 1993; Refait & Génin, 1997; Refait et al., 1998; Sandberg, 1998; Génin et al., 2001; Koleva et al., 2006; CeFrCo, 2007; Rémazeilles & Refait, 2007].

Such complexes are in the literature generally referred to as green rust with regard to the colour of the liquid, when first exposed to the atmosphere. Some authors (e.g. [Refait & Génin, 1993; Refait et al., 1998; Génin et al., 2001; Koleva et al., 2006]) distinguish further between two similar types of crystal structure for green rusts and refer to green rust one 'GR1' for iron-chloride compounds and to green rust two ('GR2') for iron-sulphate compounds. For the purpose of this thesis only 'GR1' is relevant and simply regarded as a liquid iron hydroxychloride compound involving both oxidation states of iron (+2 and +3). Reference is made to e.g. [Refait & Génin, 1993; Sagoe-Crentsil & Glasser, 1993; Refait & Génin, 1997; Refait et al., 1998; Génin et al., 2001; Koleva et al., 2006; Rémazeilles & Refait, 2007] for a detailed description or discussions on the exact chemical properties of 'GR1'.

While, due to the similar crystal structure, the solid counterpart of 'GR1' is generally regarded as fougerite [Génin et al., 2001; CeFrCo, 2007], there is a common agreement that 'GR1' is transformed into other iron compounds, when exposed to the atmosphere. In particular, goethite (FeOOH)* or magnetite are often stated as thermodynamically favoured compounds. Moreover, FeOOH and Fe_3O_4 were frequently observed by e.g. Mössbauer spectroscopy [Dickson et al., 1986] or Raman spectroscopy [Andor, 2007] as solid corrosion products formed under chloride induced corrosion [Misawa, 1973; Raharinaivo et al., 1987; Koleva et al., 2006; Marcotte & Hansson, 2007]. Thus, we take formation of FeOOH ('ΔG_f^0' = −489 kJ/mol) into consideration instead of formation of Fe_2O_3 ('ΔG_f^0' = −741 kJ/mol) for the case of chloride induced corrosion in the oxygen-deprived concrete.

From a comparison of the equilibrium lines limiting Fe_2O_3 and FeOOH in the 'SEPDs' of the Fe-H_2O system for both preselections in Figure 5.8 [A] and [B], respectively, it can observed that the two stability domains almost correspond.

* This description is simplified. In the literature, it is generally distinguished between different phases of FeOOH, e.g. goethite (α-FeOOH), akaganeite (β-FeOOH), and lepidocrocite (γ-FeOOH). This distinction is of marginal importance in the present thesis and all phases of FeOOH are referred to as goethite (cf. footnote on phases of Fe_2O_3).

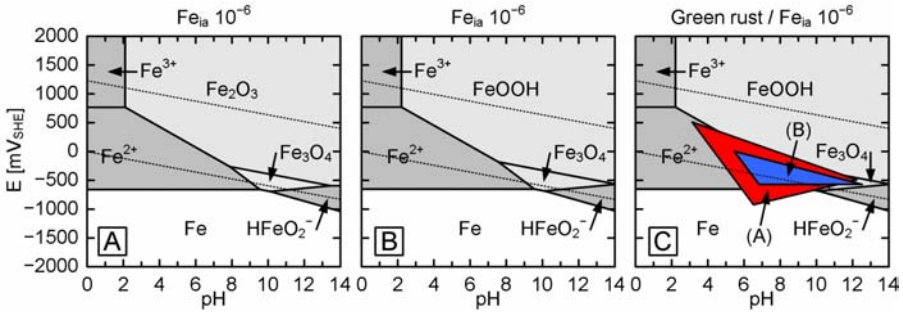

Figure 5.8: [A]: *Fe-H_2O 'SEPD' based on preselection of species according to Table 4.2 and $Fe_{ia} = 10^{-6}$ mol/L and.* [B]: *As [A], but deselection of Fe_2O_3 and preselection of FeOOH, according to Table 5.3.* [C]: *Partial 'SIPD' with [B] as underlying 'SEPD' and superimposed stability domains of 'GR1' as postulated in the literature, i.e. (A) 'GR1' domain for a $Cl_{ia} = 10^{-6}$ mol/L after [Sagoe-Crentsil & Glasser, 1993] and (B) GR1' domain for $Cl_{ia} = 0.55$ mol/L after [Refait & Génin, 1993]. Diagram [C] is for exemplification purposes only and it neither represents actual conditions nor the exact original assumptions of [Refait & Génin, 1993; Sagoe-Crentsil & Glasser, 1993].*

Table 5.3: *Species preselected for the 'SEPD' of the Fe-H_2O system considering formation of FeOOH instead of Fe_2O_3.*

Solid	Fe	Fe_3O_4	FeOOH
Soluble	Fe^{2+}	Fe^{3+}	$HFeO_2^-$

Stability domains for 'GR1' have been proposed in [Sagoe-Crentsil & Glasser, 1993] and in [Refait & Génin, 1993]. The extents of these stability domains, which correspond to chloride concentrations of (A) 10^{-6} mol/L [Sagoe-Crentsil & Glasser, 1993] and (B) 0.55 mol/L [Refait & Génin, 1993], is indicated in the partial 'SIPD' in Figure 5.8 [C]. It should be noted that the approach chosen for the underlying Pourbaix diagram, which corresponds to Figure 5.8 [B], does not exactly reflect the assumptions in the original sources. While both publications consider formation of FeOOH as favoured solid compound, the other iron species differ to a certain extent and reference is made to the original publications [Refait & Génin, 1993; Sagoe-Crentsil & Glasser, 1993] for the related theory. Neither of the two postulated 'GR1' stability domains can be favoured or rejected, but we do not expect the stability domain of 'GR1' to extent into the immunity domain (case (A), cf. also Section 5.2.3) and the suggested stability domain (A) is relatively large for a relatively low chloride concentration; in particular, in comparison with stability domain (B), which is smaller at a much higher chloride concentration.

However, in neither of the two sources [Refait & Génin, 1993; Sagoe-Crentsil & Glasser, 1993] the full thermodynamic effect of chloride is taken into account, i.e. the formation of other iron-chloride compounds is not represented in the associated Pourbaix diagrams. We think that this is thermodynamically inconsistent and suggest that the formation of 'GR1' as well as diffusion of dissolved iron ions can be consistently described, when chloride and with that all favoured iron-chloride compounds, are taken into due consideration in the establishment of the Pourbaix diagram. The thermodynamic changes we consider for the addition of chloride to the Fe-H_2O system are demonstrated in Figure 5.9.

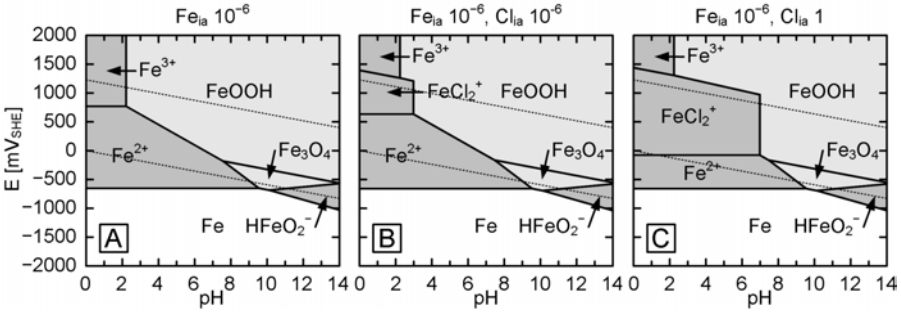

Figure 5.9: [A]: *Fe-H_2O 'SEPD' based on Table 5.3 and $Fe_{ia} = 10^{-6}$ mol/L.* [B]: *Fe-Cl-H_2O 'MEPD' based on Table 5.4 and $Fe_{ia} = 10^{-6}$ mol/L and $Cl_{ia} = 10^{-6}$ mol/L.* [C]: *As [B], but $Cl_{ia} = 1$ mol/L.*

Table 5.4: *Species preselected for the 'MEPD' of the Fe-Cl-H_2O system.*

Solid	Fe	Fe_3O_4	FeOOH	-			-
Soluble	Cl^-	ClO_4^-	Fe^{2+}	Fe^{3+}	$FeCl^+$	$FeCl_2^+$	$HFeO_2^-$

Figure 5.9 [A] corresponds to Figure 5.8 [B], i.e. it represents the 'SEPD' of the Fe-H_2O system according to Table 5.3, which can principally be also understood as the 'MEPD' of the Fe-Cl-H_2O system with a chloride ion activity of 0 mol/L. Figure 5.9 [B] and [C] represent the thermodynamic conditions, when the chloride ion activity is increased to 10^{-6} and 1 mol/L, respectively. This includes that these 'MEPDs' are based on another preselection of species, which is presented in Table 5.4.

Introduction of chloride to the system does not influence the 'ΔG_f^0' of species that do not involve chloride, i.e. Fe_3O_4 and FeOOH. In Figure 5.9 it can be observed that with increasing Cl_{ia} the stability domains of *ferric* chloride ($FeCl_2^+$), which we assume to be the most critical species in corrosion propagation, enlarges towards higher pH on the expense of stability domains of Fe_3O_4 and FeOOH. With further increment of the chloride ion activity, ferrous chloride ($FeCl^+$) replaces ferrous iron and dominates the associated stability domain. If the iron ion activity is kept at 10^{-6} mol/L, this thermodynamic shift takes place at a chloride ion activity of 1.3 mol/L. In contrast to e.g. the introduction of calcium to the Fe-H_2O system (cf. Figure 5.4 in Section 5.2.1.1),

where only solid iron-calcium complexes were taken into account, the e*quilibria in the Fe-Cl-H_2O 'MEPD' are affected by both ion activities*.

The proposed model for chloride induced corrosion is based on the 'MEPD' of the Fe-Cl-H_2O system presented in Figure 5.9 [C], i.e. an iron ion activity of 10^{-6} mol/L, as conservative choice for formation of passive domains (cf. Section 4.2.1) and a chloride ion activity of 1 mol/L, which corresponds to 35 g/L pore solution (cf. Table 4.3 in Section 4.2.1). It should be remarked that the selected chloride concentration might be regarded as arbitrary and high, but based on the theory described for pitting corrosion (cf. Section 2.3.2), migration (cf. Section 3.1.6.3), and ion mobility (cf. Section 3.1.7.4), we assume such concentration to be rather likely attained within a corrosion pit.

In Figure 5.9 [C] it can be observed that even with this relatively high chloride ion activity, corrosion propagation is thermodynamically impossible when the "global" pH of reinforcement in uncarbonated concrete, e.g. pH 13 (cf. Section 5.2.2.1), is taken into account. However, there is a general agreement in the literature that propagation of pitting corrosion involves depletion of oxygen in the pit due to the ongoing formation of anodic corrosion products as well as an associated acidification, which leads to a major localised pH drop. A macrocell is formed and dissolution of iron (i.e. the anodic reaction) takes place in the pit only, while the adjacent passive steel acts as cathode (cf. Section 3.1.8). Based on the theory described for the mobility of ions, it can be concluded that the formation of macrocells is highly favoured under the assumed conditions, i.e. high conductivity in oxygen-deprived uncarbonated concrete (cf. Section 3.1.7.4). Even if the influence of chloride ions on the conductivity is much smaller than often described in the literature (cf. Section 3.1.7.4), Cl^- contributes to macrocell formation and furthermore has a large affinity to migrate away from the cathode towards the anode, i.e. into the pit (cf. Section 3.1.6.3). We think that this argumentation supports the selected high chloride ion activity that the proposed model is based upon.

In e.g. [Broomfield, 1997; Sandberg, 1998] depletion of oxygen in the corrosion pit is attributed to the ongoing formation of ferric hydroxide, as described by the redox reaction [5.49] in the threefold reaction mechanism (cf. Section 5.2.2.1):

$$4Fe(OH)_2 + O_2 + 2H_2O \rightarrow 4Fe(OH)_3 \quad \left(\Delta G^0 = -364\,\text{kJ} \right) \qquad [5.59]$$

This ongoing process is considered to result into conditions, where the ferrous ion in the pit liquid reacts with water to form H^+, which leads to acidification of the pit:

$$Fe^{2+} + H_2O \rightarrow FeOH^+ + H^+ \quad \left(\Delta G^0 = 53\,\text{kJ} \right) \qquad [5.60]$$

The acid-base reaction [5.60] illustrates a positive 'ΔG' and we do not consider formation of ferric hydroxide to be thermodynamically favoured. Moreover, we think that due to the complex electrochemistry several anodic reactions are thermodynami-

cally possible and contribute to the acidification in a corrosion pit. With regard to the postulated dominance of FeOOH (cf. Figure 5.9 [C]), we propose the redox reaction:

$$4Fe^{2+} + 6H_2O + O_2 \rightarrow 4FeOOH + 8H^+ \quad \left(\Delta G^0 = -168\,kJ \right) \qquad [5.61]$$

as an alternative to the redox reaction [5.59] leading to depletion of oxygen.

In addition to the redox reaction [5.61], which already involves acidification, we suggest that, in principle, all mentioned anodic reactions corresponding to the equilibrium lines above neutral pH and in the vicinity of the hydrogen line can contribute to pit acidification, since most of these reactions produce hydrogen ions. Taking into account the depletion of oxygen, we think that in particular the half-cell reactions describing the formation of bihypoferrite ion, which are otherwise of rather marginal importance (cf. Section 5.2.1.2):

$$Fe + 2H_2O \rightarrow HFeO_2^- + 3H^+ + 2e^- \quad \left(E_0^0 = 391\,mV_{SHE} \right) \qquad [5.62]$$

$$Fe_3O_4 + 2H_2O + 2e^- \rightarrow 3HFeO_2^- + H^+ \quad \left(E_0^0 = -1518\,mV_{SHE} \right) \qquad [5.63]$$

$$Fe_2O_3 + H_2O + 2e^- \rightarrow 2HFeO_2^- \quad \left(E_0^0 = -941\,mV_{SHE} \right) \qquad [5.64]$$

could play a major part in the *initial* acidification of the pit (cf. Figure 5.9 [C]). Fe_3O_4 and Fe_2O_3 are, hence, not considered as favoured products, but as principal constituents of the existing passive layer (cf. Section 5.2.1.1), which is consumed in the process. In contrast to all other corrosion states described in this Chapter, we assume hydrogen ion reduction to contribute to the overall cathodic processes, since the depletion of oxygen and acidification in the pit are considered to provide for the required thermodynamic conditions (cf. Section 2.1.10).

The proposed model for chloride induced corrosion relates to the propagation stage subsequent to initial pit acidification and covers both the formation of green rust and the outwards diffusion of dissolved iron species. It is based on the above theory, additional thermodynamic considerations, and experimental observations. This model is described in detail in the following to exemplify the benefits of thermodynamic considerations based on the Pourbaix diagrams and reaction mechanisms.

The thermodynamic conditions for the proposed propagation model are identified in Figure 5.10 [B], while Figure 5.10 [A] illustrates our proposed adaptation of the representation of corrosion initiation in chloride contaminated concrete by pitting potential curves.

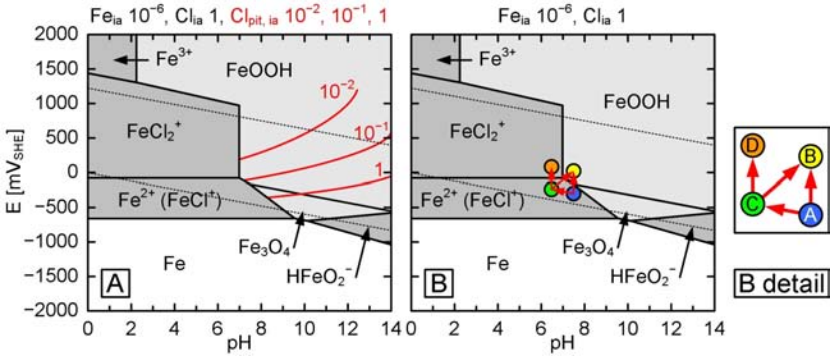

Figure 5.10: *Fe-Cl-H_2O 'MEPD' based on Table 5.4 and $Fe_{ia} = 10^{-6}$ mol/L and Cl_{ia} = 1 mol/L. $FeCl^+$, which is favoured over Fe^{2+} at higher Cl_{ia}, is included as an alternative species in the associated stability domain.* [A]: *Identification of pitting potentials for corrosion initiation based on different chloride contents based on pitting potential curves after [Nilsson et al., 1996; Sandberg, 1998].* [B]: *Identification of different thermodynamic states concerning the proposed model for corrosion propagation.*

Figure 5.10 [A] exemplifies a, in our opinion, thermodynamically more consistent representation of corrosion initiation in chloride contaminated concrete than the one shown in Figure 5.7 [A]. Instead of superimposing the pitting potential curves on the Fe-H_2O system [Nilsson et al., 1996; Sandberg, 1998], we propose to superimpose the curves on the Fe-Cl-H_2O 'MEPD'. We consider this approach to be appropriate, because it takes the thermodynamic effect of chloride on the Fe-H_2O system into due consideration and hence closes the gap between corrosion initiation and propagation.

Figure 5.10 [B] identifies the different thermodynamic states, i.e. case (A) to (D), for the proposed mechanism, which is described based on these cases and the arrows identifying reactions between them. The alternative formation of ferrous chloride at higher chloride concentration (above 1.3 mol/L), which is also indicated in Figure 5.10 [A] and [B], is covered by including the associated reactions for both Fe^{2+} and $FeCl^+$ in the model.

Initially, a pH of about 7.2 and an 'E_{corr}' of around −200 mV_{SHE} are assumed, see case (A) in Figure 5.10 [B]. The acidifying redox reaction [5.61]:

$$4Fe^{2+} + 6H_2O + O_2 \rightarrow 4FeOOH + 8H^+ \quad \left(\Delta G^0 = -168\,\text{kJ} \right) \qquad [5.65]$$

is thermodynamically possible in this state. In case of higher chloride concentrations (above Cl_{ia} = 1.3 mol/L) an alternative reaction to [5.65] is:

$$4FeCl^+ + 6H_2O + O_2 \rightarrow 4FeOOH + 8H^+ + 4Cl^- \quad \left(\Delta G^0 = -172\,\text{kJ} \right) \qquad [5.66]$$

With availability of oxygen, 'E_{corr}' is shifted into the stability domain of FeOOH (cf. case (B) in Figure 5.10 [B]) and depending on the chloride concentration a portion of the Fe^{2+} or $FeCl^{+}$ is oxidised to FeOOH as described by the redox reaction [5.65] or [5.66]. Both reactions produce hydrogen ions leading to a decrease in pH of the surrounding concrete. The effect of this acidification on the unoxidised portion of Fe^{2+} or $FeCl^{+}$ is illustrated by case (C) in Figure 5.10 [B]. A decrease to a pH of about 6.6, which is regarded to be likely surpassed, is assumed. At the pH of 6.6 and the presence of chloride ions and oxygen another oxidation reaction is thermodynamic possible to take place involving formation of hydroxyl ions. Depending on the chloride concentration this redox reaction is either described by:

$$4Fe^{2+} + 8Cl^{-} + O_2 + 2H_2O \rightarrow 4FeCl_2^{+} + 4OH^{-} \quad (\Delta G = -182\ \text{kJ}) \qquad [5.67]$$

or, in case of higher chloride concentrations, by:

$$4FeCl^{+} + 4Cl^{-} + O_2 + 2H_2O \rightarrow 4FeCl_2^{+} + 4OH^{-} \quad (\Delta G^0 = -186\ \text{kJ}) \qquad [5.68]$$

At this pH, the oxidation of Fe^{2+} or $FeCl^{+}$ with availability of Cl^{-} and O_2 is equivalent to a raise of 'E_{corr}' , which favours the formation of soluble $FeCl_2^{+}$ (case (D) in Figure 5.10 [B]). At the same time the surrounding concrete experiences a raise in pH due to the production of hydroxyl ions in [5.67] or [5.68]. With alkalinisation of the surrounding concrete or diffusion of dissolved Fe^{2+} or $FeCl^{+}$ into regions of a pH that exceeds the equilibrium line between $FeCl_2^{+}$ and FeOOH in 'MEPD' in Figure 5.10 [B], oxidation of Fe^{2+} or $FeCl^{+}$ lead to formation of FeOOH (cf. redox reaction [5.65] or [5.66]). This is illustrated by the arrow from case (C) towards case (B) in Figure 5.10 [B].

A change in species from FeOOH to $FeCl_2^{+}$ in the same oxidation state is thermodynamically described by the acid-base reaction:

$$FeOOH + 3H^{+} + 2Cl^{-} \rightarrow FeCl_2^{+} + 2H_2O \quad (\Delta G^0 = -85\ \text{kJ}) \qquad [5.69]$$

This reaction corresponds to the type III equilibrium line (vertical line, cf. Section 2.1.10) between $FeCl_2^{+}$ to FeOOH at the pH around 7 in Figure 5.10 [B]. In the considered system FeOOH is thermodynamically favoured to be transformed to $FeCl_2^{+}$ at pH values below 7. However, we assume that FeOOH precipitated in concrete is almost insoluble. Among others, this important kinetic aspect is applied in chemical coagulation processes in waste water treatment [ISA, 1995; Faust & Aly, 1998]. We verified this notion by a simple experiment, which is illustrated in Figure 5.11.

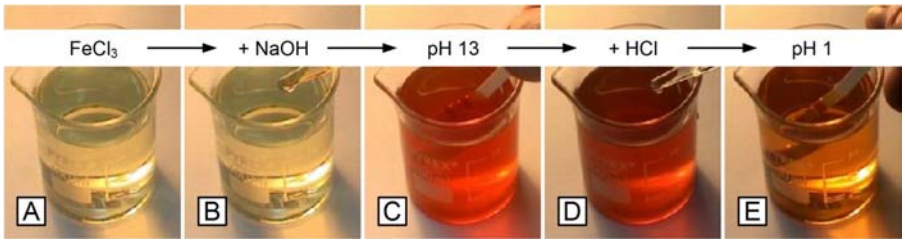

Figure 5.11: *Simple test to determine the solubility of FeOOH.* [A]: *Beaker with $FeCl_3$ solution.* [B]: *Addition of NaOH to solution.* [C]: *Solution at pH 13 with brownish colour indicating precipitation of FeOOH.* [D] *Addition of HCl to solution.* [E]: *Solution at pH 1 is diluted, but brownish colour remains indicating that FeOOH is difficult to dissolve.*

As illustrated in Figure 5.11 [A] and [B], ferric chloride solution was alkalinised by addition of sodium hydroxide, which led to precipitation of FeOOH. This is indicated by the brownish colour of the solution at pH 13, see Figure 5.11 [C], and can be described (in correspondence with [5.69]) by the acid-base reaction:

$$FeCl_2 + 3OH^- \rightarrow FeOOH + 2Cl^- + 2H_2O \quad \left(\Delta G^0 = -154\,\text{kJ} \right) \qquad [5.70]$$

The solution was then acidified by addition of hydrochloric acid, see Figure 5.11 [D]. The solution at pH 1 was diluted, but the enduring brownish colour confirmed that precipitated FeOOH is difficult to dissolve, even in very acid media. Accordingly, there is no arrow pointing from case (B) towards case (D) in Figure 5.10 [B].

The two alternative redox reactions [5.67] and[5.68] form $FeCl_2^+$. Ferric chloride in form of the liquid compound $FeCl_3$ is known to be a very reactive etching agent for metals, e.g. for printed circuit boards (PCB) and stainless steels [Walker & Tarn, 1990]. However, this compound does not exhibit thermodynamic tendency to be formed:

$$FeCl_2^+ + Cl^- \rightarrow FeCl_3 \quad \left(\Delta G^0 = 178\,\text{kJ} \right) \qquad [5.71]$$

Yet, we assume that $FeCl_2^+$ has similar etching properties on iron as $FeCl_3$. The dissolution of Fe by $FeCl_2^+$ can for instance be described by the redox reaction:

$$2FeCl_2^+ + Fe \rightarrow 3Fe^{2+} + 4Cl^- \quad \left(\Delta G^0 = -78\,\text{kJ} \right) \qquad [5.72]$$

Etching occurs under reduction of ferric ion ions and dissolution of iron to form ferrous ion. One Fe atom is dissolved by two $FeCl_2^+$ producing three Fe^{2+} under separation of the chloride ions from the complex. Therefore, both the Fe^{2+} and the Cl^- ions are available to be once more oxidised to $FeCl_2^+$, cf. [5.67] and [5.68].

We assume that by the above described reaction mechanism a self-contained (autocatalytic) loop as sketched in Figure 5.12 is established.

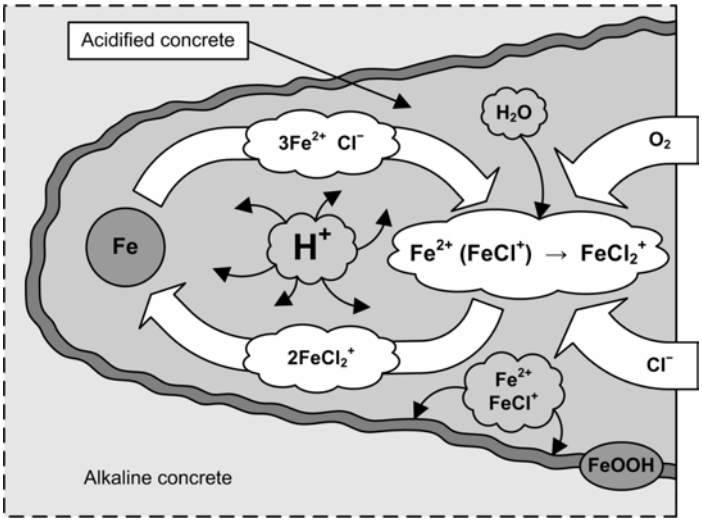

Figure 5.12: *Sketch of the proposed mechanism for chloride induced corrosion in oxygen deprived concrete. The sketch illustrates the self-contained loop between the oxidation of Fe^{2+} ($FeCl^+$) to $FeCl_2^+$ and the etching process of Fe by $FeCl_2^+$ in combination with the associated acidification and pore-blocking by precipitation of FeOOH.*

As indicated in Figure 5.12, the proposed mechanism does not require oxygen at the rebar surface. The reactants are dissolved in the pore solution and assumed to be mobile (cf. Section 3.1.7.4), so that oxidation of Fe^{2+} ($FeCl^+$) to $FeCl_2^+$ can occur at any location with sufficient supply of oxygen and a pH below the equilibrium line of $FeCl_2^+$ and FeOOH, see Figure 5.10 [B]. The $FeCl_2^+$ will diffuse from the location where it is produced towards the rebar. The anodic dissolution of Fe does not require e.g. the cathodic reduction of oxygen, since the reduction process is incorporated in the dissolution process itself [5.72].

Hydroxyl ions are generated in the oxidation reaction from Fe^{2+} ($FeCl^+$) to $FeCl_2^+$, cf. redox reactions [5.67] and [5.68], and the surrounding area experiences an increase in pH. The pH increase favours oxidation of Fe^{2+} ($FeCl^+$) to FeOOH instead of oxidation to $FeCl_2^+$ once the pH of 7 (corresponding to the equilibrium line between $FeCl_2^+$ and FeOOH) is surpassed, see Figure 5.10 [B]. Oxidation to FeOOH results in production of H^+ (cf. [5.65] and [5.66]) and the region is reacidified, as illustrated in Figure 5.12. Consequently, the pH will alternate around the equilibrium pH of 7, as illustrated in the 'MEPD' in Figure 5.10 [B].

The pH and equilibrium potential range of the proposed mechanism falls into the centre of the measured and postulated data from the literature for the formation of 'GR1' (e.g. [Refait & Génin, 1993; Sagoe-Crentsil & Glasser, 1993; Refait & Génin, 1997; Refait et al., 1998; Génin et al., 2001; Koleva et al., 2006; CeFrCo, 2007; Rémazeilles & Refait, 2007]) and hence is seen as a thermodynamic consistent description.

We performed an initial verification of acidification and precipitation of FeOOH by means of a simple experiment. As presented in Figure 5.13 [A] and [B], a chloride contaminated reinforced concrete block with a severely corroded embedded carbon steel rebar was split parallel to the rebar leaving about 3-5 cm of concrete coverage on the steel. After the cleavage phenolphthalein (cf. Section 3.1.7.2) was applied onto the split face, see Figure 5.13 [A].

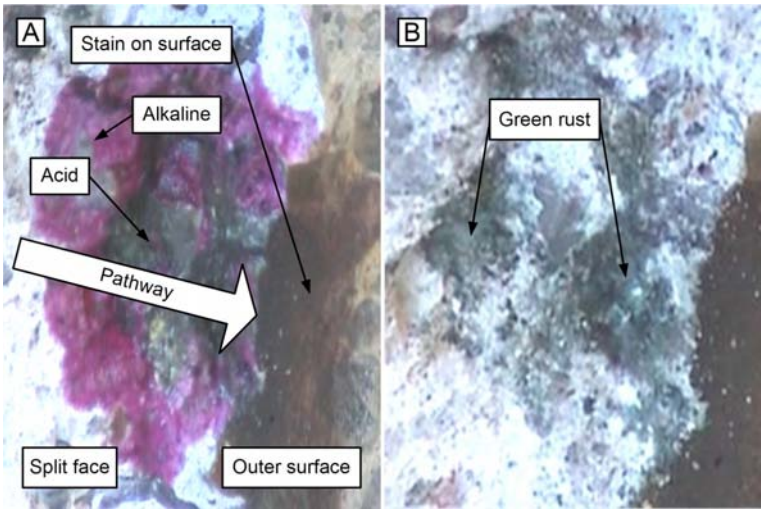

Figure 5.13: *Split chloride contaminated reinforced concrete block with a severely corroded embedded carbon steel rebar. Specimen from [Nygaard, 2003].* [A]: *Phenolphthalein applied on split face (cf. Section 3.1.7.2) and identification of regions of interest.* [B]: *Traces of green rust, also referred to as 'GR1', on the split surface before application of phenolphthalein.*

The indicator showed that the pH is (at least) below a pH of at least 9.5 (cf. Table 3.3 in Section 3.1.7.2) in designated areas. These areas appeared to connect the source of corrosion at the rebar to the rust stain on the outer surface in form of a pathway, which indicates that the dissolved ferrous ion approaches the surface by diffusion towards oxygen enriched areas. The observed low pH of the path between rebar and surface is assumed to be due to H^+ formed in the oxidation of Fe^{2+} ($FeCl^+$) to FeOOH, cf. [5.65] and [5.66]. The pathways appeared to be limited by a borderline. This is considered to be due to Fe^{2+} ($FeCl^+$) precipitating as FeOOH (cf. [5.65] and [5.66]), when diffusing out of the acidified area towards regions with a higher pH (cf. Figure 5.12), as also exemplified through the direct shift between case (C) and (B) in the 'MEPD' in Figure 5.10 [B]. We assume that this occurrence limits neutralisation of the acidified region through a densification at the "equilibrium pH line" to form acidified pathways. Otherwise, a large quantity of hydroxyl ions would be available to diffuse into the acidified area from the concrete bulk remaining at high pH.

In accordance with the 'MEPD' in Figure 5.10 [B], formation of iron oxides or hydroxides is impossible in the vicinity of the rebar, due to the low pH. Hence, Fe^{2+} ($FeCl^{+}$) and $FeCl_2^{+}$ will remain in solution and form the liquid compound, which is commonly referred to as green rust or 'GR1'. Figure 5.13 [B] shows the split face of the concrete block immediately after cleavage before application of the phenolphthalein. The predicted liquid green compound could be clearly observed to emerge from the pathway. Since stable in the absence of oxygen only, the liquid is immediately transformed to FeOOH after splitting.

The observations on the reinforced concrete block were verified by analysing the instrumented mortar specimens from 'Test II' (cf. Section 1.9.4) at the end of their exposure periods by rainbow indicator (cf. Section 3.1.7.2) and 'EDS' element mapping (cf. Section 3.2.2.2, [EDAX, 2006; FEI, 2007]). A grit-blasted carbon steel test specimen, the corresponding fresh sawn face (cut 1), and the sawn/split face (cut 2/split) with rainbow indicator applied to it are shown in Figure 5.14 [A], [B], and [C], respectively.

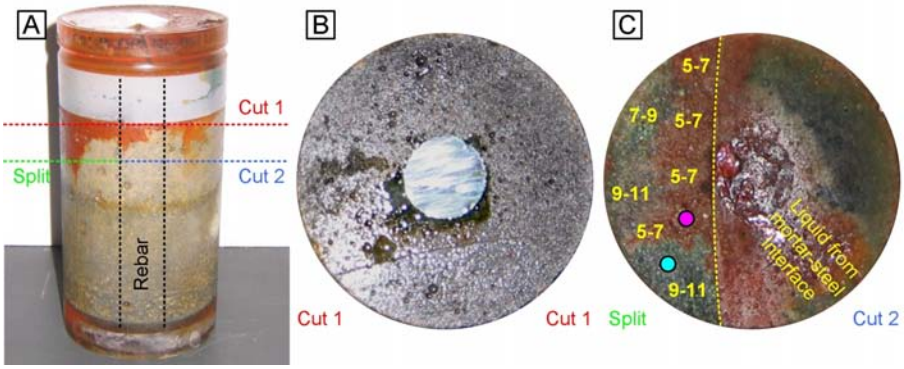

Figure 5.14: [A]: *Severely corroded (chloride induced) mortar specimen with central grit-blasted carbon steel rebar without embedded 'EEW' (specimen "C01-B", cf. Section 1.9.4) at the end of its exposure period (lead wires and O-ring removed). Identification of rebar position and of sawn face (cut 1, red) and sawn/split face (cut 2/split, blue/green).* [B]: *Fresh sawn face corresponding to cut 1 line with 'GR1' protruding from the mortar-steel interface.* [C]: *Sawn/split face with Rainbow indicator applied (cf. Section 3.1.7.2). Ranges of pH (yellow numbers) indicated on split face in accordance with the colour code of the rainbow indicator (cf. Table 3.3 in Section 3.1.7.2). Identification of measurement points used for element mapping, i.e. pink dot in low pH area (cf. Figure 5.15 and Figure 5.16) and turquoise dot in high pH area (cf. Figure 5.17).*

As mentioned in Section 1.9.2, the submersed mortar surface of 'Test II' corresponded to 60% of the total surface, which can be observed by slightly different col-

our of the lower and the upper mortar part of the specimen shown in Figure 5.14 [A]. The rust stain on the unsubmerged mortar surface close to the acrylic glass section (cf. Section 8.1.2.1) is evident. As illustrated by the cut 1 line (red) in Figure 5.14 [A], the specimen was first cut horizontally with a diamond saw just beneath the acrylic glass section. The corresponding fresh sawn face of the mortar specimen is shown in Figure 5.14 [B], where protrusion of liquid 'GR1' from the pores and in particular from the mortar-steel interface can be clearly seen. Figure 5.14 [C] shows the face corresponding to the combined cut/split face along the cut 2/split line (blue/green) indicated in Figure 5.14 [A]. For the cut/split face the specimens were cut horizontally saw to the bottom of the rebar, while the remaining part was split open with a chisel. Rainbow indicator was applied to the sawn/split face of the remaining specimen (the lower part), while the upper part, i.e. the approximately 10 mm thick section between cut 1 and cut2/split was used for 'EDS', see pink dot in low pH area and turquoise dot in high pH area in Figure 5.14 [C].

The pH ranges on the split face determined by the rainbow indicator (cf. colour code in Table 3.3 in Section 3.1.7.2) show low pH values, i.e. between 5 and 7, in the vicinity of the rebar and at designated regions connecting the rebar with the rust stains on the external surface. These regions are distinctively separated from regions of higher pH (between 9 and 11), see Figure 5.14 [C]. Regions with low pH showed relatively high Fe concentrations, which is exemplified by the element mapping in Figure 5.15 and the associated 'EDS' spectrum in Figure 5.16. Both were recorded at the measurement point identified by the pink circle in Figure 5.14 [C].

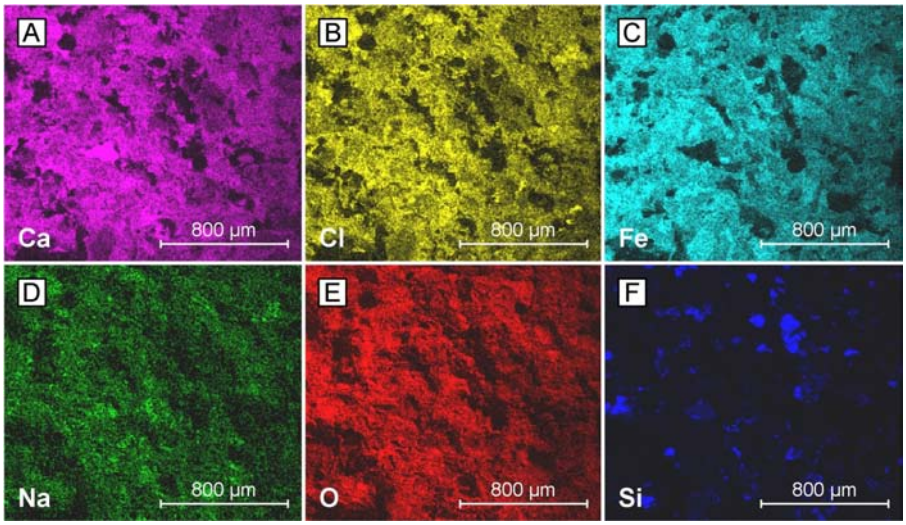

Figure 5.15: *Energy dispersive element mapping of measurement point in low pH area (Figure 5.14 [C], pink dot).* [A]: *Calcium.* [B]: *Chloride.* [C]: *Iron.* [D]: *Sodium.* [E]: *Oxygen.* [F]: *Silicon.*

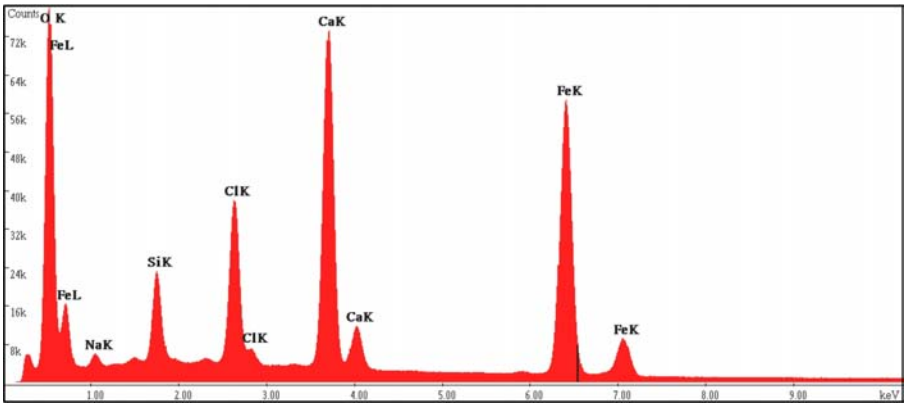

Figure 5.16: *Energy dispersive spectrum of measurement point in low pH area (Figure 5.14 [C], pink dot). X-ray energies on the X-axis and relative X-ray counts on the Y-axis.*

In contrast to the relatively high amount of iron in the low pH region, no or very little detectable iron was found in the high pH regions. This is exemplified by the 'EDS' spectrum shown in Figure 5.17, which was recorded at the measurement point identified by the turquoise circle in Figure 5.14 [C].

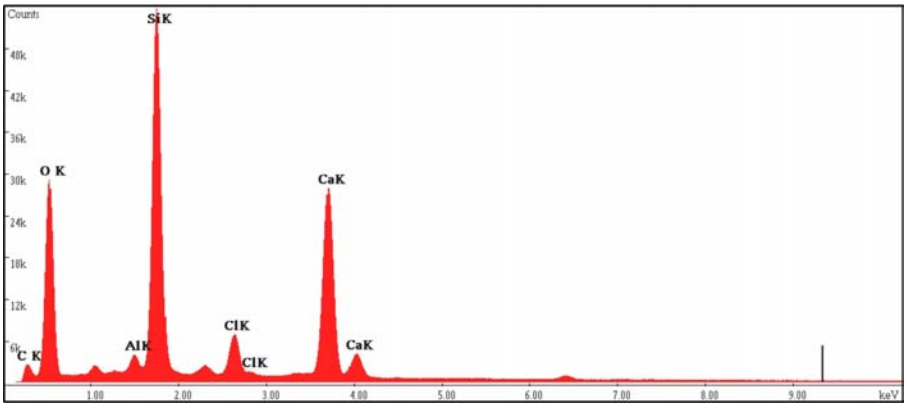

Figure 5.17: *Energy dispersive spectrum of measurement point in high pH area (Figure 5.14 [C], turquoise dot). X-ray energies on the X-axis and relative X-ray counts on the Y-axis.*

We think that the distinct occurrence and pH ranges of the regions identified with the rainbow indicator (cf. Figure 5.14 [C]) in combination with the relatively high Fe concentrations (cf. Figure 5.15 and Figure 5.16) in the low pH regions (compared to no or very low detectable iron concentration in the regions higher pH regions, cf. Figure 5.17) is a reasonable confirmation for the proposed reaction mechanism. This holds in particular with regard to the formation of acidified pathways (cf. Figure 5.10 [B], Figure 5.12, and Figure 5.13 [A]).

The physical result from chloride induced corrosion and the described mechanism in the oxygen-deprived environment differs to quite some extent from the damage types resulting from the formation of expansive corrosion products in oxygen-rich concrete (cf. Section 5.2.2.1). Chloride induced pitting and subsequent dissolution of the rebar results in a notch-like shape attack of the reinforcing steel, see Figure 5.18 [A].

Figure 5.18: [A]: *Notch-like shape corrosion attack of rebar in chloride contaminated concrete. From [COWI, 2007b]*. [B]: *Collapse of parking garage in Minnesota, USA, due to chloride induced corrosion damage. From [Borgard et al., 1990]*.

The tensional stress-strain relation of the steel changes in the corroding area and in its vicinity, when the notch grows to a sufficient size. Theoretically, if only about 8% of the cross-sectional area are corroded, a rebar can no longer be regarded as a linear-elastic or ideal-plastic material [Frederiksen & Poulsen, 1997]. The notch will take up all the deformation as tensile stress and the yield capacity of the reinforcing steel is reduced to yielding in the notch. Under these circumstances, the corroding reinforcing steel acts as a brittle material, due to the concentration of the tensile stress in the notch. The consequence of brittle behaviour of reinforcement under simultaneous exposure to heavy load can be disastrous, which is illustrated by the widely publicised photograph of the collapse of a parking garage due to chloride induced reinforcement corrosion, see Figure 5.18 [B].

Depending on the availability of oxygen, chloride induced corrosion or the combination of chloride contamination and carbonation can lead to similar damage types as described for carbonation induced corrosion (cf. Figure 5.6). However, in particular with regard to the diffusion of soluble corrosion products described throughout this Section, it is important to note that damage under chloride induced corrosion in the oxygen deprived environment is not represented by deterioration or corrosion propagation models that are based on formation of solid voluminous products at the concrete-steel interface (cf. Section 5.2.2.1).

5.2.3 Immune State

The immune state is not a corrosion state per se, but a short note on it should be given, as this thermodynamic state is of major importance in available countermeasures, e.g. concerning 'CP' (cf. Section 6.4.1), as well as in the proposed new countermeasures (cf. Chapter 7). In Figure 5.19 the Fe-H_2O 'SEPD' with $Fe_{ia} = 10^{-6}$ mol/L (Figure 5.19 [A]) is compared to the Fe-H_2O 'SEPD' with $Fe_{ia} = 1$ mol/L (Figure 5.19 [B]) and to the Fe-Cl-H_2O 'MEPD' with $Fe_{ia} = 10^{-6}$ mol/L and $Cl_{ia} = 1$ mol/L (Figure 5.19 [B]).

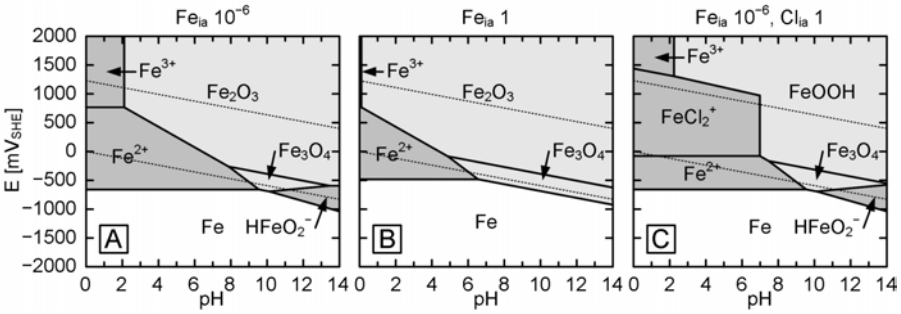

Figure 5.19: [A]: *Fe-H_2O 'SEPD' based on Table 4.2 and $Fe_{ia} = 10^{-6}$ mol/L.* [B]: *As [A], but $Fe_{ia} = 1$ mol/L.* [C]: *Fe-Cl-H_2O 'MEPD' based on Table 5.4 and $Fe_{ia} = 10^{-6}$ mol/L and $Cl_{ia} = 1$ mol/L.*

Comparing the immunity regions of the 'SEPDs' with different iron ion activities in Figure 5.19 [A] and [B], it can be concluded that an increased iron concentration has an influence on the equilibria of Fe with the adjacent species, but the effect in increasing the concentration is rather small, e.g. compared to the effect in increasing the passivity domain. From the comparison between the Fe-H_2O 'SEPD' in Figure 5.19 [A] and the Fe-Cl-H_2O 'MEPD' in Figure 5.19 [B] based on the same Fe_{ia}, it can be seen that *the addition of chloride does not affect the equilibria of Fe* with the adjacent species, i.e. the electrode potential to obtain immunity stay the same.

While the extents of the passivity domains at a certain ion activity are approximate parameters, the equilibria between Fe and oxidised species or compounds with other elements are thermodynamically exact parameters, as they reflect the inherent electrochemical properties of iron in aqueous solutions. We consider this to be an important aspect, when cathodic polarisation for corrosion protection is aimed at. Moreover, we think that it is important to point out a thermodynamic aspect of iron, which was applied, but not exclusively mentioned throughout Section 4 and 5. In Figure 5.19 it can be observed that *Fe does not have a stability domain in common with the stability domain of water and hence always "corrodes" in the active or passive state in aqueous solutions*. This thermodynamic property applies to several metals, whereas the immunity domain of some noble metals extents partly (e.g. copper, silver, platinum) or entirely (in principle, limited to gold) into the stability domain of water in the pH

range from 1-14. Related to this property, a final aspect that should be emphasised with regard to immunity of iron is that it can, consequently, only be obtained by surpassing the *theoretical* hydrogen line (cf. Section 2.1.10). Thus, *hydrogen embrittlement* (cf. Section 2.3.6) becomes an aspect of concern, when *designing for immunity*, which is discussed in relation to available countermeasures in Chapter 6 and with regard to the proposed new countermeasures throughout Chapter 7.

6 Available Corrosion Countermeasures

The exemplifications in Chapter 5 illustrated the beneficial use of thermodynamics (in particular, the use of the Pourbaix diagram in combination with reaction mechanisms) for the description of reinforcement corrosion. We think that thermodynamically consistent mechanisms are not limited to the description of corrosion processes, but can also establish the basis for the evaluation of available countermeasures (this Chapter) as well as for the design of new countermeasures (Chapter 7). Given that the established Pourbaix diagrams and the associated reaction mechanisms reflect the investigated system (cf. Section 4.2.2), a thermodynamic evaluation based on this information can be used to e.g. identify problems, possible improvements, as well as for conclusions concerning the effectiveness of the investigated countermeasure. That holds in particular for e.g. stainless steel, galvanised steel, or 'CP', which can be considered as thermodynamically based countermeasures.

However, a detailed thermodynamic evaluation of all available countermeasures goes beyond the scope of this thesis. Hence, the coverage of thermodynamic principles in this Chapter is limited to pointing out possible applications, while the particular characteristics are briefly described based on a critical review of the literature. The review is intentionally kept short and provides only a brief summary highlighting some central aspects that are considered to be important for the purposes of this thesis. Thus, it is often referred to a larger body of extensive literature dealing with the discussed countermeasures (cf. Section 6.2). Certain countermeasures are treated in more detail, because aspects of these measures are significant for the development and establishment of the proposed new countermeasures (Chapter 7). Critical shortcomings of the available countermeasures are a central input in the design aspects and requirements for our proposed new countermeasures, which is dealt with in Section 7.1. So, in combination with Chapters 2, 3, 4, and 5, this Chapter provides the background of the considerations for the development of new countermeasures.

After a short introduction to the most important general aspects of durability and service line design in Section 6.1 and to the relevant standards and guidelines as well as to selected related organisations in Section 6.2, countermeasures for new and existing structures are reviewed in Sections 6.3 and 6.4, respectively.

6.1 Durability and Service Life Design

In practice, durability is a subjective parameter and difficult to define precisely [fib, 1999a]. Therefore, the service life concept has largely replaced the non-factual concept of durability, since the service life is quantifiable and measurable quantity [Fagerlund, 1979], which is generally expressed in years. So, the time factor is introduced as a design parameter. There are different service life concepts, but the most important one for the purposes of this thesis is the *technical service life*, which can be

defined as [fib, 1999a]: *"The time in service until a defined unacceptable state of deterioration is reached."*

Proper design, i.e. a good concrete quality, a sufficiently deep concrete cover, and an adequate crack width limitation as well as appropriate execution are normally sufficient to attain the desired service life for everyday buildings and normal structures in moderate environments. The national building codes and regulations for reinforced concrete structures, e.g. Eurocode 2 [DS/EN 1992-1-1, 2005] and [ACI 201.2R, 2001; ACI 318M/318RM, 2005], ensure that the basic service life requirements are fulfilled. The service life requirements (in the order 50 years [Rostam, 2007]) in these and other national standards are generally not mentioned explicitly, but implicated by the codified design requirements. Among the crack width limitations (cf. Section 3.1.11.2), the most important design specifications from a durability point of view generally concern the maximum 'w/c', the minimum cement content (cf. Section 3.1), and a minimum concrete cover depth.

However, many special structures, such as structures under severe exposure conditions, structures with special service life requirements, or structures with architectural designs that do not allow for a sufficient cover depth*, require additional considerations and often corrosion preventive measures, i.e. countermeasures, to omit premature deterioration. Car parks and offshore structures (cf. Section 3.1.11.2) are popular examples for severe exposure conditions, but most bridges, tunnels, and other special infrastructure projects are nowadays designed for service lives of 100, 120, or even 200 years and are often also exposed to a severe environment.

With the time factor, i.e. the number of years of technical service life, introduced as a design parameter, service life design can be carried out in a similar way to the load and resistance factor design concept used for structural design [DS/EN 206-1, 2002; ACI 318M/318RM, 2005]. Nowadays, probabilistic design models, e.g. the DuraCrete approach "Probabilistic Performance based Durability Design of Concrete Structures" [Engelund et al., 2000], are often utilised in service life design of new structures as well as for the reassessment of existing structures. The DuraCrete approach takes all uncertainties regarding environmental exposure, material properties, and deterioration into account in the design phase. It has been adopted by national authorities and international associations, e.g. in the fib "Model Code for Service Life Design" [fib, 2006], which in addition to this approach provides three other durability design methodologies, i.e. the so-called "partial factor design", "deemed to satisfy design", and "avoidance of deterioration". The "Guide to Durable Concrete" [ACI 201.2R, 2001] in combination with the "Service-Life Prediction. State-of-the-Art Report" [ACI 365.1R, 2000] can be seen as the US counterpart to the above mentioned publications.

* Not only architectural requirements can favour a reduction of the cover thickness (based on appropriate countermeasures), but it is often beneficial for structural reasons, in particular with regard to crack width limitations (cf. Section 3.1.11.2).

All service life design models have in common that they are based on input parameters, which are derived from the theory of transportation mechanisms (cf. Section 3.1.6) in combination with knowledge on ingress and ion mobility parameters (cf. Section 3.1.7) and on threshold values for initiation of active corrosion (cf. Section 5.2.2).

An important concept in service life design, which came into focus during the last years, is life cycle costing ('LCC'). Life cycle costing can e.g. be formulated as an optimisation of the net present value of a concrete structure. Without a rational evaluation of future costs in a comparable manner to rate alternative solutions, service life design does often not seem to be an attractive design procedure. This is mainly due to the fact that the savings in future maintenance costs are not adequately considered to compensate for the increased initial construction costs, although such future savings can be substantial. [Val & Stewart, 2003; Rostam, 2007].

In general, it can be said that durability design for reinforced concrete structures is far more concerned about chloride induced corrosion than carbonation induced corrosion. Carbonation alone can generally be controlled with state-of-the-art concrete mixtures and design of adequate cover depths. In this respect it should be remarked that the requirements for the cover depth in the national concrete design codes [DS/EN 1992-1-1, 2005; ACI 201.2R, 2001; ACI 318M/318RM, 2005] are, in principle, based on the carbonation rate (cf. Section 3.1.7.2) for customary environments in relation to the (codified) service life of e.g. 50 years [Rostam, 2007]. So, as long as the architectural design allows for provision of sufficient cover depths, corrosion induced by carbonation is generally not an issue. However, chloride induced corrosion, alone or in combination with carbonation, is a major issue for structures exposed to such environments. Apart from the decreased extent of the initiation stage, the high corrosion rates observed under chloride induced corrosion, e.g. up to 10 times higher than for carbonation induced corrosion (cf. Section 5.1.1), as well as the possibly dangerous types of damage, i.e. the notch-like attack (cf. Section 5.2.2.2) are of concern for structures exposed to chloride environments. This is confirmed by the fact that the technical service life is often considered to correspond to the initiation phase, if chlorides are involved in the corrosion process [Costa & Appleton, 1999].

So, most of the available countermeasures for new and existing structures (cf. Sections 6.3 and 6.4, respectively) primarily aim at preventing chloride induced corrosion, where several measures, in our opinion, show (thermodynamic) deficiencies. Also, for the proposed new countermeasures (Chapter 7) focus was set on chloride induced corrosion, while resistance to carbonation was taken into account as a parameter, and all of our experimental investigations concerning corrosion resistance were based on chloride exposure (cf. Section 1.9).

Finally, it is important to note that service life design of concrete structures does not only need to provide sufficient means to avoid reinforcement corrosion, but also a

number of other deterioration mechanisms that affect the concrete directly. Some of the most important direct concrete deterioration mechanisms are:

- Freeze/thaw damage
- Thermal incompatibility of concrete components
- Sulphate attack
- Soft water or acid attack
- 'ASR' or, more general, alkali-aggregate reaction ('AAR')
- Salt recrystallisation (exfoliation).

These mechanisms are listed here, but not discussed in detail within the present thesis. Reference is made to a large body of literature that exists on the various concrete deterioration mechanisms, e.g. [Neville, 1995; ACI 201.2R, 2001; Rendell et al., 2002; Mindess et al., 2003; Richardson, 2003; Bertolini et al., 2004].

6.2 Standards, Literature, and Organisations

Great effort has been made to work out a unified European standard for protection and repair of concrete structures [Raupach, 2007]. After more than ten years of intensive discussions within different working groups the EN 1504 [DS/EN 1504-1, 2005] series of standards is now finalised and at present the European Countries are replacing their existing national standards and recommendations by the new EN 1504 series. According to [Raupach, 2007], it can be assumed that the EN 1504 series will have a significant impact on non-European countries as well. Figure 6.1 summarises the structure of the EN 1504 series, which consists of ten main standards and about 65 standards for test methods, i.e. compliance tests*.

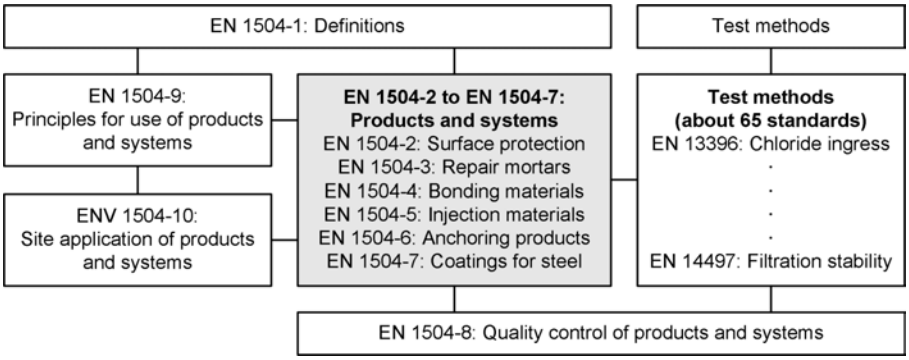

Figure 6.1: *Structure of new European standard series EN 1504 [DS/EN 1504-1, 2005]. After [Raupach, 2007].*

* The compliance tests relating to a certain countermeasure are not referred to, because the relevant test methods are listed in the associated main standard. The same holds for other test methods concerning countermeasures, e.g. published by ASTM.

As shown in Figure 6.1, the series of standards is focused on parts 2 to 7, which are the basis for CE marking of the different products and systems to be used for protection and repair of concrete structures. However, part 9 of EN 1504 is not less important, because it describes the principles for the use of the products. Furthermore, part 1 provides the definitions, part 8 regulates the quality control of the products, and part 10 provides a general guideline for site application and quality control of the execution.

The EN 1504 standard series is rather codified and therefore many national standard authorities published handbooks supplementary to the series, e.g. DS recently published "Concrete - Part 3.2: Guidance for renovation of concrete structures - Repair materials and systems according to the EN 1504 series" [DS 134.3.1, 2007].

Basically, there is no equivalent to the EN 1504 series on the US market. However, the ACI publications "Protection of Metals in Concrete Against Corrosion" [ACI 222R, 2001] in combination with the "Concrete Repair Guide" [ACI 546R, 2004], which is, among other related publications, also included in the "Concrete Repair Manual" [ACI et al., 2003], can be regarded as an equivalent to the European standard series.

Apart from these standards and guidelines as well as other relevant CEN, ASTM, and ACI publications, there are various other recommendations and guidelines published with regard to the broad field of durability design and reinforcement corrosion countermeasures by other European and US organisations. Recommendations and guidelines that we considered to be most relevant for countermeasures were published by:

- Concrete Society (CS), Blackwater, UK.
- Deutscher Ausschuss für Stahlbeton (DAfStB), German Commission for Reinforced Concrete, Berlin, Germany.
- European Federation of Corrosion (EFC), London, UK.
- Fédération Internationale du Béton (fib), International Federation for Structural Concrete Lausanne, Switzerland.*
- NACE International, formerly known as the National Association of Corrosion Engineers (NACE), Houston, TX, USA.
- International Union of Laboratories and Experts in Construction Materials, Systems, and Structures (RILEM), Bagneux, France.

In this connection, fib should be particularly mentioned, because the Model Code 78 [fib, 1978] and Model Code 90 [fib, 1993] published by fib (CEB/FIP), which are predecessors to the current "Model Code for Service Life Design" [fib, 2006] (cf. Sec-

* fib was founded in 1998 as a union between the Comité Euro-international du Béton (CEB) and the Fédération Internationale de la Précontrainte (FIP). It should be noted that in the present thesis all CEB and FIP publications are referenced as fib publications.

tion 6.1), had a major impact on the code drafting with regard to durability requirements for many national and international standardising bodies, e.g. a large part of Eurocode 2 [DS/EN 1992-1-1, 2005] is based on Model Code 90 [fib, 1993]. In relation to the important Model Code 90, extensive background information was additionally published by fib in a series of textbooks [fib, 1999c; fib, 1999a; fib, 1999b].

Besides the above mentioned standards, recommendations, and guidelines, there are other extensive publications dealing exclusively with certain countermeasures as well as several textbooks on reinforcement corrosion and/or durability design that often include detailed descriptions of various countermeasures, e.g. [Mays et al., 1992; Sarja & Vesikari, 1996; Broomfield, 1997; Bentur et al., 1997; Cigna et al., 2003; Bertolini et al., 2004; Böhni et al., 2005; Raupach et al., 2007].

6.3 Countermeasures for New Structures

As mentioned in Chapter 'TaD', countermeasures for new structures are subdivided into two groups in the present thesis:

- Concrete countermeasures

  Concrete countermeasures in this thesis include measures to reduce the permeability of the concrete bulk, concrete surface protection, integral corrosion inhibitors, and measures to improve the concrete-steel interface.

- Reinforcement countermeasures

  Reinforcement countermeasures in this thesis include non-metallic, organic-coated, more corrosion resistant, cladded, and galvanised reinforcement as well as cathodic prevention.

The most important characteristics of these two groups of countermeasures are summarised and evaluated in Sections 6.3.1 and 6.3.2.

6.3.1 Concrete Countermeasures

As described in Sections 3.1.7, the concrete properties control the ingress of carbon dioxide, chloride, and oxygen as well as the ion mobility, which all have a major effect on corrosion initiation and propagation. Besides the general measures to provide a sufficiently thick and dense concrete cover (cf. Section 6.1), the selected concrete countermeasures include:

- Mineral additions (supplementary cementitious materials) and chemical admixtures to decrease the permeability (Section 6.3.1.1)
- Post-casting densification techniques (Section 6.3.1.2)
- Concrete surface protection (Section 6.3.1.3)
- Integral corrosion inhibitors (Section 6.3.1.4)

- Electrochemical concrete-steel interface improvement (Section 6.3.1.5).

Post-casting densification techniques are only of marginal use and electrochemical concrete-steel interface improvement are, to our knowledge, not applied in practice. Apart from these, the above listed concrete countermeasures are standard techniques that are in more or less detail described in the textbooks listed in Section 6.2.

6.3.1.1 Mineral Additions and Chemical Admixtures

Concrete where the selection and proportioning of its constituents have led to improvement of one or more properties is often referred to as high performance concrete 'HPC' (Neville, 1996). Chemical admixtures in form of plasticisers and superplasticisers allow the 'w/c'* to be lowered. In practice 'w/c' ratios between 0.3 and 0.4 can be obtained in this way, while still providing for workable concretes. A further reduced permeability may be obtained when mineral additions like silica fume ('SF'), ground granulated blastfurnace slag ('GGBS'), and/or pulverised fly ash ('PFA') are used. Constituents of 'HPC' are governed by various standards: chemical admixtures [DS/EN 934-2, 2003; ASTM C494M, 2005], silica fume [DS/EN 13263-1, 2005; ASTM C1240, 2005], pulverised fly ash [DS/EN 450-1, 2005; ASTM C618, 2005], ground granulated blastfurnace slag [DS/EN 15167-1, 2006; ASTM C989, 2006], blended cements [DS/EN 197-1, 2001; ASTM C1157, 2003] and by the additional ASTM specifications for hydraulic cements [ASTM C595, 2007; ASTM C1157, 2003], which have to be applied in compliance with the associated national cement and concrete standards (cf. Section 3.1) as well as the building codes and regulations (cf. Section 6.1). Besides these standards, several guidelines and abundant other literature has been published on 'HPC' and its constituents. For instance, 'HPC' is dealt with in detail in an ACI state-of-the-art report [ACI 363R, 1992] and a guide to quality control and testing [ACI 363.2R, 1998] as well as in fib publications concerning the general application of 'HPC' [fib, 1994] and a recommended extension to the CEB/FIP Model Code 90 [fib, 1995b].

There is a general agreement that 'HPC' has a largely reduced permeability compared to ordinary concrete (e.g. from ten to thousand fold [Neville, 1995]) due to changes in the pore structure (cf. Section 3.1). If properly placed and cured, 'HPC' improves the corrosion protection of the reinforcement given the critical chloride concentration is not reduced due to a lower chloride binding capacity and/or a reduced pH of the pore solution. The beneficial effects of properly chosen and proportioned pozzolans or slags on compressive strength and corrosion related properties are illustrated in Figure 6.2.

* Technically, water-binder ratio ('w/b') would be the correct term, because different binders are used in the 'HPC' mix, which supplement or replace the Portland cement (cf. Section 3.1.1).

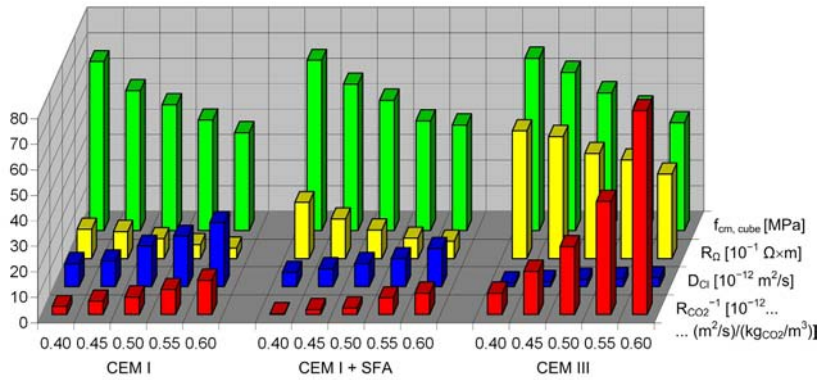

Figure 6.2: *Inverse carbonation resistance ('R_{CO2}^{-1}'), chloride migration coefficient 'D_{Cl}', electrolyte resistance 'R_{Ω}', and mean compressive cube strength ('$f_{cm,\ cube}$') for different 'w/c' ratios of Portland cement concrete ('CEM I'), Portland fly-ash cement concrete ('CEM I + SFA'), and blastfurnace concrete (CEM III). Summary of data and figures provided in [Gehlen, 2000], cf. [DS/EN 197-1, 2001] for cement types and [Gehlen, 2000] for the concrete compositions and curing conditions.*

Figure 6.2 shows the influence of both the 'w/c' and the cement type (with or without mineral additions) on the carbonation resistance 'R_{CO2}' (expressed as ('R_{CO2}^{-1}'), the chloride migration coefficient 'D_{Cl}', the electrolyte resistance 'R_{Ω}', and on the mean compressive cube strength ('$f_{cm,\ cube}$'). The influence of the 'w/c' is in good agreement with the theory described for the compressive strength, ingress, and ion mobility throughout Section 3.1. For instance, a decrement in 'w/c' increases the compressive strength, decreases permeability and the diffusion of chloride ions and CO_2, and increases the overall electrolyte resistance. Increasing electrolyte resistance largely limits the formation of macrocells (cf. Section 3.1.8) and the diffusion of dissolved corrosion products (cf. Section 5.2.2.2) is hampered as well, which was experimentally confirmed by e.g. [Hansson et al., 2006]. For a detailed discussion on the data provided in Figure 6.2 (in particular, with regard to the influence of the different cement types) reference is made to [Gehlen, 2000].

From the information summarised in Figure 6.2, it can be concluded that 'HPC' controls the essential parameters that contribute to corrosion initiation and propagation discussed throughout Section 3.1 and Chapter 5. However, 'HPC' may also have a number of less noticed adverse effects concerning the corrosion protection of reinforcement. High amounts of mineral additions may lead to lower alkalinity of the pore solution than for Portland cements, which reduces the buffer capacity to resist carbonation (cf. Section 3.1.7.2) and the chloride threshold (cf. Section 3.1.9) [Rostam, 2003]. While the influence on the chloride threshold is not represented in Figure 6.2, the decrease in carbonation resistance of CEM III mixes can be observed.

Properly produced, placed, and cured 'HPC' can provide benefits from a corrosion protection perspective. Yet, 'HPC' is sensitive towards the actual handling during production and execution, i.e. the mixing, transport, placing, compaction, and curing processes set high demands on the competence and experience of the workforce [Rostam, 1996]. Especially, the risk of cracking at early-age due to plastic shrinkage and to the combination of thermal and autogeneous deformation (cf. Section 3.1.11), is much higher for 'HPC' than for ordinary concrete [Rostam, 2003; Val & Stewart, 2003]. Early-age cracking is of particular concern, since the original benefits of 'HPC' can be compromised. In relation to this, the discussion concerning the possibility of macrocell formation in the vicinity of the crack (cf. Section 3.1.11.2) can be relevant.

For 'HPC' as a concrete countermeasure, we consider the thermodynamic influence of mineral additions and chemical admixture on iron to be more important than e.g. the influence of the decrease in permeability on 'E_{corr}'. From a corrosion protection perspective, the benefits of 'HPC' are rather kinetic than thermodynamic, although the effect of e.g. reduced 'E_{corr}' can be assessed in the Fe-H_2O 'SEPD'. The effect of mineral additions and chemical admixtures could be studied by establishment of appropriate 'MEPDs' based on the methods described in Section 4.2. However, we performed neither theoretical nor experimental investigations on mineral additions and chemical admixtures, since these aspects are marginal for the purposes of this thesis.

6.3.1.2 Post-Casting Densification Techniques

In [Neville, 1995] various options for post casting densification, e.g. treatment with silicon tetrafluoride gas, diluted water-glass wash, or magnesium fluorosilicate, are mentioned. These techniques, that, principally aim at improving the same concrete properties as 'HPC', are discussed in this separate Section, since the densification takes place in the entire concrete bulk (although there are technical limitations for the depth of penetration), rather than at or close to the surface, as e.g. concrete surface protection treatments that are briefly discussed in Section 6.3.1.3.

One proposal is to subject the concrete in a vacuum to the action of silicon tetrafluoride (SiF_4) gas. SiF_4 reacts with the calcium hydroxide to form calcium fluoride (CaF_2), which fills up the empty pores in the concrete bulk. This technique dates back to the 1950s and was originally developed to improve the acid resistance of concrete (so-called Ocrat-concrete) [Wittekindt, 1954]. The outcome with regard to acid resistance seems to be promising and, since this technique involves densification, a corrosion protection improvement similar to 'HPC' can be expected. $Ca(OH)_2$ can also be fixed by treatment with diluted water-glass (sodium silicate), where calcium silicates are formed to fill the pores. Treatment with magnesium fluosilicate is also considered as an option aiming at formation of colloidal silicofluoric gel to fill the pores. [Neville, 1995].

Application of these treatments is very marginal and we regard it to be limited to e.g. the precasting industry. However, these densifications techniques were relevant for us, since they relate to mechanisms that were implemented in the proposed new countermeasures (Chapter 7). Thus, with regard to the application of thermodynamics in this area, it can be stated the same as in Section 6.3.1.1, i.e. focus was set on the materials and the chemical processes rather than on the thermodynamic effect of the densification itself. Contrary to 'HPC' additions, however, the substances and associated formation of compounds involved in the described pore-blocking mechanisms have played a major role in our thermodynamic considerations.

6.3.1.3 Concrete Surface Protection

In contrast to 'HPC' (cf. Section 6.3.1.1) and densification (cf. Section 6.3.1.2), which aim at reducing the permeability of the concrete bulk, the focus in concrete surface protection is set on the external face of the concrete cover. We consider the beneficial action of surface protection to be related to prolonging the initiation phase only. After corrosion initiation, only those treatments that effectively impede the penetration of H_2O and O_2 reduce the corrosion rate. This may be partly efficient for carbonation initiated corrosion (cf. Section 5.2.2.1), but with regard to the mechanisms described for chloride induced corrosion (cf. Section 5.2.2.2), we do not consider surface protection as an option for repair of deteriorating structures, i.e. as a countermeasure for existing structures.

Part 2 of EN 1504 deals exclusively with surface protection systems for concrete [DS/EN 1504-2, 2005]. Moreover, extensive information on surface coatings is given in the "Guide to Durable Concrete" [ACI 201.2R, 2001] as well as in the extensive guidelines for surface protection systems published by ACI [ACI 515.1R, 1979] and CS [CS, 1997]. Besides protecting the concrete itself against chemical attack (cf. Section 6.1) and decorative applications, concrete surface treatments have largely focused on preventing reinforcement corrosion and the associated damage in special environments, especially for car parks [ACI 362.1R, 1997; ACI 365.1R, 2000; Raupach & Wolff, 2005].

A convenient way of classifying the extensive number of surface treatment types is based on the protection or benefits achieved by the treatment [Mays et al., 1992], see Figure 6.3.

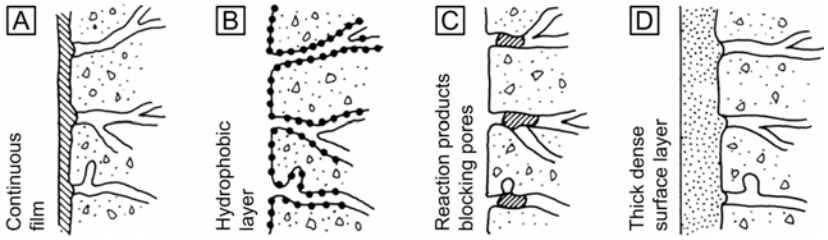

Figure 6.3: *Classes of surface treatment.* [A]: *Continuous film achieved by coatings and sealers.* [B]: *Hydrophobic layer achieved by pore-liners.* [C]: *Reaction products blocking pores achieved by pore-blockers.* [D]: *Thick dense surface layer achieved by cementitious coatings. After [Mays et al., 1992].*

These four main classes of surface treatment are described and briefly evaluated in the following:

- Continuous film achieved by coatings and sealers, see Figure 6.3 [A]

  Coatings and sealers rely upon the formation of a pinhole-free film of finite thickness over the concrete surface that acts as a barrier to the passage of water and oxygen or the diffusion of carbon dioxide and chloride ions. The materials described as sealers are supposed to penetrate into the concrete pore to a certain extent. Coatings normally have a dry film thickness of 100-300 µm applied in two or more layers, while thicker 'high build' coatings are also used. Sealers and coatings are composed of a number of constituents that are not described in detail here, and reference is made to e.g. the textbooks listed in Section 6.2. [Mays et al., 1992].

  To efficiently impede ingress, sealers and coatings must obviously have a low permeability and retain it under various degrading effects from the immediate environment as well as from e.g. temperature effect and UV light. The material properties of sealers and coatings generally differ largely from those of the concrete, e.g. concerning the modulus of elasticity and expansion due to temperature changes as well as wetting and drying. Thus, resulting stresses in the coatings may slowly degrade their barrier properties, so the long time durability of many sealers and coatings may be questioned [fib, 1995a; Rostam, 2003; Bertolini et al., 2004]. In this respect, [DS/EN 1504-2, 2005] specifies artificial weathering. Besides these concerns relating to long-term durability, it should also be noted that in extreme cases, an insufficient barrier effect can negatively influence the concrete properties, e.g. if drying out occurs at early ages, cement hydration is hampered [Cigna et al., 2003]. At the same time, coatings must allow the passage of water vapour to avoid initial disbonding [Bertolini et al., 2004].

- Hydrophobic layer achieved by pore-liners, see Figure 6.3 [B]

  Pore-lining treatments involve hydrophobic materials, which line surface pores of the concrete and repel moisture by the mechanism indicated in Figure 6.3 [B]. The

most important materials in this class are based on silicone compounds, which are synthetic chemicals produced by the chemical combination of inorganic materials containing silicon and oxygen with hydrocarbons. [Mays et al., 1992].

Hydrophobic treatments are often considered to be effective in reducing the penetration of water and chloride ions [Cigna et al., 2003]. However, it seems that the experiences vary from country to country. Whereas in some countries the application of hydrophobic treatments is mandatory for bridges exposed to deicing salts, other countries generally omit the application of silanes, etc., because the hydrophobic effect is considered to vanish after just a few months or years [Rostam, 2003].

- Reaction products blocking pores achieved by pore-blockers, see Figure 6.3 [C]

  As for densification based on exposure to gases (cf. Section 6.3.1.2), the products blocking the pores result from the reaction between a penetrant and the available calcium hydroxide. The most common penetrants are liquid silicates and silicofluorides, which are thought to lead to the formation of additional 'C-S-H' gel (cf. Section 3.1.2) and of insoluble calcium silicofluorides, respectively. [Mays et al., 1992].

  As mentioned in Section 6.3.1.3, we consider the principle of blocking pores by reaction produces to be a potent mechanism in terms of corrosion protection. However, pore-blocking based on exposure to gases cannot be applied in situ, and we consider the concept of a liquid pore-blocker applied from the surface to be doubtful for two reasons. *Firstly, the penetration depth of the pore-blocker may be insufficient to build up a barrier that provides for long-term resistance. Secondly, the densification does not take place, where we consider it to be most efficient with regard to corrosion protection, i.e. at the concrete-steel interface.* This notion is of particular importance in the development of the proposed new countermeasures (cf. Chapter 7).

- Thick dense surface layer achieved by cementitious coatings, see Figure 6.3 [D]

  Cementitious coatings, which are generally applied to the existing surface by trowelling or spraying, are based on the principles described in Section 6.1, and, in simple terms, provide an additional barrier to the existing concrete cover.

6.3.1.4 Integral Corrosion Inhibitors

Corrosion inhibitors can be applied in two different ways: as integral or as diffusion inhibitors (CBDG, 2007)[*]:

[*] Integral and diffusion inhibitors are in the literature also referred to as cast-in or admixed and migrating inhibitors, respectively. While we agree to the prefixes "cast-in" or "admixed", we consider the prefix "migration" to be misleading with regard to the actual dominating transport mechanism (cf. Section 3.1.6).

- Integral inhibitors

  Integral inhibitors are liquids or solids that are batched and mixed with the other concrete ingredients as a preventive measure for new constructions or patch repair mortars (cf. Section 6.4.2).

- Diffusion inhibitors

  Diffusion inhibitors are applied to existing reinforced concrete structures that show signs of reinforcement corrosion or need additional protection to inhibit future corrosion. Some inhibitors, e.g. sodium monofluorophosphate (Na_2PO_3F) ('MFP'), can only be used as a diffusion inhibitor due to adverse chemical reactions with fresh concrete.

Integral inhibitors and the general performance of inhibitors are dealt with in this Section, whereas the special attributes of diffusion inhibitors are briefly commented upon in Section 6.4.

The use of corrosion inhibitors is generally not specified by the national codes and standards. Besides the textbooks listed in Section 6.2, especially the broad chapters in [Böhni et al., 2005; Raupach et al., 2007], corrosion inhibitors are dealt with in extensive reports [Elsener, 2001; Thompson et al., 2000] and publications, e.g. [Hansson et al., 1998; Mammoliti et al., 1999; Trépanier et al., 2001; Gaidis, 2004].

Often the long experience with corrosion inhibitors in e.g. the oil, gas, or petroleum industry is taken as an example for the successful use of inhibitors. Also the literature on general corrosion science, e.g. [Trethewey & Chamberlain, 1995; Jones, 1996; Bardal, 2004], generally focuses on such applications, which relate to corrosion of metals in *acidic or neutral solutions* and hence mainly to uniform corrosion (cf. Section 2.3.1). In this respect, inhibitors are often classified into the following groups [Trethewey & Chamberlain, 1995; [Jones, 1996; Bardal, 2004; Trethewey & Chamberlain, 1995]:

- Anodic inhibitors (in the literature also referred to as passivators)

  Anodic inhibitors react with the ions of the corroding metal to increase its anodic polarisation, i.e. 'E_{corr}', and promote the formation of the passive layer. In principle, two types of anodic corrosion inhibitors are relevant for steel:

  - Oxidising agents (cf. Section 2.1.10), e.g. chromates, nitrites, and nitrates
  - Inhibitors that require dissolved oxygen to be effective, e.g. silicates, phosphates, molybdates, and borates.

- Cathodic inhibitors

  Cathodic inhibitors are supposed to either slow down the cathodic reaction kinetics or selectively precipitate on cathodic sites to increase the surface impedance and to limit the diffusion of reducible species to these cathodic sites.

- Adsorption inhibitors

  Adsorption inhibitors are based on long organic molecules with side chains that can limit the diffusion of oxygen to the surface, trap the metal ions on the surface, and reduce the rate of dissolution or stabilise the double layer.

Besides these three main groups, substances that retard corrosion by forming protective precipitates or by removing an aggressive constituent from the environment are also generally considered as inhibitors. However, we think that different conditions are to be considered, when inhibition of corrosion in concrete is addressed. Steel in concrete is initially passive and generally supposed to be kept in that state for several decades. As mentioned in Section 6.1, uniform corrosion as a result of carbonation can generally be regarded as marginal and the most important mechanism of corrosion inhibition should, thus, not relate to uniform corrosion phenomena, but mainly to chloride induced depassivation and pitting corrosion. Inhibitors for pitting corrosion are by far less studied and can act by [Bertolini et al., 2004]:

- Competitive surface adsorption process of inhibitor and chloride ions
- Increasing or buffering of the pH in the local (pit) environment
- Competitive migration of inhibitor and chloride ions into the pit.

Commercial inhibitors are normally blends of several compounds, and hence the inhibiting mechanisms can be multiple and difficult to identify [Bertolini et al., 2004]. Compound groups that have been used as inhibitors are primarily chromates, nitrites, phosphates, hypophosphites, alkalies, and fluorides. Moreover, new groups of organic molecules (e.g. alkanolamines and amines) have entered the market during the last years and are used as components in the complex blends that are marketed under different trade names by several producers [Bertolini et al., 2004]. Some of the blends or applied compounds have been suggested as being effective, whereas others have produced conflicting results in laboratory screening tests. Furthermore, some inhibitors, which are chemically effective in terms of corrosion protection, were observed to produce adverse effects on the physical properties of the concrete, such as a significant reduction in compressive strength [ACI 222R, 2001]. The various blends and compounds are not discussed here in detail, and reference is made to the above mentioned literature. Only calcium nitrite (commercially known as ('DCI') marketed by Grace*), which is, to our knowledge, the most extensively tested and used integral corrosion inhibitor and probably the one with the most proven success, is briefly commented upon. When applied according to the specifications and in combination with appropriate concrete and cover depths, calcium nitrite has a long and proven track record in e.g. the USA, Japan, and the Middle East [Elsener, 2001], where it is often used in parking, marine, and highway structures. However, certain disadvantages concerning calcium nitrite have also been reported. Calcium nitrite acts as a moderate set accel-

* Grace Construction Products Ltd., Cambridge, MA, USA.

erator for concrete and normally requires the additional use of water reducing and retarding admixtures. Moreover, all investigations in the literature report that calcium nitrite has to be present in sufficiently high concentration in order to be effective and that there is an increased risk of local corrosion attack in the case of insufficient inhibitor dosage.

In the literature there is a general agreement that, due to its oxidising properties, calcium nitrite acts as an anodic inhibitor leading to a stable passive layer. Yet, there are different suggestions regarding the exact mechanism. A popular description is: *"Calcium nitrite acts as a passivator due to its oxidising properties and stabilises the passive film due to its ability to oxidise ferrous ions to ferric ions, which form poorly soluble iron oxides."* [Bertolini et al., 2004]. Based on the theory on formation of (passive) anodic products (cf. Section 5.1.1) we consider such description to be doubtful from a thermodynamic perspective. Furthermore, we think that in most cases (other than carbonation induced corrosion alone) the postulated mechanism rather contributes to a high corrosion rate than inhibits corrosion, in particular for chloride induced corrosion (cf. Section 5.2.2.2). With regard to its proven track record, we obviously do not put the use of calcium nitrite into question, but suggest that other mechanisms, e.g. the formation of complex oxides between calcium nitrite and iron, result in a passive film with improved stability. A thermodynamic verification, e.g. based on the establishment of 'MEPDs' according to the methods proposed in Section 4.2.1, is principally possible. We have not performed this study, because it was marginal for the purposes of this thesis.

Nevertheless, a similar effect can be verified based on the inhibiting effect of chromates. Besides increasing 'E_{corr}' as an oxidising agent, the inhibiting effect of chromate is attributed to the formation of a tight complex oxide layer on the steel surface, which is mainly composed of hematite and chromic oxide (Cr_2O_3) and acts as an efficient passive layer preventing corrosion in certain environments [Jones, 1996; Bardal, 2004]. We think that the inhibiting effect of chromate can be conveniently represented and evaluated by means of 'SIPDs', as shown in Figure 6.4[*].

[*] The effect of chloride on chromium systems is briefly discussed in connection with thermodynamic considerations on stainless steel in Section 6.3.2.3.

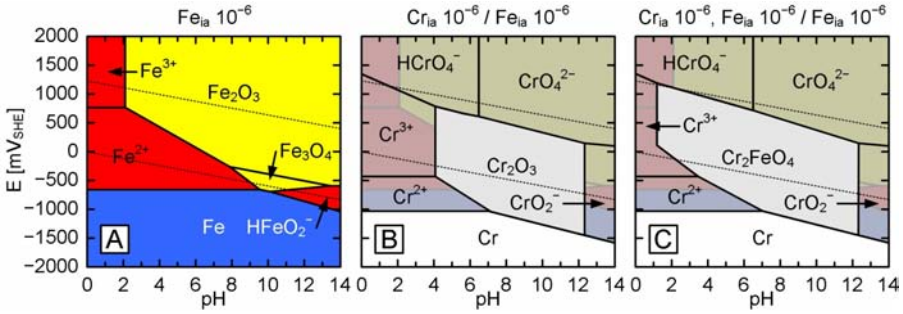

Figure 6.4: [A]: *Fe-H_2O 'SEPD' based on Table 4.2 and $Fe_{ia} = 10^{-6}$ mol/L.* [B]: *'SIPD' of the Cr-H_2O 'SEPD' based on Table 6.1 and $Cr_{ia} = 10^{-6}$ mol/L on [A].* [C]: *'SIPD' of the Cr-Fe-H_2O 'SEPD' based on Table 6.2 and $Cr_{ia} = Fe_{ia} = 10^{-6}$ mol/L on [A].*

Table 6.1: *Species preselected for the 'SEPD' of the Cr-H_2O system.*

Solid	Cr	Cr_2O_3	-	-	-
Soluble	Cr^{2+}	Cr^{3+}	CrO_2^-	CrO_4^{2-}	$HCrO4^-$

Table 6.2: *Species preselected for the 'MEPD' of the Cr-Fe-H_2O system.*

Solid	Cr	Cr_2FeO_4	Fe	Fe_3O_4	Fe_2O_3
Soluble	Cr^{2+}	Cr^{3+}	CrO_2^-	CrO_4^{2-}	Fe^{2+}
	Fe^{3+}	$HCrO4^-$	$HFeO_2^-$	-	-

Figure 6.4 [A] shows the standard Fe-H_2O 'SEPD', which corresponds to the underlying diagram for the 'SIPDs' in Figure 6.4 [B] and [C], where the Cr-H_2O 'SEPD' and the Fe-Cr-H_2O 'MEPD', respectively, are superimposed on. The species preselected for the Cr-H_2O and the Cr-Fe-H_2O system were determined based on the theoretical considerations and sources described in Section 4.2.1, which will not be discussed further, since this analysis is for exemplification purposes only.

In the 'SIPD' of the Cr-H_2O 'SEPD' superimposed on the Fe-H_2O 'SEPD' in Figure 6.4 [B] it can be observed that chrome oxide covers a critical part of the corrosion domain of iron in the stability domain of water down to a pH of around 4. Thus, it can be concluded that the addition of an appropriate amount of chromates inhibits the formation of Fe^{2+} in this decisive pH range. Even more of the corrosion domain of iron is covered, including parts of the Fe^{3+} domain down to a pH of around 2, when the formation of chromium iron oxide (Cr_2FeO_4) is taken into consideration, as shown in the 'SIPD' of the Cr-Fe-H_2O 'MEPD' superimposed on the Fe-H_2O 'SEPD' in Figure 6.4 [C]. Based on the information provided in e.g. [MinDat, 2007; MinGal, 2007; WebMin, 2007], we consider the formation of chromium iron oxide to be thermodynamically possible in most environments at moderate temperatures, such as in con-

crete. However, the conditions of formation need to be assessed, mainly concerning the required concentrations, which could e.g. be performed by means of polarisation curves (cf. Section 2.5.4). We think that in this way the function and effectiveness of many inhibitors can be assessed based on thermodynamic considerations.

Hence, we consider thermodynamic considerations based on custom-made and representative Pourbaix diagrams to be a beneficial tool concerning the evaluation of available countermeasures. With regard to the effectiveness of inhibitors for corrosion prevention, it can be concluded that, besides the uncertainty and risk concerning the correct dosage of many corrosion inhibitors (in particular, anodic inhibitors), we think that leaching and, in relation to that, outwards diffusion can impair the long-term performance of inhibitors. Apart from this, there are environmental and/or health issues related to many corrosion inhibitors, e.g. chromates and nitrites are toxic. Thus, application of calcium nitrite is not permitted for structures permanently submerged in water. Finally, with regard to the general principle of anodic inhibitors, it should be emphasised once more that, based on the thermodynamic description of active corrosion mechanisms in Section 5.2.2, raising 'E_{corr}' is an uncertain and dangerous approach in corrosion prevention, in particular with regard to chloride induced corrosion. Therefore, our approach in the design of new countermeasures is largely based on lowering the potential, i.e. cathodic polarisation, which is discussed in more detail throughout Chapter 7.

6.3.1.5 Electrochemical Concrete-Steel Interface Improvement

Electrochemical treatment of specimens during setting of the concrete has been described as an example for increasing the chloride threshold of carbon steel reinforcement in an US patent [Buenfeld et al., 2004]. This technique is included in this Chapter, although it is, to our knowledge, not applied in practice. Yet, it is an existing countermeasure and of particular relevance to the proposed new countermeasures (cf. Chapter 7).

The electrochemical treatment starts within 30 minutes after casting and consists of holding the carbon steel at −900 mV_{SCE}, i.e. −656 mV_{SHE} [RA, 2006b], for the first 18 hours. The current is then held constant at 500 mA/m^2 for the next 24 hours and finally it is reduced to 300 mA/m^2 for the next 90 hours. The results of this treatment show that the chloride threshold level is significantly increased (with a relatively small charge passed). For instance, the threshold at a void content of about 1% has increased from around 0.5% 'w/w_{ce}' to around 1.7% 'w/w_{ce}', see Figure 3.14 in Section 3.3.

So, it can be concluded that cathodic polarisation during setting of the concrete significantly improves the concrete-steel interface. While we think that impressed current cathodic polarisation during casting is not applicable in practice, in particularly for in

situ casting, we think that there are other applicable means of targeted cathodic polarisation during setting of concrete, which is discussed in Chapter 7.

6.3.2 Reinforcement Countermeasures

While the concrete countermeasures discussed in Section 6.3.1 aim at improving the concrete bulk, the following reinforcement countermeasures, which are briefly reviewed and thermodynamically evaluated in this Section, aim at improving the corrosion resistance of the reinforcement itself:

- Non-metallic reinforcement (Section 6.3.2.1)
- Organic coating of reinforcement (Section 6.3.2.2)
- Metallic reinforcement with improved corrosion resistance (Section 6.3.2.3)
- Metallic cladding of reinforcement (Section 6.3.2.4)
- Galvanised reinforcement (Section 6.3.2.5)
- Cathodic prevention (Section 6).

As for most of the concrete countermeasures, the above listed reinforcement countermeasures are standard techniques that are described to a larger or smaller extent in the textbooks listed in Section 6.2, while non-metallic reinforcement and metallic cladding are not taken into consideration by all authors. However, these approaches are included in this brief review, since non-metallic reinforcement appears to be strongly promoted for durability design by the associated industry at present and cladding relates to cost savings, which is an important issue in the construction market.

6.3.2.1 Non-Metallic Reinforcement

The term non-metallic reinforcement refers to reinforcement made of glass, aramid, or carbon fibre reinforced polymers ‘FRPs’. Besides (generally, brief) descriptions on the use of ‘FRPs’ in some of the literature mentioned in Section 6.2, ACI provides a “Guide for the Design and Construction of Concrete Reinforced with FRP Bars” [ACI 440.1R, 2003], and fib recently published “FRP reinforcement in RC structures” [fib, 2007]. Apart from strengthening of existing reinforced concrete structures, especially near-surface mounted ‘FRP’ reinforcement [DS/EN 1504-4, 2007], which also is a major research area at DTU Byg, e.g. [Rusinowski et al., 2006; Täljsten & Carolin, 2007], ‘FRP’ has, to our knowledge, not reached any practical application for concrete structures on a larger scale. Also, we consider it doubtful that ‘FRP’ reinforcement will ever replace traditional metallic reinforcement to a substantial extent. Use of non-metallic reinforcement may solve the corrosion problem, but besides compromising some of the general benefits of the concrete-steel composite system (cf. Section 1.1), ‘FRP’ reinforcement has some major practical drawbacks, which are often not acknowledged by the associated industry. For instance, ‘FRP’ cannot be adjusted on

site, most 'FRPs' are brittle and consequently sensitive to impacts from a vibrator, walking on the 'FRP' reinforcement should usually be avoided, and 'FRP' reinforcement is light and must be anchored to the formwork to avoid floating [fib, 1995a; ACI 440.1R, 2003; fib, 2007; Rostam, 2007]. Apart from these practical issues and possible structural design concerns related to the missing ductility, another major drawback of 'FRP' is the doubtful performance with regard to fire. So, we do not consider 'FRPs' as a practical alternative to traditional embedded reinforcement. However, besides the mentioned possibilities in strengthening, there might be potential within the precasting industry as well as for certain special applications where the concrete construction cannot tolerate the use of steel. For instance, magnetic resonance imaging ('MRI') requires non-magnetic structures or toll booths reading radio tags often require reinforced concrete that is transparent to radio [Wikimedia, 2007].

Application of thermodynamics pertaining to 'FRP' does not to relate to aqueous metallic corrosion* and thus beyond the scope of this thesis.

6.3.2.2 Organic Coating of Reinforcing Steel

Based on Sections 2.1 and 3, it can be concluded that *any coating that safely prevents oxygen, humidity, and aggressive ions from reaching the carbon steel surface, i.e. inhibits the electrochemical basis for the corrosion process entirely, prevents corrosion.* Thus, a potential method in protecting carbon steel in concrete is to establish an insulating barrier coating, which prevents contact of the steel with its environment. In practice, coatings that aim at that task are fusion-bonded epoxy (henceforth, epoxy) and polychloroethene (IUPAC terminology), better known as polyvinyl chloride ('PVC'), as the main thermoplastic polymer. To our knowledge, ('PVC') has been applied only marginally for reinforcement steel coatings. Epoxy has been used extensively in North America, but not as much in Europe, since it has been introduced as a new protective measure against chloride induced corrosion in the USA in the mid 1970s [fib, 1995a; Rostam, 2003; Bertolini et al., 2004; Rostam, 2007]. Thus, focus in this Section is set on epoxy-coatings.

CEN standards for epoxy-coated reinforcement steel have not been published, but ISO† provides the associated standard [ISO 14654, 2007] and ASTM publishes metric standard specification for epoxy-coated steel rebars [ASTM A775M, 2007] as well as for epoxy-coated prefabricated steel rebars [ASTM A934M, 2007].

We agree that an epoxy-coating prevents corrosion, if manufactured properly and *absolutely no damage* is introduced to the coating during placing and service. It appears to be difficult, however, to provide for entirely dense epoxy-coatings in the manufac-

* As opposed to electrically conductive polymers ('ECPs') [Rupprecht, 1999], which have been investigated as possible compounds (especially polyanilin [OMC, 2007]) for corrosion countermeasures in this project, but rejected at an early stage.

† International Organisation for Standardisation (ISO), Geneva, Switzerland.

turing process, i.e. total prevention of pinholes on a large scale, as well as to fix the coated reinforcement in place without disturbing the coating. Thus, from the early 1990s reports began to emerge indicating that chloride induced corrosion, mainly in form of crevice corrosion (cf. Section 2.3.4), developed from local pinholes and damaged the coating without necessarily causing cracking and spalling of concrete cover, but slowly disintegrating the reinforcement [Rostam, 2003; Rostam, 2007], i.e. a mechanism and damage type similar to the one described in Section 5.2.2.2. A popular case of premature deterioration related to epoxy-coated reinforcement was established by the Florida Keys Bridges, FL, USA. In 1986, only eight years after construction, the Department of Transportation observed serious cases of corrosion damage at the substructures of several bridges, which were reinforced with epoxy-coated reinforcement, see Figure 6.5. Besides the subtropical temperatures (cf. Section 3.1.10), these bridge components were continuously subjected to salt spray in the splash zone, combined with wetting and drying cycles, which produced a very corrosive environment (cf. Sections 3.1.7 and 3.1.8).

Figure 6.5: *Spalling at pier of Florida Keys Bridges, FL, USA, due to corrosion of the epoxy-coated reinforcement. From [COWI, 2007c].*

This event caused a major disturbance in North America seemingly due to pure commercial and biased reactions from the producers of epoxy-coated reinforcement and their organisations, while, at that time, the technology was slowly spreading to Europe, the Middle East, and to some parts of the Far East [Rostam, 2003; Rostam, 2007].

The first major application of epoxy-coated reinforcement in Europe was the reinforcement of the precast concrete segments for the East Tunnel of the Great Belt Link in Denmark, which was designed in 1988. Already then, the traditional technology of epoxy-coating was questioned in Denmark [Rostam, 1996; Rostam, 2007], particularly with regard to electrical insulation of the single bars from each other, which prevents the use of cathodic prevention/protection (cf. Sections 6.3.2.6/6.4.1). Apart from that, the large number of pinholes allowed by the original specifications for epoxy-coating (i.e. earlier versions of [ISO 14654, 2007] and [ASTM A775M, 2007]) was of concern as well as the need for patch repairs of all cut ends and cracks formed at

sharply bent coated bars. Hence, it was decided to apply the epoxy-coating by a fluidised bed dipping technique for 3D full-size welded reinforcement cages, while special cleaning, heating, coating and testing techniques were incorporated to minimise pinholes. In this way, 60,000 out of 62,000 segments came out without any pinholes, as determined by the wet sponge method [Rostam, 1996; Storebælt, 1997]. Hence, this technique is considered to be reliable [Rostam, 1996; Storebælt, 1997] and so far no problems have been reported from the Great Belt Link. Still, the North American experience based on the traditional technology of epoxy-coating as well as experimental studies and site investigations with unsatisfactory results, have led to epoxy-coating not gaining a strong foothold in Europe, and it is now also slowly being phased out e.g. the Middle East and the Gulf Countries [Rostam, 2007].

We agree to the described notions concerning epoxy, which principally apply to *all organic reinforcement coatings that are not affected by the concrete chemistry*. This solution provides complete corrosion protection, if it is assured that the epoxy-coating is absolutely free of damages, when the structure goes into service. However, this appears to be a difficult task, in particular when considering the general practices during construction. In general terms it can be stated that we consider the *single safety mechanism* provided by barrier coatings to be a risk, when the probability for failure is high. Because of this we decided to base the proposed new countermeasure on a combination of corrosion preventive measures. Nevertheless, barrier coatings can provide benefits for cathodic prevention/protection (cf. Sections 6.3.2.6/6.4.1).

Based on the original aim of inhibiting the electrochemical basis of corrosion processes, thermodynamics in terms of aqueous metallic corrosion does not concern organic coatings.

6.3.2.3 Metallic Reinforcement with Improved Corrosion Resistance

Metallic reinforcement with improved corrosion resistance is one alternative to inhibiting the electrochemistry of the corrosion processes on a carbon steel surface (cf. Section 6.3.2.2). It has progressed into the durability design market during the past years. When referring to metallic reinforcement with improved corrosion resistance, stainless steel dominates durability design, but recently other steel qualities, which are claimed to provide significantly improved corrosion resistance entered the market. In Section 6.3.2.3.1 the theory and background of the corrosion resistance of stainless steel is briefly reviewed and thermodynamically evaluated. Results from own investigations concerning the metallurgy and surface conditions of as-received stainless steel rebar are summarised in Section 6.3.2.3.2.

6.3.2.3.1 Theory

CEN specifications for stainless steel qualities are given in [DS/EN 10088-1, 2005], while ASTM provides particular specifications for stainless steel reinforcement

[ASTM A955M, 2007]. Besides these standards and the generally detailed chapters on stainless steel reinforcement in the literature listed in Section 6.2, a comprehensive state-of-the-art report on stainless steel in concrete was published by [Nürnberger, 1996] and extended by the same author to the largely discussed field of the performance in cracked concrete [Nürnberger & Beul, 1999]. In addition to that, several other reports and guidelines on the use of stainless steel reinforcement were published, e.g. [CS, 1998; Markeset et al., 2006].

In principle, the improved corrosion resistance of stainless steels is based on alloying chromium ($\geq 13\%$) to iron, which results in the formation of a differently structured, much tougher passive layer with excellent repassivation characteristics (cf. Section 2.1.9). Furthermore, improved resistance against a specific form of attack or certain mechanical properties can be achieved by alloying additional elements, such as nickel, molybdenum, manganese, silicon, nitrogen, carbon, phosphorus, and sulphur [Davis, 1998].* Compared to the production of carbon steel (cf. Section 3.2.1), the production process of stainless steel, which is principally based on a sophisticated process of melting and remelting [Callister & Callister, 2000], is much more complex. In combination with the more expensive raw materials, this leads to a significantly higher price for stainless steel compared to carbon steel. Nowadays, stainless steel reinforcement is commercially available in dimensions, strengths, and alloy types, which are fully compatible with the general structural requirements for reinforced concrete structures. Yet, few stainless steel grades are used for reinforcing steel, because availability and price are an issue and generally widely available types, such as 1.4436 / 316, are used.

There is a general agreement in the literature that all types of stainless steel remain passive in carbonated concrete (cf. Section 5.2.2.1), and the use of stainless steel rebars is normally associated with chloride exposure (cf. Section 5.2.2.2). Since the late 1970s, various experimental studies have been carried out in order to investigate the corrosion behaviour of stainless steel in chloride contaminated concrete. Pitting corrosion (cf. Section 2.3.2) is considered to be the dominant form of corrosion for stainless steel in chloride contaminated concrete. Intergranular corrosion (cf. Section 2.3.5) can result from welding, but it can normally be avoided by using suitable types of steel as well as an appropriate post-treatment. Scale and temper colours aggravate corrosion if not removed by pickling or grit-blasting.† Besides inhomogeneities introduced by welding, presence of mill scale or other impurities on the surface steel surface (cf. Section 6.3.2.3.2) is considered to interfere with the formation of an ideal

* The required, specified, and investigated composition of reinforcement steel of stainless steel grade 1.4436 / 316 [DS/EN 10088-1, 2005] / [ASTM DS561, 2004] is shown in Table 6.3 at the end of this Section.

† We consider pickling to be superior to grit-blasting with regard to corrosion resistance. Although not directly related to concrete reinforcement, a case in point are the corrosion problems on the grit-blasted stainless façade elements of the new opera in Copenhagen, Denmark. This illustrates that grit-blasting should not be the favoured technique for removing scale from a stainless steel surface.

passive layer and hence to affect the corrosion resistance. [Nürnberger, 1996; Cutler et al., 1997; Nürnberger & Beul, 1999; Rostam, 2003; Bertolini et al., 2004; Chowdhury, 2004; Clemeña & Virmani, 2004].

Doubts have been raised concerning the corrosion resistance of stainless steels in cracked concrete, since cracks carbonate rapidly and can act as high-velocity penetration paths for chloride ions (cf. Section 3.1.11.2). However, according to [Nürnberger & Beul, 1999], stainless steel reinforcement is generally suitable for the unfavourable case of highly chloride contaminated cracked concrete.

A prominent documentation of the performance of stainless steel reinforcement in highly chloride contaminated concrete is the concrete pier into the Mexican Gulf at Progreso, Mexico, which was opened in 1941, see Figure 6.6 [A].

Figure 6.6: *Concrete piers into the Mexican Gulf at Progreso, Mexico. From [Rambøll, 1999]*. [A]: *Perished carbon steel reinforced pier (opened in 1969) in the foreground and existing stainless steel reinforced pier (opened in 1941) in the background.* [B]: *Close up of remains of the deck of the carbon steel reinforced pier.*

Because of the severe environmental exposure of the pier and use of concrete with a relatively high porosity (due to the use of local limestone aggregate), it was decided to use stainless steel reinforcement in selected areas of the pier. Despite the harsh environment and the poor quality materials used in the construction, no considerable corrosion damage was observed at the stainless steel reinforced pier. A newer parallel pier, which was opened in 1969, was reinforced with carbon steel and perished years ago due to deterioration induced by reinforcement corrosion (see Figure 6.6 [A]) and the close-up of deteriorated remains of the deck of the pier in Figure 6.6 [B]). [Rambøll, 1999; Rostam, 2003; Rostam, 2007].

So, stainless steel reinforcement appears to grant effective corrosion protection even in harsh environments. However, the high price of stainless steel cannot always be justified. To cut costs efforts have been made to, among others, use e.g. cheaper stainless steel grades, but the performance was generally observed to decrease more than the cost. Therefore, even among the austenitic grades, where grade 1.4301 / 304 is the norm, in most projects it is considered to be cost-efficient to specify premium

grades as 1.4436 / 316 [Chowdhury, 2004]. Another recent approach has been selective use of stainless steel, i.e. application of stainless steels only in the most critical zones, while carbon steel is used for the remaining parts of the structure. Stainless steel reinforcement can be combined and *electrically connected* with carbon steel cast into concrete without risks of galvanic corrosion (cf. Section 2.3.3), because the two types of steels are nearly at the same corrosion potential when embedded in concrete [Klinghoffer, 1999; Rostam, 2003; Rostam, 2007]. This central aspect was confirmed in our investigations [Küter et al., 2005b], as illustrated in Figure 6.8 [B]. As mentioned, other approaches in the effort to develop reinforcing steel with an improved corrosion resistance included e.g. microcomposite steels ('MMFX') and tungsten doped steels [Chowdhury, 2004]. Some of these developments might be promising, but there appears to be a lack of affirmative studies and doubts with regard to the actual savings compared to stainless steel.

We think that stainless steel will further dominate the market in terms of corrosion protection achieved by improved corrosion resistance. However, the initial costs of specifying stainless steel are significantly higher than other types of corrosion protection (cf. Section 6.3.3), which makes specification difficult unless the environment is deemed to be highly corrosive. For instance, for structures subjected to carbonation only, we think that, in addition to proper design of the concrete mix and the concrete cover (cf. Section 6.1), corrosion protection can be achieved by using less expensive available countermeasures, e.g. galvanised steel (cf. Section 6.3.2.5). In severe chloride environments, stainless steel can be an attractive option based on life cycle costing (cf. Section 6.1); in particular, when selective use of stainless steel is specified. Moreover, we consider stainless steel reinforcement as an attractive option from a practical point of view, because the common construction practice remains unchanged, and the material itself is not sensitive to the design, handling, and execution, in contrast to all concrete countermeasures, 'FRPs', or organic coating of reinforcement. Moreover, with regard to design and execution, we consider the possibility for reducing the cover depth based on stainless steel reinforcement to be of great practical benefit (cf. Section 6.1).

While thermodynamic considerations based on Pourbaix diagrams and reaction mechanism are limited for high-alloyed metals (i.e. for stainless steel), we think that certain thermodynamic characteristics can nonetheless be indicated in and explained by Pourbaix diagrams; in particular, with regard to the passivation of the associated alloys and hence passivation of stainless steel in given environments. An example is presented in Figure 6.7 and Figure 6.8, which show 'MEPDs' of the principal alloys of grade 1.4436 / 316 stainless steel (cf. Section 6.3.2.3.2) and the superimposition of the stability domains of selected alloy oxides on the Fe-Cl-H_2O 'MEPD', respectively. Details for the species preselected for the establishment of the 'MEPDs' in Figure 6.7 are not described, and reference is made to the methodology described in Section 4.2.1.

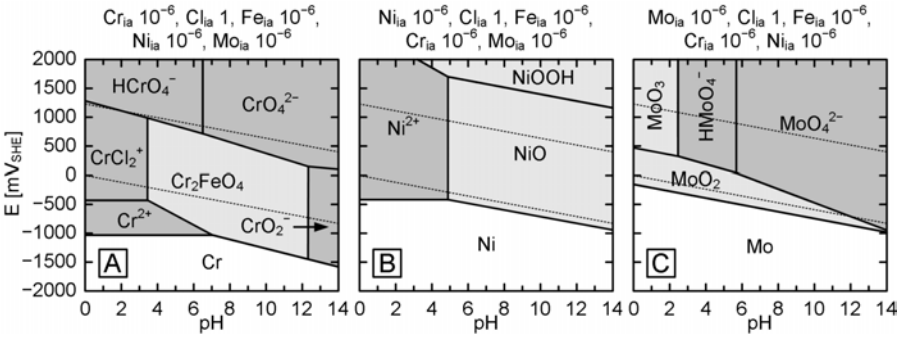

Figure 6.7: *'MEPDs' for principal alloys of grade 1.4436 / 316 [DS/EN 10088-1, 2005] / [ASTM DS561, 2004] stainless steel in the Cl-H_2O system. The ion activities of all included metals correspond to 10^{-6} mol/L and Cl_{ia} = 1 mol/L.* [A]: *Cr-Cl-Fe-Ni-Mo 'MEPD'.* [B]: *Ni-Cl-Fe-Cr-Mo 'MEPD'.* [C]: *Mo-Cl-Fe-Cr-Ni 'MEPD'.*

Figure 6.7 [A] represents the 'MEPD' of the Cr-Cl-Fe-Ni-Mo system. This diagram can be compared to the 'MEPD' of the Cr-Fe-H_2O system (cf. Figure 6.4 [C] in Section 6.3.1.4), because no compounds involving nickel and molybdenum are formed in the Cr-Cl-Fe-Ni-Mo system, when chromium is selected as the main element. The comparison shows that passivation of iron (or stainless steel) by Cr_2FeO_4 can only be maintained down to a pH of about 4, if 35 g/L of chloride are dissolved in the pore solution, compared to a pH of around 2 for chloride free concrete. In Figure 6.8 [B] the stability domain of Cr_2FeO_4 as well as the stability domains of the passivating oxides in the Ni-Cl-Fe-Cr-Mo system (Figure 6.7 [B]) and the Mo-Cl-Fe-Cr-Ni system (Figure 6.7 [C]) are superimposed on the 'MEPD' of the Fe-Cl- H_2O system.

In Figure 6.8 [B] it can be observed that even though critical regions of Fe^{2+} and $FeCl^{2+}$ are covered by passivating oxides, stainless steel has a thermodynamic tendency to corrode in a chloride environment, but the critical pH is moved away from neutrality towards a pH around 4. This aspect underlines the ideal resistance of stainless steel to carbonation induced corrosion; on the other hand, we also regard it as playing a major role in the propagation stage of chloride induced reinforcement corrosion, since the thermodynamic conditions at a around neutrality are decisive (cf. Section 5.2.2.2). However, in correspondence with chloride induced corrosion of carbon steel reinforcement, the initiation stage is not reflected, given that the involved pitting potential is considered to be a kinetic parameter (cf. Section 2.3.2). With regard to pitting corrosion, it is noteworthy that the 'SIPD' indicates the resistance of stainless steel to corrosion in oxidising acid environments, which is generally regarded to be improved by alloying molybdenum, e.g. [Davis, 1998; Møller, 2003b].

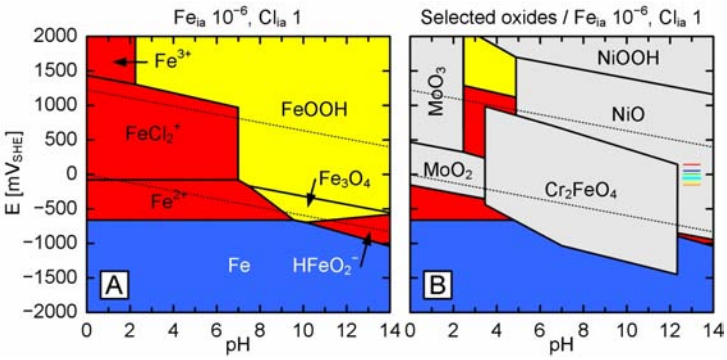

Figure 6.8: [A]: *Fe-Cl-H_2O 'MEPD' based on Table 5.4 and Fe_{ia} = 10^{-6} mol/L and Cl_{ia} = 1 mol/L.* [B]: *'SIPD' of stability domains of selected stainless steel alloy oxides from Figure 6.7 on [A]. Own corrosion potential measurements from 'Test I' of passive stainless steel embedded in mortar ("C-7A", cf. Section 1.9.3) are indicated by the thick turquoise bar and put into context with the corrosion potentials measured for passive carbon steel with different surface properties illustrated by the thin coloured lines (cf. Figure 5.4 [A] in Section 5.2.1). It should be noted that the underlying areas of the Fe-Cl-H_2O 'MEPD' are not shaded as only the passive domains are superimposed.*

Finally, Figure 6.8 [B] also exemplifies own 'E_{corr}' measurements from 'Test I' of passive stainless steel embedded in mortar. A comparison to the corrosion potentials measured for passive carbon steel with different surface properties (cf. Figure 5.4 [A] in Section 5.2.1) illustrates the thermodynamic compatibility, which is of major importance with regard to selective use of stainless steel including electrical connection to carbon steel reinforcement [Klinghoffer, 1999; Rostam, 2003; Rostam, 2007].

6.3.2.3.2 Experimental Investigations on Metallurgical Properties

In correspondence with the metallurgical investigations on carbon steel (cf. Section 3.2.2.2), the metallurgical properties of grade 1.4436 / 316 [DS/EN 10088-1, 2005] / [ASTM DS561, 2004] ribbed stainless steel rebar with a specified Cr-Ni-Mo content of 16.9-10.5-2.5 [LMG, 2004b] were investigated by 'LOM', 'SEM', and 'EDS'. Selected results are summarised after a short note on the sample preparation and measurement techniques.

- Sample preparation and measurement techniques

  The metallographic sample containing cross and longitudinal sections of as-received stainless steel rebar with a diameter of 8 mm was prepared by means of a suitable grinding and polishing sequence according to [Bjerregaard et al., 2000]. 'LOM' was performed on the specimen before and after electrochemically etching with 10% oxalic acid, as described in [Weidmann et al., 2005]. In addition to

'LOM', the metallurgical properties of the specimen have been investigated by 'SEM' and 'EDS' according to [ASTM E2142, 2001] and [ASTM E1508, 2003], respectively. Before 'SEM' and 'EDS' analyses a conducting thin film of carbon was applied on the surface of the metallographic specimen.

- Light Optical Microscopy

  In contrast to the investigated carbon steel sample (cf. Section 3.2.2.2), 'LOM' on the unetched stainless steel sample showed clear surfaces and accordingly no indications for inclusions, which was confirmed by the 'LOM' of the etched cross sections, see Figure 6.9.

Figure 6.9: *Light optical microscopy of unetched cross section of stainless steel sample.* [A]: *Middle.* [B]: *Edge of "bulk".* [C]: *Edge of rib.*

All photographs present the expected slightly deformed austenitic grain structure. The horizontal lines in Figure 6.9 [A] are a result of the sample preparation, probably remains from the grinding and polishing process. Figure 6.9 [B] shows an evenly deformed surface at the edge of the bulk of the stainless bar, whereas an uneven surface deformation from rolling is exhibited at the edge of a rib in Figure 6.9 [C]

- Scanning Electron Microscopy

  Figure 6.10 is a photograph from the secondary electron 'SEM' analysis on the edge of the etched longitudinal section of the stainless rebar. Surface defects resulting from over-rolling of the section are visible. We consider such microcracks to be crucial for corrosion initiation, and they are, therefore, considered to represent a weak spot of the stainless bar surface.

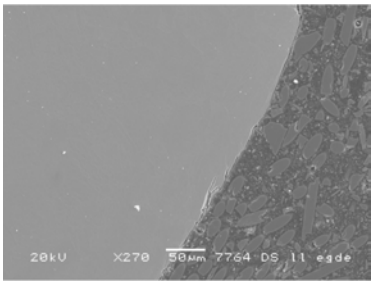

Figure 6.10: *Secondary electron scanning electron microscopy of the edge of the etched longitudinal section of the stainless rebar.*

- Energy Dispersive X-Ray Spectroscopy

  Required, specified [LMG, 2004b], and averaged measured quantities for the investigated stainless steel sample are summarised in Table 6.3. The measured values are taken from the average of the 'EDS' spectra from the middle and close to the edge of the longitudinal section.

  Table 6.3: *Required, specified [LMG, 2004b], and averaged measured composition of investigated stainless steel sample. ('LL'): Longitudinal section.*

Element	Required [LMG, 2004b]	Specified [LMG, 2004b]	Averaged measured ('LL'), middle	Averaged measured ('LL'), edge
	[%]	[%]	[%]	[%]
Iron	-	-	66.575	65.990
Chromium	16.500-18.500	16.940	17.510	17.475
Nickel	10.500-13.000	10.500	10.455	11.200
Molybdenum	2.500-3.000	2.540	2.915	2.875
Manganese	≤ 2.000	1.070	2.050	2.210
Silicon	≤ 1.000	0.400	0.480	0.500
Nitrogen	≤ 0.110	0.031	-	-
Carbon	≤ 0.050	0.043	-	-
Phosphorus	≤ 0.045	0.029	-	-
Sulphur	≤ 0.030	0.002	-	-

6.3.2.4 Metallic Cladding of Reinforcement

Another approach in improving the corrosion resistance of reinforcement is to clad carbon steel rebars with stainless steel or other metals and alloys with improved corrosion resistance. Based on the electrochemical compatibility (cf. Section 6.3.2.3), we consider stainless steel cladding as a feasible solution, but experience shows that reductions in costs have not been sufficient to make cladding an attractive option [Chowdhury, 2004]. However, a new spray coating process for manufacture of stainless steel cladding seems to provide for savings in that respect [Chesney, 2003]. Other cladding materials have been proposed and investigated in the past, but, to our knowledge, never entered the durability design market on a considerable scale. For instance, nickel and copper, which are known to provide corrosion resistance under chloride exposure, have been proposed as cladding materials, e.g. [Tripler et al., 1966; Baker, 1977] and [McDonald et al., 1996], respectively. In the related studies both nickel and copper cladded rebars showed significantly improved corrosion resistance in chloride contaminated concrete [Tripler et al., 1966; Baker, 1977; McDonald et al., 1996]. However, besides that the actual savings achieved with these techniques (especially with nickel cladding) are uncertain and that copper is known to retard cement hydration, we think that these techniques have major practical and thermodynamic

disadvantages. As it illustrated in 'SIPDs' of the Ni-Cl-H_2O 'MEPD' in Figure 6.11 [A] and the Cu-Cl-H_2O 'MEPD' in Figure 6.11 [B], which are both superimposed on the Fe-Cl-H_2O system, both nickel and copper provide improved corrosion resistance in the chloride environment compared to carbon steel*.

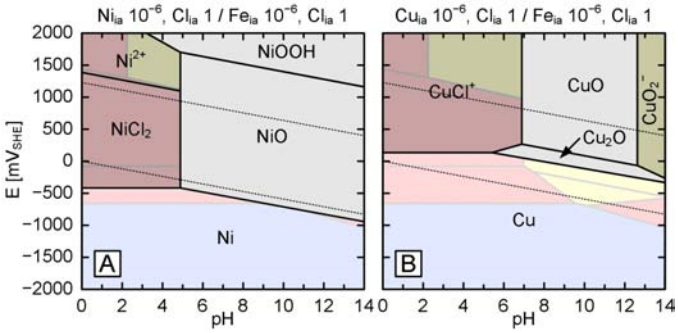

Figure 6.11: [A]: *'SIPD' of Ni-Cl-H_2O 'MEPD' with $Ni_{ia} = 10^{-6}$ mol/L and Cl_{ia} = 1 mol/L on Fe-Cl-H_2O 'MEPD' with $Fe_{ia} = 10^{-6}$ mol/L and Cl_{ia} = 1 mol/L.* [B]: *'SIPD' of Cu-Cl-H_2O 'MEPD' with $Cu_{ia} = 10^{-6}$ mol/L and Cl_{ia} = 1 mol/L on Fe-Cl-H_2O 'MEPD' with $Fe_{ia} = 10^{-6}$ mol/L and Cl_{ia} = 1 mol/L.*

However, any defect in the cladding, where carbon steel is exposed to the electrolyte, leads to increased corrosion of the carbon steel, because the 'E_{corr}' established between the nobler cladding and the steel leads to anodic polarisation of the carbon steel (cf. Section 2.1.5), which can be particularly dangerous with regard to chloride induced corrosion. From Figure 6.11 it can be concluded that the corrosion rate at defects in nickel cladding might not be considerably increased, but we consider corrosion in defects of copper cladding to be drastically accelerated. Thus, from a practical point of view, the same restrictions apply for reinforcement cladded with nickel and copper as discussed for epoxy-coated reinforcement (cf. Section 6.3.2.2), i.e. nickel and copper cladded bars cannot be adjusted on site. Yet, we assume that avoidance of initial defects is feasible for metallic cladding and that cladding provides more robustness with regard to the general construction practices. On the other hand, cladding of premanufactured reinforcement meshes or baskets, i.e. 2D or 3D cladding (cf. Section 6.3.2.2), might be feasible, but definitely not cost-efficient.

* Although these 'SIPDs' do account for all galvanic effects between the metals in the two investigated system, we consider this representation to be far more comprehensive and meaningful for conclusions regarding the thermodynamic conditions of a system than the 'EMF' series or the galvanic series.

6.3.2.5 Galvanised Reinforcement

The theoretical background of galvanised reinforcement is summarised in this Section and extended with regard to the thermodynamic characteristics of zinc in concrete in Section 7.3.1, since zinc is a central compound in the proposed new countermeasures.

The performance of galvanised steel under atmospheric conditions is well understood, and it is in extensively used for manifold applications. The extensive use of zinc is due to its twofold nature as a coating: Firstly, as a barrier coating, galvanising provides a tough, metallurgically bonded coating (in contrast to e.g. epoxy-coating, cf. Section 6.3.2.2). Secondly, the sacrificial action of zinc protects the steel even where damage or minor discontinuity occurs in the coating (in contrast to e.g. nickel and copper cladding, cf. Section 6.3.2.4), while the consumption rate of the zinc itself is relatively low (cf. exchange current density of zinc in Section 2.2.2). Similar to epoxy-coated reinforcement, galvanised, i.e. zinc coated, reinforcement is not standardised by CEN, but by ISO [ISO 14657, 2005] and ASTM [ASTM A767M, 2005]. In addition to the generally broad chapters in the textbooks listed in Section 6.2, a number of other comprehensive publications concerning galvanised steel are available, e.g. [fib, 1995a; Fratesi, 2002a; Yeomans, 2004].

Galvanised rebars have been introduced in the US about fifty years ago, where about 2% of the reinforcement is galvanised nowadays; the estimate for Europe is about 1% [Fratesi, 2002b]. In contrast to the electroplating process, which was applied for galvanisation in the experimental part of this project (cf. Sections 1.9 and 2.6.2), reinforcement is generally hot-dip galvanised in practice. In principle, the hot-dip galvanisation process consists of three steps: surface preparation, galvanising, and inspection. The surface preparation is often based on similar processes as described in Section 2.6.1, but can also be accomplished by mechanical cleaning in combination with chemical processes. After the preparation the carbon steel reinforcement is immersed in a bath of molten zinc. Typically, the zinc bath is at temperatures above 430°C and consists of 98% pure zinc [AGA, 2005; AGA, 2007]. This process produces a metallic coating composed of various layers of iron-zinc alloys. An external layer of pure zinc, left by the simple solidification of the liquid metal, is formed on top of a sequence of inner layers, which are increasingly rich in iron. The thickness of the iron-zinc layers depends on the composition of the steel, the temperature and composition of the zinc bath, and the immersion time. Moreover, the silicon content of the carbon steel has a significant effect on the reactivity between steel and zinc and thus on the thickness of these brittle layers. According to [Fratesi, 2002b], the reactivity between steel and zinc is high for silicon contents between 0.03% and 0.14% or above 0.25%. As production of carbon steel reinforcement is generally based on recycling of scrap-iron (cf. Section 3.2.1), it is practically impossible to find rebars with a silicon content less than 0.03%, so that the best choice with respect to the chemical analysis are silicon contents between 0.16% and 0.20%. For instance, the investigated carbon rebar with a Si content > 0.30% exceeds this requirement for hot-dip galvanisation.

Passivation of the external layer of pure zinc is generally considered to be the primary mechanism with regard to the corrosion resistance of galvanised reinforcement. In contact with alkaline solutions (with a pH below 13) zinc passivates with the formation of a layer of calcium hydroxyzincate. *A loss of 5-10 µm of the pure zinc layer is required prior to passivation* [Bertolini et al., 2004]. According to [Yeomans, 2004], passivity based on formation of calcium hydroxyzincate is maintained in a pH range between 8 and 12.5. As mentioned in Section 2.1.9, the passive layer on zinc does not only reduce the rate of the anodic process, but also largely impedes the cathodic reactions, i.e. oxygen and hydrogen ion reduction, which we consider to apply for passivation by calcium hydroxyzincate as well. *Due to the impeded cathodic reactions, the 'E_{corr}' of galvanised steel in concrete is much lower than the of carbon steel* (cf. Section 5.1.2). Typical values for 'E_{corr}' of galvanised steel in concrete given in the literature are mostly in the order of −500 to −300 mV_{SHE}, whereas own investigations showed even lower potentials in the order of −700 mV_{SHE} for zinc in oxygen-deprived concrete [Küter et al., 2005b].

At an early age, the bond strength of galvanised rebars is known to be lower than the one of carbon steel rebars, which is generally attributed to hydrogen evolution as well as to the dissolution of zinc from the superficial layer that delays the hydration of the cement paste at the concrete-steel interface (cf. the influence of copper in Section 6.3.2.4). However, after a few weeks the galvanised steel adheres well and its increased roughness even improves adhesion to the concrete. Improved bond is furthermore obtained due to the formation of calcium hydroxyzincate crystals that fill the interfacial porosity of the cement paste and act as bridges between the zinc coating and the concrete [Fratesi, 2002a]. In practice, however, the bond strength for ribbed galvanised rebar and ribbed carbon steel, e.g. tested according to [ASTM A944, 2005], are essentially identical, because it is mainly provided by the mechanical interlocking between the ribs and the concrete (cf. Section 3.2.1).

Galvanised bars are often chromate treated in order to inhibit zinc corrosion and to control hydrogen evolution (cf. the thermodynamic effect of chromates in Section 6.3.1.4). Hydrogen evolution is considered possible on galvanised bars, first of all during pickling before galvanisation, then in the first hours after casting and finally in hardened concrete in conditions of lack of oxygen. For this reason galvanising is not recommended as a protective measure for steel susceptible to hydrogen embrittlement, i.e. high-strength steels as often used for e.g. prestressing or post-tensioning. Galvanised steel is weldable, but loss of the zinc coating generally takes place in the welded zone. In such cases as well as for larger defects the application of a zinc-rich paint is recommended.

With regard to corrosion resistance, the performance of zinc steel in concrete is quite different from the performance of hot-dip galvanised steel in atmospheric conditions. There is a general agreement in the literature that the passive film of galvanised rebars is stable in mildly acidic environments, so that the zinc coating remains passive even

when the concrete is carbonated. The corrosion rate of galvanised steel in carbonated concrete has been estimated to 0.5-0.8 μm/y [Davis, 1998; Bertolini et al., 2004]. The corrosion rate in carbonated concrete remains negligible, even if a lower content of chloride is present. In chloride contaminated concrete, however, galvanised steel is generally considered to be affected by pitting corrosion. In most of the mentioned literature, a chloride threshold level in the range of 1-1.5% 'w/w_{ce}' is assumed for galvanised steel compared to 0.4-1% 'w/w_{ce}', which is normally considered for carbon-steel reinforcement (cf. Section 3.1.9). Other literature suggests that galvanised reinforcement resists at least 2.5 times higher chloride contents in concrete than carbon steel and that galvanisation delays the time of corrosion initiation of the underlying steel by 4-5 times, e.g. [Yeomans, 2004].

The improved resistance to chloride attack is considered to be mainly due to the lower 'E_{corr}'. Even if pitting corrosion has initiated, the corrosion rate tends to be lower for galvanised steel, because zinc acts as a poor cathode. Galvanisation reduces the effectiveness of the autocatalytic mechanism that takes place inside a corrosion pit (cf. Section 5.2.2.2) in combination with macrocell formation (cf. Section 3.1.8). Yet, it should be emphasised that a passive zinc coating does not provide *active* protection to steel as under atmospheric conditions. Therefore, cracks in the zinc coating must be avoided and repair of macroscopic defects before casting is crucial.

Considerable work has been done to identify the nature of zinc corrosion products and the effect of these on the integrity of the concrete. While the major part of the literature reports that zinc corrosion products do not interfere with the integrity of concrete, some studies present contradictory results. For instance, in [Popov, 2007] it has been postulated that zinc hydroxychloride, which occupies more than 3.5 times the volume of zinc, is the principal corrosion product of galvanised steel in chloride contaminated concrete. Consequently, it has been concluded that galvanised coatings in high chloride environments could be detrimental to the health of the structure. However, in all above mentioned sources, as well as in e.g. [Zhang, 1996; Tomlinson & Marsh, 1988; Fratesi, 2002a], zinc corrosion products are described as loose rather than bulky and as migrating away from the concrete-steel interface into the adjacent concrete bulk where they fill voids and microcracks. In contrast to iron corrosion products formed with availability of oxygen, which are relatively voluminous (cf. Table 5.2 in 5.2.2.1) and precipitate at the steel-concrete interface causing tensile stresses, these products are generally considered to cause very little disruption to the surrounding concrete bulk.

Based on the above, it can be concluded that galvanisation provides good resistance to carbonation induced corrosion, while resistance to chloride induced corrosion is improved with regard to both the initiation and the propagation stage, but still insufficient with regard to long-term durability. However, this and other critical aspects of zinc, e.g. with regard to sacrificial protection in concrete, seems not to be acknowl-

edged by the associated industry, e.g. IZA* [IZA, 2007] as well AGA† [AGA, 2005; AGA, 2007] postulate with regard to the performance of galvanised steel in concrete:

- *"... Zinc's sacrificial action offers protection where small areas of steel are exposed, such as cut edges, drill-holes, scratches, or as the result of severe surface abrasion. Cathodic protection of the steel from corrosion continues until all the zinc in the immediate area is consumed."*
- *"... Galvanised reinforcing steel can withstand exposure to chloride ion concentrations several times higher (at least 4 to 5 times) than the chloride level that causes corrosion in carbon steel reinforcement."*
- *"During curing, the galvanised surface of steel reinforcement reacts with the alkaline cement paste to form stable, insoluble zinc salts accompanied by hydrogen evolution. ... Laboratory studies indicate that this liberated hydrogen does not permeate the galvanised coating to the underlying steel and the reaction ceases as soon as the concrete hardens."*
- *"... If the cement and aggregate contain less chromate than will yield at least 100 ppm in the final concrete mix, the galvanised bars can be dipped in a chromate solution or chromates can be added to the water when the concrete is mixed."*

A comparison of these statements with the information provided in the above illustrates the common discrepancies between the point of views of industries with a marketing interest and the research community.

6.3.2.6 Cathodic Prevention

The name cathodic prevention 'CPre' was coined in [Pedeferri, 1992] to differentiate this technique from cathodic protection 'CP', which is generally considered as a countermeasure for existing structures (cf. Section 6.4.1). 'CPre', which was first used in Italy in 1989, is applied to new structures that are expected to be contaminated by chlorides. The reinforcement is cathodically polarised with the aim of increasing the chloride threshold, so that the desired service life can be attained. With regard to the pitting potential curves shown in Figure 5.10 in Section 5.2.2.2, this can be understood as maintaining the corrosion potential, so that 'E_{pit}' associated with a given maximum chloride content is not reached. Generally, current densities from 1-2 mA/m^2 are applied for cathodic prevention [Bertolini et al., 2004].

A short note on other beneficial and side effects of 'CPre', in particular with regard to migration of ions in the pore solution (cf. Sections 3.1.6.3 and 3.1.7.4) from and to the

* International Zinc Association (IZA), Brussels, Belgium

† American Galvanizers Association (AGA), Centennial, CO, USA

concrete steel interface, is given in Section 6.4.1, where electrochemical methods applied as countermeasures for existing structures are summarised.

6.3.3 Costs of Countermeasures for New Structures

For an evaluation of the effectiveness of a countermeasure considerations on its economy are of major importance, in particular when taking into account the enormous quantities used in the concrete business (cf. Section 1.1). Typical price ranges of countermeasures for new structures stated in different sources are listed in Table 6.4.

Table 6.4: *Price ranges of selected countermeasures for new structures from different sources.* [A]: *[Bertolini et al., 2004]*. [B]: *[IZA, 2007]*. [C]: *[Nürnberger, 1996]*.

Countermeasure	**Details**	**Source**		
		[A]	[B]	[C]
Concrete countermeasures (coatings in [€/m^2] and inhibitors in [€/m^3])				
Concrete surface protection	Continuous film	7-50	-	-
	Hydrophobic layer	10	-	-
Integral inhibitor	Calcium nitrite	30	-	-
Reinforcement countermeasures (based on "1" as the cost of ordinary carbon steel reinforcement, but cathodic prevention in [€/m^2])				
Epoxy	Epoxy I*	2	1.3	-
	Epoxy II*		1.5	-
	Purple epoxy*		1.8	-
Stainless steel	17 (EN 1.4016 / ASTM 430)	-	-	4.3
	18-10 (EN 1.4306 / ASTM 304)	6-8	-	5.5
	17-12-2 (EN 1.4436 / ASTM 316)	9-10	5.0	7.7
Microcomposite steel		-	1.8	-
Stainless steel cladded carbon steel*		-	3.9	-
Hot-dip galvanised steel*		2-2.5	1.5	-
Cathodic prevention		50-100	-	-

* Includes costs for coating/cladding and carbon steel.

With regard to the above listed price ranges, it is important to note that these values only reflect the *initial expenses*. We think that if actual costs of a structure are estimated, the service life is to be taken into consideration, i.e. costs should be expressed based on life-cycle costing (cf. Section 6.1). Based on life-cycle costing even expensive (but, effective) countermeasures as stainless steel and CPre (and CP) can be attractive solutions.

6.4 Countermeasures for Existing Structures

Although the focus of this project was set on the development of countermeasures for new structures rather than on repair and rehabilitation techniques, i.e. countermeasures for existing structures (cf. Section 1.6), we think that similar principles for the thermodynamic description can be used in this regard. Furthermore, specific implementations of the proposed new countermeasures (cf. Chapter 7) are applicable for repair of existing structures. So, selected countermeasures are briefly described in this Section. The following countermeasures are applied or have been proposed for rehabilitation or repair of existing structures:

- Concrete surface protection and crack injection
- Diffusion inhibitors
- Electrochemical techniques (Section 6.4.1)
  - Cathodic protection ‘CP’
  - Electrochemical realkalisation ‘ERA’
  - Electrochemical chloride removal ‘ECR’
- Concrete patch repair (Section 6.4.2)

In addition to the textbooks listed in Section 6.2, which also deal with repair and rehabilitation techniques to a smaller or larger extent, and the related standards, i.e. the EN 1504 series [DS/EN 1504-1, 2005] and [ACI et al., 2003; ACI 546R, 2004], there are other guidelines dealing exclusively with the repair of concrete damaged by reinforcement corrosion, e.g. (CS, 2002).

After a brief summary of the essential information on these repair and rehabilitation techniques the application of thermodynamics in concrete repair will be presented in Section 6.4.3. Electrochemical techniques and patch repair are dealt with separately (Sections 6.4.2 and 6.4.1, respectively) in slightly more detail, since they relate to our principles proposed in Chapter 7.

The most important background of concrete surface protection, which, in principle, also applies to crack injection and corrosion inhibitors, was already discussed in Sections 6.3.1.3 and 6.3.1.4, respectively. Therefore, only the special characteristics of their application as countermeasures for existing structures are briefly given:

- Concrete surface protection and crack injection

  Concrete surface protection and crack injection are standardised in [DS/EN 1504-2, 2005] and [DS/EN 1504-5, 2007], respectively. Besides [ACI 222R, 2001; ACI et al., 2003; ACI 546R, 2004], a relevant US publication is the ACI report on evaluation and repair of cracks in concrete structures [ACI 224.1R, 1998]. As mentioned in Section 6.3.1.3, we do not consider concrete surface protection as an option for repair of structures that are substantially contaminated by chloride or

where corrosion has already initiated, since initiation or propagation will not be prevented. The same holds for crack injection with e.g. epoxy. Sealing of cracks can, however, be an effective "first aid" to limit their contribution in accelerating the initiation and propagation of reinforcement corrosion (cf. Section 3.1.11.2), given that the cracks are not sealed only superficially, but down to the level of the reinforcement [Marcotte & Hansson, 2007].

- Diffusion inhibitors

  When inhibitors are applied to the surface of hardened concrete during the initiation phase, the mode of action is principally identical to the one of integral inhibitors, *provided that the necessary concentration at the reinforcement is attained* [Bertolini et al., 2004]. Complexes that have been proposed and tested for that purpose are mainly based on organic compounds, e.g. alkanolamines and amines, sodium monofluorophosphate, and recently also calcium nitrite [Elsener, 2001].

  In Section 6.3.1.4 it has been argued that the mode of action of some integral corrosion inhibitors as well as their contribution to durability with regard to the long service life of concrete structures may be doubtful. Furthermore, we consider that attaining and keeping of the necessary concentration is a major issue for diffusion inhibitors. The most important obstacles that interfere with the penetration of the inhibitors relate to the theory described in Section 3.1.6 and 3.1.7, e.g. poor diffusion in saturated concrete as well as possible outwards diffusion. Finally, it has been suggested that reactions between inorganic components of commercial diffusion inhibitor blends react with the cement matrix and block pores, which limits further penetration.

6.4.1 Electrochemical Techniques

Besides 'CPre', as an initial countermeasure for new structures (cf. Section 6.3.2.6), three relevant electrochemical techniques exist for rehabilitation of existing structures, i.e. 'CP', electrochemical realkalisation 'ERA', and electrochemical chloride removal 'ECR'.

'CP' is standardised in [DS/EN 12696, 2000] and described in [ACI et al., 2003; ACI 546R, 2004]. Moreover, several guidelines and handbooks provide extensive information on 'CP' of steel in concrete, e.g. [CS, 1989; Chess, 1998]. 'ERA' is standardised and 'ECR' was meant to be standardised in EN 14038 "Electrochemical realkalisation and chloride extraction treatments for reinforced concrete". Part 1 "Realkalisation" has been published [DS/CEN/TS 14038-1, 2004], whereas, according to [Gudmundsson et al., 2004], there is no mandate to work on part 2 "Chloride extraction treatment" at present and it will not be published in the foreseeable future. However, several reports and guidelines deal with 'ERA' and 'ECR', e.g. [Mietz, 1998] and [Sharp et al., 2002; Sharp & Virmani, 2006], respectively.

As for 'CPre' the steel is subjected to cathodic polarisation for 'CP', 'ERA', and 'ECR', but the applied current densities differ to a large extent. For economical reasons, the application of 'CP' is normally limited to corrosion protection in chloride contaminated concrete. The reinforcement is polarised, so that full protection is obtained, which, depending on the degree of contamination, thermodynamically corresponds to immunity or magnitudes of 'E_{corr}' close to immunity (cf. Sections 5.2.2.2 and 5.2.3.). In general, current densities between 5-20 mA/m^2 are applied during 'CP' [Bertolini et al., 2004]. Besides lowering the potential of the reinforcement, both 'CPre' and 'CP' involve ion migration in the concrete as well as cathodic reactions on the steel surface. These aspects are the basis for 'ERA' and 'ECR'. Much higher current densities, i.e. in the order of 1000-2000 mA/m^2 [Bertolini et al., 2004], are required to obtain the desired effects, i.e. to electrochemically rehabilitate the concrete, which is carbonated or chloride contaminated, respectively. The desired cathodic reactions and ionic currents in 'ERA' and 'ECR' are:

- Cathodic reactions (cf. Section 2.1.2):

$$O_2 + 2H_2O + 4e^- \rightarrow 4OH^- \quad \left(E_0^0 = 402\,\{401\}\ mV_{SHE} \right) \qquad [6.1]$$

$$2H_2O + 2e^- \rightarrow H_2 + 2OH^- \quad \left(E_0^0 = -828\,\{-828\}\ mV_{SHE} \right) \qquad [6.2]$$

  The reduction of water [6.2] only takes place at very low potentials and H_2 is formed. However, both reactions form hydroxyl ions and thus increase the local alkalinity at the concrete-steel interface.

- Ionic current (cf. Sections 3.1.6.3 and 3.1.7.4):

  Similar to corrosion processes (cf. Section 5.1.3), the circulation of current through concrete, i.e. the ionic current, is based on the migration of ions present in the pore solution, i.e. cations, e.g. H^+, K^+, Na^+, and Ca^{2+} migrate towards the steel, whereas anions, e.g. OH^-, SO_4^{2-}, and Cl^- migrate in the opposite direction.

In this connection, the major part of the circulating current is carried by hydroxyl ions (cf. Section 3.1.6.3) and thus a large portion of the hydroxyl ions produced by the cathodic reactions [6.1] and [6.2] is removed from the reinforcement surface and migrates towards the external anode. However, a certain part is balanced by sodium ions migrating towards the reinforcement and initial pH values close to 14 can be obtained [Bertolini et al., 2004]. The initial pH is balanced by the hydroxyl ions reacting with atmospheric CO_2 and generally stabilises at values around 11. [Bertolini et al., 2004].

The fraction of current carried by the chlorides is relatively small and furthermore it decreases with decreasing chloride concentration (cf. Section 3.1.7.3). Thus, high current densities are required to remove large quantities of chlorides from the reinforcement (or to prevent their ingress into new structures). [Bertolini et al., 2004].

These electrochemical reactions and transport mechanisms are the basis of 'ERA' and 'ECR', but they are also a decisive factor for the long-term operation of 'CPre' and

'CP'. Yet, the desired reactions can also involve negative side effects; in particular, hydrogen embrittlement (cf. Section 2.3.6), 'ASR' (cf. Section 6.1), and loss of bond strength.

Due to increasing field experience, the confidence in electrochemical techniques for existing concrete structure is growing. In contrast to concrete patch repair (cf. Section 6.4.2), the benefit of all these techniques is that only the physically damaged concrete cover needs to be removed and repaired, while the electrochemical techniques enable corrosion protection of the steel.

For 'CPre' and 'CP' additional installations and a provision of continuous electrical connection (cf. Section 6.3.2.2) of the reinforcement are required and, once applied, they must operate for the remaining service life of the structure. Nevertheless, based on life-cycle-costing and the existing alternatives, we consider 'CPre' or the provision for 'CP' as options for corrosion protection for certain types of structures. 'ERA' and 'ECR' need only to be applied for a limited period of time (of the order of a few weeks and a few months, respectively), and they may be effective, but we do not consider them to be effective on a large scale. However, as the original concrete surface remains unchanged, these techniques can have advantageous applications in the preservation of special architectural values, such as monuments. In that relation, research at DTU Byg showed that these techniques, in particular 'ECR', are not limited to corrosion protection of steel in concrete, but can also be used beneficially in e.g. the preservation of masonry or murals [Ottosen et al., 2007; Rörig-Dalgaard & Ottosen, 2007].

6.4.2 Concrete Patch Repair

Concrete patch (in the literature also referred to as conventional) repair is, to our knowledge, the most commonly used method for repairing localised corrosion damage of concrete. Besides the associated EN standard [DS/EN 1504-3, 2006] and US guidelines [ACI et al., 2003; ACI 546R, 2004] and most of the textbooks listed in Section 6.2, several reports, e.g. [CS, 1991], and other publications exist on the subject of patch repair. Most of the publications deal with the electrochemical incompatibility of patch repairs, e.g. [Raupach, 1996; Gu et al., 1997; Emmons & Vaysburd, 1997; Mailvaganam, 2001; Vaysburd & Emmons, 2004] and with the existence of macrocells, which has been experimentally demonstrated in e.g. [Wheat & Harding, 1993; Cusson & Mailvaganam, 1996; Schießl & Breit, 1996; Pruckner & Gjørv, 2002; Castro et al., 2003; Li & Yuan, 2003].

Patch repair includes the removal of loose concrete that has cracked, spalled, or delaminated, often the application of surface treatment on the steel, and replacement of the defective concrete with an appropriate patching material. Many patch repairs have been found to last only from a few months to a year before appearance of new corrosion damage. Corrosion damage after repair often takes place at the interface between

the patch and the unrepaired concrete substrate. This type of damage is due to the so-called ring-anode effect (in the literature also referred to as incipient anode effect). Before the repair, the corroding reinforcement acts as an anode with respect to the surrounding areas that are polarised cathodically and hence protected by the macrocell. After the repair, the newly patched area is at a higher potential than the surrounding areas, and the resulting imbalance can be as high as 500 mV [Pruckner & Gjørv, 2002]. Hence, formerly anodic sites no longer provide protection, but act as cathodes for corrosion initiation in the areas surrounding the patch, primarily the interfaces. In the literature, the resulting corrosion mechanism is often described as macrocell corrosion. However, contrary to the prevailing opinion that macrocell corrosion is the only deterioration mechanism in patch repair, both macrocell and microcell corrosion can play a significant role in inducing corrosion damage to the area surrounding the patch [Zhang & Mailvaganam, 2006].

To prevent the ring-anode effect, two techniques, which are both based on polarisation, are commonly applied in modern patch repair. The first option consists of applying zinc-rich primers to the appropriately cleaned reinforcement before patching, while the second one is based on embedding sacrificial anodes in the patch. An example for a commercially available sacrificial anode system for patch repair, which is commercially known as Galvashield XP and marketed by Fosroc[*], is shown in Figure 6.12.

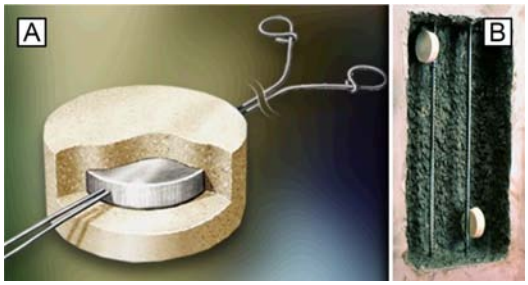

Figure 6.12: *Commercially available sacrificial anode system for patch repair. From [Qiu, 2007].* [A]: *Sketch of anode system presenting the pre-packaged zinc sacrificial anode with self-contained wire ties.* [B]: *Installed sacrificial anode system.*

Figure 6.12 [A] shows a sketch of the anode system, which is based on a pre-packaged zinc slice with wire ties. Figure 6.12 [B] presents an example for the installation before patching. The encasement is claimed to maintain the surface reactivity of zinc by a *"... highly alkaline cementitious mortar, which has a pore solution pH sufficiently high for corrosion of the anode to occur and for passive layer formation on the anode to be avoided..."* [Fosroc, 2007]. Laboratory investigations and field applications have shown that this zinc anode system can suppress the formation of incipient

[*] Fosroc A/S, Rødding, Denmark.

anodes around a patch repair. Field applications have included car parks, buildings, bridges, and other reinforced concrete structures, where conventional patch repairs could not provide acceptable performance. [Qiu, 2007].

So, the anode system seems to be working effectively, but we consider experience to be limited, since the system has been, to our knowledge, on the market only for about 10 years. In addition to that, the lifetime is limited to 20 years [Fosroc, 2007].

The proposed new countermeasures relate to both techniques of preventing the ring-anode effect and principles for alternative electrochemical active coatings and anode systems will be discussed in Chapter 7.

6.4.3 Thermodynamics of Countermeasures for Existing Structures

In relation to the traditional fundamental corrosion mechanism (cf. Figure 5.3 in Section 5.1.3), the following basic principle for repair of corrosion induced damage is often stated in the literature on reinforcement corrosion: Repair of reinforcement corrosion must aim at achieving one or more of the following objectives, e.g. [Schießl et al., 1994]:

- Stop the anodic process
- Stop the cathodic process
- Stop the electrolytic conduction process.

However, based on the theory described for formation of anodic products (cf. Section 5.1.1), the influence of anodic and cathodic processes on 'E_{corr}' (cf. Section 5.1.2), and the nature of the ionic current in concrete (cf. Section 3.1.7.4), we think that this description is not fully comprehensive and propose an alternative approach towards repair and rehabilitation of concrete structures.

Figure 6.13 shows the Pourbaix diagrams that were derived and introduced in Sections 5.2.2.1 and 5.2.2.2 as a basis for the thermodynamic description of carbonation and chloride induced corrosion, respectively. Leaving out the theory discussed for corrosion initiation of carbonation and chloride induced reinforcement corrosion, i.e. the pH drop from case (A) to case (B) in Figure 6.13 [A] and the pitting potential curves in Figure 6.13 [B], it can be concluded that a critical 'E_{corr}' and pH for corrosion propagation under both conditions is in the area of 0 mV and pH 7.

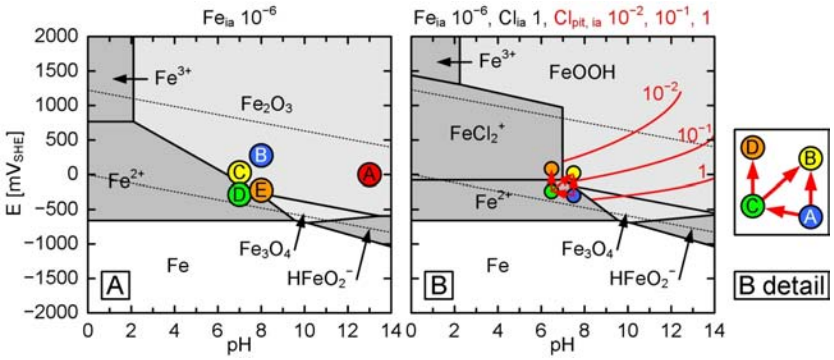

Figure 6.13: [A] *Fe-H_2O 'SEPD' based on Table 4.2 and Fe_{ia} = 10^{-6} mol/L with proposed mechanism for carbonation induced corrosion in oxygen-rich concrete (cf. Figure 5.5 in Section 5.2.2.1).* [B]: *Fe-Cl-H_2O 'MEPD' based on Table 5.4 and Fe_{ia} = 10^{-6} mol/L and Cl_{ia} = 1 mol/L with proposed mechanism for chloride induced corrosion in oxygen-deprived concrete (cf. Figure 5.10 in Section 5.2.2.2).*

This critical 'E_{corr}' and pH area are indicated by case (A) in the 'SIPD' of the Fe-H_2O 'SEPD' on the Fe-Cl-H_2O 'MEPD' in Figure 6.14.

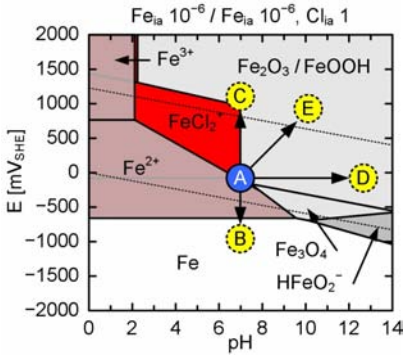

Figure 6.14: *'SIPD' of Fe-H_2O 'SEPD' on Fe-Cl-H_2O 'MEPD' with identification of critical 'E_{corr}' and pH area (A, blue dot), as identified in Figure 6.13, and illustration of potential thermodynamic approaches for repair (B, C, D, and E, yellow dots).*

Thermodynamic approaches to move the system away from the critical condition given by case (A) are illustrated by cases (B) to (E) in Figure 6.13:

- Case (B) illustrates the approach of lowering 'E_{corr}' into the immune area, while maintaining the pH. In terms of countermeasures for existing structures, this can be understood as the aim of 'CP' (while 'CP' in practice also involves realkalisation, cf. Section 6.4.1).

- Case (C) indicates the opposite approach to case (B), i.e. 'E_{corr}' is moved up into the passive domain at a constant pH, which corresponds to anodic protection aiming at the protectiveness of the passive layer. Anodic polarisation can naturally be achieved by e.g. an anodic current (which, to our knowledge, is not applied in practice), but in terms of the discussed countermeasures for existing structures it primarily relates to anodic diffusion inhibitors. *The proximity of case (C) to the critical stability domain of ferric chloride (cf. Section 5.2.2.2) in combination with the increase in "corrosion power" due to anodic polarisation (cf. Section 2.2.5) underlines our rejection of anodic protection in the chloride environment.* This does not only apply with regard to anodic inhibitors in general (cf. Section 6.3.1.4), but also with regard to e.g. noble clads (cf. Section 6.3.2.4).
- Similar to case (C), case (D) depends on the protection provided by the passive layer and illustrates the thermodynamic approach of increasing the pH of the concrete, i.e. the aim is reinstalling the initial situation of intact, uncontaminated concrete. In terms of the discussed repair methods, this approach primarily relates to 'ERA', while similar effects are obtained from 'ECR' (cf. Section 6.4.1). Nevertheless, the principal aim of 'ECR' can be understood thermodynamically to remove Cl from the Fe-H_2O, so that the stability domain of ferric chloride will be reduced (cf. Section 5.2.2.2). Patch repair relates to both these issues, but the positive effect is limited to the patched area, whereas the ring-anode effect promotes corrosion in its vicinity. The ring-anode effect can be prevented, if the patch repair strategy is combined with additional measures, e.g. corresponding to case (B).
- Finally, case (E) also aims at the protectiveness of the passive layer, but it is achieved by a combination of approaches (C) and (D), i.e. both 'E_{corr}' and the pH are increased to provide an environment for the formation of a stable passive layer. However, this concept cannot be realised in practice and, to our knowledge, no repair strategy exists that aims at this approach. Based on the theory concerning the composition of the pore solution (cf. Section 3.1.5) and migration (cf. Section 3.1.6.3), it can be thermodynamically reasoned that e.g. impressed current anodic polarisation inevitable leads to an acidification at the anode, i.e. in the vicinity of the reinforcement steel (cf. Section 6.4.1).

7 Design of Corrosion Countermeasures

As indicated in Section 1.5, the design phases of concern in this thesis correspond to the first three phases in the proposed simplified flow chart for the design and implementation of new countermeasures, see Figure 7.1.

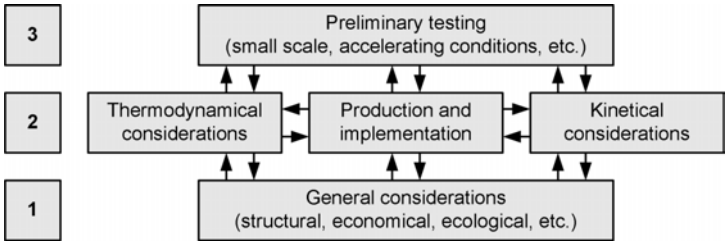

Figure 7.1: *Extract from the proposed flow chart for design of new countermeasures (cf. Figure 1.1, Section 1.5) indicating the design phases of concern in the present thesis.*

Figure 7.1 illustrates that phase 2 relates to the highly interconnected thermodynamic considerations, production and implementation processes, and kinetic considerations. This phase, which is most important in the present thesis, is preceded and largely governed by general considerations in phase 1 and succeeded by preliminary testing in phase 3. The general considerations are linked to the structural and materials properties of reinforced concrete (cf. Chapter 3). The thermodynamic and kinetic considerations as well as the production and implementation and the preliminary testing are largely based on application of the available aqueous metallic corrosion theory (cf. Chapter 2) and its adaptation to reinforcement corrosion (cf. Chapter 4). The adaptation of the theory was detailed for corrosion of carbon steel in concrete in Chapter 5 and indicated for available countermeasures throughout Chapter 6. Even though this Chapter covers the central objectives of this thesis, it is kept relatively short, since *it is mainly based on the essence of Chapters 2 to 6, which is extended to and applied in the conceptual design of new countermeasures.*

In Section 7.1 the most important design aspects and requirements we took into account in the development of the new countermeasures are listed. Our theoretical design approach is dealt with in Section 7.2, while the principal materials concepts are discussed in Section 7.3. Some remarks on the implementation of the material concepts and their application on a structural scale are given in Section 7.4. With regard to the expected patent possibilities (cf. Section 1.6), both the theoretical approach and its practical realisation are described without going into detail and thus central aspects are excluded from the associated Sections. The final Section 7.5 summarises aspects of and requirements for preliminary testing of countermeasures with focus on performance evaluation based on electrochemical testing.

It should be noted that the described strategies aim at both carbonation and chloride induced corrosion (cf. Sections 5.2.2.1 and 5.2.2.2). However, as reasoned throughout Chapter 5 and Section 6.1, chloride induced corrosion is the main concern. Hence, the models used for the descriptions of our approaches are largely based on chloride induced corrosion, i.e. on the Fe-Cl-H_2O system.

7.1 Design Aspects and Requirements

In this Section the most important design aspects and requirements that we took into account are summarised, i.e. it deals with phases 1 and 2 of our proposed design approach illustrated in Figure 7.1. Since the considerations in these phases (particularly, in phase 2) are largely interconnected, no clear distinction is made between the considerations. Instead, the subdivision is as follows:

- Aspects and requirements relating to corrosion resistance
- Aspects and requirements relating to structural and general durability performance
- Aspects and requirements relating to cracking of the concrete
- Practical aspects and requirements
- Economical aspects and requirements
- Ecological aspects and requirements

Most of these aspects and requirements relate to shortcomings of the available countermeasures, which have been indicated in Chapter 6. The shortcomings are listed in connection with the associated Bullets, which are numbered (Arabic numeral), because they are frequently referred to throughout this Chapter:

1 Aspects and requirements relating to corrosion resistance

As the fundamental basis of all considerations in phases 1 and 2 (cf. Figure 7.1) the countermeasures should provide the following for new and existing structures:

1.1 A significant improvement of the resistance of reinforcement against both carbonation and chloride induced corrosion

1.2 Reliable long-term improvement, i.e. assuring service lives of 100, 200, or more years

1.3 Protection against *all* critical forms of corrosion (cf. Section 2.3)

1.4 Effectiveness at all relevant exposure conditions (in addition to chloride contamination and carbonation), in particular all degrees of saturation (cf. Section 3.1.7.1) and normal ambient temperatures (cf. Section 3.1.10), while *special high or low temperature applications require additional considerations*.

Doubtful and/or negative examples concerning long-term effectiveness include in principle all concrete countermeasures (cf. Section 6.3.1), galvanised (cf. Section

6.3.2.5) as well as epoxy-coated steel (cf. Section 6.3.2.2), and most repair techniques other than 'CP' (cf. Section 6.4). Inhibitors (cf. Sections 6.3.1.4 and 6.4) and concrete surface protection (cf. Section 6.3.1.3) are considered to be particularly critical with regard to long-term performance (Bullet 1.2). Moreover, concrete surface protection systems are sensitive to variations in the exposure conditions (Bullet 1.4).

2 Aspects and requirements relating to structural and general durability performance

Relating to both structural and general durability performance, the below requirements are considered as crucial in the design phases 1 and 2 (cf. Figure 7.1). The countermeasures should neither interfere negatively with structural performance nor with durability aspects of the reinforcement and/or the concrete itself. This includes among others:

2.1 Strength and ductility characteristics of the *reinforcement* should not be negatively influenced.

Negative examples include 'FRP' concerning e.g. ductility (cf. Section 6.3.2.1) as well as 'ERA' and 'ECR' (cf. Section 6.4.1) with regard to a reduction in both strength and ductility due to hydrogen embrittlement (cf. Sections 2.3.6 and 6.4.1). Moreover, 'CP' (cf. Section 6.4) as well as galvanisation (cf. Section 6.3.2.5) require attention concerning hydrogen embrittlement. High-strength steels are known to be especially susceptible to hydrogen embrittlement (cf. Section 2.3.6). Thus, *high-strength steel reinforcement, which is often related to prestressing or post-tensioning, requires special design considerations.*

2.2 Strength and durability of the *concrete* should not be negatively influenced.

In practice, critical effects of countermeasures on the concrete strength or durability generally relate to interference with cement hydration (cf. Section 3.1.2) or early-age cracking (cf. Section 3.1.11.1). Most concrete countermeasures (cf. Section 6.3.1) can interfere with cement hydration, while reinforcement measures do generally not affect the chemistry of the concrete. However, the strength development of the concrete-steel interface can be affected by reinforcement countermeasures (cf. Bullet 2.3). With regard to early-age cracking, 'HPC' (cf. Section 6.3.1.1) and integral inhibitors (cf. Section 6.3.1.4) may be of concern.

2.3 Bond properties, i.e. the development of strength and chemical bond at the *concrete-steel interface* (cf. Section 3.3), should not be negatively influenced.

Negative examples include the countermeasures related to hydrogen embrittlement (cf. Bullet 2.1) as well as all concrete countermeasures affecting concrete properties (cf. Bullet 2.2). Moreover, copper cladding (cf. Section

6.3.2.4) and galvanisation (cf. Section 6.3.2.5) are known to interfere with hydration at the concrete steel interface.*

Besides the above listed requirements, the new countermeasure should generally not compromise any other of the overall benefits of the concrete-steel system, e.g. thermal compatibility (cf. Section 1.1).

3 Aspects and requirements relating to cracking of the concrete

In addition to the requirements regarding corrosion resistance and durability aspects stated in Bullets 1 and 2, the following requirements concerning cracking of the concrete are taken into account:

3.1 Since it is practically impossible to prevent the concrete cover from cracking to a lesser or larger extent (cf. Section 3.1.11), cracking is taken into consideration in the development. A crack width of 1 mm at the level of the reinforcement is proposed for the conceptual design.

3.2 Cracking due to the formation of voluminous corrosion products formed during corrosion propagation (cf. Section 5.2.2.1) is to be omitted, i.e. formation of bulky products is to be prevented.

4 Practical aspects and requirements

Practical requirements are largely interconnected with economical requirements and thus a central aspect in the general considerations. Moreover, they relate to the production and implementation and hence to both phases 2 and 3 (cf. Figure 7.1). With regard to the immense proportions and quantities produced (cf. Section 1.1), procedures during production and placing are of special concern in the concrete business. Thus, the new countermeasures should:

4.1 Not negatively interfere with the common practices and activities on site, i.e. not require special or complicated procedures during on-site performances (e.g. manufacture of the reinforcement and formwork as well as placing and curing of the concrete)

4.2 Not be sensitive to the quality of workmanship on-site and be able to tolerate a certain degree of insufficiency or damage during production and implementation†

4.3 Require only minor (or, ideally: no) attention or maintenance after implementation.

---

* However, we think that the relevance of the chemical bond between steel and concrete often seems to be overrated with regard to mechanical properties, as the major part of the force transfer is generally established by the mechanical interlocking achieved by the ribs (cf. Section 3.2.1).

† While production and implementation generally coincidence for concrete countermeasures, these phases can be distinguished for reinforcement countermeasures; considering the establishment of electrical connectivity as production for ‘CPre’ and ‘CP’ (cf. Section 6.4.1).

Except from concrete surface protection (cf. Section 6.3.1.3) and electrochemical techniques (cf. Section 6.4.1), the countermeasures listed in Section 6 fulfil requirement 4.3. However, various countermeasures conflict with requirements 4.1 and 4.2. For instance, 'HPC' (cf. Section 6.3.1.1) and concrete surface protection (cf. Section 6.3.1.3) are sensitive to the quality of workmanship. 'FRP' (cf. Section 6.3.2.1) does not allow for custom on-site practices. With regard to epoxy-coating (cf. Section 6.3.2.2) and metallic cladding (cf. Section 6.3.2.4) concerns with regard to both the sensitivity of production and execution could be raised (neither can be adjusted on-site). Moreover, post-casting densification techniques (cf. Section 6.3.1.2) as well as electrochemical concrete-steel interface improvement (cf. Section 6.3.1.5) interfere with the above practical requirements.

The possibility of combining the new countermeasure with carbon steel reinforcement, i.e. selective use of the countermeasure (cf. selective use of stainless steel in Section 6.3.2.1), is not regarded as a requirement per se, but taken into consideration in the development to account for galvanic effects due to intended or unintended electrical connection.

5 Economical aspects and requirements

As mentioned under Bullet 4, practical and economical requirements are closely interrelated. Important additional economical requirements to be taken into account relate to availability and price of the base materials as well as to the expenses for production and implementation. The countermeasure should be based on abundantly available and inexpensive raw materials and on an inexpensive production process. As illustrated in Table 6.4 in Section 6.3.3, negative examples in this connection are foremost stainless steel with regard to the price of the raw materials (cf. Section 6.3.2.1), certain types of concrete surface protection (cf. Section 6.3.1.3), as well as 'CPre' (cf. Section 6.3.2.6) and electrochemical techniques in general (cf. Section 6.4.1). Moreover, we think that, compared to the relatively low prices stated in the literature (cf. Table 6.4), proper production and implementation of epoxy-coated reinforcement requires significantly higher production costs (cf. Section 6.3.2.2).

Our overall approach with regard to economical considerations is to take carbon steel as the basis, while the upper limit is seen to be determined by the initial cost of stainless steel (cf. Table 6.4). An efficient cost saving is considered to be achieved, when the initial costs are reduced by 50%, i.e. 3-5 times the initial cost of carbon steel reinforcement, while providing for corrosion protection similar to the one of stainless steel. However, our aim is to compete with the initial price range of galvanised steel or undercutting it, i.e. to stay below twice the initial cost of carbon steel reinforcement.

6 Ecological aspects and requirements

The final design requirement relates to ecologic considerations. As mentioned in Section 6.3.1.4, calcium nitrite and chromates are toxic and application is, therefore, largely limited (at least, in Europe). In addition to avoiding such potentially critical interference in service, the new countermeasure should also aim at ecological solutions (in particular, free of personal hazards) during production and/or implementation. Besides inhibitors (cf. Sections 6.3.1.4 and 6.4) and some types of concrete surface protection (cf. Section 6.3.1.3) that may be hazardous in production and implementation, 'FRP' (cf. Section 6.3.2.1) and organic reinforcement coatings (cf. Section 6.3.2.2) are considered to pose such undesired interferences in the production stage.

7.2 Theoretical Design Approach

The description of our theoretical design approach is subdivided in thermodynamic and kinetic considerations, which are discussed in Sections 7.2.1 and 7.2.2. These considerations lead to two principles of implementation of the proposed countermeasures, i.e. based on rebar surface modification or on embedded electrodes, which will be dealt with in Section 7.2.3.

7.2.1 Thermodynamic Design Approach

With the exception of corrosion inhibitors (cf. Section 6.3.1.4), we consider concrete countermeasures (cf. Section 6.3.1) to act rather kinetically than thermodynamically. Thus, they play a more significant role in Section 7.2.2 dealing with kinetic considerations*.

Concerning reinforcement countermeasures, we ruled out 'FRP' and epoxy-coated reinforcement from our further considerations based on the major interferences with the requirements stated in Section 7.1. Hence, the available thermodynamic options for corrosion protection of new structures can be represented as illustrated in Figure 7.2.

The 'E_{corr}' and pH area in uncontaminated concrete and the critical 'E_{corr}' and pH area for corrosion initiation are identified by cases (A) and (B) in Figure 7.2 [A], [B], and [C]. Cases (C) and (D) in Figure 7.2 [A] represent cathodic and anodic polarisation with the objective of moving 'E_{corr}' away from the critical stability domains of Fe^{2+} and $FeCl_2^+$. Measures to avoid the pH decrease are indicated by the dashed line between cases (B) and (A). Apart from the marginal applications of 'ERA' in repair (cf. Section 6.4.1), this option is impractical and difficult to realise in practice. However,

* Although the implementation of electrochemical concrete-steel interface improvement is based on thermodynamic principles, its effect (i.e. the densification) is considered to act kinetically rather than thermodynamically.

options (C) and (D) are feasible thermodynamic techniques, which can be realised by cathodic and anodic polarisation, respectively.

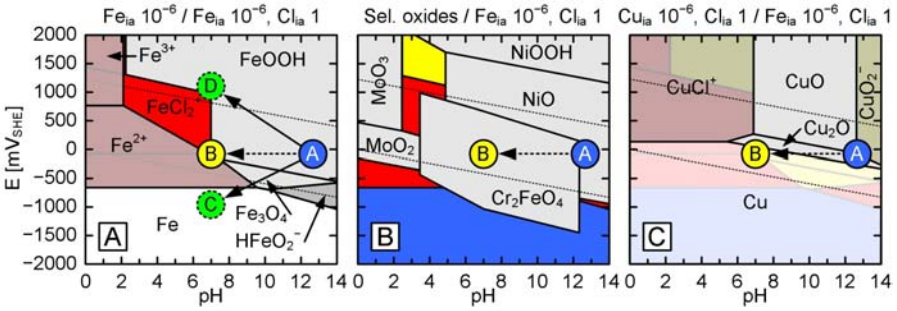

Figure 7.2: *Identification of 'E$_{corr}$' and pH area in a new structure (A, blue dot) and of critical 'E$_{corr}$' and pH area (cf. Figure 6.13) for corrosion initiation in a contaminated structure (B, yellow dot) on different 'SIPDs'.* [A]: *'SIPD' of Fe-H$_2$O 'SEPD' on Fe-Cl-H$_2$O 'MEPD' (cf. Figure 6.14) and illustration of potential thermodynamic approaches for protection (C and D, green dots).* [B]: *'SIPD' of stability domains of selected stainless steel alloy oxides (cf. Figure 6.7) on Fe-Cl-H$_2$O 'MEPD' (cf. Figure 6.8 [B]).* [C]: *'SIPD' of Cu-Cl-H$_2$O 'MEPD' on Fe-Cl-H$_2$O 'MEPD' (cf. Figure 6.11 [B]).*

In contrast to Figure 7.2 [A], which is limited to the Fe-H$_2$O system, Figure 7.2 [B] and [C] represent the thermodynamic effect of adding other metals to the system. Figure 7.2 [B] shows the 'SIPD' of stability domains of selected stainless steel alloy oxides (cf. Figure 6.7 in Section 6.3.2.3.1) on the Fe-Cl-H$_2$O 'MEPD' (cf. Figure 6.8 [B] in Section 6.3.2.3.1) and is meant to represent the combination of another metal (or element) and iron to form complexes with improved corrosion resistance, as Cr_2FeO_4 in this instance. Figure 7.2 [C] represents corrosion protection of iron by another (in this case, more noble) metal. The 'SIPD' of the Cu-Cl-H$_2$O 'MEPD' on the Fe-Cl-H$_2$O 'MEPD', which illustrates the thermodynamic conditions of copper cladding is chosen as an example for this approach (cf. Figure 6.8 [B] in Section 6.3.2.4).

Hence, Figure 7.2 represents three (interlinked) fundamental design options for countermeasures that are available from a thermodynamic point of view:

- **A** Control of 'E$_{corr}$' in the Fe-H$_2$O system (cf. Figure 7.2 [A])
- **B** Addition of other metals or elements to the Fe-H$_2$O system forming oxides with improved corrosion resistance (cf. Figure 7.2 [B])
- **C** Protection (or replacement) of the Fe-H$_2$O system by metals with improved corrosion resistance (cf. Figure 7.2 [C]).

Two principles of implementation are employed in our proposed new countermeasures (cf. Section 7.2.3). The first principle of implementation is based on a surface

modification and combines all three of the above listed thermodynamic design options, i.e. Bullets A, B, and C. Embedded electrodes are utilised for corrosion protection for the second principle of implementation, i.e. this principles is based on the first option (Bullet A) only.

With regard to the control of 'E_{corr}' and pH in the Fe-H_2O system (cf. cases (C) and (D) in Figure 7.2 [A] and Bullet A in the above list), *both principles of implementation aim at a targeted low 'E_{corr}'*[*]. In Section 6.4.3 our concerns regarding anodic polarisation for chloride contaminated concrete were indicated, e.g. concerning pitting potentials for initiation and the effects of products formed under higher 'E_{corr}' in propagation of chloride induced corrosion (cf. Section 5.2.2.2). *We consider all measures that aim at anodic polarisation (e.g. corrosion inhibitors, cf. Section 6.3.1.4) or measures that can lead to unintended anodic polarisation (e.g. noble cladding, cf. Section 6.3.2.4) as a dangerous approach towards corrosion protection in the chloride environment.*

However, from a thermodynamic perspective anodic polarisation can be beneficially utilised in preventing (or ceasing) carbonation induced corrosion, see case (D) in Figure 7.2 [A]. In this context, it is recommended in e.g. [Pourbaix, 1974a] that any reducing substance (sulphides, humic matters, etc.) should be avoided in concrete and use of oxidising cements or oxidants, e.g. chromates and nitrites (cf. Section 6.3.1.4), is recommended to form a "more protective" passive layer. The protection against carbonation induced corrosion will be enhanced, if (and only if) the anodic polarisation is sufficient to move 'E_{corr}' out of the critical region (cf. Figure 7.2 [A]) and to attain this state during the whole design service life of the structure. However, with regard to the mentioned issues with long-term performance (cf. especially Bullets 1.2 and 4.2 in Section 7.1), we think that this is a rather intricate task.

While high-strength steel reinforcement requires special considerations (cf. Bullet 2.1 in Section 7.1), we suggest addressing both carbonation and chloride induced corrosion as well as combined exposure situations with the establishment of a targeted low 'E_{corr}'. As discussed in detail in Section 5.2.1.2, we think that lowering 'E_{corr}' at high pH into the domain of $HFeO_2^-$, i.e. low potential corrosion, does not lead to problems for carbon steel reinforcement.

7.2.2 Kinetic Design Approach

As mentioned, in Section 7.2.1, we consider kinetic approaches to relate to concrete countermeasures rather than to reinforcement countermeasures. However, it should be noted that kinetic measures also have a significant effect on the thermodynamic con-

[*] The expression "low 'E_{corr}'" is used instead of cathodic protection/prevention, when referring to both principles of implementation (or, to the first principle of implementation), since the carbon steel surface treatment operates at low potentials by itself and only provides cathodic protection at e.g. discontinuities.

dition of a metallic rebar embedded in concrete. For instance, increasing the denseness or degree of saturation of the concrete limits the oxygen supply and hence lowers 'E_{corr}' (cf. Sections 3.1.7.1 and 5.1.2). At the same time, the thermodynamic condition of the rebar influences the migration of ions (cf. Sections 3.1.6.3 and 5.1.3).

Both the initiation and the propagation stage are largely influenced by the kinetic properties of the concrete bulk and the concrete-steel interface. For instance, in addition to controlling the initiation phase in terms of chloride ingress and carbonation, the properties of the concrete control the supply of oxygen and the ion mobility and thus propagation in terms of the corrosion rate. So, in continuation of the list of thermodynamic options in Section 7.2.1, the following three fundamental design options are available from a kinetic perspective:

D Improvement of the denseness of the concrete

E Concrete surface protection

F Improvement of the concrete-steel interface

In Section 7.1 it was pointed out that all techniques aiming at improving the denseness of the concrete (Bullet D) interfere with practicability (cf. Bullets 4.1 and 4.2) and that 'HPC' may also lead to an increased risk for early-age cracking (cf. Bullet 2.2). Practicability disadvantages (cf. Bullets 4.1 to 4.3) also apply to concrete surface protection (Bullet E), which further raised concerns with regard to long-term performance and sensitivity to exposure conditions (Bullets 1.2 and 1.4).

In terms of the available countermeasures (cf. Section 6), concrete-steel interface improvement (Bullet F), was covered by impressed current interface improvement. This technique does not meet our practicability requirements (cf. Bullets 4.1 and 4.2 in Section 7.1). However, we think that there are other feasible options of improving the concrete-steel interface, i.e. by self-sustaining densification processes without application of an impressed current. We suggest that this approach in combination with a workable concrete of a reasonable quality will significantly improve the concrete-steel interface (cf. Section 3.3).

7.2.3 Principles of Implementation

As mentioned in Sections 7.2.1 and 7.2.2, two diverse principles of implementation for corrosion protection, which both relate to the use of ordinary carbon steel reinforcement, have been derived based on the requirements stated in Section 7.1. The first principle of implementation (henceforth, 'Principle I') is based on a surface modification of the reinforcement, whereas the second principle of implementation (henceforth, 'Principle II') is based on the application of embedded electrodes. *Both principles follow the principal aim of attaining targeted low corrosion potentials*, which is achieved by means of the materials concepts described in Section 7.3. The materials concept of 'Principle I' also enables densification of the concrete-steel inter-

face. Interface densification is immobilised in the materials concept of 'Principle II', as cathodic protection with a high current yield is aimed at.

The concrete-steel interface improvement of 'Principle I' is achieved by electrochemical densification during the set of concrete as well by pore-blocking at later stages. While the concepts differ, the results achieved are assumed to be comparable to electrochemical densification by impressed currents (cf. Section 6.3.1.5) and formation of pore-blockers (cf. Section 6.3.1.3). In this way, a tailored dense concrete steel-interface is obtained, which is expected to significantly increase the chloride threshold (cf. Sections 3.1.9). The densified concrete-steel interface does not only limit the access to chloride ions and oxygen, but it also decreases the overall ion mobility (cf. Section 3.1.7). This limits the formation of microcells (cf. Section 3.2.2.1) and macrocells (cf. Section 3.1.8) and furthermore counteracts outwards diffusion of soluble corrosion products (cf. Section 5.2.2.2). Thus, based on this kinetic approach *the bulk denseness is improved where it is essential, i.e. where the corrosion reactions take place*. In contrast to 'HPC', possible problems related to execution and curing are avoided and, in contrast to concrete surface protection, the concrete bulk itself grants protection to the embedded barrier. Thus, *the system does not state special requirements to materials (concrete) and execution and it is maintenance-free*.

Both 'Principle I' and 'Principle II' are expected to significantly improve the corrosion protection of carbon steel reinforcement in contaminated and cracked (up to a certain crack width) concrete. Countermeasures based on combining 'Principle I' and 'Principle II' are also possible, which will be further elaborated in Section 7.4.

The principles of implementation are applicable for both new and existing structures. It should be noted that the implementation processes for 'Principle I' differ considerably between application in new and existing structures. This and other aspects of the production and implementation are discussed in Section 7.4.

7.3 Materials Concepts

In this Section the materials concepts for the production and implementation, i.e. the basis for the practical approaches to realise the theoretical concepts (cf. Section 7.2), are summarised for both principles of implementation (cf. Section 7.2.3).

Both principles of implementation are based on implementing certain portions of magnesium and zinc in the Fe-H_2O system by custom-designed processes that provide for stability in the concrete environment; also in case of carbonation and chloride contamination. The background as well as the thermodynamics of introducing zinc and magnesium to the concrete-steel system is described in Sections 7.3.1 and 7.3.2, respectively.

7.3.1 Zinc and Concrete-Steel System

Before the application of zinc in our proposed new countermeasures is reasoned, some general thermodynamic aspects of zinc are elaborated in continuation of Section 6.3.2.5. Figure 7.3 presents Zn-H_2O 'SEPDs' for different zinc ion activities.

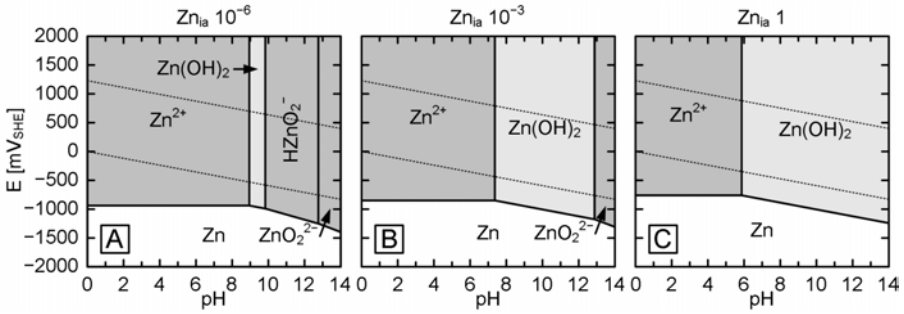

Figure 7.3: *Zn-H_2O 'SEPDs' based on Table 7.1 with different zinc ion activities.* [A]: *$Zn_{ia} = 10^{-6}$ mol/L.* [B]: *$Zn_{ia} = 10^{-3}$ mol/L.* [C]: *$Zn_{ia} = 1$ mol/L.*

Table 7.1: *Species preselected for the 'SEPD' of the Zn-H_2O system.*

Solid	Zn	$Zn(OH)_2$	-
Soluble	$HZnO_2^-$	Zn^{2+}	ZnO_2^{2-}

Based on our proposed approach towards preselection of species (cf. Section 4.2), of all oxides and hydroxides of zinc existing in aqueous solution only the most stable form, i.e. zinc hydroxide ($Zn(OH)_2$), is considered as passive compound; zinc ion, bizincate ion ($HZnO_2^-$), and zincate ion (ZnO_2^{2-}) are the selected soluble compounds, see Table 7.1.

Figure 7.3 [A] shows that zinc is thermodynamically unstable, i.e. not immune, in aqueous solutions, and tends to dissolve with the evolution of hydrogen in acid, neutral, and very alkaline solutions. Based on the assumed (lower bound) ion activity for passivation, i.e. 10^{-6} mol/L (cf. Section 4.2), zinc only passivates in a rather narrow pH range of approximately 9-10 (cf. Figure 7.3 [A]). The dissolution is considered to be most severe below pH 6 and above pH 13 [Yeomans, 2004]. However, if zinc is not galvanically connected to a metal with low hydrogen overpotential, the dissolution process generally takes place at a low rate due to the large hydrogen overpotential of zinc [Pourbaix, 1974b; Zhang, 1996].

In Figure 7.3 [B] and [C] it can be observed that the passivation domain of zinc extends in both direction with increasing ion activity. Towards higher pH values the extension firstly takes place on expense of bizincate ion and with further increment also of zincate ion. We suggest that the estimated 5-10 µm loss of the pure zinc layer on galvanised rebar prior to passivation (cf. Section 6.3.2.5) is required to increase the ion activity in the vicinity of the rebar to favour formation of $Zn(OH)_2$. Thus, it can be

concluded that *zinc is not only unstable in the concrete environment, but also initially active.*

Nevertheless, once zinc passivates with formation of calcium hydroxyzincate (cf. Section 6.3.2.5), we think that it provides beneficial corrosion protection for certain applications. Thermodynamic data of calcium hydroxyzincate has not been found available, but we assume that addition of calcium to the Zn-H_2O system will increase the extent of the passive domain. We consider the effect of calcium on the extent of the passive domain to be even more pronounced if carbon is introduced to the system, as the formation of passive compounds in connection with calcium carbonate will be favoured (cf. Figure 5.4 [C] in Section 5.2.1.1).*

The effect of adding carbon to the Zn-H_2O system can be directly estimated by the 'MEPD' of the Zn-C-H_2O system, see Figure 7.4 [A].

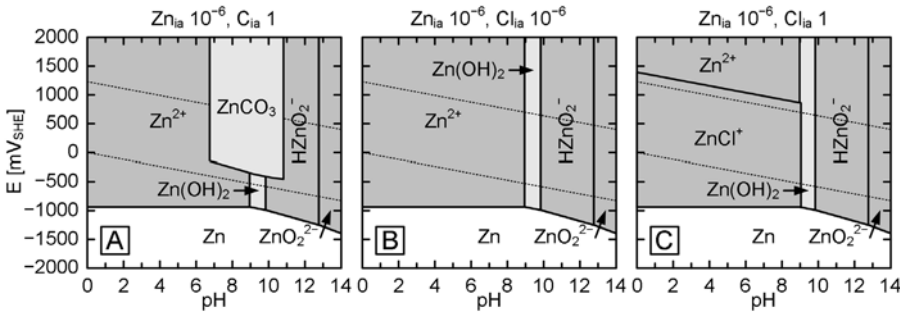

Figure 7.4: [A]: *Zn-C-H_2O 'MEPD' based on Table 7.2 and $Zn_{ia} = 10^{-6}$ mol/L and $C_{ia} = 1$ mol/L.* [B]: *Zn-Cl-H_2O 'MEPD' based on Table 7.3 and $Zn_{ia} = 10^{-6}$ mol/L and $Cl_{ia} = 10^{-6}$ mol/L.* [C]: *As [B], but with $Cl_{ia} = 1$. Based on $Zn_{ia} = 10^{-6}$ mol/L, $ZnCl^+$ is favoured over Zn^{2+} in the associated stability domain from above $Cl_{ia} = 0.7$ mol/L.*

Table 7.2: *Species preselected for the 'MEPD' of the Zn-C-H_2O system.*

Solid	C	Zn	$ZnCO_3$	$Zn(OH)_2$	-
Soluble	CO_3^{2-}	HCO_3^-	$HZnO_2^-$	Zn^{2+}	ZnO_2^{2-}

Table 7.3: *Species preselected for the 'MEPD' of the Zn-Cl-H_2O system.*

Solid	Zn	$Zn(OH)_2$	-	-	-	
Soluble	Cl^-	ClO_4^-	$HZnO_2^-$	Zn^{2+}	$ZnCl^+$	ZnO_2^{2-}

Figure 7.4 [A] indicates that formation of zinc carbonate ($ZnCO_3$) increases the passive domain of zinc from a pH range of about 9-10 to a pH range of about 7-11, which

* It is also well known that "hard water", i.e. water with high contents of $CaCO_3$, protects zinc against corrosion.

is in good agreement with e.g. measurements of zinc immersed in solutions containing CO_2 [Pourbaix, 1974b; Zhang, 1996]. We think that this increase reflects the resistance of galvanised rebar to carbonation induced corrosion (keeping in mind that the passive domain is assumed to be further increased with addition of calcium).

In Figure 7.4 [B] and [C] the influence of adding chloride to the Zn-H_2O system is illustrated. It can be observed that, contrary to iron (cf. Section 5.2.2.2), lower chloride ion activities do not have a thermodynamic effect on the extent of passive domains in the Zn-Cl-H_2O system. Based on $Zn_{ia} = 10^{-6}$ mol/L, formation of chlorozinc ion ($ZnCl^+$) is only favoured over Zn^{2+} from above $Cl_{ia} = 0.7$ mol/L. However, from Figure 7.4 [B] and [C] it can be concluded that zinc alone and hence galvanised reinforcement does not provide a satisfactory gain in corrosion protection in the chloride environment (cf. critical 'E_{corr}' and pH identified in Figure 7.2 in Section 7.2.1 and chloride thresholds of galvanised reinforcement in Section 6.3.2.5).

Nevertheless, zinc plays a role in our thermodynamic approach (cf. Section 7.2.1). Besides its contribution in the establishment of a targeted low 'E_{corr}' (Bullet A in Section 7.2.1), the most important role of zinc in 'Principle I' is the formation of stable passive compounds in combination with iron (Bullet B in Section 7.2.1), i.e. zinc ferrite ($ZnFe_2O_4$), cf. Figure 7.5.

With regard to the establishment of a targeted low 'E_{corr}', it should be noted that although zinc is generally anodic to iron* (cf. Section 6.3.2.5), zinc anodes are normally specified to strict chemical compositions, as impurities can impair the performance of the anode; the most detrimental impurity being iron [Zhang, 1996; Roberge, 2007]. According to [Roberge, 2007] iron can precipitate as intermetallic particles leading to formation of galvanic cells on a zinc anode, even if present in very low concentrations only. In combination with the formation of electrically non-conductive zinc hydroxide (cf. Section 2.1.9), we think that this can have a significant effect in reducing the anode efficiency.

The main role of zinc in 'Principle I' is to replace FeOOH by a more stable passive product. That means that the *stability of the passive layer is improved at a low 'E_{corr}'*, which we consider to be a thermodynamically consistent approach for corrosion protection.

Figure 7.5 and Figure 7.6 illustrate the thermodynamics of $ZnFe_2O_4$ at different ion activities in the Fe-Zn-Cl-H_2O system and the Zn-Fe-Cl-H_2O, respectively.

* This is true for the normal ambient temperature environments the countermeasures are designed for (cf. Bullet 1.4 in Section 7.1). However, iron becomes anodic to zinc when the temperature is raised above e.g. 60°C [Roberge, 2007].

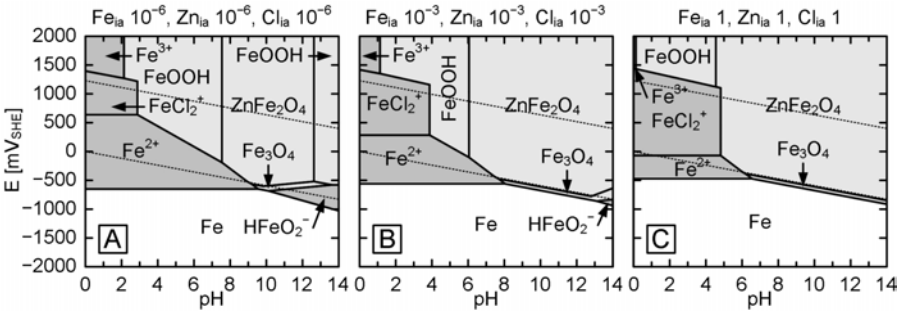

Figure 7.5: *Fe-Zn-Cl-H_2O 'MEPDs' based on Table 7.4 and different ion activities.* [A]: *$Fe_{ia} = 10^{-6}$ mol/L, $Zn_{ia} = 10^{-6}$ mol/L, and $C_{ia} = 10^{-6}$ mol/L.* [B]: *$Fe_{ia} = 10^{-3}$ mol/L, $Zn_{ia} = 10^{-3}$ mol/L, and $C_{ia} = 10^{-3}$ mol/L.* [C]: *$Fe_{ia} = 1$ mol/L, $Zn_{ia} = 1$ mol/L, and $C_{ia} = 1$ mol/L.*

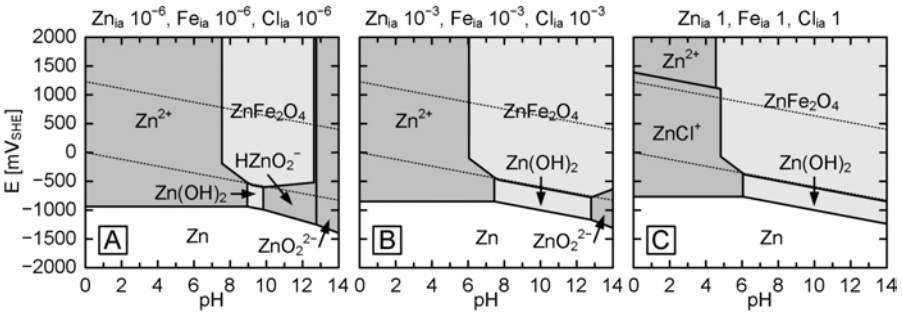

Figure 7.6: *Zn-Fe-Cl-H_2O 'MEPDs' based on Table 7.4 and different ion activities.* [A]: *$Zn_{ia} = 10^{-6}$ mol/L, $Fe_{ia} = 10^{-6}$ mol/L, and $C_{ia} = 10^{-6}$ mol/L.* [B]: *$Zn_{ia} = 10^{-3}$ mol/L, $Fe_{ia} = 10^{-3}$ mol/L, and $C_{ia} = 10^{-3}$ mol/L.* [C]: *$Zn_{ia} = 1$ mol/L, $Fe_{ia} = 1$ mol/L, and $C_{ia} = 1$ mol/L.*

The preselection for Figure 7.5 and Figure 7.6 corresponds to the species listed in Table 7.4.

Table 7.4: *Species preselected for the 'MEPD' of the Fe-Zn-Cl-H_2O and the Zn-Fe-Cl-H_2O system.*

Solid	Fe	Fe_3O_4	FeOOH	Zn	$ZnFe_2O_4$	$Zn(OH)_2$
Soluble	Cl^-	ClO_4^-	Fe^{2+}	Fe^{3+}	$FeCl^+$	$FeCl_2^+$
	$HFeO_2^-$	$HZnO_2^-$	Zn^{2+}	$ZnCl^+$	ZnO_2^{2-}	-

In Figure 7.5, i.e. in the Fe-Zn-Cl-H_2O system, it can be seen that $ZnFe_2O_4$ is favoured over a large part of the FeOOH and the Fe_3O_4 domain. Its stability domain increases on the expense of these areas as well as on the $HFeO_2^-$ domain with increasing ion activities. The stability domain of $ZnFe_2O_4$ in the Zn-Fe-Cl-H_2O system naturally corresponds to the one in the Fe-Zn-Cl-H_2O system (see Figure 7.6), which sig-

nificantly increases the extent of passivity compared to the Zn-Cl-H_2O system (cf. Figure 7.4 [B]).

The positive attributes of $ZnFe_2O_4$ in terms of corrosion protection are well known from paint systems for corrosion prevention [Patton, 1973; Abu Ayana et al., 1997]. However, to our knowledge, these beneficial attributes have so far not been adapted or acknowledged in reinforcement corrosion countermeasures. On the contrary, the intermetallic layer formed between zinc and the iron substrate in hot-dip galvanising (cf. Section 6.3.2.5) is generally considered as not providing for corrosion resistance. Yet, we think that the lack of performance of this layer is related to the dissolution of the outer zinc layer, which compromises the concrete-steel interface and hence corrupts the corrosion protection.

If, however, zinc ferrite is present at a dense interface and initial dissolution of zinc ions is prevented (cf. Section 7.3.2), we consider zinc ferrite to provide for excellent corrosion resistance for steel in concrete.

This concept was verified in 'Test I' and 'Test II' by specimens "C-6" (cf. Section 1.9.3) and specimens "C03/W03", "C04/W04" (cf. Section 1.9.4), respectively. As mentioned in Section 1.9, after pretreatment, i.e. HCl etching in 'Test I' and grit-blasting in 'Test II', the associated rebar samples were electrolytically galvanised (cf. Section 2.6.2) with a thin zinc layer of 2 µm. The performance of this galvanised rebars embedded in mortar was verified by 'E_{corr}' monitoring (cf. Section 2.5.1 and 8.4.1.1), 'EIS' (cf. Sections 2.5.6 and 8.4.1.3), and polarisation curves (cf. Sections 2.5.4 and 8.4.1.4). All measurements showed that, in contrast to the loss of 5-10 µm for passivation of a pure thick zinc layer described in the literature (cf. Section 6.3.2.5), the zinc ferrite layer remained intact and lasted during an extended period even under severe chloride exposure [Küter et al., 2005b]. The performance of the zinc ferrite layer was also verified by means of visual inspection of the associated cement paste specimens and by 'E_{corr}' measurements before and after the cement paste was applied.

To avoid *any* hydrogen evolution the rebar samples were dipped into saturated $Ca(OH)_2$ solution (curing container, cf. Figure 8.5 in Section 8.1.2.2) before the cement paste was applied. Subsequent electrochemical measurements showed that the zinc ferrite layer was fully intact and provided for a significant gain in corrosion protection, which was also verified by 'EIS' and polarisation curve measurements (cf. Sections 2.5.4 and 8.4.1.4). However, the performance gain under worst conditions, i.e. with activated macrocell (connection to activated Ti 'ECat') and chloride exposure (cf. Section 1.9.1 and 1.9.2), was relatively negligible. So, the initial 2 µm zinc layer does not provide long-term protection against chloride induced corrosion. Yet, we consider this application of zinc a simple and cost-efficient measure against carbonation induced corrosion.

For ‘Principle I’ the initial corrosion activity of zinc is compensated by magnesium, which will be dealt with in Section 7.3.2. This way, a stable passive layer is maintained in correspondence with Figure 7.6 [B]. The Zn-Fe-Cl-H_2O ‘MEPD’ of Figure 7.6 [B] is superimposed on the “standard” Fe-Cl-H_2O system in Figure 7.7 [A]. In Figure 7.7 [A] it can be observed that the passive layer covers the identified critical part for corrosion initiation and thus protects the steel from chloride induced corrosion even at high concentrations. The extended protection is due to the attainment of relatively high zinc and iron ion activities, because ion diffusion is limited by the densified concrete-steel interface (cf. Section 7.3.2).

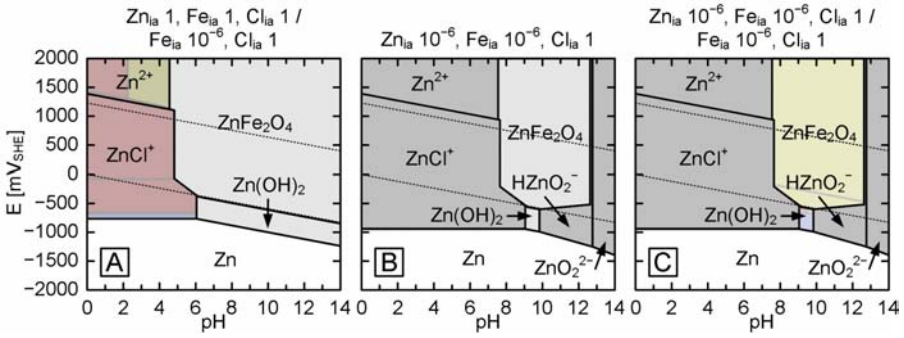

Figure 7.7: [A]: *‘SIPD’ of Zn-Fe-Cl-H_2O ‘MEPD’ based on Table 7.4 with Zn_{ia} = 1 mol/L, Fe_{ia} = 1 mol/L, and Cl_{ia} = 1 mol/L on Fe-Cl-H_2O ‘MEPD’ based on Table 5.4 and $Fe_{ia} = 10^{-6}$ mol/L and Cl_{ia} = 1 mol/L.* [B]: *Zn-Fe-Cl-H_2O ‘MEPD’ based on Table 7.4 with $Zn_{ia} = 10^{-6}$ mol/L, $Fe_{ia} = 10^{-6}$ mol/L, and Cl_{ia} = 1 mol/L.* [C]: *As [A], but with $Zn_{ia} = 10^{-6}$ mol/L and $Fe_{ia} = 10^{-6}$ mol/L for the superimposed Zn-Fe-Cl-H_2O ‘MEPD’.*

Figure 7.7 [A] represents the condition for ‘Principle I’ at an intact modified concrete-steel interface, i.e. for the general design situation. However, the condition at a discontinuity (e.g. at an unintended defect or at a cut-off) or in the vicinity of a concrete crack, where the surface modification may be compromised, is different. For these conditions as well as for the general design situation for ‘Principle II’, effective cathodic protection is aimed at. Effective cathodic protection can only be achieved if the sacrificial metal, i.e. the less noble coating or the sacrificial anode, is not passive in the critical pH and ‘E_{corr}’ range. That means that general passivation or passivation due to higher ion activities is to be prevented. The thermodynamics at a discontinuity in ‘Principle I’, which corresponds to the general design situation for ‘Principle II’, is represented by Figure 7.7 [B] and [C].

Figure 7.7 [B] illustrates the effect of the chloride ion activity on the Zn-Fe-Cl-H_2O ‘MEPD’ at low iron and zinc ion activities (10^{-6} mol/L). A comparison of Figure 7.6 [A] and Figure 7.7 [B] shows that, in contrast to systems where Fe is the main element, the appearance of stability domains in the Zn-Fe-Cl-H_2O system is almost identical for relatively low (10^{-6} mol/L) and high (1 mol/L) chloride ion activities. Hence,

zinc ferrite (in combination with magnesium, cf. Section 7.3.2) can provide for efficient cathodic protection, which is illustrated in Figure 7.7 [C].

Figure 7.7 [C] presents the superimposition of Figure 7.7 [B] on the "standard" Fe-Cl-H_2O 'MEPD', while (in contrast to Figure 7.7 [A]) sacrificial domains are shown transparently. It can be observed that sacrificial corrosion covers all critical areas when applied as a surface modification, i.e. 'Principle I'.

However, due to passivation in a pH range from 8-12, sacrificial action cannot be attained by zinc ferrite alone, when the countermeasure is based on sacrificial protection by embedded electrodes, i.e. 'Principle II'. Based on the predicted increase in passive domains with presence of calcium and/or carbon we consider that passivation can also be a problem of zinc used alone in concrete. Embedded electrodes are generally spatially separated from the defect, i.e. the area of possible corrosion initiation, and are not necessarily affected by pH changes. In our approach towards effective sacrificial anodes we provide for supplementary protection by magnesium (cf. Section 7.3.2).

We consider materials concepts, which are based on zinc as single sacrificial metal, not to be free of risks, as it is difficult to assure that zinc will be electrochemically active at any time (in particular, with regard to the general design service lives of concrete structures, cf. Section 6.1). Moreover, the mentioned precipitation of intermetallic particles leading to formation of galvanic cells on a zinc anode can compromise the anode efficiency.

In the Fosroc system (Galvashield XP, cf. Section 6.4.2) the embedded zinc slice is supposedly prevented from passivation by using a *"... highly alkaline cementitious mortar..."* [Fosroc, 2007]. While this might be an option to prevent damage after repair (e.g. for a number of years), we think that the necessary conditions are rather difficult to retain throughout customary design service lives. On the one hand, the current yield might be too low to be efficient, if the mortar is dense; on the other hand, the necessary high alkalinity, i.e. a pH above 13, is difficult to maintain in a relatively porous mortar that would allow for sufficient current yield. Thermodynamically the system is even more complex as an increasing concentration of zinc will increase the passivation domain of the zinc significantly in both directions, so that passivation of zinc can also be favoured at high pH (cf. Figure 7.3). Moreover, carbonation can largely interfere with the required high alkalinity (cf. Figure 7.4 [A]). We think that these aspects might explain that the lifetime of the Fosroc system is limited to 20 years [Fosroc, 2007].

7.3.2 Magnesium and Concrete-Steel System

From Section 7.3.1 it can be concluded that the purpose of implementing magnesium is based on densification of the concrete-steel interface, which is essential for 'Principle I', and its major contribution in lowering 'E_{corr}', which is crucial for both 'Principle I' and 'Principle II'. In addition to these benefits, the compounds formed in the

upper layer of the surface modification by the implementation processes utilised for 'Principle I' provide beneficial corrosion resistance at low 'E_{corr}'.

In this way magnesium mainly contributes to Bullets A and C concerning the thermodynamic approach, i.e. control of 'E_{corr}' and corrosion protection by other metals (cf. Section 7.2.1) as well as to Bullet F, i.e. the selected kinetic approach of improving the concrete-steel interface (cf. Section 7.2.2). Before the kinetic aspects of Mg are dealt with in the end of this Section, the thermodynamic features of magnesium in the concrete environment are discussed in the following.

The effect of increasing the magnesium ion activity is illustrated by 'SEPDs' of the Mg-H_2O system for different magnesium ion activities in Figure 7.8.

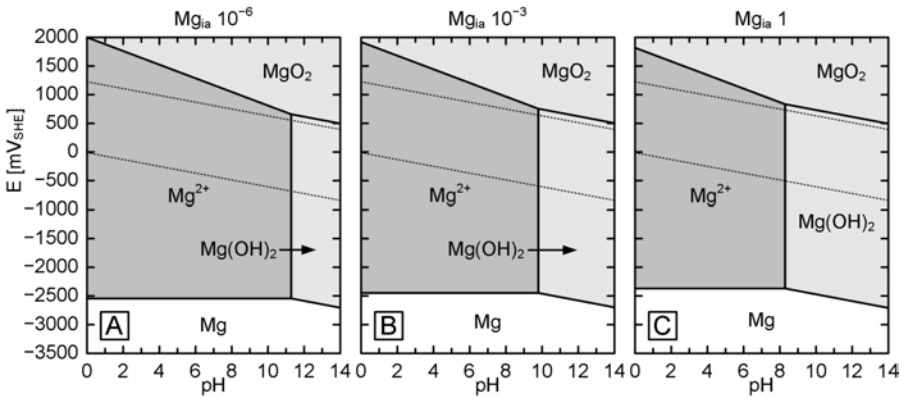

Figure 7.8: *Mg-H_2O 'SEPDs' based on Table 7.5 with different magnesium ion activities.* [A]: *$Mg_{ia} = 10^{-6}$ mol/L.* [B]: *$Mg_{ia} = 10^{-3}$ mol/L.* [C]: *Mg_{ia} = 1 mol/L.*

Table 7.5: *Species preselected for the 'SEPD' of the Mg-H_2O system.*

Solid	Mg	MgO_2	$Mg(OH)_2$
Soluble	Mg^{2+}	-	-

From Figure 7.8 [A] it can be concluded that, in contrast to zinc (cf. Figure 7.3 in Section 7.3.1), magnesium passivates at pH levels above 11.5, which makes it an interesting metal to combine with zinc for corrosion protection in concrete. Besides this favourable passivation domain, which increases towards lower pH levels with increasing ion activity (cf. Figure 7.8 [A] and [B]), the electronegativity (i.e. the very low equilibrium potential of magnesium) is of major importance in our implementation of Bullet A (and of Bullet F concerning electrochemical densification).

As illustrated in Figure 7.8, the entire immunity domain of magnesium is situated well below the stability domain of water. Thus, magnesium can be considered to be a very active metal and a powerful reducing agent (cf. Section 2.1.5). Magnesium has a high affinity to react with water, which it reduces under hydrogen evolution, when dissolv-

ing to Mg^{2+}. At pH values above 11.5, formation of a more or less protective layer of magnesium hydroxide ($Mg(OH)_2$) impedes this dissolution.

As illustrated in Figure 7.9 [A] the addition of chloride to the Mg-H_2O system does not interfere with the passive domains of Mg. Similar to the formation of $ZnCl^+$ in the Zn-Cl-H_2O 'MEPD' (cf. Figure 7.4 [B] and [C] in Section 7.3.1), formation of $MgCl^+$ is favoured in the associated region in the Mg^{2+} stability domain only.

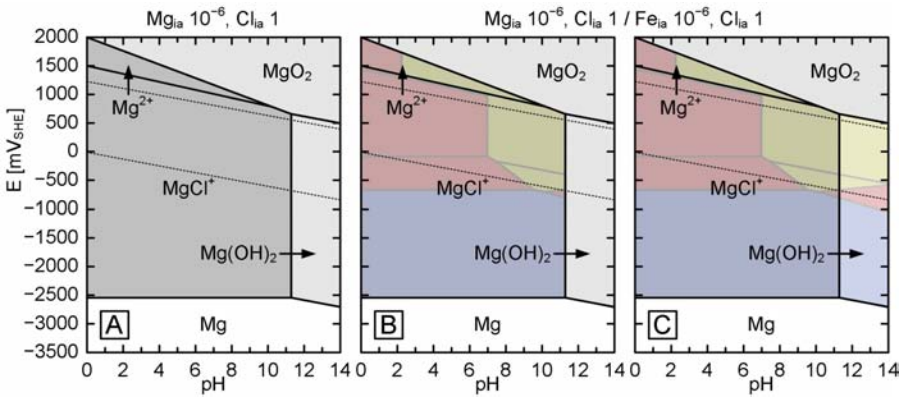

Figure 7.9: [A]: *Mg-Cl-H_2O 'MEPD' based on Table 7.6 with $Mg_{ia} = 10^{-6}$ mol/L and $Cl_{ia} = 1$ mol/L.* [B]: *'SIPD' of [A] on Fe-Cl-H_2O 'MEPD' based on Table 5.4 and $Fe_{ia} = 10^{-6}$ mol/L and $Cl_{ia} = 1$ mol/L. $MgCl^+$ domain is transparent illustrating theoretical conditions of cathodic protection with protective $Mg(OH)_2$.* [C]: *As [B], but $MgCl^+$ and $Mg(OH)_2$ domains are transparent illustrating theoretical conditions of cathodic protection with non-protective $Mg(OH)_2$.*

Table 7.6: *Species preselected for the 'MEPD' of the Mg-Cl-H_2O system.*

Solid	Mg	MgO_2	$Mg(OH)_2$	-
Soluble	Cl^-	ClO_4^-	Mg^{2+}	$MgCl^+$

In Figure 7.9 [B] and [C] the theoretical conditions for cathodic protection of iron in the chloride environment are illustrated. On the account of its electronegative nature, magnesium is generally considered to as a suitable anode for sacrificial protection of iron and other metals. The coupling of magnesium with a metal more noble than itself generally enables the 'E_{corr}' of this metal to be reduced to a value below the 'E_0' of its corrosion reaction. Thus, the galvanically connected metal can be rendered completely immune to corrosion (cf. Section 5.2.3). As for zinc, the anode efficiency of magnesium (and also that of its alloys) is closely connected to the characteristics of the passive layer. The conditions for its formation depend on the nature of the solution and on the nature of the impurities of the metal (and on the nature of the alloyed elements).

Figure 7.9 [B] and [C] represent the theoretical conditions for cathodic protection of iron by means of magnesium considering formation of protective and non-protective $Mg(OH)_2$, respectively. Industrially employed backfills for cathodic protection by magnesium have the primary objective of promoting formation of non-protective hydroxide [Pourbaix, 1974a; Pourbaix, 1974b]. Due to hydrogen evolution, the current yield at magnesium anodes rarely exceeds 30% to 50% of the theoretical yield. According to [Pourbaix, 1974a; Pourbaix, 1974b], *the current yield of magnesium anodes can be improved by surrounding them with a special chemical encapsulation (usually a mixture of gypsum and clay) or by alloying the magnesium with aluminium, zinc, or manganese.*

The proportioning of Mg, Zn, and additional compounds in combination with tailored implementation processes enable the described beneficial thermodynamic effects of Mg in the concrete environment without producing excessive amounts of hydrogen. These aspects are central in the development, but are not described in detail with regard to the expected patent possibilities (cf. Section 1.6).

An example for the importance of proper proportioning and implementation is given by the thermodynamic incompatibility of magnesium with the concrete-steel system. The incompatibility was experimentally verified, as shown in Figure 7.10.

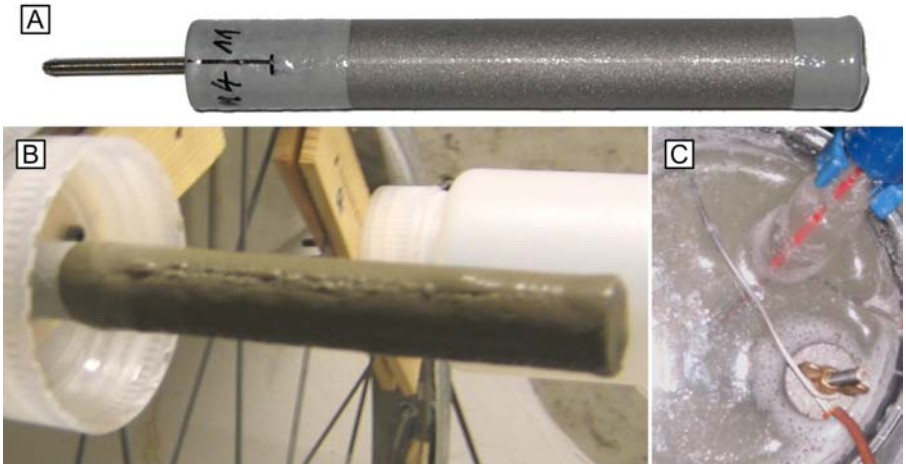

Figure 7.10: *Selected experiments concerning the interference of calcium carbonate with formation of magnesium hydroxide.* [A]: *Rebar sample prepared in correspondence with cement paste specimens (cf. Section 1.9.1) and magnesium wire [ET, 2000; ET, 2001] hammered in groves before grit-blasting.* [B]: *Rebar sample corresponding to [A] after dip-coating in cement paste (cf. Section 1.9.1 and Section 8.1.2.2).* [C]: *Rebar sample corresponding to [A] submersed in saturated calcium hydroxide solution and connected to additional magnesium wire sample.*

As discussed in the above and illustrated in Figure 7.8, magnesium should have a strong thermodynamic tendency to passivate at any 'E_{corr}' in (Portland) cement paste (cf. Section 3.1.3) as well as in saturated $Ca(OH)_2$ solution (pH 12-12.5). However, Figure 7.10 indicates that the magnesium wires embedded in a carbon steel sample (cf. Figure 7.10 [A]) do neither passivate in cement paste (cf. Figure 7.10 [B]) nor in saturated $Ca(OH)_2$ solution (cf. Figure 7.10 [C]).

The sample shown in Figure 7.10 [A] was prepared in the same way as the grit-blasted sample (cf. "C01" in Section 1.9.4), but before grit-blasting four 1 mm wide and deep longitudinal grooves were sawn with distances of 90° and magnesium wire [ET, 2000; ET, 2001] with a thickness of 1.2 mm was hammered into these grooves. When these samples were dip-coated in cement paste or submersed in saturated $Ca(OH)_2$ solution, a strong and long-lasting hydrogen evolution could be observed. The corrosion reaction lasted until a considerable amount of the magnesium wire was consumed, which is indicated by the bubbles formed along the wires in Figure 7.10 [B] and the bubbles gathering around the specimen in Figure 7.10 [C]. The corrosion reaction was only impeded after several hours by formation of a black smudge on the surface.

The performance of this rebar sample in cement paste and saturated $Ca(OH)_2$ solution was compared to submersion in other alkaline media at comparable pH levels, as e.g. saturated sodium hydroxide (NaOH). Moreover, magnesium wire was tested alone; with and without grit-blasting and with and without galvanic connection to the rebar sample in saturated $Ca(OH)_2$ and saturated NaOH solutions. The following was observed:

- Perfect passivation without visible hydrogen evolution on all samples submersed in NaOH solution
- Very little hydrogen evolution on Mg wire without grit-blasting and without connection to the rebar sample in $Ca(OH)_2$ solution
- Little hydrogen evolution on Mg wire with grit-blasting and without connection to the rebar sample in $Ca(OH)_2$ solution
- Medium hydrogen evolution on Mg wire without grit-blasting and connection to the rebar sample in $Ca(OH)_2$ solution
- Strong hydrogen evolution on Mg wire with grit-blasting and connection to the rebar sample in $Ca(OH)_2$ solution.

Hence, we postulate that the 'E_{corr}', the presence of calcium, and the surface condition of magnesium have a significant effect on the behaviour of magnesium in concrete. In the following this observation is reasoned as an interference between calcium carbonate ($CaCO_3$) and the formation of passive $Mg(OH)_2$. It is also shown that, despite the proposed thermodynamic incompatibility, thermodynamics can advantageously be applied in combination with experimental investigations, particularly measurements

of 'E_{corr}' and 'EDS' (cf. Section 3.2.2.2) to investigate and predict possible interferences.

Throughout Sections 3.1.7.2 (carbonation), 5.2.1.1 (calcite), and 7.3.1 (calcium hydroxyzincate) it was shown that calcium is a central compound in concrete. With regard to carbonation it was mentioned that calcium hydroxide reacts most readily with CO_2 (cf. Section 3.1.7.2):

$$CO_2 + Ca(OH)_2 \rightarrow CaCO_3 + H_2O \quad \left(\Delta G^0 = -73\,\text{kJ} \right) \qquad [7.1]$$

The Ca-Mg-C-H_2O and the Mg-Ca-C-H_2O system are represented by the associated 'MEPDs' in Figure 7.11 [A] and [B] to establish the thermodynamic background of the proposed mechanism. Figure 7.11 [C] to [D] illustrate the essential steps in the proposed interference between $CaCO_3$ and formation of $Mg(OH)_2$.

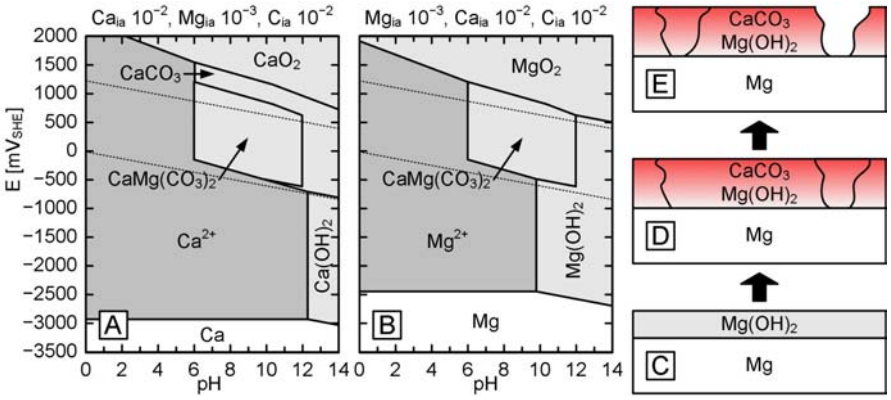

Figure 7.11: *Proposed mechanism for the interference of calcium carbonate and the formation of magnesium hydroxide.* [A]: *Ca-Mg-C-H_2O 'MEPD' based on Table 7.7 with $Ca_{ia} = 10^{-2}$ mol/L, $Mg_{ia} = 10^{-3}$ mol/L, and $C_{ia} = 10^{-2}$ mol/L.* [B]: *Mg-Ca-C-H_2O 'MEPD' with preselection and Mg_{ia}, Ca_{ia}, and C_{ia} as in [A].* [C] to [E]: *Sketches of the proposed mechanism for the inference of calcium carbonate and the formation of magnesium hydroxide.*

Table 7.7: *Species preselected for the 'MEPD' of the Ca-Mg-C system and the Mg-Ca-C-H_2O system*[*].

Solid	C	Ca	$CaCO_3$	$CaMg(CO_3)_2$	CaO
	CaO_2	$Ca(OH)_2$	Mg	MgO_2	$Mg(OH)_2$
Soluble	Ca^{2+}	$Ca(OH)^+$	CO_3^{2-}	HCO_3^-	Mg^{2+}

[*] The most notable change from the Ca-H_2O system postulated in [Pourbaix, 1974b] is that magnesium hydride (CaH_2) is not included in the preselection of elements, as it is considered to be unstable in the presence of water.

For both exposure situations shown in Figure 7.10 [B] and [C] CO_2 is available from the atmosphere and we assume that even small amounts enable the formation of $CaCO_3$. However, we expect the similar interferences to take place in absence of CO_2, e.g. based on reactions with the various calcium compounds in concrete (cf. Section 3.1.3).

While we regard the formation of calcium compounds to be favourable for the extent of passive domains for steel (cf. Section 5.2.1.1) and zinc (cf. Section 7.3.1), we think that this does not apply for magnesium. For both exposure situations shown in Figure 7.10 [B] and [C], we assume that $CaCO_3$ will deposit on the Mg or the $Mg(OH)_2$ surface. Yet, in contrast to steel and zinc, it inhibits the formation of a passive layer. As indicated in Figure 7.10 [D], we assume that $CaCO_3$ deposits on the Mg or the (imperfect) $Mg(OH)_2$ surface, which results in small cracks. $Mg(OH)_2$ is formed at the same time, but $CaCO_3$ will be integrated in the layer leading to considerable defects, e.g. due to stress release, see Figure 7.10 [E]. At these defects, hydrogen evolution can be expressed by the sum of oxidation of Mg to $Mg(OH)_2$:

$$Mg + 2OH^- \rightarrow Mg(OH)_2 + 2e^- \quad \left(E_0^0 = -2692\,mV_{SHE} \right) \qquad [7.2]$$

and the reduction of water in neutral and alkaline solutions (cf. [2.59]):

$$2H_2O + 2e^- \rightarrow H_2 + 2OH^- \quad \left(E_0^0 = -828\,\{-828\}\,mV_{SHE} \right) \qquad [7.3]$$

These reactions persist, since the interference of $CaCO_3$ hinders the formation of mechanical stable $Mg(OH)_2$ layer. When the Mg wire was not galvanically connected to the rebar, $Mg(OH)_2$ could be formed with very little or little hydrogen evolution, because $CaCO_3$ could not be formed at low 'E_{corr}' (cf. Figure 7.10 [A]). So, the worst interference takes place if the top of the layer is at a potential, which favours precipitation of $CaCO_3$. The same holds for cases, where the surface area is small and initially passive, as for Mg wires that were not grit-blasted.

The above theoretically reasoned mechanism was confirmed by 'SEM' and 'EDS' observations. The described (stress release) cracking and the black smudge, which we assume to represent the intermetallic compounds formed between Mg and Fe, can be clearly observed in the secondary electron and back-scattered 'SEM' photographs shown in Figure 7.12 [A] and [B], respectively.

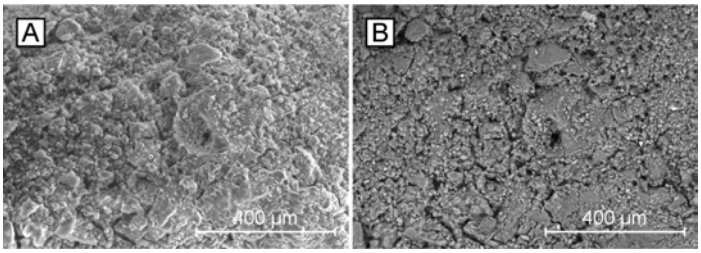

Figure 7.12: *Scanning electron microscopy of grit-blasted magnesium wire after submersion in saturated calcium hydroxide solution.* [A]: *Secondary electron.* [B]: *Back-scattered.*

The presence of both carbon and calcium in the smudge layer was verified by 'EDS' mapping (cf. Section 3.2.2.2, [EDAX, 2006; FEI, 2007]), see Figure 7.13. The associated 'EDS' spectrum is shown Figure 7.14.

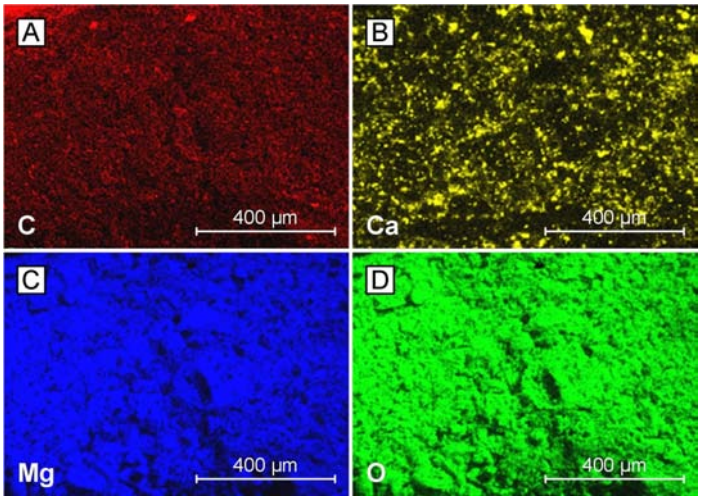

Figure 7.13: *Mapping of elements based on energy dispersive spectroscopy of area shown in Figure 7.12.* [A]: *Carbon.* [B]: *Calcium.* [C]: *Magnesium.* [D]: *Oxygen.*

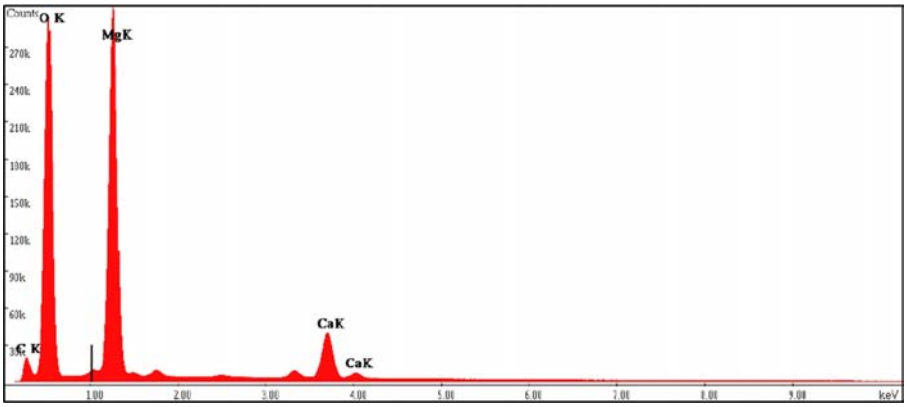

Figure 7.14: *Energy dispersive spectra for the investigated area and elements of Figure 7.13 specifying the associated X-ray energies on the X-axis and the relative X-ray counts on the Y-axis.*

In addition to the visual appearance, we think that the presence and amount of calcium (cf. Figure 7.12, Figure 7.13, and Figure 7.14) in the smudge layer is a positive indicator for the postulated mechanism.

As illustrated by the stability domain of calcium carbonate, the critical region extends throughout the theoretical water stability domain for alkaline solutions. Thus, the interference of $CaCO_3$ with the formation of a passive $Mg(OH)_2$ layer and the associated hydrogen evolution are of major importance.

Besides the thermodynamic aspects of magnesium for both 'Principle I' and 'Principle II', its kinetic effect, i.e. a significant improvement of the concrete-steel interface (cf. Bullet F in Section 7.2.2), play a major role for 'Principle I' countermeasures. The concrete-steel interface improvement is designed to be obtained in two ways: by electrochemical densification as well as by pore-blocking through precipitation of magnesium compounds. In Figure 3.14 in Section 3.3 it was indicated that according to [Buenfeld et al., 2004] the chloride threshold could be more than tripled (from 0.5% 'w/w_{ce}' to around 1.7% 'w/w_{ce}' at a void content of about 1%) by a special electrochemical treatment during the first days after casting (cf. Section 6.3.1.5). We think that the main effect of the described electrochemical treatment is obtained by the targeted cathodic polarisation during setting of the concrete, i.e. by holding the carbon steel reinforcement at around −700 mV_{SHE} for the first 18 hours after casting.

In addition to electrochemical densification, pore-blocking through products from the cement paste (cf. Section 3.1.3) and the pore solution (cf. Section 3.1.5) combining

with magnesium* plays an important role for 'Principle I'. The stability domain of calcium magnesium carbonate (dolomite, $CaMg(CO_3)_2$) is indicated in Figure 7.10 [A] and [B]. Among other minerals formed under this conditions [MinDat, 2007; MinGal, 2007; WebMin, 2007], we consider the contribution of dolomite to be most important in sealing pores (cf. Section 3.1.4) and cracks in the micro to intermediate range (cf. Table 3.5 in Section 3.1.11.1).

The benefits of the obtained interface densification in combination with the thermodynamic aspects realised by the implementation of zinc (cf. Section 7.3.1) and magnesium are the central aspects of our proposed new countermeasures. Selected indicative information on the implementation of two different principles of implementation and their intended application on a structural scale are given in Section 7.4.

7.4 Implementation and Structural Applications

In Sections 7.2.1 and 7.2.2 the thermodynamic and kinetic approaches for our proposed new countermeasures were discussed and reasoned. The two principles of implementation for the realisation were summarised in Section 7.2.3 and the most important features of the materials concepts were introduced in Section 7.3. Due to the expected patent possibilities (cf. Section 1.6), detailed information on the processes designed for the production and implementation of the countermeasures is not provided in the present thesis. However, an indicative outline of the implementation and possible structural applications is given.

The design features, i.e. the implementation of the materials concepts, for the realisation of the thermodynamic and kinetic approaches, include:

- For both 'Principle I' and 'Principle II':
  - Proper proportioning of zinc and magnesium and suitable processes for their implementation in combination with additional materials allow for operation at a targeted low 'E_{corr}' (cf. Bullet A in Section 7.2.1).
  - The processes designed for the implementation of the principal materials concepts (cf. Section 7.3) allow for controlling the thermodynamic state. This means, among others, that passivation of the implemented materials is "activated" and "deactivated" as required. Moreover, undesired effects, e.g. the interference between $CaCO_3$ and formation of $Mg(OH)_2$ (cf. Section 7.3.2), are controlled.

* In concrete technology it is well known that magnesium effectively seals surface pores, if concrete is exposed to solutions containing magnesium, e.g. seawater. Among others, this shows that also for concrete (as for steel) exposure to chloride solution differs from exposure to actual seawater (with the same chloride content), cf. corrosion properties of steel in chloride solution and sea water (cf. Section 2.3.3).

  - Low consumption rate and "on demand" consumption provide for long-term reliability and efficiency, while the system is virtually free of maintenance.

- For 'Principle I', i.e. countermeasures based on surface modifications:

  The desired 'Principle I' properties indicated in Section 7.2.3 are accomplished by custom-designed processes to obtain a *layered surface modification*. The modified reinforcement surface is zinc-rich on the inside, i.e. at the rebar interface, and has high magnesium content at the outside, i.e. at the concrete interface. Based on this approach the following features are obtained:

  - The magnesium in the top layer passivates the outer perimeter of the surface modification during and after casting (cf. Section 7.3.2) and thus protects the zinc-rich inside layer from initial dissolution. Zinc remains close to the rebar providing corrosion protection by formation of compounds with improved corrosion resistance in combination with the carbon steel surface, i.e. zinc-ferrite (cf. Bullet B in Section 7.2.1 and Section 7.3.1). This special feature of 'Principle I' is further elaborated based on Figure 7.15 and Figure 7.16 subsequent to this list.
  - The targeted 'E_{corr}' obtained by the thermodynamically stable compounds at the outer perimeter of the surface modification repels chloride ions and provides for an 'E_{corr}' range, which is well below the chloride pitting potentials of the associated compounds in alkaline concrete. This measure corresponds to protection of the Fe-H_2O system by metals with improved corrosion resistance (cf. Bullet C in Section 7.2.1 and Section 7.3.2).
  - An initial (and most significant) improvement of the concrete-steel interface (cf. Bullet F in Section 7.2.2) is achieved by electrochemical densification due to the targeted low 'E_{corr}' during setting of the concrete (cf. Sections 3.3, 6.3.1.5, and 7.3.2).
  - In case of a pH drop due to carbonation or in case of crack formation in the concrete bulk, magnesium is dissolved from the outer perimeter and precipitates in the immediate vicinity to form dolomite, which leads to a secondary densification at the concrete-steel interface (cf. Section 7.3.2). Within the densified area zinc-ferrite effectively protects the underlying carbon steel with little to no tendency of outwards diffusion (cf. Section 7.3.1). The associated regions are additionally cathodically polarised by the activated magnesium compounds (cf. Figure 7.15 and Figure 7.16 subsequent to this list).
  - Where the surface modification is discontinued, i.e. at an unintended or induced (e.g. cut-offs) defect, the exposed carbon steel surface is cathodically protected by the activated magnesium compounds (cf. Section 7.3.2) and/or the zinc-ferrite (cf. Section 7.3.1) in the vicinity of the defect.

- For 'Principle II', i.e. countermeasures based on embedded electrodes:

For the practical realisation of the intended 'Principle II' features indicated in Section 7.2.3 two dissimilar processes for the implementation of the material concepts introduced in Section 7.3 are presently under consideration. Both options are based on embedded sacrificial anodes providing for efficient cathodic protection (cf. Bullet A in Section 7.2.1). *The first option relates to a doped metal approach, while the second option is based on combining processed zinc and magnesium compounds in an electrochemical active, porous encapsulation*. The most important aspects and features of both options include:

- A process for the implementation in the materials concept designed in a way, so that the sacrificial anode can provide efficient targeted cathodic polarisation at any time (after the set of concrete). The principal materials concepts (cf. Section 7.3) are proportioned and combined with secondary compounds in the production process, so that sufficient current yield is available and electrochemical inefficiencies, e.g. due to hydrogen evolution at local cathodes, impurities, or undesired surface chemistry changes (cf. Section 7.3), are prevented.
- Initial densification of the electrode-concrete interface is *omitted* by a special surface treatment of the sacrificial anodes to allow for a high current yield.
- Secondary densification by precipitation of dissolved magnesium is *limited* by means of the special materials concept.

Based on the above it can be concluded that both principles of implementation largely benefit from the targeted 'E_{corr}' obtained by the customised processes for the implementation of the described material concepts (cf. Section 7.3). So, the real task is to "activate" and "deactivate" passivation of the implemented principal compounds, i.e. the zinc (cf. Section 7.3.1) and magnesium (cf. Section 7.3.2), as required. This also relates to the protecting function that the magnesium provides to the zinc in the layered surface modification of 'Principle I'. This mechanism is explained by means of Figure 7.15 and Figure 7.16, which illustrate protection of the zinc-rich layer by the outer magnesium-rich layer and protection of carbon steel by zinc-ferrite and magnesium, respectively.

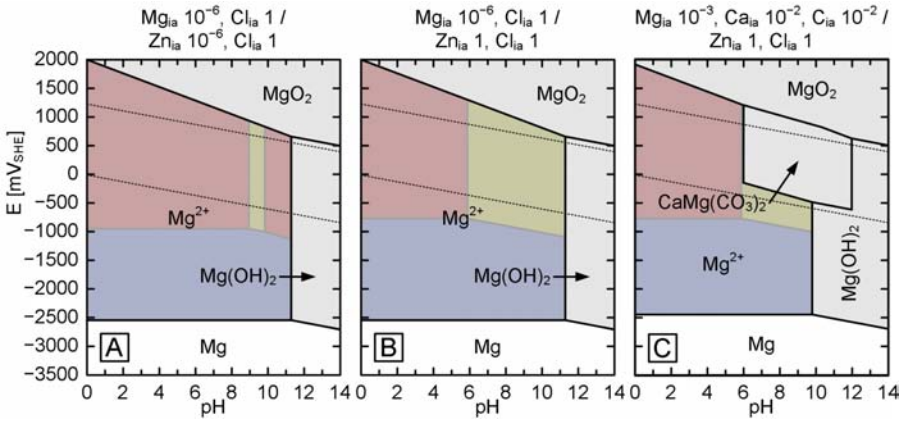

Figure 7.15: [A]: *'SIPD' of Mg-Cl-H_2O 'MEPD' based on Table 7.6 with Mg_{ia} = 10^{-6} mol/L and Cl_{ia} = 1 mol/L on Zn-Cl-H_2O 'MEPD' based on Table 7.3 with Zn_{ia} = 10^{-6} mol/L and Cl_{ia} = 1 mol/L.* [B]: *As [A], but with Zn_{ia} = 1 mol/L.* [C]: *As [B], but Mg-Cl-H_2O 'MEPD' replaced by Mg-Ca-C-H_2O 'MEPD' based on Table 7.7 with Ca_{ia} = 10^{-2} mol/L, Mg_{ia} = 10^{-3} mol/L, and C_{ia} = 10^{-2} mol/L.*

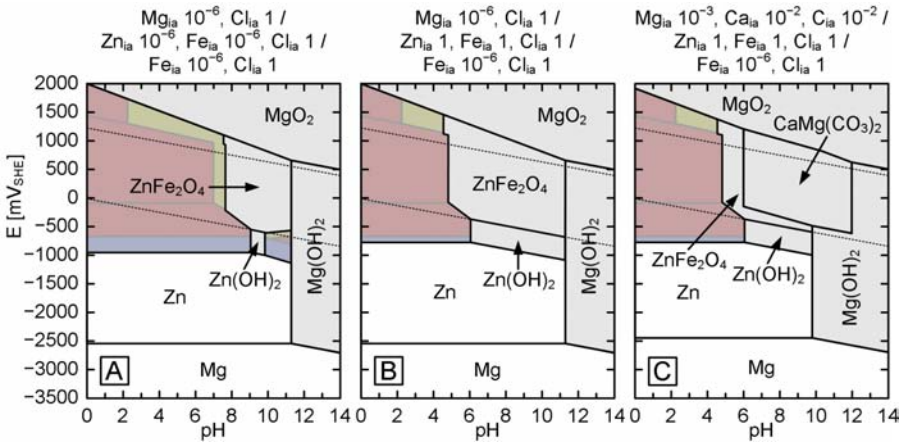

Figure 7.16: [A]: *'SIPD' of Mg-Cl-H_2O 'MEPD' based on Table 7.6 with Mg_{ia} = 10^{-6} mol/L and Cl_{ia} = 1 mol/L on Zn-Fe-Cl-H_2O 'MEPD' based on Table 7.4 with Zn_{ia} = 10^{-6} mol/L, Fe_{ia} = 10^{-6} mol/L, and Cl_{ia} = 1 mol/L on Fe-Cl-H_2O 'MEPD' based on Table 5.4 and Fe_{ia} = 10^{-6} mol/L and Cl_{ia} = 1 mol/L.* [B]: *As [A], but Zn-Fe-Cl-H_2O 'MEPD' with Zn_{ia} = 10^{-6} mol/L.* [C]: *As [B], but Mg-Cl-H_2O 'MEPD' replaced by Mg-Ca-C-H_2O 'MEPD' based on Table 7.7 with Ca_{ia} = 10^{-2} mol/L, Mg_{ia} = 10^{-3} mol/L, and C_{ia} = 10^{-2} mol/L.*

The protective function of magnesium for the lossless passivation of zinc as well as the protective function of zinc-ferrite for the underlying carbon steel, which is

achieved by the protection granted by the magnesium, is immediately obvious in Figure 7.15 and Figure 7.16, respectively. Moreover, the theoretical operational range for the targeted 'E_{corr}' achieved by proportioning of the principal material concepts can be estimated from Figure 7.16.

The processes designed for the implementation of the proposed new countermeasures differ not only between the two principles of implementation, but also with regard to the application in new and existing structures. The preliminary remarks on the intended structural application given below are subdivided in relation to their application in new and existing structures:

- 'Principle I' for new structures, i.e. initial countermeasures:

  For new structures the establishment of the layered surface modification is intended to be based on an automated sequence of three processes. The processes are relatively simple and can be assembled in a transportable device, so that they can be performed on site. Ideally, single carbon steel rebars are to be processed in convenient batch sizes (at any length), while processing of e.g. 3D cages is optional if a quality loss of the surface modification is acceptable.

  The first process in the sequence is a cleaning process based on grit-blasting. With regard to the results obtained in 'Test I' and 'Test II' (cf. Sections 1.9.3 and 1.9.4) grit-blasting is considered to be more efficient in removing corrosion products and scale, etc. from the carbon steel rebar surface (cf. Section 3.2.2) than e.g. electrochemical techniques (cf. Section 2.6.1). Moreover, 'Test II' results indicated that the increased surface area obtained with grit-blasting is advantageous in the protective function of the inner-zinc rich layer. Details on the second and third processes in the sequence are not given in this thesis with regard to the expected patent possibilities (cf. Section 1.6).

- 'Principle I' for existing structures, i.e. repair techniques

  The processes of applying 'Principle I' in the repair of existing structures are similar to the ones applied for new countermeasures with the difference that the threefold process sequence is applied to built-in rebars as opposed to batches of single rebars. The preparation and the performances following the application of the threefold application process are based on the tasks performed in conventional patch repair (cf. Section 6.4.2). In contrast to the automated sequence used for initial measures, the processes in the application of 'Principle I' for existing structures are to be performed manually one after the other. While the cleaning process is also based on grit-blasting, the application of the second and third process in repair differs from implementation for new structures. As for the previous Bullet, details on the second and third processes in the sequence are not given in this thesis with regard to the expected patent possibilities (cf. Section 1.6).

- 'Principle II' for new structures, i.e. initial countermeasures

In contrast to repair, where the installation of sacrificial anodes is generally limited to damaged regions, designing sacrificial cathodic protection as an initial measure grants various options for anode layouts and positioning. Details regarding geometry and placing are not dealt with in the present thesis, but one option under consideration should be mentioned.

Implementing the sacrificial anodes by means of concrete spacers can be a cost-efficient and practical solution for new structures. For constructive reasons a large number of spacers is generally in contact with the outer reinforcement layer, i.e. the layer that is foremost affected by corrosion. Spacers could be easily equipped with (for the doped metal option) or produced as (for the encapsulation option) sacrificial anodes and thus the reinforcement could be protected without the need for any further installations and without changing the standard practice on site.

- 'Principle II' for existing structures, i.e. repair techniques

  Repair by 'Principle II' is based on the same performances, as described for the application of the Galvashield XP anode system. The placement and possible layouts for the sacrificial anode are governed by the extent and geometry of the patch repair. Both options for the implementation of the materials concepts, i.e. the doped material and the encapsulation option, are available for repair.

Both principles of implementation are suitable for most exposure situations, while it is obvious that the concrete needs to be at a certain saturation level, so that countermeasures based on 'Principle II' are effective. This is generally the case for marine structures, but not necessarily for structures seasonally exposed to deicing salt. In such conditions combinations of the two principles of implementation could also be an option if exposure conditions are severe. That means that sacrificial anodes provide additional protection for the surface modification at increasing degree of saturation, which is generally critical in relation to chloride induced corrosion (cf. Section 5.2.2.2). For this combined application as well as for the application of 'Principle I' or 'Principle II' alone, the degree of protection can be designed to meet the requirements (i.e. the service life) by adjusting the extent of the surface modification for 'Principle I' or the amount or layout of the sacrificial anodes for 'Principle II'.

Finally, the development and implementation of effective corrosion sensors played a secondary role in our theoretical considerations and practical realisation for both principles of implementation. Corrosion monitoring may be implemented based on a modified layout of the instrumented mortar specimen in combination with the electrochemical measurements, which were briefly described in Section 1.9.1 and will be further elaborated in Sections 8.1.2.1 and 8.4.1. We consider that developments in this direction can be particularly interesting in combination with the application of 'Principle II' by means of concrete spacers aiming at the establishment of a "smart spacer" solution.

Both principles of implementation are based on using relatively small proportions of zinc and magnesium in combination with inexpensive and ecological compounds and production processes. Besides these aspects, which are central in fulfilling the two final requirements stated in Section 7.1 (cf. Bullets 5 and 6), it is evident that the other requirements concerning improved corrosion resistance for new and existing structures (cf. Bullet 1), structural performance as well as reinforcement and concrete durability (cf. Bullet 2), cracking of the concrete (cf. Bullet 3), and finally the various practical requirements (cf. Bullet 4) are also fulfilled.

Thus, we think that further development and extensive testing (cf. Section 1.5) of the proposed new countermeasures could present suitable alternatives for efficient, but expensive or impractical available countermeasures, as e.g. stainless steel (including selective use, cf. Section 6.3.2.3) and 'CPre'/'CP' (cf. Sections 6.3.2.6 and 6.4.1), in the future. While the main developments, i.e. countermeasures based on 'Principle I' and 'Principle II', generally aim at chloride exposure, we assume that carbonation alone could be efficiently addressed by the zinc-ferrite protection mechanism achieved by the thin zinc layer approach (cf. Section 7.3.1).

7.5 Preliminary Testing Aspects and Requirements

In this Section requirements and aspects that we consider to be essential in preliminary testing of new countermeasures are discussed (cf. phase 4 in Figure 7.1). Emphasis is set on electrochemical testing (cf. Section 7.5.1), while the most important additional measurement techniques are only listed and briefly commented upon (cf. Section 7.5.2). The electrochemical testing techniques are based on the theory of measurements and monitoring in aqueous metallic corrosion (cf. Section 2.5), while the listed additional techniques relate to the chemical testing as well as to the microscopic and X-ray analyses, which were introduced throughout Chapter 3. Our application of these techniques, i.e. their implementation in our experimental investigations (cf. Section 1.9) is described in more detail in Section 8.4.

7.5.1 Electrochemical Techniques

In this Section the application of the electrochemical measurement techniques available in the area of aqueous metallic corrosion (cf. Section 2.5) for our experimental purposes, i.e. for the performance evaluation of corrosion countermeasures, is discussed. The electrochemical techniques selected for our purposes include corrosion potential monitoring (Section 8.4.1.1), corrosion current monitoring (Section 8.4.1.2), 'EIS' (Section 8.4.1.3), and polarisation curves (Section 8.4.1.4).

7.5.1.1 Corrosion Potential Monitoring

Besides measuring 'E_{corr}' in order to access the thermodynamic state of the investigated system (cf. Section 2.5.1), 'E_{corr}' monitoring can also be applied for the direct

identification of corrosion initiation, since the breakdown of the passive layer is generally associated with a shift of the order of 200-500 mV to a lower 'E_{corr}' (cf. Sections 2.1.9 and 5.1.2). As discussed in Section 5.1.2, this potential drop occurs rather gradually and unsteadily, particularly for chloride-induced corrosion. This means that it is often difficult to identify the exact time of corrosion initiation using 'E_{corr}' monitoring. Another major drawback of potential monitoring is that it only reflects the thermodynamic state of the rebar. Thus, it can be estimated whether the rebar is in the passive or active state, but no information on the kinetics and consequently on the corrosion rate can be obtained. Despite these drawbacks and other inconsistencies related to 'E_{corr}' measurements (e.g. [Montemor et al., 2003]) potential mapping in accordance with e.g. [ASTM C876, 1999] can be a useful method for corrosion assessment on a structural scale, e.g. to identify areas of possible corrosion prior to destructive inspection by excavation.

For corrosion assessment on a structural scale, the 'E_{corr}' of the *same type of steel in the same type of concrete* is mapped, while taking into account the influence of exposure conditions. However, laboratory investigations generally aim at testing the effect of e.g. *different reinforcement materials, surface modifications, concrete types, or inhibitors* on corrosion initiation and propagation. These factors may have a considerable influence on 'E_{corr}' in the passive state and hence on the potential drop with corrosion initiation. On the one hand, these factors limit application of 'E_{corr}' monitoring for the assessment of the corrosion state. On the other hand, the differences observed in the passive 'E_{corr}' and in the potential drop contain useful thermodynamic information on the actual protection and corrosion mechanisms.

Details on the implementation of 'E_{corr}' monitoring in our final experimental setup (cf. Section 1.9.1) are given in Section 8.4.1.1.

7.5.1.2 Corrosion Current Monitoring

Laboratory testing usually targets at the exact time of corrosion initiation as well as at the corrosion rate. We consider current monitoring to be a more precise technique for quantifying the onset of active corrosion than 'E_{corr}' monitoring and, in contrast to 'E_{corr}' monitoring, it can provide information on the corrosion rate. In principle, there are two methods for current monitoring relevant for reinforcement corrosion testing, i.e. macrocell current monitoring (cf. Section 2.5.2) and potentiostatic monitoring (cf. Section 2.5.3).

As mentioned in Section 2.5.2, macrocell current monitoring is based on the creation of a galvanic cell and measuring of the 'i_{mac}' over a resistor or, even better, over a zero-impedance ammeter without introducing resistivity to the system. The rebar represents the anode of the galvanic cell and the cathode can either be embedded in the specimen (e.g. [Schießl & Raupach, 1990; ASTM G109, 2005]) or submerged in the exposure solution (e.g. [Buenfeld et al., 2004]). Embedding allows the use of or-

dinary carbon steel as a cathode, if the carbon steel is positioned in cathodic locations [Schießl & Raupach, 1990]. Yet, often inert cathodes, e.g. stainless steel or graphite, are used, which allows arbitrary positioning and a smaller specimen size.

As an external cathode 'ECat', i.e. a cathode submerged in the exposure solution, only materials which are inert and nobler than the passive steel rebar embedded in the test specimen can be used. For instance, activated Ti is an inert, noble, and electrochemically active material (cf. Section 8.1.1) and has been successfully used as an external cathode (e.g. [Buenfeld et al., 2004]).

The second option for current monitoring, i.e. potentiostatic monitoring, is based on monitoring the corrosion activity by measuring the current which is passed from a 'CE' to the rebar, i.e. the 'WE', to maintain its 'E_{corr}' by means of a potentiostat (cf. Section 2.5.3. The 'CE' is either embedded in the sample (e.g. [Arup & Sørensen, 1995; Sandberg, 1998]) or submerged in the exposure solution (e.g. [Nygaard & Geiker, 2005]).

Unlike the current supplied from the 'CE' to maintain the rebar potential in potentiostatic monitoring, the macrocell current reflects the corrosion current, which means that the measured current can be used for an estimation of the corrosion rate. The measured current can also be integrated and expressed as the current charge passed. However, macrocell current only represents a certain fraction of the total corrosion activity, because the localised microcell corrosion activity on the rebar itself is not accessed (cf. Sections 2.5.2 and 6.4.2).

In both configurations, potentiostatic control and macrocell creation, a sharp and defined rise in the monitored current, e.g. from a few microamps to tens and hundreds of microamps, indicates the onset of active corrosion. This means that corrosion initiation can be quantified more precisely than by 'E_{corr}' monitoring. The disadvantage of current monitoring is that it affects the thermodynamics of the rebar. The use of an embedded rebar as a cathode in defined positions has the least impact, but restricts the layout of the test specimens and exposure setup. Potentiostatic control does not allow any conclusions based on 'E_{corr}' monitoring, because 'E_{corr}' is fixed. Moreover, it is unclear how much effect a constrained 'E_{corr}' has on corrosion initiation. In contrast to potentiostatic control, macrocell creation tolerates fluctuations of the rebar potential, but a noble 'ECat' raises the 'Ecorr' of the rebar and thus has a significant effect on the thermodynamic state and accordingly on corrosion initiation and propagation.

As indicated in Section 1.9.1, we selected macrocell creation by means of a noble 'ECat' as method for current monitoring. This approach is reasoned in Section 8.4.1.2, where also its implementation in the final test setup is introduced.

7.5.1.3 Electrochemical Impedance Spectroscopy

The advantage of both potential and current measurement is that these techniques can be carried out as continuous monitoring. Another corrosion assessment technique,

'EIS', is not performed as continuous monitoring, but as individual runs. 'EIS' is based on the same principles as polarisation resistance measurement, but small potential perturbation 'ΔE_p' in the order of e.g. 10 mV is applied to the rebar at varying frequencies and the resulting density response 'Δi_p' is measured (cf. Section 2.5.6). In this way, valuable information on a number of parameters concerning the presence and characteristics of passive layers as well as on the bulk concrete (or mortar/cement paste, cf. Section 1.9.2) attributes are obtained with very limited perturbation of 'E_{corr}'. Additional background information on the application of 'EIS' for testing of reinforcement corrosion and comparisons to other electrochemical methods is available in the literature (e.g. [Berke & Hicks, 1990; Sagüés, 1991; Bentur et al., 1997; Koleva et al., 2006]).

As mentioned in Section 2.5.6, 'EIS' data can be represented by either Nyquist or Bode plots; our analysis was focused on Nyquist plots. That is due to the advantage of Nyquist plots in providing a beneficial overview of the data allowing rapid qualitative interpretations. Depending on the configuration and frequency range, Nyquist plots show fractions of two arcs separated by a cusp. The first arc represents the bulk resistivity, e.g. the resistivity of the mortar between the embedded 'REs' and the 'WE' (cf. Section 1.9.1), while the second arc represents the resistivity of the 'WE' surface, i.e. the thermodynamic state of the rebar. This illustrative representation allows for insightful comparisons of data. For instance, comparison of Nyquist plots of the same specimens at different time intervals provides information on changes in the electrochemical properties of the rebar surface and the bulk between the rebar and the 'RE'. Moreover, a lot of information can be obtained by comparing 'EIS' data from the same time interval for specimens with different properties, e.g. concrete mixes and additions, steel qualities, and steel surface properties [Küter et al., 2005b]. Conclusive identification of the corrosion state can also be achieved based on individual runs, e.g. measured in the low frequency domain around 1 mHz [Bentur et al., 1997].

To obtain representative and reproducible data is has to be assured that conditions are stable during the 'EIS' run. 'EIS' data is largely affected by the geometry and layout of the test specimen [Andrade et al., 1995b]. In particular, the position, geometry, and electrochemical properties of the 'RE' have a significant effect on the measurements [Hsieh et al., 1996; Hsieh et al., 1997]. So, with regard to stability at low frequencies and, even more importantly, in order to generally provide for reproducibility of data, special design considerations are necessary for the test specimen and the applied equipment. Our principal EIS specimen, i.e. the instrumented mortar specimen (cf. Section 1.9.1) was designed to meet these requirements. The features of the instrumented mortar specimen and our implementation of EIS measurements on the final test setup are described in more detail in Sections 8.1.2.1 and 8.4.1.3, respectively.

7.5.1.4 Polarisation Curves

The theory behind polarisation curves in aqueous metallic corrosion and their application as a measurement technique are discussed in Sections 2.2.5 and 2.5.4, respectively. It was emphasised that polarisation curves can be useful in determining the rate of the anodic and cathodic reactions that take place at a certain electrode potential. Unfortunately, determination of polarisation curves is much more complicated for metals in concrete (or mortar/cement paste, cf. Section 1.9.2) than for metals in aqueous solutions. The main problem is that diffusion phenomena in the cement paste are very slow (cf. Sections 2.2.4.2, 3.1.3, and 3.1.6.1). Besides the slow kinetics, the physical and chemical conditions of the concrete-steel interface and the bulk are being altered during the measurement (cf. Sections 5.2.2.2 and 7.3.2) or cracking may change the properties of the investigated system entirely (cf. Section 5.2.2.1). Moreover, resistance effects, i.e. the combined resistance of the solution and the concrete (or mortar/cement paste, cf. Section 1.9.2) bulk between the 'WE' and the 'RE', are of particular importance for measurements on embedded metals. Thus, the specimen layout and the measurement parameters are to be chosen with due regard to polarisation curve measurements. As mentioned in Section 2.5.4, the scan rate is an important parameter for polarisation curve measurements; due to the above mentioned aspects, it has an even more pronounced effect for measurements performed on embedded metals, e.g. concerning determination of the pitting potential 'E_{pit}' (cf. Sections 5.2.2.2).

We performed the major part of our polarisation curve measurements by means of the cement paste specimens (cf. Sections 1.9.1 and 8.1.2.2).* In addition to limiting the influence of diffusion and resistance effects, this choice was also motivated by the simple manufacture of the cement paste specimens, which allowed for a large testing matrix of destructive polarisation curve measurements.

7.5.2 Additional Measurement Techniques

In addition to the electrochemical methods described in 7.5.1, we consider the following measurement techniques to be of importance for a performance evaluation of available and new countermeasures:

- Measurement of pH and chloride content of concrete (or mortar/cement paste) and exposure solutions by chemical indicators (cf. Sections 3.1.7.2, 3.1.7.3, and 5.2.2.2)
- Light optical microscopy 'LOM' and scanning electron microscopy 'SEM' of concrete (or mortar/cement paste, cf. Section 5.2.2.2), rebar samples including

* Naturally, polarisation curve measurements can also be performed using rebars in solution, e.g. in simulated pore solution with or without the addition of chloride. Such measurements played an important role in our (preliminary) investigations. However, the crucial effects at the concrete-steel interface, i.e. electrochemical densification and pore-blocking, could only be assessed by means of testing embedded rebars.

(modified) surfaces (metallographic cross-sections, cf. Sections 3.2.2 and 6.3.2.3.2), and concrete-steel interface

- Energy dispersive X-ray spectroscopy 'EDS' based on both spectra and mapping of concrete (or mortar/cement paste, cf. Section 5.2.2.2), rebar samples including (modified) surfaces (metallographic cross-sections, cf. Sections 3.2.2 and 6.3.2.3.2), and concrete-steel interface.

These measurements are only listed here, but not described in detail, since they are largely based on standard techniques and their relevance and our application is described detail in the respective Sections. The implementation of these measurements in connection with the final test setup is described in Section 8.4.2.

8 Test Setup and Measuring Methods

This Chapter deals with the final practical realisation of the exposure conditions and measurement techniques that have been suggested in Section 7.5 for the testing of available and new countermeasures. The basic concept of the final test setup and the applied monitoring concept were outlined in Section 1.9.1. The test setup comprises three major parts that are described in this Chapter: specimens suitable for stand-alone 'E_{corr}' monitoring and 'EIS' with individual 'ECats' enabling 'i_{mac}' monitoring as well as specimens suitable for mass production (Section 8.1), a high capacity exposure setup (Section 8.2), and a monitoring system capable of logging comprehensive data from multiple specimens (Section 8.3). The implementation of the electrochemical and additional techniques proposed in Sections 7.5.1 and 7.5.2 is dealt with in Sections 8.4 and 8.4.2, respectively.

8.1 Test Specimens and External Cathodes

As mentioned in Section 1.9.1, both the embedded electrode wires 'EEWs' of the instrumented mortar specimen as well as the 'ECats' were made of activated Ti. A short description of this material is given in Section 8.1.1. The design and manufacture of the principal specimens and of the 'ECats' are described in Sections 8.1.2 and 8.1.3, respectively.

8.1.1 Activated Titanium

The embedded electrode wires 'EEWs' and the external cathodes 'ECat' (cf. Section 1.9.1) consisted of Ru/Ir mixed metal oxide ('MMO') activated titanium. In the production of activated Ti, the mixed metal oxide catalyst is thermally applied to the Ti substrate to form a chemical-resistant bond. This composition combines the stability of Ti with the conductive properties of mixed metal oxide to achieve a high and stable potential, a low consumption rate, and high current densities. Based on these properties activated Ti is often the material of choice for dimensionally stable anodes ('DSAs') in a wide range of electrochemical applications. Besides application in many electrolysis processes, activated Ti anodes are often used in connection with the electrochemical countermeasures introduced in Section 6.4.1, i.e. for 'CPre' and 'CP', which are often based on impressed currents, as well as for 'ERA' and 'ECR'.

Laboratory investigations have shown that activated Ti has no considerable sensitivity to NaCl and a steady 'E_{corr}' in solutions and concrete without pozzolanic additions. Test in concretes with high pozzolanic content showed abnormalities in the behaviour of activated Ti. Based on very low polarisation resistances determined by 'EIS' together with the development of relatively active magnitudes of 'E_{corr}', it has been con-

cluded that corrosion reactions affecting the Ti substrate were taking place.* [Castro et al., 1996].

Measured magnitudes of 'E_{corr}' of activated Ti in liquid solutions (red circles) indicate a pH dependency of 45 mV/pH, see the red line in Figure 8.1 [A] [Castro et al., 1996].

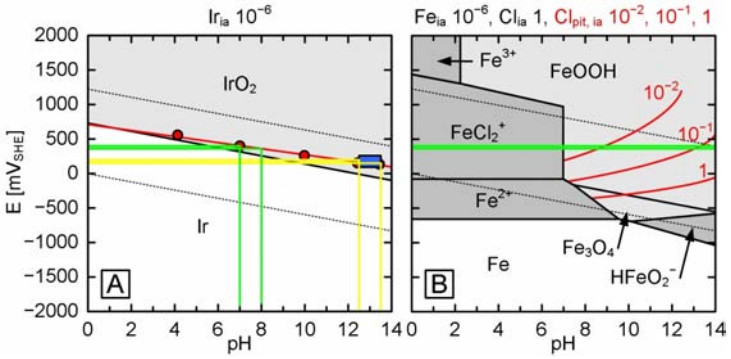

Figure 8.1: [A]: *Measured magnitudes of 'E_{corr}' of activated Ti in liquid solutions (ret dots and red line) and in concrete without pozzolanic additions (blue box) after [Castro et al., 1996]. Measured magnitudes of 'E_{corr}' superimposed on Ir-H_2O 'SEPD' and 'E_{corr}' range in the applied mortar (yellow lines) and exposure solutions (green lines).* [B]: *'E_{corr}' range of activated Ti in the applied exposure solutions (green lines) superimposed on Fe-Cl-H_2O 'MEPD' based on Table 5.4 and Fe_{ia} = 10^{-6} mol/L and Cl_{ia} = 1 mol/L.*

In [Castro et al., 1996] it is postulated that the pH dependency of activated Ti resembles the pH dependency of the oxidation of iridium-(III)-oxide (Ir_2O_3) to iridium-(IV)-oxide (IrO_2), i.e. the associated equilibrium line with a slope of 59 mV/pH. However, while we do agree to the concept that the thermodynamics of activated Ti is governed by Ir, we suggest that the pH dependency is governed by the slope of the equilibrium line (cf. Figure 8.1 [A]):

$$\begin{aligned} &IrO_2 + 4H^+ + 4e^- \rightarrow Ir + 2H_2O \quad \left(E_0^0 = 741\,mV_{SHE} \right) \\ &E_{0,\,IrO_2/Ir} = 0.741 - 0.059 \times pH \end{aligned} \qquad [8.1]$$

According to [Pourbaix, 1974b], Ir_2O_3 is practically impossible to prepare and it is thermodynamically unstable with respect to Ir and IrO_2 and hence tends to decompose to give a mixture of these substances. Besides that the mixed metal oxide catalyst is generally described to consist of IrO_2 [MAG, 2004; Hitech, 2007; KaiDa, 2007].

Figure 8.1 [A] also illustrates the pH ranges that can be expected for the 'EEWs' embedded in mortar (cf. instrumented mortar specimen in Section 8.1.2.1) (yellow lines)

* This indicates the importance of investigating the effect of pozzolanic additions on the thermodynamic conditions of metals embedded in 'HPC' (cf. Section 6.3.1.1).

and the 'ECats' (cf. Section 8.1.3) in the exposure solutions (green lines), which were kept at a pH of 7-8 (cf. Section 8.4.2). As shown in Figure 8.2 [A], after a week of submersion of the specimen the 'EEWs' were measured at a stable 'E_{corr}' of around 180 mV_{SHE} and the 'ECat' was measured at around 440 mV_{SHE}, which are both in good agreement with the pH dependency determined by [Castro et al., 1996].

To exemplify the effect of the elevated rebar 'E_{corr}', which is governed by the 'E_{corr}' of the 'ECat' (for an activated macrocell) during corrosion initiation (cf. Section 8.4.1.2), on the thermodynamics of the an embedded steel rebar in chloride contaminated concrete, the 'E_{corr}' range of the 'ECats' in solution is superimposed on the Fe-Cl-H_2O 'MEPD' in Figure 8.1 [B]. This indicates the simulated worst case conditions promoting both corrosion initiation and propagation for the specimens tested with connected 'ECat' (cf. Section 1.9.4).

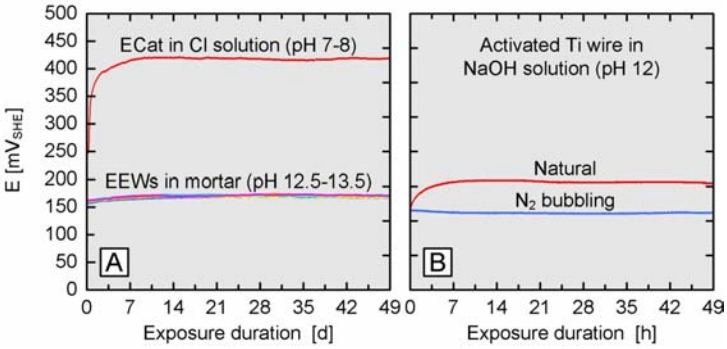

Figure 8.2: [A]: *Measured 'E_{corr}' development of embedded electrode wires 'EEWs' of the instrumented mortar specimen (cf. Section 8.1.2.1), i.e. specimen CNR-1 (cf. Section 1.9.4), and of activated Ti in exposure solution based on external cathode 'ECat' (cf. Section 8.1.3) in 10% 'w/w' chloride solution with a pH of 7-8.* [B]: *Measured 'E_{corr}' development of activated Ti wire (same as 'EEW' material) in NaOH solution with natural oxygen content and deaeration by N_2 bubbling. It should be emphasised that [A] is based on a exposure duration in days, whereas as [B] is based on hours.*

In [Castro et al., 1996] it has also been suggested that activated Ti shows only minor sensitivity to variations in the oxygen partial pressure. However, in supplementary investigations on the sensitivity of the applied 'EEW' material to oxygen, we measured 'E_{corr}' differences of about 40 mV between wires in pH 12 NaOH solution at ambient oxygen content and with deaeration, see Figure 8.2 [B]. This was also confirmed in 'Test I', where we measured 'E_{corr}' differences in the same range for 'EEWs' embedded in the same mortar, but under varying exposure conditions for the specimens [Küter et al., 2005b].

Despite its oxygen and pH sensitivity, we consider activated Ti to be a suitable embeddable electrode, in particular with regard to 'EIS' (cf. Section 8.4.1.3). A constant phase element behaviour and a very large apparent interfacial capacitance in the order of 10^{-2} F/cm^2 have been postulated for activated Ti embedded in concrete [Castro et al., 1996]. This property grants low impedance at moderate to high frequencies, which is advantageous for its use as an electrode. We verified the applicability of embedded activated Ti as 'EEW' for 'EIS' and obtained affirmative results [Küter et al., 2005b].

8.1.2 Test Specimens

Among other specimen types that were used in the experimental part of this project, the three principal types of specimens for electrochemical testing of available and new countermeasures were the instrumented mortar specimen, the simple mortar specimen, and the cement paste specimen (cf. Section 1.9). The design and manufacture of these specimens is briefly described in Sections 8.1.2.1 (mortar specimens) and 8.1.2.2 (cement paste specimens). In Section 8.4.2 variations in the layout of the mortar specimen, which were used for additional testing, are briefly summarised. As mentioned in Section 1.9.2, no chloride or other depassivating species were cast initially into the specimens, as the thermodynamic conditions during both passivity and active corrosion were to be investigated and particularly the breakdown of passivity was of interest (cf. Sections 2.1.9 and 5.2.1.1).

8.1.2.1 Mortar Specimens

The design and manufacture of the instrumented mortar specimens used in 'Test I' are described in detail in [Küter et al., 2004]. Besides investigations on the thermodynamic properties of different steel qualities and carbon steel surface treatments, 'Test I' aimed at the verification of the suitability of the specimen for 'E_{corr}' monitoring and in particular for 'EIS' (cf. Section 7.5.1). The most important results for both these objectives are summarised in [Küter et al., 2005b].

The following provides brief summary on the geometry and central features of the instrumented mortar specimen used for 'Test II', which differs from the specimens used for 'Test I' to a certain extent.

The instrumented mortar specimen was cylindrical with a diameter of 60 mm and a height of 120 mm, see Figure 8.3. The centric smooth rebar (cf. steel qualities in Section 1.9.4) had a diameter of 16 mm and a length of 100 mm. The rebar was situated in the vertical centre of the specimen, i.e. with a distance of 10 mm from the top and bottom of the specimen. A 3 mm diameter thread was inserted in the top surface of the rebar and 18.4 mm of the top circumference was dip-coated with epoxy (one layer of low viscosity and two layers of thixotropic epoxy) after application of the associated surface modification/treatment (cf. Section 1.9.4). After assembling the moulds (cf.

Figure 8.4), casting (cf. mortar compositions in Section 1.9.2), curing, and demoulding, a lead wire was connected to the rebar by a screw connection. The lead wire was connected to the associated conductor of a nine-conductor cable.

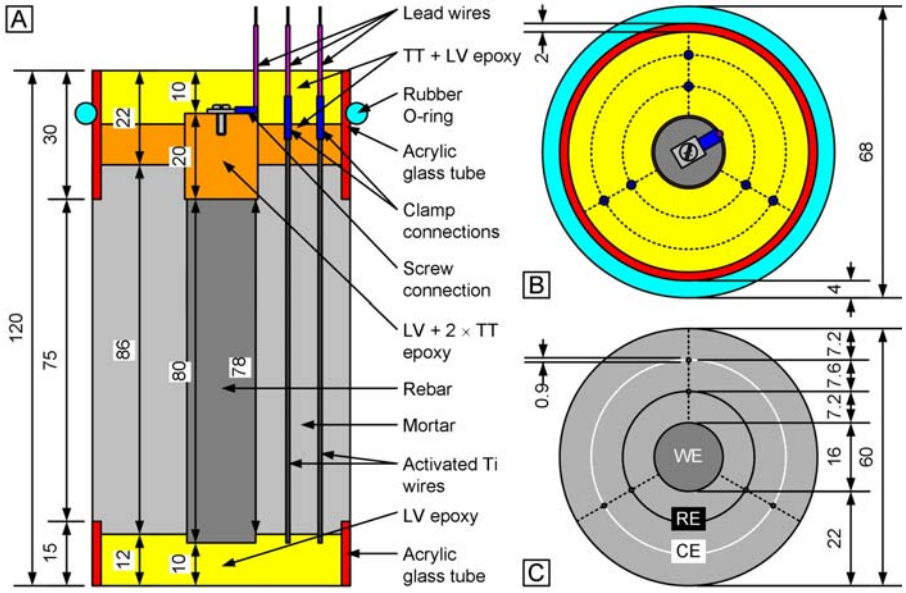

Figure 8.3: *Idealised instrumented mortar specimen. Dimensions in [mm].* [A]: *Longitudinal section. ('TT'): thixotropic and ('LV'): low viscosity epoxy.* [B]: *Top view.* [C]: *Cross-section with identification of 'EIS' electrodes. 'WE': working electrode, 'RE': reference electrode, and 'CE': counter electrode.*

The top and bottom of the specimen were filled with 22 mm and 12 mm of epoxy, respectively. 60/56 mm (outer/inner) diameter acrylic glass tube sections with a length of 30 mm at the top and 15 mm at the bottom provided moulds for the epoxy filling. The bottom layer of low viscosity epoxy was cast before demoulding and removal of the specimen with a pneumatic press 24 h after casting of the epoxy layer. After demoulding and connection of all lead wires, a first layer of thixotropic epoxy was cast and a second layer of low viscosity epoxy was cast onto that layer after hardening.

The upper acrylic glass section was circumferentially notched for the mounting of a rubber O-ring. The epoxy protected all the electrical connections, prevented ingress from the top and bottom surfaces of the specimen, and impeded outwards diffusion at the top, where the specimen was exposed to the ambient air. Moreover, the bottom epoxy filling limited the exposure length of the rebar by covering the rebar on a length of 2 mm. The total exposure length of the rebar was 79.6 mm, which corresponded to an exposed surface of exactly 4×10^3 mm^2.

The electrode wires consisted of activated Ti wire with a diameter of 0.9 mm. Two concentric circles of electrode wires were arranged so that the distances between the

rebar surface, the surface of the wires, and the surface of the specimen were of equal length. With a cover depth of 22 mm, these distances corresponded to 7.2 mm from the wire centre to both the rebar and to the specimen surface, and to 7.6 mm between the two wire centres, see Figure 8.3. Connection of the electrode wires to the lead wires was established by clamp connectors. The lead wires were connected to the associated conductors of the nine-conductor cable.

Due to the limited space of 6.7 mm between the electrode wires and the rebar and specimen surface, a maximum aggregate size of 2 mm is recommended for the mortar composition (cf. Section 1.9). The mortar was exposed to the solution over a length of 75 mm, which corresponded to an exposed mortar surface of about 14×10^3 mm^2.

The most important features of the design and manufacture of the instrumented mortar specimen are illustrated in Figure 8.4 based on the 'Test I' specimen.

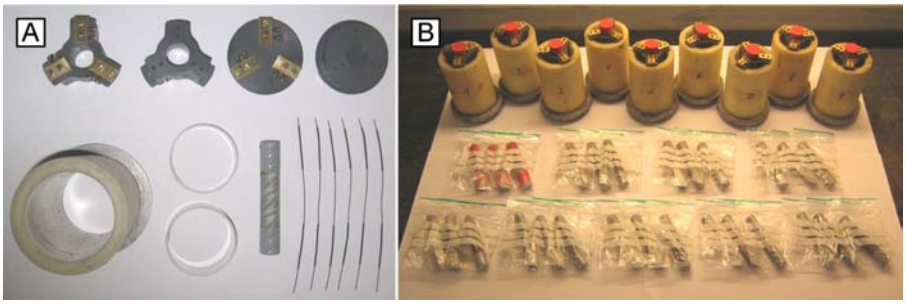

Figure 8.4: *Manufacture of the instrumented mortar specimens based on specimens used for concluding tests concerning thermodynamic properties of different steel qualities and carbon steel surface treatments (cf. Section 1.9).* [A]: *Components of moulds with top and bottom lid for positioning of rebar and embedded electrode wires and acrylic glass sections.* [B]: *Batch of mould prepared for casting and rebars with different surface treatments.*

For more information on the manufacture and testing of the instrumented mortar specimen reference is made to [Küter et al., 2004; Küter et al., 2005b]. Besides using smooth rebars instead of ribbed rebar as well as not limiting the 'EEW' surfaces by shrink tubing and the bottom of the rebar by dip-coating (cf. Figure 8.3 and Figure 8.4), some additional design changes were implemented in the manufacture of the 'Test II' specimen:

- A screw device for easier removal of the top lid and improved fixation of the rebar during vibration and a central threaded hole in the bottom lid for easier removal
- An increased overlap between the mortar and the top acrylic glass section and casting of a first layer of thixotropic epoxy (cf. Figure 8.3 [A]) to limit penetration into the joint between mortar and the acrylic glass section (for the 'Test I' specimens this was achieved by sealing the joint from the outside)

- The circumferential notch for mounting of the rubber O-ring (cf. Figure 8.3 [A]).

The instrumented mortar specimens allowed monitoring of various data in addition to the thermodynamic state of the embedded metal. All principal specimens used in 'Test I' and all specimens with indices ending with "A" in 'Test II' were based on this design (cf. Section 1.9.3 and Section 1.9.4, respectively). In addition to the instrumented mortar specimens, whose production was relatively work-intensive, simple mortar specimens with the same layout, but without 'EEWs' were used as reference specimens aiming only at the assessment of the thermodynamic state of the rebar. All specimens with indices ending with "B" used in 'Test II' were simple mortar specimens (cf. Section 1.9.4).

Besides its application in laboratory testing, we investigated possibilities for modified layouts of the instrumented mortar specimen for utilisation as embeddable corrosion sensor in connection with the electrochemical measurement techniques described in Section 7.5.1. These aspects will be evaluated in-depth in future investigations.

8.1.2.2 Cement Paste Specimens

In addition to the mortar specimens for comprehensive monitoring and the mortar specimens in the same diameter without 'EEWs' (cf. Section 8.1.2.1), another type of specimen was routinely used for various experiments including 'Test II' (cf. Section 1.9), i.e. the cement paste specimen. The production process of this type of specimens is illustrated in Figure 8.5.

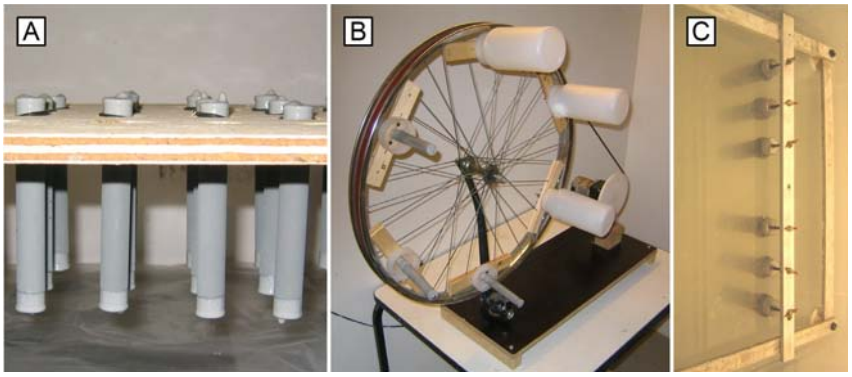

Figure 8.5: [A]: *Rebars with first layer of thixotropic epoxy dip-coating.* [B]: *Hardening of specimens after cement paste dip-coating on a spinning wheel to achieve a homogenous thickness of the cement paste layer.* [C]: *Curing of specimens in saturated $Ca(OH)_2$ solution after hardening on spinning wheel.*

The cement paste specimens were produced from the same rebars as the mortar specimens, i.e. 16 mm in diameter, but they were cut to a length of 120 mm, which corresponds to the entire length of the mortar specimen (cf. Figure 8.3 [A]). After in-

sertion of the a 3 mm diameter thread on the top surface of the rear and application of the associated surface modification/treatment the rebar was dip-coated epoxy (one layer of low viscosity and two layers of thixotropic epoxy) on length of 30 mm and 12 mm on the top and bottom, respectively, see Figure 8.5 [A]. After hardening, the epoxy coating was ground off from the top surface and a 50 mm long threaded rod with a diameter of 3 mm was screwed into the thread. Afterwards, the specimen was dip-coated with cement paste (cf. cement paste composition in Section 1.9.2) and mounted on a slowly rotating spinning wheel (to attain a homogenous coating thickness), while being sealed in a plastic bottle (to prevent drying out), see Figure 8.5 [B]. Depending on the surface modification of the rebar, the coating/curing process was repeated two to three times with an adequate number of dips to achieve a thickness of 3 ± 0.5 mm on the exposed surface, which was measured by means of a vernier calliper gauge after curing. When the desired thickness was attained and the specimens were hardened, they were moist cured in $Ca(OH)_2$ solution, see Figure 8.5 [C].

In addition to enabling mass production and obtaining quick indicative electrochemical results, we think that the cement paste specimens allowed for advantageous visual indications on the electrochemistry between the metal surface and the cement paste, i.e. principally all relevant reactive compounds in mortar or concrete (cf. Section 3.1). This could be e.g. observed in relation to the effects of hydrogen evolution at Mg wire (cf. Figure 7.10 in Section 7.3.2). Yet, not only the physical appearances of side effects, but also chemical (in terms of the rate of hydration) could be visually assessed (cf. influence of zinc on the hydration in Sections 6.3.2.5 and 7.3.1). Finally, besides these observations on the cement paste, the character of corrosion damage on the metal surface could be easily estimated by leaving the specimens to dry out for a few hours after testing (cf. pitting corrosion damage on stainless steel specimen in Figure 8.12 in Section 8.4.1.4). After drying the cement paste could be easily removed, which vice versa meant that drying out needed to be prevented before and during testing.

Besides application of cement paste specimens for various preparative and preliminary testing during the project period, the specimens with indices ending with “C” and “D” used in ‘Test II’ were based on this design (cf. Section 1.9.4).

8.1.3 External Cathodes

The external cathodes ‘ECats’ were manufactured from activated Ti tubes, 19.1 mm (0.75 in.) in diameter, see Figure 8.6 [A] for a photograph of a complete ‘ECat’ and Figure 8.6 [B] for an idealised longitudinal section.

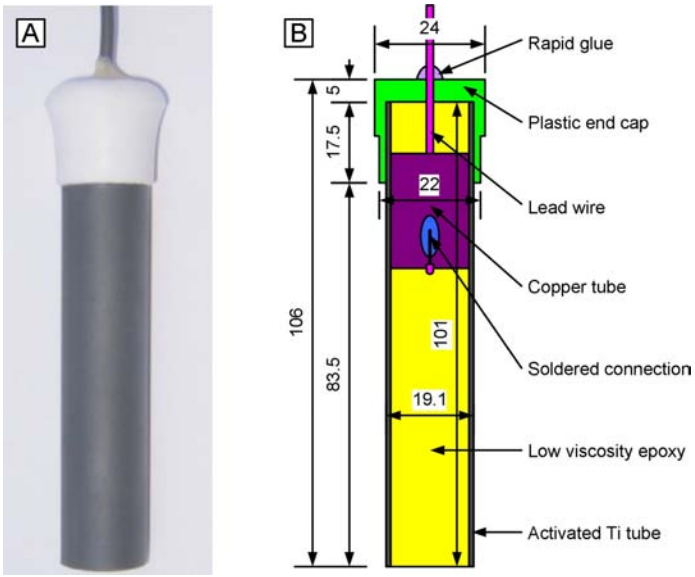

Figure 8.6: *External cathode.* [A]: *Photograph.* [B]: *Idealised longitudinal section. Dimensions in [mm].*

The usual field of application for this commercially available product is as dimensionally stable anodes ('DSAs') (cf. Section 8.1.1). The tubes were cut to a length of 101 mm under oil/water cooling. Sufficient cooling was crucial, because excessive heat affects the mixed-metal-oxide catalyst [MAG, 2004]. The tubular style provided a large surface area and allowed electrical connection in the centre of the 'ECat'. A lead wire was soldered to a section of a 16 mm diameter copper tube. The copper section was deformed into an oval, which was slightly wider than the internal circumference of the activated Ti tube, and wedged into the tube.

The top end of the tube was covered with a soft plastic end cap, whose outer diameter decreased from 24 mm at the top to 22 mm at the bottom. This layout allowed insertion and tight mounting into a hole of 22.5 mm in diameter. The lead wire was guided though a central hole in the cap and connected to two conductors from the nine-conductor cable. The hole in the cap was tightened with rapid glue. That way, it was possible to fill the entire tube with low viscosity epoxy from the bottom, which completely prevented moisture intrusion and hence protected the electrical connection.

The end cap covered the tube for a length of 17.5 mm. Thus, the total exposure length of the 'ECat' was 83.5 mm, which corresponded to an exposed surface of exactly 5×10^3 mm^2. This meant that the ratio of exposure area between rebar and 'ECat' was 0.8 (cf. Sections 8.1.2.1 and 8.1.2.2). If desired, a plastic ring with the same outer dimension as the top cap could be installed at an arbitrary position on the tube to adjust the exposure surface. In this way, the anode-to-cathode ratio could be increased.

8.2 Exposure Setup

Two exposure containers, one large and one small, were designed for positioning and submersion of the test specimens and 'ECats'. For 'Test II' the large container was used for exposure to chloride solution, while the small container was filled with potable water and functioned as reference (cf. Section 1.9.4). The required measurement techniques mentioned in Section 7.5.1 could be carried out in the same way on specimens in both containers. Each exposure container was mounted on top of a two-level cart with a reservoir container on the bottom shelf, see Figure 8.7 [A]

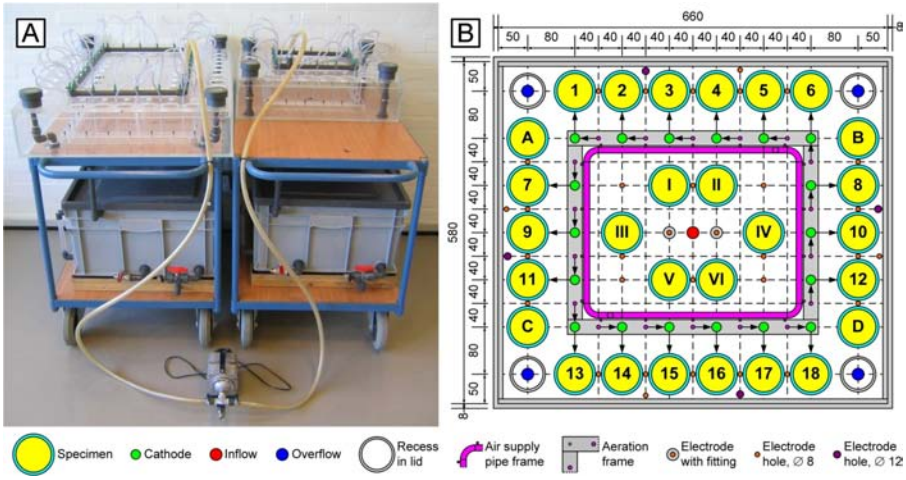

Figure 8.7: [A]: *Exposure setup on two-level carts with the acrylic glass exposure containers on the top shelf, the reservoir containers on the bottom shelf, and the air pump in front.* [B]: *Idealised top view of the fully equipped small exposure container. Dimensions in [mm].*

The exposure containers were manufactured from 8 mm thick acrylic glass. The inside dimensions of the small container were 660 mm × 580 mm, see Figure 8.7 [B]. The large container measured 1060 mm × 740 mm on the inside (cf. Figure 1.3 in Section 1.9.4). The maximum solution level from the top of the bottom plate to underneath the lid was 150 mm for both containers. Thus, the containers had a total capacity of approximately 57.4 L and 117.7 L without test specimens inserted (negligibly reduced by the aeration frame inside the container). Both containers were supplied with solution from a reservoir container. The inside dimensions of the reservoir containers were 765 mm × 565 mm and the maximum solution level is 280 mm. This corresponded to a total capacity of 121.0 L. Accordingly, 178.4 L and 238.7 L of solution were available for circulation in the small and large exposure container, respectively, when at the maximum solution level and not equipped with specimens and cathodes.

The solution was pumped from the reservoir containers into the exposure containers by a centrifugal magnetic pump through a 20 mm inlet in the centre of the bottom

plate of the exposure container. The solution flowed back into the reservoir through an overflow comprising four pipes with a diameter of 20 mm, which protruded from the bottom plate at each corner of the exposure container. The lid was recessed above each overflow pipe to enable steady flow. The recesses were created by gluing 50 mm long plastic tubes with screw caps into 60 mm diameter holes in the lid. Outflow through all four pipes and equivalent exposure conditions for all specimens were achieved by levelling the carts horizontally. The solution level could be adjusted by reducing the height of the outflow pipes. The height could be altered from underneath the lid to 30 mm below the lid by screwing the outflow pipes into their threaded fittings. Adjustment of the outflow pipes was carried out using a hard rubber rod with access through the screw caps of the recess tubes. Shorter outflow pipes could be mounted to further reduce the solution level. For 'Test II' the solution level was adjusted so that 60% of the mortar/cement paste surface (in relation to the surface of the embedded rebar) were covered by exposure solution (cf. surface of mortar specimen in Figure 5.14 [A] in Section 5.2.2.2).

If the solution had to be totally removed from the exposure container, e.g. for a drying period or solution renewal, the centrifugal pump was turned off and a two-way valve was opened, so that the solution flowed through the inflow out of the exposure container into the reservoir. The reservoir container could be emptied by means of another two-way valve, which was also used for filling. An overflow beneath the top edge prevented the reservoir container from flooding, when the depletion valve was closed and the centrifugal pump was deactivated, e.g. in the event of a power failure.

The positions of the specimens were determined by 62 mm diameter holes in the lids of the exposure containers, while 22.5 mm diameter holes determined the locations of the 'ECats'. The cement paste specimens were fixed in position by means of adapters (upper outer diameter 70 mm, lower outer diameter 62 mm, upper diameter of central hole 20 mm, and lower diameter of central hole 24 mm), where the specimens could be mounted (from below) with an O-ring (from above), so that the exposure surface of the rebar was on the same level as for the mortar specimens. The centre-to-centre distance between two adjacent specimens was 80 mm, which corresponded to a free space of 20 mm for two mortar specimens next to each other. The centre-to-centre distance between a specimen and its associated cathode were also 80 mm. This means that the surface-to-surface distance between a rebar and its associated 'ECat' was 62.5 mm for both types of specimens.

The small container had a capacity of 28 specimens altogether. 22 specimens were located on the outer circle (1-18 and A-D) and six specimens on the inner circle (I-VI). 18 specimens could be connected to an 'ECat' (1-18), whereas 10 specimens (A-D, I-VI) were not associated with an 'ECat'. The large container provided 56 positions for specimens altogether (36 on the outer and 20 on the inner circle, cf. cf. Figure 1.3 in Section 1.9.4). 32 specimens could be connected to an aerated 'ECat', while six specimens were associated with an 'ECat'. There were another 16 positions with

optional connections to unaerated 'ECats'. The unaerated 'ECats' were located within the inner circle of specimens with the same centre-to-centre distance of 80 mm to the associated specimen.

If the overflows were adjusted for maximum filling, the specimens and 'ECats' were submerged over a length of 99.0 mm and 83.5 mm, respectively. This corresponded to a solution volume of 0.28 L for the mortar specimen and 0.02 L for the 'ECat'. This means that the exposure solution volume was reduced by 8.3 L for the small container and 16.8 L for the large container, if they were fully equipped with mortar specimens and cathodes (including optional 'ECats' for the large container). Thus, the amount of exposure solution available for circulation in the two containers was reduced to 170.1 L and 221.9 L, respectively. Hence, the total area of submerged mortar surface was 0.15 m^2 for the small container and 0.29 m^2 for the large container. That led to ratios of solution volume-to-mortar surface area of 1134 L/m^2 for the small container and 765 L/m^2 for the large container. If desired, the ratios could be adjusted by lowering the solution level in the reservoir for the small container or by placing extra mortar cubes or cylinders in the unused locations of the small exposure or reservoir container. In this way effects on the mortar surface, such as leaching or surface concentration, could be evened out. For all investigations on the high capacity exposure setup a solution volume-to-mortar surface area ratio of 750 L/m^2 was used.

The 'ECats' were aerated via an aeration frame placed at the bottom of the exposure containers. Aeration conditions were equal for all specimens, because the aeration frame was mounted at the same distance between the inner and outer circle of specimens in both containers. The aeration frame was made of acrylic glass and equipped with custom-made plastic nozzles with a 1 mm diameter hole. Silicon hoses were fixed on the nozzles and connected to the air supply pipe frame, which was mounted on top of the lid, through tightly-fitting 6.3 mm diameter holes in the lid. The air supply pipe frame consisted of 20 mm diameter plastic pipes with reducing valves for each silicon hose and a connection to an air pump. Adjustment of the individual reducing valves enabled equal aeration for all 'ECats', or varying conditions, as required. The aeration in the exposure container introduced sufficient turbulence to avoid precipitation even for high chloride concentrations (cf. exposure solutions in Section 1.9.2). Precipitation in the reservoir containers was prevented by submerged circulation pumps.

Evaporation of water and crystallisation of chloride were minimised, because the solution was circulated through a closed system and the containers were fitted with lids. The lids of the exposure containers were screw-tightened to the support frame along the inside wall of the container, the 'ECats', the air supply hoses, and the adapters for the cement paste specimens were closely fitted, and the rubber O-rings around the mortar and cement specimens tightened the associated holes. The outward diffusion of exposure solution or chloride ions through the mortar was prevented by the epoxy layer on the top of the mortar specimens (cf. Section 8.1.2.1). Moreover, the reservoir

container was covered and the outflow pipes protruded into the solution down to just above the bottom of the reservoir container.

Two 8 mm diameter plastic fittings were mounted for the insertion of two permanent 'SCEs' on the centre line of the container. The height of the fittings was designed so that the tips of the 'SCEs' were in the vertical centre of the exposed surface area of the rebars in all specimens. A series of 8 mm holes and four 12 mm holes were also provided. The 8 mm holes were situated next to each specimen and at geometrically defined positions. Next to each container wall was one 8 mm and one 12 mm hole. The 8 mm holes suited most standard electrodes, while the 12 mm holes were provided for electrodes with a larger diameter, e.g. some types of ion selective and pH electrodes. A plastic adapter tube was used to bring the electrode tips to defined heights, when inserted. When not in use, rubber stoppers were inserted in the extra holes to keep the system closed.

8.3 Monitoring System

Altogether 84 specimens could be exposed simultaneously, when both containers were fully equipped (cf. Table 1.1 and Figure 1.2 in Section 1.9.4 and Figure 8.7 in Section 8.2). As mentioned in Section 1.9.1, 24 channels were monitored for the instrumented mortar specimen with 'ECat'. The number of channels was reduced to 20 for an instrumented mortar specimen without 'ECat', to six for simple mortar or cement paste specimens with 'ECat', and to two for monitoring of 'E_{corr}' only. The channel use and assignment is described in Section 8.3.3 in more detail. Using conventional datalogging to monitor the required number of channels, e.g. for the entire test batch of 'Test II' (cf. Section 1.9.4), would have been impractical as well as cost intensive. Moreover, conventional datalogging would have required individual current-to-voltage converters for each specimen, where macrocell current 'i_{mac}' was monitored.

We developed a system for monitoring of multiple specimens based on "cluster measurements". This system reduces the number of required datalogger channels to 48 and the number of current-to-voltage converters to two. The principle of cluster measurements is briefly described in Section 8.3.1 and the key features of the system, the adaptations to meet the specific requirements in the present application, and the supplementary equipment used are described in Sections 8.3.2 (switch cards), 8.3.3 (distribution terminal board and datalogger), and 8.3.4 (control routine).

8.3.1 Cluster Measurements

Conclusive evaluation of experimental testing is generally based on statistical analysis of data obtained from several specimens. Depending on the number of signals monitored for the individual specimen, the batch size is often limited by the number of available datalogger channels. This generally leads to a compromise in reducing either

the number of signals monitored per specimen or the amount of specimens (the batch size). If the numbers of signals is not to be reduced, smaller test batches are to be tested one after each other. However, sequential testing of smaller batches is often impractical or impossible for time constraints. This holds in particular for long-term testing, as e.g. tests concerning reinforcement corrosion*. Measurements or monitoring (continuous measurements) in relation to reinforcement corrosion testing is generally based on recording the same measured parameters, e.g. 'E_{corr}' and 'i_{corr}/i_{mac}' for all test specimens, which allows comparison of these parameters in relation to the test parameters, e.g. the effect of different countermeasures or exposure conditions. In such applications as well as for most other long-term monitoring a totally synchronous signal logging for all measured parameters is not important. Thus, we consider that the limitations due to the number of available datalogger channels could be conveniently addressed by diverting a larger test batch into clusters with the same measured parameters. This means that all signals of one specimen or of a group of specimens are logged before the same signals are logged for the next specimen or group of specimens until the full batch is scanned and the cluster measurement can start from the beginning at a given time. The benefits of monitoring based on cluster measurements in testing against more reference signals are exemplified in Figure 8.8 and Figure 8.9. Figure 8.8 illustrates monitoring of three "high" signals (A to C, red dots) of six specimens (1 to 6) versus three "low" reference signal (Re-1 to Re-3) in based on conventional datalogging.

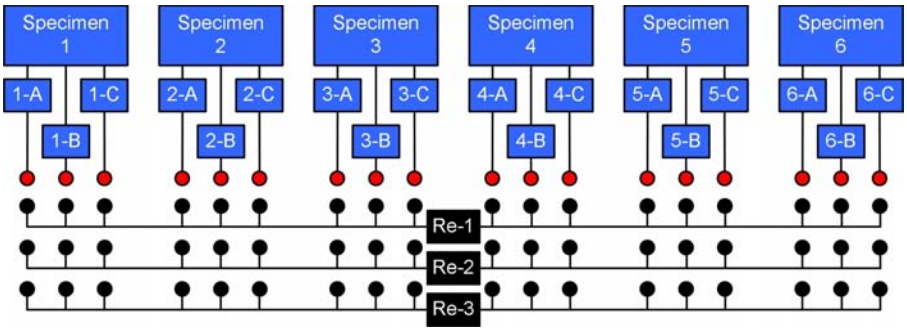

Figure 8.8: *Monitoring of three signals (A to C) from each of six specimens (1 to 6) against three reference signals (Re-1 to Re-3) by conventional datalogging.*

The black dots represent the nine "high" datalogger channels to perform the measurements for each specimen. Accordingly, 54 channels are required to monitor the matrix for the entire batch of six specimens by conventional datalogging.

* As well as for many experiments in the area of construction materials, e.g. shrinkage and relaxation monitoring. We consider cluster measurements to have beneficial applications in many areas of long-term monitoring and the modular design described in Sections 8.3.2 and 8.3.4 is conveniently adaptable to any types of measurement and batch size.

The three signals (A to C) are based on the same measured parameter, i.e. the "high" signal is measured versus the three "low" reference signals (Re-1 to Re-3) for all specimens. Thus, the measurements can be subdivided into measurement clusters (I to III), as illustrated in Figure 8.9.

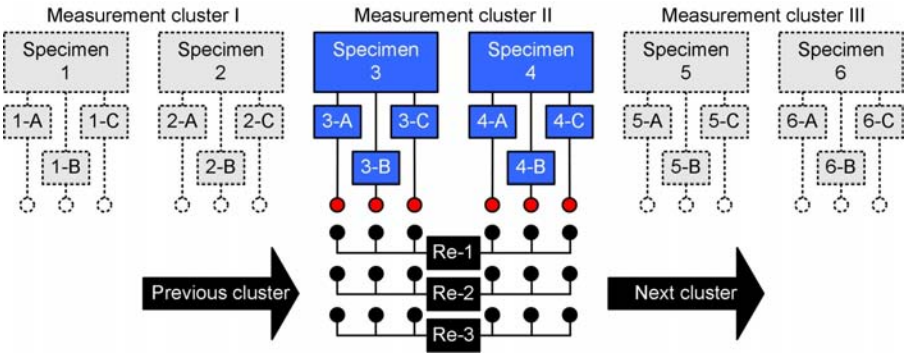

Figure 8.9: *Monitoring of three signals (A to C) from each of six specimens (1 to 6) against three reference signals (Re-1 to Re-3) by datalogging based on cluster measurements.*

One measurement cluster was chosen to comprise the "high" signals from two specimens (red dots), i.e. six signals. A distribution terminal is established where these six signals are measured versus the three "low" reference signals, i.e. 18 datalogger channels (black dots) are used in total. As illustrated by the black arrows, the clusters (I to III) corresponding to the "high" signals from the specimens (A to C) are connected to the distribution terminal one after each other and hence measured and logged versus the "low" reference signals that apply for all specimens. That way, the required number of datalogger channels can be reduced by three from 54 to 18 channels in this example. Conventional datalogging of 54 channels is still in a reasonable range and the establishing of a system for cluster measurements is not required. However, if e.g. 50 specimens are to be monitored in correspondence with the above example, 450 datalogger channels would be required using conventional logging; compared to 18 based on cluster measurements. Besides these benefits in reducing the number of required channels, we think that the application of cluster measurements is most advantageous, if certain or all signals measured within a cluster are to be processed by additional devices. Among zero-impedance-ammeters (henceforth, ammeters), as applied in the signal processing for the setup described in this Chapter, signal processing devices for other applications might include amplifiers, filters, converters (e.g. analogue-digital converters ('ADCs'), thermo converters, gauge converters), or Wheatstone bridges. If signals are to be processed using conventional datalogging, every signal to be processed requires an individual processing device connected to the associated channel. On the contrary, using cluster measurements the signal processing device only needs to be connected to the associated terminals on the connection terminal. Based on the above example and considering that e.g. signal "A" of all specimens is to be proc-

essed, this would require six processing devices for conventional datalogging and correspondingly 50 devices, when considering 50 specimens. Yet, datalogging based on cluster measurements in the same configuration would allow monitoring of a theoretically unlimited number of specimens using only two processing devices.

8.3.2 Switch Cards

In this Section as well as in Section 8.3.3, the implementation of cluster measurements for our purposes are described based on the instrumented mortar specimen with 'ECat'. With the exception of specimens where only 'E_{corr}' is monitored, connection of all other specimen types without 'ECat' and/or 'EEWs' follows the same principle, while the connections for missing components are simply left open. Specimen where only 'E_{corr}' is monitored can be connected to open 'EEWs' terminals of other specimens with 'ECat' but without 'EEWs', e.g. in 'Test II' the cement paste specimens without 'ECat' (indices ending with "D") were connected to the 'EEW 1' terminals of the cement paste specimens with 'ECat' (indices ending with "C") (cf. Section 1.9.4).

As indicated in Section 1.9.1, eight signals for each instrumented mortar specimen with 'ECat' were assessed, i.e. the rebar, the 'ECat', and the six 'EEWs' (cf. Figure 1.2 in Section 1.9.1). As the 'ECat' conductor for the establishment of the macrocell was frequently connected and disconnected from the system and 'E_{corr}' of the 'ECat' was also to be assessed during periods of disconnection, two separate 'ECat' connections ('i_{mac}' and 'E_{corr}') were required see Figure 8.10. Thus, altogether nine signals were measured from each instrumented mortar specimen with 'ECat'. One measurement cluster corresponded to two specimens (18 input signals).

As illustrated in Figure 8.10 [A] and [B], the conductors associated with each measurement cluster (two nine-conductor cables) were connected to one switch card. A switch card was based on a printed circuit board ('PCB') equipped with ten two-pole changeover relays (RL1 to RL10).

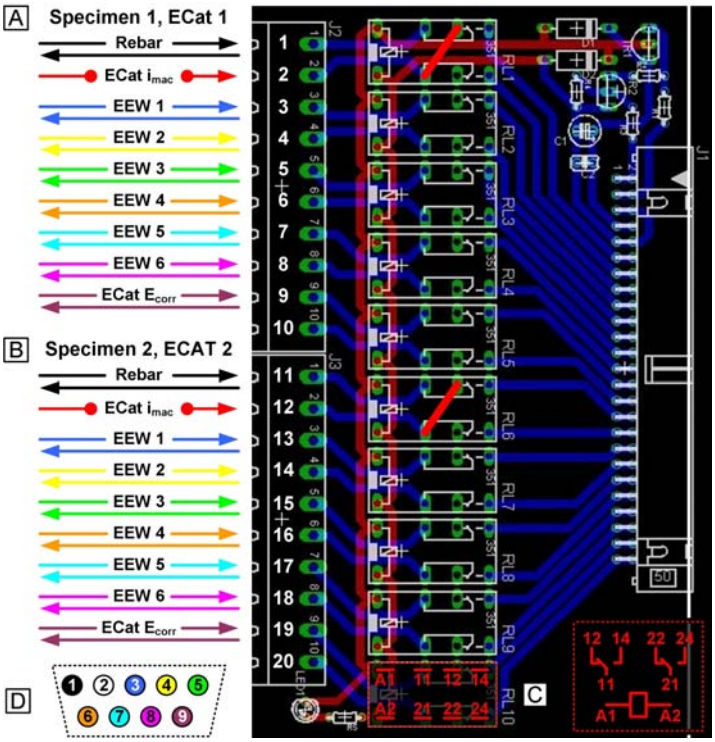

Figure 8.10: *Switch card corresponding to one measurement cluster.* [A] and [B]: *Connections for two instrumented mortar specimens with external cathode 'ECat'. 'i_{mac}': macrocell current and 'E_{corr}': corrosion potential. The colour code used for the conductors corresponds to the colours used in the scheme for the connections established on the distribution terminal board (cf. Table 8.1 in Section 8.3.3).* [C]: *Pins of two pole changeover relay and associated circuit diagram.* [D]: *Standard 9-pin plug for electrochemical impedance spectroscopy 'EIS', polarisation curves, and other supplementary electrochemical measurements (cf. Section 8.4). The colour code of the pins (1-9) corresponds to the colours of the conductors and to the colours used for the connections on the adapter terminal board customised for connection to the applied 'EIS' equipment (cf. Figure 8.11 in Section 8.4.1.3).*

Each relay allowed toggling of two input signals, so that one switch card was capable of transferring 20 signals. Two ten-pin screw terminals were installed for input connections on the left-hand side of the switch card (J2 and J3). All the relays were synchronously supplied with an excitation voltage of 12 V when the associated card was triggered by a 5 mA signal, which was supplied by a digital input/output 'I/O' board connected to an IBM compatible PC and controlled by a LabVIEW routine [NI, 2004] (cf. Section 8.3.4).

Connections for the individual trigger signal and the shared excitation voltage supply were established on pins 1-10 of the 50-pin socket on the right-hand side of the switch card (J1). Every connection on the 50-pin socket was established on two pins to ensure secure connection. The excitation voltage toggled the relay from pin 12 (22) to pin 14 (24), see Figure 8.10 [C]. In this setting the 20 input signals were connected to pins 11-50 of the output socket (J1).

The 27 switch cards were stacked in a customised plastic frame and the signal connections (pins 11-50, J1) were daisy-chained by a 40-conductor ribbon cable with 27 input plugs and an output socket for connection to a distribution terminal board as well as to an input socket for the extension of the monitoring system. As the switch cards were activated one after the other, only one switch card was transferring signals to the distribution terminal board at any one time.

While a switch card was deactivated, the current connection between the rebar and 'ECat' was established by the soldered short-circuit between relay pin 12 and pin 21 of the two associated relays (RL1 and RL6). The changeover functionality of the relays enabled connection of relay pin 11 (21) to relay pin 12 (22) in the deactivated state, see Figure 8.10 [C]. In this way, the screw terminal pins 1 (11) and 2 (12), which corresponded to the rebar and the 'ECat', respectively, were connected.

The nine-conductor cable from each specimen transferred the signals of the rebar, the six 'EEWs', and the 'ECat', see Figure 8.10. As mentioned, the 'ECat' was connected to two terminals, since the 'ECat i_{mac}' conductor was connected and disconnected at set intervals. So, the corrosion potential of the 'ECat' was exclusively monitored by the additional conductor 'ECat' 'E_{corr}'. Activation and deactivation of the 'i_{mac}' connection (the macrocell) was performed by a manual toggle switch unit. The switch unit was based on a circuit board with a series of dual in-line package ('DIP') switches connected to a set of 54 input and output screw terminals.

The conductors of all connections, except the 'ECat i_{mac}' conductor, were looped through the screw terminal and connected to a standard 9-pin plug, see Figure 8.10 [D]. Arbitrary measurement equipment, e.g. a potentiostat, a voltmeter, or an electrochemical noise analyzer ('ENA'), could be connected to this plug via customised adapters. However, during 'Test II' this plug was mainly used for connection to the 'EIS' equipment (cf. Section 8.4.1.3).

8.3.3 Distribution Terminal Board and Datalogger

The nine output signals of each of the two specimens connected to one card were diverted on the distribution terminal board into one current and 23 potential monitoring channels, see Table 8.1. In this way, 48 channels were monitored, when one cluster was measured.

Table 8.1: *Connections established on the distribution terminal board and associated datalogger channels and indices. 'ECat': external cathode, 'EEW': embedded electrode wire, 'E_{corr}': corrosion potential, 'i_{mac}': macrocell current, and 'SCE': saturated calomel electrode. The colour code for the connections corresponds to the colours used for the conductors connected to the switch card (cf. Figure 8.10 in Section 8.3.2).*

Channel		High	Low	Index
Specimen 1	**Specimen 2**			
101	201	'ECat 'i_{mac}' ('i_{mac}' high)	Rebar ('i_{mac}' low)	1
102	202	Rebar 'E_{corr}'	'SCE 1'	2
103	203	'ECat' 'E_{corr}'	'SCE 1'	3
104	204	'EEW 1'	'SCE 1'	4
105	205	'EEW 2'	'SCE 1'	5
106	206	'EEW 3'	'SCE 1'	6
107	207	'EEW 4'	'SCE 1'	7
108	208	'EEW 5'	'SCE 1'	8
109	209	'EEW 6'	'SCE 1'	9
110	210	Rebar 'E_{corr}'	'SCE 2'	10
111	211	'ECat' 'E_{corr}'	'SCE 2'	11
112	212	'EEW 1'	'SCE 2'	12
113	213	'EEW 2'	'SCE 2'	13
114	214	'EEW 3'	'SCE 2'	14
115	215	'EEW 4'	'SCE 2'	15
116	216	'EEW 5'	'SCE 2'	16
117	217	'EEW 6'	'SCE 2'	17
118	218	'ECat' 'E_{corr}'	Rebar 'E_{corr}'	18
119	219	'EEW 1'	Rebar 'E_{corr}'	19
120	220	'EEW 2'	Rebar 'E_{corr}'	20
301	305	'EEW 3'	Rebar 'E_{corr}'	21
302	306	'EEW 4'	Rebar 'E_{corr}'	22
303	307	'EEW 5'	Rebar 'E_{corr}'	23
304	308	'EEW 6'	Rebar 'E_{corr}'	24

The channels were provided by a datalogger based on analogue measurements, i.e. the channels were relay-controlled and logged individually one after the other. The datalogger was equipped with three multiplexer cards with channel numbers 101-120, 201-220, and 301-320. All the multiplexer terminals, except the ones corresponding to channel numbers 317-320, were connected to the distribution terminal board by three 40-conductor cables. That means that altogether 57 datalogger channels were made available on the distribution terminal board.

The terminal board enabled distribution of the input signals from the switch card stack connections (18 conductors) and the 'SCEs' as well as additional electrodes to the

datalogger channels, i.e. two times (high and low) 57 conductors. The distribution of signals on the terminal board was performed by connecting the switch card conductors to the associated terminals of the datalogger. The distribution terminal board consisted of a circuit board with four 40-pin sockets and seven sets of 20-pin screw terminals. One 40-pin socket was connected to the 40-conductor ribbon cable connection to the switch card stack (a single screw terminal on the switch cards was connected to two conductors) and the other three were connected to the three 40-conductor cables from the multiplexer cards. One set of 20-pin screw terminals was connected to the switch card stack socket and the other six sets were connected to the sockets corresponding to the high and low terminals of the associated datalogger channels.

Datalogger channel 101 (201) was assigned to the current channel, while channels 102-120 (202-220) and 301-304 (305-308) were the 23 channels for 'E_{corr}' monitoring of each instrumented mortar specimen with 'ECat', see Table 8.1. For monitoring of the instrumented mortar specimens without 'ECat', the current channel 101 (201) and the 'E_{corr}' channels for the 'ECat', i.e. channels 103 (203), 111 (211), and 118 (218), are left out. For simple mortar and cement paste specimens the 'EEW' channels were left out, i.e. connections were only established for channels 101-103 (201-203), 110 (210), 111 (211), and 118 (218). That way, the EEW channels were available for 'E_{corr}' monitoring of additional specimens, e.g. specimens with indices ending with "D" during 'Test II' (cf. Section 1.9.4).

The rebar, the 'ECat' and the six 'EEWs' were connected to the high terminals of channels 102-109 (302-309) and 110-117 (210-217), while the first and second 'SCE' were connected to the associated low terminals. For channels 118 (218) to 301 (304), the rebar conductor was connected to the low terminals, and the 'ECat' and the six 'EEWs' were connected to the high terminals.

The current flow between the rebar and the cathode needed to be transferred to a voltage output before connection to the corresponding datalogger terminals. The transformation was performed by two electrically separated ammeters, which were driven by two rechargeable 9 V block batteries. The batteries were automatically recharged to keep the supply voltage at a constant level. Recharging was performed after an entire batch was monitored, i.e. in the time frame between two complete scans. Charging was performed by a switch unit controlled by the digital 'I/O' board (cf. Section 8.3.4). Operation of the switch unit was based on the same principle as toggling of the switch card relays. The connections of the two battery poles was toggled between a standard charging unit and the voltage supply connections of the ammeters. In this way, the ammeters were operated with a stable supply voltage that was insulated from any perturbation sources. The ammeters provided an exact linear relation between voltage output and current input with a transformation factor of 1 V/mA. The ammeters were nulled, based on the applied supply voltage and zero current before connection to rebar and 'ECat'.

To ensure proper adjustment to the current flow of the connected specimen and cathode, an input option for a delay between switching to the associated card and logging of the active card was provided in the control routine (cf. Section 8.3.4).

Application of the current logging channels provided on the multiplexer cards was not advisable for the measured current range (0-500 μA), as resistivity and noise were very high. However, the connection to the rebar and cathode conductors could be bridged to the current input terminals of the multiplexer cards. This option was used for verification that the ammeters were functioning correctly.

Each of the two exposure containers was equipped with two individual 'SCEs'. The 'SCE' signals were independent of the output of the switch cards. Accordingly, it was necessary to switch between the two sets of two 'SCEs' of the small and large container, when the associated specimens and cathodes were monitored. This was achieved by an 'SCE' switch, which was also controlled by the digital 'I/O' board (cf. Section 8.3.4). The 'SCE' switch was operated in the same way as the charging switch unit for the ammeters. The connections of the two 'SCE' inputs on the distribution terminal were toggled between the 'SCEs' of the small container and the 'SCEs' of the large container. All the other terminal connections on the distribution terminal board were associated with the output from the activated switch card.

The digital 'I/O' board was also used to deactivate the air pump during measurements, as we considered that solution turbulence could interfere with 'E_{corr}' measurements. This was done using a 220 V supply voltage interrupter which was also triggered by a signal from the digital 'I/O' board. The delay in aeration deactivation before and reactivation after logging of the measurement cluster could be defined arbitrarily in the control routine (cf. Section 8.3.4).

The remaining channels 309-320, which were not used in the measurement clusters, could be used for supplementary measurements. The datalogger was programmed to scan these channels only once after all measurement clusters had been recorded, i.e. at the end of scan of the entire batch. Channels 309-312 were used for online verification of the four installed 'SCEs' and, in connection with the extra holes, for supplementary measurements (e.g. for quantification of the effect of the distance of the reference electrodes on measurements or in relation to solution resistance). The permanently installed 'SCEs' were connected to the high terminals and measured against the additional electrodes in the associated exposure container connected to the low terminal.

Channels 313-315 were provided for supplementary measurements with other electrode types, e.g. ion-selective, chloride, or pH electrodes. Channels 316 and 317 were configured for higher voltage ranges and used to monitor the voltage of the rechargeable batteries when disconnected from the charging unit. Channels 318-320 were configured for temperature input and equipped with thermocouple wires. Unlike all other conductors used for datalogging, the thermocouple wires were not connected to the distribution terminal board, but directly to the associated multiplexer card terminals.

The thermocouples were used to measure the solution temperature in both containers as well as the ambient air temperature.

8.3.4 Control Routine

The digital 'I/O' board and the datalogger were controlled by a LabVIEW [NI, 2004] routine. The specimens to be monitored (i.e. the clusters to be logged) could be selected in connection with the associated exposure container. This selection controlled switching between the cards and the 'SCE' switch, respectively. The time frame between logging of the entire batch and between logging of individual clusters could be specified as required. Charging of the batteries was triggered automatically after each entire batch had been logged. Moreover, the delay between switching to a card and logging of the associated cluster could be defined arbitrarily, as could the deactivation of the air pump, which toggled the 220 V supply voltage interrupter.

The LabVIEW routine created an individual text file for the selected specimens and for the extra channels. The text file for a specimen comprised tab-separated columns with a time stamp column and 24 data columns with a header according to the measurement indices, see Table 8.1. Once a measurement cluster had been logged, the measured data was saved into a new row of the text files of the associated two specimens. The routine also provided an online browser. The browser allowed monitoring of selected channels from one selected specimen or from the extra channels. The data was read from the associated text files and updated, once a new measurement cluster had been logged.

The modular layout of the monitoring system meant that extension of the monitoring capacity only required the connection of further switch cards. Additional switch cards could be conveniently daisy-chained and connected to the extension plug of the switch card cable and equipped with trigger signal connections to the available digital 'I/O' board channels. Additional measurement clusters (i.e. further specimens) could be effortlessly implemented in the control routine.

8.4 Implementation of Measurement Techniques

In this Section the implementation of the measurements techniques, which we consider to be essential in testing of the thermodynamic performance of available and new countermeasures (cf. Section 7.5), in the experimental setup is described. Emphasis is set on electrochemical techniques (cf. Section 8.4.1), while the application of the exposure setup and variations of the mortar specimens in relation to additional measurement techniques is dealt with rather briefly (cf. Section 8.4.2).

8.4.1 Electrochemical Techniques

In this Section the most important features concerning the implementation of the required electrochemical measurements stated in Section 7.5.1 into the experimental setup are described. Implementation of 'E_{corr}' monitoring, 'i_{mac}' monitoring, 'EIS' and polarisation curve measurements is described in Sections 8.4.1.1, 8.4.1.2, 8.4.1.3, and 8.4.1.4, respectively.

8.4.1.1 Corrosion Potential Monitoring

The 'E_{corr}' of the rebar and 'ECat' were monitored against the two external 'SCEs' and against the 'EEWs' during both activation and deactivation of the macrocell (cf. Table 8.1 in Section 8.3.3). Bridging of the conductors to be measured, even the 'i_{mac}' conductors, over more than one channel did not cause interference, since the multiplexer channels were electrically separated and measured one after the other. The main purpose of the 'EEWs' was to act as 'EIS' electrodes, but they also had beneficial application in the monitoring of 'E_{corr}'. Firstly, they made it possible to monitor the rebar in two directions, i.e. from the outside inwards and from the inside outwards. From the outside inwards corresponded to monitoring the rebar against the two 'SCEs', whereas from the inside outwards represented monitoring of the 'EEWs' against the rebar and against the two 'SCEs'. Based on this information an algorithm was used to adjust the 'E_{corr}' measurement of the rebar. In this way, all 'E_{corr}' deviations resulting from e.g. solution and mortar resistivity or surface and distance effects could be eliminated. The algorithm also took into account the 'ECat' and 'E_{corr}' measured against the 'SCEs' and the rebar. The individual potentials of the 'EEWs' and of the 'ECat', or 'E_{corr}' shifts, did not affect the algorithm, because these readings appeared in both measurement directions and cancelled each other out. For instance, the outer circle of electrode wires was polarised during 'EIS' and experienced an 'E_{corr}' shift; this shift was measured against both the rebar and the 'SCE' and was, therefore, cancelled out in the algorithm. Thus, the algorithm based on bidirectional measurement and input data from 23 potential readings allowed appropriate correction of the 'E_{corr}' data and many debugging options were made available.

Inaccuracies in transferring the potential values from the 'SCE' scale to the standard hydrogen electrode 'SHE' scale were minimised by measuring against two 'SCEs'. Readings from the two 'SCEs' were compared to each other as well as to the extra electrodes during monitoring. The 'SCEs' were maintained on a weekly basis. Maintenance included refilling with saturated KCl solution and KCl crystals as well as calibration against an Ag/AgCl reference electrode in a pH buffered solution. Although the above described algorithm could also be used to compensate for variations of 'E_0' of the 'SCEs' (cf. Section 2.1.7), this function was disabled. Due to the frequent maintenance and the relatively constant temperature of the exposure solutions, the 'SCE' readings were determined to be quite stable.

Monitoring of the rebar potential relative to the inner circle of electrode wires, which were not perturbed by 'EIS', was a feasible and convenient method for continuous monitoring without external electrodes, e.g. immediately after preparation or during non-submersion periods. However, due to the changes in oxygen content in the specimen (cf. Section 8.1.1), frequent calibration of the 'E_{corr}' of the electrode wires against an external reference electrode was crucial, e.g. by using a surface electrode. Such electrodes could be connected to the terminals for additional electrodes on the distribution terminal board, which were automatically logged at the end of each full scan. Calibration could be based on a limited number of representative specimens, because 'E_{corr}' of the 'EEWs' had been observed to be within a very close range for specimens with the same mortar composition and age under identical exposure conditions [Küter et al., 2005b].

The oxygen and pH sensitivity of the activated Ti wire could also be used for assessment of changes in the oxygen content and pH in the vicinity of the rebar, while the specimens were submerged. Such changes were indicated by variations in the potential of the inner circle of electrode wires against the 'SCEs' [Küter et al., 2005b].

If carbon steel wire was used instead of activated Ti wire for the 'EEWs' in the instrumented mortar specimens, the defined positions and constant distances (cf. Figure 8.3 [B] in Section 8.1.2.1) allowed for convenient non-destructive monitoring of chloride ingress. The monitoring principle was identical to the one for the rebar potential monitoring. A potential drop in the steel wire monitored against the 'SCEs' or the passive rebar indicated corrosion initiation. In this way, the chloride ingress rate could be assessed non-destructively and under exactly the same exposure conditions as for the test specimens. Furthermore, conclusive information on the bulk homogeneity of the test specimens was obtained, because the chloride ingress specimens had the same layout and were cast at the same time as the activated Ti wire specimens. Specimens with indices starting with "C-5" and "W-5" in 'Test I' (cf. Section 1.9.3) as well as "CSW" and "WSW" in 'Test II' (cf. Section 1.9.4) were based on carbon steel wires.

Additionally, specimens with activated Ti 'EEWs', but without rebar, were used in both 'Test I' and 'Test II' to quantify the 'E_{corr}' development of the activated Ti wires embedded in mortar, while the possible influence from corrosion of the rebar was eliminated. Specimens with indices starting with "C-N" and "W-N" in 'Test I' (cf. Section 1.9.3) as well as "CNR" and "WNR" in 'Test II' (cf. Section 1.9.4) were based on this layout.

8.4.1.2 Macrocell Current Monitoring

When the rebar was connected to the cathode, a mixed 'E_{corr}' was obtained and flow of 'i_{mac}' through the ammeters was enabled without introducing resistance. The mixed 'E_{corr}' and 'i_{mac}' could be influenced by reducing the exposure area of the cathode (cf. Section 8.2). As long as the rebar was passive, the impact was rather small, since the

activated Ti surface was at a much higher level of electrochemical activity than the surface of the passive rebar (cf. Section 5.1.2). However, when corrosion initiated or there was other electrochemical activity on the rebar surface, the contribution of the rebar potential to the mixed 'E_{corr}' increased largely. Hence, the potential drop, i.e. the decrement of 'E_{corr}' of the rebar (cf. Sections 5.1.2 and 8.4.1.1), could also be assessed from the decrement of the mixed 'E_{corr}' in an activated macrocell.

With rebar activity, deposition of cations yielded a calcification layer on the surface of the 'ECat', which led to an 'E_{corr}' decrement and impeded the activity of the 'ECat'. This layer could be successfully removed using HCl. The 'ECats' were removed from the exposure container and submerged in HCl for 15 min before they were resubmerged in the container at the beginning of each macrocell deactivation period.

Unlike current monitoring under potentiostatic control, the mixed potential of the rebar and 'ECat' was not preset and potential fluctuations were tolerated. The fluctuations were not affected by the state of other specimens, because each specimen was equipped with an individual cathode. We think that, besides promoting ingress of chloride ions (cf. Section 3.1.6.3), the elevated rebar 'E_{corr}' in combination with the electrochemically active 'ECat' surface under aeration created a worst case scenario for corrosion initiation and propagation. When the chloride content at the reinforcement level was sufficient to initiate corrosion, the rebar was in a thermodynamically active state at the elevated potential and under the catalysing effect of chloride ions (cf. Section 5.2.2.2).

When the rebar was in the passive state, the 'i_{mac}' was around zero micro-amperes. In the active state 'i_{mac}' was measured in the range of 100-500 µA, depending on the configuration and the corrosion state of the rebar. Since the exposure area of the rebar was well defined, the measured 'i_{mac}' allowed an estimate of the corrosion rate, while the effect of micro- or macrocells on the rebar surface could not be assessed (cf. Section 7.5.1.2). The rise in 'i_{mac}' with initiation of active corrosion was sharp and well defined, so that the onset of corrosion could be clearly identified.

The macrocell connection between rebar and 'ECat' was frequently interrupted and reactivated at set time intervals. In this way, the rebar and cathode retrieved their 'E_{corr}' when disconnected. This made it possible to draw conclusions about the thermodynamic state of the rebar. Moreover, the duration of the recovery period after deactivation and the current passed on activation of the macrocell was used to assess the corrosion state of the rebar. As in the analysis of polarisation resistance, this information could be applied to estimate the associated corrosion rate. Future publications will deal in detail with the combination of potential and current monitoring at time intervals as a quantification method for corrosion activity.

8.4.1.3 Electrochemical Impedance Spectroscopy

The 'EIS' equipment used during the initial phase of 'Test I' (at Northwestern University) was a frequency response analyzer Solartron SI 1260 [SA, 2007] in combination with an electrochemical interface Solartron SI 1287 [SA, 2007], which were daisy-chained to an IBM compatible PC and controlled by the software ZPlot [Scribner, 2004]. 'EIS' during the second phase of 'Test I' and throughout 'Test II' (at DTU Byg) was performed using a Gamry CMS 100 electrochemical measurement system [Gamry, 2007] installed in an IBM compatible PC in combination with the software Gamry Framework [Gamry, 2005].

'EIS' runs were carried out during the intervals of macrocell deactivation, after the rebar had attained its stable 'E_{corr}'. Removing of the specimens from the exposure container was not required to perform 'EIS', and 'E_{corr}' monitoring could be continued during the 'EIS' runs without interfering with the data. This provided useful information for verification purposes. All 'EIS' runs were performed at the 'E_{corr}' of the rebar with an alternating voltage perturbation of 10 mV. Ten points per frequency decade were measured. The maximum applied frequency was limited to 0.1 MHz in the equipment used. The low-frequency range was preset to 1 mHz for most runs, while some measurements down to 0.1 mHz were carried out. The standard 9-pin plug attached to the switch cards for each specimen (cf. Section 8.3.2) was connected to the 'EIS' equipment by a customised adapter. The connections established on the adapter terminal board shown in Figure 8.11 and the configuration of the pins of the 'EIS' equipment plug correspond to the Gamry CMS 100 electrochemical measurement system.

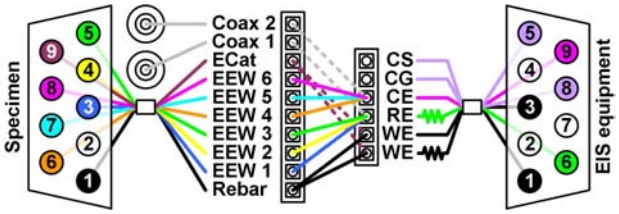

Figure 8.11: *Adapter terminal board customised for connection to the applied electrochemical impedance spectroscopy 'EIS' equipment. 'ECat': external cathode, 'EEW': embedded electrode wire, 'WE': working electrode, 'RE': reference electrode, 'CE': counter electrode, ('CS'): counter sense, and ('CG'): chassis ground. The layout of the adapter terminal board correspond to connection to a Gamry CMS 100 electrochemical measurement system [Gamry, 2007]. The colour code of the specimen connection pins corresponds to the colours used for the conductors connected to the switch card (cf. Figure 8.10 in Section 8.3.2).*

The adapter featured two 9-conductor cables with standard plugs for connection to the individual specimen plugs and the 'EIS' equipment. The associated signals were distributed by single-conductor connections between two screw terminals in the same manner as for the distribution terminal board, but on a smaller scale. The conductors of the rebar, the six 'EEWs' and the 'ECat' corresponded to the output signal from the specimen plug. Two coaxial plugs were provided for connection of external electrodes. The rebar conductor was connected to the working electrode input of the applied 'EIS' equipment. Two working electrode inputs, one equipped with a resistor, were a type-specific feature for the 'EIS' equipment used. During customary 'EIS' runs, the inner circle of 'EEWs' was connected to the 'RE' input, which was also equipped with a resistor, while the outer circle of electrode wires was connected to the 'CE' input.

Prior investigations on the instrumented mortar specimen design had shown that distortion of the 'EIS' data due to varying reference electrode positions and electrode artefacts (cf. Section 7.5.1.3) can be prevented by using activated Ti wires and the defined layout of the specimen, respectively [Küter et al., 2005b]. That way, the 'EIS' data became fully reproducible and all secondary influences were eliminated. This enabled comparison of data from different time intervals for an estimation of changes in the thermodynamic properties. Furthermore, the effect of different corrosion countermeasures could be compared based on quantitative 'EIS' data from the same time interval. Because the electrode wires could act as both 'RE' and 'CE', external electrodes were not required and 'EIS' runs could be performed before submersion of the specimens or during drying periods.

For verification runs, either one or both of the 'RE' and 'CE' connections were replaced by connections to external electrodes connected to the two coaxial plugs, see Figure 8.11. The external 'RE' and 'CE' were positioned in the additional 8 mm diameter holes next to the associated specimen (cf. Section 8.2). Any component could be connected to the 'WE' input to be electrochemically quantified by supplementary 'EIS' runs. In Figure 8.11 an example is shown of the 'ECat' used as 'WE' instead of the rebar. In this configuration, it is recommended to use an external 'RE' and 'CE'.

The counter sense ('CS') and the chassis ground ('CG') were additional type-specific features of the Gamry CMS 100. The counter sense was to be connected when the 'EIS' equipment was to be used in the zero-impedance-ammeter mode, and the chassis ground could be connected to a Faraday shield to reduce electromagnetic interference ('EMI'). The associated terminals were not connected for the 'EIS' runs, but could be used for other electrochemical measurements. For instance, the adapter could be modified to the zero-impedance-ammeter mode, which made it possible to make accurate measurements of the bulk resistivity, e.g. between two 'EEWs', or solution resistivity, e.g. between two external electrodes.

Similar connections or modified adapter terminals could be used to connect any other kind of electrochemical measuring equipment to an individual specimen, e.g. a potentiostat (cf. Section 8.4.1.4).

8.4.1.4 Polarisation Curves

The experimental setup provides different options for performing polarisation curve measurements and other potentiostatic measurements within the exposure containers (cf. Section 8.2). As mentioned in Section 8.4.1.3, the adapter terminal board (cf. Figure 8.11) could be customised, so that a potentiostat or any other electrochemical equipment could be connected to the standard 9-pin plug (cf. Section 8.3.2). That way, the instrumented mortar specimens could be conveniently tested or measurements could be performed using other specimens in combination with external electrodes. The extra holes next to the specimens provided defined positions for 'RE' and 'CE'; 'ECats' (cf. Section 8.1.3) could also be used for this purpose. As 'E_{corr}' monitoring (cf. Section 8.4.1.1) or 'EIS' (cf. Section 8.4.1.3), polarisation curve measurements could be performed before submersion or during non-submersion periods, since all required electrodes are embedded in the instrumented mortar specimens. Nevertheless, the standard (full-scale, anodic) polarisation curve measurements were performed on a supplementary three-electrode setup, see Figure 8.12 [A] and [B].

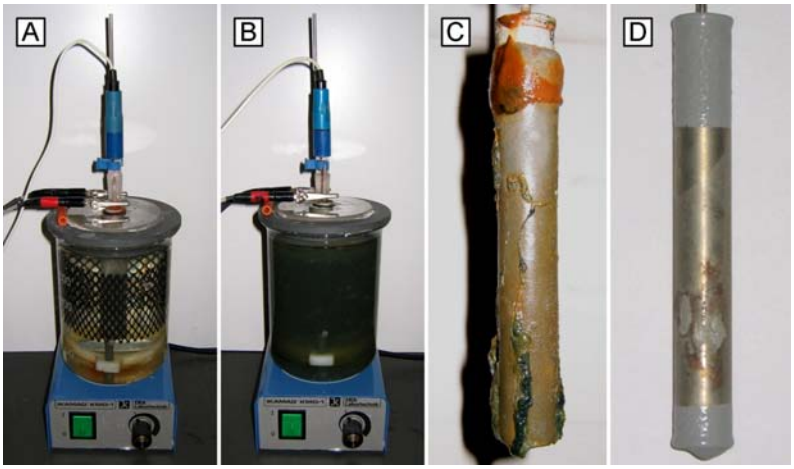

Figure 8.12: [A]: *Three-point electrode setup for destructive electrochemical testing. During testing of grit-blasted cement paste specimen (specimen "C01-G", cf. Section 1.9.4).* [B]: *As [A], but after testing of grit-blasted cement paste specimen with major precipitation of black rust.* [C]: *Grit-blasted cement paste specimen after testing with severe cracking and deposition of red/green/black rust.* [D]: *Stainless cement paste specimen (specimen "C02-J", cf. Section 1.9.4) after testing and removal of the cement layer to investigate the physical appearance of the corrosion damage showing severe pitting damage.*

The reasons for performing polarisation curves on a supplementary setup was the homogenous field supplied by the activated Ti wire mesh (see Figure 8.12 [A]) used as 'CE' and most importantly the major formation of corrosion products in full-scale anodic testing, which would have required a change of solution in the exposure setup (cf. Section 8.2) after each test. This is exemplified by the deposition of black rust in the exposure solution after testing (see Figure 8.12 [B]) and the deposition of green rust on the associated grit-blasted sample (see Figure 8.12 [C]).

The acrylic glass plate on top of the corrosion cell was used as an adapter for testing the cement paste specimens. Instrumented or plain mortar specimens could be tested on the same setup, while being supported and centred by the lower plastic ring (white), see Figure 8.12 [A]. Polarisation curve measurements as well as all other potentiostatic electrochemical measurements were performed by means of a VoltaLab 10 (PGZ100) all-in-one electrochemical laboratory [RA, 2007] connected to an IBM compatible PC; the software used was VoltaMaster 4.0 [RA, 2005]. Polarisation curves were determined in different ways, but generally based on two or more "anodic loops". The "loops" were started at an electrode potential of 100 mV below the 'E_{corr}' that was established after a predefined time of submersion on the setup (normally, 6 hours). Different maximum electrode potentials were tested and the scan rate was varied between 0.01 and 0.1 mV/s.

8.4.2 Additional Measurement Techniques

Besides these electrochemically tested (i.e. monitored) specimens, a number of the container positions which did not provide an 'ECat' connection (A-D, see Figure 5 [B]) were equipped with plain mortar specimens. Plain mortar specimens were based on the layout as the mortar test specimens, but without rebar and 'EEWs'. These specimens were split and tested for chloride ingress by means of the colour test [Frederiksen, 1997] (cf. Section 3.1.7.3). Specimens with the indices starting with "C-P" and "W-P" in 'Test I' (cf. Section 1.9.3) as well as "CPM" and "WPM" in 'Test II' (cf. Section 1.9.4) were plain mortar specimen*. The threshold for colour changes and the ingress parameters were calibrated by chloride profiles from grinding of cubical specimens (e.g. according to NT BUILD 443 [Frederiksen, 1997], cf. Section 3.1.7.3), which were stored in the free spaces of the exposure container or in the reservoir. The ratio of solution volume to the exposed mortar surface area was adjusted accordingly (cf. Section 8.2).

Wires with a higher sensitivity to chloride, e.g. Ag/AgCl wires, or with sensitivity to other parameters, e.g. graphite for oxygen sensitivity, could be employed as an alter-

* Plain mortar specimens exposed in the potable water containers provided the reference material for chemical tests, e.g. for testing of the mortar pH by phenolphthalein solution or rainbow indicator (cf. Sections 3.1.7.2 and 5.2.2.2), testing of the chloride content by the colour test (cf. Section 3.1.7.3), and for 'LOM', 'SEM', or 'EDS' analyses of the mortar.

native ‘EEW’ to obtain information on specific properties or time-dependent alterations inside the specimen. These aspects will be evaluated in future investigations.

The pH of the exposure solution was measured using standard pH indicator strips inserted through the screw caps on the exposure container. In the ongoing experiments the pH measurements were performed on a weekly basis in connection with the ‘SCE’ maintenance and calibration. Both exposure solutions (the 10% ‘w/w’ chloride exposure solution and the potable water) were replaced by new solution every five weeks, in accordance with NT BUILD 443 [Frederiksen, 1997], or when the solution pH was measured to exceeded 8 (cf. Section 1.9.2). If desired, pH sensitive electrodes could be permanently mounted in the associated extra holes and connected to the reserved channels on the distribution terminal board (channels 313-315) (cf. Sections 8.2 and 8.3.3). The same is true for ion-selective or chloride electrodes. The exposure solution and air temperatures as well as the voltage levels of the ammeter batteries are automatically monitored by the datalogger control routine.

The standard plug connector on each specimen allowed connection to virtually any kind of electrochemical measurement equipment (cf. Section 8.2). The only requirement was the appropriate adapter (cf. Section 8.3.3). Measurements could be made in connection with the ‘EEWs’ or external electrodes positioned in the associated extra holes (cf. Sections 8.2).

The design based on various small-sized specimens allowed selection of individual specimens for destructive testing based on ‘LOM’, ‘SEM’, or ‘EDS’ analyses or other techniques, e.g. testing of the mortar pH by phenolphthalein solution or rainbow indicator or testing of the chloride content by the colour test (cf. Section 7.5.2). The free specimen position could then be used for a new specimen or closed with a rubber stopper to keep the exposure system closed.

9 Conclusions and Recommendations

Existing knowledge on aqueous corrosion and reinforced concrete (Chapters 2 and 3) was extended to and applied for:

- A thermodynamically consistent description of reinforcement corrosion (Chapters 4 and 5)
- The evaluation of available corrosion countermeasures (Chapter 6)
- The establishment of a design approach for new corrosion countermeasures (Chapter 7)
- The conceptual design of two new corrosion countermeasures (Chapter 7)
- The development of suitable test setups and the adaptation of existing measurement/monitoring for conclusive performance evaluation (Chapter 8).

Brief summaries of the contents of all Chapters were given in Section 1.8. The most important findings of Chapters 4 to 8 and related recommendations for future investigations are listed in the following:

- "Application of Thermodynamics" (Chapter 4)

  Thermodynamics controls corrosion tendencies; a reaction does not occur, if thermodynamically impossible. Given that all determining parameters are taken into account, a thermodynamic model indicates how conditions can be manipulated to make corrosion (thermodynamically) impossible. Thus, appropriate models can be applied for the evaluation of available and the design of new countermeasures.

  Immunity is a definite inherent electrochemical property of a certain metal in an aqueous solution (based on a given ion activity), whereas passivation and depassivation depend on both thermodynamic and kinetic factors. The preselection of elements and the choice of ion activities are the crucial parameters for the establishment of representative Pourbaix diagrams.

  We have derived and suggested a design procedure for Pourbaix diagrams. By means of this procedure it is not only possible to establish Pourbaix diagrams for systems that can be represented by single elements, but also for systems, where formation of compounds between different elements must be taken into account. If all required thermodynamic data is available, multi-element Pourbaix diagrams can be established to represent any electrochemical system. This approach is also valid for metals in combination with substances forming soluble compounds; a case which is generally excluded from Pourbaix diagrams in the literature. Thus, it is also possible to obtain information on complex chemical systems, e.g. corrosion propagation in chloride contaminated concrete.

Conclusions regarding the corrosion tendencies can only be drawn upon Pourbaix diagrams that reflect the thermodynamics of the system; otherwise, the diagrams are meaningless.

As an important future task we suggest the establishment of a complete thermodynamic database for metals in concrete. This database should also account for mineral additions and chemical admixtures, since these factors have a significant influence on the formation of species.

- "Thermodynamics of Reinforcement Corrosion" (Chapter 5)

  Various reaction mechanisms postulated in the literature are partly erroneous or incomplete from a thermodynamic perspective. Alternative consistent descriptions based Pourbaix diagrams and reaction mechanisms were proposed in this thesis. The passive state and the immune state have been dealt with rather briefly, while active corrosion was described in detail for two situations: carbonation induced corrosion in oxygen-rich concrete and chloride induced corrosion in oxygen-deprived concrete.

  It was demonstrated that carbonation induced corrosion can be fully assessed by thermodynamic models. For chloride induced corrosion only propagation can be described thermodynamically, whereas the initiation stage is largely governed by kinetic parameters. A mechanism for the propagation stage of chloride induced was proposed. This mechanism is based on a self-contained loop between oxidation of ferrous ion to ferric chloride and the etching action of ferric chloride on iron. An associated pH decrease and pore-blocking confine acidified pathways in the concrete bulk. This mechanism was sustained by own experimental observations and found in good agreement with corrosion phenomena observed in practice.

  Protection mechanisms can be derived and described similarly as corrosion processes. Such descriptions must be based on extensive experimental investigations; much future research is required with reference to that.

- "Available Corrosion Countermeasures" (Chapter 6)

  State-of-the-art durability design and available corrosion countermeasures for new and existing structures were discussed. It was reasoned and exemplified that many of the available corrosion countermeasures are not effective; some displayed deficiencies from a thermodynamic point of view. Other countermeasures were determined to be effective, e.g. stainless steel and cathodic prevention/protection. However, it was exemplified that these available effective measures are not always applicable for economical, practical, or technical reasons.

  We concluded that new effective and in particular cost-efficient countermeasures for new and existing structures are still in demand. Therefore, the most important recommendations for future investigations relate to the development of new coun-

termeasures. Moreover, we recommend further documentation of the available effective countermeasures, e.g. corrosion performance of stainless steel welds and cathodic prevention/protection of high-strength steels.

- "Design of Corrosion Countermeasures" (Chapter 7)

  Requirements for new countermeasures were formulated based on the thermodynamic description of reinforcement corrosion as well as on the evaluation of available countermeasures.

  Two principles of implementation were derived to fulfil the formulated requirements. These principles are applicable for both new structures and repair of existing structures. They are expected to significantly improve the corrosion protection of carbon steel reinforcement in contaminated and cracked (up to a certain crack width) concrete.

  Both principles aim at obtaining targeted low corrosion potentials. The materials concept of the first principle of implementation also enables concrete-steel interface improvement by electrochemical densification during the setting of concrete and formation of pore-blockers at later stages. These actions are immobilised in the materials concept for the second principle, which aims at a high current yield for effective cathodic protection of the carbon steel reinforcement.

  The materials concepts employ magnesium and zinc in combination with supplementary electrochemically active compounds. The principle specific features are achieved by tailored proportioning of the implemented materials and customised production processes. By means of these solutions carbon steel reinforcement can be operated at targeted and long-term stable low corrosion potentials, while hydrogen evolution or any other undesired interference between the introduced materials concepts and the concrete-steel system are prevented.

  The concepts and their implementation principles are the central objective of this thesis. However, due to expected patent possibilities only limited information on the concepts is provided.

  In general, this thesis covers a very early stage of the development of new corrosion countermeasures. Much further investigation is required before the countermeasures can be implemented and tested on a structural scale. The most immediate investigations concern the fine-tuning of the production processes of the two proposed principles. Moreover, the performance of thin zinc ferrite layers, which were proposed as alternative cost-effective measures against carbonation induced corrosion, should be further evaluated.

- "Test Setup and Measuring Methods" (Chapter 8)

  A setup for comprehensive testing was developed in order to evaluate the performance of the proposed new countermeasures based on multiple specimens. Ini-

tial tests of the first principle of implementation (surface modifications) were undertaken in this setup.

The first principle of implementation was tested against available corrosion protection measures. Testing was performed by instrumented mortar specimens as well as simple mortar and cement paste specimens. The instrumented mortar specimens were equipped with embedded electrodes. This allowed for obtaining information on changes at the metal surface and at the mortar-metal interface as well as on conductivity, oxygen content, and other relevant parameters of the mortar bulk. The simple mortar and the cement paste specimens were used as reference specimens, which aimed at investigating the thermodynamic conditions of the embedded metal surface only.

The specimens were tested in a high-capacity exposure setup and monitored by an automated system, which allowed for monitoring of multiple specimens by means of cluster measurements. In the final configuration, 54 specimens could be monitored with 24 channels each. The monitoring was performed by a combination of continuous corrosion potential and macrocell current measurements. These were supplemented by frequent electrochemical impedance spectroscopy using the instrumented mortar specimens. Moreover, destructive measurements, e.g. anodic polarisation curves, were performed using a large quantity of cement paste specimens. Chemical analyses of e.g. pH alteration and chloride content as well as microscopic and X-ray analyses were used to obtain data for a comprehensive thermodynamic performance evaluation.

The setup and test methods will be applied in the investigations concerning the further development of the proposed new countermeasures. We consider the information that can be obtained from the applied electrochemical methods to be adequate for the planned investigations. With regard to microscopic and chemical analyses, expansion of the applied techniques to sample preparation and analyses in an inert atmosphere are additional objectives of future investigations. Moreover, it is planned to advance the concept of the instrumented mortar specimens in combination with the applied electrochemical methods towards comprehensive embeddable corrosion sensors. These advancements relate primarily to the second principle of implementation by means of concrete spacers, i.e. to the establishment of a “smart spacer” solution.

List of References

[Abu Ayana et al., 1997] Abu Ayana, Y. M., El-Sawy, S. M., & Salah, S. H. (1997). 'Zinc-ferrite pigment for corrosion protection'. *Anti-Corrosion Methods and Materials*, **44**(6), pp. 381–388.

[ACI 116R, 2000] ACI 116R (2000). *Cement and Concrete Terminology*. Report 116R-00 (Reapproved 2005). American Concrete Institute (ACI), Farmington Hills, MI, USA. 73 pp.

[ACI 201.2R, 2001] ACI 201.2R (2001). *Guide to Durable Concrete*. Report 201.2R-01. American Concrete Institute (ACI), Farmington Hills, MI, USA. 41 pp.

[ACI 222R, 2001] ACI 222R (2001). *Protection of Metals in Concrete Against Corrosion*. Report 222R-01. American Concrete Institute (ACI), Farmington Hills, MI, USA. 41 pp.

[ACI 224.1R, 1998] ACI 224.1R (1998). *Causes, Evaluation and Repair of Cracks in Concrete Structures*. Report 244.1R-98. American Concrete Institute (ACI), Farmington Hills, MI, USA. 22 pp.

[ACI 224R, 2001] ACI 224R (2001). *Control of Cracking in Concrete Structures*. Report 224R-01. American Concrete Institute (ACI), Farmington Hills, MI, USA. 43 pp.

[ACI 301M, 2005] ACI 301M (2005). *Metric Specifications for Structural Concrete*. Report 301M-05. American Concrete Institute (ACI), Farmington Hills, MI, USA. 49 pp.

[ACI 318M/318RM, 2005] ACI 318M/318RM (2005). *Metric Building Code Requirements for Structural Concrete and Commentary*. Standard and commentary 318M-05/318RM-05. American Concrete Institute (ACI), Farmington Hills, MI, USA. 436 pp.

[ACI 357R, 1984] ACI 357R (1984). *Guide for the Design and Construction of Fixed Offshore Concrete Structures*. Report 357R-84 (Reapproved 1997). American Concrete Institute (ACI), Farmington Hills, MI, USA. 26 pp.

[ACI 362.1R, 1997] ACI 362.1R (1997). *Guide for the Design of Durable Parking Structures*. Report 362.1R-97 (Reapproved 2002). American Concrete Institute (ACI), Farmington Hills, MI, USA. 40 pp.

[ACI 363.2R, 1998] ACI 363.2R (1998). *Guide to Quality Control and Testing of High-Strength Concrete*. Report 363.2R-98. American Concrete Institute (ACI), Farmington Hills, MI, USA. 18 pp.

[ACI 363R, 1992] ACI 363R (1992). *State-of-the-Art Report on High-Strength Concrete*. Report 363R-92 (Reapproved 1997). American Concrete Institute (ACI), Farmington Hills, MI, USA. 55 pp.

[ACI 365.1R, 2000] ACI 365.1R (2000). *Service-Life Prediction. State-of-the-Art Report*. Report 365.1R-00. American Concrete Institute (ACI), Farmington Hills, MI, USA. 44 pp.

[ACI 440.1R, 2003] ACI 440.1R (2003). *Guide for the Design and Construction of Concrete Reinforced with FRP Bars*. Report 440.1R-03. American Concrete Institute (ACI), Farmington Hills, MI, USA. 42 pp.

[ACI 515.1R, 1979] ACI 515.1R (1979). *Guide to the Use of Waterproofing, Dampproofing, Protective, and Decorative Barrier Systems for Concrete*. Report 515.1R-79 (Reapproved 85). American Concrete Institute (ACI), Farmington Hills, MI, USA. 44 pp.

[ACI 546R, 2004] ACI 546R (2004). *Concrete Repair Guide*. Report 546R-04. American Concrete Institute (ACI), Farmington Hills, MI, USA. 53 pp.

[ACI et al., 2003] ACI et al. (2003). *Concrete Repair Manual*. Collection RPMN03. American Concrete Institute (ACI), American Society of Civil Engineers (ASCE), Building Research Establishment (BRE), Construction Research Communications (CRC), Concrete Society (CS), International Concrete Repair Institute (ICRI), NACE International, The Society for Protective Coatings (SSPC), and United States Army Corps of Engineers (USACE), USA and UK. 2077 pp.

[AGA, 2005] AGA (2005). *Hot-Dip Galvanizing for Corrosion Prevention. A Guide to Specifying and Inspecting Hot-Dip Galvanized Reinforcing Steel*. Report. American Galvanizers Association, Centennial, CO, USA. 16 pp. Available online, http://www.galvanizedrebar.com, accessed: 12-May-2007.

[AGA, 2007] AGA (2007). *Corrosion Performance of Galvanized Steel in Concrete*. American Galvanizers Association, Centennial, CO, USA. Website, http://www.galvanizeit.org, accessed: 12-May-2007.

[Aldea et al., 2000] Aldea, C.-M., Ghandehari, M., Shah, S. P., & Karr, A. (2000). 'Estimation of Water Flow through Cracked Concrete under Load'. *ACI Materials Journal*, **97**(5), pp. 567–575.

[Aldea et al., 1999] Aldea, C.-M., Shah, S., & Karr, A. (1999). 'Permeability of Cracked Concrete'. *Materials and Structures*, **32**, pp. 370–376.

[Alonso et al., 1998] Alonso, C., Andrade, C., Rodriguez, J., & Diez, J. M. (1998). 'Factors controlling cracking of concrete affected by reinforcement corrosion'. *Materials and Structures*, **31**(211), pp. 435–441.

[Andor, 2007] Andor (2007). *Raman Spectroscopy*. Application notes. Andor Technology, Belfast, UK. 7 pp.

[Andrade et al., 1993] Andrade, C., Alonso, C., & Molina, F. (1993). 'Cover cracking as a function of bar corrosion: Part 1 - Experimental test'. *Materials and Structures*, **26**(162), pp. 453–464.

[Andrade et al., 1995a] Andrade, C., Merino, P., Novoa, X., Perez, M., & Soler, L. (1995a). 'Passivation of reinforcing steel in concrete'. *Materials Science Forum*, **192-194**, pp. 891–898.

[Andrade et al., 1995b] Andrade, C., Soler, L., Alonso, C., Novoa, X. R., & Keddam, M. (1995b). 'The importance of geometrical considerations in the measurements of steel corrosion in concrete by means of AC impedance'. *Corrosion Science*, **37**(12), pp. 2013–2023.

[Antunes et al., 2003] Antunes, R. A., Costa, I., & Faria, D. L. A. d. (2003). 'Characterization of corrosion products formed on steels in the first months of atmospheric exposure'. *Materials Research*, **6**, pp. 403–408.

[APA, 2001] APA (2001). *Publication Manual of the American Psychological Association*. Washington, DC, USA: American Psychological Association, 5th edition. 439 pp.

[Arup, 1983] Arup, H. (1983). 'The mechanisms of protection of steel by concrete', chapter 10, pp. 151–157. In Crane, A. P. (Ed.). *Corrosion of reinforcement in concrete construction*. Chichester, England: Horwood.

[Arup & Sørensen, 1992] Arup, H. & Sørensen, B. (1992). 'A new embeddable reference electrode for use in concrete', pp. 192/1–192/10. In *Proceedings of CORROSION/92*. Nashville, TN, USA.

[Arup & Sørensen, 1995] Arup, H. & Sørensen, H. E. (1995). 'A proposed technique for determining chloride thresholds', pp. 460–469. In *Proceedings of pro002: Chloride Penetration into Concrete. International RILEM Workshop*. Saint-Rémy-lès-Chevreuse, France.

[ASTM A615M, 2007] ASTM A615M (2007). *Standard Specification for Deformed and Plain Carbon-Steel Bars for Concrete Reinforcement*. Designation: A615M-07. ASTM International, West Conshohocken, PA, USA. 6 pp.

[ASTM A767M, 2005] ASTM A767M (2005). *Standard Specification for Zinc-Coated (Galvanized) Steel Bars for Concrete Reinforcement*. Designation: A767M-05. ASTM International, West Conshohocken, PA, USA. 4 pp.

[ASTM A775M, 2007] ASTM A775M (2007). *Standard Specification for Epoxy-Coated Steel Reinforcing Bars*. Designation: A775M-07a. ASTM International, West Conshohocken, PA, USA. 10 pp.

[ASTM A934M, 2007] ASTM A934M (2007). *Standard Specification for Epoxy-Coated Prefabricated Steel Reinforcing Bars*. Designation: A934M-07. ASTM International, West Conshohocken, PA, USA. 17 pp.

[ASTM A944, 2005] ASTM A944 (2005). *Standard Test Method for Comparing Bond Strength of Steel Reinforcing Bars to Concrete Using Beam-End Specimens*. Designation: A944-05. ASTM International, West Conshohocken, PA, USA. 4 pp.

[ASTM A955M, 2007] ASTM A955M (2007). *Standard Specification for Deformed and Plain Stainless Bars for Concrete Reinforcement*. Designation: A955M-07a. ASTM International, West Conshohocken, PA, USA. 11 pp.

[ASTM B117, 2007] ASTM B117 (2007). *Standard Practice for Operating Salt Spray (Fog) Apparatus*. Designation: B117-07. ASTM International, West Conshohocken, PA, USA. 10 pp.

[ASTM B322, 2004] ASTM B322 (2004). *Standard Guide for Cleaning Metals Prior to Electroplating*. Designation: B322-99 (Reapproved 2004). ASTM International, West Conshohocken, PA, USA. 9 pp.

[ASTM C1157, 2003] ASTM C1157 (2003). *Standard Performance Specification for Hydraulic Cement*. Designation: C1157-03. ASTM International, West Conshohocken, PA, USA. 6 pp.

[ASTM C1240, 2005] ASTM C1240 (2005). *Standard Specification for Silica Fume Used in Cementitious Mixtures*. Designation: C1240-05. ASTM International, West Conshohocken, PA, USA. 7 pp.

[ASTM C125, 2005] ASTM C125 (2005). *Terminology Relating to Concrete and Concrete Aggregates*. Designation: C125-07. ASTM International, West Conshohocken, PA, USA. 5 pp.

[ASTM C150, 2007] ASTM C150 (2007). *Standard Specification for Portland Cement*. Designation: C150-07. ASTM International, West Conshohocken, PA, USA. 8 pp.

[ASTM C1602M, 2006] ASTM C1602M (2006). *Standard Specification for Mixing Water Used in the Production of Hydraulic Cement Concrete*. Designation: C1602M-06. ASTM International, West Conshohocken, PA, USA. 4 pp.

[ASTM C33, 2007] ASTM C33 (2007). *Standard Specification for Concrete Aggregates*. Designation: C33-07. ASTM International, West Conshohocken, PA, USA. 11 pp.

[ASTM C494M, 2005] ASTM C494M (2005). *Specification for Chemical Admixtures for Concrete*. Designation: C494M-05a. ASTM International, West Conshohocken, PA, USA. 10 pp.

[ASTM C595, 2007] ASTM C595 (2007). *Standard Specification for Blended Hydraulic Cements*. Designation: C595-07. ASTM International, West Conshohocken, PA, USA. 7 pp.

[ASTM C618, 2005] ASTM C618 (2005). *Standard Specification for Coal Fly Ash and Raw or Calcined Natural Pozzolan for Use in Concrete*. Designation: C618-05. ASTM International, West Conshohocken, PA, USA. 3 pp.

[ASTM C876, 1999] ASTM C876 (1999). *Standard Test Method for Half-Cell Potentials of Uncoated Reinforcing Steel in Concrete*. Designation: C876-91 (Reapproved 1999). ASTM International, West Conshohocken, PA, USA. 6 pp.

[ASTM C989, 2006] ASTM C989 (2006). *Standard Specification for Ground Granulated Blast-Furnace Slag for Use in Concrete and Mortars*. Designation: C989-06. ASTM International, West Conshohocken, PA, USA. 5 pp.

[ASTM DS561, 2004] ASTM DS561 (2004). *Metals and Alloys in the Unified Numbering System*. West Conshohocken, PA, USA: ASTM International, 10th edition. 500 pp.

[ASTM E1508, 2003] ASTM E1508 (2003). *Standard Guide for Quantitative Analysis by Energy-Dispersive Spectroscopy*. Designation: E1508-98 (Reapproved 2003). ASTM International, West Conshohocken, PA, USA. 8 pp.

[ASTM E2142, 2001] ASTM E2142 (2001). *Standard Test Methods for Rating and Classifying Inclusions in Steel Using the Scanning Electron Microscope*. Designation: E2142-01. ASTM International, West Conshohocken, PA, USA. 16 pp.

[ASTM G102, 1999] ASTM G102 (1999). *Standard Practice for Calculation of Corrosion Rates and Related Information from Electrochemical Measurements*. Designation: G102–89 (Reapproved 1999). ASTM International, West Conshohocken, PA, USA. 7 pp.

[ASTM G106, 1999] ASTM G106 (1999). *Standard Practice for Verification of Algorithm and Equipment for Electrochemical Impedance Measurements*. Designation: G106–89 (Reapproved 1999). ASTM International, West Conshohocken, PA, USA. 11 pp.

[ASTM G109, 2005] ASTM G109 (2005). *Standard Test Method for Determining the Effects of Chemical Admixtures on the Corrosion of Embedded Steel Reinforcement in Concrete Exposed to Chloride Environments*. Designation: G109-99a (Reapproved 2005). ASTM International, West Conshohocken, PA, USA. 6 pp.

[ASTM G3, 2004] ASTM G3 (2004). *Standard Practice for Conventions Applicable to Electrochemical Measurements in Corrosion Testing*. Designation: G3-89 (Reapproved 2004). ASTM International, West Conshohocken, PA, USA. 9 pp.

[ASTM G5, 2004] ASTM G5 (2004). *Standard Reference Test Method for Making Potentiostatic and Potentiodynamic Anodic Polarization Measurements*. Designation: G5-94 (Reapproved 2004). ASTM International, West Conshohocken, PA, USA. 12 pp.

[ASTM G59, 2003] ASTM G59 (2003). *Standard Test Method for Conducting Potentiodynamic Polarization Resistance Measurements*. Designation: G59-97 (Reapproved 2003). ASTM International, West Conshohocken, PA, USA. 4 pp.

[Audenaert et al., 2007] Audenaert, K., Marsavina, L., & Schutter, G. d. (2007). *Transport Mechanisms in Cracked Concrete*. Leuven, Belgium: Acco, 1st edition. 127 pp.

[AutoLab, 2005] AutoLab (2005). *Electrochemical Impedance Spectroscopy (EIS): 1. Basic Principles*. Application note. AutoLab, Utrecht, The Netherlands. Available online, http://www.ecochemie.nl, accessed: 06-Mar-2005. 2 pp.

[Baker, 1977] Baker, E. A. (1977). 'Marine Corrosion Behavior of Bare and Metallic – Coated Reinforcing Rods in Concrete', pp. 30–50. In Tonini, D. E. Dean, S. W. J. (Ed.). *Chloride Corrosion Of Steel In Concrete*. Number ASTM STP 692. West Conshohocken, PA, USA: ASTM International.

[Bardal, 2004] Bardal, E. (2004). *Corrosion and Protection*. Engineering Materials and Processes. London, UK: Springer, 1st edition. 336 pp.

[Barin, 1993] Barin, I. (1993). *Thermodynamical Data of Pure Substances. Part 1 and Part 2*. Weinheim, Germany: VCH, 2nd edition. 1850 pp.

[Bentur et al., 1997] Bentur, A., Diamond, S., & Berke, N. S. (1997). *Steel Corrosion in Concrete. Fundamentals and Civil Engineering Practice*. Number 6 in Modern Concrete Technology. London, UK: E & FN Spon (Chapman & Hall), 1st edition. 201 pp.

[Bentz et al., 2001] Bentz, D., Geiker, M., & Hansen, K. (2001). 'Shrinkage-reducing admixtures and early-age desiccation in cement pastes and mortars'. *Cement and Concrete Research*, **31**(7), pp. 1075–1085.

[Berke & Hicks, 1990] Berke, N. S. & Hicks, M. C. (1990). 'Electrochemical Methods of Determining the Corrosivity of Steel in Concrete', pp. 425–440. In Baboian, R. & Dean, Sheldon, W. (Eds.). *Corrosion Testing and Evaluation: Silver Anniversary Volume*. Number ASTM STP 1000. West Conshohocken, PA, USA: ASTM International.

[Berke & Hicks, 1992] Berke, N. S. & Hicks, M. C. (1992). 'Estimating the Life Cycle of Reinforced Concrete Decks and Marine Piles Using Laboratory Diffusion and Corrosion Data', pp. 207–231. In Chaker, V. (Ed.). *Corrosion Forms and Control for Infrastructure*. Number ASTM STP 1137. West Conshohocken, PA, USA: ASTM International.

[Bertolini et al., 2004] Bertolini, L., Elsener, B., Pedeferri, P., & Polder, R. B. (2004). *Corrosion of Steel in Concrete. Prevention, Diagnosis, Repair*. Weinheim, Germany: Wiley-VCH, 1st edition. 409 pp.

[Bhadeshia & Honeycombe, 2006] Bhadeshia, H. & Honeycombe, R. (2006). *Steels: Microstructure and Properties*. London, UK: Butterworth-Heinemann (Elsevier), 3rd edition. 360 pp.

[Böhni et al., 2005] Böhni, H., Hunkeler, F., Schiegg, Y., Gulikers, J., Schießl, P., Nürnberger, U., Raupach, M., Rößler, G., Büchler, M., & Polder, R. B. (2005). *Corrosion in Reinforced Concrete Structures*. Cambridge, England: Woodhead, 1st edition. 264 pp.

[Bjerregaard et al., 2000] Bjerregaard, L., Geels, K., Ottesen, B., & Rückert, M. (2000). *Metalog Guide*. Ballerup, Denmark: Struers A/S, 3rd edition. 113 pp.

[Borgard et al., 1990] Borgard, B., Warren, C., Somayaji, R., & Heidersbach, R. (1990). 'Mechanisms of corrosion of steel in concrete', pp. 174–188. In Berke, N. S., Chaker, V., & Whiting, D. (Eds.). *Corrosion rates of steel in concrete*. Number ASTM STP 1065 in ASTM STP. West Conshohocken, PA, USA: ASTM International.

[Boulfiza et al., 2003] Boulfiza, M., Sakai, K., Banthia, N., & Yoshida, H. (2003). 'Prediction of Chloride Ions Ingress in Uncracked and Cracked Concrete'. *ACI Materials Journal*, **100**(1), pp. 38–48.

[Brandenburg, 2005] Brandenburg (2005). *Recyling of Reinforced Concrete*. Brandenburg Industrial Service, Chicago, Il, USA. Website, http://www.brandenburg.com, accessed: 25-Nov-2006.

[Broomfield, 1997] Broomfield, J. P. (1997). *Corrosion of Steel in Concrete. Understanding, Investigation and Repair*. London, UK: E & FN Spon (Chapman & Hall), 1st edition. 226 pp.

[Buenfeld et al., 2004] Buenfeld, N., Glass, G., Reddy, B., & Viles, F. (2004). *Process for the Protection of Reinforcement in Reinforced Concrete*. United States Patent 6685822. USPTO, Alexandria, VA, USA. 30 pp.

[Callister & Callister, 2000] Callister, W. D. & Callister, W. D. J. (2000). *Fundamentals of Materials Science and Engineering*. New York, NY, USA: Wiley, 5th edition. 552 pp.

[Campbell et al., 1991] Campbell, D. H., Sturm, R. D., & Kosmatka, S. H. (1991). 'Detecting Carbonation'. *Concrete Technology Today*, **12**(1), pp. 1–5.

[Castro et al., 2003] Castro, P., Pazini, E., Andrade, C., & Alonso, C. (2003). 'Macrocell activity in slightly chloride-contaminated concrete induced by reinforcement primers'. *Corrosion*, **59**(6), pp. 535–546.

[Castro et al., 1996] Castro, P., Sagüés, A., Moreno, E., Maldonado, L., & Genescá, J. (1996). 'Characterization of Activated Titanium Solid Reference Electrodes for Corrosion Testing of Steel in Concrete'. *Corrosion*, **52**(8), pp. 609–616.

[CeFrCo, 2007] CeFrCo (2007). *Concrete Corrosion*. Centre Français de l'anticorrosion. CEFRACOR, Paris, France. Website, http://www.concretecorrosion.net, accessed: 18-May-2007.

[CemNet, 2007] CemNet (2007). *Global Cement Report*. CemNet, Dorking, UK. Website, http://cemnet.co.uk, accessed: 04-May-2007.

[Chesney, 2003] Chesney, P. (2003). 'A new spray coating process for manufacture of stainless steel clad construction steel with resistance to corrosion by de-icing salts & seawater', pp. 5.3–5.11. In Bauckhage, K., Uhlenwinkel, V., Ziesenis, J., & Leatham, A. (Eds.). *Proceedings of the* 5th *International Conference on Spray Forming (ICSF V)*. Bremen, Germany.

[Chess, 1998] Chess, P. M. (1998). *Cathodic Protection of Steel in Concrete*. London, UK: Taylor & Francis, 2nd edition. 187 pp.

[Chowdhury, 2004] Chowdhury, P. C. (2004). 'Strategies for resisting corrosion of reinforcement in concrete'. *The Indian Concrete Journal*, pp. 46–51.

[CIEG, 2007] CIEG (2007). *Eurocode and Reinforcement*. Concrete Industry Eurocode 2 Group, Coordinator: The Concrete Centre, Blackwater, UK. Website, http://www.eurocode2.info, accessed: 17-Sep-2007.

[Cigna et al., 2003] Cigna, R., Andrade, C., Nünberger, U., Polder, R., Weydert, R., & Seitz, E. (Eds.) (2003). *EUR 20599. Cost Action 521. Corrosion of steel in reinforced concrete structures. Final Report*. Luxembourg, Luxembourg: Office for Official Publications of the European Communities, 1st edition. 238 pp.

[Clemeña & Virmani, 2004] Clemeña, G. G. & Virmani, Y. P. (2004). 'Comparing the Chloride Resistance of Reinforcing Bars'. *Concrete International*, **26**(11), pp. 39–49.

[Colwell, 1992] Colwell, J. A. (1992). *On The Mechanism of Corrosion of Composite Tubes at Ports in Kraft Recovery Boilers*. Technical Paper 440. Institute of Paper Science and Technology, Atlanta, GA, USA. 27 pp.

[Costa & Appleton, 1999] Costa, A. & Appleton, J. (1999). 'Chloride penetration into concrete in marine environment – Part II: Prediction of long term chloride penetration'. *Materials and Structures*, **32**(219), pp. 354–359.

[Cottis & Turgoose, 1999] Cottis, R. & Turgoose, S. (1999). *Electrochemical Impedance and Noise*. Corrosion Testing Made Easy. Houston, TX, USA: NACE International, 1st edition. 136 pp.

[COWI, 2007a] COWI (2007a). *Helgeland Bridge, Leirfjorden, Norway*. Personal communication. Kgs. Lyngby, Denmark, Lyngby, Denmark.

[COWI, 2007b] COWI (2007b). *Notch-like shape corrosion attack of reinforcing steel*. Personal communication. COWI A/S, Kgs. Lyngby, Denmark.

[COWI, 2007c] COWI (2007c). *Spalling at pier of Florida Keys Bridges, FL, USA, due to corrosion of the epoxy-coated reinforcement*. Personal communication. Kgs. Lyngby, Denmark, Lyngby, Denmark.

[CRSI, 2002] CRSI (2002). *Steel Reinforcing Bars: Recycled*. Special report. Concrete Reinforcing Steel Institute, Schaumburg, IL, USA. 2 pp. Available online, http://www.crsi.org/pdf/recycling_report.pdf, accessed: 12-May-2007.

[CS, 1989] CS (1989). *Cathodic Protection of Reinforced Concrete*. Report TR36. Concrete Society, Blackwater, UK. 76 pp.

[CS, 1991] CS (1991). *Patch Repair of Reinforced Concrete Subject to Reinforcement Corrosion*. Report TR38. Concrete Society, Blackwater, UK. 88 pp.

[CS, 1995] CS (1995). *The Relevance of Cracking in Concrete to Corrosion of Reinforcement*. Report TR44. Concrete Society, Blackwater, UK. 32 pp.

[CS, 1997] CS (1997). *Guide to Surface Treatments for Protection and Enhancement of Concrete*. Report TR50. Concrete Society, Blackwater, UK. 80 pp.

[CS, 1998] CS (1998). *Guidance on the use of Stainless Steel Reinforcement*. Report TR51. Concrete Society, Blackwater, UK. 56 pp.

[Cusson & Mailvaganam, 1996] Cusson, D. & Mailvaganam, N. (1996). 'Durability of repair materials'. *Concrete International*, **18**(3), pp. 34–38.

[Cutler et al., 1997] Cutler, C., Smith, F., & Cochrane, D. (1997). 'Stainless Steel Reinforcing Bars', volume 1, pp. 439–452. In *Proceedings of the* 5th *International Conference on Deterioration and Repair of Reinforced Concrete in the Arabian Gulf*. Manama, Bahrain.

[Davis, 1998] Davis, J. R. (1998). *Metals Handbook. Desk Edition*. London, UK: CRC (Taylor & Francis), 2nd edition. 1535 pp.

[DBR, 2001] DBR (2001). *Durability and Repair of Reinforced Concrete*. Personal communication. Dansk Betonråd, Taastrup, Denmark.

[Dickson et al., 1986] Dickson, D. P. E., Berry, F. J., Bauminger, E. R., Dattagupta, S., Johnson, C. E., Long, G. J., Nowik, I., Parish, R. V., & Thomas, M. F. (1986). *Mössbauer Spectroscopy*. Cambridge, UK: Cambridge University Press, 1st edition. 286 pp.

[Drissi et al., 1995] Drissi, S., Refait, P., Abdelmoula, M., & Génin, J. (1995). 'The preparation and thermodynamic properties of Fe(II)-Fe(III) hydroxide-carbonate (green rust 1). Pourbaix diagram of iron in carbonate-containing aqueous media'. *Corrosion Science*, **37**(12), pp. 2025–2041.

[DS 13080, 2001] DS 13080 (2001). *Armeringsstål - Armeringsstål i rette stænger anvendt som ikke-forspændt armering i beton-konstruktioner*. Standard DS 13080. Dansk Standard, Charlottenlund, Denmark. 4 pp. Danish language.

[DS 134.3.1, 2007] DS 134.3.1 (2007). *Concrete - Part 3.1: Products and systems for the protection and repair of concrete structures - Principles*. DS håndbog 134.3.1:2007. Dansk Standard (DS), Charlottenlund, Denmark, 1st edition. 120 pp. Partly Danish language.

[DS 2426, 2004] DS 2426 (2004). *Concrete - Materials - Rules for application of EN 206-1 in Denmark*. Application rules DS 2426:2004. Dansk Standard (DS), Charlottenlund, Denmark, 1st edition. 42 pp. Danish language.

[DS/CEN/TS 14038-1, 2004] DS/CEN/TS 14038-1 (2004). *Electrochemical realkalization and chloride extraction treatments for reinforced concrete - Part 1: Realkalization*. Standard DS/CEN/TS 14038-1:2004. Dansk Standard (DS), Charlottenlund, Denmark, 1st edition. 16 pp.

[DS/EN 10025-1, 2004] DS/EN 10025-1 (2004). *Hot rolled products of structural steels - Part 1: General technical delivery conditions*. Standard DS/EN 10025-1:2004. Dansk Standard (DS), Charlottenlund, Denmark, 2nd edition. 33 pp.

[DS/EN 10025-2, 2004] DS/EN 10025-2 (2004). *Hot rolled products of structural steels - Part 2: Technical delivery conditions for non-alloy structural steels*. Standard DS/EN 10025-2:2004. Dansk Standard (DS), Charlottenlund, Denmark, 1st edition. 34 pp.

[DS/EN 1008, 2002] DS/EN 1008 (2002). *Mixing water for concrete - Specification for sampling, testing and assessing the suitability of water, including water recovered from processes in concrete industry, as mixing water for concrete*. Standard DS/EN 1008:2002. Dansk Standard (DS), Charlottenlund, Denmark, 1st edition. 18 pp.

[DS/EN 10080, 2006] DS/EN 10080 (2006). *Steel for the reinforcement of concrete. Weldable reinforcing steel. General*. Standard DS/EN 10080:2006. Dansk Standard (DS), Charlottenlund, Denmark, 2nd edition. 69 pp.

[DS/EN 10088-1, 2005] DS/EN 10088-1 (2005). *Stainless Steels - Part 1: List of Stainless Steels*. Standard DS/EN 10088-1:2005. Dansk Standard (DS), Charlottenlund, Denmark, 2nd edition. 18 pp.

[DS/EN 12620, 2004] DS/EN 12620 (2004). *Aggregates for concrete*. Standard DS/EN 12620:2004. Dansk Standard (DS), Charlottenlund, Denmark, 2nd edition. 51 pp.

[DS/EN 12696, 2000] DS/EN 12696 (2000). *Cathodic Protection of Steel in Concrete*. Standard DS/EN 12696:2000. Dansk Standard (DS), Charlottenlund, Denmark, 1st edition. 44 pp.

[DS/EN 13263-1, 2005] DS/EN 13263-1 (2005). *Silica fume for concrete - Part 1: Definitions, requirements and conformity criteria*. Standard DS/EN 13263-1:2005. Dansk Standard (DS), Charlottenlund, Denmark, 1st edition. 28 pp.

[DS/EN 14629, 2007] DS/EN 14629 (2007). *Products and systems for the protection and repair of concrete structures. Test methods. Determination of chloride content in hardened concrete*. Standard DS/EN 14629:2007. Dansk Standard (DS), Charlottenlund, Denmark, 1st edition. 14 pp.

[DS/EN 1504-1, 2005] DS/EN 1504-1 (2005). *Products and systems for the protection and repair of concrete structures - Definitions, requirements, quality control and evaluation of conformity - Part 1: Definitions*. Standard DS/EN 1504-1:2005. Dansk Standard (DS), Charlottenlund, Denmark, 2nd edition. 8 pp.

[DS/EN 1504-2, 2005] DS/EN 1504-2 (2005). *Products and systems for the protection and repair of concrete structures - Definitions, requirements, quality control and evaluation of conformity - Part 2: Surface protection systems for concrete*. Standard DS/EN 1504-2:2005. Dansk Standard (DS), Charlottenlund, Denmark, 2nd edition. 48 pp.

[DS/EN 1504-3, 2006] DS/EN 1504-3 (2006). *Products and systems for the protection and repair of concrete structures - Definitions, requirements, quality control and evaluation of conformity - Part 3: Structural and non-structural repair*. Standard DS/EN 1504-3:2006. Dansk Standard (DS), Charlottenlund, Denmark, 2nd edition. 25 pp.

[DS/EN 1504-4, 2007] DS/EN 1504-4 (2007). *Products and systems for the protection and repair of concrete structures - Definitions, requirements, quality control and evaluation of conformity - Part 4: Structural bonding*. Standard DS/EN 1504-4:2007. Dansk Standard (DS), Charlottenlund, Denmark, 1st edition. 28 pp.

[DS/EN 1504-5, 2007] DS/EN 1504-5 (2007). *Products and systems for the protection and repair of concrete structures - Definitions, requirements, quality control and evaluation of conformity - Part 5: Concrete injection*. Standard DS/EN 1504-5:2007. Dansk Standard (DS), Charlottenlund, Denmark, 2nd edition. 38 pp.

[DS/EN 15167-1, 2006] DS/EN 15167-1 (2006). *Ground granulated blast furnace slag for use in concrete, mortar and grout - Part 1: Definitions, specifications and conformity criteria*. Standard DS/EN 15167-1:2006. Dansk Standard (DS), Charlottenlund, Denmark, 1st edition. 24 pp.

[DS/EN 196-1, 1995] DS/EN 196-1 (1995). *Methods of testing cement. Determination of strength*. Standard DS/EN 196-1:1995. Dansk Standard (DS), Charlottenlund, Denmark, 1st edition. 36 pp.

[DS/EN 197-1, 2001] DS/EN 197-1 (2001). *Cement - Part 1: Composition, Specifications and Conformity Criteria for Common Cements*. Standard DS/EN 197-1:2001. Dansk Standard (DS), Charlottenlund, Denmark, 2nd edition. 29 pp.

[DS/EN 1992-1-1, 2005] DS/EN 1992-1-1 (2005). *Eurocode 2: Design of concrete structures. Part 1-1: General rules and rules for buildings*. Standard DS/EN 1992-1-1:2005. Dansk Standard (DS), Charlottenlund, Denmark, 1st edition. 227 pp.

[DS/EN 206-1, 2002] DS/EN 206-1 (2002). *Concrete - Part 1: Specification, Performance, Production and Conformity*. Standard EN 206-1:2002. Dansk Standard (DS), Charlottenlund, Denmark, 2nd edition. 72 pp.

[DS/EN 450-1, 2005] DS/EN 450-1 (2005). *Fly ash for concrete - Part 1: Definition, specifications and conformity criteria*. Standard DS/EN 450-1:2005. Dansk Standard (DS), Charlottenlund, Denmark, 1st edition. 18 pp.

[DS/EN 934-2, 2003] DS/EN 934-2 (2003). *Admixtures for concrete, mortar and grout - Part 2: Concrete admixtures - Definitions, requirements, conformity, marking and labelling*. Standard DS/EN 934-2:2003. Dansk Standard (DS), Charlottenlund, Denmark, 3rd edition. 22 pp.

[EDAX, 2006] EDAX (2006). *Genesis Spectrum. Version 5.1*. Eds mapping screen-diplay software. EDAX Inc., Mahwah, NJ, USA.

[Edvardsen, 1999] Edvardsen, C. (1999). 'Water permeability and autogenous healing of cracks in concrete'. *ACI Materials Journal*, **96**(4), pp. 448–454.

[Elsener, 2001] Elsener, B. (2001). *Corrosion Inhibitors for Steel in Concrete. State of the Art Report*. EFC Publication 35. European Federation of Corrosion (EFC). Institute of Materials, London, UK. 448 pp.

[Emmons & Vaysburd, 1997] Emmons, P. H. & Vaysburd, A. M. (1997). 'Corrosion protection in concrete repair: Myth and reality'. *Concrete International*, **19**(3), pp. 47–56.

[EMPA, 2007] EMPA (2007). *CEMDATA. Thermodynamic data for hydrated solids in Portland cement system*. EMPA, Dübendorf, Switzerland. Website, http://www.empa.ch, accessed: 15-Sep-2007.

[Engelund et al., 2000] Engelund, S., Edvardsen, C., & Mohr, L. (2000). *General Guidelines for Durability Design and Redesign*. Document BE95-1347/R15. European Union, Luxembourg. 109 pp. Part of the Brite-EuRam III Project BE95-1347, DuraCrete, Probabilistic Performance based Durability Design of Concrete Structures.

[ESDU, 2007] ESDU (2007). *ESDU 68008. Specific heat capacity at constant pressure of ice, water and steam.* IHS ESDU International, London, UK. Website, http://www.esdu.com, accessed: 15-Sep-2007.

[ET, 2000] ET (2000). *Schweisszusätze Magnesium*. Datasheet. Drahtwerk Elisental, Neuenrade, Germany. 4 pp. German language.

[ET, 2001] ET (2001). *Werstoffdatenblatt. Draht aus Magnesiumlegierung AZ31X*. Datasheet. Drahtwerk Elisental, Neuenrade, Germany. 1 pp. German language.

[Fagerlund, 1979] Fagerlund, G. (1979). 'Service Life of Structures', pp. 199–215. In *Proceeding of Symposium on Quality Control of Concrete Structures*. Stockholm, Sweden.

[Faust & Aly, 1998] Faust, S. D. & Aly, O. M. (1998). *Chemistry of Water Treatment*. Boca Raton , FL, USA: CRC, 2nd edition. 600 pp.

[FEI, 2007] FEI (2007). *Tools for Banotech*. FEI Company, Hillsboro, OR, USA. Website, http://www.fei.com, accessed: 12-Dec-2007.

[fib, 1978] fib (1978). *International System of Unified Standard Codes of Practice for Structures. Volume 1: Common unified rules for different types of construction and material. Volume 2: CEB-FIP Model Code for concrete structures*. CEB Bulletin 124/125. International Federation for Structural Concrete (fib), Lausanne, Switzerland, 1st edition. 348 pp.

[fib, 1992] fib (1992). *Durable Concrete Structures. Design Guide*. CEB Bulletin 183. International Federation for Structural Concrete (fib), Lausanne, Switzerland, 2nd edition. 112 pp.

[fib, 1993] fib (1993). *CEB-FIP Model Code 90*. CEB Bulletin 213/214. International Federation for Structural Concrete (fib), Lausanne, Switzerland, 1st edition. 460 pp.

[fib, 1994] fib (1994). *Application of High Performance Concrete*. CEB Bulletin 222. International Federation for Structural Concrete (fib), Lausanne, Switzerland, 1st edition. 65 pp.

[fib, 1995a] fib (1995a). *Coating Protection for Reinforcement. State-of-the-Art Report*. CEB Bulletin 211. International Federation for Structural Concrete (fib), Lausanne, Switzerland, 1st edition. 51 pp.

[fib, 1995b] fib (1995b). *High Performance Concrete. Recommended Extensions to the Model Code 90 - Research Needs*. CEB Bulletin 228. International Federation for Structural Concrete (fib), Lausanne, Switzerland, 1st edition. 60 pp.

[fib, 1999a] fib (1999a). *Structural Concrete - Textbook on Behaviour, Design and Performance. Volume 3: Durability - Design for Fire Resistance - Member Design - Maintenance, Assessment and Repair - Practical Aspects*. fib Bulletin 3. International Federation for Structural Concrete (fib), Lausanne, Switzerland, 1st edition. 292 pp.

[fib, 1999b] fib (1999b). *Structural Concrete. Textbook on Behaviour, Design and Performance. Volume 1: Introduction - Design Process - Materials*. fib Bulletin 1. International Federation for Structural Concrete (fib), Lausanne, Switzerland, 1st edition. 244 pp.

[fib, 1999c] fib (1999c). *Structural Concrete. Textbook on Behaviour, Design and Performance. Volume 2: Basis of Design*. fib Bulletin 2. International Federation for Structural Concrete (fib), Lausanne, Switzerland, 1st edition. 324 pp.

[fib, 2004] fib (2004). *Environmental design*. fib Bulletin 28. International Federation for Structural Concrete (fib), Lausanne, Switzerland, 1st edition. 80 pp.

[fib, 2006] fib (2006). *Model Code for Service Life Design*. fib Bulletin 34. International Federation for Structural Concrete (fib), Lausanne, Switzerland, 1st edition. 126 pp.

[fib, 2007] fib (2007). *FRP reinforcement in RC structures*. fib Bulletin 40. International Federation for Structural Concrete (fib), Lausanne, Switzerland, 1st edition. 160 pp.

[Foley, 1970] Foley, R. T. (1970). 'Role of the Chloride Ion in Iron Corrosion'. *Corrosion-NACE*, **26**(2), pp. 58–70.

[Fosroc, 2007] Fosroc (2007). *Galvashield XP. Tied on Sacrificial Anode Units for Corrosion Prevention*. Datasheet Cl/SfB: Xh7. Fosroc Limited, Tamworth, UK. 2 pp.

[Francois & Arliguie, 1998] Francois, R. & Arliguie, G. (1998). 'Influence of service cracking on reinforcement steel corrosion'. *Journal of Materials in Civil Engineering*, **10**(1), pp. 14–20.

[Fratesi, 2002a] Fratesi, R. (2002a). 'Galvanized Reinforcing Steel Bars in Concrete', pp. 33–44. In *Final Report of COST 521 Workshop*. Luxembourg, Luxembourg.

[Fratesi, 2002b] Fratesi, R. (2002b). *Galvanized Steel Reinforcement*, chapter 1.4, pp. 28–40. In Cigna, R., Andrade, C., Nünberger, U., Polder, R., Weydert, R., & Seitz, E. (Eds.). *EUR 20599. Cost Action 521. Corrosion of steel in reinforced concrete structures. Final Report*. Luxembourg, Luxembourg: Office for Official Publications of the European Communities, 1st edition.

[Frederiksen, 1997] Frederiksen, J. M. (1997). *Chloride Penetration into Concrete. Relevant Test Methods*. HETEK Report No. 94. Danish Road Directorate, Copenhagen, Denmark. 76 pp. Partly Danish language.

[Frederiksen & Poulsen, 1997] Frederiksen, J. M. & Poulsen, E. (1997). *Chloride Penetration into Concrete. Manual*. HETEK Report No. 123. Danish Road Directorate, Copenhagen, Denmark. 48 pp.

[Freiesleben Hansen, 1995] Freiesleben Hansen, P. (1995). *Materialefysik for bygningsingeniører*. Number 183 in SBI-anvisninger. Glostrup, Denmark: Statens Byggeforskninginstitut, 1st edition. 296 pp. Danish language.

[Friedmann, 2007] Friedmann, D. (2007). *Shrinkage Cracks in Poured Concrete Slab*. InspectAPedia, Cleveland, OH. Website, http://www.inspect-ny.com, accessed: 13-Nov-2007.

[Gabrielli, 1984] Gabrielli, C. (1984). *Identification of Electrochemical Processes by Frequency Response Analysis*. Technical report 004/83. Université Pierre et Marie Curie (UPMC), Paris, France. 120 pp.

[Gaidis, 2004] Gaidis, J. M. (2004). 'Chemistry of corrosion inhibitors'. *Cement and Concrete Composites*, **26**(3), pp. 181–189.

[Gamry, 2005] Gamry (2005). *Gamry Framework. Version 4.0*. Software. Gamry Instruments, Warminster, PA, USA.

[Gamry, 2006] Gamry (2006). *Basics of Electrochemical Impedance Spectroscopy*. Application note. Gamry Instruments, Warminster, PA, USA. 29 pp.

[Gamry, 2007] Gamry (2007). *Redefining Electrochemical Measurement*. Gamry Instruments, Warminster, PA, USA. Website, http://www.gamry.com, accessed: 17-Apr-2007.

[Gautefall & Vennesland, 1983] Gautefall, O. & Vennesland, O. (1983). 'Effects of Cracks on the Corrosion of Embedded Steel in Silica-Concrete compared to Ordinary Concrete', pp. 17–28. In *Proceedings of Nordic Concrete Research Meeting*. Oslo, Norway.

[Gehlen, 2000] Gehlen, C. (2000). *Probabilistische Lebensdauerbemessung von Stahlbetonbauwerken. Zuverlässigkeitsbetrachtungen zur wirksamen Vermeidung von Bewehrungskorrosion*. DAfStb Heft 510. Deutscher Ausschuss für Stahlbeton, Berlin, Germany. 106 pp. German language.

[Geiker et al., 2007] Geiker, M. R., Nielsen, E. P., & Herfort, D. (2007). 'Prediction of Chloride Ingress and Binding in Concrete'. *Materials and Structures*, **40**(4), pp. 405–417.

[Geiker & Thaulow, 1996] Geiker, M. R. & Thaulow, N. (1996). 'Ingress of Moisture due to Freeze/Thaw Exposure', pp. 159–162. In Lindmark, S. (Ed.). *Frost Resistance of Building Materials*. Number Report TVBM-3071. Lund, Sweden: Lund Institute of Technology.

[GI, 2006] GI (2006). *Deep Purple and Rainbow Indicator*. Germann Instruments, Copenhagen, Denmark. Website, http://germann.org/, accessed: 22-Nov-2007.

[Glass & Buenfeld, 1997] Glass, G. K. & Buenfeld, N. R. (1997). 'The presentation of the chloride threshold level for corrosion of steel in concrete'. *Corrosion Science*, **39**(5), pp. 1001–1013.

[Génin et al., 2001] Génin, J.-M. R., Refaita, P., Bourriéb, G., Abdelmoulaa, M., & Trolard, F. (2001). 'Structure and stability of the Fe(II)–Fe(III) green rust "fougerite" mineral and its potential for reducing pollutants in soil solutions'. *Applied Geochemistry*, **16**(5), pp. 559–570.

[GOM, 2007] GOM (2007). *ARAMIS. System for optical 3D deformation analysis*. GOM GmbH, Braunschweig, Germany. Website, http://www.gom.com, accessed: 17-Sep-2007.

[Gonzalez et al., 2007] Gonzalez, J. A., Miranda, J. M., Otero, E., & Feliu, S. (2007). 'Effect of electrochemically reactive rust layers on the corrosion of steel in a Ca(OH)2 solution'. *Corrosion Science*, **49**(2), pp. 436–448.

[Gouda, 1970] Gouda, V. K. (1970). 'Corrosion and corrosion inhibition of reinforcing steel, I. Immersed in alkaline solutions'. *British Corrosion Journal*, **5**, pp. 198–203.

[Gouda & Halaka, 1970] Gouda, V. K. & Halaka, W. Y. (1970). 'Corrosion and corrosion inhibition of reinforceing steel, II. Embedded in concrete'. *British Corrosion Journal*, **5**, pp. 204–208.

[Gowripalan et al., 2000] Gowripalan, N., Sirivivatnanon, V., & Lim, C. (2000). 'Chloride diffusivity of concrete cracked in flexure'. *Cement and Concrete Research*, **30**(5), pp. 725–730.

[GSU, 2007] GSU (2007). *Thermodynamic Potentials*. Georgia State University, Atlanta, GA. Website, http://www.gsu.edu/, accessed: 22-Aug-2007.

[Gu et al., 1997] Gu, P., Beaudoin, J., Tumidajski, P., & Mailvaganam, N. (1997). 'Electrochemical incompatibility of patches in reinforced concrete'. *Concrete International*, **19**(8), pp. 68–72.

[Gudmundsson et al., 2004] Gudmundsson, G., Janz, M., Damgaard Jensen, A., Mehus, J., Miller, J. B., Maage, M., Pentti, M., & Poulsen, E. (2004). *Repair and Maintenance of Concrete Structures. Guidelines for manufacturers, contractors and consultants on the basis of European standards*. Presentation NORECON Task T3. Norwegian Public Roads Administration, Oslo, Norway. 58 pp.

[Gurvich, 1989] Gurvich, L. V. (1989). 'Reference books and data banks on the thermodynamic properties of individual substances'. *Pure and Applied Chemistry*, **61**(6), pp. 1027–1031.

[Hansson et al., 2006] Hansson, C., Poursaee, A., & Laurent, A. (2006). 'Macrocell and microcell corrosion of steel in ordinary Portland cement and high performance concretes'. *Cement and Concrete Research*, **36**(11), pp. 2098–2102.

[Hansson et al., 1998] Hansson, C. M., Mammoliti, L., & Hope, B. B. (1998). 'Corrosion Inhibitors in Concrete - Part I: Principles'. *Cement and Concrete Research*, **28**(12), pp. 1775–1781.

[Haung & Cuentas, 1989a] Haung, H.-H. & Cuentas, L. (1989a). 'Construction of Eh-pH and other Stability Diagrams of Uranium in a Multicomponent System with a Microcomputer - I. Domains of Predominance Diagrams'. *Canadian Metallurgical Quarterly*, **28**(3), pp. 225–234.

[Haung & Cuentas, 1989b] Haung, H.-H. & Cuentas, L. (1989b). 'Construction of Eh-pH and other Stability Diagrams of Uranium in a Multicomponent System with a Microcomputer - II. Distribution Diagrams'. *Canadian Metallurgical Quarterly*, **28**(3), pp. 235–239.

[Hausmann, 1967] Hausmann, D. A. (1967). 'Steel Corrosion in Concrete - How Does It Occur?'. *Materials Protection*, **6**, pp. 19–23.

[Herholdt et al., 1985] Herholdt, A., Justesen, C.F.P., & Nepper-Christensen, P. (1985). *Beton Bogen*. Aalborg, Denmark: Aalborg Portland A/S, 2nd edition. 731 pp. Danish language.

[Hitech, 2007] Hitech (2007). *Dimensionally Stable Anodes*. Hitech Engineering Materials and Systems Ltd., Grantham, UK. Website, http://www.hitech-me.co.uk, accessed: 21-Sep-2007.

[Hsieh et al., 1997] Hsieh, G., Mason, T. O., Garboczi, E. J., & Pederson, L. R. (1997). 'Experimental limitations in impedance spectroscopy: Part III – Effect of reference electrode geometry/position'. *Solid State Ionics*, **96**(3-4), pp. 153–172.

[Hsieh et al., 1996] Hsieh, G., Mason, T. O., & Pederson, L. R. (1996). 'Experimental limitations in impedance spectroscopy: Part II – Electrode artifacts in three point measurements on Pt/YSZ'. *Solid State Ionics*, **91**(3), pp. 203–212.

[HUJI, 2007] HUJI (2007). *Famous Scientists*. Hebrew University, Jerusalem, Israel. Website, http://www.huji.ac.il/huji/, accessed: 03-Sep-2007.

[IISI, 2007] IISI (2007). *Steel Statistical Yearbook*. International Steel and Iron Institute, Brussels, Belgium. Website, http://www.worldsteel.org, accessed: 04-May-2007.

[ISA, 1995] ISA (1995). *Gewässergüte und Abwasserwirtschaft*. Lecture notes. Institut für Siedlungswasserwirtschaft (ISA), RWTH, Aachen, Germany. German language.

[Isgor & Razaqpur, 2006] Isgor, O. B. & Razaqpur, A. G. (2006). 'Modelling steel corrosion in concrete structures'. *Materials and Structures*, **39**(287), pp. 259–270.

[ISO 14654, 2007] ISO 14654 (2007). *Epoxy-coated steel for the reinforcement of concrete*. International Standard ISO 14654:1999. International Organization for Standardization, Geneva, Switzerland. 30 pp.

[ISO 14657, 2005] ISO 14657 (2005). *Zinc-coated steel for the reinforcement of concrete*. International Standard ISO 14657:2005. International Organization for Standardization, Geneva, Switzerland. 12 pp.

[ISO 6935-1, 2007] ISO 6935-1 (2007). *Steel for the reinforcement of concrete – Part 1: Plain bars*. International Standard ISO 6935-1:2007. International Organization for Standardization, Geneva, Switzerland. 10 pp.

[ISO 6935-2, 2007] ISO 6935-2 (2007). *Steel for the reinforcement of concrete – Part 2: Ribbed bars*. International Standard ISO 6935-2:2007. International Organization for Standardization, Geneva, Switzerland. 20 pp.

[IUPAC, 1953] IUPAC (1953). *Convention of Stockholm*. International Union of Pure and Applied Chemistry, Research Triangle Park, NC, USA. Website, http://chimge.unil.ch, accessed: 15-Sep-2007.

[IUPAC, 2007] IUPAC (2007). *IUPAC Compendium of Chemical Terminology*. International Union of Pure and Applied Chemistry, Research Triangle Park, NC, USA. Website, http://goldbook.iupac.org, accessed: 14-Oct-2007.

[IZA, 2007] IZA (2007). *Galvanized Rebar Ressource Center*. International Zinc Association, Brussels, Belgium. Website, http://www.galvanizedrebar.com, accessed: 12-August-2007.

[Jensen, 1999] Jensen, O. M. (1999). *Chloride Ingress in Cement Paste and Mortar Measured by Electron Probe Micro Analysis*. Report series R, no. 51. Department of Structural Engineering and Materials, Technical University of Denmark, Kgs. Lyngby, Denmark. 60 pp.

[John, 2003] John, V. M. (2003). *On the Sustainability of the Concrete*. Extended paper. University of São Paulo, São Paulo, Brazil. 7 pp. Available online, http://www.pcc.usp.br, accessed: 12-May-2007.

[Jones, 1996] Jones, D. A. (1996). *Principles and Prevention of Corrosion*. Upper Saddle River, NJ, USA: Prentice Hall, 2nd edition. 572 pp.

[Kaesche, 1979] Kaesche, H. (1979). *Die Korrosion der Metalle*. Berlin: Springer, 2nd edition. 374 pp. German language.

[KaiDa, 2007] KaiDa (2007). *Precious Group Metal Catalysts, Compounds and Activated Titanium Anodes*. KaiDa Technology Ltd., London, UK. Website, http://www.kaida.co.uk, accessed: 21-Sep-2007.

[KAIST, 2007] KAIST (2007). *Potential - pH (Pourbaix) Diagrams*. Corrosion and Energy Storage Materials Laboratory, Korea Advanced Institute of Science and Technology, Daejeon, Korea. Website, http://corrosion.kaist.ac.kr, accessed: 15-Sep-2007.

[Kanani, 2000] Kanani, N. (2000). *Galvanotechnik: Grundlagen, Verfahren, Praxis*. Leipzig, Germany: Fachbuchverlag, 1st edition. 447 pp. German language.

[Kelly et al., 2003] Kelly, R. G., Scully, J. R., Shoesmith, D. W., & Buchheit, R. G. (2003). *Electrochemical Techniques in Corrosion Science and Engineering*. Number 18 in Corrosion Technology. New York, USA: Marcel Dekker, Inc., 1st edition. 426 pp.

[Klinghoffer, 1999] Klinghoffer, O. (1999). *Corrosion aspects of galvanic coupling between carbon steel and stainless steel in concrete*. Report. FORCE Institute, Brøndby, Denmark. 14 pp.

[Koleva et al., 2006] Koleva, D. A., Hu, J., Fraaij, A. L. A., Stroeven, P., Boshkov, N., & de Wit, J. H. W. (2006). 'Quantitative characterisation of steel/cement paste interface microstructure and corrosion phenomena in mortars suffering from chloride attack'. *Corrosion Science*, **48**(12), pp. 4001–4019.

[Kropp & Hilsdorf, 1995] Kropp, J. & Hilsdorf, H. K. (Eds.) (1995). *Performance Criteria for Concrete Durability*. Number 12 in RILEM Report. London, UK: E & FN Spon (Chapman & Hall), 1st edition. 327 pp.

[Kruger, 2001] Kruger, J. (2001). *Electrochemistry of Corrosion*. Case Western Reserve University, Cleveland, OH. Website, http://electrochem.cwru.edu, accessed: 24-Jul-2007.

[Küter, 2005] Küter, A. (2005). *Investigations on Chloride Ingress in Concrete Cracks under Cyclic Mechanical Loading*. Diplomarbeit. RWTH Aachen University, Aachen, Germany. 121 pp.

[Küter et al., 2005a] Küter, A., Geiker, M. R., Olesen, J. F., Stang, H., Dauberschmidt, C., & Raupach, M. (2005a). 'Chloride Ingress of Concrete Cracks under Cyclic Loading', 10 pp. (on CD). In *Proceedings of ConMat'05*. Vancouver, BC, Canada.

[Küter et al., 2005b] Küter, A., Mason, T. O., Møller, P., & Geiker, M. R. (2005b). 'Corrosion of Steel in Concrete – Potential Monitoring and Electrochemical Impedance Spectroscopy during Corrosion Initiation and Propagation', 12 pp. (on CD). In *Proceedings of Eurocorr 2005*. Lisbon, Portugal.

[Küter et al., 2004] Küter, A., Møller, P., & Geiker, M. R. (2004). 'Corrosion of Steel in Concrete – Specimen Design for Investigation of Interface and Bulk Conversions during Curing and Exposure', 3 pp. (on CD). In *Proceedings of Nordic Concrete Research Meeting*. Sandefjord, Norway.

[Li & Yuan, 2003] Li, G. & Yuan, Y.-S. (2003). 'Electrochemical incompatibility for patch-repaired corroded reinforced concrete'. *Zhongguo Kuangye Daxue Xuebao/Journal of China University of Mining and Technology*, **32**(1), pp. 44–47.

[Li, 2004] Li, V. (2004). *A New Research Framework for Sustainable Infrastructures*. Seminar. Department of Civil Engineering, Technical University of Denmark, Kgs. Lyngby, Denmark.

[Lide, 2002] Lide, D. R. (2002). *CRC Handbook of Chemistry and Physics*. Boca Raton, FL, USA: CRC, 83rd edition. 2664 pp.

[LMG, 2004a] LMG (2004a). *Certificeringslicens. Kamstålet K550 TS*. Datasheet 1417 H. Lemvigh-Müller A/S, Glostrup, Denmark. 2 pp. Danish language.

[LMG, 2004b] LMG (2004b). *Certifikat. Intern Kvalitetskontrol. Stålkvalitet 1.4436*. Datasheet 06-2004. Lemvigh-Müller A/S, Glostrup, Denmark. 1 pp. Danish language.

[Lothenbach & Winnefeld, 2006] Lothenbach, B. & Winnefeld, F. (2006). 'Thermodynamic modelling of the hydration of Portland cement'. *Cement and Concrete Research*, **36**(2), pp. 209–226.

[MAG, 2004] MAG (2004). *Production and further processing of MMO activated titanium*. Personal communication. MAGNETO special anodes B.V., Schiedam, The Netherlands.

[Mailvaganam, 2001] Mailvaganam, N. P. (2001). 'Concrete repair and rehabilitation: Issues and trends'. *Indian Concrete Journal*, **75**(12), pp. 759–764.

[Mammoliti et al., 1999] Mammoliti, L., Hansson, C. M., & Hope, B. B. (1999). 'Corrosion Inhibitors in Concrete Part II: Effect on Chloride Threshold Values for Corrosion of Steel in Synthetic Pore Solution'. *Cement and Concrete Research*, **29**, pp. 1583–1589.

[March, 1992] March, J. (1992). *Advanced Organic Chemistry, Reactions, Mechanisms and Structure*. New York, NY, USA: Wiley, 4th edition. 1495 pp.

[Marcotte & Hansson, 2007] Marcotte, T. & Hansson, C. (2007). 'Corrosion products that form on steel within cement paste'. *Materials and Structures*, **40**(3), pp. 325–340.

[Markeset et al., 2006] Markeset, G., Rostam, S., & Klinghoffer, O. (2006). *Guide for the use of stainless steel reinforcement in concrete structures*. Project report 405. Norwegian Building Research Institute, Oslo, Norway. 59 pp.

[Matschei et al., 2007a] Matschei, T., Lothenbach, B., & Glasser, F. P. (2007a). 'The AFm phase in Portland cement'. *Cement and Concrete Research*, **37**(2), pp. 118–130.

[Matschei et al., 2007b] Matschei, T., Lothenbach, B., & Glasser, F. P. (2007b). 'Thermodynamic properties of Portland cement hydrates in the system CaO–Al2O3–SiO2–CaSO4–CaCO3–H2O'. *Cement and Concrete Research*, **37**(10), pp. 1379–1410.

[Mays et al., 1992] Mays, G. C., Lees, T. P., Baker, A. F., Tabor, L. J., Berkeley, K. G. C., Keer, J. G., Stroud, C., Gardner, P., Boam, K. J., Dixon, J. F., Northcott, G. D. S., & Leeming, M. B. (1992). *Durability of Concrete Structures. Investigation, Repair, Protection*. London, UK: E & F Spon, 1st edition. 265 pp.

[McDonald et al., 1996] McDonald, D. B., Virmani, Y. P., & Pfeifer, D. F. (1996). 'Testing the performance of copper-clad reinforcing bars'. *Concrete International*, **18**(11), pp. 39–43.

[MEPS, 2007] MEPS (2007). *Independent Steel Industry Analysts, Consultants, Steel Prices, Reports and Publications*. MEPS Intl. Ltd., Sheffield, UK. Website, http://www.meps.co.uk/, accessed: 22-Aug-2007.

[Mietz, 1998] Mietz, J. (1998). *Electrochemical rehabilitation methods for reinforced concrete structures. State of the Art Report*. EFC Publication 24. European Federation of Corrosion (EFC). Institute of Materials, London, UK. 68 pp.

[MinDat, 2007] MinDat (2007). *MinDat.org. The Mineral and Locality Database*. MinDat, London, UK. Website, http://www.mindat.org, accessed: 22-Aug-2007.

[Mindess et al., 2003] Mindess, S., Young, J. F., & Darwin, D. (2003). *Concrete*. Upper Saddle River, NJ, USA: Prentice Hall, 2nd edition. 644 pp.

[MinGal, 2007] MinGal (2007). *The Mineral Gallery*. Amethyst Galleries, St. Augustine, FL, USA. Website, http://www.galleries.com/minerals/, accessed: 22-Aug-2007.

[Misawa, 1973] Misawa, T. (1973). 'The thermodynamic consideration for Fe-H2O system at 25°'. *Corrosion Science*, **13**, pp. 659–676.

[Møller, 2003a] Møller, P. (2003a). *Korrosion og Termodynamik*. Kgs. Lyngby, Denmark: DTU-Tryk, 1st edition. 37 pp. Danish language.

[Møller, 2003b] Møller, P. (2003b). *Korrosion (teori og teknologi)*. Lecture notes. Technical University of Denmark, Kgs. Lyngby, Denmark. Danish language.

[Møller, 2003c] Møller, P. (2003c). *Overfladeteknologi*. Ingeniøren|bøger. Copenhagen, Denmark: Ingeniøren, 1st edition. 413 pp. Danish language.

[Mohammed et al., 2001] Mohammed, T. U., Otsuki, N., Hisada, M., & Shibata, T. (2001). 'Effect of Crack Width and Bar Type on Corrosion of Steel in Concrete'. *Journal of Materials in Civil Engineering*, **13**(3), pp. 194–201.

[Molina et al., 1993] Molina, F., Alonso, C., & Andrade, C. (1993). 'Cover cracking as a function of rebar corrosion: Part 2 - Numerical model'. *Materials and Structures*, **26**(163), pp. 532–548.

[Montemor et al., 2003] Montemor, M., Simoes, A., & Ferreira, M. (2003). 'Chloride-induced corrosion on reinforcing steel: from the fundamentals to the monitoring techniques'. *Cement and Concrete Composites*, **25**(4-5), pp. 491–502.

[Naumov, 1974] Naumov, G. B. (1974). *Handbook of Thermodynamic Data*. Springfield, Virginia: National Technical Information Service. 328 pp.

[Neville, 1995] Neville, A. M. (1995). *Properties of Concrete*. Essex, UK: Longman, 4th edition. 844 pp.

[NI, 2004] NI (2004). *LabVIEW. Version 7.1*. Instrument control and signal processing software. National Instruments Corporation, Austin, TX.

[Nielsen & Geiker, 2003] Nielsen, E. & Geiker, M. (2003). 'Chloride Diffusion in Partially Saturated Cementitious Material'. *Cement and Concrete Research*, **33**, pp. 133–138.

[Nielsen et al., 2005a] Nielsen, E., Herfort, D., & Geiker, M. (2005a). 'Binding of chloride and alkalis in Portland cement systems'. *Cement and Concrete Research*, **35**(1), pp. 117–123.

[Nielsen, 2001] Nielsen, E. P. (2001). *Transport Mechanisms in Cementitious Materials. Main Report*. Master thesis. Technical University of Denmark, Kgs. Lyngby, Denmark. 104 pp.

[Nielsen, 2004] Nielsen, E. P. (2004). *The durability of white Portland cement to chemical attack*. PhD thesis. Technical University of Denmark, Kgs. Lyngby, Denmark. 208 pp.

[Nielsen et al., 2005b] Nielsen, E. P., Herfort, D., & Geiker, M. R. (2005b). 'Phase equilibria of hydrated Portland cement'. *Cement and Concrete Research*, **35**(1), pp. 109–115.

[Nilsson et al., 1996] Nilsson, L.-O., Poulsen, E., Sandberg, P., Sørensen, H. E., & Klinghoffer, O. (1996). *Chloride Penetration into Concrete. State-of-the-Art. Transport Processes, Corrosion Initiation, Test Methods and Prediction Models*. HETEK Report No. 53. Danish Road Directorate, Copenhagen, Denmark. 151 pp.

[Nilsson et al., 1997] Nilsson, L.-O., Sandberg, P., Poulsen, E., Tang, L., Andersen, A., & Frederiksen, J. M. (1997). *A System for Estimation of Chloride Ingress into Concrete. Theoretical Background*. HETEK Report No. 83. Danish Road Directorate, Copenhagen, Denmark. 170 pp.

[Nürnberger, 1996] Nürnberger, U. (1996). *Stainless Steel in Concrete. State of the Art Report*. EFC Publications 18. European Federation of Corrosion (EFC). Institute of Materials, London, UK. 28 pp.

[Nürnberger & Beul, 1999] Nürnberger, U. & Beul, W. (1999). 'Corrosion of stainless steel reinforcement in cracked concrete'. *Otto-Graf-Journal*, **10**, pp. 23–37.

[Nygaard, 2003] Nygaard, P. V. (2003). *Effect of Steel-Concrete Interface Defects on the Chloride Threshold for Reinforcement Corrosion*. Master thesis. Department of Civil Engineering, Technical University of Denmark, Kgs. Lyngby, Denmark. 142 pp.

[Nygaard, 2007] Nygaard, P. V. (2007). *Corrosion Monitoring at the Oresund Fixed Link*. Personal communication. FORCE Technology, Brøndby, Denmark.

[Nygaard & Geiker, 2005] Nygaard, P. V. & Geiker, M. R. (2005). 'A method for measuring the chloride threshold level required to initiate reinforcement corrosion in concrete'. *Materials and Structures*, **38**(278), pp. 489–494.

[OMC, 2007] OMC (2007). *Organic Metal Nanotechnology. Polyanilin*. ORMECON GmbH, Ammersbek, Germany. Website, http://www.ormecon.de, accessed: 27-Jul-2007. Partly German language.

[Ottosen et al., 2007] Ottosen, L. M., Pedersen, A. J., & Rörig-Dalgaard, I. (2007). 'Salt-related problems in brick masonry and electrokinetic removal of salts'. *Journal of Building Appraisal*, **3**(3), pp. 181–194.

[Ouku, 1999] Ouku (1999). *HSC Chemistry. Version 4*. Chemical reaction and equilibrium software. Outokumpu, Pori, Finland.

[Ouku, 2002] Ouku (2002). *HSC Chemistry. Version 5*. Chemical reaction and equilibrium software. Outokumpu, Pori, Finland.

[Page et al., 1981] Page, C. L., Short, N. R., & El-Tarra, A. (1981). 'Diffusion of Chloride Ions in Hardened Cement Paste.'. *Cement and Concrete Research*, **11**(3), pp. 395–406.

[Page & Treadaway, 1982] Page, C. L. & Treadaway, K. W. J. (1982). 'Aspects of the electrochemistry of steel in concrete'. *Nature*, **297**, pp. 109–115.

[Patton, 1973] Patton, T. C. (1973). *Pigment Handbook*. New York, NY, USA: Wiley. 256 pp.

[Pease et al., 2006] Pease, B. J., Geiker, M. R., Stang, H., & Weiss, J. (2006). 'Photogrammetric Assessment of Flexure Induced Cracking of Reinforced Concrete Beams under Service Loads', 11 pp. (on CD). In *Proceedings of the* 2nd *International RILEM Symposium. Advances in Concrete through Science and Engineering*. Québec City, Québec, Canada.

[Pedeferri, 1992] Pedeferri, P. (1992). 'Cathodic Protection of New Concrete Constructions', Paper E7190 pp. (on CD). In *Proceedings of International Conference on Structural Improvement through Corrosion Protection of Reinforced Concrete*. London, UK.

[Place Hansen de, 1999] Place Hansen de, E. J. (1999). *Holdbarhed af fiberarmeret beton. Eksperimentelle undersøgelser*. Report series R no. 63. Department of Structural Engineering and Materials, Technical University of Denmark, Kgs. Lyngby, Denmark. 136 pp. Danish language with English summary.

[Popov, 2007] Popov, B. N. (2007). *Effectiveness of Calcium Nitrite in Protecting Galvanized Steel in Concrete*. University of South Carolina., Columbia, SC, USA. Website, http://www.che.sc.edu, accessed: 17-Aug-2007.

[Pourbaix, 1974a] Pourbaix, M. (1974a). 'Applications of electrochemistry in corrosion science and practice'. *Corrosion Science*, **14**, pp. 25–82.

[Pourbaix, 1974b] Pourbaix, M. (1974b). *Atlas of Electrochemical Equilibria*. Houston, TX, USA: NACE International, 2nd edition. 644 pp.

[Poursaee & Hansson, 2007] Poursaee, A. & Hansson, C. (2007). 'Reinforcing steel passivation in mortar and pore solution'. *Cement and Concrete Research*, **37**(7), pp. 1127–1133.

[Pruckner & Gjørv, 2002] Pruckner, F. & Gjørv, O. E. (2002). 'Patch repair and macrocell activity in concrete structures'. *ACI Materials Journal*, **99**(2), pp. 143–148.

[Qiu, 2007] Qiu (2007). *Emerging Corrosion Control Technologies for Repair and Rehabilitation of Concrete Structures*. Report. Nanyang Technological University, Singapore. 9 pp. Available online, http://www.corrosionsource.com, accessed: 15-Sep-2007.

[RA, 2005] RA (2005). *Voltamaster 4. Version 5.6*. Electrochemical analysis software. Radiometer Analytical SAS, Villeurbanne, France.

[RA, 2006a] RA (2006a). *REF321. Reference Electrodes*. Datasheet. Radiometer Analytical SAS, Villeurbanne Cedex, France. 2 pp.

[RA, 2006b] RA (2006b). *XR110. Reference Electrodes*. Datasheet. Radiometer Analytical SAS, Villeurbanne Cedex, France. 2 pp.

[RA, 2007] RA (2007). *VolatLab. Making voltammetry for you*. Radiometer Analytical SAS, Villeurbanne, France. Website, http://www.radiometer-analytical.com, accessed: 19-Apr-2007.

[Raharinaivo et al., 1987] Raharinaivo, A., Génin, J. M., & Grimaldi, G. (1987). 'Mechanism of chloride actions on steel corrosion in concrete.', pp. 575–581. In *Proceedings of* 4th *International Conference on Durability of Building Materials and Components*. Singapore, Singapore.

[Rambøll, 1999] Rambøll (1999). *Pier in Progreso, Mexico. Evaluation of the Stainless Steel Reinforcement*. Inspection report. Rambøll A/S, Virum, Denmark. 62 pp.

[Randhawa & Sweety, 1998] Randhawa, B. S. & Sweety, K. (1998). 'Preparation of sodium ferrite from the thermolysis of sodium tris(maleato/fumarato)ferrates(III)'. *Journal of Radioanalytical and Nuclear Chemistry*, **238**(1), pp. 141–144.

[Raupach, 1992] Raupach, M. (1992). *Zur chloridinduzierten Makroelementkorrosion von Stahl in Beton*. DAfStb Heft 433. Deutscher Ausschuss für Stahlbeton, Berlin, Germany. 106 pp. German language.

[Raupach, 1996] Raupach, M. (1996). 'Chloride-induced macrocell corrosion of steel in concrete–theoretical background and practical consequences'. *Construction and Building Materials*, **10**(5), pp. 329–338.

[Raupach, 2007] Raupach, M. (2007). *Concrete Repair According to the New European Standard EN 1504*. Note F 892. RWTH Aachen University, Aachen, Germany. 10 pp. Available online, http://www.ibac.rwth-aachen.de, accessed: 19-Aug-2007.

[Raupach et al., 2007] Raupach, M., Elsener, B., Polder, R. B., & Mietz, J. (Eds.) (2007). *Corrosion of reinforcement in concrete. Mechanisms, monitoring, inhibitors and rehabilitation techniques*. Number 38 in European Federation of Corrosion Publications. Cambridge, UK: Woodhead, 1st edition. 312 pp.

[Raupach & Wolff, 2005] Raupach, M. & Wolff, L. (2005). *Reduktion der Bewehrungsüberdeckung bei vorhandener Beschichtung bei Parkhaus-Neubauten*. Number T 3063. Stuttgart: Fraunhofer IRB, 1st edition. 120 pp. German language.

[Refait et al., 1998] Refait, P., Abdelmoula, M., & Genin, J.-M. (1998). 'Mechanisms of formation and structure of green rust one in aqueous corrosion of iron in the presence of chloride ions'. *Corrosion Science*, **40**(9), pp. 1547–1560.

[Refait & Génin, 1997] Refait, P. & Génin, J.-M. (1997). 'The mechanisms of oxidation of ferrous hydroxychloride beta-Fe2(OH)3Cl in aqueous solution: the formation of akaganeite vs goethite'. *Corrosion Science*, **39**(3), pp. 539–553.

[Refait & Génin, 1993] Refait, P. & Génin, J.-M. R. (1993). 'The oxidation of ferrous hydroxide in chloride-containing aqueous media and pourbaix diagrams of green rust one'. *Corrosion Science*, **34**(5), pp. 797–819.

[Rehm et al., 1988] Rehm, G., Nürnberger, U., Neubert, B., & Nenninger, F. (1988). *Chloridkorrosion von Stahl in gerissenem Beton*. DAfStb Heft 390. Deutscher Ausschuss für Stahlbeton, Berlin, Germany. 156 pp. German language.

[Rendell et al., 2002] Rendell, F., Jauberthie, R., & Grantham, M. (2002). *Deteriorated Concrete - Inspection and physicochemical analysis*. London, UK: Thomas Telford, 1st edition. 208 pp.

[Richardson, 2003] Richardson, M. (2003). *Fundamentals of Durable Reinforced Concrete*. Modern Concrete Technology Series. Portland, OR, USA: Taylor & Francis, 1st edition. 208 pp.

[Rémazeilles & Refait, 2007] Rémazeilles, C. & Refait, P. (2007). 'On the formation of beta-FeOOH (akaganeite) in chloride-containing environments'. *Corrosion Science*, **49**(2), pp. 844–857.

[Roberge, 2007] Roberge, P. R. (2007). *Corrosion Doctors*. Royal Military College, Kingston, Ontario. Website, http://www.corrosion-doctors.org, accessed: 27-Aug-2007.

[Rodriguez & Hooton, 2003] Rodriguez, O. & Hooton, R. (2003). 'Influence of Cracks on Chloride Ingress into Concrete'. *ACI Materials Journal*, **100**(2), pp. 120–126.

[Roine, 2002] Roine, A. (2002). *Outokumpu HSC Chemistry. Version 5. Chemical Reaction and Equilibrium Software with Extensive Thermochemical Database. User's Guide*. Manual. Outokumpu, Pori, Finland. 414 pp.

[Rostam, 1996] Rostam, S. (1996). 'Service life design for the next century'. In Sakai, P. K. (Ed.). *Proceedings of the International Workshop Rational Design of Concrete Structures under Severe Conditions*. London, UK: E & FN Spon.

[Rostam, 2003] Rostam, S. (2003). 'Reinforced concrete structures - Shall concrete remain the dominating means of corrosion prevention?'. *Materials and Corrosion*, **54**(6), pp. 369–378.

[Rostam, 2007] Rostam, S. (2007). *Durability and Service Life Design*. Personal communication. COWI A/S, Kgs. Lyngby, Denmark.

[Rousseau & Bernheim, 2007] Rousseau, G. & Bernheim, J. (2007). *Crystallised Hydrated Potassium Ferrite prepared in the Dry Way*. Extract from article. Royal Society of Chemistry, London, UK. 2 pp. Available online, http://www.rsc.org, accessed: 12-Aug-2007.

[Rörig-Dalgaard & Ottosen, 2007] Rörig-Dalgaard, I. & Ottosen, L. M. (2007). 'Preservation of murals on salt loaded masonry vaults by electromigration', pp. 309–318. In *Proceedings of Tenth International Conference on Studies, Repairs and Maintenance of Heritage Architecture (STREMAH), Prague, Czech Republic*. Ashurst, UK.

[Rupprecht, 1999] Rupprecht, L. E. (1999). *Conductive Polymers and Plastics in Industrial Applications*. Norwich, NY, USA: Plastics Design Library, 1st edition. 302 pp.

[Rusinowski et al., 2006] Rusinowski, P., Enochsson, O., & Täljsten, B. (2006). 'Numerical analysis of two-way concrete slabs with openings strengthened with CFRP', pp. 387–390. In *Proceedings of* 3rd *International Conference on FRP Composites in Civil Engineering (CICE)*. Miami, FL, USA.

[SA, 2007] SA (2007). *Solartron Analytical Electrochemical Instrumentation*. Solartron Analytical, Farnborough, UK. Website, http://www.solartronanalytical.com, accessed: 17-Apr-2007.

[Sagoe-Crentsil & Glasser, 1989] Sagoe-Crentsil, K. K. & Glasser, F. P. (1989). 'Steel in concrete. Part I. A review of the electrochemical and thermodynamic aspects'. *Magazine of Concrete Research*, **41**(149), pp. 205–212.

[Sagoe-Crentsil & Glasser, 1993] Sagoe-Crentsil, K. K. & Glasser, F. P. (1993). '"Green rust", iron solubility and the role of chloride in the corrosion of steel at high pH'. *Cement and Concrete Research*, **23**(4), pp. 785–791.

[Sagüés, 1991] Sagüés, A. A. (1991). 'Critical Issues in Electrochemical Corrosion Measurement Techniques for Steel in Concrete', pp. Paper 141, 21 pp. In *Corrosion/91. The NACE Annual Conference and Corrosion Show*. Houston, TX.

[Sandberg, 1998] Sandberg, P. (1998). *Chloride initiated reinforcement corrosion in marine concrete*. PhD thesis (report TVBM-1015). Division of Building Materials, Lund Institute of Technology, Lund, Sweden. 86 pp.

[Saremi & Mahallati, 2002] Saremi, M. & Mahallati, E. (2002). 'A study of chloride induced depassivation of mild steel in simulated concrete pore solution'. *Cement and Concrete Research*, **32**(12), pp. 1915–1921.

[Sarja & Vesikari, 1996] Sarja, A. & Vesikari, E. (Eds.) (1996). *Durability Design of Concrete Structure*. Number 14 in Rilem Report. London, UK: E & FN Spon (Chapman & Hall), 1st edition. 165 pp.

[Schießl, 1986] Schießl, P. (1986). *Einfluß von Rissen auf die Dauerhaftigkeit von Stahlbeton- und Spannbetonbauteilen*. DAfStb Heft 370. Deutscher Ausschuss für Stahlbeton, Berlin, Germany. 129 pp. German language.

[Schießl, 1988] Schießl, P. (1988). 'Cracking of concrete and durability of concrete structures', pp. 3.1–3.8. In *Proceedings of AFREM-CCE*. St. Rémy les Chevreuse, France.

[Schießl et al., 1988] Schießl, P., Andrade, C., Bakker, R., Page, C. L., & Treadaway, K. (1988). *Corrosion of Steel in Concrete*. RILEM Technical Committee 60-CSC. New York, NY, USA: Chapman & Hall, 1st edition. 102 pp.

[Schießl et al., 1995] Schießl, P., Brauer, N., & Breit, W. (1995). *Transport-, Ausheilungs- und Korrosionsmechanismen bei Flüssigkeiten in Rissen*. Technical report F 379. RWTH Aachen University, Aachen, Germany. 155 pp. German language.

[Schießl & Breit, 1996] Schießl, P. & Breit, W. (1996). 'Local repair measures at concrete structures damaged by reinforcement corrosion – Aspects of durability'. *Special Publications of the Royal Society of Chemistry*, **183**, pp. 525–534.

[Schießl & Raupach, 1990] Schießl, P. & Raupach, M. (1990). 'Influence of concrete composition and microclimate on the critical chloride content in concrete', pp. 49–58. In Page, C. L., Treadaway, K. W. J., & Bamforth, P. B. (Eds.). *Corrosion of reinforcement in concrete*. London, UK: Elsevier Applied Science.

[Schießl & Raupach, 1995] Schießl, P. & Raupach, M. (1995). 'Influence of Temperature on the Corrosion Rate of Steel in Concrete Containing Chlorides', pp. 537–549. In Alshamsi, A. M. (Ed.). *Reinforced Concrete Materials in Hot Climates*. Portland, OR, USA: Taylor & Francis.

[Schießl & Raupach, 1997] Schießl, P. & Raupach, M. (1997). 'Laboratory Studies and Calculations on the Influence of Crack Width on Chloride-Induced Corrosion of Steel in Concrete'. *ACI Materials Journal*, **94**(1), pp. 56–62.

[Schießl et al., 1994] Schießl, P., Sørensen, B., Andrade, C., Polder, R., Isecke, B., & Page, C. (1994). 'Draft recommendation for repair strategies for concrete structures damaged by reinforcement corrosion'. *Materials and Structures*, **27**(171), pp. 415.

[Scholz et al., 1999] Scholz, W., Hiese, W., & Knoblauch, H. (1999). *Baustoffkenntnis*. Düsseldorf, Germany: Werner. 942 pp. German language.

[Schroeder, 2000] Schroeder, Daniel V., A. W. . (2000). *An Introduction to Thermal Physics*. London, UK: Addison Wesley (Pearson), 1st edition. 422 pp.

[Schutter, 1999] Schutter, G. d. (1999). 'Quantification of the influence of cracks in concrete structures on carbonation and chloride penetration'. *Magazine of Concrete Research*, **51**(6), pp. 427–435.

[Scribner, 2004] Scribner (2004). *ZPlot for Windows. Version 1.4b*. Electrochemical impedance spectroscopy software. Scribner Associates, Southern Pines, NC, USA.

[Sharp et al., 2002] Sharp, S. R., Clemeña, G. G., Virmani, Y. P., Stoner, G. E., & Kelly, R. G. (2002). *Electrochemical Chloride Extraction: Influence of Concrete Surface on Treatment*. Report FHWA-RD-02-107. Federal Highway Administration, Washington, DC, USA. 43 pp.

[Sharp & Virmani, 2006] Sharp, S. R. & Virmani, Y. P. (2006). *Factors That Influence the Efficiency of Electrochemical Chloride Extraction during Corrosion Mitigation in Reinforced Concrete Structures*. Report VTRC 06-R16. Virginia Transportation Research Council, Charlottesville, VA, USA. 30 pp.

[Shock & Helgeson, 1988] Shock, E. & Helgeson, H. C. (1988). 'Calculation of the thermodynamic and transport properties of aqueous species at high pressures and temperatures: Correlation algorithms for ionic species and equation of state predictions to 5 kb and 1000 degree C'. *Geochimica et Cosmochimica Acta*, **52**, pp. 2009–2036.

[Shock & Korezky, 1993] Shock, E. & Korezky, C. M. (1993). 'Metal-organic complexes in geochemical processes: Calculation of standard partial molal thermodynamic properties of aqueous acetate complexes at high pressures and temperatures'. *Geochimica et Cosmochimica Acta*, **57**, pp. 4899–4922.

[Shock et al., 1997] Shock, E., Sassani, D., Willis, M., & Sverjensky, D. (1997). 'Inorganic species in geologic fluids: Correlations among standard molal properties of aqueous ions and hydroxide complexes'. *Geochimica et Cosmochimica Acta*, **61**, pp. 907–951.

[Sofin & Jansen, 2005] Sofin, M. & Jansen, M. (2005). 'Synthesis, crystal structure and magnetic properties of ß-Na3FeO3'. *Solid State Sciences*, **8**(1), pp. 19–23.

[SSR, 2007] SSR (2007). *Stainless Steel Rebar. International Bulletin*. Tullmin Consulting, Kingston, Canada. Website, http://www.stainless-rebar.org, accessed: 02-Jul-2007.

[Stern & Geary, 1957] Stern, M. & Geary, A. L. (1957). 'Electrochemical polarization I. A theoretical analysis of the shape of polarization curves'. *Journal of the Electrochemical Society*, **104**(1), pp. 56–63.

[Storebælt, 1997] Storebælt (1997). *The Great Belt Link. East Tunnel. Focus on the bored tunnel for trains.* The Storebaelt Publications. Copenhagen, Denmark: Storebælt A/S, 1st edition. 179 pp.

[Straschill, 1972] Straschill, M. (1972). *Neuzeitliches Beizen von Metallen*. Schriftenreihe Galvanotechnik. Saulgau, Germany: Leuze. 180 pp. German language.

[Streeb & Hoffmann, 1969] Streeb, R. & Hoffmann, R. (1969). *Metall-Entfettung und -Reinigung*. Schriftenreihe Galvanotechnik. Saulgau, Germany: Eugen G. Leuze. 308 pp. German language.

[Østvik, 2005] Østvik, J.-M. (2005). *Thermal Aspects of Corrosion of Steel in Concrete*. PhD thesis. Norwegian University of Science and Technology (NTNU), Trondheim, Norway. 328 pp.

[Taylor, 1997] Taylor, H. F. W. (1997). *Cement Chemistry*. London, UK: Thomas Telford, 2nd edition. 480 pp.

[THDA, 2007] THDA (2007). *Thermodynamic Properties Of Inorganic Substances Inorganic Chemistry*. THERMODATA, Grenoble, France. Website, http://thermodata.online.fr, accessed: 15-Sep-2007.

[Thompson et al., 2000] Thompson, N. G., Yunovich, M., & Lankard, D. R. (2000). *Procedures for Evaluating Corrosion-Inhibiting Admixtures for Structural Concrete*. Report NCHRP Web Document 29 (Project D10-45). National Cooperative Highway Research Program, Transportation Research Board, National Research Council, Washington, DC, USA. 216 pp.

[Täljsten & Carolin, 2007] Täljsten, B. & Carolin, A. (2007). 'Near Surface Mounted Reinforcement (NSMR) to strengthen concrete structures', pp. 341–354. In *International Conference on Sustainable Bridges*. Wroclaw, Poland.

[Tomlinson & Marsh, 1988] Tomlinson, W. & Marsh, P. (1988). 'Corrosion of iron, steel, zinc, nickel and electroless nickel in concrete'. *Journal of Materials Science Letters*, **7**(8), pp. 808–810.

[Trethewey & Chamberlain, 1995] Trethewey, K. R. & Chamberlain, J. (1995). *Corrosion: For Students of Science and Engineering*. Upper Saddle River, NJ, USA: Prentice-Hall, 2nd edition. 466 pp.

[Tripler et al., 1966] Tripler, A. B., White, E. L., Haynie, F. H., & Boyd, W. K. (1966). *Methods of Reducing Corrosion of Reinforcing Steel*. Report 23. Highway Research Board, Washington, DC, USA. 22 pp.

[Trépanier et al., 2001] Trépanier, S. M., Hope, B. B., & Hansson, C. M. (2001). 'Corrosion inhibitors in concrete - Part III: Effect on time to chloride-induced corrosion initiation and subsequent corrosion rates of steel in mortar'. *Cement and Concrete Research*, **31**(5), pp. 713–718.

[Tuutti, 1982] Tuutti, K. (1982). *Corrosion of steel in concrete*. Report 4-82. Swedish Cement and Concrete Research Institute, Stockholm, Sweden. 469 pp.

[Val & Stewart, 2003] Val, D. V. & Stewart, M. G. (2003). 'Life-cycle cost analysis of reinforced concrete structures in marine environments'. *Structural Safety*, **25**(4), pp. 343–362.

[Vaysburd & Emmons, 2004] Vaysburd, A. & Emmons, P. (2004). 'Corrosion inhibitors and other protective systems in concrete repair: concepts or misconcepts'. *Cement and Concrete Composites*, **26**(3), pp. 255–263.

[VDEh, 1999] VDEh (1999). *Stahl-Eisen-Liste. Register Europäischer Stähle*. Dessau, Germany: Verein Deutscher Eisenhüttenleute (VDEh), 10th edition. 306 pp. German language.

[Volkwein, 1991] Volkwein, A. (1991). *Untersuchungen über das Eindringen von Wasser und Chlorid in Beton*. PhD thesis. Technical University of Munich, Munich, Germany. 131 pp. German language.

[Wagman et al., 1982] Wagman, D. D., Evans, W. H., Parker, V. B., Schumm, R. H., & Halow, I. (1982). 'The NBS Tables of Chemical Thermodynamic Properties. Selected Values for Inorganic and C1 and C2 Organic Substances in SI Units'. *Journal of Physical and Chemical Reference Data*, **11**, pp. 405. Supplement no. 2 to volume 11.

[Wagner & Traud, 1938] Wagner, C. & Traud, W. (1938). 'Über die Deutung von Korrosionsvorgängen durch Überlagerung von Elektrochemischen Teilvorgängen und über die Potentiallbildung an Mischelektroden'. *Zeitschrift für Elektrochemie und angewandte physikalische Chemie*, **44**(7), pp. 391–454. German language.

[Walker & Tarn, 1990] Walker, P. & Tarn, W. H. (1990). *CRC Handbook of Metal Etchants*. Boca Raton , FL, USA: CRC, 1st edition. 1415 pp.

[Wang et al., 1997] Wang, K., Jansen, D., Shah, S., & Karr, A. (1997). 'Permeability Study of Cracked Concrete'. *Cement and Concrete Research*, **27**(3), pp. 381–393.

[WebEle, 2007] WebEle (2007). *WebElements. Periodic Table*. University of Sheffield, Sheffield, UK. Website, http://www.webelements.com/, accessed: 22-Aug-2007.

[WebMin, 2007] WebMin (2007). *Mineralogy Database*. Barthelmy, David, Spring, TX, USA. Website, http://www.webmineral.com, accessed: 22-Aug-2007.

[Weidmann, 2002] Weidmann, E. (2002). *Metallographic Preparation of Zinc Coatings*. Application notes. Struers A/S, Ballerup, Denmark. 6 pp.

[Weidmann & Guesnier, 2006] Weidmann, E. & Guesnier, A. (2006). *Metallographic Preparation of Cast Iron*. Application notes. Struers A/S, Ballerup, Denmark. 6 pp.

[Weidmann et al., 2005] Weidmann, E., Guesnier, A., & Taylor, B. (2005). *Metallographic Preparation of Stainless Steel*. Application notes. Struers A/S, Ballerup, Denmark. 6 pp.

[Wheat & Harding, 1993] Wheat, H. & Harding, K. (1993). 'Galvanic corrosion in repaired reinforced concrete slabs. An update'. *Materials Performance*, **32**(5), pp. 58–62.

[Wikimedia, 2007] Wikimedia (2007). *Wikipedia. The Free Encyclopedia*. Wikimedia Foundation, St. Petersburg, FL, US. Website, http://en.wikipedia.org, accessed: 27-Aug-2007.

[Wilkins & Sharp, 1990] Wilkins, N. J. M. & Sharp, J. V. (1990). 'Localised corrosion of reinforcement in marine concrete', pp. 3–18. In Page, C. L., Treadaway, K. W. J., & Bamforth, P. B. (Eds.). *Corrosion of reinforcement in concrete*. London, UK: Elsevier Applied Science, 1st edition.

[Win et al., 2004] Win, P., Watanabe, M., & Machida, A. (2004). 'Penetration Profile of Chloride Ions in Cracked Reinforced Concrete'. *Cement and Concrete Research*, **34**, pp. 1073–1079.

[Wittekindt, 1954] Wittekindt, W. (1954). 'Acid resisting Ocrat concrete'. *Zement-Kalk-Gips*, **7**(9), pp. 337–342. German language.

[WOU, 2007] WOU (2007). *Pourbaix Diagrams*. Western Oregon University (WOU), Monmouth, OR, USA. Website, http://www.wou.edu/, accessed: 24-Aug-2007.

[Yaws, 2003] Yaws, C. L. (2003). *Yaws' Handbook of Thermodynamic and Physical Properties of Chemical Compounds*. Knovel Corporation, New York, NY, USA. Website, http://www.knovel.com, accessed: 15-Sep-2007.

[Yeomans, 2004] Yeomans, S. R. (2004). *Galvanized Steel Reinforcement in Concrete*. London, UK: Elsevier, 1st edition. 316 pp.

[Zhang & Mailvaganam, 2006] Zhang, J. & Mailvaganam, N. P. (2006). 'Corrosion of concrete reinforcement and electrochemical factors in concrete patch repair'. *Canadian Journal of Civil Engineering*, **33**(6), pp. 785–793.

[Zhang, 1996] Zhang, X. G. (1996). *Corrosion and Electrochemistry of Zinc*. New York, NY, USA: Plenum Press, 1st edition. 474 pp.

List of Figures

List of Tables

List of Chemical Species

The formulas of the most important chemical species mentioned throughout this thesis are listed alphabetically together with their corresponding names in the table below.

Formula	Name
Ag	Silver
AgCl	Silver chloride
$AgNO_3$	Silver nitrate
C	Carbon
Ca	Calcium
$CaCl_2$	Calcium chloride
$CaCO_3$	Calcium carbonate
CaF_2	Calcium fluoride
$CaMg(CO_3)_2$	Calcium magnesium carbonate (dolomite)
CaO	Calcium oxide
CaO_2	Calcium peroxide
$Ca(OH)_2$	Calcium hydroxide
$3CaO{\cdot}Al_2O_3$	Tricalcium aluminate
$4CaO{\cdot}Al_2O_3{\cdot}Fe_2O_3$	Tetracalcium ferroaluminate
$2CaO{\cdot}SiO_2$	Dicalcium silicate
$3CaO{\cdot}SiO_2$	Tricalcium silicate
$CaSiO_3$	Calcium silicate
$CaSO_4{\cdot}2H_2O$	Gypsum
$C_{20}H_{14}O_4$	Phenolphthalein
CO_3^{2-}	Carbonate ion
Cl	Chloride
Cl^-	Chloride ion
ClO_4^-	Perchlorate ion
CO_2	Carbon dioxide
Cr	Chrome
Cr^{2+}	Chromous ion
Cr^{3+}	Chromic ion
Cr_2O_3	Chromic oxide
CrO_2^-	Chromite ion
CrO_4^{2-}	Chromate ion
Cr_2FeO_4	Chromium iron oxide
Cu	Copper
Cu^{2+}	Cupric ion
$CuSO_4$	Cupric sulphate
Fe	Iron

Formula	Name
Fe^{2+}	Ferrous ion
Fe^{3+}	Ferric ion
$FeCl^+$	Ferrous chloride
$FeCl_2^+$	Ferric chloride
Fe_2O_3	Hematite
Fe_3C	Cementite
$FeCO_3$	Iron carbonate (siderite)
Fe_3O_4	Magnetite
FeO_2^-	Ferrite ion
FeOOH	Goethite
$Fe(OH)_2$	Iron-(II)-hydroxide
$Fe(OH)_3$	Iron-(III)-hydroxide
H^+	Hydrogen ion
H_2	Hydrogen
H_2O	Water
HCl	Hydrochloric acid
HCO_3^-	Hydrogen carbonate ion
$HCrO_4^-$	Hydrogen chromate ion
$HFeO_2^-$	Bihypoferrite ion
Hg	Mercury
Hg_2Cl_2	Mercury chloride (calomel)
$HZnO_2^-$	Bizincate ion
Ir	Iridium
IrO_2	Iridium-(IV)-oxide
Ir_2O_3	Iridium-(III)-oxide
K	Potassium
K^+	Potassium ion
KCl	Potassium chloride
KOH	Potassium hydroxide
Mg	Magnesium
Mg^{2+}	Magnesium ion
MgO_2	Magnesium peroxide
$Mg(OH)_2$	Magnesium hydroxide
Mo	Molybdenum

Formula	Name
Mn	Manganese
MnO_2	Manganese trioxide
Mn_2O_3	Manganese dioxide
N_2	Nitrogen
Na^+	Sodium ion
NaCl	Sodium chloride
NaOH	Sodium hydroxide
Na_2PO_3F	Sodium monofluorophosphate
Ni	Nickel
Ni^{2+}	Nickelous ion
O_2	Oxygen
OH^-	Hydroxyl
SiF_4	Silicon tetrafluoride
SiO_2	Silicon dioxide

Formula	Name
SO_4^{2-}	Sulphate ion
Ti	Titanium
Zn	Zinc
Zn^{2+}	Zinc ion
$ZnCl^+$	Chlorozinc ion
$ZnCO_3$	Zinc carbonate
$ZnFe_2O_4$	Zinc ferrite
ZnO_2^{2-}	Zincate ion
$Zn(OH)_2$	Zinc hydroxide
α-Fe	Ferrite
α- Fe_2O_3	Hematite
γ-Fe_2O_3	Maghemite
α-FeOOH	Goethite
β-FeOOH	Akaganeite
γ-FeOOH	Lepidocrocite

In this thesis a consistent thermodynamic basis is established for the description of corrosion processes as well as for the evaluation of existing and the development of new corrosion countermeasures.

The work covers: a) the adaptation of available thermodynamic principles to the area of reinforcement corrosion, b) thermodynamically consistent descriptions for the diverse corrosion states of steel in concrete, c) a review and evaluation of available measures for corrosion protection, and d) the development of theoretical concepts for new cost-efficient countermeasures.

In addition to the theoretical considerations, two implementation principles of the developed concepts are proposed and one of these tested by means of custom-designed setups and measurement methods.

DTU Civil Engineering
Department of Civil Engineering
Technical University of Denmark

Brovej, Building 118
2800 Kgs. Lyngby
Telephone 45 25 17 00

www.byg.dtu.dk

ISBN: 9788778773074
ISSN: 1601-2917